Strain rate dependency of the properties of a unidirectional thermoplastic composite material

By

Nikolaos Papadakis

A thesis submitted in partial fulfilment of the requirements for the degree of Doctor of Philosophy in Engineering

Volume 1 – Thesis

University of Warwick, School of Engineering

October 2002

Best Copy Available

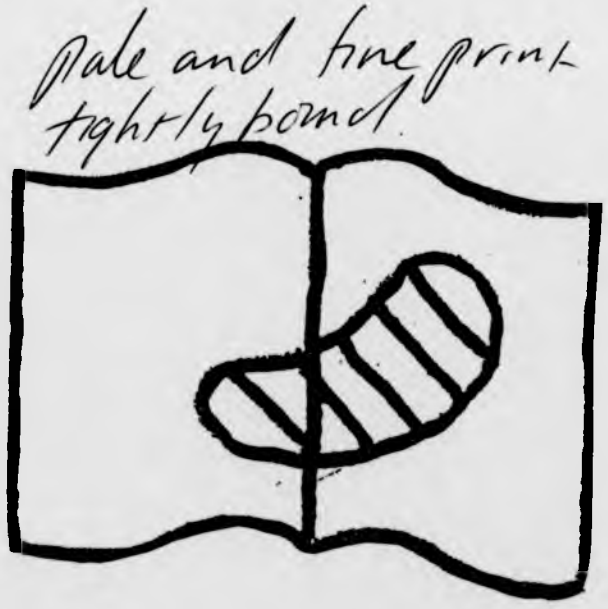

Abstract

This research work established the strain rate dependency of the the mechanical properties of a highly orientated glass fibre/thermoplastic composite lamina and validated a model for Computer Aided Engineering (CAE). The mechanical properties examined for strain rate dependency were elasticity, strength and damage evolution at a ply level.

A rigourous statistical methodology were established and implemented through mechanical testing together with processing of the results for the development of semi-empirical strain rate models.

Two different methods of data acquisition were considered, specifically strain measurement using videoextensometry and contacting extensometry. The resulting strain measurements were then computed. Video extensometry appeared to have clear advantages, however, scatter in the response was appreciably higher compared to the contacting extensometry. This was due to the much smaller scale of gauge length for strain measurement.

A rigourous validation methodology was further complemented through a statistical procedure and tool kit (utilising statistical tools and procedures like density distributions plot, hypothesis testing, analysis of variance). The statistical tool kit was developed to enable objective assessment of strain rate dependency and to establish the quality of a relationship (model) should one exist for the range of mechanical properties tested. Using this validation methodology, a semi empirical strain rate dependent model was validated for elasticity strength and damage evolution.

The effect of strain rate on the above mechanical properties was investigated for $Plytron^{TM}$. The $Plytron^{TM}$ material was supplied by Borealis as a 100mm-wide, 0.22[mm]-deep tape, comprising aligned continuous glass fibres in a polypropylene matrix. To manufacture a laminate, the tape was laid-up ply-by-ply into an unconsolidated stack. This stack was then consolidated using under pressure and heat according to a Warwick Manufacturing Group's proprietary membrane-forming process [1]. For the purposes of this study, specimens were machined in accordance with ISO-527-4 from 4 different layup sequences: $[0°]_4$, $[\pm 45°]_{2s}$, $[+45°]_8$ and $[\pm 67.5°]_{2s}$. The specimens were tested at 5, 50 and 500[mm/min] crosshead displacement rates using monotonic and cyclic loading.

From this investigation, over the examined strain rate range, the longitudinal tensile modulus increased with strain rate, while the shear modulus and Poisson's ratio decreased. The transverse tensile modulus did not exhibit any statistically significant difference. The shear failure stress and the longitudinal tensile failure strain and stress appeared to increase for increasing strain rate, while the shear failure strain were not strain rate dependent. The transverse tensile failure stress and strain did not exhibit any statistically significant strain rate dependency.

The characterisation parameters of the damage evolution were based on the global composite ply model for composites in the framework of continuum damage mechanics (CDM). This model was developed by Ladevéze et al. [2], [3], for thermosetting composites. It was established that shear damage evolution of the thermoplastic materials exhibits different behaviour compared to thermosets. It also was established that the rate of shear damage evolution decreases with increasing strain rate and that the point that shear damage initiates increases with increasing strain rate.

All testing was conducted with INSTRON 4505 universal testing machine instrumented with a 100[kN] load cell. Contacting extensometry and videoextensometry has been examined as data acquisition methods. It was established in this work that contacting extensometry provided data with less scatter, however the videoextensometry exhibited significant advantages.

Having established and validated semi-empirical rate dependent models, for the characterisation parameters to service the CDM models, CAE models were established and validated using a well known explicit FE numerical simulation. To maintain rigour, the validation methodology employed new metrics to enable objective comparison between FE and experimental results. These metrics are Pearson correlation coefficient and correlation range ratio. The comparison of experimental to FEM results revealed that the available models predict adequately well the stiffness of laminates as expected.
The onset of failure is predicted at significantly lower strains compared to the experimental results (depended on layup - usually 30% of the total failure strain). The premature failure is attributed to the failure criterion implementation at ply level and/or the definition of the boundary conditions.

Keywords : strain rate, characterisation, shear damage, mechanical properties, glass/thermoplastic composite system, FEM.

Dedication.

This is dedicated to G. Tagaras, for being an inspiration during my academic life.

And to my grandfather Nikos I. Papadakis, who never got to see the completed work.

There is surely nothing other than the single purpose of the present moment. A man's whole life is a succession of moment after moment. If one fully understands the present moment, there will be nothing else to do, and nothing left to pursue.

The end is important in all things.

Yamamoto Tsunetomo

HAGAKURE

Japan, September 1716

Acknowledgments.

I would like to thank my supervisors Dr Paul Wood and Dr Mark Pharaoh for their support and guidance during my studies and in the preparation of this research thesis. My acknowledgements also go to Neil Reynolds whose support and help throughout the PhD was invaluable. Working together with these people on the CRACTAC project has been a privilege.

I would also like to thank the technicians (especially Walter Cosgriph and Rob Bromley) in the ATC for doing such a good job cutting the specimens I've requested. (I am sorry they were so many).

A big thank you goes to every friend that helped me have a fun time in Warwick while completing this PhD. I cannot thank all of you in this section, but you know who you are.

Most of all I would like to acknowledge the contribution of my parents and grandparents to the completion of this work. Thanks for teaching me the value of hard work and persistence and for supporting my effort all these years, although I know that you've missed me as much as I did. To my only brother, Tony, thank you for listening and supporting me when I had those bad days.

Declaration.

I declare that all the work described in this report was undertaken by myself (unless otherwise acknowledged in the text) and that none of the work has been previously submitted for any academic degree. All sources of quoted information have been acknowledged by means of references.

N. Papadakis

October 2002

Contents

List of Figures

List of Tables

Abbreviations.

ATC : Advanced Technology Centre;

CAE : Computer Aided Engineering;

CCD : Charge Coupled Device;

FE : Finite Elements;

cdf : Cumulative density function;

CDR : Crosshead displacement rate;

CRR : Correlation Range Ratio;

DILA : Dynamic Interface Loading Apparatus;

GFRP : Glass fibre reinforced composite;

GFRTP : Glass fibre reinforced thermoplastic composite;

FRP : Fibre reinforced plastic;

FE : Finite Element;

Ins : Instron;

LPCC : Longitudinal Pearson's Correlation Coefficient;

LCRR : Longitudinal Correlation Range Ratio;

PCC : Pearson's Correlation Coefficient;

pdf : Probability density function;

RVE : Representative volume element;

TPCC : Transverse Pearson's Correlation Coefficient;

TCRR : Transverse Correlation Range Ratio;

UD : Uni-directional;

VE : Video-extensometry;

Notation.

- General ply properties:

  ρ^{UD} Mass density;

  t^{UD} Ply thickness;

  v_f : Fibre volume fraction;

  A : Cross-sectional area;

- Elasticity properties:

  $E^f_{t,0}$: Tensile fibre Young's modulus;

  $E^f_{c,0}$: Compressive fibre Young's Modulus;

  $E^m_{11,t,0}$, $E^m_{22,t,0}$, $E^m_{33,t,0}$: Matrix phase tensile stiffness modulii;

  $E^m_{11,c,0}$, $E^m_{22,c,0}$, $E^m_{33,c,0}$: Matrix phase compression stiffness modulii ;

  $G^m_{12,t,0}$, $G^m_{13,t,0}$, $G^m_{23,t,0}$: Matrix phase shear modulii;

  $G^m_{12,c,0}$, $G^m_{13,c,0}$, $G^m_{23,c,0}$: Matrix phase shear modulii;

  $\nu^m_{12,t}$, $\nu^m_{13,t}$, $\nu^m_{23,t}$: Matrix phase Poisson's ratio under tensile loading;

  $\nu^m_{12,c}$, $\nu^m_{13,c}$, $\nu^m_{23,c}$: Matrix phase Poisson's ratio under compressive loading;

$E_{11,t,0}$, $E_{22,t,0}$, $E_{33,t,0}$: Ply tensile stiffness modulii;

$E_{11,c,0}$, $E_{22,c,0}$, $E_{33,c,0}$: Ply compression stiffness modulii ;

$G_{12,t,0}$, $G_{13,t,0}$, $G_{23,t,0}$: Ply shear modulii;

$G_{12,c,0}$, $G_{13,c,0}$, $G_{23,c,0}$: Ply shear modulii;

$\nu_{12,t}$, $\nu_{13,t}$, $\nu_{23,t}$: Ply Poisson's ratio under tensile loading;

$\nu_{12,c}$, $\nu_{13,c}$, $\nu_{23,c}$: Ply Poisson ratio under compressive loading;

- Strength Properties

$\varepsilon_{11,f}, \varepsilon_{22,f}, \varepsilon_{33,f}$: Ply tensile failure strains.

$\varepsilon_{11,f,c}, \varepsilon_{22,f,c}, \varepsilon_{33,f,c}$: Ply compressive failure strains.

$\gamma_{12,f}, \gamma_{23,f}, \gamma_{31,f}$: Ply shear failure strains.

$\sigma_{11,f}, \sigma_{22,f}, \sigma_{33,f}$: Ply tensile failure stresses.

$\sigma_{11,f,c}, \sigma_{22,f,c}, \sigma_{33,f,c}$: Ply compressive failure strains.

$\tau_{12,f}, \tau_{23,f}, \tau_{31,f}$: Ply shear failure stresses.

- Damage evolution for Bi-Phase material:

$d_t^f(\varepsilon)$: Fibre damage law in tension;

$d_c^f(\varepsilon)$: Fibre damage law in compression;

$d_{v,t}^m(\varepsilon)$: Matrix volumetric damage under tensile loading;

$d_{s,t}^m(\varepsilon)$: Shear Damage law under tensile loading;

$d_{v,c}^m(\varepsilon)$: Matrix volumetric damage under compressive loading;

$d^m_{s.c}(\varepsilon)$: Shear Damage law under compressive loading;

- Damage parameters for the global composite model:

  d: dimensionless shear damage parameter;

  Y_0 : Initial shear damage limit;

  Y_c : Critical shear damage limit;

  Y_R : Elementary shear damage limit;

  d': dimensionless transverse damage parameter;

  Y'_0 : Initial transverse damage limit;

  Y'_c : Critical transverse damage limit;

  Y'_R : Brittle transverse damage limit;

- Coupling factors:

  A^2 : Coupling factor between transverse and shear strains ;

  b : Coupling factor between transverse and shear damage;

- Strain rate laws factors:

  $\sigma_0(\varepsilon)$: is the stress at the reference strain rate;

  $\sigma_0(\varepsilon, \dot{\varepsilon})$: is the stress at the strain rate;

  $\dot{\varepsilon}_0$: is the reference strain rate;

  $\varepsilon_u, \varepsilon_y$: are the reference strains for the Modified Jones constitutive law;

  $D, D_u, D_y, p, A, B, n_{ref}, \dot{\nu}, c$: Arbitrary constants from curve fitting.

Laminate Code.

There are slight variations but generally the following rules are followed[13]:

- The orientation of each lamina with respect to the x -axis is indicated by the angle between the fiber direction and the x-axis. Positive angles are measured counter-clockwise from the x-axis when looking toward the lay-up surface (right-hand rule).
- When indicating the lay-up of a weave, the angle is measured between the warp direction and the x-axis.
- Orientations of successive laminae with different absolute values are separated by a virgule (/). Some authors prefer comma (,) to separate the different laminas.
- Two or more adjacent laminae with the same orientation are indicated by adding a subscript, to the angle of the first such lamina, equal to the number of repetitions of laminae with that orientation.
- Laminae are listed in order from the first laid up to the last. Brackets are used to indicate the be-ginning and the end of the code.
- A subscript of 's' is used if the first half of the lay-up is indicated and the second half is

symmetric with the first. When a symmetric lay-up with an odd number of laminae is shown, the layer which is not repeated is indicated by overlining the angle of that lamina.

- A repeated set of laminae are enclosed in parentheses and the number of repetitions of the set indicated by a subscript.
- The convention used for indicating materials is no subscript for a tape ply and a subscript "f" for a weave.
- The laminate code for a hybrid has the different materials contained in the laminate indicated by subscripts on the laminae.
- Superscripts can be used to differentiate between plies of different materials.

According to the above rules the following example can be written as: $[0/(-45)^2/60/\overline{30}]$.

0
-45
-45
60
30

Chapter 1

Introduction

1.1 Definition Of A Composite Material

A composite material comprises of two or more distinct phases [1 1]. Depending on the scale at which the material is viewed, the material can be considered heterogeneous.

The higher modulus material phase is usually referred to as the reinforcement phase and the lower modulus material is referred to as the matrix phase.

The reinforcement phase is usually distinguished as either fibres (long or short), or a Particulate. Fibre reinforcements are the focus of this research work, and they may be further categorised as continuous or discontinuous.

The reinforcement phase can be almost any kind of material, from recyclable natural fibres of 10[GPa] modulus and 45[MPa] failure strength, to advanced nano-composites of 1[TPa] and 30[GPa] of tensile failure strength.

The general purpose of the composite materials is to gain advantages from the properties of

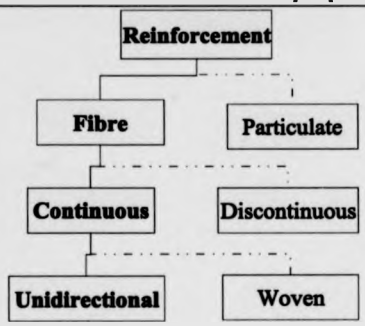

Figure 1.1: Categorisation of the reinforcement type of composite materials.

both constituent materials. Usually the reinforcement phase contributes to the stiffness, while the matrix phase contributes to the ductility and toughness of the composite material.

1.2 Historical Review

Composite materials have been used by man since the beginning of recorded history. They have been used since the time of the Egyptian Pharaohs for brick building and also for making laminated writing materials from papyrus plants. There is even indication that the ancient Egyptians were able to develop a technique for making containers of coarse fibres drawn from heat softened glass [15]. Other natural composite materials like wood have been extensively used throughout the ages both as structural materials but also as an art form.

Materials and processes such as the drawing of fine fibre glass were considered as early as the 18th century by Reaumur, but there were not commercially produced until 1939[16]. However, it was not until the second half of the 20th century that *novel, advanced* fibres were produced: boron(late 1950s) and carbon(1960s).

1.2.1 Composite Materials In Engineering

Composite materials have been employed in engineering very early mainly for masonry. Similarly today, the building industry is using reinforced concrete, one of the first examples of *new* composite materials.

During the twentieth century, recent advances in the material sciences have allowed the use of composite materials in a number of applications, which have required high performance in either structural, thermal insulation properties or a range of different properties.

Aerospace military and commercial applications have made extensive use of composite materials because of the light weight and high specific stiffness and strength properties that they provide, combined with good dimensional stabilities in a wide range of operational temperatures.

1.2.2 Composite Materials In The Automotive Industry

Composite materials have been extensively researched in the last 20 years for implementation in the automotive industry, although the cost of these materials was believed to be high compared to alternative technologies.

Initially, the use of composite materials has been extensive only in high performance automotive applications, like motor racing (Formula 1) where cost is not a primary driver.

The first motivation for the use of composite materials in the automotive industry came from the requirement for more efficient energy consumption. The low density of the materials provided a quick path to lowering the weight of a car and therefore improving energy consumption - *lean weight vehicles.*

At a later stage, aesthetic and manufacturing drivers have further increased the use of composite

materials. The ease of manufacturing and moulding of polymeric composites for non structural components compared to their metallic counterparts (using expensive press tooling) has allowed reduction of the manufacturing cost. Furthermore, the assembly time, and therefore costs, are reduced because of the possibilities of integrating more functions in one component.

Lotus car company has taken composite material usage to the next step. The extensive use of composites in their automotive chassis was perceived as a performance and marketing advantage, exhibiting technological innovation and lead in the field. Lotus has successfully managed to take advantage of this.

Another application of composite materials in automotive industry with great potential is automotive crashworthiness. Composite materials exhibit very high specific energy absorption during crushing making them ideal candidate materials for the manufacturing of sacrificial crashworthy automotive components.

Therefore the following advantages have been realised so far by the automotive industry:

- Low density which results in weight reduction;
- High specific stiffness and failure strength;
- Reduction of assembly costs through part integration;
- Use of composite technology as marketing tool;
- Low investment cost for tooling for certain operations (wood moulds).
- High energy absorption.

In today's automotive industry all automotive manufacturers utilise composite materials to some degree. So far in the mentioned applications, the use of composite materials has mainly looked

to glass fibre/thermosetting systems. The thermoset provide increased stiffness compared to thermoplastic matrix composite materials and also possess dimensional stability at increased temperatures.

However, recently because of environmental concerns, the legislation on recycling has become increasingly strict. The European commission has a passed the 2000/53/EC directive which mandates that by 2015 95% of the automotive mass will be recycled. Thermoplastic composite matrix phases provide better opportunities for recycling than their thermosetting counterparts.

Also, legislation on automotive crashworthiness is also becoming more stricter. For an automotive component to be approved in a market a number of different tests have to be carried out. As a result, significant costs and time are incurred to the design process and the number of prototypes is best if kept at a minimum. Computer Aided Engineering (CAE) enables this time and cost compression. However the numerical simulation of composite materials requires knowledge in software and hardware input, the know how on basic design with regard to the special problems of non-isotropicity and a simple reliable model for the material and experimental data for composite materials subjected to impact loading conditions[ ]. Further, implementation of CAE on dynamically loaded composite structures requires knowledge and understanding of the response of the composites to high strain-rates[ ].

1.3 Material System

The selected material system for this study is a unidirectional glass/polypropelene matrix composite. A unidirectional composite is one in which long (continuous) fibres are orientated in one direction such that the material is stronger and stiffer in that direction but relatively weak in

other directions and is usually reserved for special applications as it will give the maximum unidirectional properties in comparison to other types of composite[17]. The longitudinal properties of a unidirectional composite are primarily influenced by the fibres while the transverse properties are determined by the matrix[17].

The Glass Fibre Reinforced Polymer (GFRP) Composites consist of a thermosetting or thermoplastic polymer as a matrix phase (e.g. epoxy, polyester, urethane, polypropylene), and thin diameter glass fibres as the reinforcement phase.

1.3.1 Glass Fibres

The main types of glass fibres are E-type (also called fiberglass) and S-type. E stands for electrical, because it was originally designed for electrical applications but lately its use has been extended to other applications (see table 1.1). S-glass contains higher levels of silica, and as a result can operate at higher temperatures, and also has better fatigue properties.

Property	**Units**	**E-Glass**
Specific Gravity	$[\frac{1}{m^3}]$	2.54
Young's modulus E_{11}	[GPa]	72.40
Young's modulus E_{22}	[GPa]	72.40
Poisson's ratio v_{12}	[]	.22
Shear Modulus $G12$	[GPa]	1.17
Ultimate Tensile strength	[MPa]	3447
Typical Fibre diameter	[mm]	.01

Table 1.1: Properties of E-Glass [11] [12]

Pages
Missing
not
Available

7

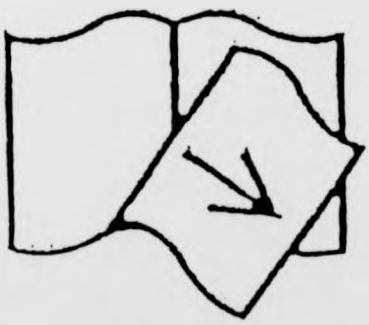

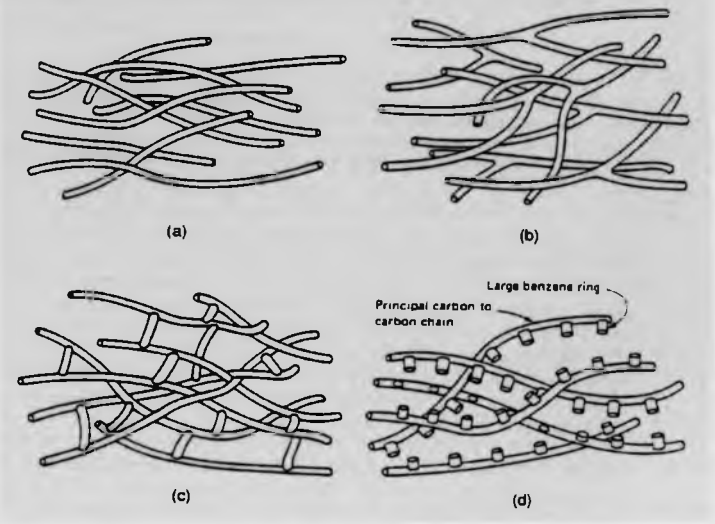

Figure 1.2: Differences of the molecular chains between a thermoset and a thermoplastic ([1, p.73]).

Thermoplastic Resins	**Thermosetting Resins**
Soften on heating and pressure	Decompose on heating
High strains to failure	Low strains to failure
Indefinite shelf life	Usually cold storage
Recyclable	Cannot be readily recycled
Easy to handle (inert, solid at 20°)	Liquid prior to processing - tacky
Short cure cycles	Long cure cycles
Can be difficult to process	Lower fabrication temperature
Excellent solvent resistance	Fair solvent resistance

Table 1.2: Comparison of thermoplastics and thermosets matrix phases [1].

Table 1.3: Properties of the E-glass/PP Plytron material according to manufacturer.

Properties	**Value**
Longitudinal tensile modulus of elasticity E_{11}	28 [GPa]
Transverse modulus of elasticity E_{22}	4 [GPa]
Shear modulusG_{12}	1.349 [GPa]
Major Poisson's ratio v_{12}	.40
Compressive modulus of elasticity $E_{11,C}$	32.5 [GPa]
Density of material ρ	1.48$[\frac{kg}{m^3}]$
Glass content	0.60 [w/w]
Volume fraction v_f	.35 []
Tensile failure strength $\sigma_{11,f}$	720 [MPa]
Transverse failure strength $\sigma_{22,f}$	11 [MPa]
Tensile failure strain $\varepsilon_{11,f}$	1.9 []
Transverse failure strain $\varepsilon_{22,f}$	0.3 []
Iosipescu shear strength $\tau_{12,f}$	19 [MPa]
Compression strength $\sigma_{11,C}$	317 [MPa]

1.4 Damage Mechanics

According to Herakovich [11, p.332], the goal of damage mechanics is to predict the response of a material in the presence of damage that initiates at some stress state. Iannucci et al.[21] state that damage mechanics proved a method which can determine accurately the full range of deterioration of a composite material from the virgin state with no damage to the fully disintegrated material

with full damage. In addition the method has the potential to predict different composite failure modes and allows an energy dissipation mechanism, due to the formation of microcracks and microvoids within the composite, to be included in the damage model[21].

The concepts which are used to define the damage evolution were initiated by Kachanov [22] and Rabotnov [23] in late 1950's and 1960's. Those concepts evolved over following two decades [24, 25, 26] and finally took the form of a formalised Damage mechanics theory in the beginning of the 1990's, following work by Lemaitre and Chaboche[27, 28], Krajcinovic[29], Bazant and Cedolin[30]. The rapid development in recent years of damage mechanics is linked to the fact that its concepts are compatible with the Finite Element Method.

At this point, the concept of damage should be defined. Damage can be associated with an number of phenomena (e.g. crack initiation and propagation, failure, degradation of mechanical properties etc). In this work, the word *damage* is associated with the mathematical (an abstract, non physical) concept of a degradation function applied to a mechanical property of the material, unless otherwise stated.

The elasticity methods, which have been described so far, assume that the materials exhibit a linear/elastic behaviour. However, this is generally not true. Almost all materials when loaded beyond a certain point begin to exhibit non linear and/or plastic behaviour, due to damage that accumulates in the material. The damage generally increases with stress up to macroscopic crack initiation or failure and also predict the conditions for failure[14, p.332].

The mechanics of damage is the study, through mechanical variables of the mechanisms involved in the progressive physical process by which materials break when they are subjected to loading [27, p. 1]. According to the damage mechanics approach, the damage of a material can be described as

an internal variable/function[27]. Krajcinovic[31] states that the history of inelastic deformation and its change may be defined by the evolution of an internal variable that depends on the expected value of the micro-defect density and therefore, the material response is both deterministic and gradual.

In principle, Damage mechanics models can be applied to porous materials weakened by micro voids of all shapes[31]. Materials with markedly different microstructure (e.g. composites, ceramics, rocks, concrete, metals and alloys) exhibit common behaviour. Damage mechanics attempt to explain material behaviour with the mechanics of continuous media and the thermodynamics of irreversible processes, which model the materials without detailed reference to the complexity of their physical microstructure[27].

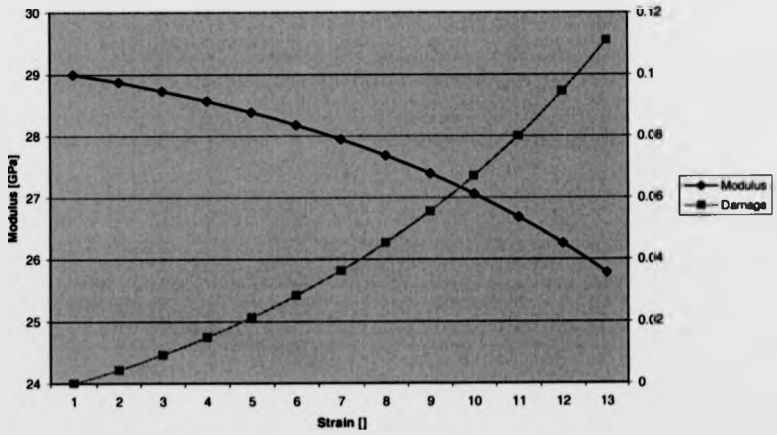

Figure 1.3: Example of damage evolution as a function of strain.

Usually, the damage function is applied to concepts like the stiffness moduli, which tends to degrade with the increase of load/strain (and therefore strain energy density) (e.g. $E(\varepsilon) = E_0 \cdot (1 - d(\varepsilon))$) - where $d(\varepsilon)$ is a damage function. In the case of modulus of elasticity, a damage function value of

0 would correspond to the stiffness of an undamaged material, while a damage value of 1 would correspond to the properties observed after catastrophic failure. Different damage functions can be defined for each mechanical property. More advanced composite materials models exist which take into consideration the failure modes[2].

The characterisation of the thermoplastic composite in this study is based on the global composite ply model proposed by Ladevéze, which is described in §2.5.4.2.

1.5 Objectives

The objectives are:

- Establish strain rate dependent mechanical properties for a Continuous Glass Fibre Reinforced thermoplastic (GFRTP) composite at ply and laminate levels, for conditions typically encountered during a vehicle crash.
- Establish a semi-empirical rate dependent model to predict the performance of ply and laminate to serve design under typical vehicle crash conditions.
- Validate rate dependent model at coupon and component level within the CAE environment.

Chapter 2

Review Of Literature Related To Strain Rate Effects in Composite Materials.

Chapter Objectives

- Review of strain rate laws for isotropic materials.
- Review experimental testing methods for composite materials.
- Literature review of the strain rate effect on material properties of composites.
- Review Finite Element (FE) methods.

2.1 Introduction

Dynamic strain rate testing had a slow beginning in the early 19th century, however a surge in the study of strain rate deformation began during World War II[7].

2.2 Constitutive Strain Rate Laws For Isotropic Materials

Table 2.1 presents a number of widely used empirical based strain rate laws used for strain rate dependent isotropic materials in commercial FE codes.

Strain Rate Law	Formulation
Cowper-Symonds	$\sigma(\varepsilon,\dot{\varepsilon}) = \sigma_0(\varepsilon)\cdot\left[1+\left(\frac{\dot{\varepsilon}}{D}\right)^{\frac{1}{p}}\right]$
Johnson-Cook	$\sigma(\varepsilon,\dot{\varepsilon}) = \sigma_0(\varepsilon)\cdot\left[1+\frac{1}{p}\ln(\max(\frac{\dot{\varepsilon}}{D},1))\right]$
Modified Jones	$\sigma(\varepsilon,\dot{\varepsilon}) = \sigma_0(\varepsilon)\cdot\left\{1+\left[\frac{(\varepsilon_u-\varepsilon_y)\dot{\varepsilon}}{D_u(\varepsilon_u-\varepsilon)+D_y(\varepsilon_u-\varepsilon)}\right]^{\frac{1}{A\varepsilon+B}}\right\}$
Left Shifted Krupkowsky	$\sigma(\varepsilon,\dot{\varepsilon}) = \sigma_0(\varepsilon)\cdot\left[\frac{\varepsilon+\varepsilon_0\left(\frac{\dot{\varepsilon}}{\dot{\varepsilon}_0}\right)^b}{\varepsilon+\varepsilon_0}\right]^{n_{ref}}$
Krupkowsky	$\sigma(\varepsilon,\dot{\varepsilon}) = \sigma_0(\varepsilon)\cdot\left\{\dot{\alpha}^a\frac{[\varepsilon+\varepsilon_0\dot{\alpha}^b]^{n_{ref}}\dot{\alpha}^c}{(\varepsilon+\varepsilon_0)^{n_{ref}}}\right\}$

Table 2.1: Formulation of strain rate analytical models used by PAM-CRASH.

where:

$\sigma_0(\varepsilon)$: is the stress at the reference strain rate;

$\sigma_0(\varepsilon,\dot{\varepsilon})$: is the stress at the strain rate;

$\dot{\varepsilon}_0$: is the reference strain rate;

$\varepsilon_u, \varepsilon_y$: are the reference strains for the Modified Jones constitutive law;

$D, D_u, D_y, p, A, B, n_{ref}, \dot{\alpha}, c$: Arbitrary constants from curve fitting.

Cowper-Symonds: The Cowper-Symonds [32] constitutive law multiplies a reference stress vs. strain curve (law) by a function of the strain rate. For this reason the factor of amplification is constant over the entire strain range. The assumption that the amplification remains constant (see figure 2.1) throughout the entire strain range is not valid for composite materials, as it does not take into account the effect of the strain rate on the physical mechanisms in the material. The Cowper-Symonds strain rate law was proposed to obtain the dynamic flow stress[33]. FE implementations use it to obtain the entire stress vs. strain curve[34].

Johnson-Cook: Like Cowper-Symonds, the Johnson-Cook method multiplies a reference stress vs. strain curve (law) by a function of the strain rate. As a result the factor of amplification is constant over the entire region[35].

Modified Jones: The modified Jones method is a generalisation of the Cowper-Symonds law. However, the modified Jones method allows for variable amplification which is defined between the yield point and ultimate failure. This provides greater flexibility, however it increases the complexity of the calibration procedure.

Left Shifted Krupkowsky: This method approximates strain rate sensitivity by shifting the reference stress vs. strain curve along the strain axis. The amplification factor decreases for increasing strain for a curve with modulus degradation.

Krupkowsky[1]: This is a generalisation of the left shifted Krupkowsky law. The hardening coefficient (k_{ref}) as well as the hardening exponent (n_{ref}) are affected independently by the strain rate.

Figure 2.1 present the factor of amplification for the different strain rate laws. In the figure, the absolute difference is given as a percentage on the y-axis and the strain on the abscissa. The figure shows that the Cowper-Symonds approach and Johnson-Cook method both amplify the stress vs strain curve by a constant factor, independent of the strain. The modified Jones, Left-Shift and Krupkowsky laws, all amplify the stress vs strain curve by a variable amplification factor. Also, it is notable that only the Modified Jones law increases for increasing strain (however it is not restricted to increasing), while the amplification factors of the Left-Shift Law and the Krupkowsky law decrease for increasing strain.

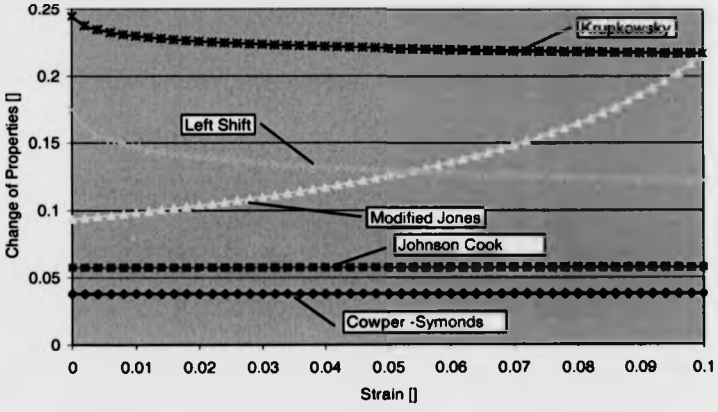

Figure 2.1: Comparison of factors of amplification vs strain for different analytical strain rate law.

Prandtl-Reuss proposed a strain rate constitutive law for a plastic material[ ]. They proposed that

$$\dot{\varepsilon}_x = \frac{3D}{2\sigma'_e}\left(\frac{\sigma'_e}{\sigma'_0} -\right)^q S'_x$$

where:

σ'_e is the equivalent, or the effective, dynamic flow stress;

ε'_e is the equivalent, or the effective, dynamic flow strain rate.

S'_x is instantaneous deviatoric stress, which is total stress minus the hydrostatic component $S'_x = \sigma'_x - \frac{\sigma'_x+\sigma'_y+\sigma'_y}{3}$.

The formulation looks very similar to the Cowper-Symonds, however, it is relative complex to implement in a FE code because of the iterations that are required for the solution.

2.2.1 Critical Stress Wave Velocity.

In order to achieve uniformity of stresses within the specimen at a high strain rate, the test duration should be long enough to ensure multiple stress wave reflections over the specimen length[36]. Many researchers[2] [38], [36], [39] assume that the axial component of the displacement is constant along the cross-section of the specimen, during wave propagation in the direction of the fibres and suggest equation 2.1, to calculate the elastic longitudinal stress wave speed.

$$c_e = \sqrt{\frac{E_{11}}{\rho}} \tag{2.1}$$

Where:

E_{11} is the modulus of elasticity of the composite material (laminate).

ρ is the density of the material.

[2]Daniel [17] suggested that $c_e = \sqrt{\frac{E'_{11}}{\rho^{\frac{1}{3}}}}$

The resulting equation for a unidirectional laminate is

$$c_e = \sqrt{\frac{E_{11}^f v_f + E_{11}^m (1 - v_f)}{\rho^f v_f + \rho^f (1 - v_f)}} = \sqrt{\frac{E_{11}^f \left(1 + \frac{(1-v_f)E_m}{v_f E_f}\right)}{\rho_f \left(1 + \frac{(1-v_f)\rho_m}{v_f \rho_f}\right)}} \tag{2.2}$$

Using the physical properties in table 1.3, the elastic longitudinal stress wave speed for fibre, matrix and composite material are respectively: $c_e^f = 5400[\frac{m}{sec}]$, $c_e^m = 2100$[m/sec] and $c_e^c = 4400$[m/sec]. For tensile testing, if the velocity increases beyond a critical value u_{cr}, failure will occur prior to any wave propagation. The resulting constraint is that of a maximum allowed testing velocity. If that velocity is exceeded a critical strain limit ε_{cr} is reached locally and local failure occurs. The critical velocity for a specimen is calculated by equation 2.3.

$$u_{cr} = \varepsilon_{cr} c_e \tag{2.3}$$

Using the physical properties in table 1.3, and setting the critical strain equal to the strain at failure of the unidirectional ply $\varepsilon_{11}^{PLY} = 1.6\%$, the critical velocity of the composite material is calculated: $u_{cr}^c = 70$[m/sec].

2.3 Testing Methods For Composite Materials At High Strain Rates

The dynamic strain rate testing activity has been reviewed by several researchers[10, 11, 12, 13, 36, 5].

The manner in which the composite materials respond to impact loading and dissipate energy is very different to that of metals[5]. Metals absorb energy through elastic and plastic

deformation[14]. Although the latter will cause some permanent structural deformation, its consequences on the load carrying capability of the component are usually small[15]. In composites however the ability to undergo plastic deformation is extremely limited with the result that energy is frequently absorbed in creating large areas of damage with ensuing reduction in both strength and stiffness[16, 17]. Furthermore, the prediction of the post impact load of a damaged composite structure is more difficult than for metals since the damage zone is generally complex in nature and consequently very difficult to characterise[18].

There is a large body of literature covering the constitutive modelling of composite materials at low strain rates[9]. Similarly, there is an even larger body of literature on the constitutive modelling of the high strain rate behaviour of metallic materials[7]. The issue that must be addressed is the development of constitutive laws for composite materials subjected to strain rates[19].

2.3.1 Dynamic Testing Problems

Hamouda and Hashmi[5] recently carried out a review of testing at high rates of strain and state that, for composite materials, where there are who or more phases present, several complication arise. They found that factors like, rate dependence of each of the constituent phases, reinforcement configuration (e.g. unidirectional or woven) are all expected to affect the strain rate dependence of the composite. A further complicating factor, for all multi-phase materials, is the presence of interfaces and hence the possibility of additional failure processes associated with the interface (e.g. interlaminar shear mechanisms).

Hamouda and Hashmi[5] identified the following factors as important strain rate testing:

- devising launch mechanisms to produce the desired stress state;

- fixture (create appropriate jigs) specimens in the test assembly;
- selection of specimen geometry;
- test duration and equilibrium time;
- complexity of composite failure mechanisms;
- measuring transient parameters accurately;
- data collection, management and interpretation.

Reliable data on the dynamic properties of composite materials are sparse because of the experimental difficulties associated with their determination[50]. Also, Cantwell and Morton[51] comment that there are no standard impact test for composites because it is hardly possible to predict their behaviour from one type of loading to another.

Conventionally, several assumptions are made (e.g. the stress state inside the specimen) in order to obtain the strain rate dependent properties of a unidirectional laminae[30]. Also, difficulties such as traveling waves, edge effects, boundary conditions etc., influence the accuracy of the results [52].

Other fracture mechanics researchers [53] suggest that the peak impact load or the energy absorbed to peak impact load might be a more meaningful measure of the impact resistance of the composite than the total work of fracture.

The noise that is inherently associated to varying degrees of significance with strain rate experiments may be removed by the implementation of appropriate filtering techniques. Finally, another issue associated with dynamic testing, is the presence of stress wave reflections at the boundaries of the different constituent phases as described by Armenakas[39].

2.3.2 Universal Testing Machines.

Universal testing machines are general purpose testing machines used to characterise the mechanical properties of a material. They may be powered by Electro-hydraulic or Hydro-pneumatic motors. Universal testing machines are commonly used for a range of mechanical tests, where load is introduced to the specimen in direct tension, compression or flexure[54]. The crosshead speed is usually limited to below 1[m/sec][3]. At high speeds sensors must be able to respond to changes within millisecs. Therefore dynamic sensors such as piezoelectric on accelerometers are called for as part of the instrumentation.

Generally, modern universal testing machines provide both load or displacement control[56]. However, there are limitations with universal testing machines. These are:

- Maximum strain rate;
- Uncertain boundary conditions;
- Resonance and ringing effects;
- Specimen distortion;
- Testing machine-specimen interaction.

The boundary conditions at the grip are uncertain because sometimes the coefficient of friction is not sufficient.

[3]There are machines with crosshead speed up to 10[m/sec], however there is a requirement for slack adaptor to allow for the nominal velocity to be reached [55].

At high strain rates, the load signals are effected due to resonance and ringing effects[5]. Specimens may be distorted due to bending/shear interaction when testing off axis laminates, that is why in those cases alignment of the grips and specimens is essential.

Finally, it has been suggested that testing machine-specimen interaction has a major influence on the strain rate[57]. Dieter[56] provided a formula for the decomposition of the observed crosshead displacement as a function of elastic and plastic displacement of the specimen and the elastic displacement of the testing machine itself. A formula for the actual strain rate was proposed. Usually, the hydraulically driven machines (also known as "soft machines" because of their low spring constants) tend to smear out the upper and lower yield point. Screw driven mechanical machines (also known as "hard machines"), tend to reproduce faithfully the shape of the stress-strain curve and the fracture behaviour.

2.3.3 Instrumented Falling Weight.

The Instrumented Falling Weight (IFW) method can be utilised to test materials in tension and compression, by converting the potential energy of a raised mass to kinetic energy, before impacting the grip of a tensile/compressive specimen [58, 59, 60, 61, 62, 50]. Alternative uses of the drop weight system let the weight drop onto a plunger which pressurises a liquid inside a tubular specimen[63, 18, 64].

The theoretical impact velocity is computed from $\sqrt{2gh}$, where g is the acceleration of gravity and h is the height. However, most modern facilities monitor the various quantities (usually acceleration using an accelerometer and load using a piezoelectric transducer) of the impactor prior and during impact The impact energy may be varied by proper adjustment of the falling mass.

Typically, strain rate ranges between $1 \rightarrow 10[s^{-1}]$ have been reported in the literature. The impact speed is limited by the height of the stucture/tower[30]. It is possible to measure load vs. displacement curves and also velocity before and after impact and calculate the energy absorbed in the specimen.

Reported disadvantages of the method are:

1. stress waves reflection;
2. localisation of the deformation (localised effects);
3. limited to failure characterisation;
4. difficulty in alignment between specimen axis and hammer movement[30].

This technique is susceptible to stress waves reflection in the tup or support anvil (where the sensors may be located). The stress waves manifest as oscillations, which are superimposed on the signal response of the specimen. Therefore, interpretation of the experimental results becomes increasingly difficult[30].

Generally, the IFW method is limited to characterisation of energy related dissipating mechanisms and specific modes of failure at moderate strain rates. Often these modes of failure are unique to this range of strain rate. Further, there are many product applications, which are designed to meet performance requirements at these strain rates (i.e. automotive crashworthiness tests).

Bramuzzo [6] developed a technique for determination of the dynamic modulus under impact conditions at strain rates higher that could be practically achieved using the universal testing machine, using a modified version of the IFW method.

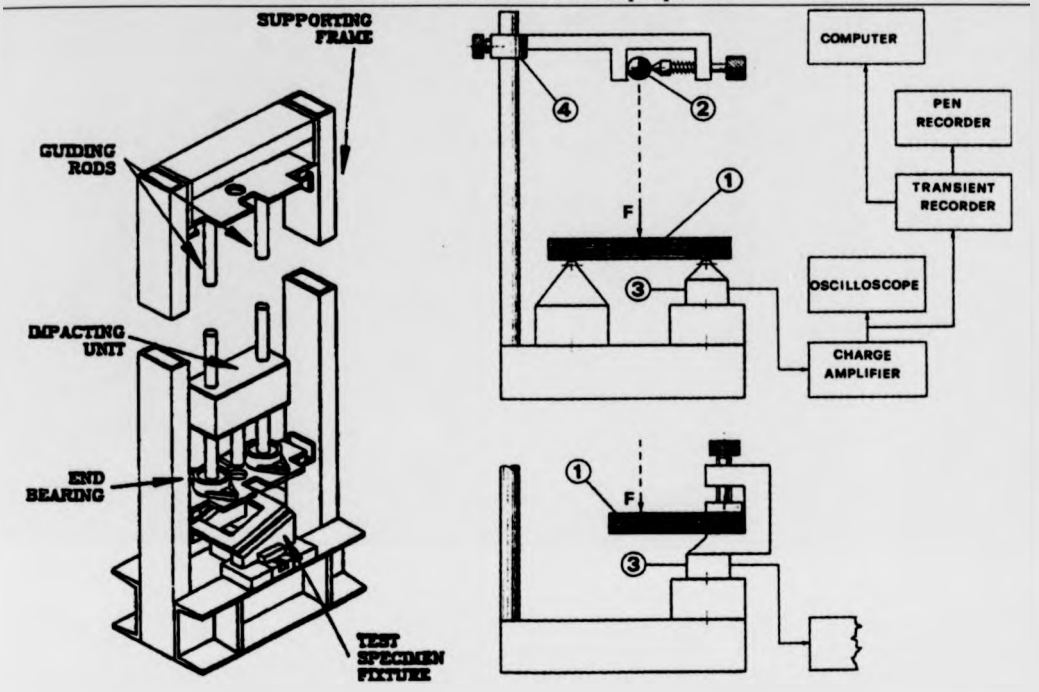

Figure 2.2: Schematic of an Instrumented Falling Weight (source Hamouda and Hashmi[ ]) testing configuration (left hand side) and the Bramuzzo (source Bramuzzo [ ]) configuration (right hand side).

The geometry of specimen may be circular, square of strip form. A circular or square placque may be simply supported or clamped at the periphery. A strip may be simply supported or clamped at both ends or clamped at one end (e.g. cantilever). A small impacting mass is dropped from a known height, as shown in figure 2.2. Assuming small displacements. the elastic dynamic modulus for the simply supported specimen is computed from:

$$E = \frac{FS^3}{f4BD^3} \tag{2.4}$$

where:

F is the measured force on the contact.

S is the span of the specimen.

B is the breadth of the specimen cross-section.

D is the depth of the specimen cross-section.

f is the deflection or displacement of the specimen at the point of impact.

The strain rate for the three point bending test is calculated using the following equation.

$$\dot{\epsilon} = \frac{6D\bar{V}}{S^2} \tag{2.5}$$

Where $\bar{V}$ is the average velocity during impact.

This test will establish the dynamic modulus of elasticity, however not the strength. There are also the following criteria maybe important:

- An impulse must be obtained which gives a symmetrical force/time curve (i.e. purely elastic deformation of the specimen no failure).
- The measurements should not reveal any inertial disturbances, which would make it difficult to interpret the curve.

2.3.4 Pendulum Type Impact Tester.

The impact load is transmitted to the specimen through a tup striking a trailing grip attached to one end of the specimen. The load is measured by a load cell connected to the opposite end[65]. Strain rates between 1 to 45$[s^{-1}]$ have been reported for this method.

Although the Charpy and Izod methods are reported to be the most extensively used tests for fracture mechanics studies[50], they are limited to the characterisation of toughness properties and furthermore the dependency of the results interpretation on the geometric dimensions[5]. The geometry of a Charpy test involves a flat rectangular specimen (see figure 2.3).

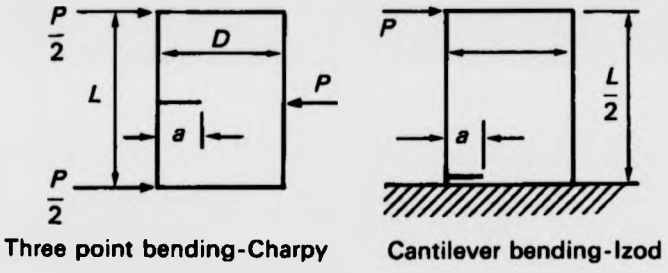

Figure 2.3: Common Charpy and Izod test geometries[5].

Usually, pendulum testing machines are used for Charpy tests, which measure the amount of energy used to break a sample[66]. Coulton [67] reports that Charpy tests have been used to characterise thermoplastic composite materials. Adams and Perry[68] used a modified impact bend test capable distinguishing between fracture initiation and fracture propagation. The main problem with the application of the Charpy tests on composite materials lies in the interpretation of the results is subject to scale effects and the layup sequence and therefore, it is not possible to relate the obtained data to a specific damage mechanism in composite materials[5].

The dependency of the results to the geometric dimensions of the specimens led Adams[68] and Philips[69] to call for "test methods that can cope with progressive changes in loading rate over the full range from creep to impact" and "test piece geometries that afford better opportunities to study the development of fracture". Furthermore, a theoretical investigation indicated that the use of the Charpy test with a V-notch specimen does not appear suitable for assessing non metallic composite impact resistance, because of the complex nature of the stress, strain and strain rates encountered throughout the specimen[70]

2.3.5 Explosively Driven Machines.

In this testing technique, one end is rigidly fixed, while the other end is attached to a fixture which is propelled by an explosive charge. Tensile strain rates up to $500[s^{-1}]$ have been reported [70]. This method, has been used for stiffness, strength and failure mode characterisation.

Armenakas and Schiamarella have also reported that slippage at the clamps can be a significant problem. Also, the use of explosives as a propellant makes impossible the accurate control of the strain rate, or constant speed.

2.3.6 Split Hopkinson Pressure Bar (SHPB).

The Split Hopkinson Pressure bar technique is a method that is used to obtain properties at very high strain rates (ballistic range). This technique uses the propagation of a wave along a bar to subject to high strain rate load to a short specimen which is sandwiched between two bars[70]. The Split Hopkinson bar has been investigated theoretically by several researchers[71, 72, 73, 74].

Several researchers have used modified versions of the Hopkinson bar for tensile impact testing of

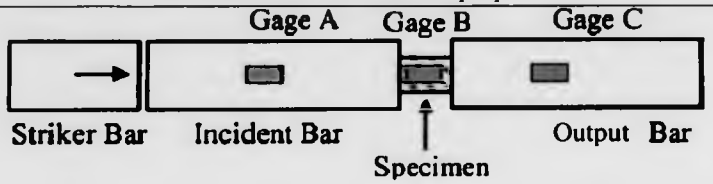

Figure 2.4: Generic representation of a compressive Split Hopkinson pressure bar apparatus [8].

composites materials[75, 76].

- Compression Split Hopkinson Bar (or Kolsky method) [77, 78, 79, 80]
- Shear Split Hopkinson Bars (for in-plane and intralaminar shear properties). [81, 82, 83]
- Tensile Split Hopkinson Bar. [84, 85, 86]

Even amongst the general categories of the split Hopkinson Bar, researchers have made modifications. Only the working principle of the compressive split Hopkinson bar are explained in this section, however the principle is applicable to the shear and tensile split Hopkinson pressure bar. A striker bar imparts an elastic stress pulse to the incident bar - see figure 2.4. A typical diameter of a Hopkinson bar apparatus is 20[mm][87]. The process produces a rectangular stress pulse in the incident bar. The propagation of the stress pulse in the specimen results in partial transmission to the output bar and partial reflection to the incident bar. The strain signals of the incident wave are recorded by three sets of strain gauges attached on the incident, output bars and the specimen[4]. The specimen strain $\varepsilon_s(t)$, strain rate $\dot{\varepsilon}_s(t)$ and stress $\sigma_s(t)$ are obtained[76].

[4] Variations of the Split Hopkinson Pressure Bar do not use a) strain gauges on the specimen in which case one-dimensional simple wave theory is used, or b) an incident bar (i.e. the stress pulse is imparted directly on the specimen).

The Split Hopkinson bar apparatus are typically used in the strain rate range of 100 and 3000[s^-1]. However, Stelly has reported using the Hopkinson bar in the range of $10^{-4} \rightarrow 10^3$ for metallic materials[].

One common problem for all material classes, associated with this method is the invalidation of the following assumptions at higher strain rates: a) the assumption of a state of uniaxial stress in the specimen, b) the assumption that radial inertia may be neglected, and, finally c) the assumption for perfect end friction[]. Hamouda and Hashmi[] question that the test assumptions have been met satisfactorily, due to conflicting results reported in the literature at strain rates near 10^4[1/sec].

The main problem of the method in conjunction with composite material testing is the small size of the testing specimens[]. Mechanical properties of a composite material are dependent on the size. The mechanical properties obtained through testing coupon size specimens may not be appropriate at larger scales, and not appropriate as design inputs to product design. The generally accepted guideline is that a specimen dimensions are relatively large compared to the characteristic length of the reinforcement[]. Arnaud and Hamelin[] have proposed a variation of the Split Hopkinson bar, which they called a *block bar*. The block bar were 80[mm] diameter thus allowing for larger, more representative composite specimens.

Also, according to Lifshitz[] the small size of the composite specimens and the small strains to failure result in short times to failure[5], causing the specimen failure to occur during the rise of the incident loading pulse. Therefore, it can no longer be taken for granted that stresses along the specimen are uniform and that the specimen is subjected to constant strain-rate loading[].

According to Hamouda, most of the studies of composite materials in the compression split Hopkinson pressure bar have in fact used short cylindrical specimens, even though these are far from

[5]The split Hopkinson bar has been designed for metallic ductile specimens which exhibit higher strains to failure.

ideal this type of material[5].

Ninan et al.[90] have reported that during off axis testing of S2-glass/epoxy systems with the use of the compressive split Hopkinson pressure bar, measurable bending waves were observed in the bars - due to extension/shear coupling. The results were in good correlation with a 2D FE numerical model. In order to minimise the bending waves, they proposed lapping and lubricating of the specimen loading faces. Finally they reported that an incident pulse with a rise time of approximately 3-4 reflection times was sufficient to produce reasonably accurate stress-strain curves in the range of small strains[90].

For intralaminar testing using the double notched specimen, Ruiz et al.[91] reported that only over a very limited range of strain does the double notch specimen deform in pure shear and that as the test proceeds a significant amount of plastic deformation appears outside the shear zone. The double-lap design is a more recent development[92]. Hamouda[4] reports that the shear stress on the interlaminar plane is not uniform and that the ends of the inter-laminar plane the stress normal to this plane is significant.

Finally, a complex study of wave propagation in composite materials is required because wave propagation effects are dominant and have to be taken into account in the strain rate range concerned[30]. It is possible that mismatch of impedance between specimen an loading bar could introduce stress wave reflections that would invalidate the Hopkinson bar analysis[4].

In conclusion the split Hopkinson bar is one of the most commonly used and favoured methods for testing at strain rates over 100[1/sec]. Although the method is mature for isotropic ductile materials, its application on highly anisotropic composite materials requires careful consideration of many factors to provide any meaningful results.

2.3.7 Gas Gun Techniques.

A pressurised gas is used to accelerate a projectile down a barrel to strike a specimen (similar in a way to explosively driven machines)[93, 94, 95]. A test setup is shown in figure 2.5. The material under investigation can be either the projectile[6] or the impacted specimen. The impact velocity is determined prior to impact using optical sensors or a break wire technique.

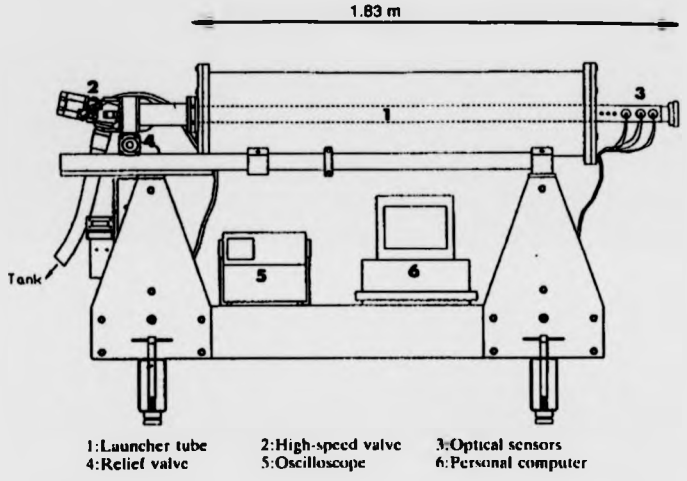

Figure 2.5: Schematic drawing of the gas-gun testing configuration (source Delfosse [9].

This technique has been used to characterise elasticity and strength properties.

The gas gun method was reported to achieve strain rates in the range of $10^{-1}[sec^{-1}]$ to $10^{4}[sec^{-1}]$)[96, 97]

The limitations of the gas gun method are:

i) It maybe used only for characterisation of compressive strength and penetration resistance.

[6] In which case it is impacted on an instrumented solid anvil

ii) Localisation of deformation at the point of impact (Non uniformity of stress distribution in the specimen).

iii) Boundary conditions have a significant effect in the interpretation of the results.

iv) Inaccurate load measurement (measurement not on point of impact but on supports).

2.3.8 Internal and External Explosive Pressurisation.

The method of internal/external explosive pressurisation uses thin walled cylindrical specimens subject to dynamic tensile/compressive hoop loading (internal pressure) to test at strain rates between $1 \rightarrow 500[sec^{-1}]$[98, 99, 100, 101, 18, 19, 102, 64, 103, 104] - see figure 2.6. An explosive charge is detonated and an internal/external pressure pulse introduces the loading, through a liquid medium.

The fixture consists of two thick walled cylinders and two disks assembled together with a composite ring specimen between them - see figure 2.6.

According to Barre[50], this testing configuration minimises unwanted wave propagation effects, because the transit time of the wave across the thickness of the specimen is very short and the liquid medium dampens unwanted harmonics.

The displacement is measured by putting strain gauges in the inside of the rings.

The method of internal/external pressurisation has the following disadvantages:

1. The strain rate decreases during the experiment (i.e. the strain rate is not constant);

2. The state of stress in the ring specimen is complex[84].

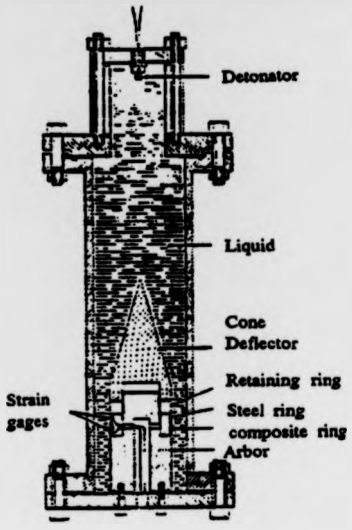

Figure 2.6: Schematic drawing of the external explosive pressurisation testing configuration (source Hamouda and Hashmi[9].

3. For the external explosive pressurisation method, one of the limitations is the acceptable failure mechanism. The specimen has to fail through crushing and not buckling, in order for the results to be representative[36].

Longitudinal tensile, transverse tensile and in-plane shear properties may be obtained testing respectively specimens of 90° hoop wound, 0° axially wound and 10° off axis[101, 105]. It has been reported in the literature that the pressurisation method has been used for strains rates in the range of 10 to 500$[s^{-1}]$.

The internal and external explosive pressurisation is also limited to a specific geometry and therefore performance testing of structural components is impractical and provides little information.

2.3.9 Summary Of Strain Rate Characterisation

Figure 2.7 compares the strain rate ranges that can be achieved with different methods of characterisation.

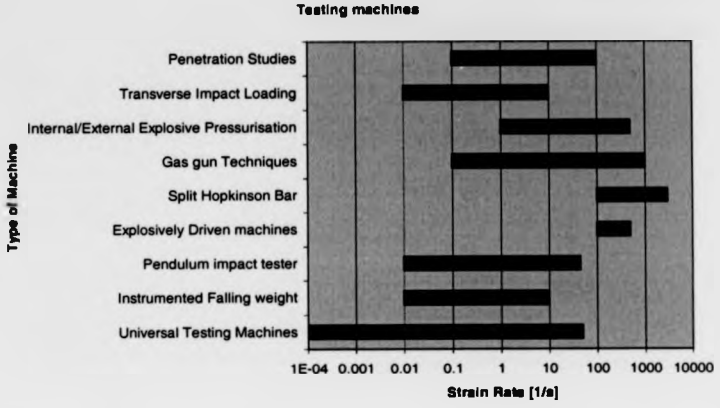

Figure 2.7: Comparison of the Strain rate range of different dynamic testing techniques.

Table 2.2 summarises the characterisation capabilities of dynamic testing machines. Only the universal testing machines offers the opportunity for characterisation of the full range of characterisation properties (elasticity, strength, damage and energy) at the desired strain rate range.

Table 2.2: Summarising table of characterisation capabilities of dynamic testing machines (✔the machine is capable of characterisation, x the machine is not capable of characterisation) .

	Stiffness	Strength	Damage	Energy
Universal Testing	✔	✔	✔	✔
Pendulum	✔	✔	x	✔
IFW	✔	✔	x	✔
Explosively Driven	✔	✔	x	✔
Split Hopkinson Bar	✔	✔	x	✔
Gas Gun	✔	✔	x	x
Internal/External Pressurisation	✔	✔	x	x
Penetration	✔	x	x	✔

2.4 Strain Rate Effect On Material Properties Of Composites

2.4.1 Strain Rate Effect On Glass Fibres.

Cameron [106] performed tensile experiments on glass fibres in the strain rate range of $1.7{\cdot}10^{-4} \rightarrow 1.7{\cdot}10^{-1}[\text{sec}^{-1}]$. Cameron found that the dynamic tensile strength of single glass fibres increased threefold with increasing strain rate up to $1.7{\cdot}10^{-2}[sec^{-1}]$.

Rotem and Lifshitz[98] carried out tests on E-glass roving fibre using a hydraulic powered machine and reported that in the strain rate range between 5 and $30[sec^{-1}]$ failure strength is nearly three times the failure strength determined under quasi-static conditions.

Armenakas and Sciamarella [30] have examined the effect of strain rate on the tensile properties of glass fibres, using an explosively driven machine. They showed that the modulus increased and failure strain decreased as the strain rate increased up to 500$[sec^{-1}]$.

Daniel and Liber[107, 108] used a hydraulic machine to compare the strain rate effect on glass and graphite reinforced composite material systems. They found that the strength in the fibre direction was affected for the glass but not for the graphite.

An interesting and relevant work by Xia [76] examined the distribution properties for the failure strength of glass fibres. Xia concluded that the failure strength of fibre bundles is satisfactorily described by a Weibull distribution. Figure 2.8 presents the proposed shape of the distribution for glass fibre strength

$$G(\sigma) = \frac{n}{N} = 1 - \exp(-\alpha\sigma^{\beta}) \tag{2.6}$$

where:

σ: is the real fibre stress;

α, β: Weibull distribution parameters, which are influenced by the material;

n,N: broken and initial number of fibres respectively.

Generally, the researchers agree that for increasing strain rate the stiffness and strength of the glass fibres increase.

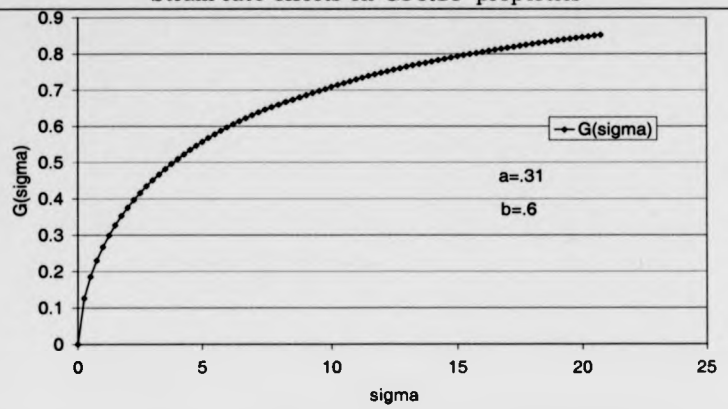

Figure 2.8: Percentage of broken glass fibres vs. real stress for Weibull distribution with parameters $\alpha = .31$ and $\beta = .6$ (taken from Xia's work).

2.4.2 Strain Rate Effect On Polymeric Matrices.

According to Shah Khan and Simpson[109] polymeric materials are known to display viscoelastic behaviour. Thermoplastic materials are known to exhibit more viscoelastic behaviour than thermosets[20]. The majority of published research work on strain rate laws of polymeric matrices has been carried out on thermosetting epoxy matrix systems.

In the author's opinion, viscoelastic behaviour is a characteristic of thermoset materials - contrary to thermoplastic materials which exhibit a visco-plastic behaviour. As mentioned in §1.3.2, an important difference between thermoset and thermoplastic materials, is the presence of rigid crosslinks between the molecular chains. In the case of thermoset plastic, the deformation is reversible while in the case of thermoplastics is only partially reversible, because slipping of the molecular chains will occur even at small loads or strains.

Most of the literature on strain rate dependence of composite material matrix phases concentrates on thermoset materials in compression[110].

Welsh and Harding[75] conducted strain rate tensile tests at a range between 0.01 to 930$[sec^{-1}]$ on unreinforced thermoset specimens and GFRP woven composites. They concluded that increasing strain rate leads to an increase of failure strength, which is accompanied by a reduction in matrix ductility. Further they concluded, rate sensitivity of modulus in fibre reinforced thermoset plastics cannot be explained solely in terms of the rate dependence of the resin modulus measured in isolation.

Agbossou et al.[110] has carried out tests on glass/epoxy systems using a screw driven and a hydraulic driven machine, at strain rates between $3 \cdot 10^{-3} \rightarrow 300[sec^{-1}]$. They established that the matrix is brittle at strain rates above $1[sec^{-1}]$.

In conclusion, it is documented that polymer matrices exhibit visco-elasticity and visco-plasticity[111, 21, 112]. The majority of published research work that considers strain rate dependency has been undertaken for thermoset matrix composite materials.

2.4.3 Strain Rate Effect On Fibre/Matrix Interface.

Research work on the effect of strain rate on the fibre/matrix interface is limited. However, Theocaris [113] postulated that mechanical behaviour of a composite material depends on the properties of the fibre/matrix interface as well as the properties of the constituent phases.

Detassis et al.[111] investigated the effect of both strain rate and temperature on the interfacial shear stress transfer in carbon/epoxy composites. They used a fragmentation test on single fibre model composites[7]. They found that the interfacial shear stress increased for increasing strain rate in the strain rate range .002→.016[1/min]. The effect was attributed to the viscoelastic behaviour

[7]A test on a single fibre composite, designed to test the interface properties.

of the epoxy matrix.

Agbossou et al.[110] reported on the testing of unidirectional epoxy composites at +45° off axis with respect to the fibre direction and found that, the interface failure stress remained constant at different strain rates, however at strain rates higher than $1[sec^{-1}]$ the failure surfaces appeared to change.

Tanoglu et al.[114] investigated the properties of fibre/matrix interface of an E-glass/epoxy composite system under high loading rates using a Dynamic Interface Loading Apparatus. They found that the local stress distribution and energy absorbing capacity of the properties of the interface are sensitive to loading rate.

Characterisation of the constituent phases of a fibre reinforced composite material contributes to an understanding of the performance of the material as a system (fibre and matrix together). However, the knowledge gained is still limited because of the complex interaction between the reinforcing fibres and matrix phase which is strain rate dependent[·]. Properties of the fibre/matrix interface are unique for different constituent phases in a composite material. In conclusion, micromechanics equations for the prediction of mechanical properties must be complemented with tests.

Generally, researchers agree that the strain rate dependency of a composite material depends on the properties of the fibre/matrix interface. Recently, Greenfield et al.[115] proposed a promising new high strain rate test of the fibre/matrix interface. There are no constitutive models of the strain rate sensitivity of fibre/matrix interface available in the published literature.

2.4.4 Strain Rate Effect On Fibrous Materials.

A composite material exhibits strain rate behaviour which has directional dependency. Consider the direction parallel and perpendicular to the fibres. In the direction of fibres, the fibres are expected to dominate the stiffness and the ultimate failure strength of the laminate. Perpendicular to the direction of fibres, the stiffness and the ultimate failure strength of the material is dominated by the matrix phase.

Behler and Sikorski[116] reviewed the literature concerning the strain rate dependent properties of woven composites and reported that strength increased with increasing strain rate. Also confirmed was that testing technique and loading conditions did not influence their observations.

Although studies have been undertaken for glass/epoxy thermosetting systems [117, 118, 119, 120], relatively few studies have been undertaken to characterise the mechanical properties of a thermoplastic composite material at high strain rate[121].

Cantwell [122] investigated the effect of loading rate on the mode II interlaminar fracture toughness for a range of thermoset composite materials. In his work a screw driven universal testing machine together with a fully instrumented drop weight carriage was used.

Al-Hassani and Kaddour[56] investigated the in-plane mechanical properties of continuous Kevlar (KRP), glass (GRP) and carbon (CFRP) fibre/epoxy composite material systems. They developed an indirect method for determination of the mechanical properties of a unidirectional composite ply by testing angle ply laminates and application of Reverse Laminate Theory (RLT). More importantly, they concluded that GRP composite materials appear to be most affected by variation of the strain rate during testing.

Weeks and Sun[123] investigated high performance carbon/ thermoplastic composite systems with

different fibre orientations using a servo-hydraulic and Split Hopkinson Pressure Bar over a strain rate range of $10^{-6} \rightarrow 1000[1/sec]$. They did not establish any strain rate dependency along the fibre direction. They reported that off axis composites and angle ply laminates exhibited significant non linear and strain rate dependent behaviour. However in their work, they did not attempt to quantify or develop a predictive model.

Trirupukuzhi and Sun[124] tested unidirectional (S2-glass) and woven (E-glass) thermoset composite material systems under monotonic loading conditions using a servo-hydraulic machine in the range of $10^{-4} \rightarrow 1[1/\text{sec}]$. For unidirectional composites, they observed that the elastic behaviour is not affected by strain rate but rate dependent behaviour is observed in the plastic deformation. Subhash et al.[125] published the only available report on the strain rate effects of braided textile composites (Spectra 1000 and Kevlar 49 fibre/Epon 862 epoxy resin). They used a servo hydraulic machine .01[1/sec] and a split Hopkinson bar at 1000[1/sec] for compressive testing. They reported strain rate dependency for uniaxial compression loading. Subhash et al. also report that the failure mechanisms are not easily reproducible due to manufacturing defects.

2.4.4.1 Fracture Appearance - Damage Micromechanisms.

At quasi-static strain rates, the fibre pull-out and fibre fractures are regarded as failure processes which occur predominantly under tension loading of unidirectional composites along the fibre direction[100]. These fibre dominated failure modes require greater energy. For tensile testing of off-axis unidirectional composites the failure is matrix dominated.

On the other hand, the splitting and delamination that have been reported to occur under compressive loading, require less energy and result in reduced structural integrity[51]. Delamination and splitting failures are also reported to occur due to stresses concentrated between the laminate

plies (interfaces)[109].

Mamalis et al.[126] have reported on the effect of the fibre orientation on the compressive behaviour of a laminate comprised of unidirectional thermoset composite lamina. They reported that axially aligned fibres were bent inwards or outwards without fracturing according to their flexibility and the constraints provided by adjacent fibres. Fibres aligned transversely can only expand outwards by fracturing and inwards by fracturing or buckling. El-Habak[127] suggested that under quasi-static and impact loading, the ultimate failure mechanism of unidirectional GRP was transverse tensile fracture owing to fibre debonding and matrix tensile failure.

Fan and Slaughter[128] report that microbuckling is an important failure mechanism for polymer matrix composites, which is supported by experimental data from several researchers[129, 130]. They identified microbuckling as a shear instability that occurred by the rotation of fibres (typically $15° - 30°$ to the fibre direction) within a kink band of with 10-20 fibre diameters[128].

Welsh and Harding [75] observed at the quasi-static rate sudden fracture of an epoxy composite specimen with no prior damage signs. The mechanisms were extensive matrix cracking, fibre debonding and fibre pull out. Similar fracture appearance was observed at intermediate rates but the damage was more extensive and the specimen shattered on fracture. It was suggested that at impact loading rates the fibre matrix interfacial bond strength was exceeded before the tensile failure strength of the glass fibres (which increases with increasing strain rate).

Espinosa et al.[131] carried out tests on woven S2-glass/epoxy composite using a pressure-shear recovery experiment to determine the out-of-plane dynamic shear resistance of composites. They reported matrix cracking and interfacial debonding in both high and low velocity impacts, while only fibre microcracking and breakage was observed at higher impact velocities. No indication of

the observed strain rates were given.

Xia et al.[76] suggested that the main failure mechanism for tensile impact testing is the cumulative breakage of fibres which is caused by the statistical distribution of the strength of brittle fibres similar to that of a brittle fibre bundle. A model was proposed based on the following assumptions:

- Every fibre behaves linearly up to fracture.
- The strength of the coated fibres is satisfactorily given by a particular probabilistic distribution.
- If the event of a single fibre failure, adjacent fibres are not affected by the event.

The third assumption implies that upon breakage of a fibre the load/stress is redistributed evenly amongst the remaining unbroken fibres and therefore no stress concentrations are present. This is not representative of the physical failure mechanisms, especially at high tensile speeds - where the system has less time to reach an equilibrium (still dynamic) stress state.

McGee and Nasser[112] have carried out bi-axial compressive testing on glass/epoxy systems using a split Hopkinson bar at a strain rate range between .0001 and 1000[1/sec][8]. They reported that kink formation was the final stage of the failure mechanism at low strain rates. Their observations indicated that kink formation was preceded by extensive micro-mechanical damage that tended to initiate at defects (e.g. voids) - although some distributed damage was recorded with no correlation to pre-existing defects. Also for dynamic testing, multiple crossing and parallel kink bands were reported.

[8]There were inconsistencies in the paper stating in one occasion that the maximum compressive strain rate was 1000[1/sec] and in other occasion 500[1/sec]

Thiruppukuzhi and Sun[124] carried out tests on unidirectional S2-glass/8553-40 material system and determined that the ultimate failure occurs always along the off-axis angle parallel to the fibre direction whilst fibre breakage occurs only for the 0° specimens. They concluded that the failure mechanism for off-axis specimens is matrix dominated. They choose accordingly a decoupled form for the implementation of the failure criteria. The failure criterion for the transverse and shear properties (matrix based) uses one parameter to determine shape - which they found to be rate independent-, and another parameter which determines size. They found that the size parameter was found to be rate dependent, i.e. the failure strengths are dependent on strain rate.

Similar tests on woven E-glass fabric materials (eight harness satin weave construction) were performed[124]. The failure mechanism observed was dominated by shear, however no distinct modes of failure where identified with orientation. Therefore, Thiruppukuzhi and Sun concluded that for woven composites the failure modes cannot be decoupled.

Shah Kahn and Simpson[109, 133] carried out compressive testing for out-of-plane and in-plane loading for E-glass/epoxy composite systems at strain rates between .001 $\rightarrow$ 10[1/sec]. They reported that for the out-of-plane loading, the failure changed from a shear mode to a crushing mode at the top surface of the specimen. For in-plane compressive loading, the researchers state that the specimen ideally deformed uniformly over the entire cross section until it fractured by intra-laminar delamination promoted by shear stresses between the plies.

Khan et al.[134] has carried out compressive tests on S2-glass/polyester resin systems using a split Hopkinson bar at a strain range between .0001[1/sec] and 1250[1/sec]. They reported that the failure modes for dynamic loading were similar to the quasi-static loading failure modes.

Okoli[135] carried out tensile tests on woven glass/epoxy 3[mm] thick composite systems using

a servo-hydraulic machine. He found that the failure modes were strain rate dependent. Okoli attributed his observation to the differences between the strain rate sensitivity of the constituent phases and the properties at their interface. Because, the fibre, matrix and the fibre/matrix interface are not expected to show consistent strain rate dependency the failure will be dominated by the yielding of the weakest link. Okoli[136] reported similar findings for 3 point bend impact testing.

Generally, the published research on the fracture appearance of composite materials suggests that the fracture surface and failure mechanisms are strain rate dependent. Further, to the author's knowledge no work has been carried out on thermoplastic composite systems.

2.4.4.2 Strain Rate Effect On The Longitudinal Tensile Properties

Most of the research work in the literature focuses on glass/thermoset systems. Only Peterson et al.[137] carried out dynamic tests on a chopped glass/thermoplastic (styrene/maleic anhydride S/MA) composite material. Peterson found that elastic modulus and strength increased between 50 to 70% over the strain rate range of $10^{-3} \rightarrow 10[sec^{-1}]$.

A number of researchers have conducted work on the tensile strength Lifshitz[91], Harding[84], Kawata[138] and recently Barre[50]. The failure tensile strength of GRP materials showed a substantial increase with increasing strain rate. Daniel's work [108] however reported a decrease in failure tensile strength of GRP materials. Kammerer and Neme[139] reported that on cyclic tensile tests in the direction of the fibres on a E-Glass/polyester system in the range of $10^{-5} \rightarrow 10^{-3}$, the material showed no strain rate dependence (they also reported linear elastic behaviour and brittle fracture).

The work by Kawata et al.[138] has been criticised by Hamouda and Hashmi[7] and Okoli[135].

Hamouda and Hasmhisuggested that the specimen fixing method had a undesirable effect on the true state of stress, and Okoli suggested that Kawata el al. ignored the inertia which affects high speed testing.

Rotem and Lifshitz[58] found that at a strain rate of 30$[sec^{-1}]$ the dynamic modulus of glass/epoxy systems is 50% higher than the quasi-static modulus, whilst the dynamic tensile strength increases as much as three times the quasi-static strength. Later, Lifshitz [60] while investigating angle ply laminates observed that the elastic modulus was unaffected, and the increase of longitudinal tensile failure stress was only 20-30%. In both occasions a hydraulic (soft) powered universal machine was used to carry out the testing. As mentioned in §2.3.2, soft machines contribute a significant portion of the measured deformation at high strain rates.

Hayes and Adams[140] carried out Charpy tests on glass/epoxy systems and found that the initial modulus and ultimate stress increased.

Welsh and Harding [84, 75] observed an increase of fracture strength and fracture strain with the increase of strain rate on woven GFRP specimens, using split Hopkinson bar test method. Also, the stress vs. strain curves departure slightly from a linear elastic response at the quasi-static rate ($10^{-4}[sec^{-1}]$), while at higher rates (10 to $10^{3}[sec^{-1}]$). A greatly extended region of non linear deformation is observed leading to a markedly increased value of both the maximum stress and strain to fracture. The non linear deformation has been associated with successive bursts of damage.

Agbossou et al.[110] carried out tensile tests using a servo-hydraulic machine on unidirectional glass fibres/epoxy composite system (10 and 40% volume fraction). They found that for strain rates lower than 1$[sec^{-1}]$ the maximum tensile stress varied linearly with the log of strain rate,

whereas for strain rate higher than $1[sec^{-1}]$ the failure strength appeared to follow an exponential power law. Agbossou et al. also observed that strain to fracture increased with increasing strain rate. Finally, they observed that the absorbed energy increased with increasing strain rate. In the author's opinion, the finding of Agbossou et al. of an exponential power law above 1[1/sec] is due to the use of a soft (hydraulic) machine and inertia, which were not taken into account. A corollary to this postulate is that power law was not been observed by any other researcher.

Barre[10] carried out tensile tests on a servo-hydraulic machine on woven E-Glass/phenolic and polyester resin materials at strain rates between $10^{-1} \rightarrow 10[sec^{-1}]$ and found that the elastic modulus and failure stress increased for increasing strain rate. They also reported contradictory conclusions for shear modulus depending on the orientation of fibre to the principal direction of loading test chosen (10° and ±45°).

Xia et al.[71] carried out tests on unidirectional GFRP composite materials using a split Hopkinson bar and observed an increase of the initial stiffness modulus and strength with increasing strain rate. From their observations, the quasi-static strain curves exhibited a linear behaviour, while the dynamic curves exhibited a non linear behaviour, however no explanation was given for this observation. Xia et al. used a load/unloading testing variation of the Hopkinson bar, but the following problems were identified:

- The secondary reflective stress waves make it impossible to obtain the complete stress strain curve after a critical strain.
- At a constant strain rate, only one loading/unloading strain rate cycle is possible.

They proposed that the nominal tensile stress (σ_{BC}) when n fibres have broken is given by:

$$\sigma_{BC} = E_0 \varepsilon_C \left(1 - \frac{n}{N}\right) \tag{2.7}$$

E_0: the initial modulus of a coated fibre;

ε_C : the strain at point where n fibres have broken;

n: the number of broken fibres;

N: the initial number of unbroken fibres in the bundle.

Using a least squares method, they fitted a linear model to the experimental results for initial modulus (E_{11}^0) in the range up to the unstable strain[9] (ε_b), versus strain and substituted in eq.2.7. They arrived at an elastic brittle damage-rate-dependent constitutive equation for a range of strain rates, which has the following form:

$$\sigma = \left(E_r + k_E \log \frac{\dot{\varepsilon}}{\dot{\varepsilon}_r}\right) \varepsilon \exp\left\{-\alpha \cdot \left[\left(E_r + k_E \log \frac{\dot{\varepsilon}}{\dot{\varepsilon}_r}\right)\right]^{\beta}\right\} \tag{2.8}$$

where:

$\dot{\varepsilon}_r, E_r$: the reference strain rate and the initial modulus at the strain rate;

α,β: Weibull distribution parameters as defined by Eqn. 2.6;

k_E: is a linear regression coefficient with units of stiffness modulus.

Wang and Xia [141] proposed a modified version of the elastic brittle damage constitutive equation of Xia [76], by introducing a double Weibull distribution function. The modified function improved correlation with the experimental results, in particular after the onset of unstable strain (which

[9]The test required that the specimens did not fail.

was a limitation in the original model). Although, the results correlated well for different types of reinforcements (Kevlar, graphite and glass), no physical explanation was offered for the adoption of a double Weibull distribution approach.

Lifshitz and Leber [80] tested E-Glass/epoxy specimens using a split Hopkinson bar at $100 \rightarrow 200$[m/sec]. They used a Hill-like failure criterion and compared the failure envelope for the quasi-static and dynamic rates; finding clear evidence of the effect of strain rate sensitivity on the failure envelope. They reported an increase of the failure envelope profile by 30%.

Todo et al.[91] investigated woven cloth glass reinforced composites and studied the effect of different matrix material phases on the micro-level damage mechanisms which develop and the effect on the fracture properties. It has been established that fracture properties increase with increasing strain rate but stabilise beyond a critical strain rate; e.g. in the case of the examined system (modified polyamide) the increase of the fracture properties stabilised at rates close to $1[sec^{-1}]$). For the strain rate effects on the tensile properties a simple regression function was assumed, defined by:

$$M = \alpha \ln \dot{\varepsilon} + \beta \tag{2.9}$$

The problem with the use of the natural logarithm is that the conversion of strain rate is not as intuitive as it would be with the use of logarithm with base 10.

Pardo et al.[112] carried out 0° and 90° tensile tests on woven E-glass/epoxy systems on a servo-hydraulic machine and reported that at a strain rate range between $10^{-4} \rightarrow 100$[1/sec]. The tests exhibited significant increases in the maximum tensile and threshold stresses, but suggested that the modulus remained constant.

In conclusion, there are contradicting reports regarding the longitudinal mechanical properties of polymer composite systems. Armenakas and Sciamarella[9] found a decrease in the tensile in ultimate strength contradicting the findings of Rotem and Lifshitz[58], Hayes and Adams[140] all of whom observed a measurable increase. Daniel and Liber[107] suggested that there was no strain rate dependency. Regarding the longitudinal modulus, a measurable increase was established by some researchers while other researchers found the longitudinal modulus to be equal for the static and dynamic case. Most of the research work agrees that the longitudinal properties are dominated by the fibre reinforcement. The majority of the research work on glass reinforced composite systems reports increase in stiffness and in strength, contrary to graphite reinforced composite systems which exhibit little or no strain rate sensitivity.

2.4.4.3 Strain Rate Effect On The Transverse Tensile Properties.

Daniel and LaBedz[105] tested unidirectional 0° and 90° graphite rings at strain rates up to 510[1/sec]. The transverse properties are dominated by the matrix and exhibited higher elastic modulus and strength than the quasi-static values. Also, they measured a significant decrease of the dynamic ultimate strain value (typically one third of the quasi-static ultimate strain).

Kaddour et al.[104] carried out tensile tests on ±67.5° Kevlar and Carbon fibre/epoxy composite systems using a internal pressurisation method for a strain rate range between .001 to 80[1/sec], and at different temperatures. They reported strain rate sensitivity of the transverse stiffness and failure strength.

Kammerer and Neme[139] studied cyclic tensile tests performed perpendicularly to the direction of the fibres on a unidirectional E-Glass/polyester system in the range of $10^{-5} \rightarrow 10^{-3}$. They found that the material showed significant strain rate dependence (they also reported non linear

behaviour and loss of specific stiffness). They reported recovery phenomena between cycles[10], which, in the author's view, indicates significant viscoelastic phenomena.

Generally, the researchers agree that the transverse stiffness and strength of polymer composite material systems increase with strain rate. It is noteworthy that the amount of published research literature on the strain rate dependency of transverse properties compared to that discussing the longitudinal properties is disproportionately small, probably because of the low failure strains observed at transverse loading and the difficulty of the instrumentation.

2.4.4.4 Strain Rate Effects On The Compressive Properties.

Most studies on the compressive failure strength of composite plates concern quasi-static loading[113, 128].

Using a compressive split Hopkinson bar Amijima et al.[94, 95], Kumar[96] concluded that compressive strength of GRP composite materials increases with increasing strain rate. Amijima[95] studied a woven and UD glass/polyester system and found that the compressive strength increase is more significant for the woven system.

Contrary to most researchers in the field, El-Habak [127] reported that the compressive strength of a glass/epoxy system exhibits little strain rate sensitivity (actually a slight decrease) up to $100[sec^{-1}]$, followed by a sharp rise in strength with increasing strain rate.

Zhao and Gary[113] carried out tests on glass/epoxy systems using a modified version of a split Hopkinson bar with the use of honeycombs as transverse complementary supports. They stated that the compressive failure strength properties are strain rate dependent at a range of $10^{-4} \rightarrow 10^{2}$. They also found higher strain rate dependency along the fibre orientation.

[10] Between unloading and reloading the plastic strains decrease.

Fan and Slaughter[128] reported that the dynamic compressive strength of fibre composites is insensitive to the strain rate up to a critical strain rate value which depends primarily on the fibre misalignment wavelength[128]. Also, the kink band width reduced for increasing strain rate until it reached a minimum value which was half of the quasi-static case.

Hsiao and Daniel [144, 145, 146] investigated the compressive behaviour of a carbon/epoxy system with different stacking sequences using a servo-hydraulic machine (strain rates up to .1[1/sec]) and an IFW testing machine (strain rates up to 120[1/sec]). They found that the longitudinal compressive modulus increased only slightly, while, the initial transverse compression modulus was found to increase by 37%. They also found that the longitudinal and transverse compressive strength at strain rates up to 120[1/sec] exhibited a significant increase compared to the static cases, respectively 79% and 100%. Further a 74% increase in the ultimate longitudinal compressive strain was observed. No strain rate dependency was established in the ultimate failure transverse compressive strain. Hsiao and Daniel[144, 145, 146] commented that the material stiffens significantly for increasing strain rates - referring to the reduced degradation of the modulus - however they did not associate this observation with damage evolution. It is the author's opinion that this lower damage evolution resulted in higher transverse compressive strengths at the same ultimate failure strain. However, because signals obtained with drop-weight or servo-hydraulic machine tests often contain perturbations which are due to the vibration of the testing machine[113].

Shan Khan and Simpson[109] carried out compressive tests on woven glass fibre/epoxy composite systems using a servo-hydraulic machine at strain rates between .001 $\rightarrow$ 10[1/sec]. They reported a 16% linear increase for the normal compressive failure stress across the examined strain rates. No strain rate dependency was reported for the in-plane failure compressive stress. Furthermore,

Shah Khan and Simpson measured an 18% increase for modulus for the normal loading. The spread of the scatter for modulus in the in-plane loading direction did not allow the researchers to make any conclusive inferences, however in a later reference, they stated that modulus for in-plane loading first increased with strain rate but then decreased markedly at higher strain rate. This observation raises questions about the methods of characterisation and their inferences. Shah Kahn and Simpson commented on failure compressive strains, reporting negligible strain rate effect.

Khan et al.[134] carried out compressive tests on S2-glass/polyester resin systems using a split Hopkinson bar at a strain range between .0001→ 1250[1/sec]. They observed that for dynamic loading, the response was significantly non linear. However they did not comment on the effect of the initial compression modulus, which appeared to increase with strain rate. They also reported higher compressive stresses for the dynamic loading condition. Because failure did not occur in all cases, the researchers did not draw any conclusions on the failure compressive stresses and strains[134].

Tsai and Sun[8] carried out off axis compressive testing on glass/epoxy composite specimens (the fibre orientations included 15°, 30°, 45°, 60°) and reported that compressive modulus is not affected by strain rate.

McGee and Nasser[135] carried out bi-axial compressive testing on glass/epoxy systems using a split Hopkinson bar at a strain rate range between .0001 → 1000[1/sec][11]. They found significant increase of the compressive strength at the higher strain rates.

[11]There were inconsistencies in the paper stating in one occasion that the maximum compressive strain rate was 1000[1/sec] and in other occasion 500[1/sec]

2.4.4.5 Strain Rate Effects On The Shear Properties.

A number of researchers have investigated the shear properties of GRP unidirectional laminates, using different test specimens and loading configurations.

Daniel et al.[108] used 10° off axis glass fibre/thermoset laminates under internal pressurisation method and found that the shear strength decreased with strain rate increasing from $1 \rightarrow 10[\sec^{-1}]$. Harding [84] used the Split Hopkinson Pressure Bar tensile results of a +45° glass/epoxy laminate and observed an 1.7 increase of shear strength with increasing strain rate over a range of $10[^{-}4] \rightarrow 930[sec^{-1}]$. Al-Salehi et al.[18] used ±45° composite laminate specimens to obtain the shear properties of the glass reinforced unidirectional laminates, and observed similar increases of laminate strength above a threshold of $10[sec^{-1}]$.

Staab and Gilat [147] carried out tensile tests on ±45° composite laminate specimens to obtain the shear properties of the unidirectional glass/epoxy composite laminates using a split Hopkinson bar, and observed 30 to 50% increase in laminate strengths (however the increase in shear failure strength was not as significant as other researchers).

Kammerer and Neme[139] reported on cyclic tensile tests of a ±45° E-Glass/polyester composite system in the range of $10^{-5} \rightarrow 10^{-3}$. The material mechanical properties showed significant strain rate dependence, plastic shear strain and degradation of the constitutive elastic properties. Although they did not quantify the change of the shear properties (shear modulus and strength), they developed a constitutive model using the elastoviscoplasticity concept (see section 2.4.6).

Hsiao and Daniel [144] investigated the shear behaviour of carbon/epoxy systems for 30° and 45° off axis. The test equipment used was a servo-hydraulic (strain rates up to .1[1/sec]) and an IFW testing machine (capable of strain rates up to 120[1/sec]). They stated that shear stress-

strain behaviour in quasi-static and dynamic strain rates is consistent. However, they observed an increase in shear failure strength by 80%, at higher strain rates using the IFW.

Kaddour et al.[103] have carried out tensile tests on ±67.5° Kevlar and Carbon fibre/epoxy composite systems using the method of internal pressurisation at a strain rate range between .001 → 80[1/sec] at different temperatures. They reported strain rate sensitivity for both shear stiffness and shear failure strength.

Okoli[135] carried out tests on woven glass/epoxy 3[mm] thick composite systems using a servo-hydraulic machine. He found shear energy to failure increased linearly with logarithm of increasing strain rate.

Generally, the researchers agree that there is a increase of the shear failure strength properties. The research work that has been carried out suggests that at increasing strain rates the shear behaviour of the composite material appears to be stiffer.

2.4.5 Strain Rate Effect On The Damage Evolution.

Lataillade et al.[112] carried out tensile tests on ±45° E-Glass epoxy laminates using a servo-hydraulic and a split Hopkinson bar in order to determine the effect of the intralaminar shear loading rate on the damage evolution of composites. Their paper provides an excellent review of recent damage mechanics approaches. They reported that the *shear damage initiation threshold* increases with increasing shear strain rate, while the *damage propagation rate* (the rate of damage evolution) decreases with increasing shear strain rate. They reported that there is an upper limit to the degradation of the mechanical properties which is associated with the existence of a crack spacing limit.

Welsh and Harding [73] using a split Hopkinson bar to test glass/polyester systems over a strain rate range of $10[^-4] \rightarrow 1000[sec^{-1}]$ and observed a change of the failure mode with increasing strain rate .

Raghavan and Meshii[148] investigated time dependent damage in the form of matrix cracking and crack density on cross-ply laminates at $10^{-6} \rightarrow 10^{-3}$[m/sec] (creep domain). They stated that time dependent damage evolution in polymer composite laminates is dependent on the viscoelastic properties of the constituent lamina and the resin rich interlaminar layer, even at very low strain rates. The parameter they selected to represent the damage evolution (crack density per unit length) is not suitable though for FE, because it would require a level of refinement of the FE mesh which would be impractical for design purposes.

Kammerer and Neme[139] reported results for tests perpendicular to the direction of the fibres in the strain rate range of $10^{-5} \rightarrow 10^{-3}$ of a Unidirectional E-Glass/polyester composite; Damage evolution showed significant strain rate dependence. However, they did not quantify this effect, instead they presented a graph of the absolute value of stiffness vs. specific stress[12]. The followed approach does not provide an intuitive interpretation of the strain rate dependency on the degradation of stiffness properties, because of the significant differences of the initial modulus.

Beligrandi and Badori [119] conducted low velocity ($.7 \rightarrow 6.28$[m/sec]) transverse impact testing on glass/epoxy composite systems and investigated a quantity they called *damage degree*. However, *damage degree* is a quantity that characterises the energy absorption and is defined as the ratio of the total energy transformed and the dissipated part of it. They found that in the considered strain rate range no sensitivity was shown to the strain rate effect. However, the researchers only considered the flexural response of the material.

[12]Stress over density

Pardo et al.[112] carried out 0° and 90° tensile tests on woven E-glass/epoxy systems on a servo-hydraulic machine and reported that at a strain rate range between $10^{-4} \rightarrow 100[1/sec]$ the observed damage mechanisms depended on strain rate.

There has been no research work carried out on the damage evolution of fibrous composite materials based on a damage mechanics framework and with strain rate dependency. The research appears to have focused on the damage evolution under static conditions.

2.4.6 Constitutive Models For High Strain Rate Response

Xia and Wang[150] carried out tests on unidirectional glass/epoxy systems at strain rates of $300[1/sec]$. They proposed a dynamic microscopic damage constitutive numerical model, taking into account thermo-mechanical coupling through statistical averaging. They suggested that thermo-mechanical coupling is necessary because at the strain rates of interest the process may be considered adiabatic.

Kammerer and Neme[151, 139, 152] proposed a constitutive model to account for the strain rate dependence of damage based on the elastoviscoplastic "*bi-material*". The "bi-material" approach considers that the ply consists of two fictitious materials (one with the behaviour of a virgin material and one with the behaviour of the damaged material just before its final breaking). The ply starts as virgin material with no damage and progressively (and irreversibly) converts to the fully damaged material. However, to obtain the parameters of the constitutive relationship, their approach required optimising the differences method between experiments and simulations[153], suggesting the predictive abilities of the method may be limited.

Kaddour et al.[103] have used a strain rate/ temperature equivalence principle to establish the

coupled effect of strain rate and temperature on shear mechanical properties. They used an Arrhenius equation to describe the variation of the shift factor with temperature. The elegance of this approach is that it is possible to construct a strain rate/temperature master curve, for which all other curves fall onto. The downside of this approach is determination of *activation energy*[154]. The *activation energy* is required to construct the master curve, is unique for each material, and in this case temperature dependent (not strain rate though). They also used a Williams-Landel-Ferry model[155] which has been used to study the relaxation process of many polymers under a wide range of test temperatures. This is an corollary to the postulation that the shear and transverse properties of the material are dominated by the matrix.

Weeks and Sun[156, 157, 123] established rate dependent constitutive models for fibrous composites for uniaxial loading using a plastic potential function[158] to provide the flow rule, which was later extended to account for the strain rate. Thiruppukuzhi and Sun[159, 124] developed further a three dimensional model for unidirectional as well as woven fabric composites for general loading condition. The model had the following form:

$$\bar{\varepsilon}^P = \chi(\dot{\bar{\varepsilon}}^P)^m(\bar{\sigma})^n \tag{2.10}$$

where:

$\bar{\varepsilon}^P$: effective plastic strain;

$\dot{\bar{\varepsilon}}^P$: effective plastic strain rate;

$\bar{\sigma}$: effective stress;

χ, m, n: parameters of viscoplasticity model.

Thiruppukuzhi and Sun[159, 124] suggested the single scalar equation for effective plastic stress, accumulated effective plastic strain and effective plastic strain rate represent the constitutive equations for orthotropic material systems for all possible orientations under multi-axial stress state.

Although, the method proposed by Thiruppukuzhi and Sun describes the stress state of the material, it is not suitable for predictive models using FE, because it creates a scalar value for each stress state. The plastic function concept and the effective function which is proposed are more suitable for the implementation in a failure criterion.

Triruppukuzhi and Sun[124] has validated their constitutive models for $[\pm 45°]_{3S}$ and $[+15°/-55°]_{3s}$ laminates via ABAQUS simulations using 4 noded layered shell finite elements. The $[\pm 45°]_{3s}$ had a good correlation (less that 5% error) for strains up to 1.5%. However, in the same paper the total range of the strain of the experimental results were not shown.

An important finding from their work was in terms of computational modelling, an estimate of the order of strain rates encountered in a particular problems should lead to reasonably good prediction of the material response, if the actual strain rate history itself is not available[159].

Tsai and Sun[8] have proposed a constitutive viscoplasticity model for characterising high strain rate behaviour of polymeric composites, based on the one parameter plastic potential function proposed by Sun and Chen[160].

As far as numerical simulation models are concerned, Iannucci et al.[21] reported a failure model for normal impact on woven glass fibre composites. Giving a detailed account of their assumptions and implementation in the PAM-CRASH explicit FE code. Okoli[136] found that prediction of material properties offered by the available micro mechanics relations are not strain rate dependent

or are too complex for the analyst to implement.

2.5 Finite Element Methods

2.5.1 Literature review

Al-Bastaki[20] has performed FE analysis of Kevlar fibre reinforced plastic tubes subjected to a dynamic internal pressure pulse using the ABAQUS code. They included strain rate effects of the transverse strength and longitudinal and transverse modulus using linear equations of the strain rate. Although, it was claimed that progressive failure was used, a rather simplistic scheme was implemented which set the transverse stiffness to zero when the transverse strength was reached. The modified values were used in the calculation of the ply Jacobian stiffness matrix. Final failure was reached when the dynamic longitudinal strength was reached.

Okoli[136] suggested failure model implemented in current FEM packages are limited by the use of non rate sensitive micro mechanics relations. However, demonstrations have shown that errors arising from this situation cannot be ignored[161].

Langlie and Cheng[162] performed numerical simulation of ballistic tests of thick composite panels.

Iannucci and Willows[163] have reported the development of a proprietary damage model. They reported accurate matrix micro cracks in the weft and warp fibre directions of a composite skin subjected to impact.

The model by Iannucci and Willows[163] was compared[164] to other FEM codes and was found to use a theory of mixtures to generate the laminate engineering constants from the constituent phases - compared to other codes that used directly the properties of the laminates. The main benefits

of the model were, that a) it used a realistic energy dissipation approach instead of complete ply failure and b) its formulation allowed for the implicit modelling of strain rate effects.[136]

Kammerer[139] have employed their elasticviscoplastic "bi-material" in the ABAQUS 5.4 finite element code, to simulate split Hopkinson tests. They compared the predictions of different material models.

Johnson and Pickett[165] reported on the impact and crash FE modelling of a helicopter subfloor composite beam structure using damage mechanics approach in PAM-CRASH FE element code. They compared different methodologies for modelling the interlaminar failure modelling.

Johnson and Simon[166] reported on the transverse impact and FE modelling of a composite plate under transverse impact using PAM-CRASH. A continuum damage mechanics model for fabric reinforced composite was implemented.

Okoli and Abdul Latif[130] carried out an FEM model of 3 point beam impact test. He discussed the limitations he found in the implementation of the Chang-Chang[167] failure criterion (significantly overestimated strength and underestimating strength for different load cases). Finally, an interactive FEM scheme was proposed, to obtain the validity of an FEM simulation based on a sensitivity analysis.

2.5.2 General Ply Representation Methods

Finite elements allow the use of different elements for the representation of physical components. Depending on the application requirements, it is possible to use either 1, 2 or 3D elements for the FE model. In the following subsections, the benefits of the different methods will be briefly discussed.

2.5.2.1 1-D FE Ply Representation Methods

The common one dimensional elements (otherwise known as beam elements) are consisted of two nodes connected. These elements are the most basic elements, and there are not usually preferred for composites unless in very specific conditions.

Beam elements may be used for the modelling of highly orientated composites to simulate the reinforcement effect. In this case the matrix phase can be constituted by another set of elements (usually shell or brick elements) and the beam elements share nodes with the matrix phase. The Bi-phase model follows the principle of this approach.

2.5.2.2 2-D FE Ply Representation Methods.

Two dimensional elements present an more attractive method of modelling laminated composite materials. In some cases, like those of laminated composites, they are even preferable to three dimensional composites, because of the computational efficiency. In explicit FE codes, where the maximum timestep for a stable solution is proportionate to the minimum dimension of the element, the computational gains of using 2-D elements are even greater.

Low order 2D elements consist of 3 or 4 nodes (triangular or rectangular elements respectively). The planar geometry of the element resembles the geometry of a thin plate. This geometric similarity between physical object and abstract representation has a number of advantages. The main benefit is the easy of creating laminate layups, with elements with reasonable aspect ratios, without increasing the computational requirements.

The difference between a triangular and a rectangular mesh is quite significant for low order shell elements. The formulation of the triangular shell elements allows only a constant stress state

throughout the element. In the case of the rectangular element a linear gradient of the stress or strain are allowed throughout the specimen. The effects on the accuracy of the solution because this could be quite significant, especially in locations where the stress gradients vary (e.g. near stress concentration points).

Higher order rectangular shell elements consist of 8 nodes (3 nodes define each side of the rectangle) and allow for quadratic shapes of the boundary. Higher order shell elements are only implement in implicit FE codes.

2.5.2.3 3-D FE Representation Methods

Three dimensional FE elements (also known as solid or brick elements) provide the most dimensionally accurate representation of a physical object, at the expense of increased computational processing requirements for the solution. As a result, three dimensional elements are very rarely used.

2.5.3 2D laminate FE Representation Methods.

In this subsection, the advantages and disadvantages of different laminate representations will be discussed.

2.5.3.1 Single Layer Of Elements

Many FE code allow one element to include a layup sequence. Then using Classical laminate theory the stiffness matrix of the element is calculated and updated according to the stresses and strains observed in the material.

Although, in most cases the geometric offset of the plies is taken into account during the calculation

(therefore there is no loss of geometric stiffness), it is not possible to account for delaminations and intralaminar failure, which is a significant factor is certain cases of materials.

The advantages of this approach are the simplicity of definition, and the low computational requirements. An efficient use of this approach is for stiffness studies at the concept stage. The approach would be totally inappropriate for any representation of post-failure studies of laminate.

2.5.3.2 Multiple Layer Of Elements For Each Individual Ply With Shared Nodes.

This approach is based on duplicate elements shells. Duplicate elements are two elements that share the same nodes, and therefore occupy the same space in three dimension.

- No delamination (perfect bonding).
- Not accurate representation of geometric stiffness in most FE code implementations (possible to offset the midplane of each layer), especially for bending.
- Individual ply failure (more accurate representation).
- Increased number of elements (high computational requirements).
- No intralaminar stresses.

This is one of the least favourable methods, because of the poor geometric representation and the increased computational requirements. This method is recommended mainly in studies where there are no out of plane loads.

2.5.3.3 Multiple Layer Of elements Offset And Constrained With Rigid Links

The FE model consists of multiple layers of shell elements, each one representing one of the plies in the layup sequence. Each layer is offset according to the ply thickness so that the model matches the physical component. The nodes of corresponding elements are connected using rigid beam elements (therefore there is a stiffness which allows a degree of relative movement for the ply layers.

- Delamination is possible (definition of cutoff strength).
- Accurate representation of geometric stiffness in all implementations (possible to offset the midplane of each layer).
- Individual ply failure (more accurate representation).
- The introduction of loads can be cumbersome, in order to avoid singularities.
- Difficult to define cutoff strengths for the rigid links for irregular meshes.
- Cumbersome to define the geometry of FE model (rigid links).
- Possible to obtain intralaminar stresses.

The offset layers with rigid links methodology represents better the physical laminate. Compared to the previously mentioned representation methods it has significant advantages for out of plane loading conditions, and also allows for delaminations. The disadvantages are the increased computational requirements because of the increased element number (compared to the single layer method) and also the difficult of the element preparation which makes the method, prohibitive for industrial environments.

This method is advised for any type of loading, and is able to represent the failure and post failure of a laminate very accurately.

2.5.3.4 Multiple Layer Of Elements Offset And Constrained With Contact Definition.

Like the previous method, the FE model consists of multiple layers of shell elements, each one representing one of the plies in the layup sequence and each layer is offset according to the ply thickness so that the model matches the physical component. The difference is that the layers are in this case constrained using a contact definition between each set of layers.

The contact definition is the equivalent of a interphase between the layers. It has a stiffness and a cut-off load. Therefore, relative movement is allowed between the nodes, and also when a level of load is exceeded the interphase fails, essentially creating a delamination location.

- Relative movement of plies. Reorientation possible (scissoring of fibres).
- Delamination is possible (definition of cutoff strength).
- Accurate representation of geometric stiffness in all implementations (possible to offset the midplane of each layer).
- Individual ply failure (more accurate representation).
- The introduction of loads can be cumbersome, in order to avoid singularities.
- Cutoff strengths is defined over the entire area, therefore it is more convenient than rigid links for irregular meshes.

- Relatively easy to define the geometry of FE model.
- Possible to obtain intralaminar stresses.

The offset layers with constrains methodology represents very well the physical laminate. It has similar advantages to the multiple offset layers with rigid links approach, but in addition it is a lot more convenient to define. The main disadvantage is are the increased computational requirements because of the increased element number (compared to the single layer method) and the presence of contact definitions.

This method is advised for any type of loading, and is able to represent the failure and post failure of a laminate very accurately.

2.5.4 Material Models For Composites

2.5.4.1 Bi-phase Orthotropic Model

The Bi-phase model for unidirectional composite plies was one of the first models developed based on the concept of the degradation of mechanical properties. The model was developed for Civil engineering in the 1970's for designing studies using steel reinforced concrete.

The model incorporates the concept of degradation of mechanical properties however there is no account for the physical mechanisms of failure in the composite material. The Bi-phase model consists of a matrix phase (shell or solid elements) superimposed by a reinforced beam element. All the stiffness properties have associated damage evolution functions with respect to the strain.

Required Parameters for Bi-phase calibration. The parameters, which are required for complete definition of the bi-phase ply definition, are presented in table 2.3.

Card	Quantity	Symbol
Generality		
	Mass Density	ρ^{UD}
Orthotropy		
	Orthotropy Directions	{x,y,z}
	Ply thickness	t^{UD}
Ply/Matrix	*Tension*	
	Stiffness Modulii	$E^m_{11,t,0}$, $E^m_{22,t,0}$, $E^m_{33,t,0}$
	Shear Modulii	$G^m_{12,t,0}$, $G^m_{13,t,0}$, $G^m_{23,t,0}$
	Poisson's ratio	$\nu^m_{12,t}$, $\nu^m_{13,t}$, $\nu^m_{23,t}$
	Volumetric Damage	$d^m_{v,t}(\epsilon)$
	Shear Damage	$d^m_{s,t}(\epsilon)$
Fibre	*Tension*	
	Young's Modulus	$E^f_{t,0}$
	Damage law	$d^f_t(\epsilon)$
	Volume fraction	$v_{f,t}$
Ply/Matrix	*Compression*	
	Stiffness Modulii	$E^m_{11,c,0}$, $E^m_{22,c,0}$, $E^m_{33,c,0}$
	Shear Modulii	$G^m_{12,c,0}$, $G^m_{13,c,0}$, $G^m_{23,c,0}$
	Poisson's ratio	$\nu^m_{12,c}$, $\nu^m_{13,c}$, $\nu^m_{23,c}$
	Volumetric Damage	$d^m_{v,c}(\epsilon)$
	Shear Damage	$d^m_{s,c}(\epsilon)$
Fibre	*Compression*	
	Young's Modulus	$E^f_{c,0}$
	Damage law	$d^f_c(\epsilon)$
	Volume fraction	$v_{f,c}$

Table 2.3: Parameters required for the complete definition of the bi-phase ply definition.

Required Testing There are no standardised calibrated procedures for the bi-phase ply definition. Table 2.4 presents tests that can be carried out to assist in the evaluation of the bi-phase parameters.

Test	Laminate	Parameters
ASTM D3039	UD90	$E^m_{22,t,0}$,$E^m_{33,t,0}$, $d^m_{v,t}(\epsilon)$
	UD00	$E^f_{11,t,0}$,$E^m_{11,t,0}$ $d^f_t(\epsilon)$, $\nu^m_{12,t}$
Iosipescu	UD90	$G^m_{12,t,0}$=$G^m_{13,t,0}$=$G^m_{23,t,0}$, $d^m_{s,t}(\epsilon)$
		$G^m_{12,c,0}$=$G^m_{13,c,0}$=$G_{23,c,0}m$, $d_{sm,c}(\epsilon)$

Table 2.4: Parameters that are obtained through a standardised test procedure.

Strategy There are no standardised calibration procedures for the Bi-phase orthotropic model. The approach that is usually followed is that the material is calibrated for a certain layup and a certain loading condition based on test data. Although the material is relatively simple to calibrate for simple loading conditions (uniaxial loading), it is very difficult to calibrate for a generic loading conditions (complex stress state). The reason for this is that there is no underlying physical reasoning and the damage evolution laws are based on uniaxial testing results. However, it is well documented that the failure processes and mechanisms of laminated composite materials are complex and there are interactions between normal (dilational) and shear (deviatoric) parameters. Therefore, a coupling of the ply different damage evolution laws is essential to provide an representative description of the mechanisms of damage. In the case of the bi-phase this coupling is not provided, and therefore its usefulness as a predictive tool is limited.

The estimation of the stiffness of a composite ply laminate in the explicit element code $PAMCRASH^{TM}$

is based on the Classical laminate theory. Therefore, the governing equation is equation 2.11:

$$\begin{bmatrix} \sigma_{11} \\ \sigma_{22} \\ \tau_{12} \end{bmatrix} = C^{UD} \begin{bmatrix} \epsilon_{11} \\ \epsilon_{22} \\ \gamma_{12} \end{bmatrix} \tag{2.11}$$

The stiffness matrix for the UD ply C_{UD} is given by the following equation 2.12

$$C^{UD} = C^m + C^f \tag{2.12}$$

$$\begin{bmatrix} \frac{E_{11}^{UD}}{N^{UD}} & \frac{v_{21}^{UD} E_{22}^{UD}}{N^{UD}} & 0 \\ \frac{v_{21}^{UD} E_{11}^{UD}}{N^{UD}} & \frac{E_{22}^{UD}}{N^{UD}} & 0 \\ 0 & 0 & G_{12}^{UD} \end{bmatrix} = \begin{bmatrix} \frac{E_{11}^m}{N^m} & \frac{v_{21}^m E_{22}^m}{N^m} & 0 \\ \frac{v_{21}^m E_{11}^m}{N^m} & \frac{E_{22}^m}{N^m} & 0 \\ 0 & 0 & G_{12}^m \end{bmatrix} + \begin{bmatrix} E_{11}^f & 0 & 0 \\ 0 & 0 & 0 \\ 0 & 0 & 0 \end{bmatrix}$$

Volumetric Matrix Damage law The Bi-phase model superimposes the effect of the a stiff 1-Dimensional reinforcement on a isotropic matrix. The fibre contributes only in the direction of fibres. The matrix properties are required to characterise the ply properties in the plane normal to the direction of the fibres (both in-plane and out-of-plane).

The recorded longitudinal load (P_L) and displacement (Δl) of a UD laminate tested at 90° degrees tension are required to obtain the Volumetric Matrix Damage law. The load and displacement are transformed to the material axes to stress ($\sigma_{22} = \frac{P_L}{Area}$) and strain ($\epsilon_{22} = \frac{\Delta l}{l_0}$). The transverse modulus $E_{22,i}$ at each observation is the quotient of stress divided by strain$\left(\frac{\sigma_{22,i}}{\epsilon_{22,i}}\right)$.

According to the bi-phase model, the transverse properties of a composite ply are calculated by equation 2.13.

$$E_{22}^{ply}(\epsilon) = E_{22,0}^m \cdot [1 - d_v^m(\epsilon)] \cdot (1 - v_f) \tag{2.13}$$

Where:

Initial Transverse stiffness modulus $E^m_{22,0}$ is the initial modulus and is calculated by $\max_{i=1,2..N}(E^m_{22,i})$.

N is the number of observations (data points).

The volumetric damage curve (as a function of strain) is obtained using:

$$d^m_v(\epsilon) = 1 - \frac{E^{ply}_{22}(\epsilon)}{E^m_{22,0} \cdot (1 - v_f)} \tag{2.14}$$

Once the volumetric damage curve is obtained, the input parameters of PAMCRASH are selected:

Initial strain ($\epsilon_{22,i}$) is the transverse when degradation of the transverse properties initiates.

Intermediate damage and strain ($d^m_{v,1}$,$\epsilon_{22,1}$) an intermediate value of damage, and the corresponding strain, selected to represent the damage curve as closely as possible.

Ultimate damage and strain ($d^m_{v,u}$, $\epsilon_{22,u}$) the value of shear damage at failure, and the corresponding strain.

Therefore, to obtain the matrix volumetric damage law, the tensile test results of a UD specimen tested in 90^o are required.

Once the matrix volumetric damage law is obtained, the ply effectively has an isotropic volumetric damage law; because of the different stiffness moduli, different stiffnesses are observed in the different directions. The properties degradation behaviour in the direction of the fibres is expected to be markedly different to the direction transversely to the fibres.

Fibre Damage law In the cyclic loading of UD material in the direction of the fibres, there is no stiffness degradation. Therefore, the fibre damage law is used to calibrate the response in the direction of the fibres.

The modulus of elasticity for the UD ply in the fibre direction (for tension and compression) is given by the :

$$E_{11}^{UD}(\epsilon) = E_{11,0}^{m} \cdot [1 - d_v^m(\epsilon)] \cdot (1 - v_f) + E_0^f \cdot \left[1 - d^f(\epsilon)\right] \cdot v_f \tag{2.15}$$

Where:

$E_{11}^{UD}(\epsilon)$ is the stiffness modulus of the composite ply in the fibre direction as a strain function.

$E_{11,0}^{m}$ is the initial stiffness modulus of the matrix/ply in the fibre direction as a strain function.

E_0^f is the initial stiffness modulus of the fibres in the fibre direction as a strain function.

The tensile modulus of the UD ply in tension $E_{11}^{UD}(\epsilon)$ is described in terms of the damage degradation stiffness modulus of the UD :

$$E_{11}^{UD}(\epsilon) = E_{11,0}^{UD}[1 - d^{UD}(\epsilon)] \tag{2.16}$$

The degradation of the stiffness modulus of the UD can be easily obtained from the experimental results.

Substituting equation 2.16, the fibre damage law is obtained.

$$d^f(\epsilon) = 1 - \frac{E_{11,0}^{UD}[1 - d^{UD}(\epsilon)] - E_{11,0}^{m} \cdot [1 - d_v^m(\epsilon)] \cdot (1 - v_f)}{E_0^f \cdot v_f} \tag{2.17}$$

Deviatoric Matrix Damage law For the calibration of the Deviatoric Matrix damage law, the $[\pm 45]_{2s}$ results will be used. The process requires recording of both the longitudinal (ϵ_L) and the transverse strain (ϵ_T). Using laminate theory the tensile load and the recorded strains in the global axis (experiment) are transformed to stress and strain in the local (material) axis (1), (2).

$$\begin{bmatrix} \sigma_{11} \\ \sigma_{22} \\ \tau_{12} \end{bmatrix} = \begin{bmatrix} 0 \\ 0 \\ \sigma_L/2 \end{bmatrix} \quad and \quad \begin{bmatrix} \epsilon_{11} \\ \epsilon_{22} \\ \gamma_{12} \end{bmatrix} = \begin{bmatrix} 0 \\ 0 \\ \epsilon_L - \epsilon_T \end{bmatrix}$$

For each measurement i a value of the shear modulus $G_{12,i}$ is obtained ($G_{12,i} = \frac{\gamma_{12}}{\tau_{12}}$). A damage curve is obtained based on the following equation:

$$d_s^m(\gamma_{12}) = 1 - \frac{G_{12,i}}{G_{12,0}} \tag{2.18}$$

Once the damage curve is available, the input parameters of PAMCRASH are selected:

Initial strain ($\gamma_{12,i}$) is the shear strain when degradation of the shear properties initiates.

Intermediate damage and strain ($d_{s,1}^m$,$\gamma_{12,1}$) an intermediate value of damage, and the corresponding strain, selected to represent the damage curve as closely as possible.

Ultimate damage and strain ($d_{s,u}^m$, $\gamma_{12,u}$) the value of shear damage at failure, and the corresponding strain.

This material model has been one of the few damage mechanics models available in explicit Finite Element codes. Its continued used is based more on its simplicity of concept and ease of use than on validity or rationale and predictive capabilities.

2.5.4.2 Ladevéze model Theoretical Formulation

The Ladevéze composite ply material model is a more recent advance[2, 168]. The composite ply material model has been developed to characterise and simulate the basic building block. The Ladédeze composite ply material model is suitable for Finite Element Method approach, because

angle plies of a specific material can be simulated by changing the orthotropy directions of the basic composite material ply.

The main benefit of the Ladevéze composite material ply compared to other available model suitable is that it characterises the damage evolution in a way which is compatible to the continuous medium assumption of the FE method. Other method of damage characterisation employ quantities like crack density which are not suitable for FE material because they impose upper limits on the geometrical size of the elements (with negative effects on the simulation run time).

Damage Model. The original model assumes plain stress state. The strain energy density of the damaged material has the following form:

$$E_D = \frac{1}{2}\left[\frac{\sigma_{11}^2}{E_{11}^0} - \frac{2\nu_{12}}{E_{11}^0}\sigma_{11}\sigma_{22} + \frac{\langle\sigma_{22}\rangle_+^2}{E_{22}^0(1-d')} + \frac{\langle\sigma_{22}\rangle_-^2}{E_{22}^0} + \frac{\tau_{12}^2}{2G_{12}^0(1-d)}\right] \tag{2.19}$$

d and d' are respectively dimensionless scalar shear and transverse damage variables that remain constant throughout the ply thickness. The strain energy density E_D units $[ML^{-1}T^{-2}]$.

Notice that only the transverse and the shear modulus are assumed to be degraded by the damage. The $\langle\alpha\rangle$ has the following mathematical meaning.

$$\begin{cases} \langle\alpha\rangle_+ = \alpha \text{ if } \alpha \geq 0\text{; otherwise } \langle\alpha\rangle_+ = 0. \\ \langle\alpha\rangle_- = \alpha \text{ if } \alpha \leq 0\text{; otherwise } \langle\alpha\rangle_- = 0. \end{cases}$$

The transverse stress is therefore decomposed to tensile and compressive stress. The theory suggests that microcracks initiate in the 90^o of the unidirectional ply. Tensile transverse stresses will result in opening of the microcracks and therefore degradation of properties. Compressive transverse stresses will close up the microcracks, and therefore have no effect on the behaviour of the

transverse direction.

The elastic law ($\varepsilon^e = K^{-1}\sigma$) after the inclusion of the above described damage model, is then formulated as:

$$\varepsilon^e = K^{-1}\sigma \Leftrightarrow \begin{cases} \varepsilon^e_{11} = \frac{\sigma_{11}}{E^0_{11}} - \frac{\nu^0_{12}}{E^0_{11}}\sigma_{22} \\ \varepsilon^e_{22} = \frac{\langle\sigma_{22}\rangle_+}{E^0_{22}(1-d')} + \frac{\langle\sigma_{22}\rangle_-}{E^0_{22}} - \frac{\nu^0_{12}}{E^0_{11}}\sigma_{11} \\ \gamma^e_{12} = \frac{\tau_{12}}{2G^0_{12}(1-d)} \end{cases} \tag{2.20}$$

The shear and transverse damage variables d and d' (and therefore the damage development) are governed by the conjugate quantities Y_d and $Y_{d'}$ (like energy release rates govern the crack propagation). They are defined as:

$$Y_d = \left.\frac{\partial E_D}{\partial d}\right|_{\bar{\sigma},d'} = \frac{1}{2}\frac{\tau^2_{12}}{G^0_{12}(1-d)^2} \tag{2.21}$$

$$Y_{d'} = \left.\frac{\partial E_D}{\partial d'}\right|_{\bar{\sigma},d} = \frac{1}{2}\frac{\langle\sigma_{22}\rangle^2_+}{E^0_{22}(1-d')^2} \tag{2.22}$$

where $\bar{\sigma}$ is the effective stress.

$$\bar{\sigma} = \begin{bmatrix} \sigma_{11} \\ \frac{\langle\sigma_{22}\rangle_+}{1-d'} + \langle\sigma_{22}\rangle_- \\ \frac{\sqrt{2}\tau_{12}}{1-d} \end{bmatrix} \tag{2.23}$$

Y_d and $Y_{d'}$ are the partial derivatives of the strain energy density with respect to the damage parameters d and d' and represent respectively the pure shear and transverse effect.

Two ply degradation mechanisms are identified that contribute to damage development:

- Matrix microcracking.
- Fibre matrix debonding.

Quantities $\underline{Y}$ and $\underline{Y}'$ are introduced in order to describe the damage development.

$$\underline{Y} = \sup_{\tau \leq t}(\sqrt{Y_d(\tau) + bY_{d'}(\tau)}) \tag{2.24}$$

$$\underline{Y}' = \sup_{\tau \leq t}(\sqrt{Y_{d'}(\tau)}) \tag{2.25}$$

$\underline{Y}$ and $\underline{Y}'$ provide respectively the Master Shear and Transverse Damage Curves. Cyclic testing is used in order to obtain the $\underline{Y}$ and $\underline{Y}'$ and the respective d and d' damage quantities. Therefore, the Master Damage Curves are approximated by a piece-wise linear curves. More detailed presentation is available in §3.4.

Fibre Direction Behaviour Finally in the fibre direction, a brittle linear elastic behaviour in tension and a non linear elastic behaviour in compression is assumed. The compressive stiffness loss (see equation 2.26)is based on the compressive stiffness constant γ which is a material characteristic.

$$E_{11}^{c} = E_{11,0}^{c}(1 + \gamma\langle\sigma_{11}\rangle_{-}) \tag{2.26}$$

$$\begin{cases} \varepsilon_{11}^{e} = \frac{\sigma_{11}}{E_{11}^{0}(1+\gamma\langle\sigma_{11}\rangle_{-}} - \frac{\nu_{12}^{0}}{E_{11}^{0}}\sigma_{22} \\ \varepsilon_{22}^{e} = \frac{\langle\sigma_{22}\rangle_{+}}{E_{22}^{0}(1-d')} + \frac{\langle\sigma_{22}\rangle_{-}}{E_{22}^{0}} - \frac{\nu_{12}^{0}}{E_{11}^{0}}\sigma_{11} \\ \gamma_{12}^{e} = \frac{\tau_{12}}{2G_{12}^{0}(1-d)} \end{cases} \tag{2.27}$$

2.5.4.3 Other Models

Other proven explicit FE solver like LS-DYNA use composite model with damage which are based on the Chang-Chang composite failure material model[169, 167].

The MAT_COMPOSITE_DAMAGE (material model 22) was the first one developed. It uses four strength measurements[170]:

- longitudinal tensile strength;
- transverse tensile strength;
- shear tensile strength;
- transverse compressive strength;

and also α a nonlinear shear stress parameter. In plane stress, the strain is given in terms of the stress as:

$$\begin{aligned} \varepsilon_1 1 &= \frac{1}{E_{11}}(\sigma_{11} - v_1 2\sigma_{22}) \\ \varepsilon_2 2 &= \frac{1}{E_{22}}(\sigma_{11} - v_1 2\sigma_{22}) \\ 2\varepsilon_1 2 &= \frac{1}{G_{12}}\tau_{12} - \alpha\tau_{12}^3 \end{aligned} \tag{2.28}$$

The third equation defines the non-linear shear stress parameter α. This parameter is used in a fibre matrix shearing term $\bar{\tau}$ to predict failure. The fibre matrix shearing term is essentially a ratio of the shear stress to the shear strength and is computed by the following equation:

$$\bar{\tau} = \frac{\frac{\tau_{12}^2}{2G_{12}} + \frac{3}{4}\alpha\tau_{12}^4}{\frac{\tau_{12,f}^2}{2G_{12}} + \frac{3}{4}\alpha\tau_{12,f}^4} \tag{2.29}$$

The $\bar{\tau}$ is used to compute whether one of the three proposed modes of failure is satisfied (i.e. $F > 1$). The three modes of failure are: Matrix cracking $F_{matrix} = \left(\frac{\sigma_{22}^2}{\sigma_{22,f}^2}\right)^2 + \bar{\tau}$, compression failure criteria $F_{comp} = \left(\frac{\sigma_{22}^2}{\sigma_{22,f}^2}\right)^2 + \left[\frac{\sigma_{22,Comp,f}^2}{2\bar{\tau}_{12,f}^2} - 1\right]\frac{\sigma_{22}^2}{2\sigma_{22,Comp,f}} + \bar{\tau}$ and fiber breakage $F_{fibre} = \left(\frac{\sigma_{11}^2}{\sigma_{11,f}^2}\right)^2 + \bar{\tau}$. Depending on the failure mode that is satisfied different elastic constants are set to zero. This material model does not have a progressive failure damage.

The Enhanced Composite Damage Model (ECDM) is an enhanced version of the composite model material type 22. It proposes a tensile and compressive fibre failure mode, and a tensile and compressive matrix failure mode. The matrix failure mode is determined by a Chang-Chang criterion or a Tsai-Wu criterion[171]. Arbitrary orthotropic materials, e.g., unidirectional layers in composite shell structures can be defined. This model is only valid for thin shell elements. The model allows after damage a user defined load carrying capacity by the fibres and them matrix.

Both the models mentioned so far do not allow for progressive degradation of the material properties. Probably the most suitable models provided by LS-DYNA for damage modelling is the Laminated Composite Fabric Model (LMFM) and Laminated Composite Failure Option Model(LCFOM). Compared to the previous models it allows for non linear stress vs. strain response, however in the author's opinion, the quantities do not necessarily correlate to physical quantities/characteristics of the material. The derivation of the properties is independent of physical properties like energy in the material and appears to be more empirical, limiting the application of the models for predictive modelling.

2.6 Summary Of Literature Related To Strain Rate Effects In Composite Materials

The majority of the researchers in the field of strain rate effects on the material properties of composite materials agree on the following points:

- For increasing strain rate the stiffness and strength of the glass fibres increase, contrary to carbon fibres that do not exhibit any strain rate dependency.
- The fracture appearance of composite materials suggests that the fracture surface and failure mechanisms are strain rate dependent.
- The strain rate dependency of a composite material depends on the properties and strain rate dependency of the fibre/matrix interface.
- The longitudinal stiffness and strength of a fibre reinforced composite material are predominantly dominated by the fibre reinforcement.
- The transverse stiffness and strength of polymer composite material systems increase with strain rate. Also, it is noteworthy that the published research literature on the strain rate dependency of transverse properties comparatively to the longitudinal properties is disproportionate, indicating that the issues arising from the weak nature of this class of materials.
- The shear failure strength and stiffness increased with strain rate.
- There has been only one published research work carried out on the damage evolution of thermoset fibrous composite materials based on a damage mechanics framework and with

strain rate dependency. The research work reported that for increasing strain rates the shear behaviour of the composite material appears to be stiffer.

It is noteworthy that a significant majority of the strain rate research work has been undertaken for thermoset system composite materials.

From the review of the testing equipment, the universal testing machine is a configuration suitable for strain rate testing over a few orders of strain rate magnitude. Therefore, it is suitable for characterisation of elasticity, strength and damage evolution properties of a composite material under variable strain rate loading.

Finally, in this author's opinion, the abstract approach of LMFM and LCFOM of LS-DYNA or the Bi-Phase model in PAM-CRASH is suitable for a generic FE material model, however it is limiting the predictive ability to material system configurations that have already been extensively tested. An approach that is developed taking into account on the actual physical processes and quantities (e.g. energy) of the material is more suitable for actual predictive modelling (i.e. the Ladevéze global composite ply model), in the author's opinion.

Chapter 3

Experimental Methods.

Chapter Objectives

- Describe test specimen manufacture.
- Describe the displacement measurement techniques used for testing.
- Present the processing methodology for test data.

3.1 Introduction.

The selection of an efficient testing technique, requires the following considerations:

- Critical stress wave speed.
- Range of strain-rate required.
- Specimen dimensions.
- Accuracy of measuring and deformation loads.
- Filtering of raw data.

The literature suggests that glass fibres have marked strain rate dependence, which is expected to contribute to the strain rate dependence of glass fibre reinforced composite materials.
Tensile tests at different strain rates are conducted to establish the level of strain rate dependence on the following properties of a thermoplastic composite material:

1. Elasticity;
2. Strength;
3. Damage evolution;
4. Strain energy absorption at failure;
5. Coupling factors between transverse and shear (damage and strain).

Characterising the mechanical properties of the thermoplastic composite is based on the global composite ply model proposed by Ladevèze, which is described in the §2.5.4.2. Statistical methods

are implemented to examine the difference of the properties at different strain rates [1] (hypothesis testing) because composite materials exhibit great variation in their properties than other engineering materials.

The *null hypothesis* H_0 is that there is no strain rate sensitivity and that the mechanical properties remain the same. Rejection of the null hypothesis automatically leads to acceptance of the alternative hypothesis H_1, i.e. the mechanical properties are statistically different for increasing strain rates.

3.2 Test Specimen Manufacture

The material is a thermoplastic glass-polypropylene composite laminate material called $Plytron^{TM}$ [172]. The properties of the Plytron can be seen in table 1.3. The material is supplied by Borealis as a 100mm-wide tape (approximately .22[mm] thick, comprising aligned continuous glass fibres in a polypropylene matrix. To manufacture a laminate, the tape is laid-up ply-by-ply into an unconsolidated stack.

The stack is consolidated under pressure and heat using Warwick Manufacturing Group's proprietary membrane-forming process [1]. The process involves the enclosure of the ply stacking sequence between two silicon membranes (each silicon membrane is attached to a rectangular frame - see figure 3.1). A vacuum pump removes the air between the two membranes applying almost one bar pressure. The vacuum former is then placed in the infra-red oven until the temperature reaches 200°(approximately for ten minutes), so that the polypropelene melts. Then the

[1] To achieve an acceptable level of confidence, the high strain rate experiments have to be repeated. However, two or more mechanical properties can be obtained by the same tests, which reduces the overall number of tests.

vacuum former is removed from the oven and is allowed to cool down.

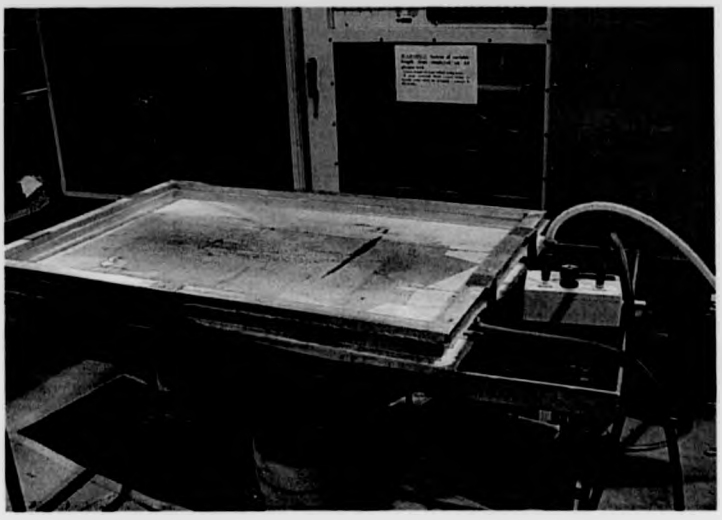

Figure 3.1: Vacuum former configuration.

Because the prepreg tape is supplied fully dense, and the process does not introduce any voids the material is not expected to have any voids. All the test specimens were created personally by the author.

One 4 layer and three 8-layer lay-up sequences were used for the purposes of this study.

The specimens were machined out of the consolidated plaques in accordance with ISO 527-4 revision 1994 specimen Type 1B dimensions[179] (see figure 3.2).

Mechanical test for the global composite model calibration involves the following:

- Uni-directional 4-ply ($[0°]_4$) laminate tested at 0° under monotonic tension loading;
- Uni-directional 8-ply ($[0°]_8$) laminate tested at 45° under cyclic tension loading;
- Laminate $[+45°, -45°]_{2s}$ tested at 0° under cyclic tension loading;

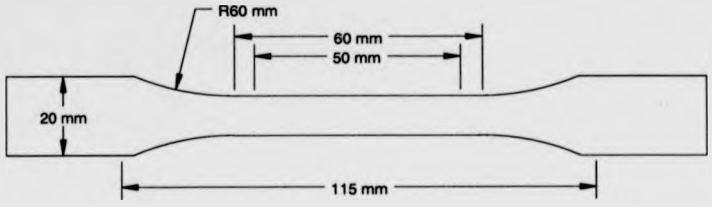

Figure 3.2: ISO-527-4 1994, Type 1B specimen.

- Laminate $[+67.5°, -67.5°]_{2s}$ tested at 0° under cyclic tension loading.

Cyclic loading is carried out in order to quantify the damage evolution. The number of cycles must not exceed five or six, in order to avoid low cycle fatigue phenomena.

The size of the test specimens follows the equivalent test standard unless specifically stated.

3.2.1 Testing Machine

The university of Warwick has an INSTRON 4505 Universal testing machine which has a maximum crosshead displacement rate of $1[\frac{m}{min}]$. On a test specimen with 100[mm] gauge length, testing at full speed would yield a strain rate of $10^{-1}[sec^{-1}]$.

The test work was conducted on an INSTRON 4505 universal testing machine instrumented with a 10 and a 100[kN] load cell. The specimens were loaded uniaxially in tension at three different crosshead displacement rates: 5, 50 and 500[mm/min]. Table 3.1 presents the table with the number of the experiments for each laminate and crosshead displacement rate.

Table 3.1: Table with the number of experiments for each crosshead displacement rate and stacking sequence.

Crosshead Displacement Rate	5	50	500
Laminate Layup	[mm/min]	[mm/min]	[mm/min]
$[0°]_4$	28	33	33
$[\pm 45°]_{2s}$	23	21	20
$[+45°]_4$	18	25	24
$[\pm 67°]_{2s}$	12	11	11

3.3 Displacement Measurement Techniques

The ability to accurately measure deformation and displacement is critical to the testing and characterisation of composite materials. This section reviews the two different techniques that were used to measure deformations to establish local strain in a composite specimen. Strain sensor classification is discussed in ASTM E 83[174].

A number of sensing techniques have evolved to measure displacement:

1. LVDT (Linear Variable Differential Transformer) deflectometers.
2. Contacting extensometers.
3. Optical methods of extensometry.

3.3.1 Linear Variable Differential Transformer (LVDT)

LVDTs are electromagnetic devices designed so that as a ferromagnetic core is displaced within a transformer (consisting of three windings), a linearly varying a.c. voltage and phase shift are

produced, this signal is demodulated to produce a varying d.c. output. LVDTs are available in both linear and angular configurations. LVDTs are available in lengths to 3[m], their output linearity is about 0.1%, and their maximum resolution is 25[μ m]. The accuracy of a given LVDT is commonly limited to 0.01% of total travel.

High temperature LVDTs are generally used with extensions or linkages to avoid exposing them to hostile environments. LVDTs must be calibrated at the temperature to which they will be exposed in use.

3.3.2 Contacting Extensometers

Contacting extensometers and compressometers are devices that are used to determine the relative displacements of two points on a specimen. The initial distance between the two points is referred to as the gauge length. The contact extensometer must be clamped to the specimen surface in such a way that the contact points cannot slip, and that the extensometer does not affect the test. Extensometers are relatively complex devices which rely on integral strain gauges or LVDTs to convert the relative displacements of their attachment points into linearly related outputs.

Extensometers are available in a range of fixed gage lengths from 12 - 50[mm], their output linearity is 0.1%, and they can resolve displacement to 25[μ m]. This resolution does not imply accuracy or calibration. A well-made contact extensometer is accurate to 0.01% of full scale, and can measure strain up to 100%.

Repeatability of contacting extensometers is dependent on their maintaining a constant initial gage length, therefore, when a zero stop is provided it should always be used when attaching the extensometer to a specimen.

The weight and method of attachment of a contacting displacement device can influence both the results obtained and the point of rupture;

3.3.3 Optical Methods Of Extensometry.

A number of strain measurement methods based on optical phenomena, exist:

1. Photo-elasticity.
2. Moiré interferometry.
3. Laser extensometry.
4. Video-extensometry.

Methods 1 and 2 can be used to verify Finite element Analysis results, because they creates strain maps, which can be used to investigate stress distributions on test specimens or structures.

Laser extensometry is a non contact method, which is utilised in the cases of high temperatures, small radii and rough surfaces.

Video extensometry is a non-contact displacement measurement method, which in real time processes a charge coupled device (CCD) camera image. The CCD camera image is digitised and the resulting grey scale values (0-255) of each pixel stored in a frame buffer. Using the buffer data, it is possible to produce a grey scale (contrast) diagram for every horizontal scan line and for every vertical column of pixels. High contrast targets (i.e. black and white self-adhesive strips - see figure 3.3) are attached to the specimen. Both the longitudinal and transverse strains can be determined by the change in distance between the marked targets. The theoretical maximum resolution is

directly related to the field of view (e.g. a 50 [mm] field of view results in a resolution of 0.4 [μm]). The accuracy of the strains is subject to the alignment of the specimen in the grips.

During the testing, it is important that the distance between camera and specimen remains constant and that there are adequate lighting conditions: a change in contrast levels between target and surroundings may confuse the software.

Figure 3.3: Marked Video extensometry specimen.

The sampling frequency is also another issue. The PAL system that the video extensometry employs has a frequency of 25[Hz]. The sampling frequency on the data acquisition equipment cannot exceed half of this frequency (12.5[Hz]). So depending on the system used there is a maximum data-sampling rate.

Another potential problem is the change in shape or position of the targets during the test. This is comparable to slipping for contact extensometers or failure of the adhesive substrate for bondable strain gauges.

3.3.4 Actual Displacement Measurement Configuration

The displacement measurements were obtained using videoextensometry apparatus [177] and a two contacting extensometers. A reference grid consisting of two white self adhered targets is used to monitor the longitudinal extension (d_L) along the direction of the specimen. The videoextensometry also captures the transverse contraction (d_T) during the tensile test. The gauge length

between the videoextensometry targets approximately is 10[mm], and for the contacting extensometers it is 50[mm]. The location of the failure is categorised according to the partition of a dogbone specimen in figure 3.4 [2].

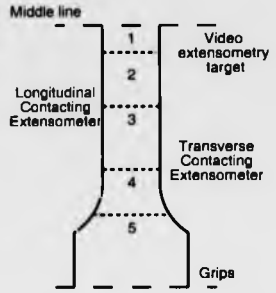

Figure 3.4: Failure location partitions for the ASTM dogbone.

3.4 Results processing

Once the raw test data for each test were obtained, the following procedure was followed to compute the characterisation properties.

3.4.1 Monotonic Tensile Test On $[0]_4$ Ply Stack

Using the transformation equations A.7 and A.8 yield the following for this test:

$$\begin{bmatrix} \sigma_{11} \\ \sigma_{22} \\ \tau_{12} \end{bmatrix} = \begin{bmatrix} \sigma_L \\ 0 \\ 0 \end{bmatrix} \quad and \quad \begin{bmatrix} \epsilon_{11} \\ \epsilon_{22} \\ \gamma_{12} \end{bmatrix} = \begin{bmatrix} \epsilon_L \\ \epsilon_T \\ 0 \end{bmatrix}$$

[2]The failure location did not apply to the unidirectional specimens

This test allows to obtain:

- The tensile initial Young's modulus in the direction of the fibers $E^f_{t,11}$;

$$E^f_{t,11} = \frac{\sigma_L}{\epsilon_L}$$

- The Poisson's ratio in plane (1,2) ν^0_{12};

$$\nu^0_{12} = -\frac{\epsilon_T}{\epsilon_L}$$

The flowchart in figure 3.5 presents the relation between the different quantities in a graphical manner.

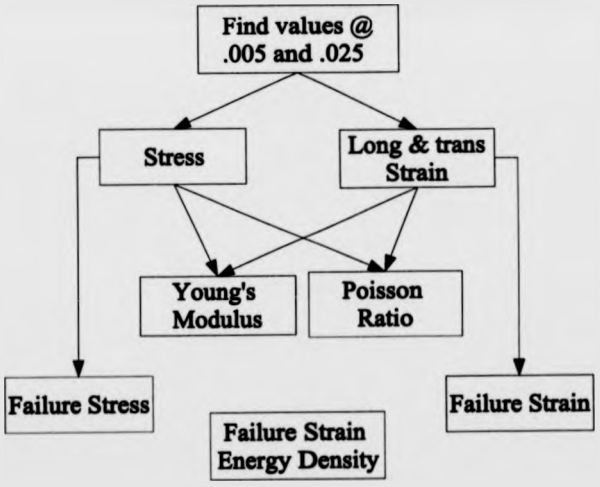

Figure 3.5: Flowchart of the calculation dependencies of the procedure to obtain the Ladevèze parameters from the $[0°]_4$ laminate specimens.

3.4.2 Tensile Test On $[\pm 45]_{2s}$ Ply Stack

Using the transformation equations A.7 and A.8 yield the following for this test:

$$\begin{bmatrix} \sigma_{11} \\ \sigma_{22} \\ \tau_{12} \end{bmatrix} = \begin{bmatrix} 0 \\ 0 \\ \sigma_L/2 \end{bmatrix} \quad and \quad \begin{bmatrix} \epsilon_{11} \\ \epsilon_{22} \\ \gamma_{12} \end{bmatrix} = \begin{bmatrix} 0 \\ 0 \\ \epsilon_L - \epsilon_T \end{bmatrix}$$

For elastic damaging behaviour, this test allows to obtain:

- the shear modulus in plane (1,2), $G_{12,0}$;
- the critical shear damage limit, Y_c;
- the initial shear damage limit, Y_0^*;
- the elementary shear damage fracture limit, Y_R.

For each load/unload cycle i, a value of Y_i is obtained, which is used in the estimation of the shear damage evolution law using the following equations:

$$\left.\begin{aligned} d_i &= 1 - \frac{G_{12,i}}{G_{12,0}} \\ Y_i &= \sqrt{\tfrac{1}{2} G_{12,0} \gamma_{12,i}^e} \end{aligned}\right\} \quad Y_i = Y_c d_i + Y_0 \tag{3.1}$$

The resulting system of non linear equations is solved and the values for $G_{12,0}$, Y_c, Y_0^* and Y_R are obtained. The elementary shear damage fracture limit Y_R is taken as the maximum of the shear damage limit values Y_i. The material constants G_{12}, $\gamma_{12,fail}$ and $\tau_{12,fail}$ are then obtained by the curve of shear stress vs. shear strain on the material coordinate system ($\tau_{12} = f(\gamma_{12})$).

The flowchart in figure 3.6 present the relation between the different quantities in a graphical manner - the quantities in bold represent the characterisation parameters that will be considered.

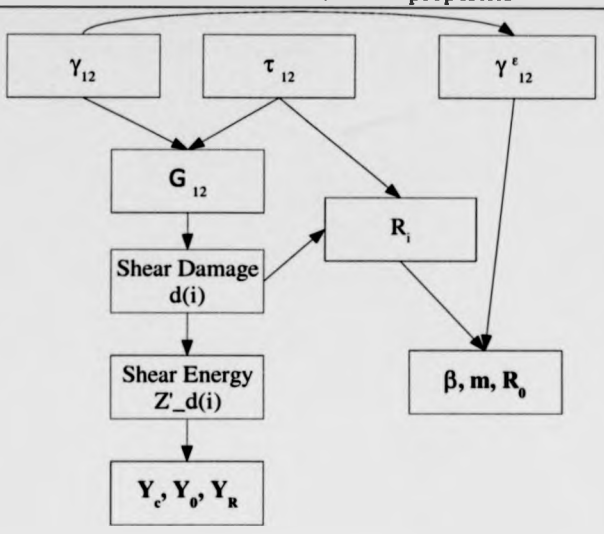

Figure 3.6: Flowchart of the calculation dependencies of the procedure to obtain the Ladevéze parameters from the $[\pm 45°]_{2s}$ laminate specimens.

3.4.3 Tensile Test On $[+45]_8$ Ply Stack

Using the transformation equations A.7 and A.8 yield the following for this test:

$$\begin{bmatrix} \sigma_{11} \\ \sigma_{22} \\ \tau_{12} \end{bmatrix} = \begin{bmatrix} 0 \\ \sigma_L/2 \\ \sigma_L/2 \end{bmatrix} \quad \textit{and} \quad \begin{bmatrix} \epsilon_{11} \\ \epsilon_{22} \\ \gamma_{12} \end{bmatrix} = \begin{bmatrix} 0 \\ \epsilon_L + \epsilon_T \\ \epsilon_L - \epsilon_T \end{bmatrix}$$

This test allows to obtain:

- The coupling factor between transverse and the shear plastic strains, A^2.
- The transverse elastic modulus, E_{22}.

For each load/unload cycle i, a values of A^2 is obtained:

$$A^2 = \frac{(\epsilon^p_{22,i} - \epsilon^p_{22,i-1})(1 - d'_i)^2}{(\gamma^p_{12,i} - \gamma^p_{12,i-1})(1 - d_i)^2} \tag{3.2}$$

The flowchart in figure figure 3.7 present the relation between the different quantities in a graphical manner.

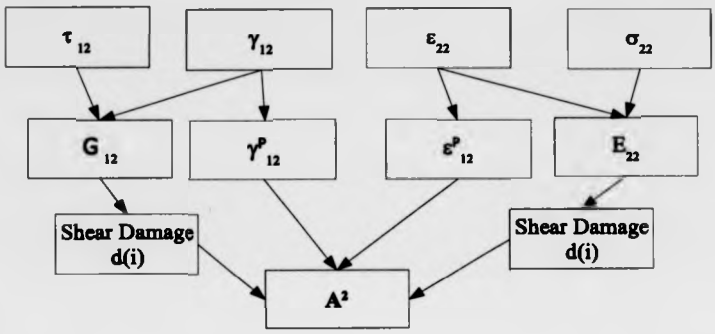

Figure 3.7: Flowchart of the calculation dependencies of the procedure to obtain the Ladevéze parameters from the $[+45°]_8$ laminate specimens.

3.4.4 Tensile Test On $[\pm 67.5]_{2s}$ Ply Stack

This test needed to be carried out last, because the following quantities are required for the calculations: $E_{11,0}$, $E_{22,0}$, $\nu_{12,0}$ and $G_{12,0}$. The strain rate models from the previous tests are used to interpolate (or extrapolate) for the values of the elasticity parameters.

The transformation equations A.7 and A.8 are used to convert the experimental results (obtained on the global frame referencing system) to a coordinate system suitable for the analysis (on the

local frame referencing system). The transformation yields the following:

$$\begin{bmatrix} \sigma_{11} \\ \sigma_{22} \\ \tau_{12} \end{bmatrix} = \begin{bmatrix} S_1 \\ S_2 \\ S_3 \end{bmatrix} \sigma_L \qquad and \qquad \begin{bmatrix} \epsilon_{11} \\ \epsilon_{22} \\ \gamma_{12} \end{bmatrix} = Q_1 \begin{bmatrix} \epsilon_L \\ \epsilon_T \\ 0 \end{bmatrix}$$

For elastic damaging behaviour, the $[\pm 67.5°]_{2s}$ test yield the following characterisation parameters:

- the critical transverse damage limit, Y_c'.
- the initial transverse damage limit, Y_0'
- the brittle transverse damage limit for the fiber-matrix interface, Y_S'.
- the coupling factor between transverse and shear damage, b.

For each load/unload cycle i, the following computations are performed:

$$\left.\begin{aligned} d_i &= 1 - \tfrac{G_{12,i}}{G_{12,0}} \\ d_i' &= 1 - \tfrac{E_{22,i}}{E_{22,0}} \end{aligned}\right\} \Rightarrow \begin{aligned} Z_{d,i}' &= \tfrac{1}{2} G_{12,0} (\gamma_{12,i}^e)^2 \\ Z_{d,i} &= \tfrac{1}{2} E_{22,0} (\nu_{12,0} \epsilon_{11,i}^e + \epsilon_{22,i}^e)^2 \end{aligned} \tag{3.3}$$

Z_d and Z_d' quantities are only introduced for the convenience of the computation and essentially they represent the pure shear and transverse energy.

Once the Z_d and Z_d' values for each cycle are obtained, the coupling factor between transverse and shear damage is estimated using:

$$b_i = \frac{(Y_c d_i + Y_0)^2 - Z_{d,i}}{Z_{d,i}'} \tag{3.4}$$

Once the b value for each cycle is obtained, a set of equations is formed using the following equation:

$$Y'_c d'_i + Y'_0 = \sqrt{Z_{d,i} + b_i Z'_{d,i}} \tag{3.5}$$

The solution of the above non linear system, will provide the values of Y'_c and Y'_0 and b. Because there are five cycles, therefore five equations may be derived, it is possible to calculate different values depending on the set of equation that are used to constrain the solution.

The brittle transverse damage limit for the fiber-matrix interface, Y'_S is taken as the maximum of the Z'_d values.

The flowchart in figure figure 3.8 present the relation between the different quantities in a graphical manner.

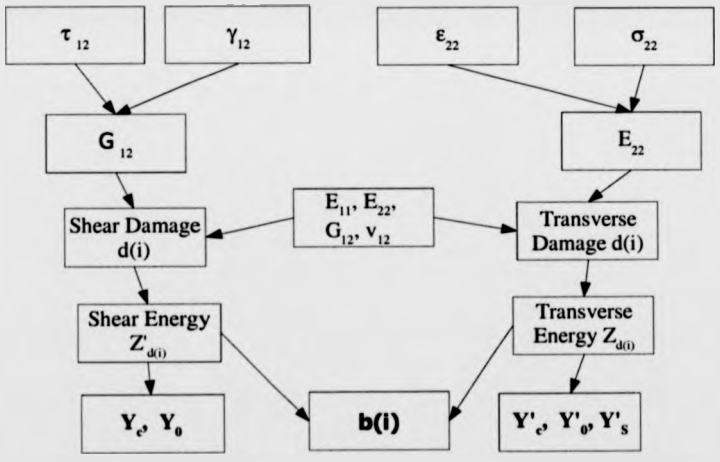

Figure 3.8: Flowchart of the calculation dependencies of the procedure to obtain the Ladevéze parameters from the $[\pm 67°]_{2s}$ laminate specimens.

3.5 Statistical Processing.

In this section, the implementation of the above prove procedure will be explained.

Automation of data processing will be implemented through computer program taking the from of scripts. The Matlab environment was selected as the most appropriate software. The experimental data will be processed using a Matlab scripts which are presented in Appendix C.1.1. Two versions of the computer code have been generated to serve the two different displacement measuring methods (i.e. Instron contacting extensometer and Video-extensometry).

The flowchart for the Instron raw data preprocessing is presented in figure 3.9 and for the videox-tensometry raw data the equivalent flowchart is presented in figure 3.10.

A lowpass digital signal filter will be applied to remove the inherent noise of dynamic experimental testing. The filtered data was compared to the unfiltered experimental dynamic values to establish a suitable filter. The filtered results are used to obtain the characterisation properties which are used in the statistical analysis.

The filtering methodology is generic for all experimental results and is presented in the flowchart in figure 3.11. The load data is used to determine the start and termination of each experiment (less noise in the load channel compared to displacement channel).

An appropriate filter is applied to all the longitudinal and transverse displacement channels before they are converted to stains on the material axes.

3.5.1 Statistical Processing Of The Results.

The experimental results will be processed using the methodology which is presented in figure 3.12, to determine the strain rate sensitivity of the material and derive a semi empirical strain

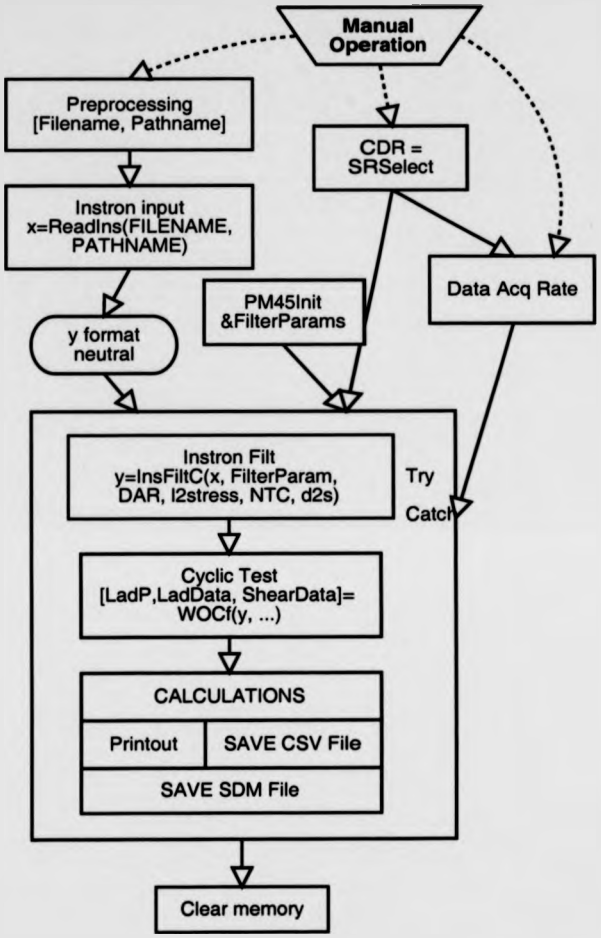

Figure 3.9: Instron raw data processing methodology flowchart.

rate model.

The processing of the results commences with the calculation of the statistics for the different crosshead displacement rates. Routines have been added for the removal of the observations which are identified as being outliers. The calculated statistic values are: the average, the standard

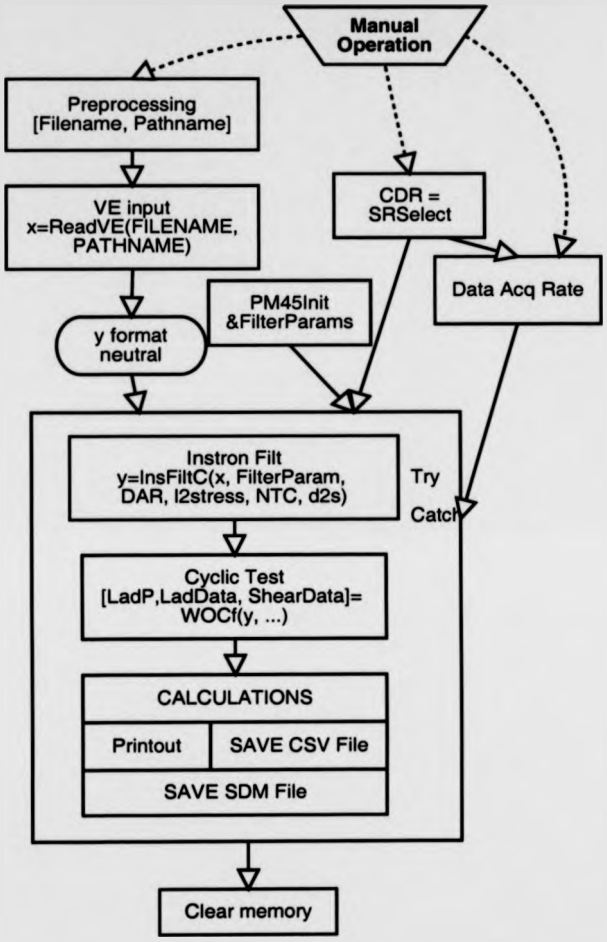

Figure 3.10: Instron raw data processing methodology flowchart.

deviation of the sample set of observations and the coefficient of variance.

The second step is to check whether the average of the properties is statistically different for the different material properties. In order to ascertain this, a test of equality of two means with unknown variance will be used (*t-test*). The procedure of the *t-test* is described in [170, sec.11-

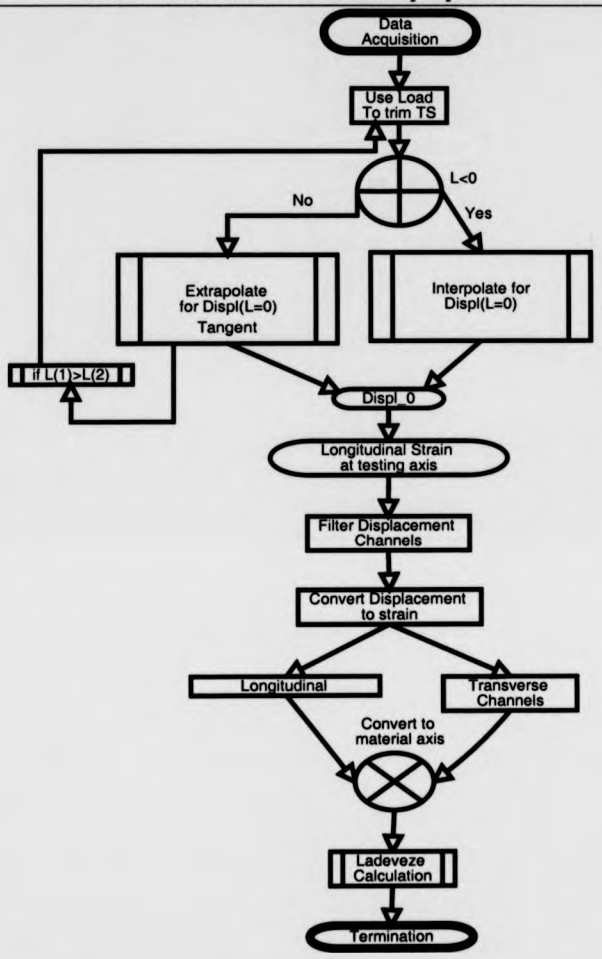

Figure 3.11: Filtering methodology flowchart.

5.2, p10]. The null hypothesis H_0 is that there is no strain rate sensitivity. Rejection of the null hypothesis (from a statistical point of view) is equivalent to the following statement: "there is a strong indication that there is strain rate dependence of the examined mechanical property". If the test indicates that at least one compared pair of averages of the mechanical properties is different

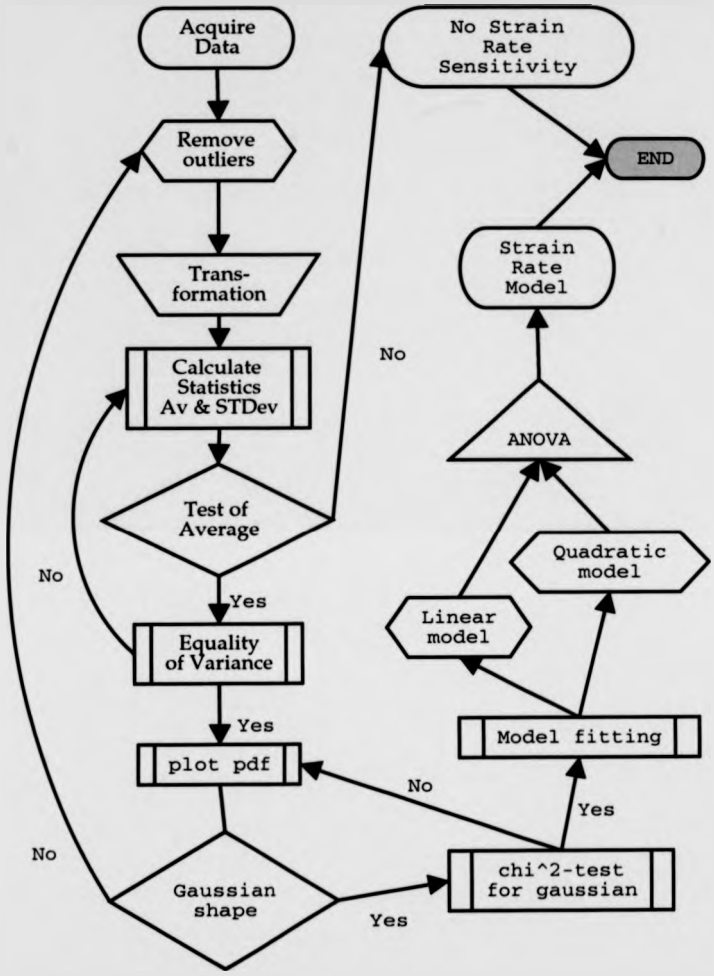

Figure 3.12: Analysis of results methodology.

(i.e. the property under investigation is statistically different at different strain rate levels) then the estimation of a semi empirical material model can follow.

The distribution of the mechanical properties at different levels of crosshead displacement rate is

examined, before proceeding to the development of a semi-empirical strain rate model, because normal distribution is a fundamental assumption for regression analysis. *Probability density (p.d.f.)* plots of the mechanical properties are plotted. A normal distribution plot for each of the different crosshead rates is expected. A χ^2-*test* [170, sec.11-11] is used to quantify the Goodness-Of-Fit of the distribution of the acquired response values at each level of crosshead displacement rate.

Regression analysis will be used for the development of the semi empirical strain rate material model. The regressor variable is the logarithm with base 10 of the strain rate and the response variable is the mechanical property under investigation (in some cases an appropriate transformation might be required for the mechanical property under investigation). A linear and a quadratic model with respect to the logarithm of the strain rate will be fitted. ANalysis Of VAriance (ANOVA 5% α type error) was used to select which is the appropriate order for the strain model (which model describes the variability of the measured data adequately).

The appropriate transformations for each of the response variables (i.e. mechanical properties) are enforced by the constraints/assumptions of regression analysis. In order to decide on the appropriate transformation, the above process has to be iterated one or more times and certain tests had to be carried out (plot of residuals vs. response and regressor variable etc).

Chapter 4

Experimental Results

Chapter Objectives

- Presentation of the experimental results for mechanical testing of composites using contacting extensometers.
- Presentation of the experimental results for mechanical testing of composites using videoextensometry.

4.1 Strain Measurement Using Contacting Extensometry

4.1.1 Tensile Results For $[0°]_4$ Laminate.

The suggested eight layered composite laminate was discarded in favour of the four layer composite laminate, because the eight layer specimen tensile loads exceeded the gripping load of the test machine(i.e. low coefficient of friction even with the use of sandpaper). Figure 4.1 presents typical failed four-layered specimens at different strain rates.

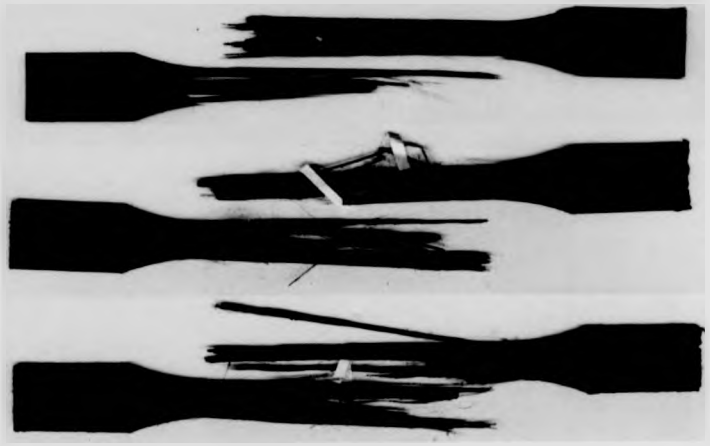

Figure 4.1: Typical failed unidirectional specimens at different strain rates - 5(top), 50(middle) and 500(bottom)[mm/min] crosshead displacement rate.

Figure 4.2 compares typical curves for the stress vs. the longitudinal and transverse strain for a $[0°]_4$ laminate at 5, 50 and 500 [mm/min] crosshead displacement rates, as obtained from the contacting extensometer.

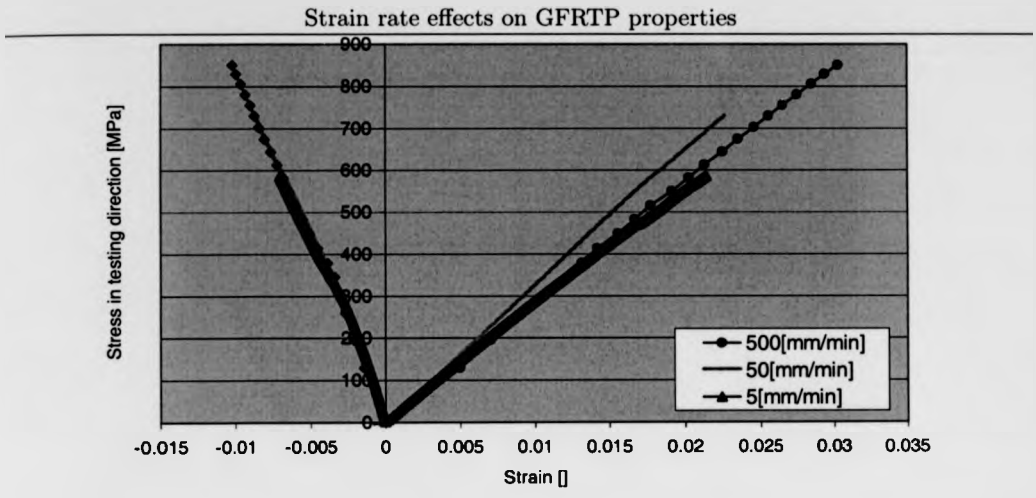

Figure 4.2: Comparison of representative stress vs. longitudinal and transverse strain curves of $[0°]_4$ laminated specimens at 5, 50 and 500 [mm/min] crosshead displacement rates as obtained using the Contacting Extensometers. The longitudinal strain (along the testing direction) are positive, whilst transverse strains are negative.

4.1.2 Tensile Results For $[\pm 45°]_{2s}$ Laminate.

Figure 4.3 present typical failed $[\pm 45]_{2s}$ laminate specimens at different crosshead displacement rates. Also in the same figure a magnification of fracture surface of the tested laminate specimen at 5[mm/min].

Figure 4.4 compares typical curve for the stress vs. the longitudinal and transverse strain for $[\pm 45]_{2s}$ Plytron laminate specimens at 5, 50 and 500 [mm/min] crosshead displacement rate, as obtained from the contacting extensometers.

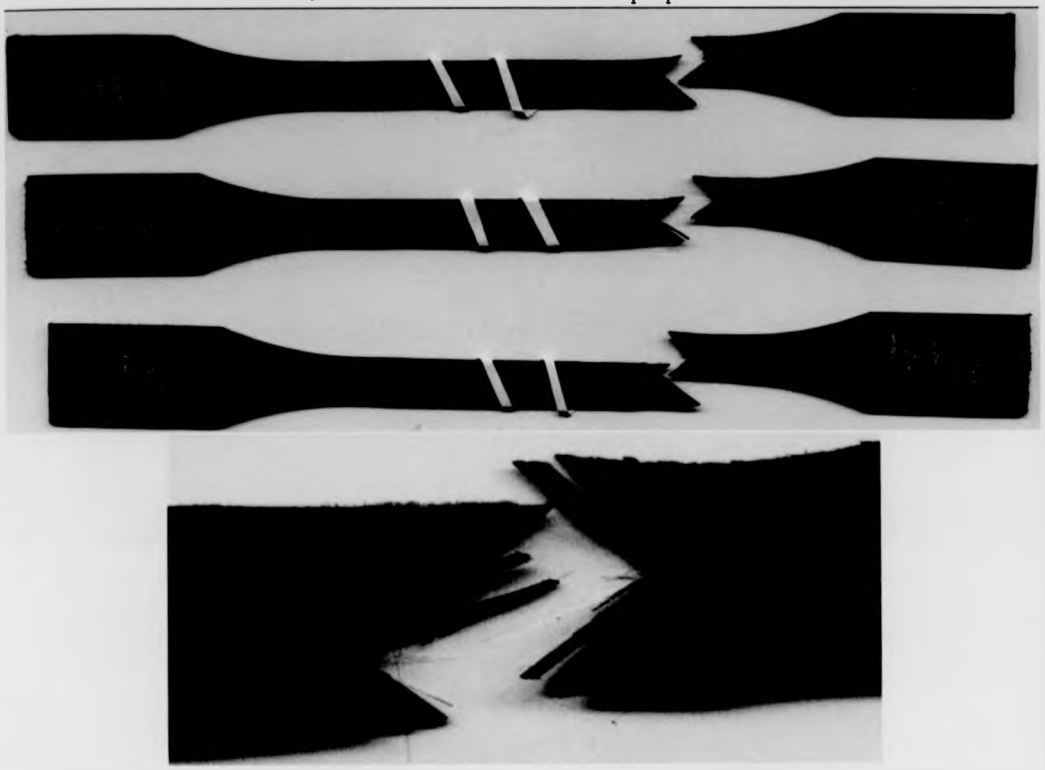

Figure 4.3: Failed $[\pm 45°]_{2s}$test specimen and magnification of the failure surface.

4.1.3 Tensile Results For $[+45°]_8$ Laminate.

Figure 4.5 presents the typical failure of $[+45°]_8$ uniaxially loaded dogbone specimens at different crosshead displacement rates. A magnification of a 5[mm/min] crosshead displacement rate failed specimen at the location of failure is also presented. The failure is in the form of a crack which propagates 45° along the direction of the fibers. Therefore, the failure is dominated by the matrix properties (transverse properties of the unidirectional ply).

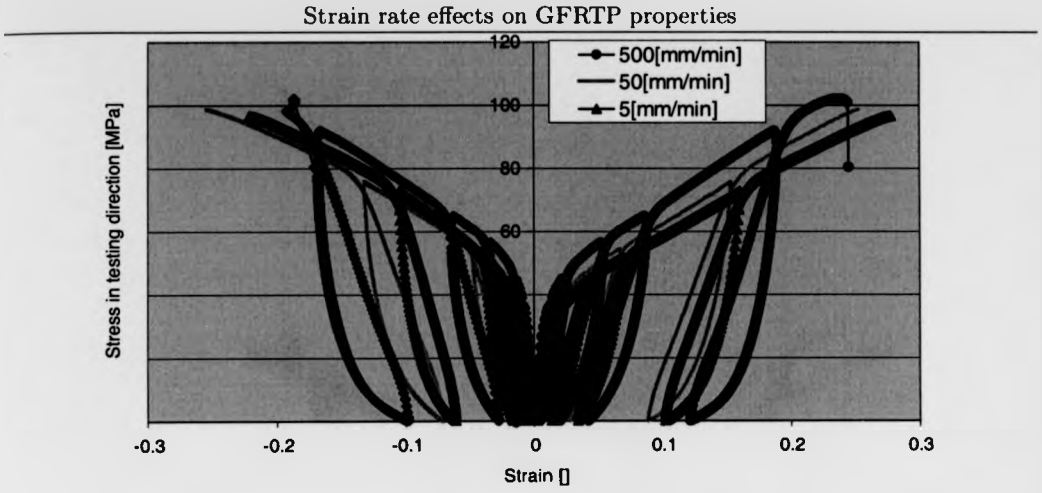

Figure 4.4: Comparison of representative stress vs. longitudinal and transverse strain curves of $[\pm 45°]_{2s}$ laminated specimens at 5, 50 and 500[mm/min] crosshead displacement rates as obtained using the Contacting Extensometers.

Figure 4.6 compares typical curve for the stress vs. the longitudinal and transverse strain for $[+45]_8$ Plytron laminate specimens at 5, 50 and 500 [mm/min] crosshead displacement rates, as obtained from the contacting extensometers.

4.1.4 Tensile Results For $[\pm 67.5°]_{2s}$ Laminate.

Figure 4.7 presents the typical failure of $[\pm 67.5°]_{2s}$ uniaxially loaded dogbone specimen at different crosshead displacement rates. Also a magnification of the failed specimen at 5[mm/min] crosshead displacement rate is presented. The specimen failed by crack propagation along the fibres on each ply level. Delamination between the layers is associated with this type of failure. The specimen has delaminated and gradual failure of each ply led to final failure of the laminate. The failure

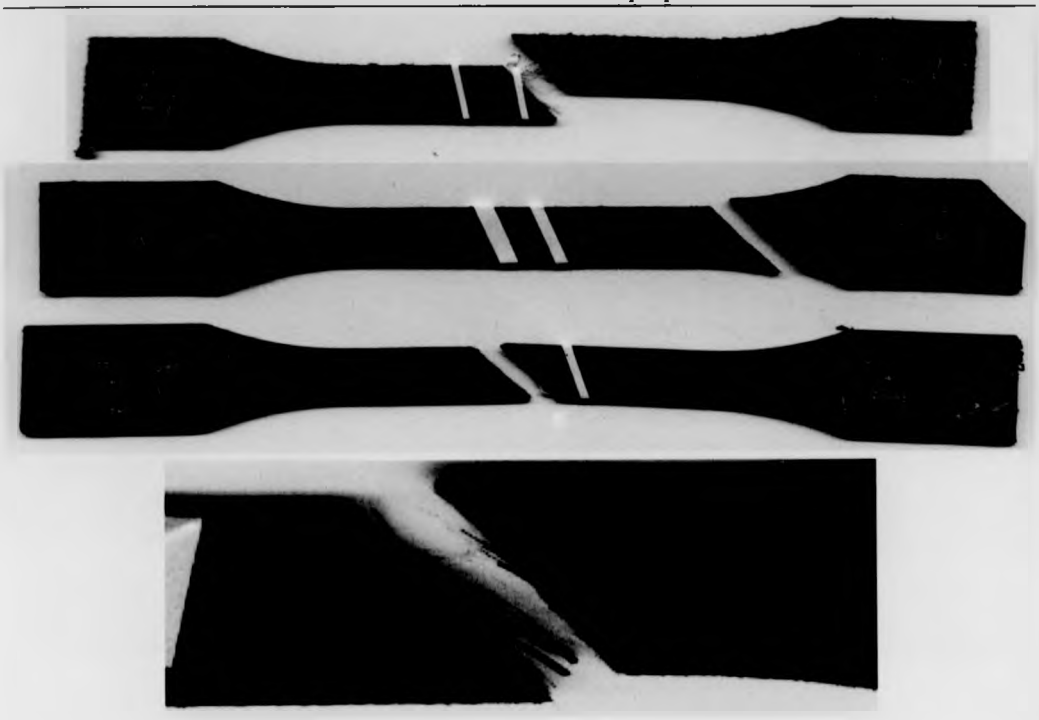

Figure 4.5: Typical failure of a $[+45°]_8$ uniaxially loaded dogbone specimen.

was a gradual process where the matrix phase of the material failed gradually.

Figure 4.8 compares typical curve for the stress vs. the longitudinal and transverse strain for $[\pm 67.5]_{2s}$ laminate specimens at 5, 50 and 500 [mm/min] crosshead displacement rates, as obtained from the contacting extensometers.

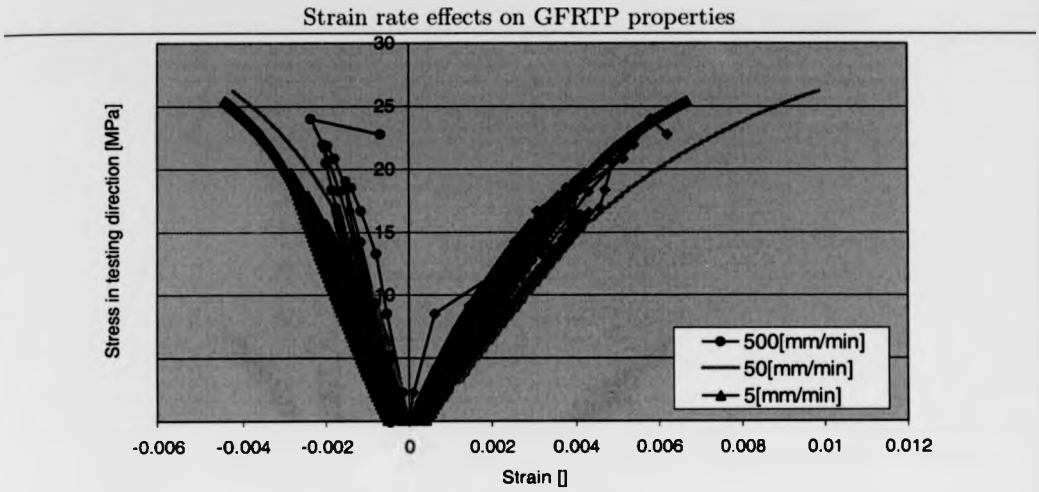

Figure 4.6: Comparison of representative stress vs. longitudinal and transverse strain curves of $[+45]_8$ at 5, 50 and 500 [mm/min] crosshead displacement rates as obtained using the Contacting Extensometers.

4.2 Strain Measurement Using Video Extensometry

4.2.1 Tensile Results For $[0°]_4$ Laminate.

Figure 4.9 compares typical curves for the stress vs. the longitudinal and transverse strain for a $[0°]_4$ laminate at 5, 50 and 500 [mm/min] crosshead displacement rates, as obtained from the videoextensometry apparatus.

Comparison of the results in figures 4.2 the specimens exhibit linear elastic brittle behaviour. The only exception is at the 500[mm/min] crosshead displacement rate for the video extensometry results for the $[0°]_4$. In this case the material exhibits non linear behaviour. For the longitudinal strain (positive strains), the initial stiffness (up to .005 units of strain) appear to be lower than in

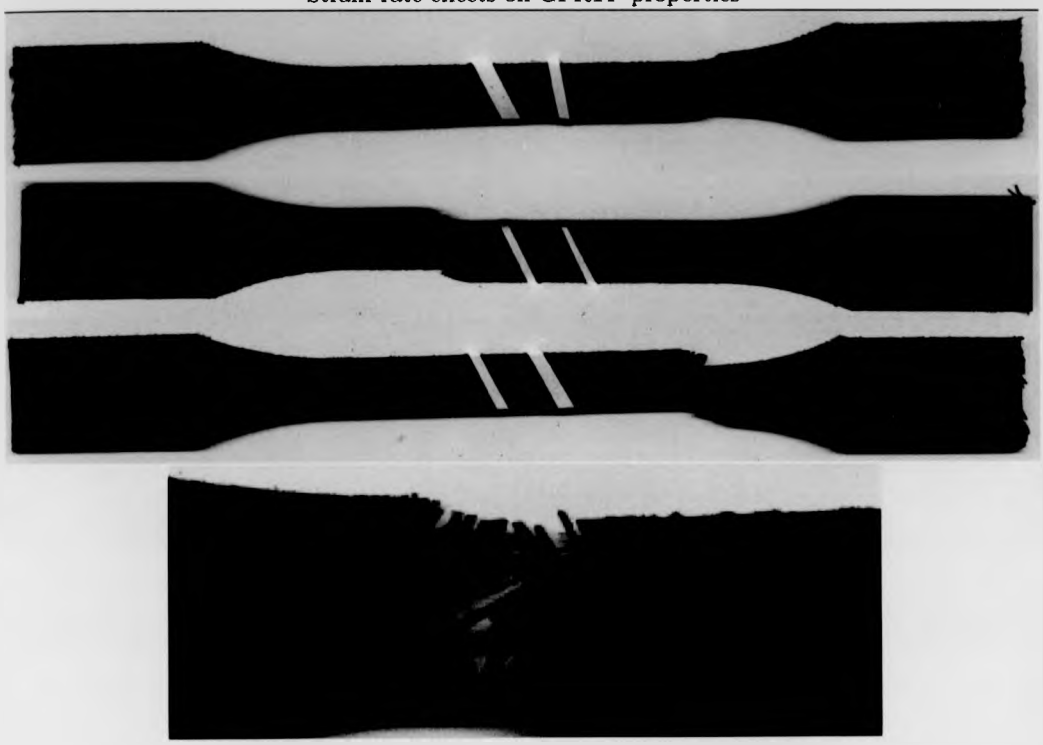

Figure 4.7: Typical failure of a $[\pm 67.5°]_{2s}$ uniaxially loaded dogbone specimen.

the other crosshead displacement rates. However, between .005 and .01 units of strain the specimen appears to be significantly stiffer.

4.2.2 Tensile Results For $[\pm 45°]_{2s}$ Laminate.

Figure 4.10 compares typical curves for the stress vs. the longitudinal and transverse strain for a $[\pm 45°]_{2s}$ laminate at 5, 50 and 500 [mm/min] crosshead displacement rates, as obtained from the videoextensometry apparatus.

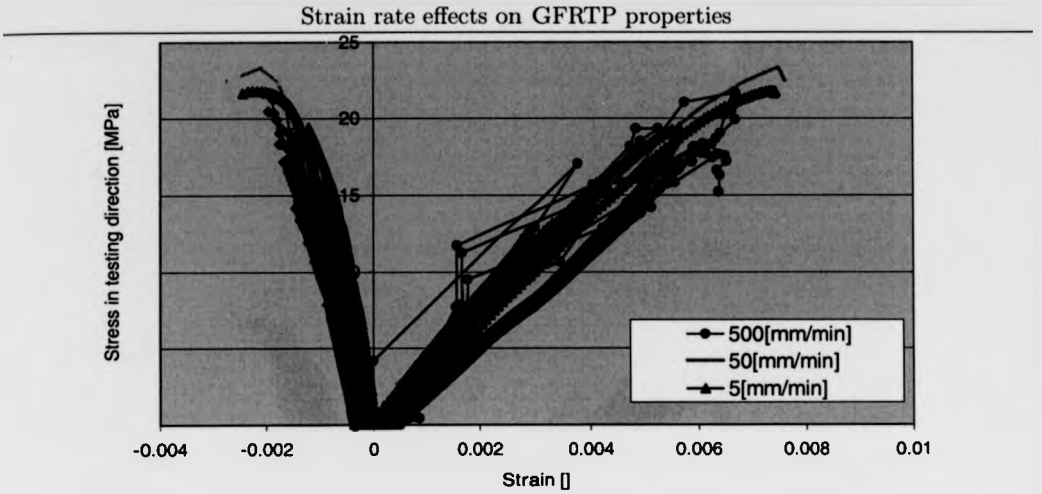

Figure 4.8: Comparison of representative stress vs. longitudinal and transverse strain curves at 5, 50 and 500 [mm/min]crosshead displacement rates as obtained using the contacting extensometers.

Comparison of the results in figures 4.4 and 4.10 does not reveal any marked difference in behaviour between the different displacement data acquisition methods.

4.2.3 Tensile Results For $[+45°]_8$ Laminate.

Figure 4.11 compares typical curves for the stress vs. the longitudinal and transverse strain for a $[+45°]_8$ laminate at 5, 50 and 500 [mm/min] crosshead displacement rates, as obtained from the videoextensometry apparatus.

Comparison of the results in figures 4.6 and 4.11 reveal that there is marked difference in the recorder results for different displacement data acquisition methods. Contrary to the contacting extensometer results which appear to be without any noise, the videoextensometry results appear to be heavily influenced by strain rate. Similar trends were observed for the other $[+45°]_8$ spec-

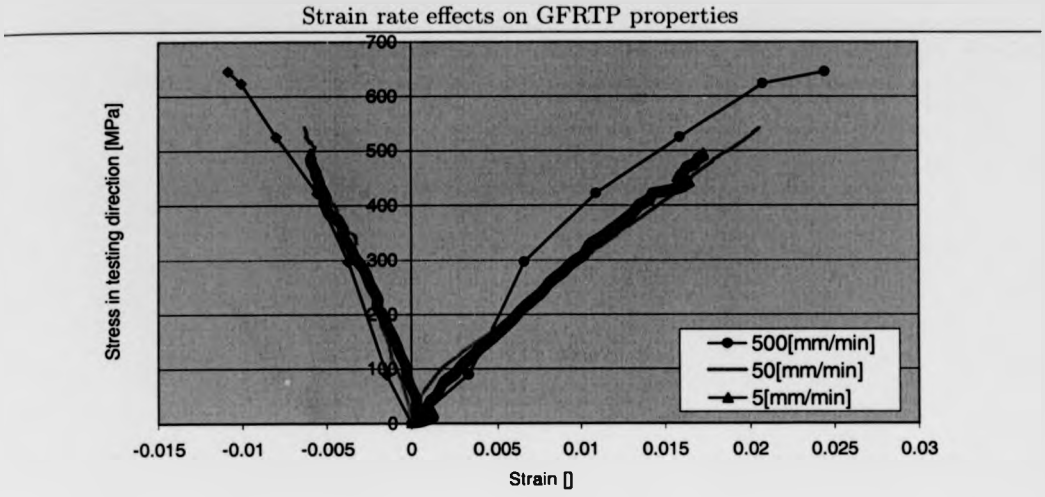

Figure 4.9: Comparison of representative stress vs. longitudinal and transverse strain curves of $[0°]_4$ laminated specimens at 5, 50 and 500 [mm/min] crosshead displacement rates as obtained from videoextensometry apparatus.

imens. The effect is attributed to the small displacements which cannot be measured accurately with the videoextensometry apparatus.

4.2.4 Tensile Results For $[\pm 67.5°]_{2s}$ Laminate.

Figure 4.12 compares typical curves for the stress vs. the longitudinal and transverse strain for a $[\pm 67.5°]_{2s}$ laminate at 5, 50 and 500 [mm/min] crosshead displacement rates, as obtained from the videoextensometry apparatus.

Comparison of the results in figures 4.8 and 4.12 reveal that there is marked difference in the recorder results for different displacement data acquisition methods, similar to that observed for the $[\pm 67.5°]_{2s}$ specimens. This is a corollary to the postulate that the videoextensometry apparatus

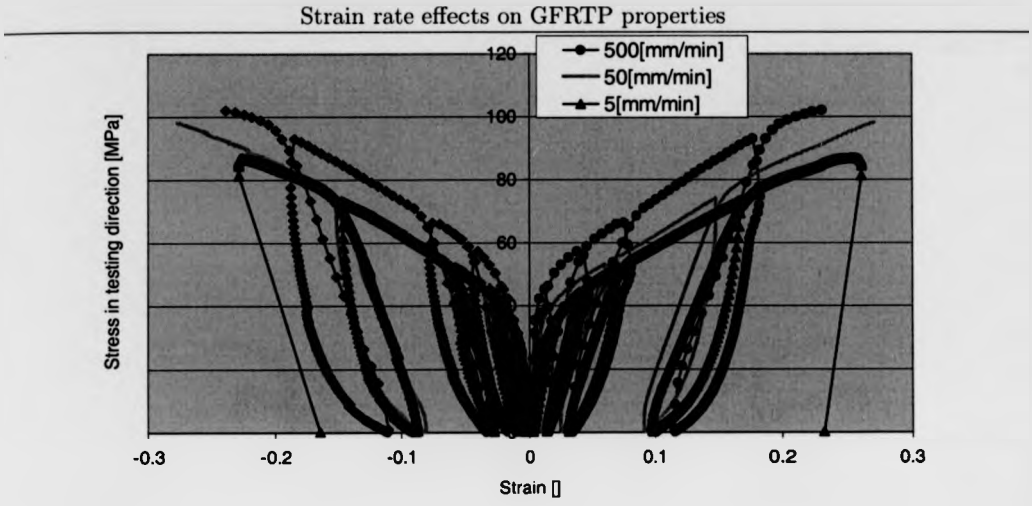

Figure 4.10: Comparison of representative stress vs. longitudinal and transverse strain curves of $[\pm 45^\circ]_{2s}$ laminated specimens at 5, 50 and 500 [mm/min] crosshead displacement rates as obtained from videoextensometry apparatus.

cannot be used to obtain strain measurements lower than .01 units of strain under high strain rates.

4.2.5 Displacement Measurement Comparison.

The two methods of data acquisition will be discussed only for the longitudinal tensile modulus (E_{11}) quantity. However, similar observations could be made for other quantities.

Figure 4.13 presents a conditional plot for the two methods of data acquisition (e.g. contacting extensometry and video extensometry). The longitudinal tensile modulus along direction 11 vs. the logarithm of the strain rate with respect to the method of data acquisition. The video extensometry apparatus is referred by the abbreviation VE, while for the contacting extensometry data

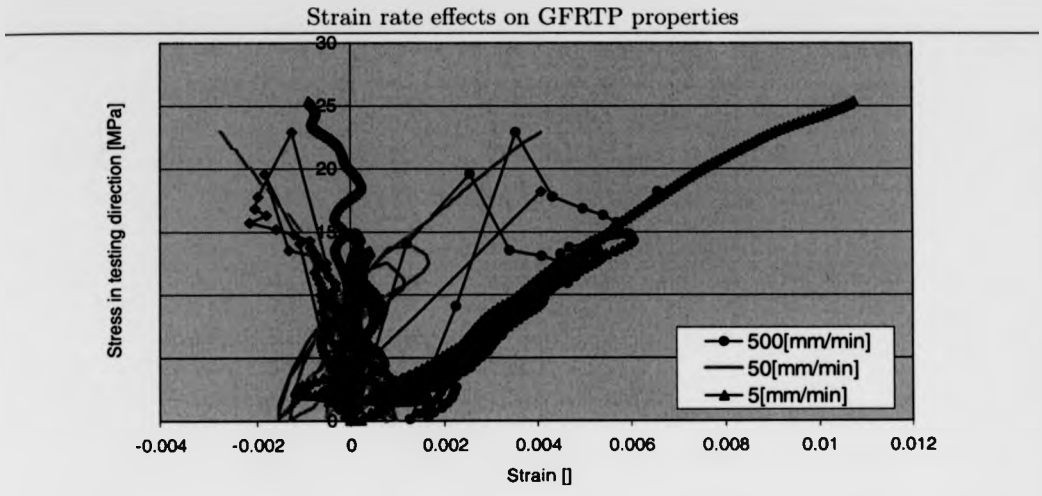

Figure 4.11: Comparison of representative stress vs. longitudinal and transverse strain curves of $[+45°]_8$ laminated specimens at 5, 50 and 500 [mm/min] crosshead displacement rates as obtained from videoextensometry apparatus.

acquisition method the abbreviation Ins is used[1]. The circles, triangles and crosses in the figure 4.13 represent respectively tests at 5, 50 and 500[mm/min] crosshead displacement rates.

It is observed from figure 4.13, that there is no discernable difference in the location (i.e. centre of the cloud) of the 5 and 50[mm/min] crosshead displacement rates (there is difference as far as scatter is concerned), however for the 500[mm/min] crosshead displacement rate a discrepancy between VE and Ins in the location is found.

Contrary to the location, the scatter (i.e. spread and size of the data points cloud) appears to be affected by the data acquisition method at all crosshead displacement rates. The video extensometry results (VE) appear to be significantly less concentrated (i.e. more scatter). This observation is attributed to the scale effects.

[1]The abbreviation is used because the contacting extensometer is supplied as part of the INSTRON machine.

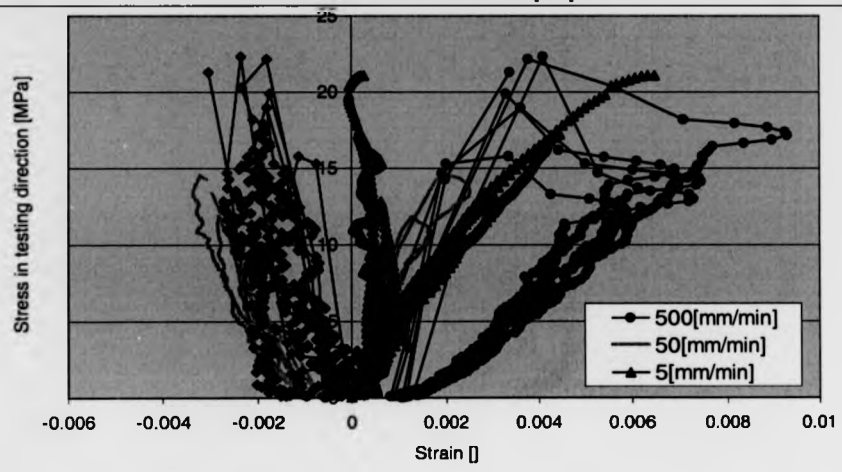

Figure 4.12: Comparison of representative stress vs. longitudinal and transverse strain curves of $[\pm 67.5°]_{2s}$ laminated specimens at 5, 50 and 500 [mm/min] crosshead displacement rates as obtained from videoextensometry apparatus.

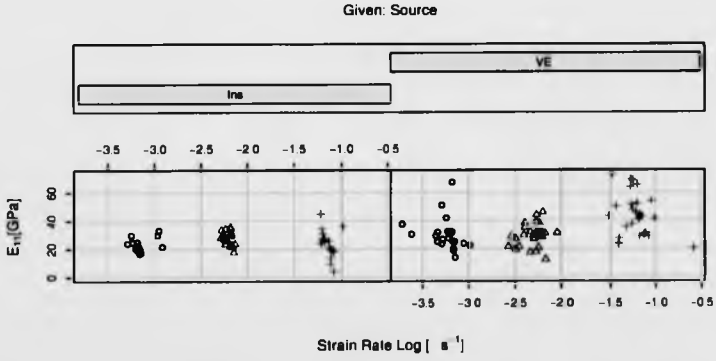

Figure 4.13: Unidirectional Plytron tensile longitudinal Young's Modulus vs. logarithm of strain rate.

Also, the difference in scatter between the two data acquisition methods appears to decrease and then increase for increasing strain rate. The videoextensometer at the 500[mm/min] crosshead displacement rate is capable of capturing only 4-5 points during the entire test of 0° laminate. In some cases, results must be discarded because of the low data resolution and especially for the cyclic testing of +45° and ±67.5° laminates which fail at comparatively low strains.

4.2.6 Equality Of Means Testing

The null hypothesis (H_0) is that the computed longitudinal tensile modulus (E_{11}) from the two methods of data acquisition is not statistically different. Therefore, the mean (which is associated with the location of the cloud of data points) of the longitudinal tensile modulus for each method of data acquisition is equal, e.g. $H_0 : \overline{E}_{11,VE} = \overline{E}_{11,Ins}$. The alternative hypothesis is that the longitudinal tensile modulus (E_{11}) is dependent on the method of data acquisition $H_1 : \overline{E}_{11,VE} \neq \overline{E}_{11,Ins}$.

The statistics for the equality of means test are presented in table 4.1. The table presents the calculated test statistic t_0, α-type error probability, degrees of freedom df and the calculated critical value t_{crit}. Finally, the level of confidence is presented (i.e. the value of α-type error probability for which the calcuated critical value (t_{crit}) is equal to the statistic (t_0)).

Table 4.1: Hypothesis testing statistics for the equality of means of longitudinal Young's modulus.

VE vs. Ins	t_0	α	df	t_{crit}	Level
5	2.834	0.05	29	1.699	0.996
50	0.73	0.05	44	1.68	0.765
500	5.73	0.05	43	1.68	1

The critical test statistic t_{crit} is calculated using the degrees of freedom and the α-type probability from the relevant statistic tables. The test statistic is calculated based on the standard deviation of the sample and the mean of both samples. The null hypothesis, is rejected if the test statistic is greater than the critical statistic $t_0 > t_{crit}$. The information is summarised under the Level value. If the Level value is higher than .95[2] then the null hypothesis should be rejected.

The longitudinal tensile modulus computed by Video extensometer at 5[mm/min] and 500[mm/min] crosshead displacement rate is statistically different to the longitudinal tensile modulus computed by the Instron contacting extensometry data acquisition method at respective crosshead displacement rates at a 5% α-type error. There is strong indication that the measured longitudinal tensile modulus of unidirectional Plytron *is* dependent on the data acquisition method.

4.2.7 Equality Of Variances

The statistics for the equality of variances test are presented in table 4.2. The table presents the calculated test statistic F_0, the α-type error probability, the degrees of freedom $df1$ and $df2$ and the calculated critical value F_{crit}. In the last column, the level of confidence is presented (i.e. the value of α-type error probability for which the calculated critical value (F_{crit}) is equal to the statistic (F_0)).

The critical test statistic F_{crit} is calculated using the degrees of freedom from both samples and the α-type error probability from the relevant statistic tables. The test statistic F_0 is calculated based on the standard deviation of the sample and the number of specimens in both samples. The null hypothesis, is rejected if the test statistic is greater than the critical statistic $F_0 > F_{crit}$. The

[2]More accurately, since different values of the α-type error probability are possible, if the Level plus the α-type probability are higher than one.

Table 4.2: Hypothesis testing for equality of variances statistics of longitudinal Young's modulus.

VE vs. Ins	F_0	α	df_1	df_2	F_{crit}	Level
5	6.53	0.05	22	17	2.26	1
50	2.771	0.05	27	19	2.134	0.986
500	2.3	0.05	26	18	2.18	0.96

information is summarised under the Level value. If the Level value is higher than .95 (again see footnote of page 116) then the null hypothesis should be rejected.

The results presented in table 4.2 suggest that the variance of the Video extensometry calculated tensile modulus at all crosshead displacement rate is not equal to the variance of the Instron contacting extensometer calculated longitudinal Young's modulus.

4.2.8 Conclusion

Statistical analysis showed that both the centre of location (i.e. mean) and the scatter (i.e. variance) of the quantities are affected by the data acquisition method. This is in accordance to the trends observed in figure 4.13. Only the results for the mean at 50[mm/min] crosshead displacement rate remain unaffected by the method of the data acquisition method.

The observation is partly attributed to the observation area of each data acquisition method. As discussed in the methodology chapter 3, the Videoextensometry measures the strains over a small area - approximately square 10[mm] by 10[mm]; at a maximum data acquisition frequency of 25[Hz]. The longitudinal Instron contacting extensometer measures the strain over a 50[mm] gauge length; at a maximum data acquisition frequency of 50[Hz]. Therefore, the video extensometry measures longitudinal strain at a much smaller volume scale compared to the contacting

extensometer (5 times less). As a result, the longitudinal effect is averaged over a larger area for the contacting extensometer, therefore resulting in lower scatter.

Also, the failure location with respect to the area of observation may have a significant effect. Failure of the specimen is almost certainly contained within the gauge length of the contacting extensometer (because of the greater area of observation) while this is not the case for the Videoextensometry. In the case that yielding of the material occurs in a localised area within both gauge lengths, the longitudinal strain computed by the displacement measurement of videoextensometry method is greater than the longitudinal strain computed by the contacting extensometer method, because the initial gauge length is greater [3]. If yielding occurs outside the videoextensometry gauge length but inside the contacting extensometry gauge length, then the displacement data of videoextensometry method computes lower longitudinal strain. Therefore greater scatter is expected and is confirmed in the longitudinal strains videoextensometry. Therefore, the methods

[3] The Cauchy definitions of stress and strain are:

$$\varepsilon_{eng} = \frac{l - l_0}{l_0} = \frac{\Delta l}{l_0}$$

where:

l_0 The initial length of the specimen or the initial gauge length of the specimen.

l The length of the specimen or the gauge length to the specimen, at a certain point in time.

However, the above definition of stress and strain are only valid for small strains. For large strains the definitions of stress and strain are:

$$\varepsilon_{true} = \int_{l_0}^{l} \frac{dl}{l} = \ln\left(\frac{\Delta l}{l_0}\right) \tag{4.1}$$

The latter definition is more applicable to thermoplastics, which can generally exhibit large strains. Strain is a unit-less quantity. It may be perceived as a percentage change in length.

record over the surface areas that are likely to exhibit different behaviour; as a result the measurements are affected. The effect of the location of failure is relevant in the cases that failure is localised, i.e. all the examined laminates except from the $[0°]_4$ ply-stack.

Concerning transverse displacement measurement, the videoextensometry obtains measurements from a 10[mm] area in the same area that the longitudinal measurements are made. Also, the videoextensometry software is capable of tracking necking along that area. The contacting extensometry method (*Ins*) uses a separate contacting extensometer for the transverse measurement. Furthermore, contrary to the videoextensometry method, the transverse contacting extensometer measures at a single gauge length along the longitudinal testing axis.

Moreover, the location of the transverse displacement measurement affects the measurement because occurrence of the failure within one transverse gauge length area is mutually exclusive for the other because of the way the extensometer were positioned. As a result, in the event that failure occurs with in the transverse gauge of one of the measuring methods, the measured values from the different methods vary significantly. The effect is particularly significant for the coupling factors.

In the author's opinion, the fact that Videoextensometry captures displacement data over a localised square area is more appropriate (local properties) for characterisation purposes, provided that it obtains always information on the failure area. However, the location of failure cannot be guaranteed within the measuring area. As a result, the measurements lead to increased scatter.

Further, at higher crosshead displacement rates, data acquisition rate has increasing importance and the Videoextensometry data acquisition method has only half the sampling rate of the contacting extensometer.

The scatter is not desirable because it is difficult to make statistical inferences. As a result, since the contacting extensometer appears to provide less scatter in the experimental results only the Instron results will be examined in the §8.1.

The effect of data acquisition method on the longitudinal tensile modulus was investigated using statistical tools. It was found that the longitudinal tensile modulus is dependent on the data acquisition method. Similar effects can be observed for other quantities of characterisation.

4.3 Strain Rate Dependent Mechanical Properties

4.3.1 Mechanical Test Results From $[0°]_4$ Test Specimens.

Tables 4.3, 4.4 and 4.5 present the Ladevéze composite material model parameters as obtained from the Plytron $[0°]_4$ laminated specimens at respectively 5, 50 and 500[mm/min] INSTRON crosshead displacement rate .

Table 4.3: Ladevéze composite material model parameters as obtained from the Plytron $[0°]_4$ laminated specimens at 5[mm/min] crosshead displacement rate.

ID	E_{11} [GPa]	ε_{11} []	σ_{11} [GPa]	ν_{12} []	ε_{22} []	SR_{11} $[s^{-1}]$	NRG $[J/m^2]$	Fail
UD.1.v1	26.774	0.027	0.649	0.155	-0.0064	0.0005	0.0093	Cat
UD.1.v2	31.803	0.027	0.756	0.370	-0.0086	0.0005	0.0107	Cat
UD.1.v3	25.369	0.025	0.582	0.353	-0.0075	0.0007	0.0076	Cat
UD.1.v4	30.383	0.022	0.646	0.347	0.0074	0.0002	0.0073	Cat
UD.1.v5	29.326	0.022	0.583	0.456	-0.0636	0.0004	0.0066	Cat
UD.1.v6	27.614	0.025	0.601	0.172	0.0002	0.0006	0.0086	Cat
UD.1.v7	24.973	0.025	0.561	0.345	-0.0094	0.0005	0.0074	Cat
UD.1.v8	22.530	0.027	0.560	-2.403	0.0014	0.0010	0.0077	Cat
UD.1.v9	37.498	0.018	0.594	3.112	-0.0480	0.0002	0.0056	Cat
UD.1.v11	23.642	0.024	0.636	0.141	-0.0082	0.0005	0.0078	Cat
UD.1.v14	43.571	0.017	0.495	0.181	-0.0059	0.0006	0.0046	Slip
UD.1.v15	31.989	0.023	0.573	0.281	-0.0082	0.0006	0.0065	Slip
UD.1.v16	42.031	0.022	0.538	0.421	-0.0018	0.0006	0.0067	Cat
UD.1.v17	18.918	0.022	0.385	0.091	-0.0062	0.0007	0.0043	Cat

Table 4.3: (continued)

ID	E_{11} [GPa]	ε_{11} []	σ_{11} [GPa]	ν_{12} []	ε_{22} []	SR_{11} $[s^{-1}]$	NRG $[J/m^2]$	Fail
UD.1.v18	67.180	0.018	0.572	1.567	0.0029	0.0007	0.0058	Cat
UD.1.v19	13.892	0.021	0.378	0.351	-0.0067	0.0007	0.0041	Cat
UD.1.v20	25.168	0.018	0.327	0.582	-0.0074	0.0007	0.0033	Cat
UD.1.v21	32.068	0.020	0.406	0.471	-0.0061	0.0007	0.0052	Cat
UD.1.v22	30.662	0.020	0.386	0.650	-0.0081	0.0006	0.0043	Cat
UD.1.v23	31.877	0.019	0.539	0.573	-0.0085	0.0005	0.0059	Slip
UD.1.v24	32.130	0.020	0.416	0.646	-0.0070	0.0006	0.0047	Cat
UD.1.v25	32.450	0.017	0.405	0.751	-0.0090	0.0006	0.0036	Cat
UD.1.v26	50.996	0.017	0.537	0.541	-0.0062	0.0005	0.0046	Cat
UD.1.v27	20.194	0.021	0.377	0.189	-0.0075	0.0007	0.0046	Cat
UD.1.v28	23.847	0.021	0.493	0.438	0.0045	0.0009	0.0075	Cat
UD.1.8i	21.662	0.024	0.560	0.424	-0.0085	0.0012	0.0066	Cat
UD.1.9i	29.697	0.022	0.588	0.235	-0.0071	0.0011	0.0065	Cat
UD.1.10i	33.239	0.022	0.703	0.375	-0.0099	0.0011	0.0080	Cat
UD.1.i11	24.024	0.025	0.646	0.303	-0.0094	0.0005	0.0083	Cat
UD.1.i12	24.741	0.027	0.612	0.542	-0.0135	0.0006	0.0087	Cat
UD.1.i13	20.921	0.025	0.509	0.581	-0.0147	0.0006	0.0064	Cat
UD.1.i15	25.849	0.022	0.573	0.171	-0.0046	0.0006	0.0062	Slip
UD.1.i16	22.336	0.025	0.538	0.286	-0.0053	0.0006	0.0070	Cat
UD.1.i17	16.918	0.022	0.384	0.383	-0.0072	0.0007	0.0043	Cat
UD.1.i18	24.990	0.022	0.572	0.332	-0.0067	0.0006	0.0063	Cat
UD.1.i20	17.490	0.019	0.325	0.299	-0.0068	0.0007	0.0031	Cat
UD.1.i21	21.800	0.021	0.405	0.548	-0.0080	0.0007	0.0043	Cat
UD.1.i22	18.891	0.021	0.383	0.424	-0.0147	0.0007	0.0041	Cat
UD.1.i23	29.176	0.020	0.538	0.458	-0.0074	0.0005	0.0055	Slip
UD.1.i24	20.263	0.021	0.415	0.400	-0.0086	0.0007	0.0044	Cat
UD.1.i25	21.508	0.020	0.402	0.584	-0.0078	0.0006	0.0041	Cat
UD.1.i26	29.770	0.019	0.531	0.270	-0.0066	0.0006	0.0051	Cat
UD.1.i27	20.442	0.021	0.375	0.381	-0.0072	0.0007	0.0040	Cat
UD.1.i28	20.196	0.022	0.492	0.583	-0.0096	0.0006	0.0055	Cat

Table 4.4: Ladevéze composite material model parameters as obtained from the Plytron $[0°]_4$ laminated specimens at 50[mm/min] crosshead displacement rate.

ID	E_{11} [GPa]	ε_{11} []	σ_{11} [GPa]	ν_{12} []	ε_{22} []	SR_{11} $[s^{-1}]$	NRG $[J/m^2]$	Fail
UD.2.v2	27.225	0.022	0.576	0.016	-0.0092	0.0032	NA	Cat
UD.2.v3	17.913	0.029	0.579	0.286	0.0020	0.0054	0.0096	Cat
UD.2.v4	21.476	0.025	0.555	0.358	-0.0112	0.0035	0.0079	Cat
UD.2.v5	38.648	0.023	0.705	0.407	-0.0070	0.0019	0.0091	Slip
UD.2.v6	29.815	0.025	0.663	0.451	-0.0095	0.0039	0.0087	Cat
UD.2.v7	19.371	0.021	0.528	0.234	-0.0092	0.0032	0.0063	Cat

Table 4.4: (continued)

ID	E_{11} [GPa]	ε_{11} []	σ_{11} [GPa]	ν_{12} []	ε_{22} []	SR_{11} $[s^{-1}]$	NRG $[J/m^2]$	Fail
UD.2.v8	21.476	0.025	0.555	0.358	-0.0112	0.0035	0.0079	Cat
UD.2.v9	27.121	0.021	0.673	0.338	-0.0057	0.0038	0.0078	Slip
UD.2.v10	17.576	0.023	0.568	0.228	-0.0088	0.0047	0.0077	Cat
UD.2.v11	28.878	0.020	0.627	0.357	-0.0082	0.0029	0.0059	Cat
UD.2.v12	38.359	0.026	0.786	0.066	-0.0045	0.0027	0.0104	Slip
UD.2.v13	38.361	0.027	0.735	0.365	-0.0102	0.0041	0.0107	Cat
UD.2.v15	35.165	0.026	0.705	0.550	-0.0079	0.0041	0.0099	Cat
UD.2.v16	32.058	0.028	0.677	0.379	-0.0084	0.0047	0.0099	Cat
UD.2.v17	21.506	0.027	0.639	0.191	0.0126	0.0027	0.0089	Cat
UD.2.v19	20.806	0.017	0.411	0.345	-0.0075	0.0057	0.0033	Cat
UD.2.v20	46.076	0.022	0.450	0.894	-0.0081	0.0064	0.0054	Cat
UD.2.v21	32.108	0.021	0.420	1.006	-0.0086	0.0062	0.0053	Cat
UD.2.v22	29.416	0.021	0.611	0.421	-0.0082	0.0050	0.0074	Cat
UD.2.v23	27.116	0.023	0.609	0.532	-0.0082	0.0051	0.0079	Cat
UD.2.v24	31.076	0.022	0.410	0.623	-0.0034	0.0067	0.0048	Cat
UD.2.v25	39.382	0.022	0.637	0.035	-0.0108	0.0054	0.0072	Cat
UD.2.v26	31.340	0.034	0.592	0.280	-0.0120	0.0091	0.0141	Cat
UD.2.v27	33.552	0.023	0.581	0.451	-0.0075	0.0059	0.0074	Cat
UD.2.v28	31.379	0.021	0.579	0.485	-0.0065	0.0054	0.0068	Cat
UD.2.v29	12.400	0.024	0.460	0.104	-0.0077	0.0068	0.0054	Cat
UD.2.v30	28.497	0.023	0.472	0.290	-0.0059	0.0063	0.0057	Cat
UD.2.v31	44.055	0.022	0.643	0.527	-0.0062	0.0055	0.0071	Cat
UD.2.v32	30.613	0.021	0.442	0.589	-0.0068	0.0062	0.0049	Cat
UD.2.v33	37.734	0.021	0.542	0.458	-0.0063	0.0059	0.0062	Cat
UD.2.11i	29.333	0.023	0.636	0.258	-0.0078	0.0066	0.0075	Cat
UD.2.12i	38.771	0.024	0.785	0.260	-0.0092	0.0061	0.0096	Slip
UD.2.13i	29.338	0.025	0.708	0.391	-0.0091	0.0064	0.0092	Cat
UD.2.15i	34.720	0.027	0.709	0.413	-0.0069	0.0066	0.0097	Cat
UD.2.16i	35.517	0.026	0.697	0.263	-0.0078	0.0066	0.0093	Cat
UD.2.17i	30.912	0.026	0.653	0.321	-0.0095	0.0067	0.0088	Cat
UD.2.i18	33.561	0.021	0.662	0.428	-0.0080	0.0052	0.0070	Cat
UD.2.i19	21.999	0.023	0.411	0.344	-0.2715	0.0068	0.0064	Cat
UD.2.i20	22.676	0.023	0.454	0.446	-0.0077	0.0067	0.0054	Cat
UD.2.i22	23.597	0.024	0.611	0.511	-0.0105	0.0057	0.0075	Cat
UD.2.i23	28.018	0.024	0.609	0.404	-0.0123	0.0052	0.0074	Cat
UD.2.i24	17.689	0.023	0.408	0.484	-0.0078	0.0071	0.0049	Cat
UD.2.i25	30.350	0.022	0.639	123.457	-0.2730	0.0055	0.0070	Cat
UD.2.i26	34.266	0.022	0.595	0.470	-0.0144	0.0058	0.0073	Cat
UD.2.i27	28.099	0.022	0.584	0.307	-0.0074	0.0057	0.0065	Cat
UD.2.i28	26.776	0.022	0.579	0.274	-0.0061	0.0056	0.0065	Cat
UD.2.i29	23.571	0.023	0.458	0.292	-0.0082	0.0074	0.0059	Cat
UD.2.i31	27.913	0.022	0.641	0.219	-0.0066	0.0056	0.0074	Cat
UD.2.i32	22.155	0.022	0.445	0.313	-0.0071	0.0066	0.0051	Cat

Table 4.4: (continued)

ID	E_{11} [GPa]	ε_{11} []	σ_{11} [GPa]	ν_{12} []	ε_{22} []	SR_{11} $[s^{-1}]$	NRG $[J/m^2]$	Fail
UD.2.i33	25.942	0.021	0.553	0.262	-0.0072	0.0060	0.0061	Cat

Table 4.5: Ladevéze composite material model parameters as obtained from the Plytron $[0°]_4$ laminated specimens at 500[mm/min] crosshead displacement rate.

ID	E_{11} [GPa]	ε_{11} []	σ_{11} [GPa]	ν_{12} []	ε_{22} []	SR_{11} $[s^{-1}]$	NRG $[J/m^2]$	Fail
UD.3.v1	27.611	0.037	0.665	0.022	-0.0149	0.0393	NA	Cat
UD.3.v2	37.663	0.014	0.465	0.776	-0.0078	0.0545	0.0040	Cat
UD.3.v3	19.984	0.017	0.385	0.817	-0.0120	0.0799	0.0038	Slip
UD.3.v4	24.708	0.015	0.412	0.815	-0.0044	0.0548	0.0039	Slip
UD.3.v5	65.390	0.016	0.752	0.923	-0.0086	0.0623	0.0087	Cat
UD.3.v6	43.326	0.022	0.758	0.522	-0.0083	0.0691	0.0107	Cat
UD.3.v7	31.070	0.019	0.516	0.547	-0.0059	0.0775	0.0064	Cat
UD.3.v8	37.222	0.023	0.554	0.620	-0.0231	0.0981	0.0093	Slip
UD.3.v9	47.723	0.019	0.771	0.692	-0.0091	0.0554	0.0090	Cat
UD.3.v10	43.398	0.017	0.702	1.071	-0.0111	0.0304	0.0071	Cat
UD.3.v11	40.926	0.019	0.739	Na	Na	0.0648	0.0094	Cat
UD.3.v12	28.855	0.024	0.653	0.410	-0.0066	0.0658	0.0095	Cat
UD.3.v13	29.081	0.015	0.492	0.433	-0.0003	0.0835	0.0047	Cat
UD.3.v14	20.460	0.038	0.497	0.501	0.0102	0.2569	0.0147	Cat
UD.3.v15	42.233	0.020	0.628	0.507	-0.0054	0.0656	0.0088	Cat
UD.3.v16	23.849	0.018	0.555	1.093	-0.0205	0.0388	0.0045	Cat
UD.3.v17	30.317	0.019	0.533	0.418	-0.0028	0.0738	0.0067	Cat
UD.3.v18	53.857	0.031	0.399	0.132	0.0288	0.0890	0.0089	Cat
UD.3.v19	90.790	0.019	0.699	0.810	-0.0084	0.0456	0.0084	Cat
UD.3.v20	99.005	0.018	0.441	0.625	-0.0078	0.0514	0.0051	Cat
UD.3.v21	69.303	0.021	0.643	0.633	0.0121	0.0529	0.0078	Cat
UD.3.v22	63.825	0.024	0.645	0.681	-0.0108	0.0523	0.0098	Cat
UD.3.v23	41.586	0.031	0.435	1.752	0.0003	0.0962	0.0094	Cat
UD.3.v24	138.058	0.018	0.630	1.180	-0.0048	0.0484	0.0071	Cat
UD.3.v25	72.961	0.015	0.451	0.712	-0.0078	0.0331	0.0043	Cat
UD.3.v26	51.285	0.020	0.416	0.632	-0.0046	0.0533	0.0054	Cat
UD.3.v27	52.310	0.021	0.458	0.664	-0.0084	0.0621	0.0063	Cat
UD.3.v28	149.031	0.013	0.539	1.486	-0.0061	0.0391	0.0048	Cat
UD.3.v29	50.099	0.012	0.357	0.905	0.0094	0.0363	0.0025	Cat
UD.3.v30	45.789	0.023	0.480	0.580	-0.0087	0.0605	0.0065	Cat
UD.3.v31	44.566	0.024	0.509	0.439	-0.0077	0.0655	0.0074	Cat
UD.3.v32	35.866	0.015	0.382	0.539	-0.0064	0.0472	0.0036	Cat
UD.3.v33	68.407	0.023	0.671	0.551	-0.0043	0.0557	0.0099	Cat
UD.3.11i	25.836	0.029	0.829	0.281	-0.0100	0.0734	0.0123	Cat
UD.3.12i	25.049	0.031	0.805	0.361	-0.0085	0.0655	0.0133	Cat

Table 4.5: (continued)

ID	E_{11} [GPa]	ε_{11} []	σ_{11} [GPa]	ν_{12} []	ε_{22} []	SR_{11} $[s^{-1}]$	NRG $[J/m^2]$	Fail
UD.3.13i	NA	NA	NA	NA	NA	NA	NA	Cat
UD.3.14i	26.968	0.024	0.605	-1.555	-0.1675	0.0663	0.0074	Cat
UD.3.17i	36.222	0.025	0.666	0.352	-0.0095	0.1032	0.0110	Cat
UD.3.i18	-123.079	0.027	0.424	-3.283	-0.0671	0.0843	0.0056	Cat
UD.3.i19	27.355	0.026	0.730	0.259	-0.0082	0.0631	0.0098	Cat
UD.3.i20	19.635	0.026	0.463	0.284	-0.0101	0.0760	0.0062	Cat
UD.3.i21	30.512	0.023	0.626	0.345	-0.0116	0.0637	0.0072	Cat
UD.3.i22	26.431	0.025	0.652	0.186	-0.0091	0.0664	0.0082	Cat
UD.3.i23	19.207	0.024	0.416	0.167	-0.0091	0.0810	0.0053	Cat
UD.3.i24	34.369	0.023	0.645	0.209	-0.0095	0.0624	0.0081	Cat
UD.3.i25	24.387	0.027	0.473	0.231	-0.0266	0.0613	0.0069	Cat
UD.3.i26	21.612	0.024	0.439	0.150	-0.0111	0.0746	0.0066	Cat
UD.3.i27	17.983	0.028	0.476	0.301	-0.2781	0.0824	0.0071	Cat
UD.3.i28	-313.815	0.021	0.557	-3.612	-0.0083	0.0570	0.0060	Cat
UD.3.i29	13.591	0.022	0.391	0.156	-0.0065	0.0769	0.0043	Cat
UD.3.i30	4.286	0.032	0.503	0.049	-0.0170	0.0825	0.0074	Cat
UD.3.i31	9.347	0.028	0.512	-0.103	-0.0101	0.0764	0.0067	Cat
UD.3.i32	19.289	0.025	0.416	-0.005	-0.0176	0.0774	0.0053	Cat
UD.3.i33	44.904	0.024	0.656	0.604	-0.0106	0.0605	0.0079	Cat

4.3.2 Mechanical Test Results From $[\pm 45°]_8$ Test Specimens.

Tables 4.6, 4.7 and 4.8 present the mechanical properties as obtained from $[\pm 45]_{2s}$ Plytron laminate experimental results at 5[mm/min], 50[mm/min] and 500[mm/min] crosshead displacement rates, respectively.

Table 4.6: Mechanical properties as obtained from $[\pm 45]_{2s}$ Plytron laminate experimental results at 5[mm/min] crosshead displacement rate.

ID	G_{12} $[GPa]$	γ_{12} $[rad]$	τ_{12} $[MPa]$	Y_0 $[GPa]$	Y_c $[GPa]$	Y_R $[GPa]$	SR_{12} $[s^{-1}]$	m	β	R_0 $[GPa]$	FailLoc
PM45.1.v1	1.161	0.413	0.0424	0.0039	0.0442	0.0441	0.0018	0.573	0.476	-0.002	3
PM45.1.v2	1.460	0.432	0.0396	0.0025	0.0412	0.0447	0.0019	0.668	0.721	-0.002	3
PM45.1.v3	1.970	0.400	0.0366	0.0007	0.0402	0.0463	0.0016	0.758	1.374	-0.006	3
PM45.1.v4	1.181	0.385	0.0397	0.0033	0.0453	0.0462	0.0019	0.500	0.390	-0.008	3
PM45.1.v5	1.130	0.484	0.0456	0.0034	0.0466	0.0442	0.0017	0.344	0.276	-0.023	3
PM45.1.v6	1.151	0.395	0.0396	0.0026	0.0461	0.0476	0.0020	0.318	0.268	-0.020	3
PM45.1.v7	1.249	0.316	0.0387	0.0027	0.0461	0.0466	0.0017	0.505	0.420	-0.008	3
PM45.1.v9	1.618336	0.5773	0.04714	0.00391	0.037704	0.041842	0.001573	1.268138	3.150435	0.021078	2
PM45.1.v10	1.229	0.585	0.0456	0.0025	0.0422	0.0464	0.0019	0.254	0.404	-0.080	3
PM45.1.v11	1.189	0.471	0.0434	0.0025	0.0464	0.0482	0.0017	0.341	0.342	-0.033	2
PM45.1.v12	3.684	0.500	0.0378	0.0214	-0.0043	0.0386	0.0014	0.938	6.068	-0.185	1
PM45.1.v13	3.482	0.506	0.0431	0.0027	0.0300	0.0412	0.0016	1.009	7.107	0.005	3
PM45.1.v14	2.934	0.528	0.0443	0.0032	0.0293	0.0389	0.0016	1.203	6.643	0.038	3
PM45.1.v15	2.678	0.373	0.0389	0.0037	0.0305	0.0405	0.0014	0.984	3.686	0.025	4
PM45.1.v16	2.113	0.536	0.0470	0.0039	0.0326	0.0410	0.0017	1.284	4.902	0.036	3
PM45.1.v18	2.029	0.564	0.0482	0.0045	0.0314	0.0386	0.0016	0.708	0.940	0.014	3
PM45.1.v19	1.745	0.486	0.0409	0.0044	0.0345	0.0413	0.0016	0.952	1.451	0.019	3
PM45.1.v20	2.762	0.405	0.0403	0.0029	0.0304	0.0381	0.0013	1.766	32.700	0.039	1
PM45.1.v21	2.096	0.452	0.0441	0.0040	0.0320	0.0393	0.0015	0.723	1.214	0.015	2
PM45.1.v22	2.169	0.411	0.0424	0.0043	0.0318	0.0392	0.0015	0.532	0.799	-0.028	3
PM45.1.v23	1.945	0.423	0.0419	0.0047	0.0329	0.0395	0.0016	0.637	0.779	-0.002	2
PM45.1.i18	1.710	0.489	0.0481	0.0046	0.0348	0.037734	0.001315	1.129	1.925	0.026	3
PM45.1.i19	1.648	0.443	0.0410	0.0044	0.0356	0.039842	0.001509	1.391	3.529	0.031	3
PM45.1.i20	1.952	0.409	0.0404	0.0040	0.0334	0.038803	0.001471	1.387	4.577	0.030	1
PM45.1.i21	1.266	0.529	0.0481	0.0051	0.0405	0.040913	0.001539	1.038	1.047	0.024	2
PM45.1.i22	1.655	0.376	0.0425	0.0047	0.0361	0.040152	0.001444	1.085	1.727	0.027	3
PM45.1.i23	1.742	0.379	0.0421	0.0048	0.0351	0.03947	0.001391	1.130	2.010	0.032	2

Table 4.7: Mechanical properties as obtained from $[\pm 45]_{2s}$ Plytron laminate experimental results at 50[mm/min] crosshead displacement rate.

ID	G_{12} $[GPa]$	γ_{12} $[rad]$	τ_{12} $[MPa]$	Y_0 $[GPa]$	Y_c $[GPa]$	Y_R $[GPa]$	SR_{12} $[s^{-1}]$	m	β	R_0 $[GPa]$	FailLoc
PM45.2.v1	3.203	0.164	0.0311	0.0039	0.0250	0.0310	0.0177	0.553	2.005	-0.044	3
PM45.2.v2	2.021	0.334	0.0408	0.0050	0.0283	0.0314	0.0168	0.518	1.008	-0.025	3
PM45.2.v3	1.932	0.381	0.0441	0.0024	0.0410	0.0524	0.0191	0.370	0.764	-0.048	3
PM45.2.v4	2.120	0.358	0.0443	0.0021	0.0419	0.0526	0.0185	0.301	0.675	-0.079	3
PM45.2.v5	2.008	0.467	0.0518	0.0025	0.0405	0.0487	0.0170	0.453	0.808	-0.047	3
PM45.2.v6	3.206	0.285	0.0380	0.0035	0.0255	0.0307	0.0168	0.615	2.155	-0.013	3
PM45.2.v7	1.963	0.399	0.0459	0.0174	-0.0034	0.0315	0.0165	0.421	0.850	-0.050	2
PM45.2.v8	2.770	0.390	0.0443	0.0012	0.0399	0.0529	0.0184	0.436	1.115	-0.033	3
PM45.2.v9	1.424	0.534	0.0493	0.0021	0.0431	0.0485	0.0168	0.522	0.761	-0.011	3
PM45.2.v10	1.415	0.547	0.0491	0.0017	0.0428	0.0485	0.0163	0.645	1.121	0.010	3
PM45.2.v11	1.610	0.553	0.0530	0.0014	0.0435	0.0488	0.0153	0.140	0.495	-0.179	2
PM45.2.v12	3.067	0.482	0.0450	0.0001	0.0346	0.0457	0.0133	0.699	3.389	-0.002	3
PM45.2.v13	2.285	0.451	0.0458	0.0035	0.0340	0.0422	0.0132	1.495	15.730	0.044	2
PM45.2.v14	2.952	0.406	0.0411	0.0002	0.0355	0.0464	0.0148	0.415	1.413	-0.035	2
PM45.2.v15	1.858	0.382	0.0407	0.0010	0.0415	0.0492	0.0153	0.578	1.069	-0.004	2
PM45.2.v16	2.644	0.363	0.0414	0.0058	0.0324	0.0460	0.0140	1.398	21.864	0.071	2
PM45.2.v17	1.192	0.530	0.0505	0.0027	0.0490	0.0501	0.0176	NA	NA	NA	2
PM45.2.v18	1.859	0.462	0.0438	0.0012	0.0411	0.0490	0.0165	0.195	0.472	-0.099	1
PM45.2.v19	1.784	0.536	0.0427	0.0005	0.0436	0.0514	0.0174	0.831	2.729	-0.002	1
PM45.2.v20	2.978	0.477	0.0459	0.0006	0.0347	0.0451	0.0139	0.368	1.287	-0.092	2
PM45.2.v21	1.892	0.421	0.0414	0.0015	0.0396	0.0487	0.0171	0.041	1.561	-1.215	2
PM45.2.i9	1.175	0.507	0.0494	0.0032	0.0474	0.0488	0.0155	NA	NA	NA	3
PM45.2.i10	1.338	0.506	0.0496	0.0023	0.0446	0.0474	0.0150	0.392	0.459	-0.020	3
PM45.2.i11	1.211	0.470	0.0531	0.0028	0.0483	0.0496	0.0152	0.345	0.376	-0.022	2
PM45.2.i12	1.328	0.435	0.0447	0.0027	0.0443	0.0470	0.0148	0.384	0.437	-0.025	3
PM45.2.i13	1.355	0.442	0.0450	0.0025	0.0455	0.0479	0.0149	0.415	0.510	-0.023	2
PM45.2.i14	1.230	0.371	0.0411	0.0028	0.0464	0.0470	0.0146	0.307	0.375	-0.043	2
PM45.2.i15	1.501	0.331	0.0406	0.0025	0.0442	0.0480	0.0149	0.462	0.577	-0.015	2
PM45.2.i16	1.350	0.349	0.0409	0.0029	0.0454	0.0488	0.0160	0.407	0.468	-0.015	2
PM45.2.i17	1.385	0.386	0.0468	0.0027	0.0466	0.0479	0.0149	0.366	0.422	-0.021	2

Table 4.7: (continued)

ID	G_{12} $[GPa]$	γ_{12} $[rad]$	τ_{12} $[MPa]$	Y_0 $[GPa]$	Y_c $[GPa]$	Y_R $[GPa]$	SR_{12} $[s^{-1}]$	m	β	R_0 $[GPa]$	FailLoc
PM45.2.i18	1.425	0.370	0.0431	0.0024	0.0452	0.0485	0.0156	0.358	0.461	-0.027	1
PM45.2.i19	1.354	0.340	0.0417	0.0029	0.0447	0.0473	0.0146	0.398	0.453	-0.019	1
PM45.2.i20	1.248	0.416	0.0456	0.0028	0.0475	0.0491	0.0149	0.374	0.403	-0.016	2
PM45.2.i21	1.389	0.350	0.0401	0.0024	0.0453	0.049516	0.016287	0.472	0.586	-0.010	2

Table 4.8: Mechanical properties as obtained from $[\pm 45]_{2s}$ Plytron laminate experimental results at 500[mm/min] crosshead displacement rate.

ID	G_{12} $[GPa]$	γ_{12} $[rad]$	τ_{12} $[MPa]$	Y_0 $[GPa]$	Y_c $[GPa]$	Y_R $[GPa]$	SR_{12} $[s^{-1}]$	m	β	R_0 $[GPa]$	FailLoc
PM45.3.v1	1.963	0.473	0.0532	0.0099	0.0379	0.0513	0.0910	1.287	2.869	0.067	3
PM45.3.v2	4.262	0.519	0.0585	0.0057	0.0411	0.0602	0.1019	0.689	5.501	0.028	3
PM45.3.v3	2.764	0.417	0.0525	0.0050	0.0442	0.0576	0.0811	1.651	37.510	-0.039	3
PM45.3.v5	4.521	0.440	0.0471	0.0059	0.0413	0.0625	0.0981	0.247	4.903	-1.274	3
PM45.3.v6	3.814	0.463	0.0509	0.0060	0.0376	0.0541	0.0907	NA	NA	NA	3
PM45.3.v7	3.504	0.461	0.0523	0.0016	0.0450	0.0606	0.1020	NA	NA	NA	3
PM45.3.v8	2.779	0.504	0.0501	0.0008	0.0429	0.0535	0.0984	2.517	664.155	0.037	3
PM45.3.v9	3.615	0.444	0.0486	0.0011	0.0366	0.0464	0.0912	0.887	6.360	-0.009	2
PM45.3.v10	1.575	0.455	0.0464	0.0056	0.0450	0.0488	0.1005	1.866	25.399	0.025	2
PM45.3.v11	2.833	0.468	0.0511	0.0007	0.0431	0.0535	0.0897	1.402	25.599	0.017	2
PM45.3.v12	3.471	0.365	0.0463	0.0045	0.0357	0.0487	0.0740	2.627	744.098	0.075	1
PM45.3.v13	2.333	0.409	0.0487	0.0022	0.0426	0.0508	0.0853	1.222	9.793	0.021	2
PM45.3.v14	2.631	0.470	0.0466	0.0035	0.0380	0.0463	0.1065	0.816	3.143	-0.023	2
PM45.3.v15	3.127	0.509	0.0515	0.0012	0.0387	0.0498	0.1018	0.547	2.074	-0.087	3
PM45.3.v16	2.601	0.458	0.0471	0.0065	0.0376	0.0526	0.1123	0.485	1.624	-0.112	2
PM45.3.v17	2.127	0.402	0.0445	0.0030	0.0419	0.0500	0.0931	0.931	3.126	0.003	2
PM45.3.v18	2.139	0.400	0.0457	0.0070	0.0395	0.0541	0.1036	1.981	40.667	0.079	3
PM45.3.v19	1.977	0.499	0.0493	0.0080	0.0387	0.0510	0.1188	NA	NA	NA	2
PM45.3.v20	3.369	0.500	0.0489	0.0007	0.0393	0.0506	0.1089	0.036	5.359	-4.466	2
PM45.3.i8	1.103	0.419	0.0510	0.0073	0.0532	0.0548	0.1044	0.545	0.408	0.006	3
PM45.3.i9	1.152	0.425	0.0490	0.0065	0.0531	0.0546	0.1031	0.618	0.511	0.000	2

Table 4.8: (continued)

ID	G_{12} $[GPa]$	γ_{12} $[rad]$	τ_{12} $[MPa]$	Y_0 $[GPa]$	Y_c $[GPa]$	Y_R $[GPa]$	SR_{12} $[s^{-1}]$	m	β	R_0 $[GPa]$	FailLoc
PM45.3.i10	1.007	0.425	0.0466	0.0082	0.0525	0.0533	0.1135	0.365	0.285	-0.014	2
PM45.3.i11	1.024	0.456	0.0517	0.0075	0.0569	0.0561	0.1096	0.342	0.280	-0.018	2
PM45.3.i12	1.290	0.371	0.0466	0.0066	0.0508	0.0527	0.0988	0.518	0.425	-0.007	1
PM45.3.i13	0.984	0.421	0.0489	0.0080	0.0562	0.0555	0.1086	0.344	0.265	-0.017	2
PM45.3.i14	1.012	0.438	0.0473	0.0080	0.0529	0.0551	0.1107	0.420	0.335	-0.011	2
PM45.3.i15	1.174	0.339	0.0451	0.0093	0.0357	0.0344	0.1010	0.445	0.377	-0.007	3
PM45.3.i16	1.015	0.418	0.0472	0.0079	0.0529	0.0531	0.1105	0.195	0.296	-0.093	2
PM45.3.i17	0.989	0.448	0.0474	0.0078	0.0532	0.0542	0.1112	0.369	0.282	-0.015	2
PM45.3.i18	1.184	0.418	0.0466	0.0074	0.0497	0.0520	0.1068	0.495	0.432	-0.013	3
PM45.3.i19	1.125	0.427	0.0494	0.0072	0.0535	0.0534	0.1027	0.643	0.475	0.010	2
PM45.3.i20	0.985	0.490	0.0492	0.0084	0.0523	0.0540	0.1168	0.402	0.303	-0.013	2

4.3.3 Mechanical Test Results From $[+45°]_8$ Test Specimens.

Tables 4.9, 4.10 and 4.11 present the mechanical properties as obtained from $[+45]_8$ Plytron laminate experimental results at 5[mm/min], 50[mm/min] and 500[mm/min] crosshead displacement rates, respectively.

Table 4.9: Mechanical properties as obtained from $[+45]_8$ Plytron laminate experimental results at 5[mm/min] crosshead displacement rate.

ID	E_{22} [GPa]	ε_{22} []	σ_{22} [MPa]	A^2 []	SR_{22} [1/s]	SR_{12} [1/s]	Fail. Type	Fail. Loc.
P45.1.v1	2.52	0.0026	5.29	0.82	0.00094	0.0012	Premature	3
P45.1.v2	3.20	0.0364	13.17	2.85	0.00065	0.001168	Cat	3
P45.1.v3	20.12	0.0030	7.16	1.48	0.00069	0.001294	Premature	3
P45.1.v5	2.52	0.0024	4.13	6.44	0.00060	0.000983	Premature	3
P45.1.v8	12.15	0.0011	6.58	2.59	0.00017	0.000487	Premature	2
P45.1.v9	6.40	0.0050	12.13	2.57	0.00047	0.000985	Cat	2
P45.1.v11	9.95	0.0065	14.03	1.22	0.00046	0.00101	Cat	3
P45.1.v12	28.67	0.0033	13.25	1.58	0.00054	0.001037	Cat	3
P45.1.v13	3.37	0.0019	13.30	1.43	0.00037	0.000833	Cat	2
P45.1.v14	3.53	0.0047	13.52	1.15	0.00040	0.001093	Cat	2
P45.1.v15	10.03	0.0034	14.69	6.59	0.00018	0.000705	Cat	1
P45.1.v16	32.66	0.0000	14.52	4.85	0.00007	0.000762	Cat	1
P45.1.v17	5.65	0.0058	15.77	1.28	0.00028	0.000631	Cat	1
P45.1.v18	16.20	0.0000	12.44	0.38	0.00053	0.000667	Cat	1
P45.1.i1	9.22	0.0011	5.25	0.37	0.00023	0.000769	Premature	3
P45.1.i2	8.92	0.0025	13.12	0.46	0.00022	0.000969	Cat	3
P45.1.i3	3.78	0.0022	7.04	0.34	0.00043	0.000952	Premature	3
P45.1.i4	8.00	0.0012	6.19	0.39	0.00025	0.000838	Cat	3
P45.1.i5	3.17	0.0014	4.12	0.49	0.00046	0.00087	Premature	3
P45.1.i6	4.89	0.0013	6.35	1.05	0.00029	0.000826	Premature	3
P45.1.i7	4.46	0.0014	6.39	0.84	0.00031	0.000879	Premature	3
P45.1.i8	3.42	0.0016	6.31	1.26	0.00039	0.000918	Premature	2
P45.1.i9	8.59	0.0019	11.62	1.66	0.00022	0.000835	Cat	2
P45.1.i10	6.19	0.0033	13.24	1.32	0.00027	0.000905	Cat	3
P45.1.i11	3.76	0.0044	13.99	0.81	0.00039	0.000963	Cat	3

Table 4.10: Mechanical properties as obtained from $[+45]_8$ Plytron laminate experimental results at 50[mm/min] crosshead displacement rate.

ID	E_{22} [GPa]	ε_{22} []	σ_{22} [MPa]	A^2 []	SR_{22} [1/s]	SR_{12} [1/s]	Fail. Type	Fail. Loc.
P45.2.v5	6.76	0.0013	13.19	1.56	0.00194	0.002651	Cat	3
P45.2.v6	23.93	0.0021	13.36	1.33	0.00323	0.005267	Cat	3
P45.2.v7	29.50	0.0066	14.99	0.73	0.00058	0.000843	Cat	3
P45.2.v8	25.30	0.0085	13.32	1.17	0.00051	0.002541	Cat	3
P45.2.v9	33.64	0.0000	8.12	8.10	0.00030	0.001443	Premature	2
P45.2.v10	22.09	0.0045	15.26	1.56	0.00142	0.000663	Cat	2
P45.2.v11	78.60	0.0074	13.38	4.14	0.00100	0.002194	Cat	2
P45.2.v12	16.00	0.0074	14.42	6.50	0.00234	0.001696	Cat	2
P45.2.v13	14.16	0.0051	14.11	0.55	0.00116	0.001433	Cat	3
P45.2.v14	61.04	0.0053	14.54	1.64	0.00055	0.000693	Cat	3
P45.2.v15	109.61	0.0028	13.43	0.73	0.00066	0.001144	Cat	3
P45.2.v16	178.66	0.0030	15.13	80.61	0.00126	0.000486	Cat	3
P45.2.i73	3.69	0.0056	13.12	0.90	0.00425	0.008938	Cat	3
P45.2.i74	4.46	0.0051	12.54	0.37	0.00425	0.008132	Cat	2
P45.2.i76	4.13	0.0045	11.64	0.37	0.00448	0.008641	Cat	3
P45.2.i77	9.95	0.0016	11.71	0.46	0.00155	0.009181	Cat	2
P45.2.i78	5.44	0.0042	13.19	0.54	0.00298	0.008151	Cat	5
P45.2.i79	14.86	0.0007	7.09	0.42	0.00121	0.007451	Cat	4
P45.2.i80	13.27	0.0007	5.40	1.82	0.00125	0.005148	Cat	5
P45.2.i81	34.33	0.0037	11.84	22.04	0.00294	0.006698	Cat	2
P45.2.i73	4.81	0.0134	13.07	1.10	0.00188	0.00388	Cat	3
P45.2.i74	6.51	0.0004	12.44	2.21	0.00222	0.004384	Cat	2
P45.2.i75	38.26	0.0000	6.90	8.94	0.00102	0.0026	Premature	2
P45.2.i76	13.17	0.0013	11.45	5.90	0.00169	0.004125	Cat	3
P45.2.i77	722.01	0.0021	11.36	61.38	0.00048	0.005098	Cat	2
P45.2.i78	56.33	0.0016	13.13	28.86	0.00056	0.003964	Cat	5
P45.2.i79	23.83	0.0051	7.13	1.03	0.00403	0.00143	Cat	4
P45.2.i80	43.59	0.0003	5.48	1.30	0.00138	0.002183	Cat	5
P45.2.i81	7.64	0.0038	11.51	23.04	0.00229	0.006475	Cat	2

Table 4.11: Mechanical properties as obtained from $[+45]_8$ Plytron laminate experimental results at 500[mm/min] crosshead displacement rate.

ID	E_{22} [GPa]	ε_{22} []	σ_{22} [MPa]	A^2 []	SR_{22} [1/s]	SR_{12} [1/s]	Fail. Type	Fail. Loc.
P45.3.v2	4.89	0.0042	13.34	0.61	0.01179	0.012398	Cat	3
P45.3.v4	8.86	0.0028	14.16	4.37	0.00668	0.012538	Cat	3
P45.3.v5	5.33	0.0061	14.80	1.02	0.00876	0.010944	Cat	2
P45.3.v6	15.03	0.0045	13.52	2.28	0.00858	0.010739	Cat	1
P45.3.v7	26.72	0.0025	13.03	3.34	0.00482	0.005532	Premature	2
P45.3.v8	5.34	0.0019	13.14	0.10	0.00618	0.007827	Premature	3
P45.3.v9	8.84	0.0016	15.07	0.90	0.00780	0.004439	Cat	3
P45.3.v10	7.12	0.0022	12.03	0.82	0.00745	0.003147	Cat	3
P45.3.v11	11.33	0.0030	10.91	3.59	0.00654	0.003368	Cat	2
P45.3.v12	3.19	0.0042	12.36	0.57	0.01055	0.006102	Premature	2
P45.3.v13	7.93	0.0018	8.37	1.64	0.00695	0.006844	Cat	3
P45.3.v14	7.12	0.0015	13.57	1.78	0.00977	0.009208	Cat	3
P45.3.i72	2.34	0.0032	8.47	0.90	0.03897	0.05503	Premature	1
P45.3.i82	7.35	0.0020	11.35	0.11	0.01138	0.042416	Cat	1
P45.3.i83	3.62	0.0035	12.00	0.19	0.02211	0.042282	Cat	2
P45.3.i84	21.27	0.0010	12.94	1.03	0.00485	0.048028	Cat	4
P45.3.i86	15.33	0.0010	11.47	3.53	0.00653	0.041337	Cat	5
P45.3.i89	3.65	0.0042	12.82	0.20	0.01985	0.057753	Cat	5
P45.3.i90	0.89	0.0043	2.18	NA	0.03574	0.047087	Premature	1
P45.3.i72	0.17	0.0245	2.415	NA	0.10437	0.044345	Premature	1
P45.3.i82	13.68	0.0107	9.09	1.05	0.00326	0.006673	Cat	1
P45.3.i83	10.73	0.0047	5.54	1.51	0.00440	0.013236	Cat	2
P45.3.i84	13.08	0.0022	10.59	2.06	0.00299	0.014548	Cat	4
P45.3.i86	8.30	0.0000	7.614	1.06	0.00661	0.004233	Cat	5
P45.3.i87	10.66	0.0000	8.239	1.93	0.00126	0.006098	Cat	5
P45.3.i88	0.24	0.0008	0.568	NA	0.00562	0.028945	Cat	3
P45.3.i89	23.72	0.0014	12.93	21.93	0.00292	0.013405	Cat	5

4.3.4 Mechanical Test Results From $[\pm 67.5°]_8$ Test Specimens.

Tables 4.12, 4.13 and 4.14 present the mechanical properties as obtained from $[+45]_8$ Plytron laminate experimental results at 5[mm/min], 50[mm/min] and 500[mm/min] crosshead displacement rates, respectively.

Table 4.12: Mechanical properties as obtained from $[\pm 67.5°]_{2s}$ Plytron laminate experimental results at 5[mm/min] crosshead displacement rate.

ID	Y'_0 [Gpa]	Y'_c [Gpa]	Y'_s [Gpa]	b []	SR_{22} [1/sec]	SR_{12} [1/sec]	Y_0 [Gpa]	Y_c [Gpa]	Fail Loc.
PM67.1.v3	0.003352	0.00010	0.00471	0.981	0.00019	0.00026	0.00246	0.00181	3
PM67.1.v4	0.002967	0.00005	0.00719	1.004	0.00045	0.00036	0.00166	0.00007	2
PM67.1.v5	0.000753	0.00755	0.00792	0.194	0.00063	0.00047	0.00167	0.00384	4
PM67.1.v6	0.041109	-0.06142	0.01028	0.335	0.00087	0.00089	-0.00993	0.02605	1
PM67.1.v7	0.000448	0.00761	0.00963	0.589	0.00077	0.00069	0.00181	0.00181	1
PM67.1.v8	0.059542	-0.09045	0.01137	0.331	0.00094	0.00080	-0.01699	0.04472	3
PM67.1.v9	-0.003313	0.01380	0.01823	0.271	0.00171	0.00131	-0.00926	0.01895	4
PM67.1.v10	0.020107	-0.02193	0.01208	0.193	0.00109	0.00088	-0.00309	0.01120	2
PM67.1.v11	0.012554	0.00148	0.01470	1.299	0.00056	0.00233	0.06130	-0.06396	2
PM67.1.i3	-0.009483	0.03821	0.00806	0.504	0.00058	0.00058	0.00038	0.00940	3
PM67.1.i4	0.017711	-0.02795	0.00864	0.576	0.00064	0.00065	0.00923	-0.01672	2
PM67.1.i5	-0.00322	0.02495	0.00694	0.695	0.00053	0.00058	0.00089	0.00604	4
PM67.1.i6	0.003052	0.00513	0.00567	0.749	0.00044	0.00048	0.00179	0.00278	1
PM67.1.i7	0.002923	0.00512	0.00550	0.945	0.00041	0.00050	0.00179	0.00050	1
PM67.1.i8	0.001811	0.00434	0.00507	0.695	0.00043	0.00043	0.00150	0.00041	3
PM67.1.i9	0.003016	0.00420	0.00591	0.819	0.00046	0.00052	0.00121	0.00462	4
PM67.1.i10	0.003088	0.00001	0.00529	1.308	0.00039	0.00049	0.00162	0.00075	2
PM67.1.i11	0.002338	0.00302	0.00572	0.731	0.00047	0.00045	0.00152	0.00159	2
PM67.1.i12	-0.014624	0.03791	0.00703	0.743	0.00061	0.00055	-0.00126	0.00860	2

Table 4.13: Mechanical properties as obtained from $[\pm 67.5°]_{2s}$ Plytron laminate experimental results at 50[mm/min] crosshead displacement rate.

ID	Y'_0 [Gpa]	Y'_c [Gpa]	Y'_s [Gpa]	b []	SR_{22} [1/sec]	SR_{12} [1/sec]	Y_0 [Gpa]	Y_c [Gpa]	Fail Loc.
PM67.2.v1	0.002395	0.00335	0.00600	0.190	0.00416	0.00213	0.00193	0.00071	4
PM67.2.v2	0.003254	0.00000	0.00544	2.482	0.00144	0.00441	0.00188	-0.00098	3
PM67.2.v3	0.009906	0.00655	0.01946	0.788	0.00530	0.02026	-0.00237	0.01218	NA
PM67.2.v4	0.002562	0.00002	0.00311	2.161	0.00066	0.00340	0.00115	0.00570	NA

Table 4.13: (continued)

ID	Y'_0 [Gpa]	Y'_c [Gpa]	Y'_s [Gpa]	b []	SR_{22} [1/sec]	SR_{12} [1/sec]	Y_0 [Gpa]	Y_c [Gpa]	Fail Loc.
PM67.2.v5	0.00287	0.00077	0.00417	0.691	0.00086	0.00195	0.00120	0.00018	2
PM67.2.v6	0.001055	-0.00007	0.00234	1.305	0.00102	0.00144	0.00097	0.00003	2
PM67.2.v7	0.003008	0.00019	0.00464	1.118	0.00166	0.00354	0.00146	0.00110	2
PM67.2.v10	0.007234	0.00019	0.00525	2.606	0.00029	0.00368	0.00138	0.00326	2
PM67.2.v11	0.002316	0.00100	0.00375	0.720	0.00275	0.00216	0.00110	0.00006	3
PM67.2.i1	0.002994	0.00165	0.00687	0.564	0.02219	0.02330	0.00162	0.00165	4
PM67.2.i2	0.003033	0.00056	0.00815	0.432	0.03000	0.02979	-0.00046	0.00723	3
PM67.2.i3	0.008064	-0.01024	0.00731	0.484	0.02896	0.02885	0.00381	-0.00511	NA
PM67.2.i4	0.000005	0.00000	0.00001	0.325	0.00004	0.00005	0.00000	0.00000	NA
PM67.2.i5	0.007845	-0.00918	0.00729	0.425	0.02865	0.02916	0.00387	-0.00475	2
PM67.2.i6	0.005805	-0.00607	0.00672	0.379	0.02714	0.02612	0.00272	-0.00290	2
PM67.2.i7	0.006226	-0.00821	0.00716	0.422	0.02546	0.02497	0.00283	-0.00425	2
PM67.2.i9	0.006705	-0.00934	0.00683	0.488	0.02666	0.02721	0.00330	-0.00534	2
PM67.2.i10	0.002212	0.00398	0.00575	0.403	0.02049	0.02251	0.00129	0.00201	2
PM67.2.i11	0.001342	0.00950	0.00554	0.332	0.02052	0.02259	0.00085	0.00471	3

Table 4.14: Mechanical properties as obtained from $[\pm 67.5^\circ]_{2s}$ Plytron laminate experimental results at 500[mm/min] crosshead displacement rate.

ID	Y'_0 [Gpa]	Y'_c [Gpa]	Y'_s [Gpa]	b []	SR_{22} [1/sec]	SR_{12} [1/sec]	Y_0 [Gpa]	Y_c [Gpa]	Fail Loc.
PM67.3.v2	0.001912	-0.00305	0.00585	0.288	0.00763	0.00573	0.00134	0.00043	3
PM67.3.v3	0.001588	0.00026	0.00253	0.309	0.00431	0.00732	0.00093	0.00010	2
PM67.3.v6	0.001034	-0.00002	0.00204	0.692	0.00534	0.00355	0.00080	0.00005	2
PM67.3.v9	0.00036	-0.00023	0.00238	0.127	0.00287	0.00199	0.00057	0.00002	2
PM67.3.v10	0.008009	0.00036	0.01431	2.157	0.00200	0.00549	0.00281	0.00361	2
PM67.3.i1	-0.001963	0.01861	0.00845	0.361	0.02512	0.02589	-0.00013	0.00986	3
PM67.3.i2	0.001971	0.01305	0.00855	0.396	0.02307	0.02569	0.00078	0.00863	3
PM67.3.i3	0.003151	0.00973	0.00808	0.383	0.02292	0.02417	0.00188	0.00599	2
PM67.3.i6	0.001219	0.01422	0.00937	0.368	0.03314	0.03275	0.00157	0.00682	2
PM67.3.i7	0.000058	0.01544	0.01311	0.321	0.04002	0.03914	0.00078	0.00869	2

Table 4.14: (continued)

ID	Y'_0 [Gpa]	Y'_c [Gpa]	Y'_s [Gpa]	b []	SR_{22} [1/sec]	SR_{12} [1/sec]	Y_0 [Gpa]	Y_c [Gpa]	Fail Loc.
PM67.3.i9	-0.006041	0.02973	0.01046	0.346	0.03824	0.03767	-0.00030	0.01154	2
PM67.3.i10	0.003669	0.00590	0.01146	0.317	0.03874	0.03681	0.00206	0.00428	2

4.4 Strain Rate Effect On Elastic Properties

Only the statistical analysis of the longitudinal tensile modulus will be presented in the main body of the work, so that the method and rigour of the procedure is presented. To avoid repetition, all the statistical results and data processing is given in the appendix D.

4.4.1 Longitudinal Tensile Modulus E_{11}.

Figure 4.14 is a plot of the longitudinal tensile modulus along direction 11 vs. strain rate and a quadratic model of the log of the strain rate are fitted. Those labeled observations were not included in the statistical treatment.

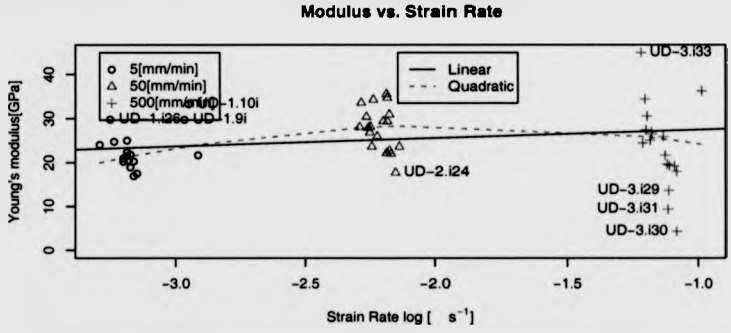

Figure 4.14: Longitudinal tensile modulus vs. logarithm of strain rate.

Statistics: Table 4.15 presents the statistics of the longitudinal tensile modulus at different crosshead displacement rates of unidirectional laminate composite material.

The mean of the longitudinal tensile modulus increases with an increase of the crosshead displacement rate from 5 to 50[mm/min]. Further increase of the crosshead displacement rate to 500[mm/min] results in a decrease for longitudinal tensile modulus compared to the 50[mm/min]

Table 4.15: Statistics for longitudinal tensile modulus at different crosshead displacement rates rates.

Crosshead Rate		5	50	500
Mean	[GPa]	21	28	25
Standard Deviation	[GPa]	2.4	4.4	5.6
Coef. of Variance	[]	0.12	0.16	0.22

value. The lowest standard deviation is observed at the 5[mm/min] crosshead displacement rate results and the highest is observed at the 500[mm/min] crosshead displacement rate. The coefficient of variance is lowest for the 5[mm/min] crosshead displacement rate and highest at the 500[mm/min] crosshead displacement rate however they are still in the same order of magnitude. The mean of the longitudinal tensile modulus appears to increase and then decrease, although the decrease can be explained statistically due to the scatter. The following tests are carried out to determine the strain rate sensitivity of the longitudinal tensile modulus.

Hypothesis testing: The null hypothesis (H_0) is that the longitudinal tensile modulus is not strain rate dependent. Therefore, the mean of the longitudinal tensile modulus for one crosshead displacement rate results should be equal to the mean of the longitudinal tensile modulus for another crosshead displacement rate, e.g. $H_0 : \overline{E}_{11,5} = \overline{E}_{11,50}$. The alternative hypothesis is that longitudinal tensile modulus is strain rate dependent, $H_0 : \overline{E}_{11,5} \neq \overline{E}_{11,50}$.

The statistics for the equality of means test are presented in table 4.16. The table presents the calculated test statistic t_0, the α-type error probability, the degrees of freedom df and the calculated critical value t_{crit}. Finally, the level of confidence is presented (i.e. the value of α-type error

probability for which the calculated critical value (t_{crit}) is equal to the statistic (t_0)). The use of the table is similar to the table 4.1 under §4.2.6.

Table 4.16: Hypothesis testing statistics for the equality of means of longitudinal tensile modulus.

Crosshead Rate	t_0	α	df	t_{crit}	Level
5 vs. 50	5.79	0.05	28	1.7	1
50 vs. 500	1.596	0.05	25	1.708	0.938
5 vs. 500	2.56	0.05	18	1.73	0.99

The longitudinal tensile modulus at 5[mm/min] crosshead displacement rate is statistically different to the other crosshead displacement rates at a 5% α-type error. Therefore, there is strong indication that longitudinal tensile modulus *is* dependent on the strain rate.

The statistics for the equality of variances test are presented in table 4.17. The table presents the calculated test statistic F_0, the α-type error probability, the degrees of freedom $df1$ and $df2$ and the calculated critical value F_{crit}. In the last column, the level of confidence is presented (i.e. the value of α-type error probability for which the calculated critical value (F_{crit}) is equal to the statistic (F_0)). The use of the table is similar to the table 4.2 under §4.2.7.

Table 4.17: Hypothesis testing for equality of variances statistics of longitudinal tensile modulus.

Crosshead Rate	F_0	α	df1	df2	F_{crit}	Level
5 vs. 50	3.303	0.05	18	14	2.499	0.983
50 vs. 500	1.62	0.05	14	18	2.353	0.826
5 vs. 500	5.35	0.05	14	14	2.577	0.998

The results presented in table 4.17 suggest that the variance of the longitudinal tensile modulus

at 5[mm/min]crosshead displacement rate is not equal to the variance of the 50 and 500[mm/min] crosshead displacement rates. This result is expected, because of the inherent problems encountered in strain rate testing.

Distribution: Figure 4.15 presents the probability density function plots of the longitudinal tensile modulus (E_{11}) at different crosshead displacement rates. Figure 4.15(a) present the p.d.f. of the complete data set. Figures 4.15 (b),(c) and (d) group the data set according to the crosshead displacement rate: 5, 50 and 500[mm/min] respectively.

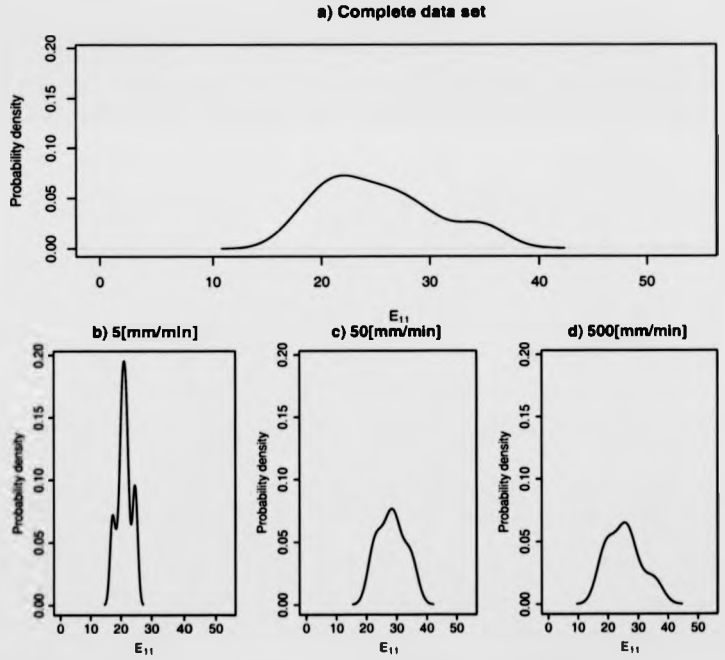

Figure 4.15: Density plots of the longitudinal tensile modulus at a) all displacement rates, and b),c) and d) at each different crosshead displacement rate separately.

The p.d.f. of the longitudinal tensile modulus which is presented in figure 4.15(a) appears to have a primary peak and two secondary points of inflection. The p.d.f. of the longitudinal tensile modulus grouped at different crosshead displacement rates appear to generally follow a normal distribution, and more specifically the p.d.f. of longitudinal tensile modulus results at 5 [mm/min] crosshead displacement rate (see figure 4.15(b)) appears to have two secondary peaks. The p.d.f. of longitudinal tensile modulus results at 50 and 500 [mm/min] crosshead displacement rate(see figure 4.15(c) and 4.15(d) respectively) appear to follow a slightly skewed distribution with a primary peak and 2 secondary points of inflection.

The χ^2 Goodness of Fit test [176, sec.11-11] is used to determine whether the results of the longitudinal tensile modulus for each strain rate are adequately described by a normal distribution. The procedure requires computation of the chi-squared statistic (see equation 4.2 for continuous distributions:

$$\chi_0^2 = \sum_{i=1}^{8} \frac{(O_i - E_i)^2}{E_i} \tag{4.2}$$

where:

E_i: are the expected frequencies of the hypothesised (normal) distribution of the i-th class interval.

O_i: are the observed frequencies in the i-th class interval.

Class intervals: If the mean and standard deviations are known for a continuous distribution, the common practice for construction of class intervals is to select the cell boundaries so that the expected frequencies are equal for all cells[170]. The observed frequencies use the same cell boundaries.

The computed values of the χ_0^2 statistic for the complete data set and for the different crosshead

displacement rates are presented in table 4.18.

Table 4.18: Statistics for the Goodness-of-Fit of longitudinal tensile modulus probability density distribution.

Crosshead Rate	χ_0^2	α	# of Classes	χ_{crit}^2	Level
ALL	4.087	0.05	6	7.815	0.748
5	3.14	0.05	6	7.81	0.63
50	4	0.05	6	7.815	0.739
500	4	0.05	6	7.815	0.739

If the computed χ_0^2 statistic is smaller than the χ_{crit}^2 the conclusion is that there is no reason to believe that the distribution of the longitudinal tensile modulus results is *not* normally distributed. Therefore, according to the data presented in table 4.18, the longitudinal tensile modulus results appears to follow the normal distribution. However, this may be attributed to the fact that beyond 50[mm/min] crosshead displacement rate the longitudinal tensile modulus does not exhibit statistically significant strain rate dependency.

Model fitting: A linear model of the longitudinal tensile modulus with respect to the logarithm of the strain rate has the following form:

$$E_{11}(\dot{\varepsilon}_{11}) = 29.31 + 1.88 \cdot \log_{10}(\dot{\varepsilon}_{11}) \tag{4.3}$$

A quadratic model of the longitudinal tensile modulus with respect to the logarithm of the strain rate has the following form:

$$E_{11}(\dot{\varepsilon}_{11}) = 10.68 - 18.21 \cdot \log_{10}(\dot{\varepsilon}_{11}) - 4.68 \cdot \log_{10}(\dot{\varepsilon}_{11})^2 \tag{4.4}$$

The *null* hypothesis for the analysis of variance is that the linear model explains the behaviour as adequately as the quadratic model. The statistics for the comparison of the two strain rate models of the longitudinal tensile modulus are presented in table 4.19. The probability that the null hypothesis is true but is rejected nevertheless, is only 0.06% (see table table 4.19). Therefore the null hypothesis can be rejected, i.e. the equation for the quadratic model (eq. 4.4) describes better the given set of results.

Table 4.19: ANOVA results for the selection of the strain rate model order for the longitudinal tensile modulus.

Model	Res.Df	RSS	Df	Sum of Sq	F	$Pr(>F)$
Linear	44	1114				
Quadratic	43	849	1	265	13.4	0.00068

The coefficient of determination R^2 for the quadratic model of the longitudinal tensile modulus with respect to the logarithm of the strain rate is 0.269. The R^2 gives a metric of the amount of variability in the data explained or accounted for by the regression model. Therefore in this case 26.9% of the variability in the data is accounted for by the model[4]. It might appear at first sight that the quadratic model fits the data set adequately for the data sets tested.

It is the author's opinion that there will be upper and lower limits for the longitudinal tensile modulus for a wider range of strain rates. The linear and the regression model are abstract mathematical concepts easy to handle for regression analysis purposes, however they have no limit

[4]Normally the coefficient of determination increases as the number of terms added to the model increases (i.e. perfect fit for a *n-1* polynomial). In the confines of this work, an adjusted value of the coefficient of determination is used which takes into account the number of degrees of freedom.

(the quadratic has neither an upper nor a lower limit). For example using the linear model and using a value of strain rate equal to $10^{-15.59}$[1/s] (or lower) would result in prediction of a zero (or negative) longitudinal tensile modulus[5]. Respectively for the quadratic model, using a strain rate value of .5[1/s] (or higher) would result to a value of longitudinal tensile modulus equal to zero (or negative). Therefore, the linear and quadratic models may not necessarily be appropriate, if the model is applied beyond its validated range.

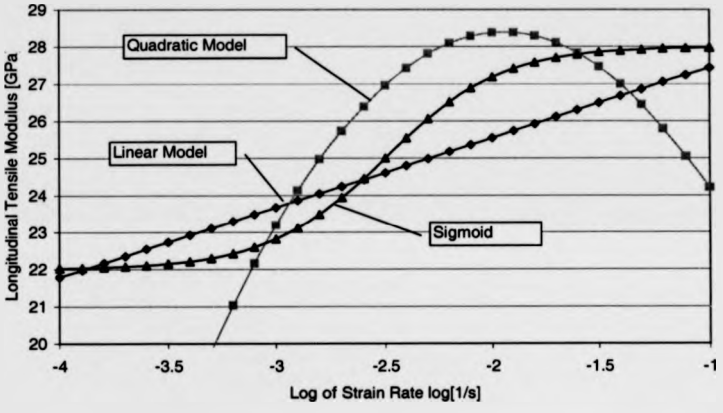

Figure 4.16: Various curve fitted models to experimental data.

In figure 4.16, three different models are proposed, a linear, a quadratic and a sigmoid. It is the author's opinion, that the sigmoid model is more appropriate for describing the strain rate dependency of the longitudinal tensile modulus, and in general the mechanical properties. However, it may be costly to calibrate the model, requiring tests over a wider range of strain rates.

Finally, the author considers that the longitudinal tensile modulus does increase linearly between 5 and 50[mm/min] crosshead displacement rate. Beyond the 50[mm/min] crosshead displacement

[5] However from a philosophical point of view one might argue that extremely low strain rates are equivalent to degradation imposed by corrosion and disintegration over time, which leaves a material with no stiffness.

rate a slight decrease is observed at 500[mm/min] crosshead displacement rate. However, a difference between 50 and 500[mm/min] crosshead displacement rate is not statistically significant, whilst the 5 and 500[mm/min] crosshead displacement rates are statistically different.

4.4.2 Transverse Tensile Modulus E_{22}

Figure 4.17 is a plot of the transverse tensile modulus vs. strain rate and two models (a linear and a quadratic model) of the logarithm of the strain rate are fitted. Those labeled observations on figure 4.17 were regarded outliers and were not included in the statistical treatment. It should be noted that the linear model appears almost like a flat line, suggesting no strain rate sensitivity.

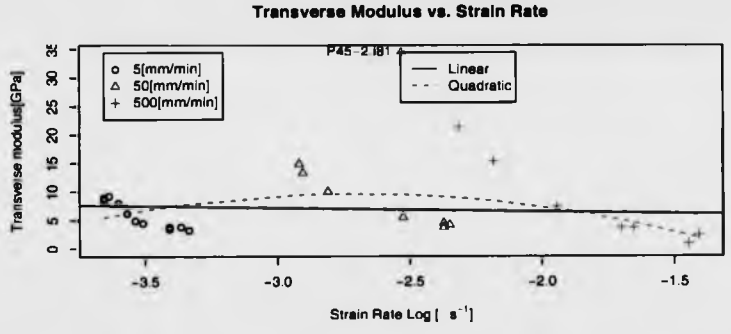

Figure 4.17: Transverse tensile modulus vs. logarithm of strain rate as obtained from the tensile testing of a $[+45]_8$ laminate.

One important feature of the graph is that for a given crosshead displacement rate the transverse failure strength increases for increasing values of the calculated strain rate. This is attributed to the fact that specimens with lower transverse tensile modulus deform more and as a result a higher level of strain rate is calculated.

Statistics: Table 4.20 presents the statistics of the transverse tensile modulus at different crosshead displacement rates as obtained from a $[+45]_8$ laminate.

Table 4.20: Statistics for the transverse tensile modulus at different crosshead displacement rates as obtained from a $[+45]_8$ laminate.

Crosshead Rate		5	50	500
Mean	[GPa]	5.8	8	7.8
Standard Deviation	[GPa]	2.4	4.7	7.6
Coef. of Variance	[]	0.41	0.59	0.98

The mean of the transverse tensile modulus appears to initially increase for increasing crosshead displacement rate and the decrease for further increase - suggesting that there is no constant trend. The standard deviation of the transverse tensile modulus is lowest at the 5[mm/min] crosshead displacement rate. The coefficient of variance is lowest for the 5[mm/min] crosshead displacement rate and highest at the 500[mm/min] crosshead displacement rate.

No strain rate sensitivity could be determined statistically (see appendix §D.3.2.1 for detailed statistical analysis), therefore the transverse tensile modulus mean of all observed values is proposed as the value of the transverse tensile modulus at all crosshead displacement rates. The calculated value is 7.0[GPa].

4.4.3 Shear Modulus G_{12}

Figure 4.18 is a plot of the Shear modulus vs. shear strain rate and two models (a linear and a quadratic model) of the logarithm of the shear strain rate are fitted. Those labeled observations on figure 4.18 were regarded outliers and were not included in the subsequent statistical treatment.

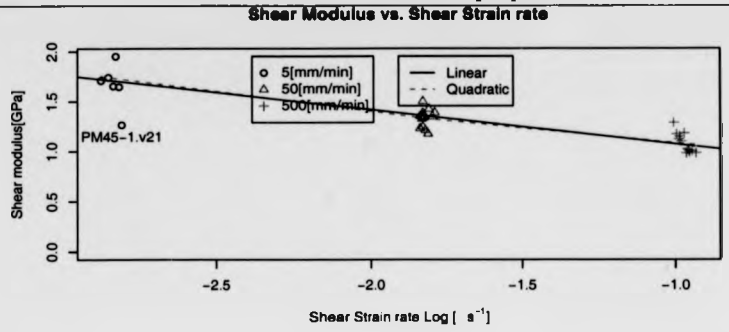

Figure 4.18: Shear modulus vs. logarithm of shear strain rate as obtained from the tensile testing of a $[\pm 45]_{2s}$ laminate.

Statistics: Table 4.21 presents the statistics of the shear modulus at different crosshead displacement rates as obtained from a $[\pm 45]_{2s}$ laminate.

Table 4.21: Statistics for shear modulus at different crosshead displacement rates as obtained from a $[\pm 45]_{2s}$ laminate.

Crosshead Rate		5	50	500
Mean	[GPa]	1.74	1.33	1.08
Standard Deviation	[GPa]	0.12	0.092	0.098
Coef. of Variance	[]	0.071	0.069	0.091

The mean of the shear modulus appears to decrease for increasing crosshead displacement rate. The standard deviation of the 50[mm/min] is the lowest. The standard deviation is lowest for the 50[mm/min] crosshead displacement rate and highest for the 5[mm/min] crosshead displacement rate. Similarly the coefficient of variance is lowest at the 50[mm/min] crosshead displacement rate and highest at 500[mm/min] crosshead displacement rate.

Model fitting: A linear model of the shear modulus with respect to the logarithm of the shear strain rate has the following form:

$$G_{12}(\dot{\gamma}_{12}) = 0.731 - 0.344 \cdot \log_{10}(\dot{\gamma}_{12}) \tag{4.5}$$

This is supported by figure 4.18, where it can be seen that the shear modulus decreases linearly. The coefficient of determination R^2 value for the linear model is 0.85, which is very high, and indicates good correlation.

It is noteworthy that this linear model cannot be extrapolated to strain rates beyond the validated range. Similar to the discussion in §4.4.1, there is a physical limit to the decrease of the shear modulus as strain rate becomes insignificant.

4.4.4 Major Poisson's ratio v_{12}

Figure 4.19 is a plot of the Major Poisson's ratio along vs. strain rate log and a linear and a quadratic model of the log of the strain rate are fitted. Those labeled observations have been identified as outliers and have not be included in the statistical treatment.

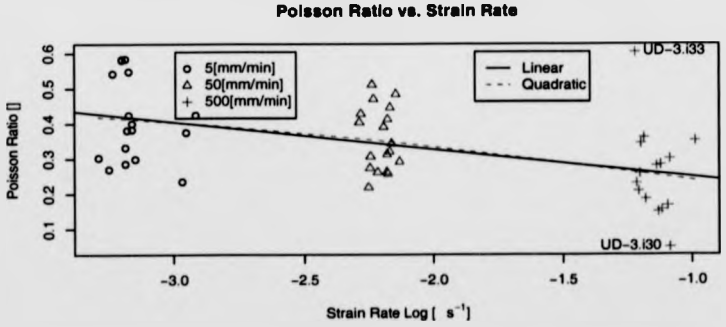

Figure 4.19: Major Poisson's ratio vs. strain rate logarithm.

Statistics: Table 4.22 presents the statistics of the major Poisson's ratio at different crosshead displacement rates of unidirectional laminate composite material.

Table 4.22: Statistics for the major Poisson's ratio at different crosshead displacement rates.

Crosshead Rate		5	50	500
Mean	[]	0.41	0.36	0.25
Standard Deviation	[]	0.12	0.09	0.076
Coef. of Variance	[]	0.29	0.25	0.30

The mean of the major Poisson's ratio appears to decrease and for increasing displacement rate. The standard deviation is lowest again for the 500[mm/min] crosshead displacement rate and highest at the 5 [mm/min] crosshead displacement rate. The lowest coefficient of variance is for the 50[mm/min] crosshead displacement rate and highest at the 500 [mm/min] crosshead displacement rate, however the figures are quite comparable indicating that the scatter of the results is comparable.

A linear model of the major Poisson's ratio with respect to the logarithm of the longitudinal strain rate was fitted the following form:

$$\nu_{12}(\dot{\varepsilon}_{11}) = 0.1716 - 0.0777 \cdot \log_{10}(\dot{\varepsilon}_{11}) \tag{4.6}$$

The coefficient of determination R^2 value for the quadratic model is .282. The low value of R^2 is because of the high scatter observed at each crosshead displacement rate. The statistical analysis of the major Poisson's ratio data (see appendix §D.1.2.1) indicated that only the 500[mm/min] crosshead displacement rate was statistically different. Therefore, at 5 and 50[mm/min] the value of the major Poisson's ratio remains unchanged, while further increase of the crosshead displacement

rate results in a statistically significant decrease. Again, it is obvious that the major Poisson's ratio has a physical lower limit[6] which in this case would be zero, therefore the rate of decrease should tail off.

4.5 Strain Rate Effect On Strength Properties

4.5.1 Longitudinal Tensile Failure Strain $\varepsilon_{11,f}$

Figure 4.20 is a plot of the longitudinal tensile failure strain vs. strain rate log and a linear and a quadratic model of the log of the strain rate are fitted. Those labeled observations has been identified as an outlier and has not been included in the statistical treatment. Both fitted models suggests that there is an increase of the longitudinal tensile failure strain with increasing strain rate.

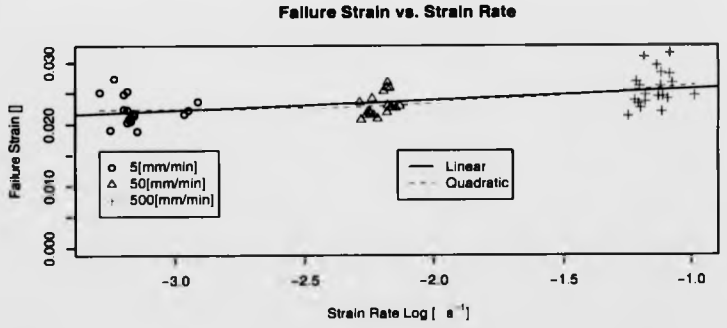

Figure 4.20: Longitudinal tensile failure strain vs. strain rate logarithm.

[6]Auxetic materials have negative major Poisson's ratio, due to their unique internal structure

Statistics: Table 4.23 presents the statistics of failure strain at different crosshead displacement rates of unidirectional laminate composite material.

Table 4.23: Statistics for the failure strain at different crosshead displacement rates

Crosshead Rate		5	50	500
Mean	[]	0.022	0.023	0.026
Standard Deviation	[]	0.0023	0.0018	0.0028
Coef. of Variance	[]	0.104	0.077	0.11

The mean of the longitudinal tensile failure strain increases with increasing crosshead displacement rate. The standard deviation is lowest for the 50[mm/min] crosshead displacement rate results and highest for the 500 [mm/min] crosshead displacement rate. Similarly, the coefficient of variance is lowest for the 50[mm/min] crosshead displacement rate results and highest at the 500 [mm/min] crosshead displacement rate.

The statistical analysis indicated that only the longitudinal tensile failure strain 500[mm/min] crosshead displacement rate was statistically different to the longitudinal tensile failure strain at other crosshead displacement rates. The longitudinal tensile failure strain exhibits strain rate dependency beyond the 50[mm/min] crosshead displacement rate.

Model fitting: A linear model of the failure strain with respect to the logarithm of the strain rate has the following form:

$$\varepsilon_{11,f}(\dot{\varepsilon}_{11}) = 0.0274 + 0.00172 \cdot \log_{10}(\dot{\varepsilon}_{11}) \tag{4.7}$$

The coefficient of determination R^2 value for the linear model for failure strain is 0.26. This value

is low, which is to be expected since the longitudinal tensile failure strain was only proven to be strain rate dependent above 500[mm/min] crosshead displacement rate. However, the high values of the test of hypotheses (see appendix §D.1.3.1), suggest that the longitudinal failure is strain rate dependent.

4.5.2 Longitudinal Tensile Failure Stress $\sigma_{11,f}$.

Figure 4.21 is a plot of the longitudinal tensile failure stress vs. strain rate log and a linear and a quadratic model of the log of the strain rate are fitted.

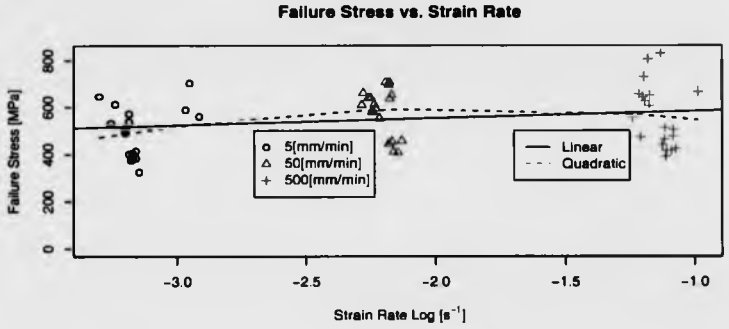

Figure 4.21: Longitudinal tensile failure stress vs. strain rate logarithm.

It is noteworthy that at each crosshead displacement rate two different groups can be discerned. It is also possible to identify them in the probability distribution functions (see appendix§D.1.3.2). The groupings are attributed to variability in manufacture.

Statistics: Table 4.24 presents the statistics of the tensile failure stress at different crosshead displacement rates of unidirectional laminate composite material.

The mean of the longitudinal tensile failure stress increases initially for increasing crosshead dis-

Table 4.24: Statistics for the longitudinal tensile failure stress at different crosshead displacement rates.

Crosshead Rate		5	50	500
Mean	[MPa]	496	581	564
Standard Deviation	[MPa]	110	100	133
Coef. of Variance	[]	0.22	0.17	0.24

placement rate from 5 to 50[mm/min]. Further increase of the crosshead displacement rate to 500[mm/min] crosshead displacement rate resulted in a decrease of the longitudinal tensile failure stress. In figure 4.21, both models appear to increase for increasing strain rate. The standard deviation is lowest for the 50[mm/min] crosshead displacement rates and highest at the 500 [mm/min] crosshead displacement rate. Similarly, the coefficient of variance is lowest for the 50[mm/min] crosshead displacement rate and highest at the 500 [mm/min] crosshead displacement rate.

Model fitting: A linear model of the longitudinal tensile failure stress with respect to the logarithm of the strain rate has the following form:

$$\sigma_{11}(\dot{\varepsilon}_{11}) = 612 + 29 \cdot \log_{10}(\dot{\varepsilon}_{11}) \tag{4.8}$$

The coefficient of determination R^2 value for the linear model is 0.0247, which is extremely low. The fitted model only explains 2.47% of the variability of the data. Therefore, other factors (like choice of manufacturing route) effect the longitudinal tensile failure stress more significantly. This outcome indicates the importance of manufacturing quantity on the material properties.

Despite the fact that the variability was significant, the statistical process captured the strain rate dependency. This is supported by figure 4.21 where it is possible to observe that the highest values

of longitudinal tensile failure stress for each crosshead displacement rate appear to increase with strain rate.

This outcome is in agreement with most of the research work on strain rate dependency of glass fibre composite systems.

4.5.3 Transverse Tensile Failure Strain $\varepsilon_{22,f}$

Figure 4.22 is a plot of the transverse tensile failure strain vs. strain rate log and a linear and a quadratic model of the log of the strain rate is fitted.

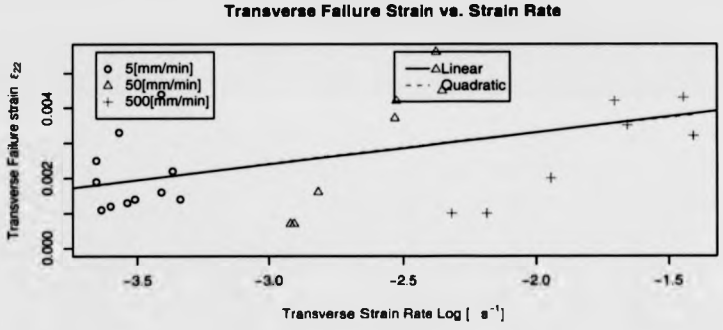

Figure 4.22: Transverse tensile failure strain vs. strain rate logarithm.

One important feature of the graph is that for a given crosshead displacement rate the transverse tensile failure strain increases for increasing values of the calculated strain rate. This is attributed to the fact that the specimens at a given crosshead displacement rate fail at the same stress. Higher observed values of the strain rate are equivalent to lower modulus. The assumption of Hooke's law[7] suggests that for lower modulus specimens, higher strains are required to obtain a given stress level.

[7]Hooke's law is suitable for the transverse properties because of the linear/brittle failure of the material.

Statistics: Table 4.25 presents the statistics of transverse tensile failure strain at different crosshead displacement rates.

Table 4.25: Statistics for the transverse tensile failure strain at different crosshead displacement rates

Crosshead Rate	5	50	500	
Mean	[]	0.0027	0.0033	0.0024
Standard Deviation	[]	0.0012	0.002	0.0015
Coef. of Variance	[]	0.47	0.60	0.62

The mean of transverse tensile failure strain initially increases for increasing crosshead displacement rate and decreases for increasing crosshead displacement rate. The standard deviation is lowest at the 5[mm/min] crosshead displacement rate and highest at the 50[mm/min] crosshead displacement rate. The coefficient of variance is lowest at the 5 [mm/min] crosshead displacement rate and highest at the 500[mm/min] crosshead displacement rate.

The transverse tensile failure strain at different crosshead displacement was not statistically different, despite the fact that both the fitted models exhibited an increase with strain rate in the figure 4.22. This is attributed to manufacturing and also in the instrumentation, due to the very low strains to failure which can be observed for this class of laminates.

Since no strain rate dependency was statistically determined for the transverse tensile failure strain, the mean value of the complete data set is used. This value was computed 0.0028[].

4.5.4 Transverse Tensile Failure Stress $\sigma_{22,f}$

Figure 4.23 is a plot of the transverse tensile failure stress vs. strain rate log and a linear and a quadratic model of the log of the strain rate is fitted. Those labeled observations are removed as outliers from the statistical treatment.

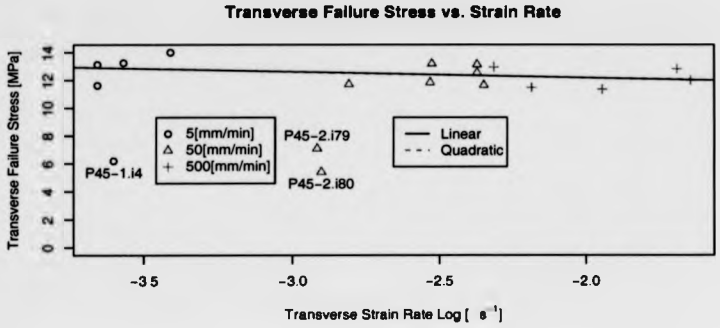

Figure 4.23: transverse tensile failure stress vs. strain rate logarithm.

It should be noted that the specimens which failed prematurely were already removed from the analysis. However, three distinct values between 5 an 6[MPa] (1 for the 5[mm/min] and 2 for the 50[mm/min] crosshead displacement rates) may be observed. These values are attributed to manufacturing inconsistencies, i.e. resin rich areas. This observation indicates the importance of manufacturing route to the strength properties of these materials.

Statistics: Table 4.26 presents the statistics of transverse tensile failure stress at different crosshead displacement rates of $[+45]_8$ laminate.

The mean of transverse tensile failure stress decreases for increasing crosshead displacement rate. The standard deviation is lowest at the 50[mm/min] crosshead displacement rate and highest at the 5[mm/min] crosshead displacement rate. The coefficient of variance is lowest for the 50[mm/min]

Table 4.26: Statistics for the transverse tensile failure stress at different crosshead displacement rates

Crosshead Rate		5	50	500
Mean	[MPa]	13	12	12
Standard Deviation	[MPa]	1.0	0.7	0.7
Coef. of Variance	[MPa]	0.076	0.057	0.061

crosshead displacement rate and highest for the 5[mm/min] crosshead displacement rate.

The transverse tensile failure stress at different crosshead displacement was not statistically different, which is in accordance to observations in the figure 4.23.

Since no strain rate dependency was statistically determined for the transverse tensile failure stress, the mean value of the complete data set is used. This value was computed 12.4[MPa].

4.5.5 Shear Failure Strain $\gamma_{12,f}$

Figure 4.24 is a plot of the shear failure strain vs. shear strain rate log and a linear and a quadratic model of the log of the shear strain rate is fitted. The fitted models indicate that there is little or no strain rate sensitivity.

Statistics: Table 4.27 presents the statistics of shear failure strain at different crosshead displacement rates of $[\pm 45°]_{2s}$ laminate.

The mean of shear failure strain decreases from 44% to 41% and further inreases to 42% for increasing crosshead displacement rate. The standard deviation is lowest at the 500[mm/min] crosshead displacement rate and is highest at the 5 and 50[mm/min] crosshead displacement rate.

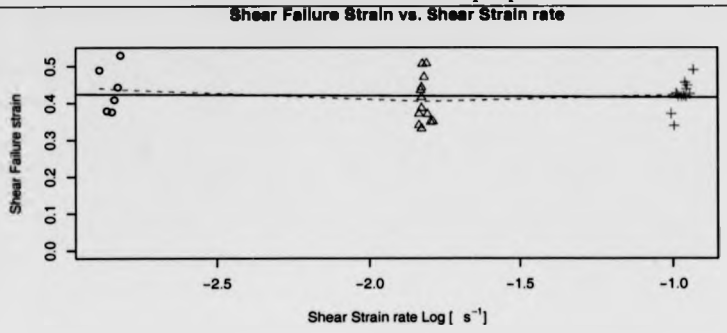

Figure 4.24: Shear failure strain of vs. shear strain rate logarithm.

Table 4.27: Statistics for the shear failure strain at different crosshead displacement rates

Crosshead Rate		5	50	500
Mean	[]	0.44	0.41	0.42
Standard Deviation	[]	0.062	0.062	0.037
Coef. of Variance	[]	0.141	0.152	0.087

The coefficient of variance is lowest for the 500 [mm/min] crosshead displacement rate and highest for the 50[mm/min] crosshead displacement rate.

However, the statistical analysis showed that the variations of the failure strain did not appear to be statistically significant.

Model fitting: The shear failure strain at different crosshead displacement was not statistically different, which is in accordance to observations in the figure 1.24.

Since no strain rate dependency was statistically determined for the shear failure stress, the mean value of the complete data set is used. This value was computed 42[].

4.5.6 Shear Failure Stress $\tau_{12,f}$

Figure 4.25 is a plot of the shear failure stress vs. shear strain rate log and a linear and a quadratic model of the log of the shear strain rate are fitted. Those labeled observations were regarded outliers and were not included in the subsequent statistical treatment. The fitted models suggest that there is an increase of the shear strain at failure.

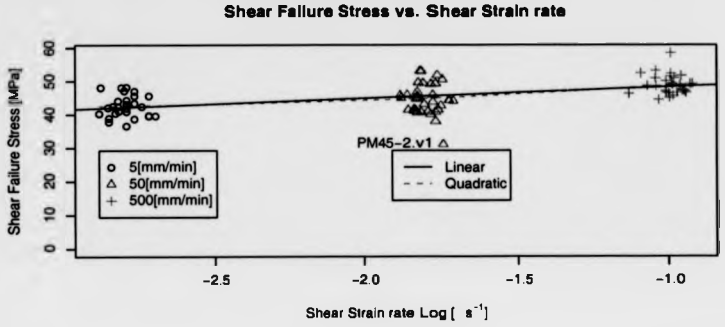

Figure 4.25: Shear failure stress vs. shear strain rate logarithm.

Statistics: Table 4.28 presents the statistics of the shear failure stress at different crosshead displacement rates.

Table 4.28: Statistics for the shear failure strain at different crosshead displacement rates.

Crosshead Rate		5	50	500
Mean	[GPa]	42	45	49
Standard Deviation	[GPa]	3.3	4	2.9
Coef. of Variance	[GPa]	0.078	0.089	0.059

The mean of the shear failure stress increases with crosshead displacement rate. The standard

deviation of the shear failure stress at 500[mm/min] crosshead displacement rate is lowest and the highest standard deviation for the shear failure stress is at the 50[mm/min] crosshead displacement rate. Similarly the lowest coefficient of variance of the shear failure stress is at 500[mm/min] crosshead displacement rate and the highest is at 50[mm/min] crosshead displacement rate.

The statistical analysis confirmed that the shear failure stress is statistically different at all crosshead displacement rates.

Model fitting: A linear model of the shear failure stress with respect to the logarithm of the shear strain rate has the following form:

$$\tau_{12}(\dot{\gamma}_{12}) = 51.81 + 3.44 \cdot \log_{10}(\dot{\gamma}_{12}) \tag{4.9}$$

The coefficient of determination R^2 value for the linear model is 0.341. Although, the increase does not appear to be significant, the level of confidence from the statistical analysis was significant. When this result is viewed in conjunction with the results for the shear failure strain and shear modulus, an inconsistency appears. Although the initial modulus appears to decrease and the shear failure strain remains constant, the shear failure stress appears to increase. The observed increase of the shear failure stress can only be attributed to the damage evolution of the shear modulus. This is a first indication that the shear damage evolution is strain rate dependent.

4.6 Strain Rate Effect On Shear Damage Evolution

It is pertinent at this stage to review the shear damage evolution characterisation parameters in brief.

The critical shear damage limit is a quantity related to the rate of damage development. In

figure 4.26 the relationship is given. The figure presents the shear damage (degradation of shear modulus) vs. the shear damage pseudo-force. The pseudoforce describes the elastic shear energy density stored in the specimen. Historically, this is the convention that the Master Damage Curves are presented[108]. The initial and critical shear damage limit are defined as intercept and slope of the Shear pseudoforce (as ordinate) vs shear damage (as abscissa). It is noteworthy that the ordinate and the abscissa are reversed compared to figure 4.26. Therefore, high values of the critical shear damage limit are equal to low rate of damage evolution.

Similar to the discussion under §4.4.1, there is a lower and an upper limit for the rate of damage evolution. According to Iannucci[21], the rate of damage evolution limit is determined by the speed of sound through the material.

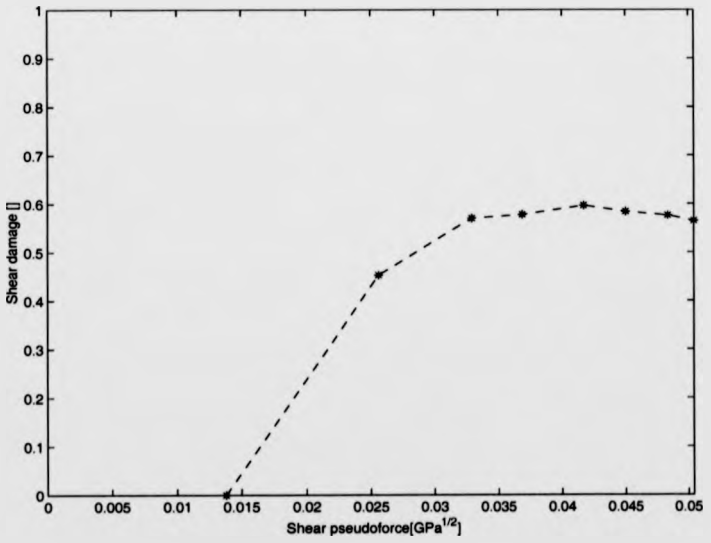

Figure 4.26: Master Shear Damage Law Graph for thermoplastic.

Figure 4.26 reveals another issue. The global composite ply model §2.5.4.2 was created for ther-

moset composite which exhibit a more brittle behaviour. For those materials, the relationship between shear damage and shear pseudoforce is linear. The initial shear damage limit represents the amount of energy stored/absorbed before degradation is initiated for thermosetting materials

.

It can be observed in the figure 4.26 that, the relationship of shear damage and shear pseudoforce for a thermoplastic composite material is highly non linear. This is attributed to the ductility of the thermoplastic matrix. The shear elastic properties of the thermoplastic matrix degrade linearly with increasing shear pseudoforce. Once a critical value of the shear pseudoforce is reached, the damage evolution stops. This is attributed to scissoring of the fibres.

The nonlinearity of the Master Shear Damage Curve for thermoplastic composite materials has a significant effect on the initial shear damage limit. Because the initial shear damage limit is a quantity originally conceived for the description of a linear behaviour, its application to a non linear relationship is dependent on other factors (i.e. the slope/rate of the curve and the maximum shear pseudoforce). Therefore, the initial shear damage limit is only an approximation the amount of energy stored/absorbed before degradation is initiated for thermosetting materials.

4.6.1 Initial Shear Damage Limit Value Y_0

Figure 4.27 is a plot of the initial shear damage limit value vs. shear strain rate log and a linear and a quadratic model of the log of the shear strain rate is fitted. Those labeled observations were regarded outliers and were not included in the subsequent statistical treatment.

Statistics: Table 4.29 presents the statistics of the initial shear damage limit value at different crosshead displacement rates .

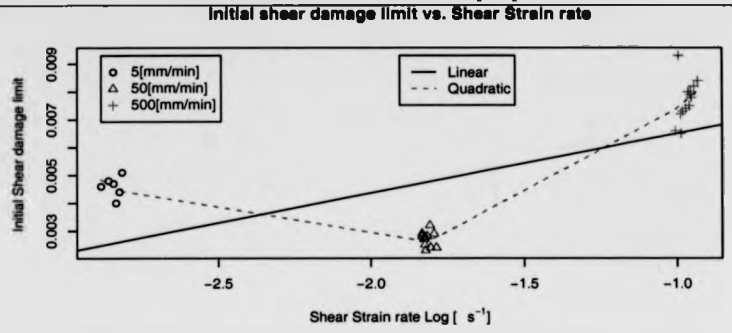

Figure 4.27: Initial shear damage limit value vs. shear strain rate logarithm.

Table 4.29: Statistics for the initial shear damage limit value at different crosshead displacement rates.

Crosshead Rate		5	50	500
Mean	$[\sqrt{GPa}]$	0.0046	0.0027	0.0077
Standard Deviation	$[\sqrt{GPa}]$	0.00037	0.00025	0.00075
Coef. of Variance	[]	0.0813	0.0948	0.0972

The mean of the initial shear damage limit value appears to decrease initially for increasing crosshead displacement rate from 50 to 500[mm/min] crosshead displacement rate. Further increase to 500[mm/min] crosshead displacement rate results to a significant increase of the mean value of the shear damage limit value. The standard deviation of the initial shear damage limit value is lowest at the 50[mm/min] displacement rate and highest at the 500[mm/min] displacement rate. The coefficient of variance is the lowest for the 5[mm/min] crosshead displacement rate, and highest for the 500[mm/min] crosshead displacement rate.

The statistical analysis of the initial transverse damage limit at different crosshead displacement found it to be statistically different between all possible pairs, with a high degree of confidence.

Model fitting: A quadratic model of the Initial shear damage limit value with respect to the logarithm of the shear strain rate has the following form:

$$Y_0(\dot{\gamma}_{12}) = 0.021 + 0.018 \cdot \log_{10}(\dot{\gamma}_{12}) + 0.0042 \cdot \log_{10}(\dot{\gamma}_{12})^2 \tag{4.10}$$

The coefficient of determination R^2 value for the linear model is 0.955. This is a very high value which indicates good correlation between the model and the physical measurements. This in conjunction with the statistical analysis results suggest that the initial shear damage limit is strain rate dependent.

The decrease of the initial shear damage value at 50[mm/min] crosshead displacement rate has not been explained. However, it is obvious from the results that there is small margin attributed to error. Therefore, the hypothesis which forms takes into consideration the discussion on the effect of the critical Y_c and elementary Y_R shear damage limit on the initial shear damage limit Y_c are taken into consideration. At this point the discussion will continue with the presentation of the statistical results for the critical Y_c and elementary Y_R shear damage limit, and the discussion on the inconsistency of the initial shear damage limit Y_0 is resumed at the end of section §8.1.3.

4.6.2 Critical Shear Damage Limit Value Y_c

Figure 4.28 is a plot of the critical shear damage limit value vs. shear strain rate log and a linear and a quadratic model of the log of the shear strain rate is fitted. Those labeled observations were regarded outliers and were not included in the subsequent statistical treatment. The fitted models suggest that the critical shear damage increases for increasing strain rate.

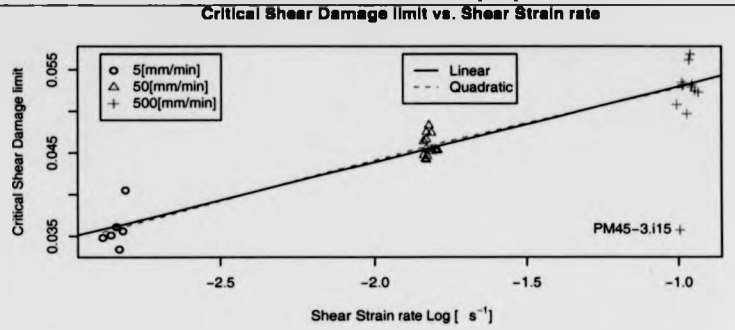

Figure 4.28: Critical shear damage limit value vs. shear strain rate logarithm.

Statistics: Table 4.30 presents the statistics of the critical shear damage limit value at different crosshead displacement rates.

Table 4.30: Statistics for the critical shear damage limit value at different crosshead displacement rates.

Crosshead Rate		5	50	500
Mean	$[\sqrt{GPa}]$	0.036	0.046	0.053
Standard Deviation	$[\sqrt{GPa}]$	0.0024	0.0013	0.002
Coef. of Variance	[]	0.0675	0.029	0.037

The mean of the critical shear damage limit value appears to increase for increasing crosshead displacement rate. The standard deviation of the critical shear damage limit value is lowest at the 50[mm/min] displacement rate and highest at the 5[mm/min] displacement rate. Similarly, the coefficient of variance is lowest at the 50[mm/min] crosshead displacement rate, and highest at the 5[mm/min] crosshead displacement rate.

The statistical analysis confirmed that the critical shear damage is statistically different at different

crosshead displacement rates.

Model fitting: A linear model of the critical shear damage limit value with respect to the logarithm of the shear strain rate has the following form:

$$Y_c(\dot{\gamma}_{12}) = 0.062 + 0.0091 \cdot \log_{10}(\dot{\gamma}_{12}) \tag{4.11}$$

The coefficient of determination R^2 value for the linear model is 0.927. This is a high value which indicates good correlation between the model and the physical measurements. This in conjunction with the statistical analysis results suggest that the initial shear damage limit is strain rate dependent.

4.6.3 Elementary Shear Damage Limit Value Y_R

Figure 4.29 is a plot of the elementary shear damage limit value vs. shear strain rate log and a linear and a quadratic model of the log of the shear strain rate is fitted. Those labeled observations were regarded outliers and were not included in the subsequent statistical treatment. The fitted models suggest that the elementary shear damage increases for increasing strain rate.

Statistics: Table 4.31 presents the statistics of the elementary shear damage limit value at different crosshead displacement rates.

The mean of the elementary shear damage limit value appears to increase for increasing crosshead displacement rate. The standard deviation of the elementary shear damage limit value is lowest at the 50[mm/min] displacement rate and highest at the 500[mm/min] displacement rate (nearly 7 fold increase). The coefficient of variance is lowest for the 50[mm/min] crosshead displacement rate, and it is highest at the 5[mm/min] crosshead displacement rate.

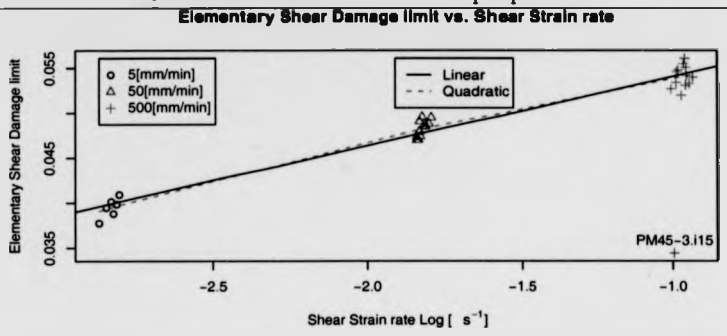

Figure 4.29: Elementary shear damage limit value vs. shear strain rate logarithm.

Table 4.31: Statistics for the elementary shear damage limit value at different crosshead displacement rates.

Crosshead Rate		5	50	500
Mean	$[\sqrt{GPa}]$	0.04	0.048	0.054
Standard Deviation	$[\sqrt{GPa}]$	0.0011	0.0009	0.0012
Coef. of Variance	[]	0.028	0.019	0.022

The statistical analysis confirmed that the critical shear damage is statistically different at different crosshead displacement rates.

Model fitting: A quadratic model of the elementary shear damage limit value with respect to the logarithm of the shear strain rate has the following form:

$$Y_R(\dot{\gamma}_{12}) = 0.059 + 0.0043 \cdot \log_{10}(\dot{\gamma}_{12}) - 0.00092 \cdot \log_{10}(\dot{\gamma}_{12})^2 \tag{4.12}$$

The coefficient of determination R^2 value for the quadratic model is 0.966. This is a very high value which indicates good correlation between the model and the physical measurements. This in conjunction with the statistical analysis results suggest that the initial shear damage limit is

strain rate dependent.

4.7 Strain Rate Effect On Transverse Damage Evolution

The transverse damage evolution characterisation parameters are briefly reviewed. As with the respective shear damage evolution parameters, the initial and critical transverse damage limit are defined as intercept and slope of the transverse pseudoforce vs transverse damage. Again, high values of the critical transverse damage limit are equal to a low rate of transverse damage evolution. Also, high values of the initial transverse damage limit indicate a delayed degradation of properties.

4.7.1 Initial Transverse Damage Limit Y_0'

Figure 4.30 is a plot of the initial transverse damage limit vs. strain rate and two models (a linear and a quadratic model) of the logarithm of the strain rate are fitted. Those labeled observations on figure 4.30 were regarded outliers and were not included in the statistical treatment. It is noteworthy that the results for the initial transverse damage limit at 50 and 500[mm/min] crosshead displacement rate appear to be similar order of magnitude.

Statistics: Table 4.32 presents the statistics of the initial transverse damage limit at different crosshead displacement rates as obtained with the $[\pm 67]_{2s}$ laminate.

The mean of the initial transverse damage limit appears to increase for increasing crosshead displacement rate and then decrease. The standard deviation of the 5[mm/min] crosshead displacement rate is the lowest and is highest at the 5[mm/min] crosshead displacement rate. The

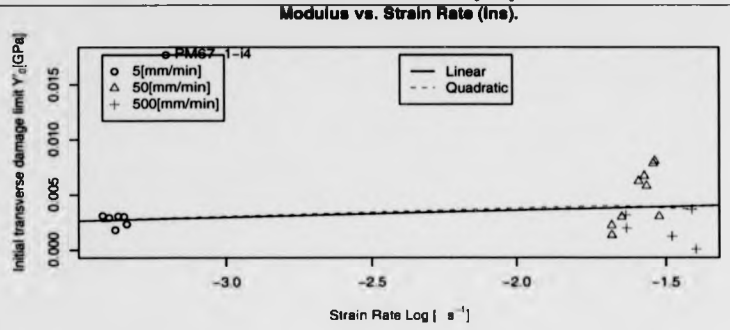

Figure 4.30: Initial transverse damage limit vs. logarithm of strain rate as obtained from the tensile testing of a $[\pm 67]_{2s}$ laminate.

Table 4.32: Statistics for the initial transverse damage limit at different crosshead displacement rates as obtained from a $[\pm 67]_{2s}$ laminate.

Crosshead Rate		5	50	500
Mean	$[\sqrt{GPa}]$	0.0027	0.0049	0.0020
Standard Deviation	$[\sqrt{GPa}]$	0.00052	0.0025	0.00146
Coef. of Variance	[]	0.192	0.52	0.72

coefficient of variance is lowest for the 5[mm/min] crosshead displacement rate and highest at the 5[mm/min] crosshead displacement rate.

The statistical analysis showed that only the 500[mm/min] crosshead displacement rate appear to be statistically different. However, the variances at all crosshead displacement rates appear to be statistically different, suggesting that the result might be inconclusive.

Model fitting: A linear model of the initial transverse damage limit with respect to the logarithm of the strain rate has the following form:

$$Y_0'(\dot{\varepsilon}_{22}) = 0.004879 + 0.000643 \cdot \log_{10}(\dot{\varepsilon}_{22}) \tag{4.13}$$

The coefficient of determination R^2 value is very low (.00777) which suggests that the initial transverse damage limit is dominated by other factors. The low value of the coefficient of determination R^2 in conjunction with the statistical analysis results which indicated that only one crosshead displacement rate appeared to be statistically different and that the variance was different at all crosshead displacement rates, suggests that the results are inconclusive.

4.7.2 Critical Transverse Damage limit Y_c'

Figure 4.31 is a plot of the critical transverse damage limit vs. strain rate log and a linear and a quadratic model of the log of the strain rate is fitted. Also a magnified version is presented when the outliers are removed. Those labeled observations are removed as outliers and they are not included in the statistical treatment. It is noteworthy that the results for the critical transverse damage limit at 50 and 500[mm/min] crosshead displacement rate appear to be in the same order of magnitude.

Statistics: Table 4.33 presents the statistics of critical transverse damage limit at different crosshead displacement rates of $[\pm 67.5]_{2s}$.

The mean of critical transverse damage limit increases with increasing crosshead displacement rate. The standard deviation is lowest at the 5[mm/min] crosshead displacement rate and is highest at the 500[mm/min] crosshead displacement rate. The absolute value of the coefficient of variance is lowest at the 500 [mm/min] crosshead displacement rate and highest at the 50[mm/min] crosshead displacement rate.

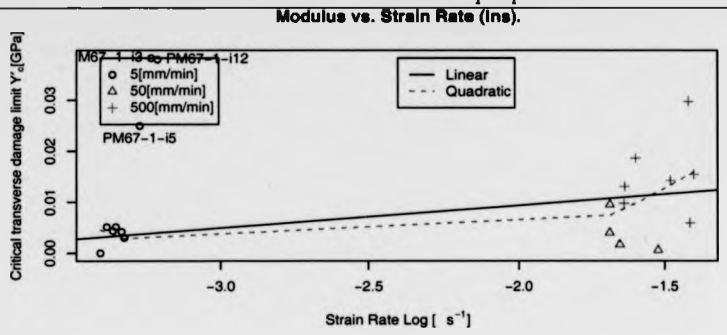

Figure 4.31: Critical transverse damage limit vs. strain rate logarithm.

Table 4.33: Statistics for the critical transverse damage limit at different crosshead displacement rates

Crosshead Rate		5	50	500
Mean	$[\sqrt{GPa}]$	0.0036	0.0039	0.015
Standard Deviation	$[\sqrt{GPa}]$	0.002	0.004	0.0076
Coef. of Variance	[]	0.53	1.	0.5

The statistical analysis showed that only the 500[mm/min] crosshead displacement rate appear to be statistically different. However, the variances at 50 and 500[mm/min] crosshead displacement rates appear to be statistically different, suggesting that the result might be inconclusive at the strain rates of interest.

Furthermore the coefficient of variance is one of the highest. The increased scatter of the the critical transverse damage limit is attributed to brittle behaviour exhibited by unidirectional composite ply under transverse loading. Unidirectional plies fail at significantly low strain, and as a result the standard deviation of the results is more dependent on the the error introduced by the data acquisition method or by error of displacement introduced by the testing machine (at high strain

rate tests it is difficult to control accurately the displacement of the machine).

Model fitting: A linear model of the critical transverse damage limit with respect to the logarithm of the strain rate has the following form:

$$Y_c'(\dot{\varepsilon}_{22}) = 0.018 + 0.0044 \cdot \log_{10}(\dot{\varepsilon}_{22}) \tag{4.14}$$

The coefficient of determination R^2 is a moderate value (.214). Although this value gives a degree of confidence on the suitability of the model, the difference in the variance of the critical transverse modulus and the proximity of the results of the 50 and 500[mm/min] crosshead displacement rate, introduce a level of uncertainty.

It is the author's opinion that the critical transverse shear damage is indeed strain rate dependent, however the quantitative model which is proposed should only be seen as an trend.

4.7.3 Brittle Transverse Damage Limit Y_S'

Figure 4.32 is a plot of the brittle transverse damage limit vs. strain rate log and a linear and a quadratic model of the log of the strain rate is fitted. Those labeled observations are removed as outliers and they are not included in the statistical treatment. It is noteworthy that the results for the brittle transverse damage limit at 50 and 500[mm/min] crosshead displacement rate appear to be in the same order of magnitude.

Statistics: Table 4.34 presents the statistics of Brittle transverse damage limit at different crosshead displacement rates of $[\pm 67.5]_{2s}$.

The mean of brittle transverse damage limit increases with increasing crosshead displacement rate.

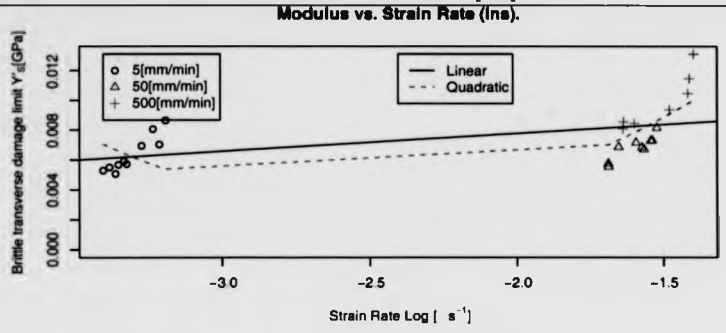

Figure 4.32: Brittle transverse damage limit vs. strain rate logarithm.

Table 4.34: Statistics for the brittle transverse damage limit at different crosshead displacement rates

Crosshead Rate		5	50	500
Mean	$[\sqrt{GPa}]$	0.0064	0.0069	0.01
Standard Deviation	$[\sqrt{GPa}]$	0.0012	0.0008	0.00186
Coef. of Variance	[]	0.19	0.12	0.19

The standard deviation is lowest again at the 50[mm/min] crosshead displacement and highest at the 500[mm/min] crosshead displacement rate. The coefficient of variance is lowest for the 50 [mm/min] crosshead displacement rate and highest at the 5[mm/min] crosshead displacement rate. The statistical analysis showed that only the 500[mm/min] crosshead displacement rate appear to be statistically different. However, the variances at 50 and 500[mm/min] crosshead displacement rates appear to be statistically different, suggesting that the result might be inconclusive at the rates of interest.

Model fitting: A linear model of the brittle transverse damage limit with respect to the logarithm of the strain rate has the following form:

$$Y'_S(\dot{\varepsilon}_{22}) = 0.01016 + 0.00119 \cdot \log_{10}(\dot{\varepsilon}_{22}) \tag{4.15}$$

The coefficient of determination R^2 value for the linear model is relatively high (.39), only compared with the transverse damage evolution properties. Although this value gives a degree of confidence on the suitability of the model, the difference in the variance of the critical transverse modulus and the proximity of the results of the 50 and 500[mm/min] crosshead displacement rate, introduce a high level of uncertainty. It is the author's opinion that the brittle transverse shear damage is indeed strain rate dependent, however the quantitative model which is proposed should only be seen as an trend.

4.8 Strain Rate Effect On Coupling Factors

4.8.1 Coupling Factor Between Plastic And Shear Strains A^2.

Figure 4.33 is a plot of the coupling factor between plastic and shear strains vs. strain rate log and a linear and a quadratic model of the log of the strain rate is fitted. Those labeled observations are removed as outliers from the statistical treatment.

Statistics: Table 4.35 presents the statistics of coupling factor between plastic and shear strains at different crosshead displacement rates of $[+45]_8$ laminates.

The mean of coupling factor between plastic and shear strains decreases for increasing crosshead displacement rate. The standard deviation is lowest at the 50[mm/min] crosshead displacement

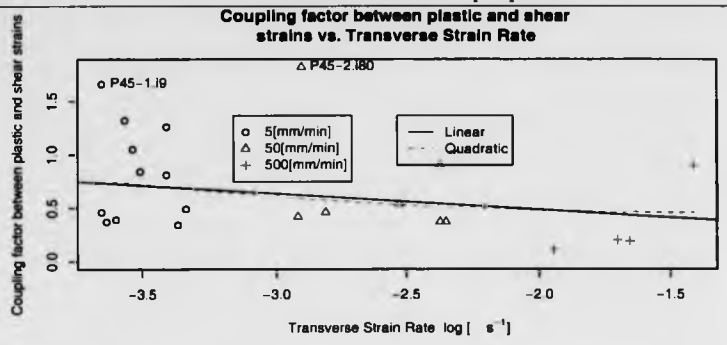

Figure 4.33: Coupling factor between plastic and shear strains vs. strain rate logarithm.

Table 4.35: Statistics for the coupling factor between plastic and shear strains at different crosshead displacement rates

Crosshead Rate		5	50	500
Mean	[]	0.73	0.51	0.47
Standard Deviation	[]	0.38	0.20	0.44
Coef. of Variance	[]	0.51	0.40	0.91

rate and highest at the 500[mm/min] crosshead displacement rate. The coefficient of variance is lowest for the 50[mm/min] crosshead displacement rate and highest for the 500[mm/min] crosshead displacement rate.

Model fitting: No strain rate sensitivity could be determined statistically, therefore the mean of all observed values of the coupling factor between plastic and shear strains is proposed as the value at all crosshead displacement rates. The calculated value is 0.61.

4.8.2 Coupling Factor Between Plastic And Shear Damage b

Figure 4.34 is a plot of the coupling factor between transverse and shear damage vs. strain rate log and a linear and a quadratic model of the log of the strain rate is fitted. Those labeled observations are removed as outliers and they are not included in the statistical treatment. Figure 4.34 is a plot of the coupling factor between the transverse and shear damage after the outliers have been removed.

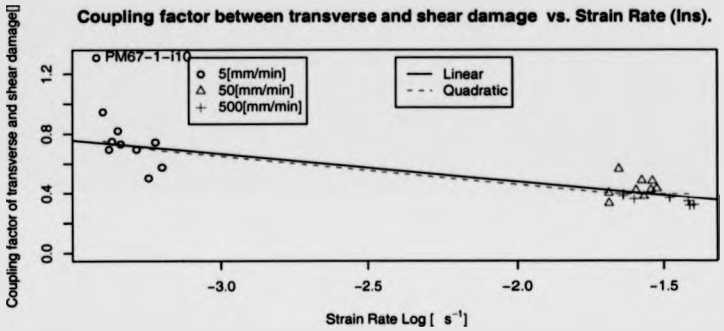

Figure 4.34: Coupling factor between transverse and shear damage vs. transverse strain rate logarithm.

Statistics: Table 4.36 presents the statistics of coupling factor between transverse and shear damage at different crosshead displacement rates of $[\pm 67.5]_{2s}$.

The mean of the coupling factor between transverse and shear damage decreases with increasing crosshead displacement rate. The standard deviation is lowest at the 500[mm/min] crosshead displacement rate and highest at the 5[mm/min] crosshead displacement rate. The coefficient of variance is lowest for the 500 [mm/min] crosshead displacement rate and highest for the 5[mm/min] crosshead displacement rate.

Table 4.36: Statistics for the coupling factor between transverse and shear damage at different crosshead displacement rates

Crosshead Rate		5	50	500
Mean	[]	0.78	0.44	0.36
Standard Deviation	[]	0.22	0.07	0.03
Coef. of Variance	[]	0.286	0.156	0.084

The statistical analysis of the results suggested that at all crosshead displacement rates the means of the coupling factor between transverse and shear damage appear to be statistically different at a high degree of confidence. However, similar observation were made for the variances of the coupling factor between transverse and shear damage, thus reducing the validity of the result.

Model fitting: A linear model of the coupling factor between transverse and shear damage with respect to the logarithm of the strain rate has the following form:

$$b(\dot{\epsilon}) = 0.055 - 0.22 \cdot \log_{10}(\dot{\epsilon}) \tag{4.16}$$

The coefficient of determination R^2 value for the linear model is quite high(.655). This is a very high value which indicates that the model explains most of the variability in the experimental measurements. This observation, in conjunction with the statistical analysis results suggest that the coupling factor between transverse and shear damage is strain rate dependent, however the validity of the quantitative model decreases since at all crosshead displacement rates the variances are statistically different.

Chapter 5

Finite Element Modelling

Chapter Objectives

- Presentation of the Ladevéve calibration.
- Description of the Finite Element model.

5.1 Introduction

5.1.1 Hardware.

The computer hardware used for the current study is a Silicon Graphics ®Octane ™workstation. The workstation is a dual R12000 processor workstation (at 300MHz) with 512MB RAM and two hard disks of 4 and 9GB capacity.

5.1.2 Software.

The Altair®HyperMesh™computer software is used for the creation of the finite element mesh. ESI's®PAM-Generis™was used to input the material definitions and boundary conditions.
The PAM-CRASH™explicit Finite Element solver was used to obtain the results. The code has been developed by ESI and is based on the public domain version of the DYNA-2D explicit finite element code.

5.2 Calibration Of Ladevéze Material Model

Table 5.1 presents the summary of the mechanical properties, required for the modelling of the Plytron unidirectional ply.

5.2.1 Analysis.

Apart from the cards which are used for the initialisation of the file, each section starts with a keyword followed by a forward slash /. Each line in a section is called a card.
The TITLE keyword gives a name to the model.

Property	Notation	Units	5 $\left[\frac{mm}{min}\right]$	50 $\left[\frac{mm}{min}\right]$	500 $\left[\frac{mm}{min}\right]$
Longitudinal tensile modulus	E_{11}	[MPa]	21000	28000	25500
Transverse tensile modulus	E_{22}	[MPa]	6986	6986	6986
Shear modulus	G_{12}	[MPa]	1740	1330	1080
Poisson's ratio	v_{12}	[]	0.41	0.36	0.25
Long. failure strain	ε_{11}	[]	.022	.023	0.026
Trans. failure strain	ε_{22}	[]	0.0028	0.0028	0.0028
Shear. failure strain	γ_{12}	[rad]	0.42	0.42	0.42
Long. failure stress	σ_{11}	[MPa]	508	572	564
Trans. failure stress	σ_{22}	[MPa]	12	12	12
Shear. failure stress	τ_{12}	[MPa]	42	44	48
Initial shear damage limit	Y_0	$[\sqrt{GPa}]$	0.0046	0.027	.0078
Critical shear damage limit	Y_c	$[\sqrt{GPa}]$	0.036	0.046	0.053
Elementary shear damage limit	Y_R	$[\sqrt{GPa}]$	0.040	0.048	0.054
Initial transverse damage limit	Y_0'	$[\sqrt{GPa}]$	0.0027	0.005	0.002
Critical transverse damage limit	Y_c'	$[\sqrt{GPa}]$	0.0036	0.0039	0.015
Brittle transverse damage limit	Y_S'	$[\sqrt{GPa}]$	.0064	0.007	0.01
Coupling factor between shear and transverse strains	A^2	[]	0.61	0.61	0.61
Coupling factor between shear and transverse damage	b	[]	0.78	0.44	0.36

Table 5.1: Ladevéze characterisation of Plytron at different strain rates.

The CTRL is the control keyword and is used for termination time, number of output states, initial timestep, global damping coefficients etc.

```
  CTRL  /      0.005      100S      100S   .1   10     1e-05     0.1     0 0 0
               1.2       0.06       0       0.9       0       0.3         1
               200         0        0         0    0         1    0    2    0
```

The MATER keyword informs that a material definition will follow. In the first line, an ID is given followed by the material type model and the density of the material. The following lines are depended on the material type model. The material keyword also the element formulation is defined. The Hughes-Tezduyar element formulation is used, which is more expensive but eliminates the hourglassing [1] energy problem.

```
 $
 $  MATERIAL DATA CARDS
 $
 $---5---10----5---20----5---30----5---40----5---50----5---60----5---70----5---80
MATER /        3     131        1.48e-09       1

 4 Ply laminate
         0         0                                    0.01      0.01      0.01     0.8333
    1    1    1    1    0    0    0    0    0    0    0    0    0    0    0    0
    0    0    0    0    0    0    0    0    0    0    0    0    0    0    0    0
    0    0    0    0    0    0    0    0    0    0    0    0    0    0    0    0
     0.019    10    1         0
    0    0    0    0    0    0    0    0    0    0    0    0    0    0    0    0
    0    0    0    0    0    0    0    0    0    0    0    0    0    0    0    0
    0    0    0    0    0    0    0    0    0    0    0    0    0    0    0    0
    0    0    0    0    0    0    0    0    0    0    0    0    0    0    0    0
    0    0    0    0    0    0    0    0    0    0    0    0    0    0    0    0
    0    0    0    0    0    0    0    0    0    0    0    0    0    0    0    0
```

The PLY keyword informs that a ply definition will follow. Again an exclusive ID number is given followed by the ply definition type (1 in the case of a Ladevéze composite global ply model),

[1] Hourglassing is a zero energy deformation pattern. These modes produce rigid body motion and the mesh starts self-straining, consequently the solution is destroyed.

the density and a logical (0 or 1) indicating whether ply failure criteria will be evaluated. The following cards are depended on the ply definition model that will be used. Different ply definitions are given because of the different orthotropy directions (laminates at angle).

```
PLY   /     1     1  1.48e-09     1
 Plytron_0_Ladeveze
     21160       6986
      1740       1740                0.409     0.887     0.887
     1.135     0.1455     0.1151     0.853     0.776    0.2017     1.243       0.65
     0.025

    3          1          0          0                                        0.22




       508     12.439     12.439     42.57     42.57     42.57       0.5
    0.0223    0.00284    0.00284     0.438     0.438     0.438
      -508    -12.439    -12.439    -42.57    -42.57    -42.57
   -0.0223   -0.00284   -0.00284    -0.438    -0.438    -0.438
```

On the ply definition, it is possible to define failure criteria. The failure criterion selected for this study were the Tsai-Wu (see appendix B). The values used for the Tsai-Wu is 10^{-7} which is equivalent to small interaction between the different modes of failure. The failure criteria are defined at a ply level, however, the effect is on the entire laminate because each shell element represents the entire ply. As a result, if the failure criteria are satisfied for one of the plies the entire laminate is deleted (effective stiffness equal to zero - no load carrying capacity).

5.3 Finite Element Model

5.3.1 Mesh

The geometrical dimensions of the physical specimen are given in figure 3.2. The Finite Element mesh of the FE model is given in figure 5.1.

Figure 5.1: Representation of Finite element model with the nodes involved on the grip boundary conditions.

5.3.1.1 Longitudinal Strains.

In figure 5.2, the locations and numbers of the nodes which are used for the strain and stress computations are presented.

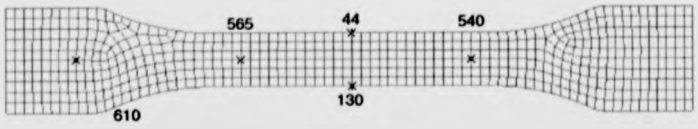

Figure 5.2: Nodes used to compute the longitudinal strain, transverse strain and longitudinal force.

The nodes 565 and 540 are used to monitor the longitudinal displacement. The distance between the two nodes ($d_{x,0}$) is 50[mm][2] corresponding to the length of the longitudinal contacting exten-

[2]Precision is 49.9816[mm] and is the value that will be used for the calculations.

someter. Longitudinal strain ε_L is computed by measuring the displacement of each node ($d_{x,565}$ and $d_{x,540}$), subtracting and dividing by ($d_{x,0}$) (see equation 5.2).

$$\varepsilon_L = \frac{d_{x,565} - d_{x,540}}{d_{x,0}} \tag{5.1}$$

5.3.1.2 Transverse Strains.

The node positions are used to monitor the transverse displacement. These nodes are 44 and 130 and they are presented in figure 5.2.

The distance between the two nodes ($d_{y,0}$) is 10[mm][3] corresponding to the length of the transverse contacting extensometer. Transverse strain ε_T is computed by measuring the coordinate of each node ($d_{y,44}$ and $d_{y,130}$) and subtracting and dividing by 10[mm] (see equation 5.2).

$$\varepsilon_T = \frac{d_{y,44} - d_{y,130}}{d_{y,0}} \tag{5.2}$$

5.3.1.3 Longitudinal Stress.

An energy method is used to obtain the longitudinal stress. The internal energy of the specimen is recorded at each timestep. The internal energy of the deformed specimen vs the total displacement of the deformed specimen has the form shown in figure 5.3.

The internal energy is assumed to equal the external work. The external work is generally distributed between the internal and kinetic energy. In the examined case, the specimen's kinetic energy is independent of the internal energy because the artificial boundary condition of a constant displacement rate is applied (in which infinite energy is available for the system - similarly

[3]Precision is 10.0017[mm] and is the value that will be used for the calculations.

to the experiment). The assumption that all external work is converted to internal energy is equivalent to a static equilibrium/testing assumption.

The force is computed as the differential of the internal energy of the specimen with respect to the deformed specimen's total displacement.

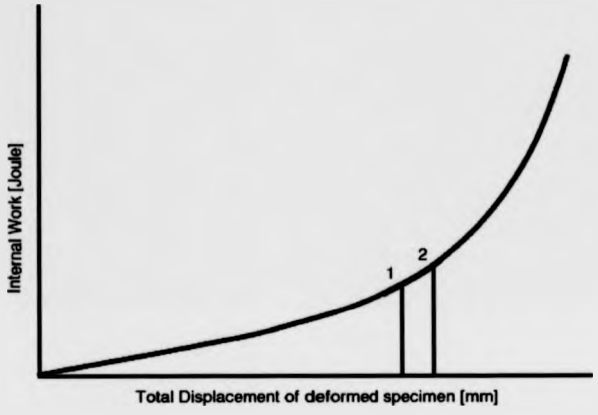

Figure 5.3: Internal energy vs. total displacement of deformed specimen.

Given the total displacement of the deformable part of the composite specimen part (see figure 5.2 node 610), the force/load P may be computed by the following equation.

$$P = \frac{IE_{n+1} - IE_n}{Td_{n+1}} \tag{5.3}$$

where Td_n is the total deformed specimen displacement at timestep n. It is node 610 which is used to establish Td_n and its location within the FE mesh is shown in figure 5.2[4].

[4]The selected node for the total deformed specimen displacement calculation could be any of the moving grip nodes, because of the applied boundary conditions.

The force is converted to stress using a conversion factor based on the initial cross-section of the specimen. The cross-section depends on the initial width ($d_{y,0} \simeq 10[mm]$ - see §5.3.1.2), number of plies (n) and the thickness of each ply (t_0=.22[mm]) (in the given case the conversion factor is given by equation 5.4.

$$load2stress = d_{y,0} \cdot n \cdot t \quad [mm^2] \tag{5.4}$$

Using equations 5.3 and 5.4, the equation for the stress is obtained.

$$\sigma_T = \frac{IE_{n+1} - IE_n}{Td_{n+1} \cdot d_{y,0} \cdot n \cdot t} \quad [MPa] \tag{5.5}$$

5.3.1.4 Direct Shell Measurements.

Although stresses and strains may be obtained directly from shell elements, the preferential coordinate system is the principal axis directions, which generally does not coincide with the direction of load applied in the test.

5.3.2 Boundary Conditions

5.3.2.1 Stationary Grip.

To simulate the stationary grip on the specimen, a set 99 nodes are selected (see figure 5.1 right side) and all their translational degrees of freedom are fixed. Rotational degrees of freedom are however, permitted.

It is important to note that, in the respective area that the grip of the universal testing machine is attached to the specimen, all relevant nodes in the FE model are constrained (see figure 5.1. If

the nodes were not constrained, they would contribute to the internal energy, and influence the results obtained.

5.3.2.2 Moving Grip.

In order to simulate the moving grip a set of 99 nodes are fixed (see figure 5.1 left side), the out of plane (z) and lateral (y) translational degrees of freedom are fixed. Rotational degrees of freedom are permitted.

A constant displacement rate (velocity) boundary condition is applied along the x direction at the moving grip.

To improve the computational efficiency of the explicit code the displacement boundary condition has been altered 60 fold, so instead of minutes the time unit is second. The increase is compensated by the introduction of a global nodal damping parameter to critically dampen the response.

As in the case of the stationary grip, in the respective zone that the universal testing machine grip is attached to the physical specimen, all the relevant nodes of the FE model are constrained (see figure 5.1).

5.3.3 Output

There are different outputs from the PAMCRASH FE element code.

5.3.3.1 Graphical.

The graphical output consists of mesh plots (see figure 6.2) at distinct points in time. The recording frequency may be arbitrarily set.

5.3.3.2 Nodal Output.

Nodal properties may be recorded throughout the FE simulation at a preset frequency. Typical properties are displacement, coordinate, nodal forces etc.

5.3.3.3 Element Output.

Element properties may be recorded during the simulation at a preset frequency. Typical properties are element stress, element strain, material damage, energy (hourglass, internal and kinetic) etc.

5.3.3.4 Material Output

Certain material properties like the hourglass, internal, kinetic and total energy are recorded in the THF file by default.

5.3.3.5 Output File.

The nodal and element properties are directed to an ASCII file which is given a .dc extension. The file includes for six (6) set of time-history curves. Each curve is preceded by a 7 line header and then the actual time-history data follow.

The output file is processed by a Excel macro and automatically produces the stress vs strain curves and plots the corresponding charts.

Chapter 6

Finite Element Modelling Results

Chapter Objectives

- Presentation of the qualitative FEM results.
- Presentation of the stress vs. strain FEM results.

6.1 Presentation Format

The FEM results are presented in four different sections, according to the laminate sequence. In each section the following data are presented for the different crosshead displacement rates:

1. the predicted FEM stress vs. strain curves.
2. a FEM principal stress contour plot of the developed stress state in the specimen.
3. a FEM plot of the first element elimination.

The FEM principal stress contour plot of the developed stress state in the specimen (item 2 of the above list) is a snapshot of the stress contour plot of the specimen taken a few states before the failure initiation (at $90 \pm 2\%$ of the simulation time).

Similarly, a FEM plot of the first element elimination (item 3 of the above list) is taken immediately after the first element elimination - when the failure criteria are satisfied. The element elimination was used to determine the location of failure initiation.

Both the plots are used for comparative reasons. In all cases the FEM predicted failure at a significantly lower strain (usually less than half of the observed experimental). Therefore, the visual comparison is not proposed for any quantitative purpose, rather it is used to identify potential qualitative similarities.

6.2 Results For The $[0°]_4$ Laminate.

Figures 6.1 compares the FEM predicted stress vs strain curves of $[0°]_4$ specimen for 5, 50 and 500[mm/s] crosshead displacement rate mechanical properties.

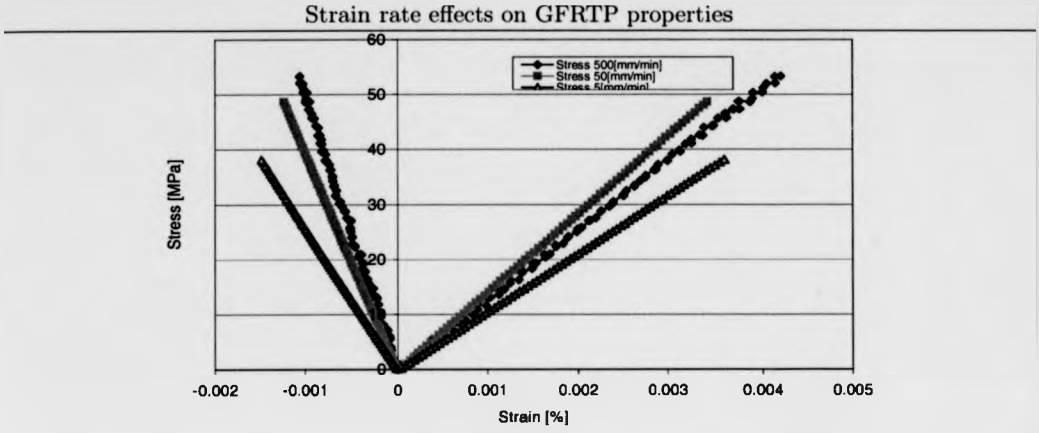

Figure 6.1: FEM stress vs. strain curves of $[0°]_4$ specimen at 5, 50 and 500 [mm/min] crosshead displacement rate mechanical properties.

A linear behaviour is observed for each simulation. The longitudinal behaviour at 50[mm/s] crosshead displacement rate appears to be stiffer than its counterpart at 500[mm/s] crosshead displacement rate. This is consistent with the experimental result regarding the longitudinal tensile modulus observed at the statistical analysis in chapter 8. The transverse response of the specimen at 500[mm/s] appears to be stiffer than the 50[mm/s] analysis. This observation may be attributed to the significant change in Poisson's ratio. The typical set of curves shown in figure 4.2 exhibit a similar behaviour. However, the transverse response does not appear to be consistent.

Figure 6.2 presents the principal stress in the $[0°]_4$ specimen prior to failure as predicted by the FEM at different crosshead displacement rates.

Similar stress contours develop in each simulation. Notably a high stress gradient is observed at the shoulder of each specimen. This might suggest that for a UD test the straight specimen might be preferable - as is suggested in the ASTM standard.

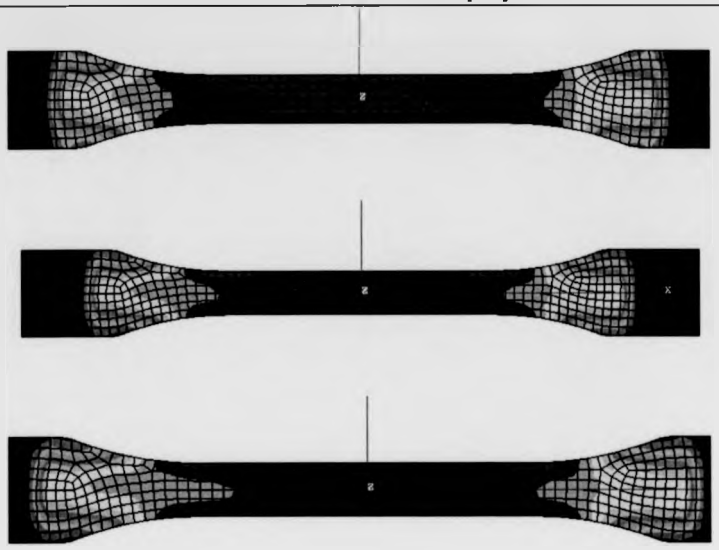

Figure 6.2: Principal stress contour plot of $[0°]_4$ specimen prior to first element elimination at different crosshead displacement rates (presented from top to bottom 5, 50 and 500[mm/min] crosshead displacement rates)

Figure 6.3 presents the first state with eliminated elements as predicted by the FEM of $[0°]_4$ specimen for the different crosshead displacement rates (presented from top to bottom 5, 50 and 500[mm/min]).

The FEM results predict global catastrophic failure for the $[0°]_4$ ply stack. The catastrophic failure process occurs so rapid that it was not possible to obtain a state with partial damage for the 5 and 50[mm/s] crosshead displacement rates simulations. The 500[mm/s] crosshead displacement rate simulation shows that failure starts from one grip side and propagates along the length of the specimen.

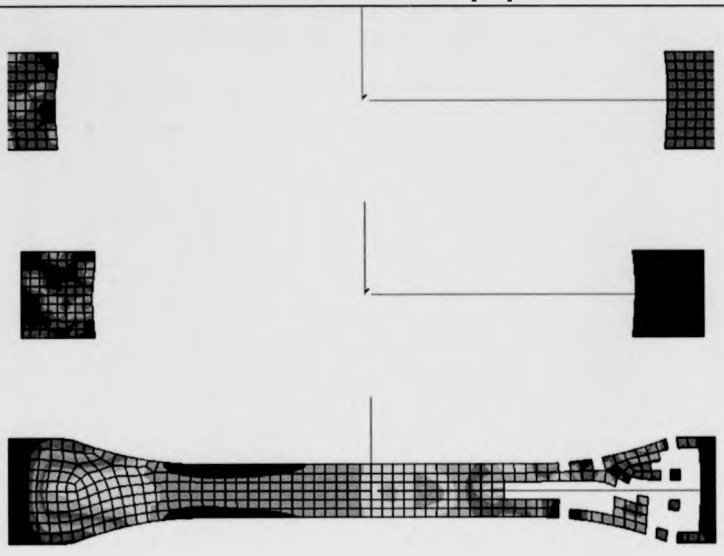

Figure 6.3: FEM plot of $[0°]_4$ laminate after the first element elimination at different crosshead displacement rates (presented from top to bottom 5, 50 and 500[mm/min] crosshead displacement rates).

The failure near the boundary condition indicates potential issues with the definition of the boundary condition. This assumption is inconclusive though due to the inability to monitor the progressive failure at the experimental testing.

6.3 Results For The $[\pm 45°]_{2s}$ Laminate.

Figures 6.4 compares the FEM predicted stress vs strain curves of $[\pm 45°]_{2s}$ specimen at 5, 50 and 500[mm/s] crosshead displacement rates.

A linear behaviour is observed for every curve in the graph. Comparison with the experimental

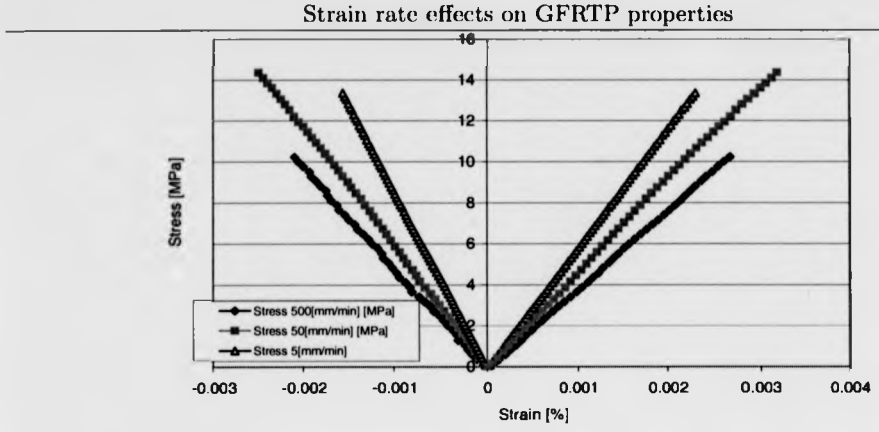

Figure 6.4: FEM stress vs. strain curves of $[\pm 45°]_{2s}$ specimen at 5, 50 and 500 [mm/min] crosshead displacement rate mechanical properties.

results in figure 4.10 (page 113), reveals that the strain rate curve is completely different - exhibiting highly non linear behaviour for large strains. The FEM predicted failure at significantly lower strains compared to the experimental results.

As expected the behaviour appears to be less stiff for increasing strain rate, since the observed results are at the linear portion of the stress vs strain curve, where the response is dominated by the elastic shear modulus. This was described in chapter 8, where elastic shear modulus decreased with increasing strain rate.

Figure 6.5 presents the FEM results for a numerical simulation of the $[\pm 45]_{2s}$ specimen with no implemented failure criterion for element elimination.

The difference between figure 6.4 and 6.5 are obvious. The FE analysis without the failure criterion for element elimination predicts a nonlinear behaviour similar to the experimental suggesting that the inclusion of the failure criterion and/or the boundary conditions is not appropriate.

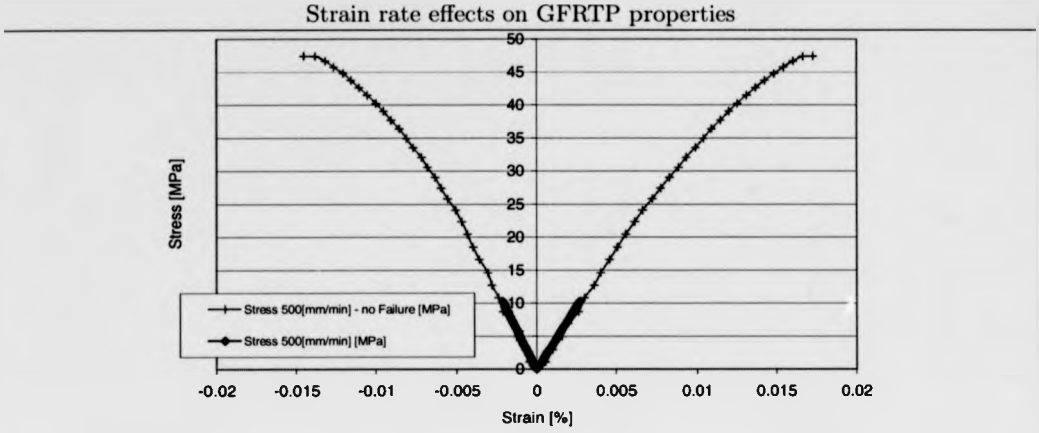

Figure 6.5: Comparison of FEM Stress vs. strain curves $[\pm 45°]_{2s}$ Plytron specimen at 500 [mm/min] crosshead displacement rate mechanical properties with and without implementation of failure criterion.

Figure 6.6 presents the principal stress of the $[\pm 45]_{2s}$ in the material prior to failure as predicted by the FEM at different crosshead displacement rates.

The stress contours which develop in each simulation show similar patterns. The numerical simulations predict stress patterns forming along the 45 direction. This is an artifact of the simulation, because it presents the stress state on the outermost ply, for which the principal direction is along the 45°.

Figure 6.7 presents the first state with eliminated elements as predicted by the FEM for the different crosshead displacement rates (presented from top to bottom 5, 50 and 500[mm/min]).

FEM predicts failure very prematurely, at less than 5% the experimentally observed failure strain. Also, failure initiation location predicts the location of failure is next to the grip constraints. It is the author's opinion that this is an artifact of the way that failure criterion is implemented in the

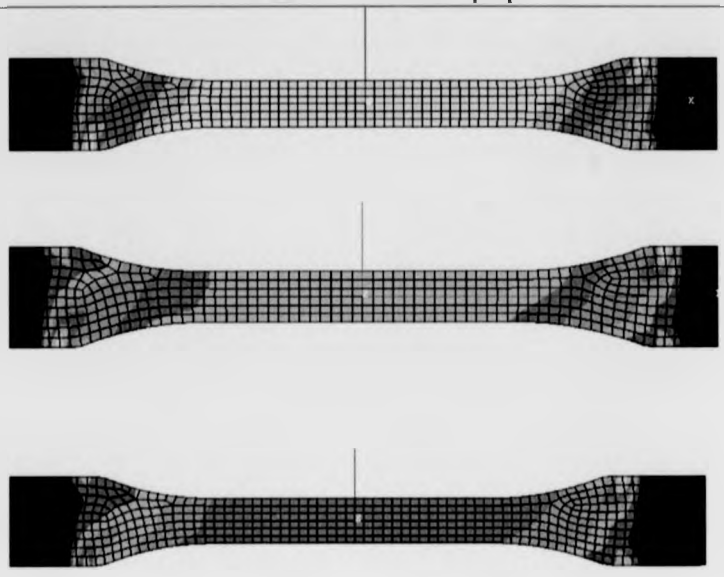

Figure 6.6: Principal stress contour plot of $[\pm 45°]_{2s}$ specimen prior to first element elimination at different crosshead displacement rates (presented from top to bottom 5, 50 and 500[mm/min] crosshead displacement rates)

code on a ply level and also the definition of the boundary conditions.

As mentioned earlier, the element includes all plies but elimination of the element is determined if failure occurs at ply level - the weakest link. In the regard to experimentations, microcracks are formed on a ply, and their propagation would be inhibited/arrested by neighbouring plies; this feature prevents catastrophic failure.

Even duplicating the elements is not an adequate solution, because even when one ply fails the load capacity of the element reduces to zero and the loads are redistributed to the neighbouring plies. This is not appropriate because unless many fibres fail the composite has some load carrying

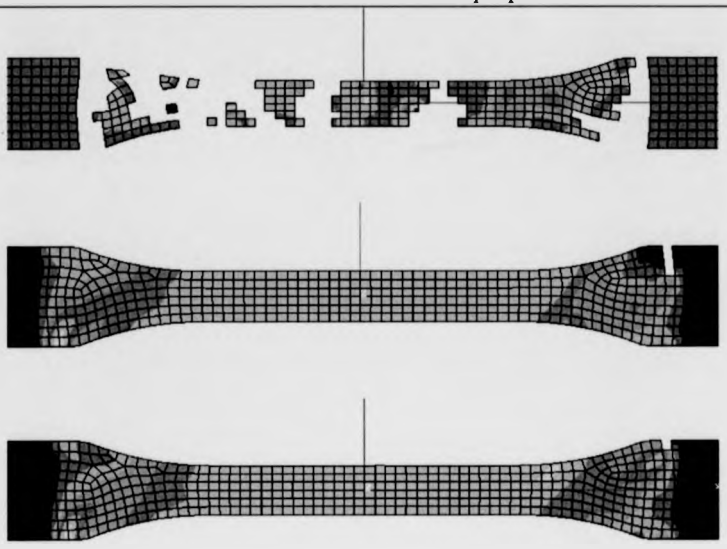

Figure 6.7: FEM plot of $[\pm 45°]_{2s}$ Plytron specimen after the first element elimination at different crosshead displacement rates (presented from top to bottom 5, 50 and 500[mm/min] crosshead displacement rates).

capacity.

6.4 Results For The $[+45°]_8$ Laminate.

Figures 6.4 compares the FEM predicted stress vs strain curves for $[+45°]_8$ laminate at 5, 50 and 500[mm/s] crosshead displacement rates.

A linear behaviour is observed for every simulation for every curve in the graph. Comparison with the experimental results in figure 4.11 (page 114), reveals that failure is predicted prematurely, at approximately 2/3 of the experimental failure stress. As expected the behaviour appears to be

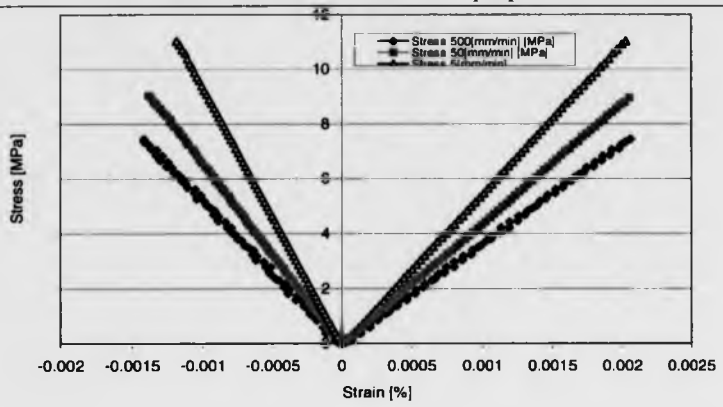

Figure 6.8: FEM stress vs. strain curves of $[+45°]_8$ specimen at 5, 50 and 500 [mm/min] crosshead displacement rate mechanical properties.

less stiff for increasing strain rate, since the observed results are at the linear range of the stress vs strain curve. Over the linear range, the specimen response is affected by the transverse tensile modulus (which remains constant) and shear modulus (which decreases with increasing strain rate).

Figure 6.9 presents the principal stress contours in the $[+45]_8$ specimen prior to failure as predicted by the FEM at different crosshead displacement rates.

Similar patterns of stress contours can be observed for each numerical simulations.

Figure 6.10 presents the first state with eliminated elements as predicted by the FEM for the different crosshead displacement rates (presented from top to bottom 5, 50 and 500[mm/min]).

FEM predicts failure prematurely. It predicts that the location of failure is next to the grip constraints. Failure initiation location predicts the location of failure is next to the grip constraints. This is a corollary to the assumption that the definition of the boundary conditions is not appro-

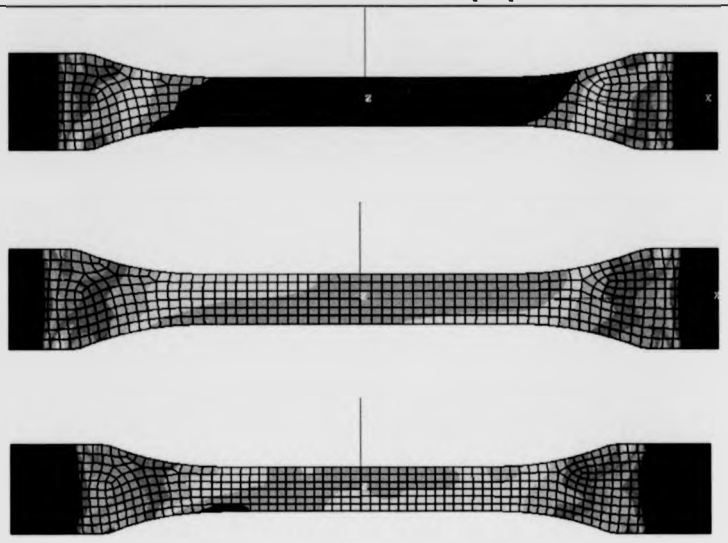

Figure 6.9: Principal stress contour plot of $[+45°]_8$ specimen prior to first element elimination at different crosshead displacement rates (presented from top to bottom 5, 50 and 500[mm/min] crosshead displacement rates)

priate, and/or that the failure criterion implementation is not appropriate.

6.5 Results For The $[\pm 67°]_{2s}$ Laminate.

Figures 6.11 compares the FEM predicted stress vs strain curves for for $[\pm 67°]_{2s}$ laminate at 5, 50 and 500[mm/s] crosshead displacement rates.

A linear behaviour is observed for each simulation. The stiffness of the response appeared to decrease for increasing strain rate. Comparison with the experimental results in figure 4.12 (page 115), reveals that failure is predicted prematurely, at approximately 1/4 of the experimental failure

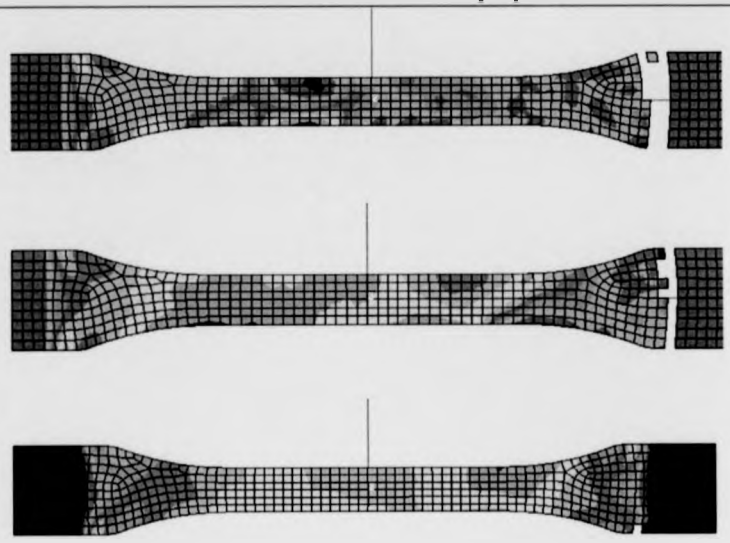

Figure 6.10: FEM plot of $[+45°]_8$ Plytron specimen after the first element elimination at different crosshead displacement rates (presented from top to bottom 5, 50 and 500[mm/min] crosshead displacement rates).

stress.

Figure 6.12 presents the principal stress in the $[\pm 67°]_{2s}$ specimen prior to failure as predicted by the FEM at different crosshead displacement rates.

Similar patterns of stress development are observed for each simulation. A 67° angle to the testing direction can be observed.

Figure 6.13 presents the first state with eliminated elements as predicted by the FEM simulation of $[\pm 67°]_{2s}$ laminate at the different crosshead displacement rates (presented from top to bottom 5, 50 and 500[mm/min]).

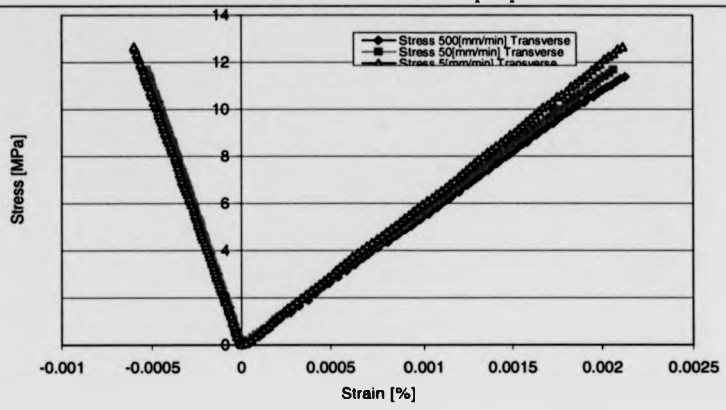

Figure 6.11: FEM stress vs. strain curves of $[\pm 67°]_{2s}$ specimen at 5, 50 and 500 [mm/min] crosshead displacement rate mechanical properties.

The FEM predicts failure near the shoulders of the specimen, but still within the gauge. Failure appears to propagate along the transverse direction as expected and there is an indication that it follows the fibre direction. It appears that the failure is premature although the problem is not as significant as it is for the $[\pm 45°]_{2s}$ laminate.

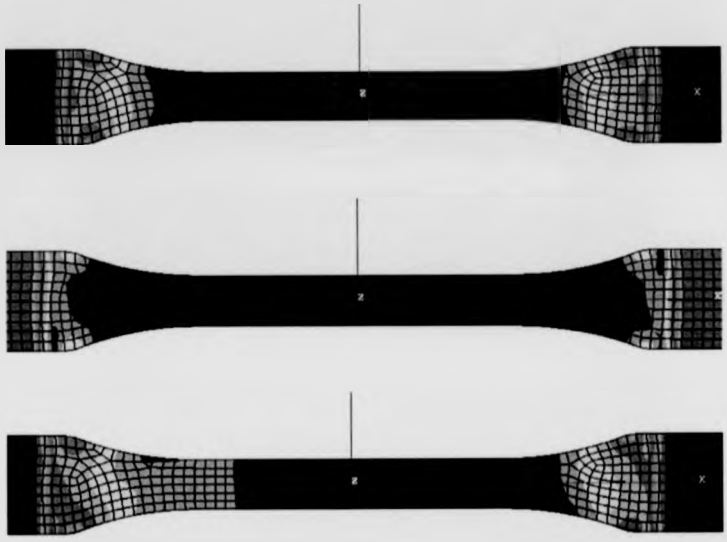

Figure 6.12: Principal stress contour plot of $[\pm 67°]_{2s}$ specimen prior to first element elimination at different crosshead displacement rates (presented from top to bottom 5, 50 and 500[mm/min] crosshead displacement rates)

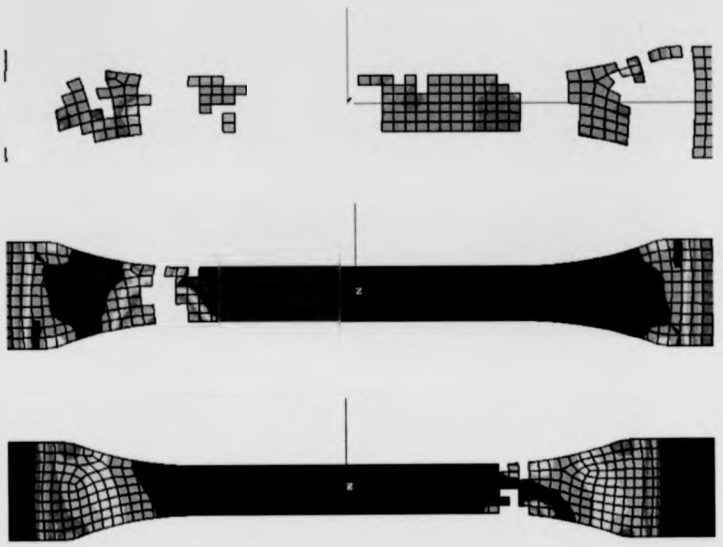

Figure 6.13: FEM plot of $[\pm 67°]_{2s}$ Plytron specimen after the first element elimination at different crosshead displacement rates (presented from top to bottom 5, 50 and 500[mm/min] crosshead displacement rates).

Chapter 7

Statistical Comparison Of Experimental And FE Results

Chapter Objectives

- Description of comparison methodology and presentation of metrics used.
- Present quantitative comparison data.

7.1 Methodology.

The experimental and FEM results will be compared quantitatively and graphically. The methodology is discussed:

7.1.1 Qualitative Comparison

The final stages of the loaded composite specimens are used to compare typical failed surfaces obtained from experiments to the predicted results of the FEM numerical simulations.

7.1.2 Quantitative Comparison

In order to compare the stress vs. strain curves quantitatively, a Pearson correlation coefficient is used [176, p.129], [177, p.97] together with a *correlation range ratio*. The methodology presented in the flowchart in figure 7.1 is used.

The Pearson coefficient reflects the extent of a linear relationship between two data sets, and takes values between [-1,1]. Therefore, a value of unity of the Pearson coefficient indicates that there is a linear relationship between the two data sets (i.e. for data set x and y, they follow $y = a_0 x + a_1$[1]). It is obvious that the correlation coefficient does not account for offsets and scaling factors, but for the shape of the curve - see figure 7.2.

To implement the Pearson correlation coefficient, the experimental and FE analysis vectors[2] need to have the same number of data points. For this reason, the data are transformed using an interpolation method, over an linearly spaced stress vector.

[1] Where a_0 and a_1 are scalar coefficients.

[2] Matrices with a single dimension.

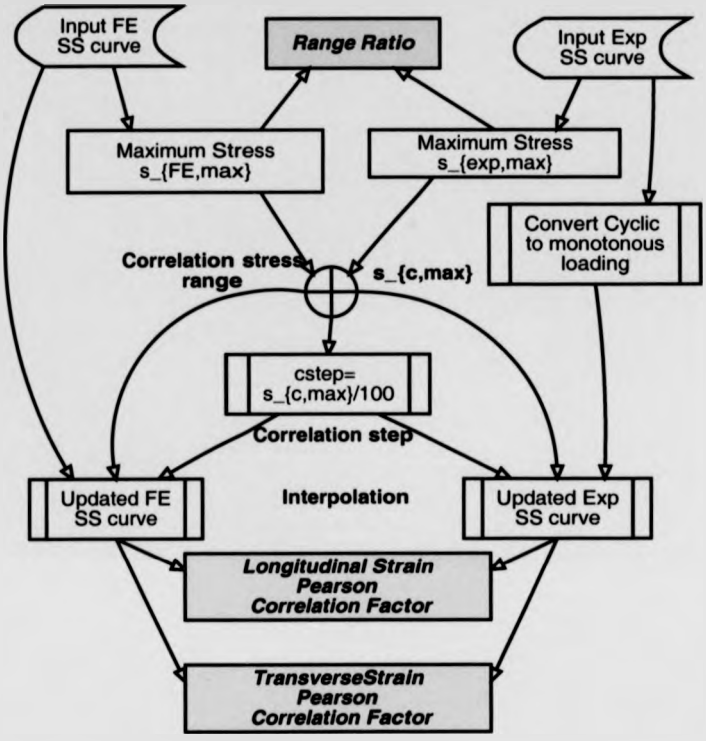

Figure 7.1: Correlation methodology.

The maximum stress is set as a cutoff point for both curves ($\sigma_{FE,max}$ and $\sigma_{exp,max}$). The minimum of the two maximum stresses is used as the maximum stress $\sigma_{c,max}$ over which the correlation takes place.

Two updated curves for the experimental and FE analysis data with the same length are produced (see figure 7.3), so that the examined vectors can be used on the Pearson correlation coefficient (PCC). The vectors (longitudinal strain, transverse strain and stress) consist of 101 points (including the 0,0), linearly spaced. The vectors have as limit points: zero and the respective value

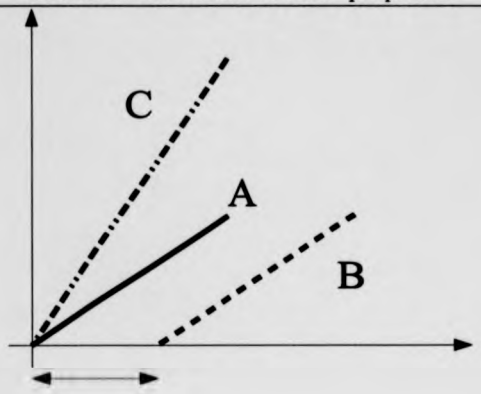

Figure 7.2: Issues concerning the Pearson coefficient - Scaling and translation.

at the maximum correlation stress ($\sigma_{c,max}$), as previously calculated. The intermediate points are calculated using a linear interpolation method.

In the case of the experimental results, the unloading and part of the reloading cycles of the cyclic loading for $[+45°]_8$, $[\pm 45°]_{2s}$ and $[\pm 67.5°]_{2s}$ are removed (as a result the original cyclic stress vector is replaced by a monotonic stress vector).

It is deemed acceptable because, in $[+45°]_8$, $[\pm 45°]_{2s}$ and $[\pm 67.5°]_{2s}$ cases, the offset will be zero, as all curves start from zero.

Also, because the method selects a common maximum stress value, it is not possible to have any scaling effects, although it seems at first glance to be more significant.

Examples of the interpretation of the Pearson correlation coefficient values are presented in figure 7.4.

Another metric used to compare the experimental vs. the FEM results is the *Correlation range ratio* (CRR) . Although, the Pearson coefficient gives a good indication of the association between the two variables (i.e. experimental and FE analysis stress vector) it is limited because of the

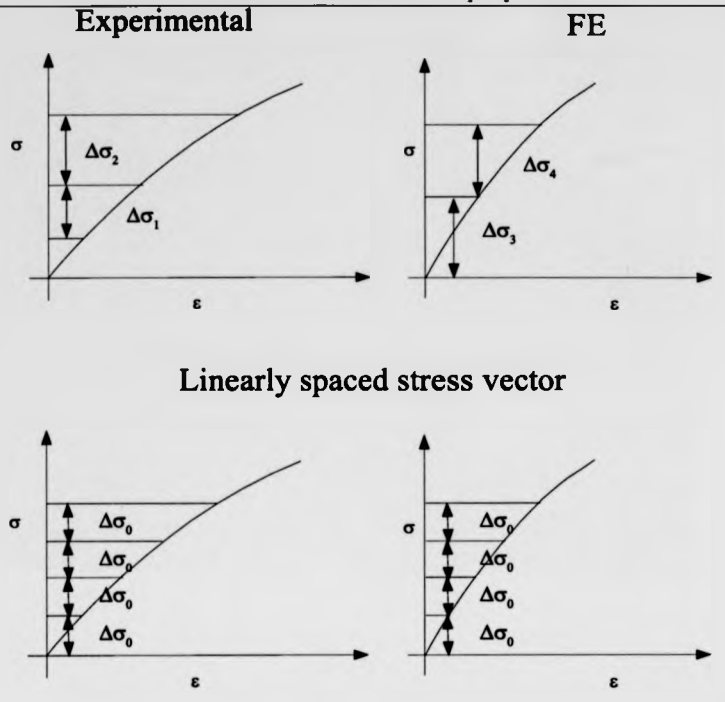

Figure 7.3: How a linearly spaced stress vector is used on the experimental and numerical simulation data to obtain data suitable for computation of the Pearson correlation coefficient.

limited range over which the comparison is taking place. Therefore, a longitudinal and a transverse ratio of the maximum strain obtained by the FEM over the maximum strain values obtained experimentally are used to quantify the range of correlation (see figure 7.5 for a graphical example of the longitudinal Correlation Range Ratio). A ratio close to the unity indicates that the Pearson correlation coefficient used a larger percentage of the data for the comparison.

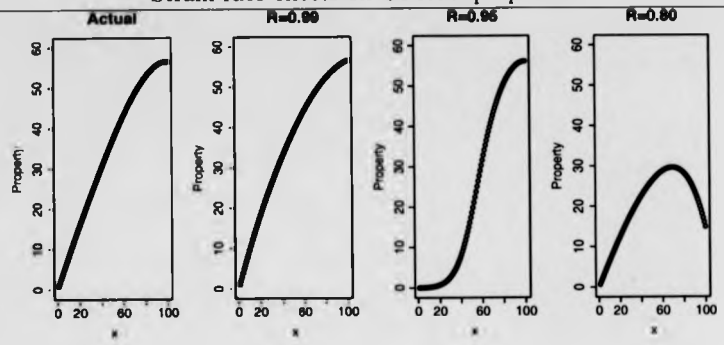

Figure 7.4: Comparison of the Pearson correlation coefficient for different curves.

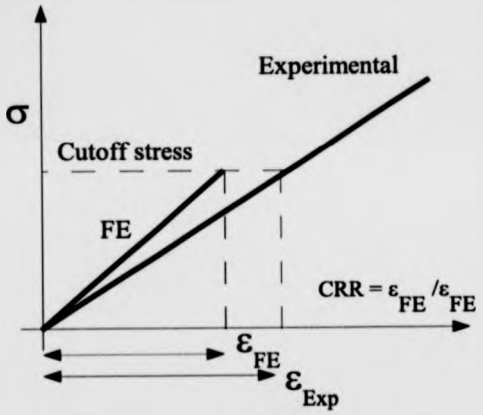

Figure 7.5: Correlation range ratio explanation.

7.2 Quantitative Comparison

7.2.1 Experimental vs FE Comparison For $[0°]_4$ Test Specimens.

Table 7.1: Quantitative metrics for the comparison between experimental and FEM results for the $[0°]_4$ specimens at 5[mm/min] crosshead displacement rates.

Specimen	PCC1	CRR1	PCC2	CRR2
UD0.32	0.9954	0.1555	0.9831	0.1644
UD0.33	NA	NA	NA	NA
UD0.34	0.9998	0.1656	0.9864	0.1978
UD0.35	0.9510	0.1749	0.0065	-0.3303
UD0.97	0.9996	0.1441	0.8957	0.1362
UD0.98	0.9991	0.1318	0.9969	0.1094
UD0.99	0.9989	0.1432	0.9845	0.0973
UD0.50	NA	NA	NA	NA
UD0.51	0.9949	0.1606	0.9922	0.3202
UD0.52	0.9984	0.1424	0.9905	0.2892
UD0.53	0.9996	0.1636	0.9777	0.1844
UD0.54	0.9874	0.1565	0.2425	NA
UD0.55	0.9587	0.1627	0.3309	NA
UD0.56	0.9990	0.1939	0.9978	0.2206
UD0.57	0.9994	0.1748	0.9969	0.1796
UD0.58	0.9996	0.1696	0.9926	0.0983
UD0.59	0.9972	0.1749	0.9909	0.1937

Table 7.1: (continued)

Specimen	PCC1	CRR1	PCC2	CRR2
UD0.60	0.9931	0.1691	0.9969	0.1797
UD0.61	0.9996	0.1787	0.3664	0.0431
UD0.62	0.9974	0.1831	0.9940	0.2261
UD0.63	0.9982	0.1705	0.9920	0.2088
UD0.64	0.9969	0.1567	0.9739	0.1496
Average	0.9932	0.1636	0.8344	0.1482
St. Deviation	0.0135	0.0153	0.3141	0.1371
Coef. of Variance	0.0136	0.0936	0.3765	0.9246

Table 7.2: Quantitative metrics for the comparison between experimental and FEM results for the $[0°]_4$ specimens at 50[mm/min] crosshead displacement rates.

Specimen	PCC1	CRR1	PCC2	CRR2
UD0.43	0.9998	0.1496	0.5389	0.0909
UD0.44	0.9992	0.1406	0.4032	0.0683
UD0.45	0.9986	0.1266	0.8276	0.0961
UD0.46	0.9975	0.1047	0.1733	0.0063
UD0.47	0.9970	0.1250	0.5828	0.0812
UD0.48	0.9979	0.1301	NA	NA

Table 7.2: (continued)

Specimen	PCC1	CRR1	PCC2	CRR2
UD0.49	0.9999	0.1329	NA	NA
UD0.65	0.9981	0.1649	0.9973	0.1519
UD0.66	0.9943	0.1422	0.9992	0.0045
UD0.67	0.9997	0.1507	0.9990	0.1552
UD0.68	0.9995	0.1450	0.9974	0.1681
UD0.69	0.9969	0.1395	0.9868	0.1148
UD0.70	0.9965	0.1436	0.9624	0.0998
UD0.71	0.9976	0.1466	0.9877	0.1669
UD0.72	0.9946	0.1561	0.7532	0.0045
UD0.73	0.9986	0.1581	0.9886	0.0857
UD0.74	0.9967	0.1578	0.9950	0.1653
UD0.75	0.9987	0.1543	0.9791	0.2027
UD0.76	0.9999	0.1477	0.9996	0.1481
UD0.77	0.1154	NA	NA	NA
UD0.78	0.7846	0.1533	0.9924	0.1617
UD0.79	0.9995	0.1555	0.9980	0.1679
UD0.80	0.9937	0.1631	0.9988	0.1707
Average	0.9502	0.1449	0.8580	0.1155
St. Deviation	0.1873	0.0143	0.2424	0.0605

Table 7.2: (continued)

Specimen	PCC1	CRR1	PCC2	CRR2
Coef. Of Variance	0.1971	0.0988	0.2825	0.5233

Table 7.3: Quantitative metrics for the comparison between experimental and FEM results for the $[0°]_4$ specimens at 500[mm/min] crosshead displacement rates.

Specimen Number	PCC1	CRR1	PCC2	CRR2
UD0.36	0.9738	0.1278	0.8006	0.1363
UD0.34	0.9806	0.1269	NA	NA
UD0.37	0.9935	0.1762	NA	NA
UD0.38	0.9929	0.1747	NA	NA
UD0.39	0.9881	0.1467	0.8646	0.0973
UD0.40	0.9692	0.1409	0.4823	0.0627
UD0.41	0.9919	0.1648	0.5382	0.0672
UD0.42	0.9801	0.1551	0.9898	0.0162
UD0.81	0.9986	0.1631	0.9974	0.1284
UD0.82	0.9907	0.1677	0.9983	0.1090
UD0.84	0.9986	0.1877	0.9985	0.0913
UD0.85	0.9983	0.1639	0.9818	0.0951
UD0.86	0.9996	0.1685	0.9825	0.1147

Table 7.3: (continued)

Specimen Number	PCC1	CRR1	PCC2	CRR2
UD0.87	0.9996	0.1825	0.9058	0.1102
UD0.88	0.9979	0.1555	0.9936	0.0248
UD0.89	0.9995	0.1764	0.9942	0.1000
UD0.90	0.9998	0.1527	0.9988	0.0039
UD0.91	0.7558	0.1902	0.9985	0.1291
UD0.92	0.9953	0.1857	0.9973	0.1600
UD0.93	0.9471	0.1383	0.9977	0.0636
UD0.94	0.9930	0.1515	0.6314	0.1558
UD0.95	0.9996	0.1741	0.6539	0.0608
UD0.96	0.9940	0.1677	0.9949	0.0935
Average	0.9799	0.1625	0.8900	0.0910
St. Deviation	0.0505	0.0181	0.1721	0.0434
Coef. Of Variance	0.0515	0.1113	0.1934	0.4774

7.2.2 Experimental vs FE Comparison For $[\pm 45°]_8$ Test Specimens.

Table 7.4: Quantitative metrics for the comparison between experimental and FEM results for the $[\pm 45°]_{2s}$ specimens at 5[mm/min] crosshead displacement rates.

Specimen	PCC1	CRR1	PCC2	CRR2
PM45-33	0.9959	0.0084	NA	NA
PM45-34	0.9937	0.0115	0.9951	0.0064
PM45-35	0.9955	0.0112	0.9968	0.0077
PM45-36	0.9946	0.0089	0.9963	0.0058
PM45-37	0.9947	0.0117	0.9990	0.0087
PM45-38	0.9958	0.0118	0.9986	0.0086
Average	0.9950	0.0106	0.9972	0.0074
St. Deviation	0.0009	0.0015	0.0016	0.0013
Coef. Of Variance	0.0009	0.1432	0.0016	0.1731

Table 7.5: Quantitative metrics for the comparison between experimental and FEM results for the $[\pm 45°]_{2s}$ specimens at 50[mm/min] crosshead displacement rates.

Specimen	PCC1	CRR1	PCC2	CRR2
PM45-39	0.9988	0.0125	0.9993	0.0098
PM45-40	0.9979	0.0117	0.9973	0.0105
PM45-41	0.9970	0.0118	0.9993	0.0123

Table 7.5: (continued)

Specimen	PCC1	CRR1	PCC2	CRR2
PM45-42	0.9970	0.5781	0.9999	0.5017
PM45-43	0.9248	0.0003	NA	NA
PM45-44	0.9051	0.0003	NA	NA
PM45-45	0.9014	0.0003	NA	NA
PM45-46	0.9066	0.0003	NA	NA
PM45-47	0.9391	0.0002	NA	NA
PM45-48	0.9204	0.0003	NA	NA
PM45-49	0.9174	0.0003	NA	NA
PM45-50	0.9287	0.0003	NA	NA
PM45-51	0.9111	0.0003	NA	NA
Average	0.9420	0.0474	0.9990	0.1336
St. Deviation	0.0400	0.1595	0.0011	0.2454
Coef. Of Variance	0.0424	3.3625	0.0011	1.8375

Table 7.6: Quantitative metrics for the comparison between experimental and FEM results for the $[\pm 45°]_{2s}$ specimens at 500[mm/min] crosshead displacement rates.

Specimen	PCC1	CRR1	PCC2	CRR2
PM45-52	0.9929	0.0126	0.9906	0.0124

Table 7.6: (continued)

Specimen	PCC1	CRR1	PCC2	CRR2
PM45-53	0.9627	0.0133	0.9915	0.0117
PM45-54	0.9891	0.0131	0.9910	0.0115
PM45-55	0.9839	0.0123	0.9904	0.0107
PM45-56	0.9897	0.0138	0.9919	0.0151
PM45-57	0.9908	0.0126	0.9910	0.0124
PM45-58	0.9920	0.0124	0.9906	0.0116
PM45-59	0.9917	0.0163	0.9893	0.0145
PM45-60	0.8980	0.0003	NA	NA
PM45-61	0.9034	0.0003	NA	NA
PM45-62	0.8993	0.0003	NA	NA
PM45-63	0.9055	0.0003	NA	NA
PM45-64	0.9111	0.0002	NA	NA
Average	0.9546	0.0083	0.9908	0.0125
St. Deviation	0.0429	0.0067	0.0008	0.0015
Coef. Of Variance	0.0449	0.8059	0.0008	0.1217

7.2.3 Experimental vs FE Comparison For $[+45°]_8$ Test Specimens.

Table 7.7: Quantitative metrics for the comparison between experimental and FEM results for the $[+45°]_8$ specimens at 5[mm/min] crosshead displacement rates.

Specimen	PCC1	CRR1	PCC2	CRR2
P45-1	0.9904	1.0901	0.9840	0.8024
P45-2	0.9980	0.2732	0.3163	0.0417
P45-3	0.9966	0.5025	0.9932	0.7252
P45-4	0.9937	0.6949	0.9933	0.6678
P45-5	0.9947	0.9350	0.9943	1.5817
P45-6	0.9947	0.6432	0.9911	0.6751
P45-7	0.9942	0.5990	0.9893	0.6021
P45-8	0.9987	0.5826	0.9920	0.6554
P45-9	0.9957	0.3292	0.9963	0.2805
P45-10	0.9976	0.2594	0.9974	0.2610
P45-11	0.9996	0.2153	0.9975	0.2361
Average	0.9958	0.5568	0.9313	0.5935
St. Deviation	0.0026	0.2823	0.2040	0.4116
Coef. Of Variance	0.0026	0.5070	0.2190	0.6935

Table 7.8: Quantitative metrics for the comparison between experimental and FEM results for the $[+45°]_8$ specimens at 50[mm/min] crosshead displacement rates.

Specimen	PCC1	CRR1	PCC2	CRR2
P45-15	0.9966	0.8649	0.9965	0.6446
P45-16	0.9956	2.2093	0.9956	1.6465
P45-17	0.9371	5.5534	0.9375	4.1388
P45-18	0.9970	0.6504	0.9969	0.4847
P45-19	0.9743	0.3143	0.9741	0.2342
P45-20	0.9972	0.2355	0.9972	0.1755
P45-21	0.9980	0.1977	0.9980	0.1474
P45-22	0.9958	0.2120	0.9958	0.1580
P45-23	0.9801	0.4163	0.9802	0.3103
P45-24	0.9870	0.2010	0.9869	0.1498
P45-25	0.9808	0.2536	0.9808	0.1890
P45-26	0.9944	0.1856	0.9944	0.1383
P45-27	0.9907	0.2115	0.9907	0.1577
P45-28	0.9917	0.2146	0.9917	0.1599
P45-29	0.9972	0.2368	0.9972	0.1765
P45-45	0.9976	0.1790	0.9974	0.1334
Average	0.9882	0.7585	0.9882	0.5653

Table 7.8: (continued)

Specimen	PCC1	CRR1	PCC2	CRR2
St. Deviation	0.0155	1.3764	0.0154	1.0258
Coef. Of Variance	0.0157	1.8146	0.0156	1.8146

Table 7.9: Quantitative metrics for the comparison between experimental and FEM results for the $[+45°]_8$ specimens at 500[mm/min] crosshead displacement rates.

Specimen	PCC1	CRR1	PCC2	CRR2
P45-30	0.9826	0.3935	0.9801	0.3053
P45-31	0.9671	0.2391	0.9648	0.1855
P45-32	NA	NA	NA	NA
P45-33	0.9743	0.2525	0.9719	0.1959
P45-34	NA	NA	NA	NA
P45-35	0.9395	0.2246	0.9374	0.1743
P45-36	0.9656	0.2381	0.9633	0.1847
P45-37	0.9704	0.2830	0.9681	0.2195
P45-38	0.7956	0.2508	0.7943	0.1945
P45-39	0.9785	0.2704	0.9760	0.2098
P45-40	0.9598	0.3955	0.9575	0.3069
P45-41	0.9737	0.3243	0.9713	0.2516

Table 7.9: (continued)

Specimen	PCC1	CRR1	PCC2	CRR2
P45-42	0.9315	0.3152	0.9294	0.2446
P45-43	0.9590	0.2922	0.9568	0.2267
Average	0.9498	0.2899	0.9476	0.2249
St. Deviation	0.0508	0.0577	0.0505	0.0448
Coef. Of Variance	0.0535	0.1990	0.0533	0.1990

7.2.4 Experimental vs FE Comparison For $[\pm 67.5°]_8$ Test Specimens.

Table 7.10: Quantitative metrics for the comparison between experimental and FEM results for the $[\pm 67°]_{2s}$ specimens at 5[mm/min] crosshead displacement rates.

Specimen	PCC1	CRR1	PCC2	CRR2
PM67-1	0.9997	0.2878	0.9808	0.2369
PM67-2	0.9990	0.2691	0.9881	0.2349
PM67-3	0.9995	0.2935	0.9137	0.1558
PM67-4	0.9979	0.3182	0.9985	0.3901
PM67-5	0.9980	0.3139	0.9991	0.2930
PM67-6	0.9991	0.2683	0.9960	0.4038
PM67-7	0.9989	0.3161	0.9936	0.3082

Table 7.10: (continued)

Specimen	PCC1	CRR1	PCC2	CRR2
PM67-8	0.9945	0.2952	0.9960	0.1289
PM67-9	0.9979	0.2673	0.9953	0.2255
PM67-10	0.9996	0.2157	0.9886	0.4177
Average	0.9984	0.2845	0.9850	0.2795
St. Deviation	0.0015	0.0312	0.0257	0.1014
Coef. Of Variance	0.0015	0.1095	0.0261	0.3627

Table 7.11: Quantitative metrics for the comparison between experimental and FEM results for the $[\pm 67°]_{2s}$ specimens at 50[mm/min] crosshead displacement rates.

Specimen	PCC1	CRR1	PCC2	CRR2
PM67.12	0.9847	0.2750	0.9943	0.2528
PM67.13	0.9929	0.2375	0.9892	0.3130
PM67.14	0.9208	0.4108	NA	NA
PM67.15	NA	NA	NA	NA
PM67.16	0.9948	0.2000	0.9964	0.2655
PM67.17	0.9939	0.2435	0.9903	0.3112
PM67.18	NA	NA	NA	NA
PM67.19	NA	NA	NA	NA

Table 7.11: (continued)

Specimen	PCC1	CRR1	PCC2	CRR2
PM67.20	0.9995	0.2685	0.9994	0.3143
PM67.21	0.9976	0.3451	0.9983	0.3220
PM67.22	0.9989	0.3604	0.9987	0.3343
Average	0.9854	0.2926	0.9952	0.3019
St. Deviation	0.0265	0.0719	0.0041	0.0304
Coef. Of Variance	0.0269	0.2459	0.0041	0.1007

Table 7.12: Quantitative metrics for the comparison between experimental and FEM results for the $[\pm 67°]_{2s}$ specimens at 500[mm/min] crosshead displacement rates.

Specimen	PCC1	CRR1	PCC2	CRR2
PM67.23	0.9889	0.3346	0.9852	0.3075
PM67.24	0.9920	0.2881	0.9827	0.2066
PM67.25	0.9886	0.2812	0.9867	0.2794
PM67.26	0.9552	0.2725	0.9585	0.2836
PM67.27	0.9675	0.2223	0.9544	0.2430
PM67.28	0.9792	0.2519	0.9776	0.2876
PM67.29	NA	NA	NA	NA
PM67.30	NA	NA	NA	NA

Table 7.12: (continued)

Specimen	PCC1	CRR1	PCC2	CRR2
PM67.31	NA	NA	NA	NA
PM67.32	NA	NA	NA	NA
PM67.33	NA	NA	NA	NA
Average	0.9786	0.2751	0.9742	0.2680
St. Deviation	0.0145	0.0376	0.0141	0.0366
Coef. Of Variance	0.0149	0.1367	0.0145	0.1368

7.2.5 Longitudinal Pearson Correlation Coefficient

Figure 7.6 presents the mean values of the Longitudinal Pearson Correlation Coefficient (LPCC) for different stacking sequences and crosshead displacement rates.

The mean of the longitudinal Pearson Correlation Coefficient is greater than .94 in all examined cases. This indicates, generally a good correlation between two σ vs. ε curves for all laminates.

LPCC is affected by the crosshead displacement rate. The simulations correlate well with the experimental data at the 5[mm/min] crosshead displacement rate for all laminates. The minimum value of the LPCC at 5[mm /min] crosshead displacement rate is .993 indicating a very good correlation. At increasing crosshead displacement rates the LPCC decreases in all cases.

The $[\pm 67]_{2s}$ laminate [PM67] exhibited the highest LPCC values at all crosshead displacement rates from the different stacking sequences. The remaining laminates showed an significant decrease for the LPCC at 50 or 500[mm/min] crosshead displacement rate.

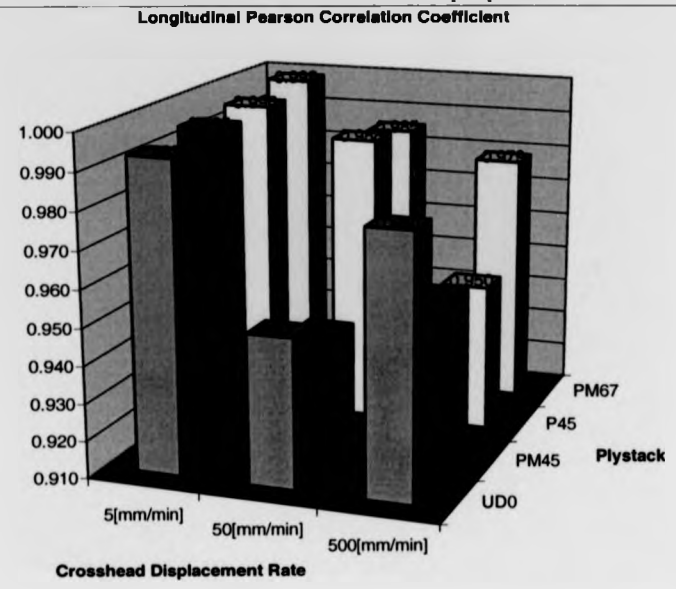

Figure 7.6: Longitudinal Pearson Correlation Coefficient results for different stacking sequences and different crosshead displacement rates.

7.2.6 Transverse Pearson Correlation Coefficient

Figure 7.7 presents the mean values of the Transverse Pearson Correlation Coefficient (TPCC) for different stacking sequences and crosshead displacement rates.

The mean of the Transverse Pearson Correlation Coefficient (TPCC) is greater than .93 in all examined cases except from the $[0°]_4$ laminate; thus indicating good correlation between transverse stress vs. strain curves obtained.

Contrary to the LPCC which appeared to be affected by crosshead displacement rate, the TPCC appeared to be affected primarily by the layup sequence. The $[\pm 45°]_{2s}$ and $[\pm 67°]_{2s}$ laminates exhibited the highest values of TPCC. The $[0°]_4$ laminates exhibit the lowest value of the TPCC,

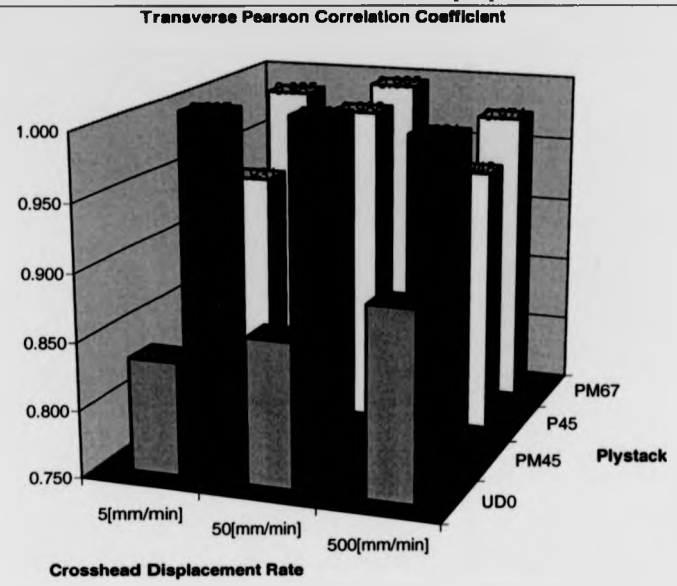

Figure 7.7: Transverse Pearson Correlation Coefficient results for different stacking sequences and different crosshead displacement rates.

indicating lower level of correlation of the transverse stress vs. strain curve. This observation is in agreement to what was stated in §6.2.

The $[\pm 45°]_{2s}$, $[45°]_8$ and $[\pm 67°]_{2s}$ laminate exhibited the highest TPCC values at 50[mm/min] crosshead displacement rates. The $[0°]_4$ laminate exhibited higher TPCC values with increasing crosshead displacement rates.

7.2.7 Longitudinal Correlation Range Ratio

Figure 7.8 presents the mean values of the Longitudinal Correlation Range Ratio (LCRR) for different stacking sequences and crosshead displacement rates.

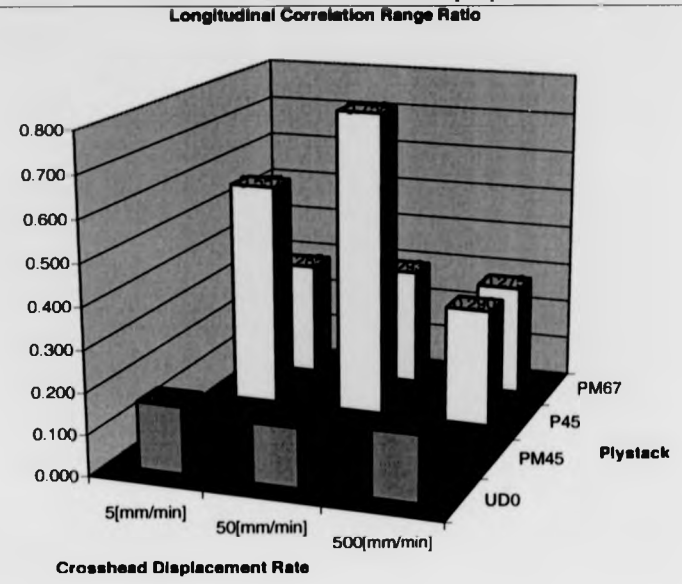

Figure 7.8: Longitudinal Correlation Range Ratio results for different stacking sequences and different crosshead displacement rates.

The mean of the Longitudinal Correlation Range Ratio (LCRR) exhibited great variation in both strain rate and laminate.

Generally, the LCRR appears to be affected mainly by the stacking sequence. The $[\pm 45^\circ]_{2s}$ laminate appears to have the lowest values of LCRR, almost an order of magnitude higher than the values of LCRR for the $[0^\circ]_4$ laminates. The $[\pm 67^\circ]_{2s}$ laminates have similar values but slightly higher. The $[45^\circ]_8$ laminates appear to have the highest values. However, the average value for the $[45^\circ]_8$ laminate increased because a few outliers (premature failure of the specimen). Normally, the LCRR ratios are similar to those of the $[\pm 67^\circ]_{2s}$ laminates.

Strain rate appears to have an mixed effect on the LCRR. For all angle laminates ($[\pm 45^\circ]_{2s}$,

$[45°]_8$ and $[\pm 67°]_{2s}$) it appears that the highest values are observed for the 50[mm/min] crosshead displacement rate. In the case of the $[0°]_4$ laminate the effect is reversed.

It is noteworthy that the numerical simulation at $[45°]_8$ at 50[mm/min] crosshead displacement rate resulted in 75.8% Correlation Range Ratio, which indicated that the correlation coefficient was applicable to over 3/4 of the longitudinal strain range. The numerical simulation of the $[45°]_8$ laminate at 5[mm/min] crosshead displacement rate also showed high value of Correlation Range Ratio (55.7%).

7.2.8 Transverse Correlation Range Ratio

Figure 7.9 presents the mean values of the Transverse Correlation Range Ratio (TCRR) for different stacking sequences and crosshead displacement rates.

The mean of the Transverse Correlation Range Ratio (LCRR) exhibited great variation in both strain rate and laminate stacking sequence.

Like the LCRR, the TCRR appears to be affected mainly by the stacking sequence. The $[\pm 45°]_{2s}$ laminate appears to have the lowest values of TCRR. The $[0°]_4$ laminate generally has greater values of Correlation Range Ratio than the $[\pm 45°]_{2s}$ laminate, with the only exception for 50[mm/min] crosshead displacement rates. The results for the $[\pm 67°]_{2s}$ laminate have TCRR values close to 30%. Finally, the $[45°]_8$ appears to have the highest values, for the 5 and 50[mm/min] crosshead displacement rate, however there is a sudden drop for the 500[mm/min] crosshead displacement rate.

Strain rate does not appear to have any consistent trend on the TCRR. Generally, the TCRR values for the 50[mm/min] crosshead displacement rate appear to be lower than the respective

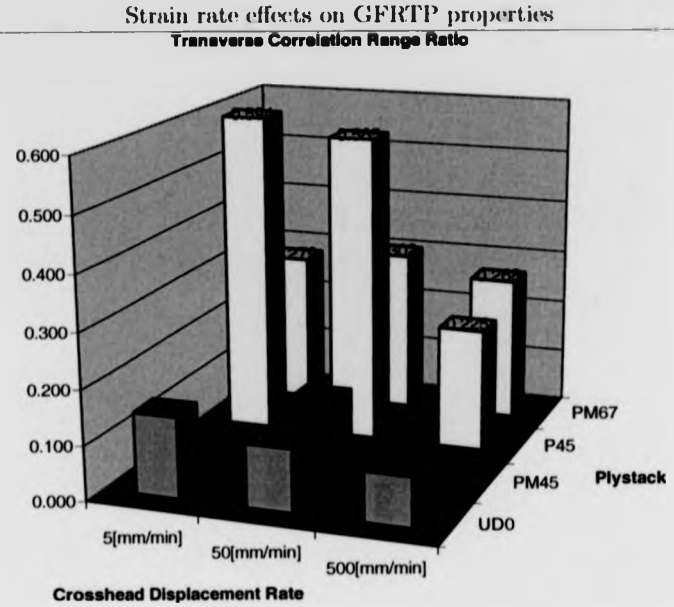

Figure 7.9: Transverse Correlation Range Ratio results for different stacking sequences and different crosshead displacement rates.

values for the 500[mm/min] crosshead displacement rate.

Chapter 8

Discussion.

Chapter Objectives

- Discuss the strain rate effect on the material properties based on the statistical experiments.
- Discuss the correlation between experimental and FEM results.

8.1 Strain Rate Effects On Mechanical properties

8.1.1 Discussion On Elasticity Properties

The longitudinal tensile modulus increases linearly between 5 and 50[mm/min] crosshead displacement rate and then no further increase is observed. This is in accordance to the majority of the researchers in the field, and it is attributed to the dominating effect of the glass-fibre reinforcement strain rate dependency on the performance of the composite material along the direction of the fibres.

The transverse tensile modulus did not exhibited statistical difference over the examined strain rate range. This is was an unexpected result since similar research work on thermosetting composites reported marked strain rate dependency, and because the thermoplastic matrix phase is well known for its viscoelastic properties. This observation may be attributed to the variability of the material which is linked to the processing route.

The shear modulus decreases linearly over the examined range of the strain rate. From all the elasticity properties that were examined the correlation factor was the highest indicating confidence about the result.

Finally, although the rest of the elasticity properties have been investigated at a great extent, there is little research work carried out on the strain rate dependency of the major Poisson's ratio. Also, it is a common the assumption in numerical studies that the Poisson's ratio remains constant. In this case, it was showed that the value of the Poisson's ratio at 5 and 50[mm/min] crosshead displacement rates remains unchanged, while further increase of the crosshead displacement rate to 500[mm/min] results in a statistically significant decrease.

8.1.2 Conclusions On Strength Strain Rate Dependency

The longitudinal tensile failure strain appears to increase for increasing strain rate, which is consistent with the findings of Xia[ ] that also reported increase of the longitudinal failure strain. The longitudinal tensile failure stress appeared to increase for increasing strain rate. This outcome is in agreement with most of the research work on strain rate dependency of glass fibre composite systems. Also it was found that the fitted model explained only a small percentage of the variability and it is suggested that the variability due to manufacturing effects the results.

The transverse tensile failure strain at different crosshead displacement was not statistically different, however, there were indications of possible increase. The transverse tensile failure stress at different crosshead displacement was not statistically different. In both cases, the results were statistically inconclusive and that may be attributed to the brittle nature of the material in transverse loading. The unidirectional composite systems fails in low transverse strain and stress, and as a result this makes the accuracy of the instrumentation an important factor which contributes to the variability of the data[1].

The shear failure strain did not appear to be strain rate dependent over the strain rate range examined, contrary to the shear failure stress that appeared to increase for increasing strain rate. This result is quite important because in conjunction with the results for the strain rate dependency of shear failure strain and shear modulus leads to the conclusion that the shear damage evolution is strain rate dependent.

[1] At higher strain this is not so much a problem

8.1.3 Conclusion On Shear Damage Evolution Strain Rate Dependency

The critical shear damage limit appears to increase with increasing strain rate. As discussed earlier in this section, higher values of the critical shear damage are equivalent to a lower rate of shear degradation. The result is in accordance with the work by Latallaide[112] (the only published work so far which investigates the effect of strain rate on the shear damage evolution of thermosetting epoxy systems). This observation further explains the findings for the longitudinal failure strength. Figure 8.1 compares the shear master curves of three typical specimen at different crosshead displacement rates. It can be seen from the figure that for increasing crosshead displacement rate, the curves are shifted towards the right, therefore at the same amount of energy absorbed in the system less degradation of properties has occurred.

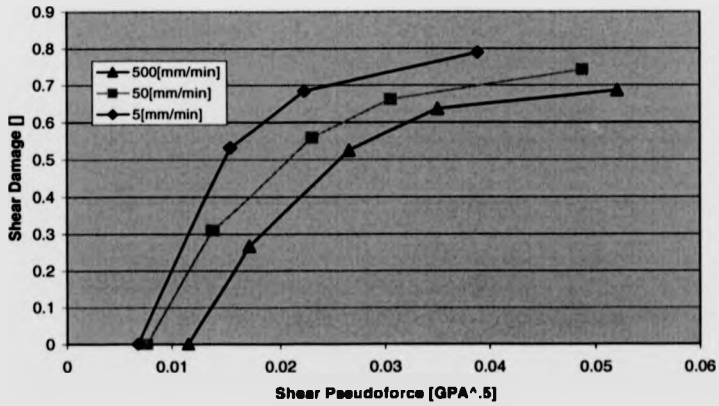

Figure 8.1: Comparison of three typical Master shear law curves at 5, 50 and 500[mm/min] crosshead displacement rate as obtained from the mechanical testing of $[\pm 45^{\circ}]_{2s}$ laminate.

The elementary shear damage limit appears to increase for increasing strain rate. The maximum

value at which degradation occurs before failure. An increased value of the elementary shear damage is equivalent to higher strain energy absorption before shear failure of the material. This is consistent with the findings, of the shear failure strength.

Finally, the initial shear damage limit appears to initially decrease and then increase for increasing strain rate. The result appears to contradict with the work by Latallaide[112], that found that the initial shear damage limit increases consistently with strain rate. It was suggested that this inconsistency is attributed to the effect of the critical Y_R and elementary Y_R shear damage limit. From figure 8.1 it is possible to compare three typical damage evolution curves.

It may be observed that the value of the shear pseudoforce that damage initiates are close for both the 5 and the 50[mm/min] crosshead displacement rates (the value for the 500[mm/min] crosshead displacement rate is significantly increased). Also, it may be observed that the final value (value before failure) for the 50[mm/min] crosshead displacement rate is significantly higher than the 5[mm/min]. It may be deducted[2] (and also observed from the figure) that the gradient of the best linear fit for 5[mm/min] crosshead displacement rate is higher that the respective gradient for 50[mm/min] crosshead displacement rate. All the above features in the apparent initial decrease on the initial shear damage limit. Therefore the hypothesis of the sensitivity of the initial shear damage limit is appropriate. Therefore, according to the graphical data, the value of the shear pseudoforce at which damage initiates consistently increases with crosshead displacement rate (at the rates examined).

An increase of the initial shear damage limit indicates that the material is able to absorb more strain energy before degrading the shear properties. This would partly explain the findings about the shear strength in the previous section8.1.2.

[2] Since both functions are monotonic and at no point intersect.

8.1.4 Conclusions On The Transverse Damage Strain Rate Dependency.

The characterisation properties of transverse damage evolution feature a high value for the coefficient of variance, therefore rendering the results of the statistical analysis for the determination of the strain rate dependency questionable. The high coefficient of variance is attributed to problems of testing such brittle materials under cyclic loading at strain rate loading. The issues with testing unidirectional composites transversely are reflected in the low volume of research work on the strain rate dependency of the transverse properties.

Also another issue, is that the results for the transverse damage evolution are based on the $[\pm 67^{\circ}]_{2s}$ laminate. To obtain the material axis results, the elastic properties from the previous tests were used for the transformation of the measured stresses and strains to the material axis. Any error on this properties is additive to the error of the testing.

The low value of the coefficient of determination R^2 for the initial transverse damage limit in conjunction with the statistical analysis results for the means and variance, suggests that the results are inconclusive.

The critical transverse damage limit appeared to be strain rate dependent and increase with strain rate. This suggests that with increasing strain rate the rate of the transverse damage evolution decreases. However, the author suggests that the quantitative model should not be used for extrapolation beyond the validated range of strain rate.

The brittle transverse damage limit appeared to be strain rate dependent. This suggests that with increasing strain rate the brittle transverse damage limit value decreases. The author suggests that the quantitative model should not be used for extrapolation beyond the validated range of

strain rate.

It is noteworthy that the results for all the parameters that describe the transverse damage at 50 and 500[mm/min] crosshead displacement rate appear to be in the same order of magnitude. A possible explanation for this observation is that there is a coupling between the transverse and shear damage (which are both present with the $[\pm 67^\circ]_{2s}$ laminate) which effects the deformation of the specimen.

8.1.5 Conclusion On Coupling Factors Strain Rate Dependency.

It was not possible to draw conclusive results for the coupling factor for transverse and shear strains.

The coupling factor between transverse and shear damage is strain rate dependent, however the validity of the quantitative model decreases since at all crosshead displacement rates the variances are statistically different. This is in accordance to the findings for the evolution of the transverse damage.

The coupling factor between transverse and shear damage is obtained from the $[\pm 67^\circ]_{2s}$ laminate like the transverse damage evolution properties. As a result the same issues are applicable as those discussed in §8.1.4, regarding testing issues of transversely loaded unidirectional composite materials and transformation of the measured stresses and strains along the testing axis to the material coordinate system.

8.2 Conclusions On Qualitative Comparison Of FEM Vs. Experimental Results

8.2.1 $[0°]_4$ Laminates.

Figure 8.2 compare the experimentally observed failure of an $[0°]_4$ laminate at 500[mm/min] crosshead displacement rate (top figure), with an FEM plot of the developed principal stress state in the specimen (middle figure) and a FEM plot of the specimen after the first elements have been eliminated (bottom figure).

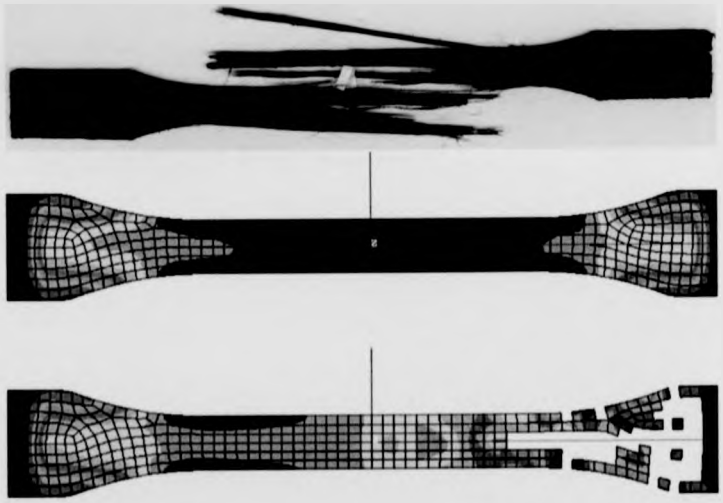

Figure 8.2: Top: Experimental failure of $0°]_4$ laminate at 500[mm/min] crosshead displacement rate, Middle: principal stress state contour plot obtained by an FEM analysis, Bottom: FEM plot of a specimen with eliminated elements (failure onset).

Comparing mechanical test results at 500[mm/min] crosshead displacement rate to FEM results at 500[mm/s] crosshead displacement rate suggests that the predicted FEM failure appears to be global and catastrophic as in the mechanical testing results. Element elimination is predicted at a significantly lower stress state, and therefore the results cannot be used as the only tool.

The failure in both cases initiates close to the area that the width of the specimen changes (shoulders of the specimens). The high stress gradients near the shoulders - as obtained by the FEM numerical simulation - can be observed in the experimental results. In some cases, a shear failure of the specimen along the fibre direction near the shoulders may be observed, see figure 8.3.

Figure 8.3: Detail of the shear failure observed at tensile testing of $0°]_4$ laminate at 500[mm/min] crosshead displacement rate.

8.2.2 $[\pm 45°]_{2s}$ Laminates.

Figure 8.4 compare the experimentally observed failure of an $[\pm 45°]_{2s}$ laminate at 500[mm/min] crosshead displacement rate (top figure), with an FEM plot of the developed principal stress state in the specimen (middle figure) and a FEM plot of the specimen after the first elements have been eliminated (bottom figure).

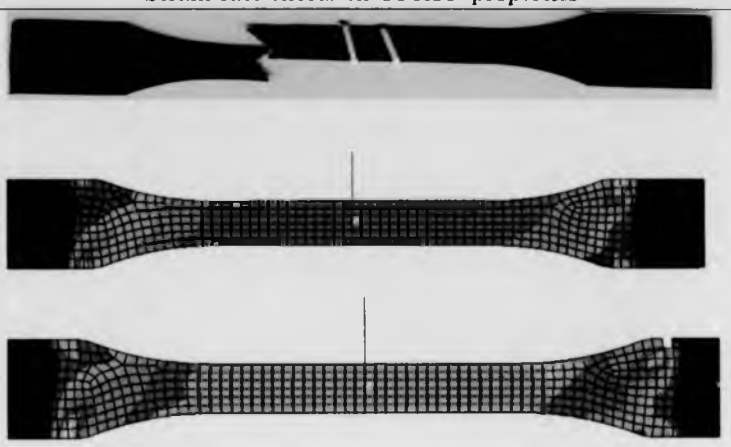

Figure 8.4: Top: Experimental failure of $[\pm 45°]_{2s}$ laminate at 500[mm/min] crosshead displacement rate, Middle: principal stress state contour plot obtained by an FEM analysis, Bottom: FEM plot of a specimen with eliminated elements (failure onset)

Comparing mechanical testing to FEM results at 500[mm/s] crosshead displacement rate exposes significant difference in the failure mode. It is noteworthy, that element elimination occurred prematurely in the FE analysis.

Significant difference can be observed in the failure location. The FEM predicted failure initiates at the location that the grip constraints (boundary conditions) are applied, contrary to the results of the experimental work where failure of the $[\pm 45°]_{2s}$ laminates initiated in all cases within the gauge length.

Further, the stress state appears to be different than expected. The principal stress contour develops at an angle of 45°. These stress patterns are expected by a unidirectional 45° laminate.

8.2.3 $[+45°]_8$ Laminates.

Figure 8.5 compare the experimentally observed failure of an $[+45°]_8$ laminate at 500[mm/min] crosshead displacement rate (top figure), with an FEM plot of the developed principal stress state in the specimen (middle figure) and a FEM plot of the specimen after the first elements have been eliminated (bottom figure).

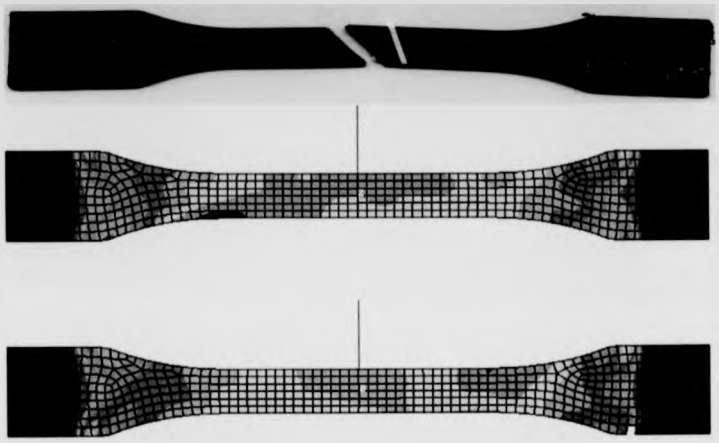

Figure 8.5: Top: Experimental failure of $[+45°]_8$ laminate at 500[mm/min] crosshead displacement rate, Middle: principal stress state contour plot obtained by an FEM analysis, Bottom: FEM plot of a specimen with eliminated elements (failure onset)

Comparing mechanical testing results at 500[mm/min] crosshead displacement rate to FEM results at 500[mm/s] crosshead displacement rate exposes significant difference in the failure location. The FEM predicted failure location initiates at the nodes that the boundary conditions (displacement constraints) were applied.

The principal stress develops along the fibre direction (45°), which is correlates well with the experimental failure mode (the experimentally observed failure occurs at 45°). FEM numerical simulations with the failure criteria not implemented showed that the degradation of properties resulted in softening the material (by damage degradation) along the fibre direction.

Similar observations are made for the 5 and 50[mm/min] crosshead displacement rates. In all FEM analyses the element elimination occurs at significantly lower strains compared to the experimental results, reducing the validity of the qualitative comparison.

8.2.4 $[\pm 67.5°]_8$ Laminates.

Figure 8.6 compare the experimentally observed failure of an $[\pm 67°]_{2s}$ laminate at 500[mm/min] crosshead displacement rate (top figure), with an FEM plot of the developed principal stress state in the specimen (middle figure) and a FEM plot of the specimen after the first elements have been eliminated (bottom figure).

Comparing mechanical testing results at 500[mm/min] crosshead displacement rate to the corresponding FEM results suggests adequate correlation for the failure location and failure mode. Failure location in both the experimental and the FEM results initiates near the shoulders transversely to test direction.

Similar observation can be made for the 5 and 50[mm/min]crosshead displacement rate. Again, element elimination of the FEM initiates significantly earlier, therefore reducing the validity of the above qualitative comparison.

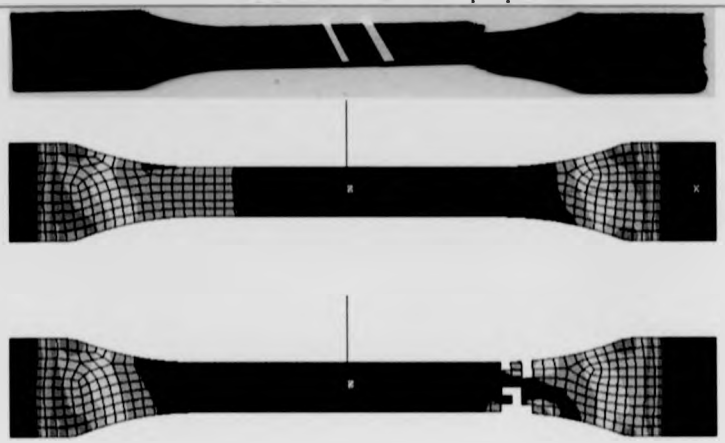

Figure 8.6: Top: Experimental failure of $[\pm 67^{\circ}]_{2s}$ laminate at 500[mm/min] crosshead displacement rate, Middle: principal stress state contour plot obtained by an FEM analysis, Bottom: FEM plot of a specimen with eliminated elements (failure onset)

8.2.5 Discussion On Qualitative Comparison

According to the Qualitative comparison in §8.2, the observed failure is significantly different to the failure predicted by the FE. It appears that in most of the cases the failure initiates near the grip constrains of the FE models. The validity of the comparison results is reduced, because the results of the qualitative comparison involve mainly the failure type and failure initiation location and the predicted FEM failure was at considerably lower strain.

It is the author's view that this behaviour can be attributable to the one or more of the following:

- the failure criteria implementation on the unidirectional ply.

- the definition of the boundary conditions (constraints at grip).
- to the inherent variability of the mechanical properties of the composite material at stiffness and strength.

8.3 Conclusions On Quantitative Comparison Of FEM Vs. Experimental Results

Figure 8.7, 8.8, 8.10 and 8.11 compares stress strain curves for the different laminates.

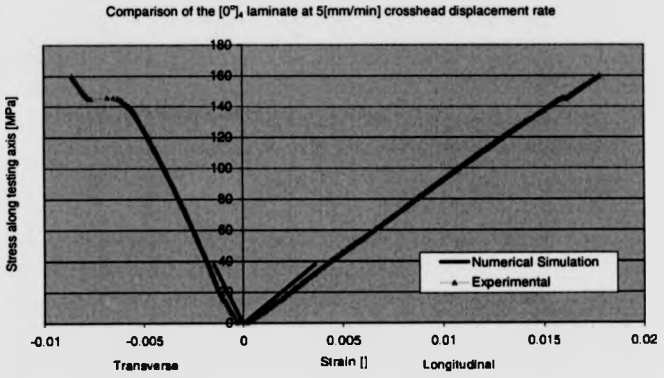

Figure 8.7: Comparison of experimental vs FEM predicted stress vs. strain curves for $[0°]_4$ laminate at 5[mm/min] crosshead displacement rate.

The correlation between experimental and FEM numerical simulation in figure 8.7 for the $[0°]_4$ laminate is good for stiffness predictions. In the comparison region, the longitudinal and transverse responses are linear for both the experimental and the FEM results. This is supported by the results in §7.2.5 and §7.2.6 - the LPCC of the $[0°]_4$ laminate exhibits high correlation values (above .95

for the longitudinal behaviour and above .83 for the transverse behaviour).

The onset of failure is predicted prematurely by the FEM numerical simulation. The results in §7.2.7 and 7.2.8 indicate that the first element is eliminated only at 10-17% of the experimentally observed failure strain (longitudinal and transverse).

The correlation between experimental and FEM numerical simulation in figure 8.8 for the $[\pm 45°]_{2s}$ laminate is good for stiffness predictions. However, the comparison region is very small for the $[\pm 45°]_{2s}$; FEM failure strain is only 1-2% of the experimental failure strain - see §7.2.7 and 7.2.8. Therefore, the high correlation coefficients in §7.2.5 and §7.2.6 are not representative of the correlation between experimental and analytical results.

Figure 8.9 present the comparison of the FEM numerical simulation without a failure criterion for the $[\pm 45°]_{2s}$ laminate.

The FEM results of the $[\pm 45°]_{2s}$ laminate without a failure criteria correlate well with the experimental results over the linear range. They also predict accurately the strain onset of the nonlinearity. However, beyond this point the numerical simulation becomes unstable. At this point it is unclear whether this is due to the effect of the calibration of the transverse damage evolution, or due to the numerical method not being able to capture the physical process. In the experiment multiple parallel cracks formed along the direction of the fibres, giving a ragged texture on the side of the specimen. This suggests that in the experiment there is a level of transverse damage evolution involved, however it is unclear at this stage the extent of its effect.

Compared to the respective $[\pm 45°]_{2s}$ FEM simulation with failure criterion (see figure 8.8), the simulation without a failure criterion failed at significantly higher strain. This indicated that the failure criterion has a significant effect on the numerical simulation of the $[\pm 45°]_{2s}$ laminate.

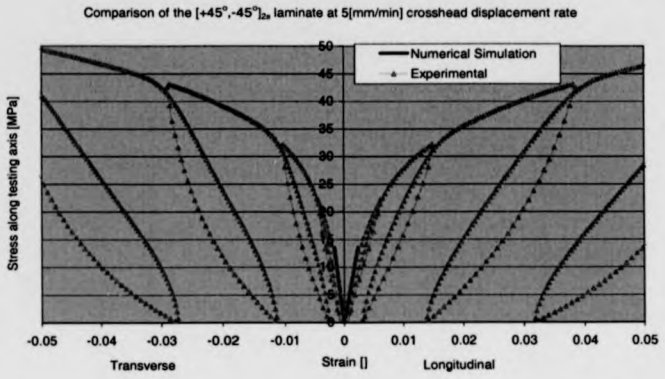

Figure 8.8: Comparison of experimental vs FEM predicted stress vs. strain curves for $[\pm 45°]_{2s}$ laminate at 5[mm/min] crosshead displacement rate.

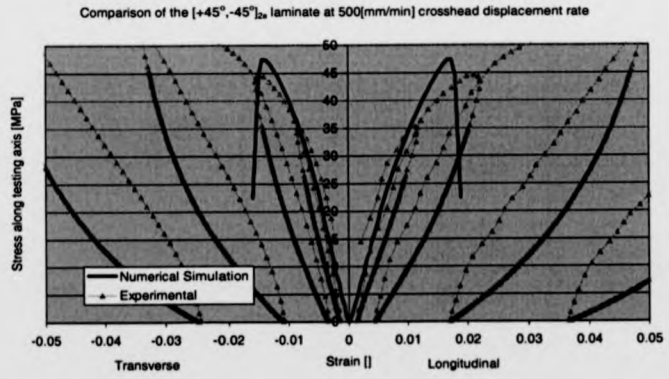

Figure 8.9: Comparison of experimental vs FEM predicted stress vs. strain curves for $[\pm 45°]_{2s}$ laminate at 5[mm/min] crosshead displacement rate - without a failure criterion.

The correlation between experimental and FEM numerical simulation in figure 8.10 for the $[+45°]_8$ laminate is good for stiffness predictions. In the comparison region, the longitudinal and transverse responses are linear for both the experimental and the FEM results. This is supported by the results in §7.2.5 and §7.2.6 - the LPCC exhibits high correlation values (above .95 for the longitudinal behaviour and above .93 for the transverse behaviour) for the $[+45°]_8$ laminate.

The onset of failure is predicted prematurely by the FEM numerical simulation. The results in §7.2.7 and 7.2.8 indicate that the first element in the numerical simulation is eliminated as early as 30% of the longitudinal and 22% of the transverse experimentally observed failure strain. Although, the values for the $[+45°]_8$ laminate are the highest of all laminates, they are still quite low. This fact reduces the validity of the high correlation coefficients.

The correlation between experimental and FEM numerical simulation in figure 8.11 for the $[\pm 67.5°]_{2s}$ laminate is good for stiffness predictions. In the comparison region, the longitudinal and transverse responses are linear for both the experimental and the FEM results. This is supported by the results in §7.2.5 and §7.2.6 - the LPCC exhibits high correlation values (above .97 for both the longitudinal and transverse behaviour) for the $[\pm 67.5°]_{2s}$ laminate.

The onset of failure is predicted prematurely by the FEM numerical simulation. The results in §7.2.7 and 7.2.8 indicate that the first element in the numerical simulation is eliminated between 27-30% of the longitudinal and transverse experimentally observed failure strain. Again, the low LCRR and TCRR values of the $[\pm 67.5°]_{2s}$ laminate reduces the validity of the high correlation coefficients.

As a conclusion, the quantitative analysis showed that the FEM predicted failure initiation at significantly lower strains compared to the experimental observations. Within the comparison range

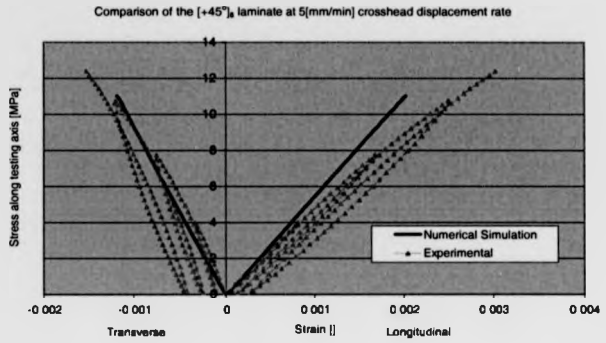

Figure 8.10: Comparison of experimental vs FEM predicted stress vs. strain curves for $[+45°]_8$ laminate at 5[mm/min] crosshead displacement rate.

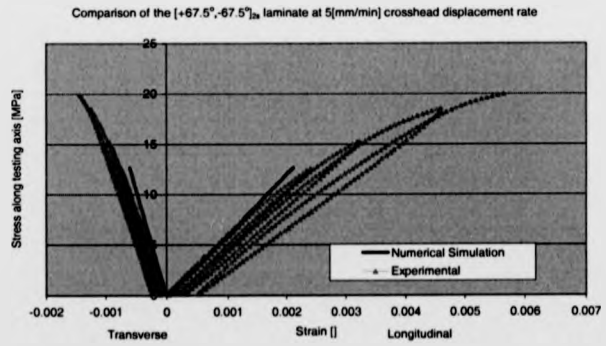

Figure 8.11: Comparison of experimental vs FEM predicted stress vs. strain curves for $[\pm 67°]_{2s}$ laminate at 5[mm/min] crosshead displacement rate.

the results correlated well, however that was expected because the data is based on experimental results and the comparison range does not exhibit non linearity. This suggests that the FEM model which was used has exhibited significant deficiencies.

Chapter 9

Conclusions

This research work has investigated the influence of strain rate dependency on the characterisation properties of a unidirectional glass fibre/thermoplasic composite system. The literature review revealed that little or no research has been done on characterising the strain rate dependency of mechanical properties of these composite systems. Characterisation properties for elasticity, strength and damage evolution of the unidirectional glass/thermoplastic composite system were established.

The principal aim was to extend the understanding and establish/validate a CAE model to simulate shear and transverse damage in a thermoplastic composite material for a certain strain rate range. Some of the findings of this investigation challenge conventional assumptions on evolution and elasticity (i.e. Poisson's ratio and shear damage master curve behaviour).

The conclusions of this research work are listed in categories in order to present them most effectively.

9.1 Conclusions For Characterisation Methodology

Validation methodology for processing the results :

- A rigourous validation methodology was developed to enable objective assessment of strain rate dependency on the properties of a unidirectional glass fibre/ thermoplastic composite material.
- The validation methodology was implemented through a statistical procedure and toolkit.
- The validation methodology verified strain rate dependency at a 5% level of significance for those mechanical properties which exhibited strain rate dependency.
- For those mechanical properties which exhibited strain rate dependency, the validation methodology established a semi-empirical model together with the quality of the relationship for the range of strain rates tested.
- A minimum sample size of ten (10) specimens at each crosshead displacement rate was found to be sufficient in most cases to establish a strain rate dependency. However, sample sizes double the minimum size are generally preferable. Also, it is noteworthy that the minimum sample size is considerably larger than the sample size suggested by testing standards.

Data acquisition method comparison :

- Video extensometry was identified as being promising because it is able to focus on a specific area and obtain simultaneous data from several locations on the specimen.

- Videoextensometry and contacting extensometer testing data computed similar averages for 5 and 50[mm/min] crosshead displacement rate. Significant differences were observed for the averages at 500[mm/min] crosshead displacement rate. This was attributed to the a limitation on the acquisition rate of the two methods.
- Videoextensometry exhibited consistently higher variability compared to contacting extensometry. This is attributed to the size of the gauge length and the data acquisition rate.

9.2 Strain rate dependency of composites

The literature review revealed that past research work investigating strain rate dependency had been undertaken mainly on thermosetting composite systems, compared to thermoplastic composite materials that have received considerably less attention.

For the fibre reinforced thermoplastic composite UD ply:

Effects on Elasticity :

- The longitudinal tensile modulus increases linearly between 5 and 50[mm/min] crosshead displacement rate and then no further increase is observed. This is in agreement to the majority of the reported finding in the field. The strain rate dependency is attributed to the dominating effect of the glass-fibre reinforcement on the longitudinal tensile performance of a unidirectional composite material. The strain rate dependency of glass-fibre is well established.
- The transverse tensile modulus did not exhibit statistically significant difference over

the examined strain rate range. This was an unexpected result since, similar research work on thermosetting composites reported marked strain rate dependency. It is well known that the mechanical properties of the thermoplastic matrix phase (in isolation) exhibit significant viscoelastic properties. This observation may be attributed to the variability of the material, linked to the processing route. Further, the transverse tensile modulus appeared to be higher than virgin polypropylene material.

- The shear modulus decreases linearly over the examined range of strain rate. Considering all the elasticity properties in this study, that were examined the correlation factor was the highest (.847) for shear modulus indicating a high confidence in the result.
- Finally, the Poisson's ratio was found to decrease for increasing strain rate. The strain rate dependency of the Poisson's ratio is a subject that has received much less attention comparatively to the strain rate dependency of other elastic properties. Also, a common assumption in numerical studies is that the Poisson's ratio remains constant.

Effects on strength :

- The longitudinal tensile failure strain increases for increasing strain rate. This is consistent with the reported findings of other research work on the strain rate dependency of glass fibre polymer composite systems. This is attributed to the dominating effect of the glass fibre reinforcement in the longitudinal tensile performance of a unidirectional composite material.
- The longitudinal tensile failure stress increases for increasing strain rate. This outcome is in agreement with most of the research work on strain rate dependency of glass fibre

composite systems. It was found that the fitted model explained only a small percentage of the variability and is suggested that the results were affected by the manufacturing variability.

- The transverse tensile failure strain at different strain rates did not exhibit statistically significant difference, however, there were indications of possible increase. The transverse tensile failure stress at different strain rates did not exhibit statistically significant difference. In both cases, the results were statistically inconclusive and that may be attributed to the brittle nature of the material when loaded transversely to the direction of the fibres. The unidirectional composite fails at low transverse strain and stress. This makes the accuracy and resolution of the instrumentation an important contributor to the variability of the observed results.
- The shear failure strain did not appear to be strain rate dependent over the strain rate range examined, contrary to the shear failure stress that appeared to increase for increasing strain rate. This result is an important finding because in conjunction with the results confirming the strain rate dependency of shear failure strain and shear modulus, this concludes that the shear damage evolution is strain rate dependent.

Effects on shear damage evolution :

- A non-linear behaviour was observed for the shear damage evolution for the thermoplastic composite material. The conventional linear model of the shear damage curve was found to be inadequate for Plytron Material. The effect of the linear approximation (conventional model) on the shear damage evolution of the Plytron material were established.

- The critical shear damage limit increases with increasing strain rate, and therefore the rate of shear modulus degradation decreases.
- The elementary shear damage limit increases for increasing strain rate, therefore, shear failure occurs at higher stress values.
- The initial shear damage limit appears to initially decrease and then increase for increasing strain rate. However, the initial shear damage limit was found not to be representative of the shear pseudoforce at which damage initiates. It is proposed that for thermoplastics or other material systems exhibiting a non-linear response, that the shear pseudoforce value is more appropriate.
- The value of the shear pseudoforce at which damage initiates increases with strain rate, i.e. damage initiates at later.

Effects on transverse damage evolution :

- The characterisation properties of transverse damage evolution exhibited a high value for the coefficient of variance. Therefore characterisation for strain rate dependency is not robust. The high coefficient of variance is attributed to problems of testing such inherently weak materials under cyclic transverse loading, especially at higher strain rates.
- The high coefficient of variance was attributed (apart from the testing issues on transverse composites) to the inconclusive results of the characterisation of the transverse tensile modulus from the previous tests. Because the transverse tensile modulus was set equal at all strain rates, it is speculated that it affected the transformation from

the testing to the material coordinate system. A corollary to this is the proximity of the strain rates in the results of the [±67°] laminates.

- The low value of the coefficient of determination R^2 for the initial transverse damage limit in conjunction with the statistical analysis results for the means and variance, suggests that the results are not conclusive.
- The critical transverse damage limit appeared to increase with strain rate, therefore the rate of transverse damage evolution decreases with strain rate. It is suggested that the quantitative model is not however extrapolated beyond the validated range of strain rate.
- The brittle transverse damage limit appeared to increase with strain rate therefore the maximum value at which transverse failure occurs increases with strain rate. It is suggested that the quantitative model is not however extrapolated beyond the validated range of strain rate.

Effects on coupling factors :

- Although the coupling factor for transverse and shear strains appears to decrease with increase of the strain rate, it was not possible to establish statistically, strain rate dependency.
- The coupling factor between transverse and shear damage is strain rate dependent and appears to decrease with increasing strain rate. However, the validity of the quantitative model is questioned since at all crosshead displacement rates the variances are statistically different.

9.3 Conclusions For FEM

Validation methodology :

- A comparison methodology has been proposed for the validation of the experimental and FEM results. The methodology included qualitative and statistical tools. From the results, the comparison methodology appeared to be representative and robust.

FEM validation :

- In general, it is possible to obtain a high correlation coefficient for stiffness properties obtained by mechanical testing and the ply model in the FEM code. This was expected because experimental data were used as material input data.
- Damage evolution is predictable, but the complexity of the characterisation computation demands small margins of testing error. Consistency and repeatability of the testing results has paramount importance.
- The strain rate dependency is very high, so strain rate characterisation for this class of materials is very important for accurate numerical modelling.
- Failure is predicted prematurely. It was suggested that this maybe attributed to the implementation of the failure criterion, the variability of the results and/or the definition of the grip constraint in the material model.
- The FEM exhibited significant deficiencies in the prediction of the composite laminate behaviour.

9.4 Recommendation For Further Work

In view of the outcomes of this research work, the following further investigations are proposed.

Recommendation of characterisation methodology :

- Extend the strain rate range and the material types. A database of strain rate dependent characterisation properties would be an important resource for CAE for crashworthiness studies.
- The statistical analysis revealed significant scatter for transverse properties, which was attributed to both the material and the data acquisition method. Therefore a method of characterisation for transverse properties requires further investigation to identify principal sources of scatter.
- Formulation of an appropriate characterisation methodology for damage evolution, based on the principles of continuum damage mechanics. It was established that characterisation which assumes a linear master damage curve does not adequately describe the response and is susceptible to error.
- Establish and validate a model of the rate dependent mechanical properties extended across a broader range of strain rates. As an example, an asymptotic (sigmoid) empirical model was proposed, but not implemented.

Recommendations for further work on FEM :

- Validate an FEM model with a or more than one failure criteria implemented at laminate level. It was established that ply level failure criteria tend to predict failure premature for laminates.

- Development of an FEM material mode capable of taking into account the non-linear behaviour of the shear damage evolution.

Recommendations on data acquisition methods :

- Investigation of other non-contacting extensometer methods suitable for strain rate testing. Strain mapping techniques offer significant advantages for the testing of composites (e.g. possibility to obtain data from the entire gauge specimen and focus on the area of interest after the effect).

7

DX

230953

vol.1

DX

230953

vol.2

Strain rate dependency of the properties of a unidirectional thermoplastic composite material

By

Nikolaos Papadakis

A thesis submitted in partial fulfilment of the requirements for the degree of Doctor of Philosophy in Engineering

Volume II– References and Appendices

University of Warwick, School of Engineering

October 2002

Pale and fine print
tightly bound

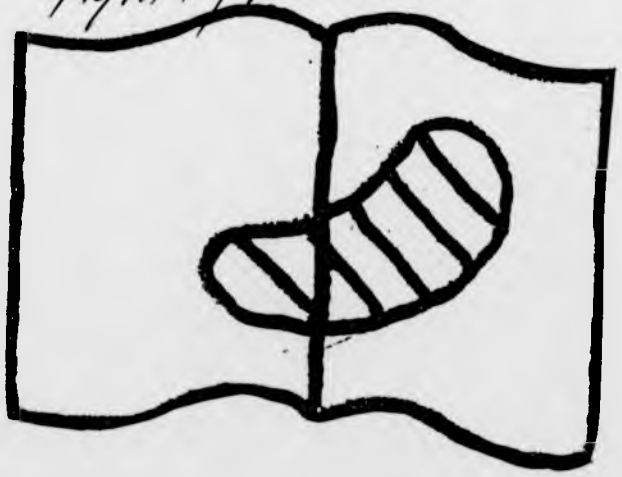

Bibliography

[1] N. Reynolds, M. Pharaoh, D. Fleming, N.Papadakis, and G. Smith. The evaluation of progressive impact damage in reinforced thermoplastic composite laminate materials. *Proceedings of Automotive Composite and Plastics 2000*, 2000.

[2] P. Ladevéze. Damage modelling of the elementary ply for laminated composites. *Composites Science and Technology*, 43:257–267, 1981.

[3] P. Ladevéze and E. Le Dantec. Damage modelling of the elementary ply for laminated composites. *Composites Science and Technology*, 43:257–267, 1992.

[4] N.E. Dowling. *Mechanical Behaviour of Materials.* Prentice Hall International Editions, N.J. 07632, 1993.

[5] A.M.S. Hamouda and M.S.J. Hashmi. Testing of composite materials at high rates of strain: Advances and challenges. *Journal of Materials Processing Technology*, 77:327–336, 1998.

[6] M. Bramuzzo. Dynamic elastic modulus in bending: A new determination technique in impact and rebound conditions. *Polymer Testing*, 5:439–454, 1985.

[7] F.L. Matthews and R.D. Rawlings. *Composite Materials: Engineering and science.* Woodhead Publishing Limited and CRC press, 2nd edition, 1999.

[8] J. Tsai and C.T. Sun. Constitutive model for high strain rate response of polymeric composites. *Composite Science and Technology*, 62:1289–1297, 2002. Received 5 October 2001; received in revised form 7 March 2002; accepted 12 March 2002 (In press).

[9] D. Delfosse, G. Pageau, R. Bennett, and A. Poursartip. Instrumented impact testing at high velocities. *Journal of Composites Technology and Research, JCTRER*, 15(1):38–45, 1993.

[10] F. Dubois and R. Keunings. Dcb testing of thermoplastic composites: A nonlinear micro-macro numerical analysis. *Composites Science and Technology*, 57:437–450, 1997.

[11] J.C. Halpin. *Primer on Composite Materials Analysis.* Technomic Publishing AG, 851, New Holland Avenue, Lancaster, Pennsylvania, USA, 2nd edition, 1992.

[12] A.K. Kaw. *Mechanics of Composite Materials.* CRC Press LLC, New York, 1997.

[13] MIL-HDBK-17-2E. Military handbook. World Wide Web, December 1998. http://www.mil17.org/download.htm.

[14] C. Herackovich. *Mechanics of Fibrous Composites.* John Wiley & Sons, Inc, 1998.

[15] D.R. Hartman, M.E. Greenwood, and D.M. Miller. High strength glass fibers. Technical report, Owens-Corning Fiberglass corporation, Toledo, Ohio, US, 1994.

[16] C.E. Knox. *Handbook of composites*, chapter Fiberglass reinforcement. Van Nostrand Reinhold, New York, 1982.

[17] M. Pinfold. *Composite Mechanical Properties for Use in Structural Analysis.* Phd thesis, Warwick Manufacturing Group, University of Warwick, April 1995.

[18] F.A.R. Al-Salehi, S.T.S. Al-Hassani, and M.J. Hinton. An experimental investigation into the strength of angle gfrp tubes under high rate of loading. *Journal of Composite Materials*, 23:288–305, 1989.

[19] F.A.R. Al-Salehi, S.T.S. Al-Hassani, N.M. Bastaki, and M.J. Hinton. Rate effects on aramid fibre/epoxy (krp) tube under hoop loading. *Applied Composite Materials*, 24(9):894–917, 1990.

[20] N.M.S. Al-Bastaki. Design of fibre reinforced composite structures subjected to high strain rates using finite element analysis. *Applied Composite Materials*, 5:223–236, 1998.

[21] L. Iannucci, R. Dechaene, W. Willows, and J. Degrieck. A failure model for the analysis of thin woven glass composite structures under impact loadings. *Computers and Structures*, 79:785–799, 2001.

[22] L.M. Kachanov. Time of the rupture process creep conditions. *Izn Akad Nauk S.S.R. Otd, Tech Nauk*, 8:pp:26–31, 1958.

[23] Y.N. Rabotnov. Creep rupture. In *Proceedings of 12 International Cong. Applied Mechanics.* Stanford Springer, 1968.

[24] J. Lemaitre and J.L. Chaboche. A nonlinear model of creep-fatigue damage cumulation and interaction. In *Proceedings IUTAM. Symposium on Mechanics of Visco-elastic Media and Bodies.* Springer, Gothenberg, 1974.

[25] J.Hult. *On Topics in Applied Continuum Mechanics.* Springer, New York, 1974.

[26] S. Murakami. Notion of continuum damage mechanics and its application to anisotropic creep damage theory. *Journal of Engineering Material Technology*, 105:99–105, 1983.

[27] J. Lemaitre. *A course on Damage Mechanics.* Springer-Verlag, 2nd edition, July 1996. ISBN:3-540-60980-6.

[28] J. Lemaitre and J.L. Chaboche. *Mechanics of Solid Materials.* Cambridge University Press, Cambridge, 1990.

[29] D. Krajcinovic. Damage mechanics. *Mechanics of Materials*, 8:117–197, 1989.

[30] Z.P. Bazant and L. Cedolin. *Stability of Structures*, chapter 13. Oxford University Press, New York, 1991.

[31] D.Krajcinovic. Damage mechanics: accomplishments, trends and need. *International Journal of Solids and Structures*, 37:267–277, 2000.

[32] G.R. Cowper and P.S. Symonds. Strain hardeingn and strain rate effects in the impact loading of cantilever beams. Report 28, Brown University, Division of Applied Mathematics, September 1957.

[33] N. Jones. *Structural Impact*, chapter Strain rate sensitive behaviour of materials, pages 348–355. Cambridge University Press, 1989. First paperback edition 1997.

[34] ESI. *PAM-CRASH Solver Notes*, solver manual Ply Data, pages Ply Data – 2. ESI, level 18 edition, 2000.

[35] M.A. Meyers. *Dynamic Behavior of Materials.* John Wiley and Sons, 1994.

[36] S.T.S. Al-Hassani and A.S. Kaddour. Strain rate effects on GRP, KRP and CFRP composite laminates. *Key Engineering Materials*, 141-143:427–452, 1998.

[37] I.M. Daniel, T. Liber, and R.H. LaBedz. Wave propagation in transversely impacted composite laminates. *Experimental Mechanics*, 19:9–16, 1979.

[38] B.W. Abbot and L.J. Broutman. Elastic longitudinal stress wave speed. *Experimental Mechanics*, 6:383, 1966.

[39] A.E. Armenákas and C.A. Sciammarella. Response of glass -fibre reinforced epoxy specimens to high rates of tensile loading. *Experimental Mechanics*, 13:433–440, October 1973.

[40] R.H. Cooper and J.D. Campbell. Testing of materials at medium rates of strain,. *Journal of Mechanical Engineering and Science*, 9:278, 1967.

[41] J.D. Campbell. Dynamic plasticity: macroscopic and microscopic aspects. *Materials Science and Engineering*, 12:3, 1973.

[42] P.S. Follansbee. *ASM Handbook*, volume 8, chapter High-strain-rate testing. ASM, 1990.

[43] J. Harding. *Shock-Wave and High Strain Rate Phenomena in Materials*, chapter Mechanical behaviour of composite materials under impact loading, page 21. Number 0-8247-8579-7. Dekker, 1992.

[44] P.J. Shadbolt. A preliminary investigation of plate perforation by projectiles in the subordance range. Report 1372:81, Oxford University, Oxford, 1981.

[45] F.J. Bradshaw. Impact resistance of carbon reinforced plastics. Technical Report 72240, Royal Aircraft Establishment, MOD, 1972.

[46] P.W. Manders and W.C. Harris. A parametric study of composite performance in compression-after-impact testing. *Journal of Society American Plastic Engineers SAMPE*, 22:47, 1986.

[47] A. Rotem. Residual flexural strength of frp composite specimens subjected to transverse impact loading. *Journal of Society of American Plastic Engineers*, 24:19, 1988.

[48] J.G. Avery. Design manual for impact damage tolerant aircraft structures. AGARDograph 238, NATO, 1981.

[49] A.M.S. Hamouda and M.S.J. Hashmi. *Advanced Composites*, chapter High strain rate constitutive equation for aluminium metal matrix composites, page 1119. TMS, 1993.

[50] S. Barre, T. Chotard, and M.L. Benzeggagh. Comparative study of strain rate effects on mechanical properties of glass fibre-reinforced thermoset matrix composites. *Composites Part A*, 27(A):1169–1181, 1996.

[51] W.J. Cantwell and J. Morton. The impact resistance of composite materials - a review. *Composites*, 22:347–362, 1991.

[52] F.A.R. Al-Salehi, S.T.S. Al-Hassani, N.M. Bastaki, and M.J. Hinton. Extracting dynamic basic ply properties from test data on angle ply laminates - 1. theoretical procedures. *Journal of Composite Materials*, 26:2454–2476, 1992.

[53] D.F. Adams and J.L. Perry. Instrumented charpy impact test of sever unidirectional composite materials. *Fibre Science and Technology*, 8:275–302, 1975.

[54] M. Todo, K. Takahashi, P. Béguelin, and H.H. Kausch. Strain rate dependence of the tensile fracture behaviour of woven cloth reinforced polyamide composites. *Composite Science and Technology*, 60:763–771, 2000.

[55] C. Wolff and A.R. Brunsell. Developments in the science and technology of composite materials. ECCM4 Proceedings, page 653, 25-28 September 1990.

[56] G.E. Dieter. *Mechanical Metallurgy*, chapter Applications to mechanical testing, pages 304–305. Materials Science & Engineering S. McGraw-Hill, 1986.

[57] M.A. Hamstad and P.P. Gillis. *Material Research Standards*, 6:569–573, 1966.

[58] A. Rotem and I.M. Lifshitz. Time-dependent longitudinal strength of unidirectional fibrous composites. 26th Annual Technical Conference, Reinforced Plastics/Composite Division, Soc. Plastics Industry, Section 10-6, February 1971.

[59] T. Fujii and M. Miki. Symposium on Mechanical Behaviour of Materials, Soc. Mat. Sci., Kyoto, Japan, 1973. 83.

[60] J.M. Lifshitz. Impact strength of angle ply fiber reinforced materials. *J. Composite Materials*, 10:92–101, 1976.

[61] J.M. Lifshitz and A. Gilat. Experimental determination of the nonlinear shear behaviour of fiber-reinforced laminae under impact loading. *Experimental Mechanics*, 19:444–449, 1979.

[62] J.D. Winkel and D.F. Adams. *Composites*, 16:268, 1985.

[63] M.N. Nahas. Survey of failure and post-failure theories of laminated fiber-reinforced composites. *Journal of Composites Technology and Research*, 8(4):138–153, 1986.

[64] N.M. Al-Bastaki. *PhD Thesis.* PhD thesis, Applied Mechanics Division, UMIST, Manchester, UK, 1989.

[65] D.F. Adams and L.G. Adams. *Journal of Composite Materials*, 24:256, 1990.

[66] British Standards. Bs2782 part 3 - method 360 determination of charpy impact strength of rigid materials. British Standards, Methods for Testing Plastics.

[67] J. Coulton. *Effect of elevated strain rates on the mechanical performance of polyethylene structures.* PhD Thesis, School of Engineering, University of Warwick, May 1996.

[68] D.F. Adams. In *Proceedings of the Fourth International Conference on Composite Materials Testing and Design*, page 1977. ASTM, 1977.

[69] M.G. Phillips. *Fibre Composite Hybrid Materials*, chapter 4. Number 0853349282. Applied Science Publishers, London, February 1981.

[70] R.L. Sierakowski. *Dynamic Constitutive Failure Models*, chapter : High strain rate resting of composites. Number AFWAL-TR-88-4229,. 1988.

[71] E.D. Davies and S.C. Hunter. The dynamic compression testing of solids by the method of split hopkinson pressure bar. *Journal of Mechanics and Physics of Solids*, 11:155–179, 1963.

[72] J.Z. Malinowski and J.R. Kkeoaczko. A unified numerical and analytical approach to specimen behaviour in the split hopkinson bar. *International Journal of Mechanical Sciences*, 28(6):381–391, 1986.

[73] L.D. Bertholf and C.H. Karnes. Two dimensional analysis of split hopkinson pressure bar. *Journal of Mechanics and Physics of Solids*, 23:1–19, 1975.

[74] T. Nicholas. *Impact Dynamics*, chapter Material behaviour at high strain rates. John Wiley and Sons, New York, 1982.

[75] L.M. Welsh and J. Harding. Dynamic tensile response of unidirectionally reinforced carbon epoxy and glass epoxy composites. *Proceedings 5th International Conference on Composite Materials ICCM V*, pages 1517–1531, 1985. TMS-AIME.

[76] Y. Xia and X. Wang. Constitutive equation for unidirectional composites under impact. *Composite Science and Technology*, 56:155–160, 1996.

[77] H. Kolsky. An investigation of the mechanical properties of materials at very high rates of loading. *Proceedings of Physics Society, London*, B(62):767, 1949.

[78] C.A. Ross and R.L. Sierakowsky. Dynamic compressive properties of a metal matric composite material. In *Proceedings of the 16th SAMPE National symposium*, pages 109–121, Anaheim, 1971.

[79] L.J. Griffiths and D.J. Martin. A study of the dynamic behaviour of carbon fiber composite using the Split Hopkinson bar. *Journal of Physics D: Applied Physics*, 7:229–2341, 1974.

[80] Y.L. Bai and J. Harding. Fracture initiation in glass reinforced plastic under impact loading: Mechanical properties at high rates of strain. In *Institute of Physics conference*, pages 339–350, Oxford, 1984.

[81] J.D. Campbell and J.L. Lewis. The development and use of a torsional split hopkinson bar for testing material at shear strain rates up to 1500[1/s]. Report No 1080, 69, University of Oxford, Department of Engineering Science, 1969.

[82] K.A. Hartley, J. Duffy, and R.H. Hawley. *Metals Handbook*, volume 8, chapter The torsional Kolsky (split Hopkinson) bar, page 218. American Society of Metals, 9th edition edition, 1985.

[83] S.M. Werner and C.K.H. Dharan. The dynamic response of graphite fibre-epoxy laminate at high shear strain rate. *Journal of Composite Materials*, 20:365, 1986.

[84] J. Harding and L.M. Welsh. A tensile testing technique for fibre reinforced composites at impact rates of strain. *Journal of Materials Science*, 18:1810–1826, 1983.

[85] C.A. Ross, W.H. Cook, and L.L. Wilson. Dynamic tensile tests of composite materials sing a split Hopkinson pressure bar. *Experimental Techniques*, (8):30–33, 1984.

[86] Z.G. Liu and C.Y. Chiem. A new technique for tensile testing of composite materials using a split Hopkinson pressure bar. *Experimental Techniques*, (12):20–21, 1988.

[87] P. Arnaud and P. Hamelin. Dynamic characterisation of structures: A study of energy absorption in composite tubes. *Composites Science and Technology*, 58:709–715, 1998.

[88] M. Stelly. Comportement méchanique des matériaux sollicités á grande vitesse: premiére partie: Défomration dynamique. *Matériaux et Techniques*, pages 485–493, 1986.

[89] J.M. Lifshitz and H.Leber. Response of fibre reinforced polymers to high strain rate loading in interlaminar tension and combined tension/shear. *Composite Science and Technology*, 58:987–996, 1998.

[90] L. Ninan, J. Tsai, and C.T. Sun. Use of split Hopkinson pressure bar for testing off-axis composites. *International Journal of Impact Engineering*, 25:291–313, 2001.

[91] D.J. Ruiz. High strain rate testing of materialsa fully validated test calibration by a hybrid numericalexperimental technique. *J. de Physique, IV*, page 465, 1991.

[92] J. Harding and L. Dong. The effect of strain rate on the interlaminar shear strength of woven reinforced laminates,. In J. Fuller et al., editor, *Proc. ECCM-4 Developments in the Science and Technology of Composite Materials*, page 517, London, 1990. Elsevier Applied Science.

[93] W.J. Cantwell. Phd thesis, University of London, 1985.

[94] S. Amijima, T. Fujii, S. Siba, and H. Tanioka. *Proceedings of Japanese Conference on Material Research.*, page 251, September 1978. Society of Materials Science.

[95] S. Amijima, T. Fujii, S. Siba, and H. Tanioka. Compressive strength and fracture characteristics of fiber composites under impact loading. *Proceedings of 3rd Int. Conf. on Composite materials ICCM-3.*, pages 399–413, 1980.

[96] P. Kumar, A. Garg, and B.D. Agarwal. Dynamic compressive behaviour of unidirectional gfrp for various fibre orientations. *Materials Letters*, 4(2):111, 1986.

[97] P. Kumar and A. Garg. *Journal Material Science*, 23:2305–2309, 1988.

[98] AMMRC. *Proceedings of Army symposium on Solid Mechanics*, number ACC No. P2229.67, 1976.

[99] I.M. Daniel, R.H. LaBedz, and T. Liber. New method for testing composites at very high strain rates. *Experimental Mechanics*, 21:71–77, 1981.

[100] I.M. Daniel, R.H. LaBedz, and W.G. Hamilton. *Composite Materials: Testing and Design 6th Conference*, ASTM STP:p.393, 1982.

[101] C.C. Chamis and G.T. Smith. Environmental and high strain rate effects on composites for engine applications. *Journal of American Institute of Aeronautics and Astronautics*, 22(1), 1984.

[102] F.A.R. Al-Salehi, S.T.S. Al-Hassani, N.M. Bastaki, and M.J. Hinton. Derived dynamic ply properties from test data on angle ply laminates. *Applied Composite Materials*, 4(3):157–172, 1997.

[103] A.S. Kaddour, F.A.R. Al-Salehi, S.T.S. Al-Hassani, and M.J. Hinton. Simultaneous determination of in-plane shear and transverse moduli of unidirectional composite laminae at different strain rates and temperatures. *Composite Science Technology*, 53(4):431–444, 1995.

[104] A.S. Kaddour, F.A.R. Al-Salehi, S.T.S. Al-Hassani, and M.J. Hinton. Burst behaviour of $\pm 75^{\circ}$ filament wound kevlar/epoxy and carbon/epoxy tubes at high loading rates. *Composite Science Technology*, 56(10):1151–1159, 1996.

[105] I.M. Daniel and R.H. LaBedz. *Compression testing of homogeneous materials and Composites*, page 121. STP 808. American Society for Testing and Materials, 1983.

[106] N.M. Cameron. *PhD thesis*. PhD thesis, University of Illinois, 1965.

[107] I.M. Daniel and T. Liber. Strain rate effects on the mechanical properties of fiber composites, part 3. Report CR-135087, NASA, 1976.

[108] I.M. Daniel and T. Liber. Testing fiber composites at high strain rates. *Proceedings of 2nd International Conference on Composite Materials(ICCM2)*, pages 1003–1018, April 1978. Toronto.

[109] M.Z. Shah Khan and G. Simpson. Mechanical properties of a glass reinforced plastic naval composite material under increasing compressive strain rates. *Material Letters*, 45:167–174, 2000.

[110] A. Agbossou, I. Cohen, and D. Muller. Effects of interphase and impact strain rates on tensile off axis behaviour of unidirectional glass fibre composite: Experimental results. *Engineering Fracture Mechanics*, 52(5):923–934, 1995.

[111] M. Detassis, A. Pegoretti, and C. Migliaresi. Effect of temperature and strain rate on interfacial shear stress transfer in carbon/epoxy model composites. *Composite Science and Technology*, 53:39–46, 1995.

[112] J.L. Lataillade, M. Delaet, F. Collombet, and C. Wolff. Effects of the intralaminar shear loading rate on the damage of multi-ply composites. *International Journal of Impact Engineering*, 18(6):679–699, 1996.

[113] P.S. Theocaris. *The Mesophase Concept in Composites*. Springer, 1987.

[114] M. Tanoglu, S.H. McKnight, G.R. Palmese, and J.W. Gillspie. A new technique to characterise the fiber/matrix interphase properties under high strain rates. *Composites Part A*, 31:1127–1138, 2000.

[115] M.J. Greenfield, A. Pedicini, and L.S. Penn. Development of single fiber fragmentation test for high strain rates. *International Journal of Adhesion and Adhesives*, 20:403–407, 2000.

[116] F.J. Behler and S. Sikorski. Impact behaviour of carbon fiber reinforced. *J. de Physique IV*, (283), 1991.

[117] O.I. Okoli and G.F. Smith. High speed performance of composite materials. *Engineering Polymers Integrated Capability (EPIC) Conference*, March 1996. Work Area 2d, University of Warwick.

[118] O.I. Okoli, G.F. Smith, and A. Abdul-Latif. The impact response of Glass Fibre Reinforced Composites: A comparison between Finite Element results and Experimental Data. *Proceedings of Society of Plastic Engineers Annual Technical Conference*, 2:2504–2509, May 1996. Advanced Polymer Composites Division.

[119] O.I. Okoli. *Experimental Determination of Transient Dynamic Response of Fibre Reinforced Polymer Composites.* Phd thesis, Engineering, University of Warwick, 1996.

[120] O.I. Okoli and G.F. Smith. The effects of strain rate and fibre content on the Poisson's ratio of Glass/Epoxy composites. *Journal of Materials Science*, pages 5415–5422, 1998.

[121] S.M. Walley, J.E. Field, P.H. Pope, and N.A. Safford. The rapid deformation behaviour of various polymers. *Journal of Physics III*, Not Applicable(1):1889–1925, 1991.

[122] W.J. Cantwell. The influence of loading rate on the mode ii interlaminar fracture toughness of composite materials. *Journal of Composite Materials*, 31(4):1364–1380, 1997.

[123] C.A. Weeks and C.T. Sun. Modelling non linear rate dependent behaviour in fiber reinforced composites. *Composites Science and Technology*, 58:603–611, 1998.

[124] Thiruppukuzhi S.V. and C.T. Sun. Models for the strain-rate-dependent behaviour of polymer composites. *Composites Science and Technology*, 61:1–12, 2001.

[125] G. Subhash, S. Suibhavi, and M.A. Zirky. Influence of strain rate on the uniaxial compressive behaviour of 2-d braided textile composites. *Composites: Part A*, 32:1583–1591, 2001.

[126] A.G. Mamalis, D.E. Manolakos, G.A. Demosthenous, and M.B. Ioannidis. Collapse of fibreglass composite automotive frame rails. *Composite Structures*, 34:77–90, 1996.

[127] A.M.A. El-Habak. *Journal of Composite Technology Research*, 15:311, 1990.

[128] J. Fan and W.S. Slaughter. High strain rate compression of fiber composites. *Journal of Mechanics and Physics of Solids*, 45(5):731–751, 1997.

[129] M.R. Piggot and B. Harris. Compression strength of carbon, glass and Kevlar-49 fibre reinforced polyester resins. *Journal of Material Science*, 15:2523–2538, 1980.

[130] P.M. Jelf and N.A. Fleck. Compressive failure of unidirectional composites. *Journal of Composite Materials*, 26:2706–2726, 1992.

[131] H.D. Espinosa, Y. Xu, and H.C. Lu. Inelastic behaviour of fiber composites subjected to out-of-plane high strain rate shearing. *Acta Mater*, 45(11):4855–4865, 1997.

[132] J.D. McGee and S. Nemat-Nasser. Dynamic bi-axial testing of woven composites. *Material Science and Engineering*, A317:135–139, 2001.

[133] M.Z. Shah Khan, G. Simpson, and E.P. Gellert. Resistance of glass fibre reinforced polymer composites to increasing compressive strain rates and loading rates. *Composites Part A*, 31:57–67, 2000.

[134] A.S. Khan, O.U. Colak, and P. Centala. Compressive failure strengths and modes of woven s2-glass reinforced polyester due to quasi static and dynamic loading. *International Journal of Plasticity*, 18:1337–1357, 2002.

[135] O.I. Okoli. The effects of strain rate and failure modes on the failure energy of fibre reinforced composites. *Composite Structures*, 54:299–303, 2001.

[136] O.I. Okoli and A. Abdul-Latif. Failure in composite laminates: overview of an attempt at prediction. *Composites Part A*, 33:315–321, 2002.

[137] B.L. Peterson, R.N. Pangborn, and C.G. Pantano. Static and high strain rate response of glass fiber reinforced thermoplastic. *Journal of Composite Materials*, 25:887–906, 1991.

[138] K. Kawata, A. Hondo, S. Hashimoto, N.Tokeda, and H.L. Chung. Dynamic behaviour analysis of composite materials. *Japan-US conference on Composite Materials proceedings*, pages 2–11, 1981. Tokyo.

[139] C. Kammerer and A. Neme. Plane behaviour at high strain rates of a quasi unidirectional e-glass/polyester composite: application to ballistic impacts. *Journal of Mechanics and Solids*, 17(3):461–477, 1998.

[140] S.V. Hayes and D.F. Adams. Rate sensitive tensile impact properties of fully and partially loaded unidirectional composites. *Journal of Testing Evaluation*, 10(2):61–68, 1982.

[141] Y. Wang and Y. Xia. A modified constitutive equation for unidirectional composites under tensile impact and the dynamic tensile properties. *Composite science and Technology*, 60:591–596, 2000.

[142] S Pardo, D. Baptiste, D.Decobert, J.Fitoussi, and R. Joannic. Tensile dynamic behaviour of quasi unidirectional e-glass/polyester composite. *Composite Science and Technology*, 62:579–584, 2002.

[143] H.Zhao and G. Gary. An experimental investigation of compressive failure strength of fibre reinforced polymer matrix composite plats under impact loading. *Composite Science and Technology*, 57:287–292, 1997.

[144] H.M. Hsiao and I.M. Daniel. Strain rate behaviour of composite materials. *Composites Part B*, 28(B):521–533, 1998.

[145] H.M. Hsiao, I.M. Daniel, and R.D. Cordes. Dynamic compressive behaviour of thick composite materials. *Experimental Mechanics*, 38:172-180, 1998.

[146] H.M. Hsiao, I.M. Daniel, and R.D. Corder. Strain rate effects on the transverse compressive and shear behaviour of unidirectional composites. *Journal of Composite Materials*, 33:1620-1642, 1999.

[147] G.H. Staab and A. Gilat. High strain response of angle-ply glass/epoxy laminates. *Journal of Composite Materials*, 29:1308–1320, 1995.

[148] J. Raghavan and M. Meshii. Time dependent damage in carbon fibre reinforced polymer composites. *Composites Part A*, 27(A):1223, 1227 1996.

[149] G. Belingardi and R. Vadori. Low velocity impact tests of laminate glass fiber epoxy matrix composite material plates. *International Journal of Impact Engineering*, 27:213–229, July 2002.

[150] Y. Xia and Z. Wang. A dynamic Monte Carlo microscopic damage model incorporating thermo-mechanical coupling in a unidirectional composite. *Composite Science and Technology*, 59:947–955, 1999.

[151] C. Kammerer and A. Neme. Thermodynamic constitutive model for the damageable elastoviscoplastic behaviour of e-glass/polyester unidirectional plies. In *In proceedings of 5th International Symposium on Plasticity*, pages 969–972, Osaka, 1995. Dynamic plasticity and structure behaviours.

[152] C. Kammerer and A. Neme. Plane behaviour of an e-glass/polyester composite at high strain rates. *Composite Science and Technology*, 58:717–725, 1998.

[153] C. Kammerer. *Plane constitutive model of a E-glass/polyester quasi unidirectional composite under low and high strain rates: application to impact tests.* PhD thesis, Université de Paris XIII, Villetaneuse, 1996.

[154] Y. Miyano, M. Kanemitsu, T. Kunio, and M. Miki. Influence of matrix resin on ultimate strength of unidirectional CFRP. In *Proceedings of 4th international Conference on Mechanical Behaviour of Materials*, volume 1, pages 473–479, 1983.

[155] M.L. Williams, R.F. Landel, and J.D. Ferry. *Journal of American Chemical Society*, 77:3701, 1955.

[149] G. Belingardi and R. Vadori. Low velocity impact tests of laminate glass fiber epoxy matrix composite material plates. *International Journal of Impact Engineering*, 27:213–229, July 2002.

[150] Y. Xia and Z. Wang. A dynamic Monte Carlo microscopic damage model incorporating thermo-mechanical coupling in a unidirectional composite. *Composite Science and Technology*, 59:947–955, 1999.

[151] C. Kammerer and A. Neme. Thermodynamic constitutive model for the damageable elastoviscoplastic behaviour of e-glass/polyester unidirectional plies. In *In proceedings of 5th International Symposium on Plasticity*, pages 969–972, Osaka, 1995. Dynamic plasticity and structure behaviours.

[152] C. Kammerer and A. Neme. Plane behaviour of an e-glass/polyester composite at high strain rates. *Composite Science and Technology*, 58:717–725, 1998.

[153] C. Kammerer. *Plane constitutive model of a E-glass/polyester quasi unidirectional composite under low and high strain rates: application to impact tests.* PhD thesis, Université de Paris XIII, Villetaneuse, 1996.

[154] Y. Miyano, M. Kanemitsu, T. Kunio, and M. Miki. Influence of matrix resin on ultimate strength of unidirectional CFRP. In *Proceedings of 4th international Conference on Mechanical Behaviour of Materials*, volume 1, pages 473–479, 1983.

[155] M.L. Williams, R.F. Landel, and J.D. Ferry. *Journal of American Chemical Society*, 77:3701, 1955.

[156] C.A. Weeks. *Non linear rate dependent response of thick section composite laminates.* Phd thesis, Purdue University, USA, 1995.

[157] C.A. Weeks and C.T. Sun. Non linear rate dependent response of thick section composite laminates. In *International Mechanical Congress and Exposition*, San Francisco, November 1995.

[158] J.L. Chen and C.T. Sun. A plastic potential function suitable for anisotropic fiber composites. *Journal of Composite materials*, 27:1379, 1993.

[159] S.V. Thiruppukuzhi and C.T. Sun. Testing and modelling high strain rate behaviour of polymeric composites. *Composites Part B*, 29(B):535–546, 1998.

[160] C.T. Sun and J.L. Chen. A simple flow rule for characterising nonlinear behaviour of polymer composites. *Journal of Composite Materials*, 23(1009-1020), 1989.

[161] O.I. Okoli and G.F. Smith. Development of semi-empirical method for obtaining the dynamic Young's modulus in random continuous reinforced glass/epoxy composites. *Journal of Reinforced Plastic Composites*, 19(4):292–300, 2000.

[162] S. Langlie and W. Cheng. Numerical simulation of high velocity impact on fibre reinforced composites. *ASME P.V. and P.*, 59(1):51–64, 1989.

[163] L. Iannucci and M. Willows. Simulation of ice impact onto composite sandwich panels. Dyna3D User Conference, 1994.

[164] M. Willows and L. Iannucci. A comparison between the standard dyna3d composite material model and an in-house developed composite damage model. Dyna3D User Conference, 1994.

[165] A. F. Johnson and A.K. Pickett. Impact and crash modelling of composite structures: A challenge for damage mechanics. Technical report, German Aerospace Center (DLR)and Engineering Systems International GmbH, Institute of Structures and Design, Stuttgart, Germany and Eschborn, Germany, 1999.

[166] A.F. Johnson and J. Simon. Modelling fabric reinforced composites under impact loads. In *EUROMECH 400: Impact and damage tolerance modelling of Composite materials and structures*, Imperial College of Science and Technology & Medicine, London, 27-29 September 1999. German Aerospace Centre (DLR), institute of Structures and Design.

[167] K. Chang and K.Y. Chang. A progressive damage model for laminated composites containing stress concentrations. *Journal Composite Materials*, 21:834–855, 1987.

[168] P.Ladevz'eze and E. Le Dantec. Damage modelling of the elementary ply for laminated composites. *Composites Science and Technology*, 43:pp. 257–267, January 1992.

[169] K. Chang and K.Y. Chang. Post-failure analysis of bolted composite joints in tension or shear-out mode failure. *Journal Composite Materials*, 21:809–833, 1987.

[170] J. Hallquist. *LS-Dyna3D Theory Manual.* Livermore Software Technology Corporation, Livermore Software Technology Corporation, 2876 Waverley Way, Livermore, California, 94550-7612, 1998.

[171] S.W. Tsai and E.M. Wu. A general theory of strength for anisotropic materials. *J. of composite Materials*, 5:58–80, 1971.

[172] Borealis. Plytron data book. Borealis report.

[173] ISO. Standard test method for tensile properties of polymer matrix composite materials. American Society of Testing Methods, June 1995.

[174] ASTM-E83. Practice for verification and classification of extensometers. American Society for Testing and Materials, Annual Book of ASTM Standards, West Conshohocken,PA, 1994.

[175] N. Papadakis, N. Reynolds, M. Pharaoh, P. Wood, and G. Smith. Experimental issues regarding the characterisation of shear properties and shear damage evolution within a unidirectional composite laminate material. *Materials Research Conference Proceedings*, May 2001.

[176] W.W. Hines and D.C. Montgomery. *Probability and statistics in Engineering and Management Science*, chapter 11, pages 301–303. John Wiley & Sons, 3rd edition, 1990.

[177] I. Doltsinis. *Stochastic Analysis of Multivariate Systems in Computational Mechanics and Engineering.* International Center for Numerical Methods in Engineering (CINME), Gran Capitan, Barcelona, Spain, 1st edition, September 1999.

[178] J.E. Ashton, J.D. Halpin, and P.H. Petit. *Primer on composite materials: Analysis.* Technomic Publishing, West Port, CT, 1969.

[179] R.F. Foral and W.D. Humphrey. *Journal A.I.A.A.*, 22:111, 1984.

[180] G.J. Dvorak and N. Law. Analysis of progressive matrix cracking in composite laminates. *J. of Composite Materials*, 21:309–329, 1987.

[181] E.M. Wu. Optimal experimental measurements of anisotropic failure tensors. *J. of Composite Materials*, 6:472–489, 1972.

[182] S.C. Cowin. On the strength anisotropy of bone and wood. *Trans. ASME J. Applied Mechanics*, 46 (4):832–838, 1979.

[183] R.C. Tennyson, D. McDonald, and A.P. Nanyaro. Evaluation of the tensor polynomial failure criterion for composite materials. *J. Composite Materials*, 12:63–75, 1978.

[184] R.C. Tennyson, A.P. Nanyaro, and G.E. Wharram. Application of the cubic polynomial strength criterion to the failure analysis of composite materials. *J. Composite Materials supplement*, 14:28–41, 1980.

[185] C.T. Herakovich and D.A. O'Brian. Failure analysis of an idealised composite damage zone. Presented at the MFPG Symposium on Advanced Composites: Design and Applications, 1979.

Appendix A

Review Of Classical Laminate Theory (CLT)

Chapter Objectives

- Basic definitions of elastic equations of a Lamina.
- Introduction to Laminate Analysis.

A.1 Introduction To Laminate Analysis.

Hooke's law provides the constitutive equation between stress and strain. The generic form is given by equation A.1.

$$\sigma = \mathbf{Q}\varepsilon \tag{A.1}$$

where:

σ : is the stress vector;

ε : is the strain vector;

$\mathbf{Q}$: is the *stiffness* matrix.

There are two strain vector representations: the engineering ε and the true $\bar{\varepsilon}$ strain vector. The relationship between the engineering and the true strain vector is presented in equation A.2 :

$$\varepsilon = \begin{bmatrix} \varepsilon_{11} \\ \varepsilon_{22} \\ \varepsilon_{33} \\ \gamma_{23} \\ \gamma_{31} \\ \gamma_{12} \end{bmatrix} = R\bar{\varepsilon} = \begin{bmatrix} 1 & 0 & 0 & 0 & 0 & 0 \\ 0 & 1 & 0 & 0 & 0 & 0 \\ 0 & 0 & 1 & 0 & 0 & 0 \\ 0 & 0 & 0 & 2 & 0 & 0 \\ 0 & 0 & 0 & 0 & 2 & 0 \\ 0 & 0 & 0 & 0 & 0 & 2 \end{bmatrix} \begin{bmatrix} \varepsilon_{11} \\ \varepsilon_{22} \\ \varepsilon_{33} \\ \varepsilon_{23} \\ \varepsilon_{31} \\ \varepsilon_{12} \end{bmatrix} \tag{A.2}$$

The representation ε of the strain is the one suitable for use in the generalised Hooke's Law. The benefit of the $\bar{\varepsilon}$ strain representation is that the strains can be readily transformed to another coordinate system. $\mathbf{R}$ is the Reuters matrix which is used for the conversion between the two strain vector forms.

A.1.1 Hooke's Law For Orthotropic Materials.

The general form of Hooke's Law for an orthotropic material is presented in equation A.3. Orthotropic material have three mutually perpendicular planes of elastic symmetry[12, 11].

$$\begin{bmatrix} \sigma_{11} \\ \sigma_{22} \\ \sigma_{33} \\ \tau_{23} \\ \tau_{31} \\ \tau_{12} \end{bmatrix} = \begin{bmatrix} Q_{11} & Q_{12} & Q_{12} & 0 & 0 & 0 \\ Q_{12} & Q_{22} & Q_{23} & 0 & 0 & 0 \\ Q_{12} & Q_{23} & Q_{33} & 0 & 0 & 0 \\ 0 & 0 & 0 & Q_{44} & 0 & 0 \\ 0 & 0 & 0 & 0 & Q_{55} & 0 \\ 0 & 0 & 0 & 0 & 0 & Q_{66} \end{bmatrix} \begin{bmatrix} \varepsilon_{11} \\ \varepsilon_{22} \\ \varepsilon_{33} \\ \gamma_{23} \\ \gamma_{31} \\ \gamma_{12} \end{bmatrix} \tag{A.3}$$

The *stiffness* matrix **Q** can be presented as a function of the material constants (see A.4

$$\mathbf{Q} = \begin{bmatrix} \frac{1-\nu_{23}\nu_{32}}{E_{22}E_{33}\Delta} & \frac{\nu_{21}+\nu_{23}\nu_{31}}{E_{22}E_{33}\Delta} & \frac{\nu_{31}+\nu_{21}\nu_{32}}{E_{22}E_{33}\Delta} & 0 & 0 & 0 \\ \frac{\nu_{21}+\nu_{23}\nu_{31}}{E_{22}E_{33}\Delta} & \frac{1-\nu_{13}\nu_{31}}{E_{11}E_{33}\Delta} & \frac{\nu_{32}+\nu_{12}\nu_{31}}{E_{11}E_{33}\Delta} & 0 & 0 & 0 \\ \frac{\nu_{31}+\nu_{21}\nu_{32}}{E_{22}E_{33}\Delta} & \frac{\nu_{32}+\nu_{12}\nu_{31}}{E_{11}E_{33}\Delta} & \frac{1-\nu_{12}\nu_{21}}{E_{11}E_{22}\Delta} & 0 & 0 & 0 \\ 0 & 0 & 0 & G_{23} & 0 & 0 \\ 0 & 0 & 0 & 0 & G_{13} & 0 \\ 0 & 0 & 0 & 0 & 0 & G_{12} \end{bmatrix} \tag{A.4}$$

where $\Delta = \frac{(1-\nu_{12}\nu_{21}-\nu_{23}\nu_{32}-\nu_{13}\nu_{31}-2\nu_{12}\nu_{21}\nu_{21})}{E_{11}E_{22}E_{33}}$.

The *compliance* matrix **S** is defined as $\mathbf{S} = \mathbf{Q}^{-1}$.

A.1.2 Hooke's Law For Transversely Isotropic Materials

A *transversely isotropic* material is defined as a material whose effective properties are isotropic in one of its planes[11]. A unidirectional fibrous composite with the fibres in direction 1, exhibits

isotropic properties in the 2-3 plane.

The general form of Hooke's Law for a transversely isotropic material is presented in equation A.5 [12, 14].

$$\begin{bmatrix} \sigma_{11} \\ \sigma_{22} \\ \sigma_{33} \\ \tau_{23} \\ \tau_{31} \\ \tau_{12} \end{bmatrix} = \begin{bmatrix} Q_{11} & Q_{12} & Q_{12} & 0 & 0 & 0 \\ Q_{12} & Q_{22} & Q_{23} & 0 & 0 & 0 \\ Q_{12} & Q_{23} & Q_{22} & 0 & 0 & 0 \\ 0 & 0 & 0 & \frac{Q_{22}-Q_{23}}{2} & 0 & 0 \\ 0 & 0 & 0 & 0 & Q_{55} & 0 \\ 0 & 0 & 0 & 0 & 0 & Q_{55} \end{bmatrix} \begin{bmatrix} \varepsilon_{11} \\ \varepsilon_{22} \\ \varepsilon_{33} \\ \gamma_{23} \\ \gamma_{31} \\ \gamma_{12} \end{bmatrix} \tag{A.5}$$

A.2 Lamina Characterisation

A.2.1 Hooke's Law For A 2D Unidirectional Lamina

The fundamental assumption is that of a thin unidirectional composite lamina under plane stress condition ($\sigma_{33} = 0$, $\tau_{31} = \tau_{23} = 0$)[12], [14, p. 78]. Then, Hooke's law for a unidirectional lamina under plane stress conditions is presented in equation A.6 [12, 14]:

$$\begin{bmatrix} \sigma_{11} \\ \sigma_{22} \\ \tau_{12} \end{bmatrix} = \begin{bmatrix} \frac{E_{11}}{1-\nu_{21}\nu_{12}} & \frac{\nu_{12}E_{22}}{1-\nu_{21}\nu_{12}} & 0 \\ \frac{\nu_{12}E_{22}}{1-\nu_{21}\nu_{12}} & \frac{E_{22}}{1-\nu_{21}\nu_{12}} & 0 \\ 0 & 0 & G_{12} \end{bmatrix} \begin{bmatrix} \varepsilon_{11} \\ \varepsilon_{22} \\ \gamma_{12} \end{bmatrix} \tag{A.6}$$

The Hooke's law is expressed in terms of the material axis. In the following section, the transformation to global axis will be discussed.

A.2.2 Hooke's Law For A 2D Angle Lamina

In section §A.2.1, the Hooke's law was obtained for a coordinate system which coincides with a coordinate system defined by the fibre orientation. When a different orthogonal coordinate system is used the coordinate system transformation needs to be undertaken.

Two coordinate systems of a unidirectional ply are presented in figure A.1. The coordinate system defined by axes (1-2) is known as *local* or material coordinate system (also called *principal* or *specially orthotropic* coordinate system). The coordinate system defined by (L,T) axes is called *global* coordinate system, and is an arbitrary coordinate system, usually a coordinate system defined by the testing axis.

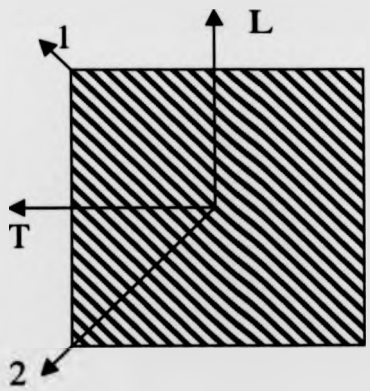

Figure A.1: Local (material) and global (testing) axes of an angle lamina.

The global and local stresses in a angle lamina are related to each other through equation A.7.

$$\begin{bmatrix} \sigma_{11} \\ \sigma_{22} \\ \tau_{12} \end{bmatrix} = [T] \times \begin{bmatrix} \sigma_L \\ \sigma_T \\ \tau_{LT} \end{bmatrix} \tag{A.7}$$

where **T** is the *transformation matrix.*

$$\mathbf{T}(\theta) = \begin{bmatrix} \cos^2\theta & \sin^2\theta & 2\cos\theta\sin\theta \\ \sin^2\theta & \cos^2\theta & -2\cos\theta\sin\theta \\ -\cos\theta\sin\theta & \cos\theta\sin\theta & \cos^2\theta - \sin^2\theta \end{bmatrix}$$

The global and local strains in a angle lamina are related to each other through equation A.8.

$$\begin{bmatrix} \varepsilon_{11} \\ \varepsilon_{22} \\ \varepsilon_{12} \end{bmatrix} = [\mathbf{T}] \times \begin{bmatrix} \varepsilon_x \\ \varepsilon_y \\ \varepsilon_{xy} \end{bmatrix} \tag{A.8}$$

Substituting the appropriate forms of equations A.8 and A.7 in equation A.6, the equation A.9.

$$\sigma_{LT} = [\mathbf{T}]^{-1}[Q][R][\mathbf{T}][R]^{-1}\varepsilon_{LT} \Leftrightarrow \sigma_{LT} = \bar{\mathbf{Q}}_{LT}\varepsilon_{LT} \tag{A.9}$$

where:

$\bar{\mathbf{Q}}$: is the reduced transformed stiffness matrix.

$$\left[\bar{\mathbf{Q}}\right] = [T]^{-1}[\mathbf{Q}][R][T][R]^{-1} \tag{A.10}$$

R: is an appropriate Reuter matrix.

The reduced transformed stiffness matrix is a symmetric matrix with the following form:

$$\mathbf{Q} = \begin{bmatrix} \# & \# & 0 \\ \# & \# & 0 \\ 0 & 0 & \# \end{bmatrix} \tag{A.11}$$

where # represents a non negative number.

Figure A.2 presents an example of the variation of a single stiffness parameters (Q_{11}) for an symmetric angle laminate. The graph presents the variation of one of the stiffness parameters as the angle of each ply changes from $-\frac{\pi}{2}$ to $\frac{\pi}{2}$. The effect of the angles can be quite significant on the stiffness parameters, and can be used for obtaining characterisation parameters.

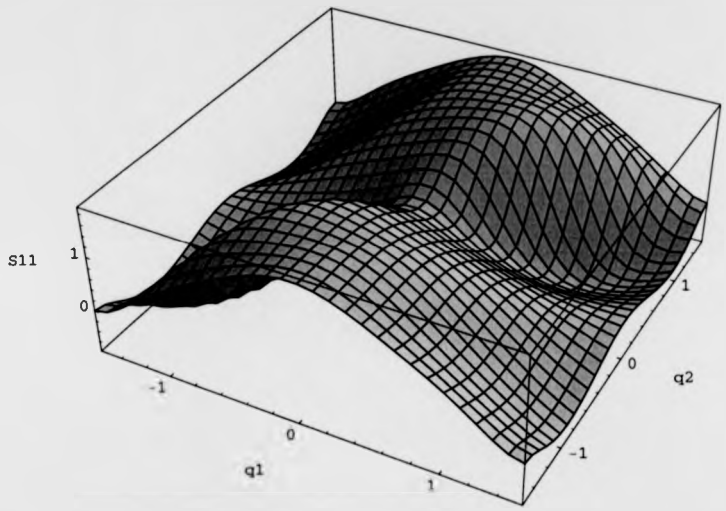

Figure A.2: Example of the change of stiffness parameters with fibre angle orientation.

A.2.3 In-Plane Loading And Bending Of A Lamina

The following assumptions are made to develop the strain-displacement relationships for a lamina under in-plane and bending loads [12, 178, 11].

- Each lamina is orthotropic.

- Each lamina is homogeneous.
- A line straight and perpendicular to the middle surface remains straight and perpendicular to the middle surface during deformation ($\gamma_{xz} = \gamma_{yz} = 0$). This assumption results in an overstiff result for FEM.
- A straight line in the z-direction remains of constant length ($\varepsilon_{zz} = 0$).
- The laminate is thin and is loaded only in its plane (plane stress) ($\sigma_{zz} = \tau_{xz} = \tau_{yz} = 0$).
- Displacements are continuous and small throughout the laminate ($\max(|u|, |v|, |w|) \ll$ laminate thickness).
- Each lamina is elastic.
- No slip occurs between the lamina interfaces.

Rotational moments are created in a lamina due to in-plane loads, because the lamina has a finite thickness. For a single lamina under in plane load it maybe proven that the bending moments above and below the midplane of the lamina cancel out. The stress-strain/curvature relationship for a laminate under in-plane loads is given through equation A.12[12, p. 230].

$$\begin{bmatrix} \sigma_{11} \\ \sigma_{22} \\ \tau_{12} \end{bmatrix} = \left[\bar{\mathbf{Q}}\right] \begin{bmatrix} \varepsilon_x \\ \varepsilon_y \\ \gamma_{xy} \end{bmatrix} \tag{A.12}$$

$$\begin{bmatrix} \varepsilon_x \\ \varepsilon_y \\ \gamma_{xy} \end{bmatrix} = \begin{bmatrix} \varepsilon_x^0 \\ \varepsilon_y^0 \\ \gamma_{xy}^0 \end{bmatrix} + z \begin{bmatrix} \kappa_x \\ \kappa_y \\ \kappa_{xy} \end{bmatrix} \tag{A.13}$$

where

$\bar{\mathbf{Q}}$: is the reduced transformed stiffness matrix, is obtained from equation A.10.

κ: is the vector of midplane curvatures $= \begin{bmatrix} \kappa_x \\ \kappa_y \\ \kappa_{xy} \end{bmatrix}$.

z: is the distance from the midplane of the lamina.

A.3 Laminate Analysis

Structures usually utilise laminates. It is possible to obtain the stresses and strain in the local and global axes of each ply when the applied in-plane loads are known through Classical Laminate Theory (CLT).

Different analysis approaches distinguish three levels of representative volume element of a material:

Microscale

Mesoscale

Macroscale

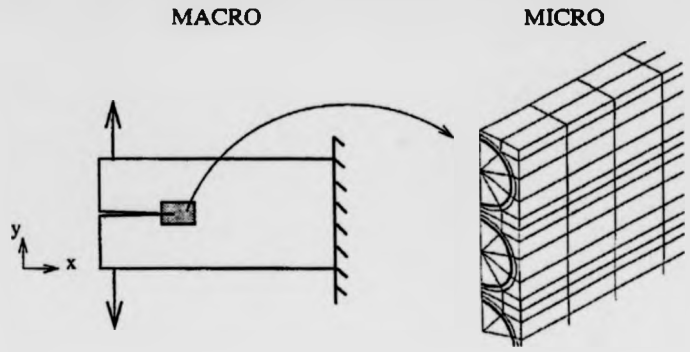

Figure A.3: Comparison of macro vs. micro computational levels [10].

A.3.1 Classical Laminate Theory For A Laminate.

The assumptions for the strain-displacement relationships of a lamina, which were presented in §A.2.3, apply equally to a laminate.

The thickness h of an n-laminae laminate is

$$h = \sum_{k=1}^{n} t_k$$

Where:

$\mathbf{t_k}$: the thickness of the k-th lamina.

The relationship between the *forces* and *moments* of a laminate in terms of the midplane *strain* and *curvatures* is presencted in equation A.14 [11, 11].

$$\begin{bmatrix} N_x \\ N_y \\ N_{xy} \\ M_x \\ M_y \\ M_{xy} \end{bmatrix} = \left[\begin{array}{ccc|ccc} \overbrace{A_{11} & A_{12} & A_{16}}^{\mathbf{A}} & \overbrace{B_{11} & B_{12} & B_{16}}^{\mathbf{B}} \\ A_{12} & A_{22} & A_{26} & B_{12} & B_{22} & B_{26} \\ A_{16} & A_{26} & A_{66} & B_{16} & B_{26} & B_{66} \\ \hline B_{11} & B_{12} & B_{16} & D_{11} & D_{12} & D_{16} \\ B_{12} & B_{22} & B_{26} & D_{12} & D_{22} & D_{26} \\ \underbrace{B_{16} & B_{26} & B_{66}}_{\mathbf{B}} & \underbrace{D_{16} & D_{26} & D_{66}}_{\mathbf{D}} \end{array}\right] \begin{bmatrix} \varepsilon_x^0 \\ \varepsilon_y^0 \\ \gamma_{xy}^0 \\ \kappa_x \\ \kappa_y \\ \kappa_{xy} \end{bmatrix} \tag{A.14}$$

$$A_{ij} = \sum_{k=1}^{n} [\bar{Q}_{ij}]_k (h_k - h_{k-1}), \quad i,j = 1,2,6 \tag{A.15}$$

$$B_{ij} = \frac{1}{2} \sum_{k=1}^{n} [\bar{Q}_{ij}]_k (h_k^2 - h_{k-1}^2), \quad i,j = 1,2,6 \tag{A.16}$$

$$D_{ij} = \frac{1}{3} \sum_{k=1}^{n} [\bar{Q}_{ij}]_k (h_k^3 - h_{k-1}^3), \quad i,j = 1,2,6 \tag{A.17}$$

Where

A: is the extensional stiffness matrix

B: is the coupling stiffness matrix

D: is the bending stiffness matrix

Inversion of equation A.14 results in equation A.18

$$\left[\begin{array}{c} \varepsilon^0 \\ \hline \kappa \end{array}\right] = \left[\begin{array}{c|c} A & B \\ \hline B & D \end{array}\right]^{-1} \begin{bmatrix} N \\ M \end{bmatrix} = \left[\begin{array}{c|c} A^* & B^* \\ \hline C^* & D^* \end{array}\right] \begin{bmatrix} N \\ M \end{bmatrix} \tag{A.18}$$

where

ε^0: is the extensional strain vector in the midplane of the laminate.

κ: is vector of curvatures in the midplane of the laminate.

$[\mathbf{A}^*]$: is called the extensional compliance matrix.

$[\mathbf{B}^*]$: is called the coupling compliance matrix and $[\mathbf{C}^*] = [\mathbf{B}^*]^{\mathbf{T}}$.

$[\mathbf{D}^*]$: is called the bending compliance matrix;

N: is vector of normal and shear forces per unit length [N/m].

M: is vector of bending and twisting moments per unit length [N].

The effective in-plane stiffness properties of a laminate can be predicted using the coefficients of the extensional compliance matrix $[\mathbf{A}^*]$[12, pp. 245-247].

$$E_{11}^{Lam} = \frac{1}{hA_{11}^*} \tag{A.19}$$

$$E_{22}^{Lam} = \frac{1}{hA_{22}^*} \tag{A.20}$$

$$G_{12}^{Lam} = \frac{1}{hA_{66}^*} \tag{A.21}$$

$$\nu_{12}^{Lam} = -\frac{A_{12}^*}{A_{11}^*} \tag{A.22}$$

$$\nu_{21}^{Lam} = -\frac{A_{12}^*}{A_{22}^*} \tag{A.23}$$

A.3.2 Reverse Laminate Theory.

Foral and Humphrey [179] and Dvorak and Law [180] attempted to determine some of the lamina properties from the behaviour of multidirectional laminates using Classical Laminate Theory. Similarly, Lataillade[112] have used a ±45° laminate in order to characterise the intralaminar

shear properties. Several other researchers have used similar approach to characterise indirectly a composite material.

Al-Bastaki [64] used a similar technique and referred to this approach as application of Reverse Laminate Theory (RLT). In effect, RLT assumes prior knowledge of the laminate properties, loading direction and lay-up, in order to derive the mechanical properties of the individual lamina that constitutes the laminate. The RLT methodology of RLT has been described by Al-Salehi[92] and Kaddour [104, 103]

RLT has been extensively used for characterisation of the elasticity and strength mechanical properties (i.e. $E_{11}, E_{22}, G_{12}, v_{12}$ and the corresponding strengths and strains at failure) of composite materials.

Appendix B

Failure theories

The following criteria will be reviewed:

- Maximum Strain Theory
- Petit-Waddoups Theory
- Maximum Stress Theory
- Modified Puck
- Hill Theory
- Marin Theory
- Norris Theory
- Tsai-Hill Theory
- Gol'denblat and Kopnov Theory

- Ashkenazi Theory
- Malmeister Theory
- Hankinson Formula
- Tsai-Wu Theory
- Cowin Theory
- Tennyson Theory
- Hoffman Theory
- Fischer Theory
- Chamis Theory
- Sandu Theory
- Griffith-Baldwin Theory
- Puppo-Evensen Theory
- Wu-Scheublein Theory

For a laminate the failure criterion is applied to the individual laminae (plies). At the ply level, the failure theories are not based on the principal normal stresses and maximum shear stresses but on the stresses in the material local axes (axes defined by the orientation of the fibers). The sign of the shear stress (positive or negative) has an effect on the strength of an angle lamina. [12] As a result, the implemented failure criterion does not influence the material behaviour. It acts only as indicator of failure. Their use is limited to a purely linear elastic predictive tool used

to approximate loads and displacements leading to failure of the structure once a corresponding preset limit is attained.

B.0.3 Tsai-Wu Theory

In an effort to more adequately predict experimental results, Tsai and Wu [171] proposed a lamina failure criterion having additional stress terms not appearing in theories such as the Hill analysis. The Tsai Wu theory is based on the total strain energy failure by Beltrami. The failure surface in stress space is of the form:

$$f(\sigma) = \sum_{i=6}^{6} F_i \sigma_{ii} + \sum_{i,j=6}^{6} F_{ij} \sigma_{ii} \sigma_{jj} = 1 \tag{B.1}$$

The F_i and F_{ij} are second and fourth order lamina strength tensors. The linear stress terms account for possible differences in tensile and compressive strengths. The quadratic stress terms are similar to those in the Tsai-Hill formulation, and describe an ellipsoid in stress space. Off-diagonal terms of the strength tensor provide independent interactions among the stress components. Under plane-stress conditions, the Tsai-Wu failure criterion is implemented in PAM-CRASH as:

$$\begin{aligned} &F_1\sigma_{11} + F_2\sigma_{22} + F_{11}\sigma_{11}^2 + 2F_{12}\sigma_{11}\sigma_{22} + \\ &+ F_{22}\sigma_{22}^2 + F_{44}\tau_{23}^2 + F_{55}\tau_{13}^2 + F_{66}\tau_{12}^2 = 1 \end{aligned} \tag{B.2}$$

where

$$
\begin{aligned}
F_1 &= \frac{1}{\sigma^t_{11,f}-\sigma^c_{11,f}} \quad , \quad F_2 = \frac{1}{\sigma^t_{22,f}-\sigma^c_{22,f}} \\
F_{11} &= \frac{1}{\sigma^t_{11,f}\sigma^c_{11,f}} \quad , \quad F_{22} = \frac{1}{\sigma^t_{22,f}\sigma^c_{22,f}} \\
F_{44} &= \frac{1}{\tau^p_{23,f}\tau^n_{23,f}} \quad , \quad F_{55} = \frac{1}{\tau^p_{13,f}\tau^n_{13,f}} \\
F_{66} &= \frac{1}{\tau^p_{12,f}\tau^n_{12,f}} \quad , \quad F_{12} = k\sqrt{F_{11}F_{22}}
\end{aligned}
\tag{B.3}
$$

where σ^t_{11}, σ^t_{22}, σ^c_{11}, σ^c_{22}, remain the lamina longitudinal and transverse strengths in tension and compression, respectively[1]. The shear failure stresses $\tau_{12,f}, \tau_{23,f}$ and $\tau_{13,f}$ are the positive (superscript p) and negative (superscript n) ultimate shear strengths. These strength values are not sufficient to determine coefficients such as F_{12}. For its determination, biaxial tests are required. The latter have to be selected carefully to obtain accurate values for such interaction terms [1-1]). The value $k = \frac{1}{2}$ is proposed by the PAM-CRASH manual.

The Tsai-Wu tensor strength theory is more general than the Tsai-Hill analysis. Specific advantages include:

1. invariant under rotation of coordinates,
2. transforms according to established tensorial laws,
3. symmetrical strength properties akin to those of stiffnesses and compliances, and
4. provides independent interactions among stress components.

In strength theories such as the Tsai-Hill analysis, the stress interactions are fixed or implied (not independent). In the maximum stress or maximum strain criteria, simultaneous equations are required and interactions are not included. Like the modified Tsai-Hill criterion, the Tsai-Wu

[1] In this theory, as with those of maximum stress, etc., compressive strengths X', Y' and S' are taken as positive numbers

analysis employs tensile and compressive lamina strengths. While it is a stress criterion, linear-elastic lamina response is typically assumed in the accompanying lamination theory. The criterion predicts the imminency of failure but nothing about the failure mode (tensile or compressive longitudinal, transverse or shear). The most inconvenient aspect of this theory is the determination of F_{12}.

Cowin [182] subsequently formulated a similar theory although he again restricted the interaction by expressing F_{12} in terms of uniaxial normal and shear strengths. Tennyson et al. [183], [184] extended the Tsai-Wu concept to include cubic terms. The Tsai-Wu theory has received quite extensive use, e.g., Herakovich and O'Brien [185] have recently employed the three-dimensional form of Equation B.2 to analyse damage zones in a composite.

Appendix C

Programming Scripts

Scripts have been developed in MATLAB, R and Visual Basic for applications in Excel.

C.1 Processing Of Raw Data.

C.1.1 Matlab.

C.1.1.1 Calculations For $[0°]_4$ laminate

```
1  function ans = UD0Calc(y, FILENAME, PATHNAME, NoTransChan, spmn);
2  % Ladeveze calculation for [+45]_{8} and printout to disk .CSV and .SDM
3  % Suitable for video extensometry AND INSTRON input
4  % function ans = UD0Calc(y, FILENAME, PATHNAME, NoTransChan, spmn);
5  % Input
6  %   y             : Matrix of observations
7  %   FILENAME      : Original Filename
8  %   PATHNAME      : Original Pathname
9  %   NoTransChan   : NoTransChan
10 %   spmn          : optional argument for specimen number
11 % Output
12 %   ans           : return exit code
13
14 try
15     %------------------- Calculations -------------------
```

```
16  %-------------------------------------------------------------------
17  % Calculation of Modulus
18  i(1)=1; %Finding the strain value at
19  while y(4,i(1))<0.0005
20      i(1)=i(1)+1;
21  end
22  if i(1)>2, %make sure that the it's not the first element of the ...
        matrix.
23      i(1)=i(1)-1;
24  end
25
26  i(2)=i(1)+1;
27  while (y(4,i(2))<0.0025 & i(2) <= length(y(4,:)))
28      i(2)=i(2)+1;
29  end
30  if (i(2)-i(1))>1, %make sure that the it's not the first element of ...
        the matrix.
31      i(2)=i(2)-1;
32  end
33
34  E0 = (y(2,i(2)) - y(2,i(1)) )/( (y(4,i(2)) - y(4,i(1)) ));
35
36  % Poisson Ratio
37  nu0 = -(y(NoTransChan+6,i(2)) - y(NoTransChan+6,i(1)) )/( (y(4,i(2)) ...
        - y(4,i(1)) ));
38
39  % Maximum Stress Strain
40  [fsts,fi] = max( y(2,:));
41  fsts= fsts *1000 % Convert [GPa] to [MPa]
42  fstrn = y(4,fi);
43  StrNrg = trapz(y(4,:), y(2,:));
44  s22= y(NoTransChan+6,fi);
45  SR = mean(y(3,2:fi));% y(3,fi)
46
47  disp(['_Results_for_',FILENAME]);
48  disp('-------------------------------------------------------------');
49  disp(['Stiffness_modulus_[GPa]_____E11:_', num2str( E0 )]);
50  disp(['Poisson_Ratio_____________v12:_', num2str( nu0 )]);
51  disp(['Maximum_Strain_failure_____e11:_', num2str( fstrn)]);;
52  disp(['Maximum_Stress_failure_[MPa]_s11:_', num2str( fsts )]);
53  disp(['Strain_energy_up_to_failure__SNR:_', num2str( StrNrg)]);
54  disp(['Strain_rate_____________SR:_', num2str( SR )]);
55  %
56  % Open file name
57  FILENAME=lower(FILENAME);
58  try %try for INSTRON when spcm is defined
59      spmn;
```

```
60          i = findstr(FILENAME, '.csv');
61          specFILENAME = [ FILENAME(1:(i-1)),'i',num2str(spmn),'.CSV' ];
62          newPATHNAME = PATHNAME;
63          feval('cd',newPATHNAME);
64          fid = fopen(specFILENAME, 'wr');
65          disp('Insron .csv and .SDM files are written');
66      catch     %try for VE when spcm is defined
67          i = findstr(FILENAME, '.dat');
68          specFILENAME = [ FILENAME(1:(i-1)),'v.CSV' ];
69          newPATHNAME = PATHNAME;
70          feval('cd',newPATHNAME);
71          fid = fopen(specFILENAME, 'wr');
72          disp('VE .csv and .SDM files are written');
73      end
74      %
75      %
76      %---------------------SAVE contents of .csv FILE ...
            ------------------------------------------
77      count1 = fprintf(fid,'E0 , Fail. Strain , Fail. Stress , Poisson ...
            Ratio , Transverse F Strain , SR , Strain NRG\n');
78      count1 = fprintf(fid,'%f , %f , %f , %f , %f , %f , %f\n', E0, ...
            fstrn, 1000*fsts, nu0, s22, SR, StrNrg );
79      % values used in calculation
80      count1 = fprintf(fid,'Time[sec] , Stress [MPa] , Long[] , Aver Trans ...
            , Strain Rate[s^(-1)]\n');
81      n=length(y(1,:));
82      for i = 1:n,
83          count1 = fprintf(fid,'%f , %f , %f , %f , %f\n', y(1,i), y(2,i), ...
                y(4,i), y(6+NoTransChan,i), y(3,i));
84      end
85      fclose(fid);
86      disp('.csv and .SDM files completed');
87      disp(' ');
88      ans=0;
89  end
```

C.1.1.2 Calculations For $[\pm 45°]_{2s}$ laminate

```
1  function ans = PM45Calc(y, LadP, LadData, RawData, SRvec, FILENAME, ...
       PATHNAME, NoTransChan, spmn);
2  % Ladeveze calculation for [+/- 45]_{2s} and printout to disk .CSV and . ...
       SDM
3  % Input
4  %   y            : Matrix of observations
5  %   LadP         : Number of cycles
6  %   LadData      : Matrix with material coordinate system (1-2) data
7  %   RawData      : Matrix with testing coordinate system (L-T) data
```

```
8  %   SRvec        : Vector of Strain rates 2 for LT and 3 for material ...
       axis
9  %   FILENAME     : Original Filename
10 %   PATHNAME     : Original Pathname
11 %   NoTransChan  : NoTransChan
12 %
13
14 try
15     %-------------------------------------------------------------------------

16     %-------------------------------- LADAVEZE CALCULATIONS ...
                 ------------------------

17     %-------------------------------------------------------------------------

18     % LadCalc=zeros(14,6);
19     % Row 1: elastic portion of shear strain
20     % Row 2: shear stress (high)
21     % Row 3: shear Modulus
22     % Row 4: shear damage
23     % Row 5: Y(I)
24     LadCalc = LadData(8,1:(LadP/2 -1)) - LadData(7,2:(LadP/2));
25     LadCalc(2,:) = LadData(14,1:(LadP/2 -1));
26     LadCalc(3,:) = LadCalc(2,:)./LadCalc(1,:) ;
27     LadCalc(4,:) = 1- LadCalc(3,:)./max(LadCalc(3,:)) ;
28     LadCalc(5,:) = sqrt(1/2* (LadCalc(3,:).*(LadCalc(1,:).^2)) );
29     % Plasticity parameters
30     % Row 6: elastic plastic strain (\int epsilon_12 (1-d_i) )
31     % Row 7: Li=R(i)+R0
32     LadCalc(6,:)=zeros(size(LadCalc(1,:)));
33     LadCalc(6,1)=LadData(7,2)*(LadCalc(4,1));
34     for j=2:(LadP/2 -1)
35         LadCalc(6,j)=LadCalc(6,j-1) + LadData(7,j+1)*(1- (LadCalc(4,j))) ...
               ;
36     end
37     LadCalc(7,:) = LadCalc(2,:)./(1-LadCalc(4,:));
38     % Calculation of Plasticity parameters.
39     % initial value for m
40     m=5;
41     [m,beta,R0]=Brackm(LadCalc(7,2:4),LadCalc(6,2:4), m);
42
43     j = glmfit(LadCalc(4,:)', LadCalc(5,:)');
44     Yc = j(2);
45     Y0 = j(1);
46     YR = max(LadCalc(5,:)); % Elementary Shear damage fracture limit.
47     G0 = max(LadCalc(3,:)); % Calculation of Shear modulus
48     % ADD shear modulus criterion++++++++++++++++++++++++++++++++++++++++++++++
```

```
49      [fsts , i] = max( [LadData(13,:) , LadData(14,:)]);
50      fsts = 1000 * fsts;
51      [fstrn , j] = max( [LadData(7,:) , LadData(8,:)]);
52      notes=[];
53      if (i~=j)
54          notes='THE HIGHEST VALUE OF FAILURE STRESS is not observed at ...
                FAILURE STRAIN';
55      end
56      disp(['Results for ',FILENAME]);
57      disp('-------------------------------------------------------');
58      disp(['Shear Modulus---------------------------[GPa] G12:  ', num2str ...
            ( G0 )])
59      disp(['Shear strain at failure -----------------[]    g12:  ', num2str ...
            ( fstrn)])
60      disp(['Shear stress at failure -----------------[MPa] t12:  ', num2str ...
            ( fsts )])
61      disp(['Initial Shear damage limit --------------[GPa] Y0:  ', num2str ...
            ( Y0)])
62      disp(['Critical Shear damage limit -------------[GPa] Yc:  ', num2str ...
            ( Yc)])
63      disp(['Elementary Shear damage fracture limit -[GPA] YR:  ', num2str ...
            ( YR)])
64      disp(['Shear Strain rate-----------------------SR12:  ', num2str( ...
            SRvec(5))])
65      if ~isempty(m)
66          disp(['Plasticity parameter m-----------------------m:  ', num2str ...
                ( m)])
67          disp(['Plasticity parameter beta----------------beta:  ', num2str ...
                ( beta)])
68          disp(['Plasticity parameter R0------------------R0:  ', num2str ...
                ( R0)])
69      end
70
71      disp(notes);
72
73      %
74                  % Plot results
75  %     subplot(2,1,1)
76      plot( LadCalc(5,:)',LadCalc(4,:)', 'b*--');
77      axis([0 max(LadCalc(5,:)) 0 1 ]);
78      xlabel( 'Shear pseudoforce [GPa^{1/2}]' ); ylabel( ['Shear damage []' ...
            ] );
79  %     subplot(2,1,2)
80  %     plot(LadCalc(13,:)', LadCalc(10,:)');
81  %     axis([0 max(LadCalc(13,:)) 0 1]);
82  %     xlabel( 'Y(t) [GPa]' ); ylabel( ['Transverse damage[]'] );
83      pause
```

```
84
85      %
86      %
87      %------------------------ Open FILE ------------------------------------
88      FILENAME = lower(FILENAME);
89      try % INSTRON variation
90          spmn;
91          % open csv file
92          i = findstr(FILENAME, '.csv');
93          newFILENAME = [ FILENAME(1:(i-1)), '-',num2str(spmn),'i.CSV' ];
94          newPATHNAME = PATHNAME;
95          feval('cd',newPATHNAME);
96          fid = fopen(newFILENAME, 'wr');
97          % open sdm file
98          i = findstr(FILENAME, '.csv');
99          newFILENAME = [ FILENAME(1:(i-1)), '-',num2str(spmn),'i.SDM' ];
100         fid2 = fopen(newFILENAME, 'wr');
101         % open LAD file
102         i = findstr(FILENAME, '.csv');
103         newFILENAME = [ FILENAME(1:(i-1)), '-',num2str(spmn),'i.LAD' ];
104         fid3 = fopen(newFILENAME, 'wr');
105         disp('Instron .csv and .sdm files will be written');
106     catch % VE variation
107         % open csv file
108         i = findstr(FILENAME, '.dat');
109         newFILENAME = [ FILENAME(1:(i-1)), 'v.CSV' ];
110         newPATHNAME = PATHNAME;
111         feval('cd',newPATHNAME);
112         fid = fopen(newFILENAME, 'wr');
113         % open sdm file
114         i = findstr(FILENAME, '.dat');
115         newFILENAME = [ FILENAME(1:i), 'SDM' ];
116         fid2 = fopen(newFILENAME, 'wr');
117         % open LAD file
118 i = findstr(FILENAME, '.dat');
119         newFILENAME = [ FILENAME(1:i), 'LAD' ];
120         fid3 = fopen(newFILENAME, 'wr');
121         disp('Video Ext .csv and .sdm files will be written');
122     end
123     %------------------------ Save Contents of .csv FILE ...
        ------------------------------------
124     count1 = fprintf(fid,'G0 , Fail. Strain , Fail. Stress ,  Y0 , Yc, YR ...
            , SSR , m, beta , R0 \n');
125     if ~isempty(m)
126         count1 = fprintf(fid,'%f ,%f ,%f ,%f ,%f ,%f ,%f ,%f ,%f ,%f ...
                \n', G0, fstrn, fsts, Y0, Yc, YR, SRvec(5), m, beta, R0 );
127     else
```

```
128         count1 = fprintf(fid,'%f␣,␣%f␣,␣%f,␣%f␣,␣%f␣,␣%f,␣%f␣␣\n', G0,  ...
                fstrn, fsts, Y0 , Yc, YR, SRvec(5) );
129     end
130     count1 = fprintf(fid,'Time[sec]␣,␣Stress␣[MPa]␣,␣Long[]␣,␣Aver␣Trans ...
            ␣,␣LT␣Strain␣Rate[s^(-1)]\n');
131     n = length(y(1,:));
132     for i = 1:n,
133         count1 = fprintf(fid,'%f␣,␣%f␣,␣%f␣,␣%f,␣%f\n', y(1,i), y(2,i),  ...
                y(4,i), y(NoTransChan +6,i), y(3,i));
134     end
135     fclose(fid);
136     %---------------------- Save Contents of .sdm FILE ...
                ------------------------------
137     %   1 - Time frame [msec]
138     %   2 - Load [kN]
139     %   3 - useless channel (for biaxial loads)
140     %   4 - Longitudinal distance of targets [mm]
141     %   5 - Transverse distance 1 [mm]
142     %   6 - Transverse distance 2 [mm]
143     %   7 - Transverse distance 3 [mm]
144     %   8 - Transverse distance 4 [mm]
145     count1 = fprintf(fid2,'Time␣,␣Load␣,␣SR␣,␣␣L1␣,␣T4␣\n');
146     for i = 1:length(RawData(1,:)),
147         count1 = fprintf(fid2,'%f␣,␣%f␣,␣%f␣,␣%f,␣%f\n', RawData(1,i),  ...
                RawData(2,i), RawData(3,i), RawData(4,i) ,RawData( ...
                NoTransChan +6,i));
148     end
149     fclose(fid2);
150     %---------------------- Save Contents of .LAD FILE ...
                ------------------------------
151     %   LADCALC
152     outputString= '%f';
153     for i = 2:length(LadCalc(:,1)),
154       outputString= [outputString ',␣%f'];
155     end
156     outputString = [outputString '\n'];
157
158     outString2= 'LadCalc(1,i)';
159     for i = 2:length(LadCalc(:,1)),
160       outString2= [outString2 ',␣LadCalc(' num2str(i) ',i)'];
161     end
162
163     count1 = fprintf(fid3,['gamma␣{12}^{elastic},␣tau␣{12}␣␣,␣G12' ...
164         '␣,␣damage␣,␣Y(I),␣Plastic␣Shear␣Strain,' ...
165          '␣Plasticity␣␣\n']);
166     for i = 1:length(LadCalc(1,:)),
167   eval(['count1␣=␣fprintf(fid3,outputString,' outString2 ');']);
```

```
168     end
169     fclose(fid3);
170
171     disp('.csv and .sdm files were written successfully.');
172     ans =0;
173 catch
174     disp(lasterr);
175 end
```

C.1.1.3 Calculations For $[45°]_8$ laminate

```
1  function ans = P45Calc(y, LadP, LadData, RawData, SRvec, FILENAME, ...
       PATHNAME, NoTransChan,spmn);
2  % Ladeveze calculation for [+45]_{8} and printout to disk .CSV and .SDM
3  % Input
4  %   y            : Matrix of observations
5  %   LadP         : Number of cycles
6  %   LadData      : Matrix with material coordinate system (1-2) data
7  %   RawData      : Matrix with testing coordinate system (L-T) data
8  %   SRvec        : Vector of Strain rates 2 for LT and 3 for material ...
       axis
9  %   FILENAME     : Original Filename
10 %   PATHNAME     : Original Pathname
11 %   NoTransChan  : NoTransChan
12 %   spmn         : specimen number
13 %
14 try
15     %-------------------------------------------------------------------------

16     %------------------------------ LADAVEZE CALCULATIONS ...
                 ------------------------------------------

17     %-------------------------------------------------------------------------

18     % Row 1: elastic portion of strain perpendicular to fibres.
19     % Row 2: elastic portion of shear strain
20     % Row 3: Transverse stress
21     % Row 4: Shear Stress
22     % Row 5: Transverse Modulus
23     % Row 6: shear Modulus
24     % Row 7: Transverse damage d'(i)
25     % Row 8: Shear damage d(i)
26     % Row 9: Z'(d) Zprime
27     LadCalc = abs(LadData(6,1:(LadP/2 -1)) - LadData(5,2:(LadP/2)));    % ...
           eps_{22}
28     LadCalc(2,:) = abs(LadData(8,1:(LadP/2 -1)) - LadData(7,2:(LadP/2))) ...
           ; % eps_{12}^e
```

```
29      LadCalc(3,:) = LadData(12,1:(LadP/2 -1)) - LadData(11,2:(LadP/2)); ...
            % s22(i)
30      LadCalc(4,:) = LadData(14,1:(LadP/2 -1)) - LadData(13,2:(LadP/2)); ...
            % t12(i)
31      LadCalc(5,:) = LadCalc(3,:)./LadCalc(1,:) ;          % E22(i)
32      LadCalc(6,:) = LadCalc(4,:)./LadCalc(2,:) ;          % G12(i)
33      LadCalc(7,:) = 1- LadCalc(5,:)/max(LadCalc(5,:));    % d'(i)
34      LadCalc(8,:) = 1- LadCalc(6,:)/max(LadCalc(5,:));    % d(i)
35      LadCalc(9,:) = zeros(size(LadCalc(8,:)));
36      LadCalc(9,2:(LadP/2 -1) ) = ((LadData(5,3:(LadP/2)) - LadData(5,2:(( ...
           LadP/2)-1)) ).*( 1-LadCalc(7,2:((LadP/2-1))) ) )./( (LadData ...
           (7,3:(LadP/2)) - LadData(7,2:((LadP/2)-1)) ).*( 1-LadCalc(8,2:(( ...
           LadP/2)-1)) ) );
37      %-------10--------20--------30--------40--------50--------60--------70-------

38      %
39      E22 = max(LadCalc(5,:));
40      [fsts , i] = max( [LadData(11,:), LadData(12,:)]);
41      fsts = 1000* fsts          % Converst [GPa] to [MPa]
42      [fstrn , j] = max( [LadData(5,:), LadData(6,:)]);
43      A=LadCalc(9,:);
44
45      % Print results
46      disp(['_Results_for_',FILENAME]);
47      disp('-------------------------------------------------------');
48      disp( ['Transverse_Modulus_____________[GPa]_____E22:__', num2str( ...
           E22 )])
49      disp( ['Transverse_strain_at_failure___________eps22:__', num2str( ...
           fstrn)])
50      disp( ['Transverse_stress_at_failure__[MPa]_____s22:__', num2str( ...
           fsts )])
51      disp( ['C.F.__of_shear_and_transverse_strains_____A:__', num2str( ...
           LadCalc(9,2:(LadP/2-1)) )  ] );
52      disp( ['Mean_value_of_A_____________________Abar:__', num2str( ...
           mean( abs(A(2:(LadP/2-1) ) ))) ] );
53      disp( ['Transverse_Strain_rate_____[s^(-1)]__SR22:__', num2str( ...
           SRvec(4) )]);
54      disp( ['Shear_Strain_rate_____________[s^(-1)]__SR12:__', num2str( ...
           SRvec(5) )]);
55      %
56      %
57      %------------------- Open FILE ----------------------------------------
58      FILENAME = lower(FILENAME);
59      try % INSTRON variation
60          spnn;
61          % open csv file
62          i = findstr(FILENAME, '.csv');
```

```
63          newFILENAME = [ FILENAME(1:(i-1)), 'i', num2str(spmn), '_.CSV' ...
                ];
64          newPATHNAME = PATHNAME;
65          feval('cd',newPATHNAME);
66          fid = fopen(newFILENAME, 'wr');
67          % open sdm file
68          i = findstr(FILENAME, '.csv');
69          newFILENAME = [ FILENAME(1:(i-1)), 'i', num2str(spmn), '_.SDM' ...
                ];
70          fid2 = fopen(newFILENAME, 'wr');
71          disp('Instron_.csv_and_.sdm_files_will_be_written');
72      catch % VE variation
73          % open csv file
74          i = findstr(FILENAME, '.dat');
75          newFILENAME = [ FILENAME(1:(i-1)), 'v.CSV' ];
76          newPATHNAME = PATHNAME;
77          feval('cd',newPATHNAME);
78          fid = fopen(newFILENAME, 'wr');
79          % open sdm file
80          i = findstr(FILENAME, '.dat');
81          newFILENAME = [ FILENAME(1:(i-1)), 'v.SDM' ];
82          fid2 = fopen(newFILENAME, 'wr');
83          disp('Video_Ext_.csv_and_.sdm_files_will_be_written');
84      end
85      % Save contents of .csv file
86      count1 = fprintf(fid,'E22_,_eps22,_s22,_A,_SR22,_SR12_\n');
87      count1 = fprintf(fid,'%f_,_%f_,_%f,_%f,_%f,_%f_,_\n', E22, fstrn, ...
            fsts, mean( abs(A(2:(LadP/2-1)))), SRvec(4), SRvec(5));
88      InputStrg = '%f';
89      if (LadP/2-1)>=3
90          for i = 3:(LadP/2-1)
91              InputStrg = [InputStrg ',_%f'];
92          end
93      end
94      InputStrg = [InputStrg ',_\n'];
95      count1 = fprintf(fid, InputStrg, A(2:(LadP/2-1)));
96      count1 = fprintf(fid,'Time[sec]_,_Stress_[MPa]_,_Long[]_,_Aver_Trans ...
            _,_Strain_Rate[s^(-1)]_\n');
97      n = length(y(3,:));
98      for i = 1:n,
99          count1 = fprintf(fid,'%f_,_%f_,_%f_,_%f_,_%f_\n', y(1,i), y(2,i) ...
                , y(4,i), y(6+NoTransChan,i), y(3,i));
100     end
101     fclose(fid);
102     % Save contents of .sdm file
103     count1 = fprintf(fid2,'Time_,_Load_,_SR_,_L1_,_Taverage_\n');
104     for i = 1:length(RawData(1,:)),
```

```
105         count1 = fprintf(fid2, '%f␣,␣%f␣,␣%f␣,␣%f␣,␣%f␣\n', RawData(1,i) ...
                , RawData(2,i), RawData(3,i), RawData(4,i) , RawData(6+ ...
                NoTransChan,i));
106     end
107     fclose(fid2);
108     disp('Video␣Ext␣.csv␣and␣.sdm␣files␣were␣written␣successfully.');
109     ans=0;
110 catch
111     ans=lasterr;
112 end
```

C.1.1.4 Calculations For $[\pm 67.5°]_{2s}$ laminate

```
1  function ans = PM67Calc(y, LadP, LadData, RawData, SRvec, FILENAME, ...
       PATHNAME, NoTransChan, plyInfo, plyThick, plies,theta, spmn);
2  % Ladeveze calculation for [+45]_{8} and printout to disk .CSV and .SDM
3  % function ans = PM67Calc(y, LadP, LadData, RawData, SRvec, FILENAME, ...
       PATHNAME, NoTransChan, E11i, E22i, G12i, v12i, Y0, Yc, spmn);
4  % Input
5  %   y            : Matrix of observations
6  %   LadP         : Number of cycles
7  %   LadData      : Matrix with material coordinate system (1-2) data
8  %   RawData      : Matrix with testing coordinate system (L-T) data
9  %   SRvec        : Vector of Strain rates 2 for LT and 3 for material ...
       axis
10 %   FILENAME     : Original Filename
11 %   PATHNAME     : Original Pathname
12 %   NoTransChan  : NoTransChan
13 %   plyInfo      :
14 %   plyThick     :
15 %   plies        :
16 %   theta        :
17 %   spmn         : Specimen number (optional)
18
19 try
20     R=[1,0,0;0,1,0;0,0,2];
21     % Variation from
22     [E11i,E22i,G12i,v12i,Y0,Yc]=MechSelSR(SRvec);
23     v21i=v12i*E22i/E11i;
24
25     Axy= LamtSM(E11i, E22i, v12i, G12i, plyThick, plyInfo);
26     Axy=Axy(1:3,1:3)/(plies*plyThick);
27     %    Stiffness matrix
28     SMcv = LamStiff(E11i, E22i, v12i, G12i, 0)*R*Transtheta(theta)*inv(R ...
           )*inv(Axy);
29     i = 1;
30     while i < (LadP/2 +1),
```

```
31          LadData(9,i) = SMcv(1,1) * RawData(2,2*(i-1)+1);
32          LadData(10,i) = SMcv(1,1) * RawData(2,2*(i-1)+2);
33          LadData(11,i) = SMcv(2,1) * RawData(2,2*(i-1)+1);
34          LadData(12,i) = SMcv(2,1) * RawData(2,2*(i-1)+2);
35          LadData(13,i) = SMcv(3,1) * RawData(2,2*(i-1)+1);
36          LadData(14,i) = SMcv(3,1) * RawData(2,2*(i-1)+2);
37          i=i+1;
38      end
39
40      %-------------------------------------------------------------------
41      % LadCalc
42      % Row 1: elastic portion of shear strain
43      % Row 2: shear stress (high)
44      % Row 3: shear Modulus
45      % Row 4: shear damage
46      % Row 5: Z'(d) Zprime
47      LadCalc = abs(LadData(8,1:(LadP/2 -1))- LadData(7,2:(LadP/2)));     % ...
            eps_{12}^e
48      LadCalc(2,:) = abs(LadData(14,1:(LadP/2 -1)));              % tau_12
49      LadCalc(3,:) = LadCalc(2,:)./LadCalc(1,:) ;               % G12(i)
50      LadCalc(4,:) = 1- LadCalc(3,:)/G12i;                      % d(i)
51      LadCalc(5,:) =  G12i/2*(LadCalc(1,:).^2) ;               % Z_d(i) Shear
52      j= glmfit(LadCalc(4,:)', sqrt(LadCalc(5,:)'));
53      Ycc = j(2);             % Critical transverse damage limit
54      Y0c = j(1);             % Initial transverse damage limit
55
56      % Row 6: elastic portion of strain along fibres.
57      % Row 7: elastic portion of strain perpendicular to fibres.
58      % Row 8: Transverse Stress
59      % Row 9: Transverse Modulus
60      % Row 10: Transverse damage d'
61      % Row 11: Z'd
62      % Row 12: Coupling factor between transverse and shear damage b.
63      % Row 13: Y(t) Pseudo force
64      LadCalc(6,:) = abs(LadData(4,1:(LadP/2 -1)) - ...
65          LadData(3,2:(LadP/2)));    % eps_{11} elastic portion
66      LadCalc(7,:) = abs(LadData(6,1:(LadP/2 -1)) - ...
67          LadData(5,2:(LadP/2)));    % eps_{22} elastic portion
68      LadCalc(8,:) = abs(LadData(12,1:(LadP/2-1 )));    % s22(i) Changed it
69                                                  % from 13,1:(LadP/2-1)
70                                                  % -> 12,1:(LadP/2-1)
71      LadCalc(9,:) = LadCalc(8,:)./LadCalc(7,:) ; % E22(i)
72      LadCalc(10,:) = 1- LadCalc(9,:)/E22i;       % d'(i)
73      LadCalc(11,:) = 1/2 * E22i * (v12i*LadCalc(6,:) + ...
74  LadCalc(7,:)).^2;  % Z'_d(i)
75      LadCalc(12,:) = ( (Ycc*LadCalc(4,:) +Y0c).^2 + ...
76          LadCalc(5,:) )./LadCalc(11,:);          % b(i)
```

```
77      LadCalc(13,:) = sqrt( LadCalc(5,:) + ...
78          LadCalc(12,:).*LadCalc(11,:) );        % Y(t_i)
79
80
81      % Exclude first point from calculation
82      j = glmfit(LadCalc(10,:)', LadCalc(13,:)');
83      Ycp = j(2);            % Critical transverse damage limit
84      Y0p = j(1);            % Initial transverse damage limit
85      YSp = max( sqrt(LadCalc(11,:)) );        % Brittle transvesre damage ...
            limit for fiber matrix interface
86      bcf = mean(LadCalc(12,2:(LadP/2-1) ));  % coupling factor between ...
            transverse and shear damage.
87      %
88              % Plot results
89      subplot(2,1,1)
90      plot( LadCalc(5,:)',LadCalc(4,:)');
91      axis([0 max(LadCalc(5,:)) 0 1 ]);
92      xlabel( 'Shear pseudoforce[GPa]' ); ylabel( ['Shear damage []'] );
93      subplot(2,1,2)
94      plot(LadCalc(13,:)', LadCalc(10,:)');
95      axis([0 max(LadCalc(13,:)) 0 1]);
96      xlabel( 'Y(t) [GPa]' ); ylabel( ['Transverse damage []'] );
97      pause
98
99      %
100     %
101     %
102     disp(['Results for ',FILENAME]);
103     disp('-------------------------------------------------------');
104     %     disp(['Shear Modulus                                G0:   ', ...
            num2str( G0 )])
105     %     disp(['Maximum shear strain at failure is          g12:   ', ...
            num2str( fstrn )])
106     %     disp(['Maximum shear stress at failure is          t12:   ', ...
            num2str( fsts )])
107     disp(['Initial transverse damage limit ----------[GPa]--Y'0:--', ...
            num2str( Y0p )]);
108     disp(['Critical transverse damage limit ----------[GPa]--Y'c:--', ...
            num2str( Ycp )]);
109     disp(['Comparison of initial shear damage limit --[GPa]---Y0:-', ...
            num2str( Y0 ), ', (Calc):--', num2str( Y0c )]);
110     disp(['Comparison of critical shear damage limit -[GPa]---Yc:-', ...
            num2str( Yc ), ', (Calc):--', num2str( Ycc )]);
111     disp(['Elementary Shear damage fracture limit ----[GPa]--Y'S:--', ...
            num2str( YSp )]);
112     disp(['C.F. between transverse shear strain -------[GPa]----b:--', ...
            num2str( bcf )]);
```

```
113     disp([' ------------------Individual numbers------[GPa]----b:  ', ...
            num2str( LadCalc(12,:) )   ] );
114     disp(['Transverse Strain rate-------------------[s^(-1)] SR22:  ', ...
            num2str( SRvec(4) )]);
115     disp(['Shear Strain rate-----------------------[s^(-1)] SR12:  ', ...
            num2str( SRvec(5) )]);
116     %
117     %
118     FILENAME=lower(FILENAME);
119     try %try for INSTRON when spcm is defined
120         spmn;
121         %
122         %------------------------ SAVE FILE ...
                ------------------------------------
123         %
124         % Place Filtered data in a similar filename with .csv extension.
125         %
126         %
127         % Open CSV file stream
128         i = findstr(FILENAME, '.csv');
129         specFILENAME = [ FILENAME(1:(i-1)),'i',num2str(spmn),'.CSV' ];
130         newPATHNAME = PATHNAME;
131         feval('cd',newPATHNAME);
132         fid = fopen(specFILENAME, 'wr');
133
134         % Open SDM file for Instron
135         i = findstr(FILENAME, '.csv');
136         specFILENAME = [ FILENAME(1:(i-1)),'i',num2str(spmn),'.SDM' ];
137         fid2 = fopen(specFILENAME, 'wr');
138         disp('Instron .csv and .SDM files are written');
139     catch  % If spmn not defined then it is a Video extensometry file.
140         %------------------------ SAVE FILE ...
                ------------------------------------
141         %
142         % Place Filtered data in a similar filename with .csv extension.
143         %
144         i = findstr(FILENAME, '.dat');
145         newFILENAME = [ FILENAME(1:(i-1)), 'v.CSV' ];
146         fid = fopen(newFILENAME, 'wr');
147
148         % open SDM file for VE
149         i = findstr(FILENAME, '.dat');
150         newFILENAME = [ FILENAME(1:(i-1)), 'v.SDM' ];
151         fid2 = fopen(newFILENAME, 'wr');
152         disp('VE .csv and .SDM files are written');
153     end
154     %-------------------------------------
```

```
155     % Information to be inputed on .csv
156     count1 = fprintf(fid,'Y'0 ,Y'c,Y'S,b,SR22,SR12,Y0,Yc\n');
157     count1 = fprintf(fid,'%f,%f,%f,%f,%f,%f,%f,%f\n', Y0p , ...
            Ycp, YSp, bcf, SRvec(4), SRvec(5), Y0c, Ycc );
158     InputStrg = '%f';
159     if (LadP/2-1)>=3
160         for i = 3:(LadP/2-1)
161             InputStrg = [InputStrg ',%f'];
162         end
163     end
164     InputStrg = [InputStrg '\n'];
165     count1 = fprintf(fid, InputStrg , LadCalc(12,2:(LadP/2-1)) );
166     % Assumed Values
167     count1 = fprintf(fid,'E11,E22,v12,G12,Y0,Yc\n');
168     count1 = fprintf(fid,'%f,%f,%f,%f,%f,%f\n', E11i , E22i, ...
            v12i, G12i , Y0, Yc );
169     % values used in calculation
170     count1 = fprintf(fid,'Time[sec],Stress[MPa],Long[],AverTrans ...
            ,Strain Rate[s^(-1)]\n');
171     n=length(y(1,:));
172     for i = 1:n,
173         count1 = fprintf(fid,'%f,%f,%f,%f,%f\n', y(1,i), y(2,i), ...
                y(4,i), y(6+NoTransChan,i), y(3,i));
174     end
175     fclose(fid);
176
177     %-----------------------------------
178     % Information to be inputed on .sdm
179     count1 = fprintf(fid2,'Time,Load,SR,L1,T1\n');
180     for i = 1:length(RawData(1,:)),
181         count1 = fprintf(fid2,'%f,%f,%f,%f,%f\n', RawData(1,i) ...
                , RawData(2,i), RawData(3,i), RawData(4,i), RawData(6+ ...
                NoTransChan,i));
182     end
183     fclose(fid2);
184     disp('.csv and .SDM files completed.');
185     disp(' ');
186
187     ans =0;
188
189 catch
190     ans = lasterr
191 end
```

C.1.2 Matlab Auxiliary Scripts.

C.1.2.1 Bisection Script For Calculation Of The Plasticity Exponent

```
function [m,beta,R0]= Brackm(Rmat, epmat, m);
% bisection method used to obtain the m parameter.
% Input
%   Rmat        : R vector (3 points)
%   epmat       : plastic strain vector (length =3)
%   m           : upper bound of m
% Output
%   m         : Plasticity parameter m
%   beta      : Plasticity parameter beta
%   R0        : initial Yield stress

% constants
MaxIt=100;  % Maximum iterations
Es= .0002;  % Stopping criterion

% initial value
mL= 1E-7;
mU=m;

iter=0;
Ea=1.1*Es;
try
    while ((Ea>Es) & (iter<MaxIt))
        m = (mL+mU)/2;
        iter=iter+1;
        if (mL+mU)~=0
            Ea=abs((mU+mL)/(mL+mU));
        end
        test = mPlasFnc(Rmat,epmat,mL)* mPlasFnc(Rmat,epmat,m);
        switch sign(test)
        case 0
            Ea=0;
        case -1
            mU=m;
        case 1
            mL=m;
        end
    end

    beta=( Rmat(3)-Rmat(1) ) / (epmat(3)^m - epmat(1)^m);
    R0= Rmat(3) - beta *epmat(3)^m;
catch
    disp('m did not converge!');
```

C.1.2 Matlab Auxiliary Scripts.

C.1.2.1 Bisection Script For Calculation Of The Plasticity Exponent

```
function [m,beta,R0]= Brackm(Rmat, epmat, m);
% bisection method used to obtain the m parameter.
% Input
%   Rmat        : R vector (3 points)
%   epmat       : plastic strain vector (length =3)
%   m           : upper bound of m
% Output
%   m         : Plasticity parameter m
%   beta      : Plasticity parameter beta
%   R0        : initial Yield stress

% constants
MaxIt=100;  % Maximum iterations
Es= .0002;  % Stopping criterion

% initial value
mL= 1E-7;
mU=m;

iter=0;
Ea=1.1*Es;
try
    while ((Ea>Es) & (iter<MaxIt))
        m = (mL+mU)/2;
        iter=iter+1;
        if (mL+mU)~=0
            Ea=abs((mU+mL)/(mL+mU));
        end
        test = mPlasFnc(Rmat,epmat,mL)* mPlasFnc(Rmat,epmat,m);
        switch sign(test)
        case 0
            Ea=0;
        case -1
            mU=m;
        case 1
            mL=m;
        end
    end

    beta=( Rmat(3)-Rmat(1) ) / (epmat(3)^m - epmat(1)^m);
    R0= Rmat(3) - beta *epmat(3)^m;
catch
    disp('m did not converge!');
```

```
44      m=[];
45      beta=[];
46      R0=[];
47  end
48
49  if iter>=MaxIt
50      disp('m did not converge!');
51      m=[];
52      beta=[];
53      R0=[];
54  end
```

C.1.2.2 Computation Of Individual Laminate Stiffness

```
1  function Qbar = LamStiff(E11,E22,v12,G12,theta);
2  % Calculates the transformed stiffness matrix of a lamina.
3  % Argument order
4  %    1) E11   [GPa]     Longitudinal tensile modulus of ply
5  %    2) E22   [GPa]     Transverse tensile modulus of ply
6  %    3) v12   []        Poisson ratio
7  %    4) G12   [GPa]     Shear modulus of ply
8  %    5) theta [rad]  Angle formed by the global (loading/testing) axis ...
       and the local (material) axis.
9  if (~isreal([E11,E22,v12,G12,theta]))
10     error('Inputs must be real numbers.')
11 end
12 v21=v12*E22/E11;
13 R=[1,0,0;0,1,0;0,0,2];
14 S12 = [1/E11, -v21/E22, 0; -v12/E11,1/E22, 0; 0, 0, 1/G12];
15 Q12 = inv(S12);
16 Qbar = inv(TransTheta(theta))*Q12*R*TransTheta(theta)*inv(R);
```

C.1.2.3 Calculation Of Laminate Stiffness Based On Individual Plies

```
1  function Qlambar = LamtSM(E11, E22, v12, G12, plyThick, plyInfo);
2  % Calculates the transformed stiffness matrix of a laminate.
3  % Argument order
4  %    1) E11   [GPa]        Longitudinal tensile modulus of ply
5  %    2) E22   [GPa]        Transverse tensile modulus of ply
6  %    3) v12   []           Poisson ratio
7  %    4) G12   [GPa]        Shear modulus of ply
8  %    5) plythick [mm]      Ply thickness
9  %    6) plyInfo matrix     Angle formed by the global (loading/testing) ...
       axis and the local (material) axis.
10 %              col.1        col.2
11 %              height       angle
```

```
12 if (~isreal([E11,E22,v12,G12]))
13     error('Inputs must be real numbers.')
14 end
15
16 i=size(plyInfo);
17 if (i(2)~=2)
18     error('Invalid plyInfo format.')
19 end
20
21 Ars = zeros(3);
22 Brs = zeros(3);
23 Drs = zeros(3);
24 for i=1:length(plyInfo(:,1))
25     Ars = Ars + LamStiff(E11, E22, v12, G12, plyInfo(i,2) )*( (plyInfo(i ...
       ,1)+plyThick/2) - (plyInfo(i,1)-plyThick/2)  );
26     Brs = Brs + LamStiff(E11, E22, v12, G12, plyInfo(i,2) )*( (plyInfo(i ...
       ,1)+plyThick/2)^2 - (plyInfo(i,1)-plyThick/2)^2  );
27     Drs = Drs + LamStiff(E11, E22, v12, G12, plyInfo(i,2) )*( (plyInfo(i ...
       ,1)+plyThick/2)^3 - (plyInfo(i,1)-plyThick/2)^3  );
28 end
29 Brs=.5*Brs;
30 Drs=1/3*Drs;
31 Qlambar = [Ars Brs; Brs Drs];
```

C.1.2.4 File With Properties Dataset

```
1 % Properties datasheet
2 %
3 %-----------Elasticity and Strength-----------
4 E11=[-3, -2, -1; ...
5       21.160, 28.360, 25.350];
6 %eps11f=[-3, -2, -1; ...
7 %     .0223, .0231, .0256];
8 %s11f=[-3, -2, -1; ...
9 %     508.41 , 572.13 , 564.65];
10 %SEf=[-3, -2, -1; ...
11 %     0.00821, .00803, .00910];
12 E22=[   -3,     -2,      -1; ...
13       6.986,   6.986,   6.986];
14 %eps22f=[-3, -2, -1; ...
15 %     0.0028389, 0.0028389, 0.0028389];
16 %s22f=[-3, -2, -1; ...
17 %     12.439, 12.439, 12.439];
18 v12=[-3, -2, -1; ...
19       .409, .356, .252];
20 G12=[  -3,          -2,         -1; ...
21       1.740, 1.330, 1.080];
```

```
%g12f=[-3,   -2,      -1; ...
%      .438, .406, .423];
%t12f=[-3,     -2,      -1; ...
%      42.57,  44.87, 47.70];

%-----------Damage Evolution-----------
%
%------Shear Damage
Y0m=[-3,          -2,          -1; ...
      0.00263, 0.00326,  0.00422];
Ycm=[   -3,       -2,      -1; ...
      0.0442,   0.0377, 0.0299];
%YR=[   -3,    -2,      -1; ...
%      .0458, .0407, .0368];
%------Transverse Damage
%Y0tm=[-3,       -2,      -1; ...
%      0.00263,    .3,      .3];
%Yctm=[-3,       -2,      -1; ...
%      0.0442,     .3,      .3];
%YSt=[-3,        -2,      -1; ...
%      .0458,      .3,      .3];
```

C.1.2.5 Function Used By Bisection Method

```
function m = mPlasFnc(Rmat,epmat,m)
% Plasticity function used in bisection method
% As obtained from [+/- 45]_{2s} ladeveze theory.
%
m= log( ( Rmat(3)-Rmat(1) )*( epmat(2)^m - epmat(1)^m ) /(Rmat(2)-Rmat ...
    (1)) + epmat(1)^m ) /log(epmat(3))-m;
```

C.1.2.6 Initialisation File For $[0°]_4$ laminate

```
% Filtering
switch CDR
case 5
     saFreq = DAR/2;      % Sampling Frequency [Hz]
     coFreq = .5;    % cutoff frequency [Hz]
     Forder = 9;
     AveOrd = 25;          % number of averaging entries.
     AvOr = floor(AveOrd/2)+1;
case 50
     saFreq = DAR/2;      % Sampling Frequency [Hz]
     coFreq= 10;   % cutoff frequency [Hz]
     Forder = 5;
     AveOrd = 11;          % number of averaging entries.
```

```
14      AvOr = floor(AveOrd/2)+1;
15  case 500
16      saFreq = DAR/2;       % Sampling Frequency [Hz]
17      coFreq= .999*saFreq;  % cutoff frequency [Hz]
18      Forder = 1;
19      AveOrd = 1;           % number of averaging entries.
20      AvOr = floor(AveOrd/2)+1;
21  end
22
23
24
25  % CONSTANTS
26  %----------
27  %
28  R=[1,0,0;0,1,0;0,0,2];
29  thet = 0;
30  plyThick= .22;
31  plies= 4;
32  plyInfo=zeros(plies,2);
33  for i=1:plies/2
34      plyInfo(i,:) = [ (i-plies/2)*plyThick-plyThick/2 , thet*(-1)^i   ];
35      plyInfo(plies+1-i,:)= plyInfo(i,:).*[-1,1];
36  end
37  d2s=[50,10];
38  l2stress = 10 *plyThick *plies;    % [mm^2]
```

C.1.2.7 Initialisation File For $[\pm 45°]_{2s}$ laminate

```
1  % Initialisation File for [PM45]_{2s}
2  %
3  % Requires CDR as global variable
4  % Provides:
5  %           Filtering parameters saFreq, coFreq, Forder, AveOrd, AvOr;
6  %           laminate sequence: PlyInfo, plyThick, plies, theta
7  %           Displacement to Strain parameter (required for instron) d2s
8  % Calculates
9  %           Load to stress conversion factor:  l2stress [mm^2]
10 %           Strain and Stiffness conversion matrices.
11
12 switch CDR
13 case 5
14     saFreq = DAR/2;       % Sampling Frequency [Hz]
15     coFreq = .5;      % cutoff frequency [Hz]
16     Forder = 9;
17     AveOrd = 25;          % number of averaging entries.
18     AvOr = floor(AveOrd/2)+1;
19 case 50
```

```
20      saFreq = DAR/2;       % Sampling Frequency [Hz]
21      coFreq= 3;  % cutoff frequency [Hz]
22      Forder = 5;
23      AveOrd = 25;          % number of averaging entries.
24      AvOr = floor(AveOrd/2)+1;
25  case 500
26      saFreq = DAR/2;       % Sampling Frequency [Hz]
27      coFreq= .999*saFreq;  % cutoff frequency [Hz]
28      Forder = 3;
29      AveOrd = 15;          % number of averaging entries.
30      AvOr = floor(AveOrd/2)+1;
31  end
32
33  % CONSTANTS
34  %---------
35  %
36  R=[1,0,0;0,1,0;0,0,2];
37  thet = pi/4;
38  plyThick= .22;
39  plies= 8;
40  plyInfo=zeros(plies,2);
41  for i=1:plies/2
42      plyInfo(i,:)= [ (i-plies/2)*plyThick-plyThick/2 , thet*(-1)^i   ];
43      plyInfo(plies+1-i,:)= plyInfo(i,:).*[-1,1];
44  end
45  d2s=[50,10];
46  l2stress = 10*plyThick*plies;    % [mm^2]#
47
48
49  % CALCULATIONS
50  %-------------
51  % Strain Conversion Matrix
52  %SnMcv= (inv(TransTheta(thet)))';
53  SnMcv= [ 0 , 0 , 0; 1 , 1 , 0; 1 , -1 , 0];
54  %Axy= LamtSM(E11i, E22i, v12i, G12i, plyThick, plyInfo);
55  %Axy=Axy(1:3,1:3)/(plies*plyThick);
56  %    Stiffness matrix
57  %SMcv = LamStiff(E11i, E22i, v12i, G12i, 0)*R*TransTheta(thet)*inv(R)* ...
        inv(Axy);
58  SMcv= [ 0 , 0 , 0; 1/2 , 0 ,0; 1/2 , 0 ,0];
59  %SMcv = [0 , 0 , .5 ];   % Stiffness matrix conversion factor (PAM-CRASH ...
        manual ply -data 26
```

C.1.2.8 Initialisation File For $[+45°]_8$ laminate

```
1  % Initialisation File for [P45]_8
2  %
```

```
% Requires CDR as global variable
% Provides:
%           Filtering parameters saFreq, coFreq, Forder, AveOrd, AvOr;
%           laminate sequence: PlyInfo, plyThick, plies, theta
%           Displacement to Strain parameter (required for instron) d2s
% Calculates
%           Load to stress conversion factor:  l2stress [mm^2]
%           Strain and Stiffness conversion matrices.

switch CDR
case 5
    saFreq = DAR/2;      % Sampling Frequency [Hz]
    coFreq = .5;     % cutoff frequency [Hz]
    Forder = 9;
    AveOrd = 11;          % number of averaging entries.
    AvOr = floor(AveOrd/2)+1;
case 50
    saFreq = DAR/2;      % Sampling Frequency [Hz]
    coFreq= 10;   % cutoff frequency [Hz]
    Forder = 5;
    AveOrd = 3;          % number of averaging entries.
    AvOr = floor(AveOrd/2)+1;
case 500
    saFreq = DAR/2;      % Sampling Frequency [Hz]
    coFreq= .999*saFreq;  % cutoff frequency [Hz]
    Forder = 3;
    AveOrd = 1;          % number of averaging entries.
    AvOr = floor(AveOrd/2)+1;
end


% CONSTANTS
%----------
%
R=[1,0,0;0,1,0;0,0,2];
thet = pi/4;
plyThick= .22;
plies= 8;
plyInfo=zeros(plies,2);
for i=1:plies/2
    plyInfo(i,:) = [ (i-plies/2)*plyThick-plyThick/2 , thet   ];
    plyInfo(plies+1-i,:)= plyInfo(i,:).*[-1,1];
end
d2s=[50,10];
l2stress = 10*plyThick*plies;    % [mm^2]

```

```
50
51
52 % CALCULATIONS
53 %-----------
54 % Strain Conversion Matrix
55 %SnMcv= (inv(TransTheta(thet))) ';
56 SnMcv= [ 0 , 0 , 0; 1 , 1 , 0; 1 , -1 , 0];
57 %Axy= LamtSM(E11i, E22i, v12i, G12i, plyThick, plyInfo);
58 %Axy=Axy(1:3,1:3)/(plies*plyThick);
59 %    Stiffness matrix
60 %SMcv = LamStiff(E11i, E22i, v12i, G12i, 0)*R*TransTheta(thet)*inv(R)* ...
       inv(Axy);
61 SMcv= [ 0 , 0 , 0; 1/2 , 0 ,0; 1/2 , 0 ,0];
```

C.1.2.9 Initialisation File For $[\pm 67.5°]_8$ laminate

```
1  % Filtering
2  switch CDR
3  case 5
4      saFreq = DAR/2;      % Sampling Frequency [Hz]
5      coFreq = .5;     % cutoff frequency [Hz]
6      Forder = 9;
7      AveOrd = 15;          % number of averaging entries.
8      AvOr = floor(AveOrd/2)+1;
9  case 50
10     saFreq = DAR/2;      % Sampling Frequency [Hz]
11     coFreq = 10;    % cutoff frequency [Hz]
12     Forder = 5;
13     AveOrd = 5;          % number of averaging entries.
14     AvOr = floor(AveOrd/2)+1;
15 case 500
16     saFreq = DAR/2;      % Sampling Frequency [Hz]
17     coFreq= .999*saFreq;  % cutoff frequency [Hz]
18     Forder = 3;
19     AveOrd = 1;          % number of averaging entries.
20     AvOr = floor(AveOrd/2)+1;
21 end
22
23
24
25 % CONSTANTS
26 %----------
27 %
28 R=[1,0,0;0,1,0;0,0,2];
29 thet = pi*3/8;
30 plyThick= .22;
31 plies= 8;
```

```
plyInfo=zeros(plies,2);
for i=1:plies/2
    plyInfo(i,:)= [ (i-plies/2)*plyThick-plyThick/2 , thet*(-1)^i   ];
    plyInfo(plies+1-i,:)= plyInfo(i,:).*[-1,1];
end
d2s=[50,10];
l2stress = 10 *plyThick *plies;    % [mm^2]


% CALCULATIONS
%-----------
% Strain Conversion Matrix
SnMcv= (inv(TransTheta(thet)))';
%Axy= LamtSM(E11i, E22i, v12i, G12i, plyThick, plyInfo);
%Axy=Axy(1:3,1:3)/(plies*plyThick);
%    Stiffness matrix
SMcv = zeros(3);%TransTheta(thet);
```

C.1.2.10 Strain Rate Selection File

```
CDR=[];
while isempty(CDR)% Define static test heading for these checkboxes
    txt_axes = uicontrol( gcf ,...
        'Style', 'text',...
        'Units', 'normalized',...
        'Position', [.0 .20 .20 .05],...
        'String', 'Strain Rate');
    % Define the 5 [mm/sec] radio box
    speed1 = uicontrol( gcf, ...
        'Style', 'radio', ...
        'Units', 'normalized',...
        'Position', [.0 .15 .20 .05],...
        'Value', 0,...
        'String', '5mm/min',...
        'Callback', [...
            'set(speed1,''Value'',1),' ,...
            'set(speed2,''Value'',0),' ,...
            'set(speed3,''Value'',0),' ,...
            'CDR=5;']);
    % Define the 50[mm/sec] radio box
    speed2 = uicontrol( gcf, ...
        'Style', 'radio', ...
        'Units', 'normalized',...
        'Position', [.0 .10 .20 .05],...
        'String', '50mm/min',...
        'Callback', [...
            'set(speed1,''Value'',0),' ,...
```

```
28              'set(speed2,''Value'',1),'  ,...
29              'set(speed3,''Value'',0),'  ,...
30              'coFreq=3;␣Forder␣=␣5;␣CDR=50;']);
31      % Define the 500[mm/sec] radio box
32      speed3 = uicontrol( gcf, ...
33          'Style', 'radio', ...
34          'Units', 'normalized',...
35          'Position', [.0 .05 .20 .05],...
36          'String', '500mm/min',...
37          'Callback', [...
38              'set(speed1,''Value'',0),'  ,...
39              'set(speed2,''Value'',0),'  ,...
40              'set(speed3,''Value'',1),'  ,...
41              'CDR=500;']);
42
43      pause;
44  end
45  CDR=CDR;
46  close(gcf);
47  clear txt_axes speed1 speed2 speed3;
48  clear plies1 plies2;
```

C.1.2.11 Function For Transformation Of Angles.

```
1  function T = TransTheta(theta)
2  % (3x3) Transformation matrix for laminate stiffness.
3  % theta is the angle of the matrix.
4  % Non-vector input results in an error.
5  if (~isreal(theta))
6      error('Input␣must␣be␣a␣real␣number.')
7  end
8  T =  [cos(theta)^2, sin(theta)^2 , 2*cos(theta)*sin(theta);  sin(theta) ...
       ^2, cos(theta)^2 , -2*cos(theta)*sin(theta); -cos(theta)*sin(theta), ...
      cos(theta)*sin(theta), cos(theta)^2-sin(theta)^2];   % Stiffness ...
      matrix conversion factor (PAM-CRASH manual ply-data 26
```

C.1.2.12 Matrix Trimming Function.

```
1  function RawData = trimMat(yTemp, ans, symbl)
2  % Input
3  %   yTemp    : Matrix to be trimmed
4  %   ans      : Input string
5  %   symbl    : separator symbol - default
6  %
7
8  % set default symbl
```

```
try
    symbl;
catch
    symbl='-';
end

flag = findstr(ans,symbl);

if isempty(flag)
    ans =str2num(ans);
    n = length( yTemp(2,:) );
    RawData = zeros( size(yTemp) - [0 1] );
    for i=1:(ans-1)
        RawData(:,i) = yTemp(:,i);
    end
    for i=(ans+1):n
        RawData(:,i-1) = yTemp(:,i);
    end
    disp('present at the nowhere');
else
    n = length(yTemp(2,:));
    switch length(num2str(ans))<= flag
    case  1% - at the end
        j = str2num(ans(1:(flag-1)));
        RawData = [yTemp(:,1:(j-1)) , yTemp(:,n)];
    case  0% - in the middle
        j = str2num(ans(1:(flag-1)));
        k = str2num( ans((flag+1):length(ans)) );
        RawData = [yTemp(:,1:(j-1)) , yTemp(:,(k+1):n)];
    end
end
```

C.1.3 Video Extensometry Specific Scripts

C.1.3.1 Cyclic Loading Weedout Function

```
% Selection of maximum and minimum curves points
%  and conversion from test axis to material axis

% Requires the following global variables:
%   y
%   NoTransChan : Number of transverse channels
%   SnMcv    strain matrix conversion from global to local
%   SMcv     Load matrix conversion from global to local
%        Dload variable is used to check for the Lad nums
%        ShearData array stores the Lad nums obtained by the process.
```

```
DLoad= y(2, 2:length(y(2,:))) - y (2, 1: ( length( y(2,:) )-1 ) );
j=2;
ShearData(:,1) = y(:,1);
for i = 1:(length(y(2,:))-2),
    flagProd = DLoad( i ) * DLoad( i+1 ) ;
    if flagProd <= 0
        ShearData(:,j) = y(:,i);
        j=j+1;
    end;
end
ShearData(:,j) = y(:,length(y(2,:)));

% plotting the ShearData array in order to be able to cut off the not ...
   needed pieces.
i = gcf;  close(i);                % close open window.
plot(ShearData(2,:));      xlabel('Lad Number'); ylabel('Stress [MPa]')

% selection routine
LadP=[];
while isempty(LadP),
    LadP = input('What is the maximum no of Ladaveze numbers: ');
    if (LadP<12 | LadP>length(ShearData(2,:)) )
        LadP=length(ShearData(2,:)) ;
    end
end
ShearData=ShearData(:,1:LadP);  % truncation of the ShearData matrix.

ans = 1;
while ans~=0
    LadTemp = ShearData;
    plot(LadTemp(2,:))
    ans= input('Add observation #remove obs or Enter for continue: ');
    if (isempty(ans) | ans==0)
        ans =0;
    else
        n = length( LadTemp(2,:) );
        ShearData = zeros( size(LadTemp) - [0 1] );
        for i=1:(ans-1)
            ShearData(:,i) = LadTemp(:,i);
        end
        for i=(ans+1):n
            ShearData(:,i-1) = LadTemp(:,i);
        end
    end
end

i = gcf;  close(i);                % close open window.
```

```
57 plot(ShearData(2,:));              % making sure of the 5 distinctive peaks ...
58 xlabel('Observation'); ylabel('Stress [MPa]')
59 pause
60 LadP = length( ShearData(2,:) );
61
62 % Conversion of longitudinal stress to shear stress.
63 %   LadData contains the values which will be used in the calculations ...
      in a friendly format.
64 LadData=zeros(14,(LadP/2));
65 % Row 1: Time index
66 % Row 2: Time index
67 % Row 3: Low longitudinal strain = eps_{11}^p
68 % row 4: High Longitudinal strain
69 % row 5: Low transverse strain = eps_{22}^p
70 % row 6: High transverse strain
71 % row 7: Low shear strain = eps_{12}^p
72 % row 8: High shear strain
73 % Row 9: Low longitudinal Stress
74 % row 10: High Longitudinal Stress
75 % row 11: Low transverse Stress
76 % row 12: High transverse Stress
77 % row 13: Low shear Stress
78 % row 14: High shear Stress
79 i = 1;
80 while i < (LadP/2 +1),
81     LadData(1,i) = ShearData(1,2*(i-1)+1);  %time
82     LadData(2,i) = ShearData(1,2*(i-1)+1+1);
83
84     LadData(3,i) = SnMcv(1,1) * ShearData(4,2*(i-1)+1) + SnMcv(1,2) * ...
          ShearData(6+NoTransChan,2*(i-1)+1);
85     LadData(4,i) = SnMcv(1,1) * ShearData(4,2*(i-1)+2) + SnMcv(1,2) * ...
          ShearData(6+NoTransChan,2*(i-1)+2);
86     LadData(5,i) = SnMcv(2,1) * ShearData(4,2*(i-1)+1) + SnMcv(2,2) * ...
          ShearData(6+NoTransChan,2*(i-1)+1);
87     LadData(6,i) = SnMcv(2,1) * ShearData(4,2*(i-1)+2) + SnMcv(2,2) * ...
          ShearData(6+NoTransChan,2*(i-1)+2);
88     LadData(7,i) = SnMcv(3,1) * ShearData(4,2*(i-1)+1) + SnMcv(3,2) * ...
          ShearData(6+NoTransChan,2*(i-1)+1);
89     LadData(8,i) = SnMcv(3,1) * ShearData(4,2*(i-1)+2) + SnMcv(3,2) * ...
          ShearData(6+NoTransChan,2*(i-1)+2);
90
91     LadData(9,i) = SMcv(1,1) * ShearData(2,2*(i-1)+1);
92     LadData(10,i) = SMcv(1,1) * ShearData(2,2*(i-1)+2);
93     LadData(11,i) = SMcv(2,1) * ShearData(2,2*(i-1)+1);
94     LadData(12,i) = SMcv(2,1) * ShearData(2,2*(i-1)+2);
95     LadData(13,i) = SMcv(3,1) * ShearData(2,2*(i-1)+1);
```

```
96      LadData(14,i) = SMcv(3,1) * ShearData(2,2*(i-1)+2);
97      i=i+1;
98  end
```

C.1.3.2 Read Video Extensometry File Function

```
1  function [x1, NTC] = ReadVE(FILENAME, PATHNAME);
2  % Reads a csv Instron file and converts the array to a multidimensional ...
       array
3  %
4  % Creates strains
5  % Presents a plot of the transverse strains to select
6  %   which will be used for the average transersal strain
7  % Use PSTRE M-script file to view files.
8  %-------------------------------------------------------------
9  % Read in from a .csv file
10 % The format of the input file is
11 %   1 - Time in msec
12 %   2 - Load [kN]
13 %   3 - Biaxial Load
14 %   4 - Longitudinal Channel 1
15 %   5 - Transverse distance
16 %   6 - ...
17 %   7 - ...
18 %   . - ...
19 %   NTC+5 - Final transverse
20 %
21 % Output data in a x1 1-D array
22 %   1 - Time in msec
23 %   2 - Load [kN]
24 %   3 - Biaxial Load
25 %   4 - Longitudinal Channel 1
26 %   5 - Transverse distance
27 %   6 - ...
28 %   7 - ...
29 %   . - ...
30 %   NTC+5 - Final transverse
31
32 feval('cd',PATHNAME);
33 fid = fopen(FILENAME, 'r');
34 fgetl(fid);
35 y=fgetl(fid);
36 k = length(findstr(y,char(9)))+1;
37 NTC=k-5;
38 fseek(fid,0,-1);
39 fgetl(fid);
40 [x1,count] = fscanf(fid,'%f ',[k,inf/k]);
```

```
fclose(fid);


% convert from N to kN
if max(x1(2,:))>100
    x1(2,:) = x1(2,:) /1000;
    disp('The load channel has been converted from N to kN');
end
```

C.1.3.3 Video Extensometry Filtering Function

```
% Script for filtering and conversion to stress and strain from VE raw ...
    data
% Arguments InsaFreqilt(x, coFreq, saFreq)
%   x:       The actual data.      6+NoTransChan matrix
%   coFreq:      The CutOff frequency  [Hz]
%   saFreq:      Sampling frequency    [Hz]
%   Forder:   Butterworth filter order    [Integer]
%   AvOr:   AvOraging number for filter
%   l2stress:   Load to stress conversion factor
%   NoTransChan:         Number of transverse channels.


nFreq = coFreq/saFreq;  % Normalised Frequency []
if nFreq >0
    [b,a]=butter(Forder, nFreq); % Calculate Filtfilt butter filter ...
        parameters
end

%-----------Data Manipulations and Filtering ...
    ------------------------------
%
% Conversion of msec to [sec];
x(1,:) = x(1,:)/1000;

j = 1;
while j ~= 0,
    n=length(x(1,:));
    plot( x(2,:),'r-')
    xlabel( 'Observations [#]' ); ylabel( ['Load [kN]'] );
    j = input('Set number for starting [0 or enter to continue]: \n Use ...
        ###- to trim the end: ', 's');
    if (isempty(j) | j ==0)
        j =0;
    elseif (~isempty(j) & isempty(findstr(j, '-')) )
        j= str2num(j);
        x= x( :,j:n);
```

```
33      elseif (~isempty(j) & ~isempty(findstr(j, '-')) )
34          j= str2num( j(1:(findstr(j, '-')-1)) );
35          x= x( :,1:j);
36      end
37      k =gcF;
38      close(k);
39  end
40
41  y = x;
42  n = length(y(1,:));
43
44  % 2 - Load [kN] to stress [MPa].
45  y(2,:) = x(2,:);
46  if ( coFreq < 1 & coFreq >0)
47      i = AvOr;
48      while (i+ AvOr) < length( y(2,:) -1 ),
49          i=i+1;
50          y(2,i) = mean( y(2, (i-AvOr):(i+AvOr) ) );
51      end
52  end
53  y(2,:) =   y(2,:)  / l2stress;
54
55  if y(2,1)<=0
56      i=1;
57      disp('Interpolation')
58      while y(2,i)<=0
59          i=i+1;
60      end
61      y=y(:,(i-1):length(y(2,:)));
62      y(:,1) = - (y(:,1) - y(:,2)) / (y(2,1) - y(2,2))* y(2,2)+  y(:,2);  ...
            %Check this
63  else
64      disp('Extrapolation')
65      while y(2,1)>y(2,2)
66          disp('Not possible to extrapolate. Please trim Load Channel ...
                again; Use with caution!')
67          n = length(y(1,:));
68          y = y(:,2:n);
69      end
70      try
71          i=1;
72          while y(2,i)<=y(2,i+1)
73              i=i+1;
74          end
75      catch
76          disp('Error in the extrapolation procedure of first cycle');
```

```
77          disp('␣Presence␣of␣Monotonous␣Load␣function␣equals␣no␣cyclic␣ ...
                testing.');
78          disp('␣Extrapolation␣procedure␣continues␣but␣use␣results␣with␣ ...
                caution.');
79          i = length(y(2,:));
80      end
81      ans = y(:,1) - (y(:,i) - y(:,1)) * y(2,1)/ (y(2,i) - y(2,1));
82      y= [ans, y];
83  end
84
85  % Reset the time
86  y(1,:) = y(1,:)- y(1,1);
87
88
89  for i = 4:(5+NoTransChan),
90      y(i,:) = ( y(i,:) - y(i,1) ) /y(i,1);
91  end
92
93  % Filtering of Displacement channels [mm]
94  for i = 4:(5+NoTransChan),
95      if nFreq >0
96          y(i,:) = filtfilt(b,a,y(i,:));
97      end
98  end
99  % Converstion of Longitudinal Displacement to strain
100
101 % call SelT subroutine to select transversal strains
102 % Plot Transversal strains to aid selection.
103 for i = 5:(5+NoTransChan),
104     subplot(2,ceil((NoTransChan+1)/2),i-4);
105     plot( y(1,:), y(i,:),'r-')
106     axis([min(y(1,:)) max(y(1,:)) min(min(y(5:(5+NoTransChan),:))) max( ...
            max(y(5:(5+NoTransChan),:)))]);
107     xlabel( 'Time[sec]' ); ylabel( ['Transverse-', num2str(i-4), '␣ ...
            strain␣[%]'] );
108     %   legend('y-.', 'Strain');
109     title( ['Tr-', num2str(i-4), '␣strain'] );
110 end
111
112 SelT2;
113 pause;
114 y(6+NoTransChan,:) = y(5,:)* sel(1);
115 for j= 2:length(sel),
116     y(6+NoTransChan,:) = y(6+NoTransChan,:) + y( 4+ j,:) * sel(j);
117 end
118 y(6+NoTransChan,:) = y(6+NoTransChan,:)/sum(sel);
119
```

```
% 3 - useless channel (for biaxial loads) - Replaced by Tangential ...
    strain Rates
y(3,1)=(y(4,2)-y(4,1))/y(1,2);
n = length(y(3,:));
y(3,n)=(y(4,n)- y(4,n-1))/(y(1,n) - y(1,n-1));
for i = 2:n-1,
    y(3,i) = abs((y(4,i+1) - y(4,i-1))/(y(1,i+1) - y(1,i-1)));
end



%-------------------------------------------------------------
% Plot Stress vs. Strain results
clf;
subplot(2,1,1);
plot(y(4,:),y(2,:),y(6+NoTransChan,:),y(2,:));
xlabel('Strain'); ylabel('Stress');
subplot(2,1,2);
plot(y(1,:),y(3,:));
xlabel('Time [sec]'); ylabel('Strain Rate');
pause;
```

C.1.4 Instron Contacting Extensometer Specific Scripts

C.1.4.1 Cyclic Loading Weedout Function

```
function [LadP, LadData, RawData, SRvec] = WOCyf(y, NTC, SnMcv, SMcv);
% WeedOut Cyclic selection function
%
% [LadP, LadData, RawData, SRvec] = WOCyf(y, NTC, SnMcv, SMcv)
% Input:
%   y matrix
%   NTC             : Number of transverse channels
%   SnMcv           : Global to material Strain conversion matrix
%   SMcv            : Global to material stress conversion matrix
% Output
%   LadP            : Number of cycles
%   LadData         : Matrix with material coordinate system (1-2) data
%   RawData         : Matrix with testing coordinate system (L-T) data

% Finds the local maxima and minima for the given load curves.
% The data points are transfered in the RawData matrix (testing axis L,T ...
    ).
% and then to LawData transformed to Material axis (1-2).
% Selection of maximum and minimum curves points
%  and conversion from test axis to material axis
```

```
%
% Requires the following global variables:
%   y
%   NTC:     Number of transverse channels
%   SnMcv    strain matrix conversion from global to local
%   SMcv     Load matrix conversion from global to local
%        Dload variable is used to check for the Lad nums
%        RawData array stores the Lad nums obtained by the process.
DLoad= y(2, 2:length(y(2,:))) - y (2, 1: ( length( y(2,:) )-1 ) );
j=2;
RawData(:,1) = y(:,1);
for i = 1:(length(y(2,:))-2),
    flagProd = DLoad( i ) * DLoad( i+1 ) ;
    if flagProd <= 0
        RawData(:,j) = y(:,i);
        j=j+1;
    end;
end
RawData(:,j) = y(:,length(y(2,:)));

% plotting the RawData array in order to be able to cut off the not ...
   needed pieces.
i = gcf;  close(i);                % close open window.
plot(RawData(2,:));      xlabel('Lad Number'); ylabel('Stress [MPa]')

% selection routine
LadP=[];
while isempty(LadP),
    LadP = input('What is the maximum no of Ladaveze numbers: ');
    if (LadP<12 | LadP>length(RawData(2,:)) )
        LadP=length(RawData(2,:)) ;
    end
end
RawData=RawData(:,1:LadP);  % truncation of the RawData matrix.

ans = 1;
while ans~=0
    LadTemp = RawData;
    i = gcf;  close(i);                % close open window.
    plot(LadTemp(2,:))
    ans= input('Add observation # remove obs (valid ##- or ##-##) or \n ...
       Enter for continue ','s');
    if (isempty(ans) | ans==0)
        ans =0;
    else
        RawData = trimMat(LadTemp,ans);
    end
```

```
65 end
66
67 i = gcf;  close(i);                    % close open window.
68 plot(RawData(2,:));                   % making sure of the 5 distinctive peaks.
69 xlabel('Observation'); ylabel('Stress [MPa]')
70 pause
71 LadP = length( RawData(2,:) );
72
73 % Conversion of longitudinal stress to shear stress.
74 %  LadData contains the values which will be used in the calculations ...
      in a friendly format.
75 LadData=zeros(14,(LadP/2));
76 % Row 1: Time index
77 % Row 2: Time index
78 % Row 3: Low longitudinal strain = eps_{11}^p
79 % row 4: High Longitudinal strain
80 % row 5: Low transverse strain = eps_{22}^p
81 % row 6: High transverse strain
82 % row 7: Low shear strain = eps_{12}^p
83 % row 8: High shear strain
84 % Row 9: Low longitudinal Stress
85 % row 10: High Longitudinal Stress
86 % row 11: Low transverse Stress
87 % row 12: High transverse Stress
88 % row 13: Low shear Stress
89 % row 14: High shear Stress
90 i = 1;
91 while i < (LadP/2 +1),
92     LadData(1,i) = RawData(1,2*(i-1)+1);  %time
93     LadData(2,i) = RawData(1,2*(i-1)+1+1);
94
95     LadData(3,i) = SnMcv(1,1) * RawData(4,2*(i-1)+1) + SnMcv(1,2) * ...
          RawData(6+NTC,2*(i-1)+1);
96     LadData(4,i) = SnMcv(1,1) * RawData(4,2*(i-1)+2) + SnMcv(1,2) * ...
          RawData(6+NTC,2*(i-1)+2);
97     LadData(5,i) = SnMcv(2,1) * RawData(4,2*(i-1)+1) + SnMcv(2,2) * ...
          RawData(6+NTC,2*(i-1)+1);
98     LadData(6,i) = SnMcv(2,1) * RawData(4,2*(i-1)+2) + SnMcv(2,2) * ...
          RawData(6+NTC,2*(i-1)+2);
99     LadData(7,i) = SnMcv(3,1) * RawData(4,2*(i-1)+1) + SnMcv(3,2) * ...
          RawData(6+NTC,2*(i-1)+1);
100    LadData(8,i) = SnMcv(3,1) * RawData(4,2*(i-1)+2) + SnMcv(3,2) * ...
          RawData(6+NTC,2*(i-1)+2);
101
102    LadData(9,i) = SMcv(1,1) * RawData(2,2*(i-1)+1);
103    LadData(10,i) = SMcv(1,1) * RawData(2,2*(i-1)+2);
104    LadData(11,i) = SMcv(2,1) * RawData(2,2*(i-1)+1);
```

```
105     LadData(12,i) = SMcv(2,1) * RawData(2,2*(i-1)+2);
106     LadData(13,i) = SMcv(3,1) * RawData(2,2*(i-1)+1);
107     LadData(14,i) = SMcv(3,1) * RawData(2,2*(i-1)+2);
108     i=i+1;
109 end
110
111 SRvec = median(RawData(3,2:length(RawData(3,:))));  % Longitudinal ...
      modulus
112 SRvec(2) = median(RawData(3,2:length(RawData(3,:))));  % Longitudinal ...
      modulus
113 SRvec(3) = median(abs((LadData(4,:) - LadData(3,:))./(LadData(2,:) - ...
      LadData(1,:))));
114 % Longitudinal modulus (material axis)
115 SRvec(4) = median(abs((LadData(6,:) - LadData(5,:))./(LadData(2,:) - ...
      LadData(1,:))));  % Transverse modulus  (material axis)
116 SRvec(5) = median(abs((LadData(8,:) - LadData(7,:))./(LadData(2,:) - ...
      LadData(1,:))));  % Shear modulus (material)
```

C.1.4.2 Read Instron Contacting Extensometer File Function

```
1  function x1 = ReadIns(FILENAME, PATHNAME);
2  % Reads a csv Instron file and converts the array to a multidimensional ...
     array
3  %
4  % Creates strains
5  % Presents a plot of the transverse strains to select
6  %   which will be used for the average transersal strain
7  % Use PSTRE M-script file to view files.
8  %-------------------------------------------------------------
9  % Read in from a .csv file
10 % The format of the input file is
11 %   1 - observation number
12 %   2 - Longitudinal displacement (over 50[mm] gauge length)
13 %   3 - Load [kN]
14 %   4 - Transverse distance of targets (over 10[mm] gauge length)
15 %
16 % Output data in a x1 multidimensional array
17 %   1 - observation number
18 %   2 - Longitudinal displacement (over 50[mm] gauge length)
19 %   3 - Load [kN]
20 %   4 - Transverse distance of targets (over 10[mm] gauge length)
21
22
23 feval('cd',PATHNAME);
24 fid = fopen(FILENAME, 'r');
25 InputStrg= '%i,␣%f,␣%f,␣%f␣';
26 [x,count1] = fscanf(fid,'%f,␣%f,␣%f,␣%f',[4,inf/4]);
```

```
fclose(fid);

j=1;
spec=1;
x1=zeros(size(x));
while (j~=length(x(1,:)))
    disp(['Now processing specimen #',num2str(spec),'.']);
    i=j;
    while (x(1,j+1)>x(1,j) & (j+1)~=length(x(1,:)))
        j=j+1;
    end

    k = x(:,i:j);
    k = cat(2, k , zeros(size(x1(:,:,1)) - [0, length(k(1,:))] ));
    x1(:,:,spec)= k;
    disp(['     from #',num2str(i),' to #',num2str(j)]);
    j=j+1;
    spec=spec+1;
end

x1= x1(:,1:max(max(x1(1,:,:))),:); % minimize the length of the matrix ...
   using

%catch
%disp('Prob ');
%end
```

C.1.4.3 Instron Contacting Extensometer Filtering Function

```
function y=InsFiltC(x, cF, sF, FOrd, Aver, DAR, l2stress, NTC, d2s)
% Function for conversion to stress and strain from Instron raw data
% Arguments InsFilt(x, coFreq, saFreq)
%   x:        The actual data.       6+NoTransChan matrix
%   cF:       The CutOff frequency   [Hz]
%   sF:       Sampling frequency     [Hz]
%   Ford:     Butterworth filter order     [Integer]
%   Aver:     Averaging number for filter
%   DAR:      Data Acquisition Rate [points/sec]=[Hz]
%   l2stress:    Load to stress conversion factor
%   NTC:         Number of transverse channels.
%   d2s       Data matrix with extensiometer distances.
%         d2s(1) longitudinal
%         d2s(2) transverse


nFreq = cF/sF;  % Normalised Frequency //
[b,a]=butter(FOrd, nFreq); % Calculate Filtfilt butter filter parameters
```

```
%----------Data Manipulations and Filtering ...
%
% Conversion of msec to [sec];
x(1,:) = x(1,:)/DAR;

j = 1;
while j ~= 0,
    n=length(x(1,:));
    plot( x(2,:),'r-')
    xlabel( 'Observations [#]' ); ylabel( ['Load [kN]'] );
    j = input('Set number for starting [0 or enter to continue]: \n Use ...
       ### to trim the end: ', 's');
    if (isempty(j) | j ==0)
        j =0;
    elseif (~isempty(j) & isempty(findstr(j, '-')) )
        j= str2num(j);
        x= x( :,j:n);
    elseif (~isempty(j) & ~isempty(findstr(j, '-')) )
        j= str2num( j(1:(findstr(j, '-')-1)) );
        x= x( :,1:j);
    end
    k =gcf;
    close(k);
end

y = x;
n = length(y(1,:));

% 2 - Load [kN] to stress [MPa].
y(2,:) = x(2,:);
if ( cF < 1 & cF >0)
    i = Aver;
    while (i+ Aver) < length( y(2,:) -1 ),
        i=i+1;
        y(2,i) = mean( y(2, (i-Aver):(i+Aver) ) );
    end
end
y(2,:) =   y(2,:)  / 12stress;

if y(2,1)<=0
    i=1;
    disp('Interpolation')
    while y(2,i)<=0
        i=i+1;
    end
    y=y(:,(i-1):length(y(2,:)));
```

```
64      y(:,1) = - (y(:,1) - y(:,2)) / (y(2,1) - y(2,2))* y(2,2)+  y(:,2);  ...
            %Check this
65  else
66      disp('Extrapolation')
67      if y(2,1)>y(2,2)
68          disp('Not possible to extrapolate. Please trim Load Channel ...
                again;')
69          finish;
70      else
71          try
72              i=1;
73              while y(2,i)<=y(2,i+1)
74                  i=i+1;
75              end
76          catch
77              disp('Error in the extrapolation procedure of first cycle');
78              disp(' Presence of Monotonous Load function equals no cyclic ...
                    testing.');
79              disp(' Extrapolation procedure continues but use results ...
                    with caution.');
80              i = length(y(2,:));
81          end
82          ans = y(:,1) - (y(:,i) - y(:,1)) * y(2,1)/ (y(2,i) - y(2,1));
83          y= [ans, y];
84      end
85  end
86
87  % Reset the time
88  y(1,:) = y(1,:)- y(1,1);
89
90  % Converstion of Longitudinal Displacement to strain and filtering
91  y(4,:) = ( y(4,:) - y(4,1) ) /d2s(1);
92  y(4,:) = filtfilt(b,a,y(4,:));
93
94  y(6+NTC,:) = ( y(6+NTC,:) - y(6+NTC,1) ) /d2s(2);
95  y(6+NTC,:) = -filtfilt(b,a,y(6+NTC,:));
96
97  % 3 - useless channel (for biaxial loads) - Replaced by Tangential ...
        strain Rates
98  y(3,1)=(y(4,2)-y(4,1))/y(1,2);
99  n = length(y(3,:));
100 y(3,n)=(y(4,n)- y(4,n-1))/(y(1,n) - y(1,n-1));
101 for i = 2:n-1,
102     y(3,i) = abs((y(4,i+1) - y(4,i-1))/(y(1,i+1) - y(1,i-1)));
103 end
104
105
```

```
106
107 %-------------------------------------------------------------------
108 % Plot Stress vs. Strain results
109 clf;
110 subplot(2,1,1);
111 plot(y(4,:),y(2,:),y(6+NTC,:),y(2,:));
112 xlabel('Strain'); ylabel('Stress');
113 subplot(2,1,2);
114 plot(y(1,:),y(3,:));
115 xlabel('Time [sec]'); ylabel('Strain Rate');
116 pause;
```

C.1.4.4 Conversion Instron Data To Neutral Format Function

```
1  function x=Ins2Calc(y, NTC);
2  % Converts a 4 row matrix to a matrix suitable for the calculation.
3  % Arguments are Ins2Calc(y, NTC)
4  %       y:      a 4 row matrix
5  %           y(1) observation
6  %           y(2) Longitudinal displacement
7  %           y(3) Load
8  %           y(4) Transverse displacement
9  %       NTC:    is the number of transverse channels [integer]
10 %
11 %       DAR:    Data Acquisition Rate [obs/sec];
12
13 i = size(y);
14 if i(1)==4
15     x=y(1,:);
16     x(2,:)=y(3,:);
17     x(3,:)=zeros(1,length(y(3,:)));
18     x(4,:)=y(2,:);
19     x(5:(5+NTC),:)=zeros(NTC+1,length(y(3,:)));
20     x(6+NTC,:)=y(4,:);
21 else
22     disp('The input matrix is not valid for Ins2Calc');
23 end
```

C.2 Statistical Processing - R

R is an integrated suite of software facilities for data manipulation, calculation and graphical display. Among other things it has

- an effective data handling and storage facility;
- a suite of operators for calculations on arrays, in particular matrices,
- a large, coherent, integrated collection of intermediate tools for data analysis,
- graphical facilities for data analysis and display either directly at the computer or on hard-copy, and
- a well developed, simple and effective programming language which includes conditionals, loops, user defined recursive functions and input and output facilities. (Indeed most of the system supplied functions are themselves written in the S language.)

Sample scripts will be provided for each of the different laminates, because of the length of the scripts. All the scripts have a similar basic structure and differ only in minor cosmetic changes mainly in the output.

C.2.1 Listing For Generic Functions

```
1  options(digits=5)  #increase accuracy
2  RawD<-read.csv('UD0.csv')  # Read file.
3
4  RawD$CR<- factor(RawD$CR)   # Convert numbers to factors for a candlestick
       bar
5  RawD$FailType<- factor(RawD$FailType)   # Convert FailType to Factor
6  # Colume     1   2   3       4      5      6       7      8      9       10   11
7  #Names       No  CR  E11   eps11   s11    v12     e22    SR     X  FailType  X
8
9  # ------------------------------------CLEARING
       ------------------------------------------------
10 #Clear from slipped and failed specimens.
11 CI <- ( RawD$FailType =="Cat" | RawD$FailType == "Premature") & (!is.na(
       RawD$SR) & !is.na(RawD$FailType =="Cat" | RawD$FailType == "Premature")
       ) # Creates index Vector
12 RawD <- RawD[CI,]
```

```
13
14 RD.bak  <- RawD
15 # Transformations
16 RawD$SR <- log10(RawD$SR)
17
18 #------------------------ Equality of Means-------------------------------
19 t0.func <- function(CR1,CR2,alpha=.05, Property="E11", Dataset = "RawD"){
20     x1 <- eval(parse(text= paste("mean(",Dataset,"$",Property,"[",Dataset,
          "$CR==",CR1,"])",sep="" ) ))
21     x2 <- eval(parse(text= paste("mean(",Dataset,"$",Property,"[",Dataset,
          "$CR==",CR2,"])",sep="" ) ))
22     s1 <- eval(parse(text= paste("sd(",Dataset,"$",Property,"[",Dataset,"$
          CR==",CR1,"])",sep="" ) ))
23     s2 <- eval(parse(text= paste("sd(",Dataset,"$",Property,"[",Dataset,"$
          CR==",CR2,"])",sep="" ) ))
24     n1 <- eval(parse(text= paste("length(",Dataset,"$",Property,"[",
          Dataset,"$CR==",CR1,"])",sep="" ) ))
25     n2 <- eval(parse(text= paste("length(",Dataset,"$",Property,"[",
          Dataset,"$CR==",CR2,"])",sep="" ) ))
26     nu  <- as.integer( ( (s1^2)/n1 + (s2^2)/n2 )^2/( ( (s1^2)/n1 )^2 /(n1
          +1) + ( (s2^2)/n2 )^2 /(n2+1)  ) )-2
27     tper <- qt( (1-alpha) , df = nu)
28     t0  <- abs(x1-x2)/sqrt(((s1^2)/n1) + ((s2^2)/n2))
29     t0.level <- pt(t0, df=nu )
30 # Print out statistics.
31     cat("Degrees of freedom", nu,"\n")
32     cat("t(alpha =",alpha,", df =",nu,") =", tper, ".\n")
33     cat("The statistic t0 =", t0, ".\n")
34     t0.values <- c(t0= t0, alpha=round(alpha,digits=2), df1=round(nu), ta=
          round(tper,digits=3), Level= round(t0.level,digits=3))
35     if(tper<t0) cat("*****The Null hypothesis IS rejected.\n")
36     if(tper>t0) cat("*****The Null hypothesis is NOT rejected.\n")
37     cat("The critical probability is :", 1-t0.level, ".\n\n")
38     return(t0.values)
39 }
40
41                                          # Sources Equality of Means
42 t0.src <- function(CR1, alpha=.05, Property="E11", Dataset = "RawD", SRC1=
       "VE", SRC2="Ins"){
43     x1 <- eval(parse(text= paste("mean(",Dataset,"$",Property,"[",Dataset,
          "$CR==",CR1,"& ",Dataset,"$Source=='",SRC1,"'])",sep="" ) ))
44     x2 <- eval(parse(text= paste("mean(",Dataset,"$",Property,"[",Dataset,
          "$CR==",CR1,"& ",Dataset,"$Source=='",SRC2,"'])",sep="" ) ))
45     s1 <- eval(parse(text= paste("sd(",Dataset,"$",Property,"[",Dataset,"$
          CR==",CR1,"& ",Dataset,"$Source=='",SRC1,"'])",sep="" ) ))
46     s2 <- eval(parse(text= paste("sd(",Dataset,"$",Property,"[",Dataset,"$
          CR==",CR1,"& ",Dataset,"$Source=='",SRC2,"'])",sep="" ) ))
```

```
47      n1 <- eval(parse(text= paste("length(",Dataset,"$",Property,"[",
            Dataset,"$CR==",CR1,"&",Dataset,"$Source=='",SRC1,"']",sep="" )
            ))
48      n2 <- eval(parse(text= paste("length(",Dataset,"$",Property,"[",
            Dataset,"$CR==",CR1,"&",Dataset,"$Source=='",SRC2,"']",sep="" )
            ))
49      nu  <- as.integer( ( (s1^2)/n1 + (s2^2)/n2 )^2/( ( (s1^2)/n1 )^2 /(n1
            +1) + ( (s2^2)/n2 )^2 /(n2+1)  ) )-2
50      tper <- qt( (1-alpha) , df = nu)
51      t0  <- abs(x1-x2)/sqrt(((s1^2)/n1) + ((s2^2)/n2))
52      t0.level <- pt(t0, df=nu )
53      # Print out statistics.
54      cat("Degrees of freedom", nu,"\n")
55      cat("t(alpha =",alpha,", df =",nu,") =", tper, ".\n")
56      cat("The statistic t0 =", t0, ".\n")
57      # Returned value
58      t0.values <- c(t0= t0,
59                     alpha=round(alpha,digits=2),
60                     df1=round(nu),
61                     ta=round(tper,digits=3),
62                     Level= round(t0.level,digits=3))
63      if(tper<t0) cat("*****The Null hypothesis IS rejected.\n")
64      if(tper>t0) cat("*****The Null hypothesis is NOT rejected.\n")
65      cat("The critical probability is :", 1-t0.level, ".\n\n")
66      return(t0.values)
67  }
68
69                                                  #    Equality of Variances
70  Var.f <- function(CR1,CR2,alpha=.05, Property="E11", Dataset = "RawD"){
71      s1 <- eval(parse(text= paste("sd(",Dataset,"$",Property,"[",Dataset,"$
            CR==",CR1,"])",sep="" ) ))
72      s2 <- eval(parse(text= paste("sd(",Dataset,"$",Property,"[",Dataset,"$
            CR==",CR2,"])",sep="" ) ))
73      n1 <- eval(parse(text= paste("length(",Dataset,"$",Property,"[",
            Dataset,"$CR==",CR1,"])",sep="" ) ))
74      n2 <- eval(parse(text= paste("length(",Dataset,"$",Property,"[",
            Dataset,"$CR==",CR2,"])",sep="" ) ))
75      if(s1>s2) {
76          F0 <- s1^2/s2^2
77          Fper <- qf( (1-alpha), n1-1, n2-1)
78          F0.level <- pf(F0, n1-1, n2-1 )
79          cat("F(alpha =",1-alpha,", df1 =",n1-1 ,", df2 =", n2-1,") =",
                Fper, ".\n")
80          F0.values <- c(F0= F0, alpha=alpha, df1=n1, df2=n2, Fa=Fper, Level
                = F0.level)
81      } else {
82          F0 <- s2^2/s1^2
```

```
83          Fper <- qf( (1-alpha) , n2-1, n1-1)
84          F0.level <- pf(F0, n2-1, n1-1 )
85          cat("F(alpha=",1-alpha ,",df1=",n2-1 ,",df2=", n1-1,")=",
                Fper , ".\n")
86          F0.values <- c(F0= F0, alpha=alpha , df1=n2, df2=n1, Fa=Fper , Level
                = F0.level)
87          }
88      # Print out statistics.
89      cat("The statistic F0=" , F0, ".\n")
90      if(Fper<F0) cat("*****The Null hypothesis IS rejected.\n")
91      if(Fper>F0) cat("*****The Null hypothesis is NOT rejected.\n")
92      cat("The critical probability is :", 1-F0.level , ".\n")
93      return(F0.values)
94  }
95
96
97                                                  #     Equality of Variances
98
99  Var.src <- function(CR1, alpha=.05, Property="E11" , Dataset = "RawD" , SRC1
        ="VE" , SRC2="Ins"){
100     cat("Equality of variances for the different sources at" ,CR1,"CDR.\n"
            )
101     s1 <- eval(parse(text= paste("sd(" ,Dataset ,"$" ,Property ,"[" ,Dataset ,"$
            CR==" ,CR1," &" ,Dataset ,"$Source==" ,SRC1," ])" ,sep="" ) ))
102     s2 <- eval(parse(text= paste("sd(" ,Dataset ,"$" ,Property ,"[" ,Dataset ,"$
            CR==" ,CR1," &" ,Dataset ,"$Source==" ,SRC2," ])" ,sep="" ) ))
103     n1 <- eval(parse(text= paste("length(" ,Dataset ,"$" ,Property ,"[",
            Dataset ,"$CR==" ,CR1," &" ,Dataset ,"$Source==" ,SRC1," ])" ,sep="" )
            ))
104     n2 <- eval(parse(text= paste("length(" ,Dataset ,"$" ,Property ,"[",
            Dataset ,"$CR==" ,CR1," &" ,Dataset ,"$Source==" ,SRC2," ])" ,sep="" )
            ))
105     if(s1>s2) {
106         F0 <- s1^2/s2^2
107         Fper <- qf( (1-alpha) , n1-1, n2-1)
108         F0.level <- pf(F0, n1-1, n2-1 )
109         cat("F(alpha=",1-alpha ,",df1=",n1-1 ,",df2=", n2-1,")=",
                Fper , ".\n")
110         F0.values <- c(F0= F0, alpha=alpha , df1=n1, df2=n2, Fa=Fper , Level
                = F0.level)
111     } else {
112         F0 <- s2^2/s1^2
113         Fper <- qf( (1-alpha) , n2-1, n1-1)
114         F0.level <- pf(F0, n2-1, n1-1 )
115         cat("F(alpha=",1-alpha ,",df1=",n2-1 ,",df2=", n1-1,")=",
                Fper , ".\n")
```

```
116         F0.values <- c(F0= F0, alpha=alpha, df1=n2, df2=n1, Fa=Fper, Level
                = F0.level)
117         }
118     # Print out statistics.
119     cat("The statistic F0*=", F0, ".\n")
120     if(Fper<F0) cat("*****The Null hypothesis IS rejected.\n")
121     if(Fper>F0) cat("*****The Null hypothesis is NOT rejected.\n")
122     cat("The critical probability is :", 1-F0.level, ".\n\n")
123     return(F0.values)
124 }
125
126
127
128 #------------------------------------ Goodness of Fit
        ------------------------------
129 chi2.Prop <- function(CR1, alpha=.05, cl=6, Property="E11", Dataset="RawD"
        ){
130     chi2.crit <- qchisq(1-alpha, cl -3, ncp=0, log = FALSE)    #Chi
            Squared
131     if(!CR1==0) {
132         cat("CR1<>0")
133         # Observed frequencies
134         X1<- eval(parse(text= paste("hist(",Dataset,"$",Property,"[",
                Dataset,"$CR==",CR1,
135             "], breaks=qnorm(c(10^-6,1:(cl-1)/cl,1-10^-6), mean(",
                    Dataset,"$",Property,"[",Dataset,"$CR==",CR1,
136             "])), sd(",Dataset,"$",Property,"[",Dataset,"$CR==",CR1,"]))))$
                    count", sep="" )))
137     } else {
138         cat("CR1=0\n")
139         # Observed frequencies
140         X1<- eval(parse(text= paste("hist(",Dataset,"$",Property,
141             ", breaks=qnorm(c(10^-6,1:(cl-1)/cl,1-10^-6), mean(",Dataset
                    ,"$",Property,
142             "), sd(",Dataset,"$",Property,")))$count", sep="" )))
143     }
144     Est.freq <- 1/cl *sum(X1)
145     chi2.stat <- sum( (X1 - Est.freq)^2/Est.freq )
146     chi2.level <- pchisq(chi2.stat, cl -3, ncp=0, log = FALSE)    #Chi
            Squared
147     cat("chi-squared value for alpha=",alpha," and df=", cl-3," is :",chi2
            .crit, "\n")
148     cat("The sum of chi-squared statistic is :  ",chi2.stat, "\n")
149     if(chi2.stat<chi2.crit) cat("There is NO reason to believe that the
            output is not normally distributed\n")
150     if(chi2.stat>chi2.crit) cat("There IS reason to believe that the
            output is not normally distributed\n")
```

```
151     chi2.values <- c(chi20= chi2.stat, alpha=alpha, df=cl, chi2.crit=chi2.
            crit, Level= chi2.level)
152     return(chi2.values)
153 }
```

C.2.2 Listing For Young Modulus Obtained From $[0\circ]_4$ Laminate

```
1  rm(list=ls())
2  source('D:/current/Program/R/Ud0/Ud0-gen.R')
3  Src.const  <- "VE"
4  # ------------------------------ Young's Modulus E
       [11]------------------------
5  CI <- !is.na(RawD$E11) & RawD$E11 >0 & RawD$E11 <80
6  RawD <- RawD[CI,]
7  xcut  <- c(min(RawD$SR), max(RawD$SR))
8  ycut  <- max(RawD$E11 )
9  # Co Plot with respect to Source
10 win.graph(width = 7, height = 3.5,pointsize=10)
11 coplot(RawD$E11~RawD$SR|RawD$Source, data=RawD,
12     xlab=c(expression(paste("Strain Rate log [mi",n^{-1},"]")), "Given:
           Source")),
13     ylab = expression(paste(E[11],"[GPa]")), ylim=c(0,ycut),
14     pch=as.integer(RawD$CR), col=as.integer(RawD$CR))
15 CI <- RawD$Source == Src.const
16 RawAll <- RawD
17 RawVE <- RawD[CI,]
18 RawIns <- RawD[!CI,]
19 # Plot vs. Sustained Strain Rate
20 for (counter in c("All","VE", "Ins")) {
21     RawD <- eval(parse(text=paste("Raw",counter, sep="")))
22     cat("Calculations for", counter, ".\n")
23     win.graph(width = 7, height = 3.5,pointsize=10)
24     plot(RawD$SR,RawD$E11, main=paste("Modulus vs. Strain Rate(", counter
           ,").", sep=""),
25          xlab=expression(paste("Strain Rate log [mi",n^{-1},"]")),
26          ylab = "Young's modulus[GPa]", ylim=c(0,ycut),
27          pch=as.integer(RawD$CR), col=as.integer(RawD$CR))
28     legend(xcut[1], ycut, c("5[mm/min]", "50[mm/min]", "500[mm/min]"),
29          pch=as.integer(labels(RawD$CR)), col=as.integer(labels(RawD$Source
               )))
30     legend(mean(xcut), ycut, c("Linear","Quadratic"),lty=1:2, col=1:2)
31
32     wrong <- identify( RawD$SR,RawD$E11,labels=RawD$ID)
33     CI <- rep(TRUE, length(RawD$CR))
34     CI[wrong] <- c(FALSE)
35     RD.bak  <- RawD
```

```
36  RawD <- RawD[CI,]
37
38  # model Fitting
39  SR.ord_order(RawD$SR)   #vector with ascending order of the Strain
        rate
40  E11.lm <- lm(E11~RawD$SR, data=RawD)
41  E11.lm2 <- lm(E11~RawD$SR+ I((RawD$SR)^2), data=RawD)
42  E11.hat2 <- predict(E11.lm2)
43  lines(RawD$SR[SR.ord], E11.hat2[SR.ord], lty=2, col=2)
44  abline(lsfit(RawD$SR, RawD$E11), lty=1, col=1)
45  eval(parse(text=paste("rm(RD.stats.E11.",counter,")", sep="")))
46  eval(parse(text=paste("RD.stats.E11.",counter,"<-list(CR=c
        (5,50,500),",
47            "ave=c(mean(RawD$E11[RawD$CR==5]),mean(RawD$E11[RawD$CR
                ==50],na.rm=TRUE),",
48                  "mean(RawD$E11[RawD$CR==500],na.rm=TRUE)),",
49            "sd=c(sd(RawD$E11[RawD$CR==5]),sd(RawD$E11[RawD$CR==50]),sd
                (RawD$E11[RawD$CR==500]))", sep="")))
50  eval(parse(text=paste("RD.stats.E11.",counter, "$CV","<-",
51      "RD.stats.E11.",counter, "$sd/RD.stats.E11.",counter, "$ave",sep="
            ")))
52
53  RD.stats.E11 <-  eval(parse(text=paste("RD.stats.E11.",counter,sep="")
        ))
54      # EQUALITY OF MEANS
55  t1 <- list(f1 =as.vector(t0.func(5,50,alpha=.05, Property="E11")),
56          f2 = as.vector(t0.func(50,500,alpha=.05, Property="E11")),
57          f3 =as.vector(t0.func(5,500,alpha=.05, Property="E11")) )
58
59      # EQUALITY OF Variances
60  f1 <- list(f1 =as.vector(Var.f(5,50,alpha=.05, Property="E11")),
61          f2= as.vector(Var.f(50,500,alpha=.05, Property="E11")),
62          f3 =as.vector(Var.f(5,500,alpha=.05, Property="E11")) )
63
64  win.graph(width = 7, height = 3.5,pointsize=10)
65  ypdf <- c(0,max(c(density(RawD$E11[RawD$CR==5])$y,
66          density(RawD$E11[RawD$CR==50])$y,
67          density(RawD$E11[RawD$CR==500])$y)))
68  par(mfrow=c(1,1))
69  plot(density(RawD$E11),
70      main=paste("a)Complete data set(",counter,").", sep=""),
71      xlab=expression(paste( E[11])),
72      ylab="Probability density",
73      xlim=c(0,1.5*ycut), ylim=ypdf)
74
75  win.graph(width = 6, height = 3,pointsize=12)
76  par(mfrow=c(1,3))
```

```
77      plot(density(RawD$E11[RawD$CR==5]),
78           xlab=expression(paste(E[11])),
79           ylab="Probability density",
80           main=paste("b) 5[mm/min] (", counter,").", sep=""),
81           xlim=c(0,1.5*ycut), ylim=ypdf)
82      plot(density(RawD$E11[RawD$CR==50]),
83           xlab=expression(paste(E[11])),
84           ylab="Probability density",
85           main=paste("c) 50[mm/min] (", counter,").", sep=""),
86           xlim=c(0,1.5*ycut), ylim=ypdf)
87      plot(density(RawD$E11[RawD$CR==500]),
88           xlab=expression(paste(E[11])),
89           ylab="Probability density",
90           main=paste("d) 500[mm/min] (", counter,").", sep=""),
91           xlim=c(0,1.5*ycut), ylim=ypdf)
92
93      # GOODNESS OF FIT
94      win.graph(width = 7, height = 3.5,pointsize=10)
95      chi2.Prop(0,alpha=.01,cl=9,Property="E11", Dataset="RawD")
96      chi2.Prop(5,alpha=.05,cl=4,Property="E11", Dataset="RawD")
97      chi2.Prop(50,alpha=.05,cl=4,Property="E11",Dataset="RawD")
98      chi2.Prop(500,alpha=.05,cl=4,Property="E11",Dataset="RawD")
99      chi2.E11 <-  list(chi0 =as.vector(chi2.Prop(0,alpha=.05,cl=6,Property=
          "E11", Dataset="RawD")),
100                chi1=as.vector(chi2.Prop(5,alpha=.05,cl=6,Property="E11",
                     Dataset="RawD")),
101                chi2=as.vector(chi2.Prop(50,alpha=.05,cl=6,Property="E11",
                     Dataset="RawD")),
102                chi3=as.vector(chi2.Prop(500,alpha=.05,cl=6,Property="E11"
                     ,Dataset="RawD")) )
103
104     #ANOVA of the two different models
105     anova(E11.lm, E11.lm2)
106     anova(E11.lm2, E11.lm)
107
108     #---------------------  OUTPUT  ------------------------------
109     outfile <- paste("UD0_E11_",counter,".txt",sep="")
110     cat("          Tensile Modulus
          \n", file=outfile)
111     cat("                                                                \
          n", file=outfile, append = TRUE)
112     cat("Crosshead Rate\t\t", RD.stats.E11[[1]] ,"\\\\ \n" , file=outfile
          , sep="&\t",append = TRUE)
113     cat("Mean\t\t\t", format(RD.stats.E11[[2]] , digits=3,nsmall=2),"
          \\\\ \n" , file=outfile, sep="&\t",append = TRUE)
114     cat("Standard Deviation\t", format(RD.stats.E11[[3]] , digits=3,nsmall
          =2),"\\\\ \n" , file=outfile, sep="&\t",append = TRUE)
```

```
115  cat("Coef. of Variance\t\t", format(RD.stats.E11$sd/RD.stats.E11$ave
         , digits=3,nsmall=2),"\\\\ \n" , file=outfile , sep="&\t",append
         = TRUE)
116  cat("----------------------------------------------------------\
         n", file=outfile , append = TRUE)
117  cat("---------Coefficients Mean testing---------\n",
         file=outfile , append = TRUE)
118  cat("Crosshead Rate&\t $t_0$&\t $\\alpha$ \t&df &\t $t_{crit}$
         \t&\t Level\\\\ \n" , file=outfile , append = TRUE)
119  cat("5 vs. 50\t", format(t1[[1]] , digits=3,nsmall=2),"\\\\ \n" , file
         =outfile , sep="&\t",append = TRUE)
120  cat("50 vs. 500\t", format(t1[[2]] , digits=3,nsmall=2),"\\\\ \n" ,
         file=outfile , sep="&\t",append = TRUE)
121  cat("5 vs. 500\t", format(t1[[3]] , digits=3,nsmall=2),"\\\\ \n" ,
         file=outfile , sep="&\t",append = TRUE)
122  cat("---------Coefficients Variance testing---------\n"
         , file=outfile , append = TRUE)
123  cat("Crosshead Rate&\t $F_0$&\t $\\alpha$ \t&df1 \t&df1 &\t F_
         {crit}&\t Level\\\\ \n" , file=outfile , append = TRUE)
124  cat("5 vs. 50\t", format(f1[[1]] , digits=3,nsmall=2),"\\\\ \n" , file
         =outfile , sep="&\t",append = TRUE)
125  cat("50 vs. 500\t", format(f1[[2]] , digits=3,nsmall=2),"\\\\ \n" ,
         file=outfile , sep="&\t",append = TRUE)
126  cat("5 vs. 500\t", format(f1[[3]] , digits=3,nsmall=2),"\\\\ \n" ,
         file=outfile , sep="&\t",append = TRUE)
127  cat("---------Normality Check---------\n", file=outfile
         , append = TRUE)
128  cat("Crosshead Rate\t&$\\chi^2_0$&$\\alpha$&df\t&$\\chi^2_{
         crit}&Level\\\\ \n" , file=outfile , sep="", append = TRUE)
129  cat("ALL\t\t\t", format(chi2.E11[[1]] , digits=3,nsmall=2),"\\\\ \n"
         , file=outfile , sep="&\t",append = TRUE)
130  cat("5\t\t\t", format(chi2.E11[[2]] , digits=3,nsmall=2),"\\\\ \n" ,
         file=outfile , sep="&\t",append = TRUE)
131  cat("50\t\t\t", format(chi2.E11[[3]] , digits=3,nsmall=2),"\\\\ \n" ,
         file=outfile , sep="&\t",append = TRUE)
132  cat("500\t\t\t", format(chi2.E11[[4]] , digits=3,nsmall=2),"\\\\ \n"
         , file=outfile , sep="&\t",append = TRUE)
133  cat("----------------------------------------------------------\
         n", file=outfile , append = TRUE)
134  cat("---------Coefficients of Material Models---------\
         n", file=outfile , append = TRUE)
135  cat("Model\t\t&Intercept&\t log(SR)&\t log^2(SR) \t&$R^2$ \n",
         file=outfile , append = TRUE)
136  cat("MC.lm1\t",format(E11.lm$coe , digits=3,nsmall=2)," ", format
         (summary(E11.lm)[8], digits=3),"\\\\ \n", file=outfile , sep=" +\t",
         append = TRUE)
```

```
137     cat("MC.lm2\t",format(E11.lm2$coe ,digits=3,nsmall=2), format(summary(
            E11.lm2)[8],digits=3),"\\\\ \n" , file=outfile, sep="+\t", append
            = TRUE)
138     cat("---------ANOVA----------\n", file=outfile, append
            = TRUE)
139     cat(names(anova(E11.lm, E11.lm2)),"\\\\ \n" , file=outfile, sep="&\t
            ",append = TRUE)
140     write.table(format(anova(E11.lm, E11.lm2), digits=3,nsmall=2), file =
            outfile,
141                 quote=FALSE, sep = "&", append =TRUE, col.names = FALSE)
142 }
143
144 RawD <- RawAll
145
146 t1.src <- list(f5 =as.vector(t0.src(5,alpha=.05, Property="E11")),
147          f50 = as.vector(t0.src(50,  alpha=.05, Property="E11")),
148          f500 = as.vector(t0.src(500, alpha=.05, Property="E11")) )
149
150 f1.src <- list(f1 =as.vector(Var.src(5,alpha=.05, Property="E11")),
151              f2= as.vector(Var.src(50,alpha=.05, Property="E11")),
152              f3 =as.vector(Var.src(500,alpha=.05, Property="E11")) )
153
154 outfile <- "UD0_E11_Src.txt"
155 cat("------Comparison of Source for Tensile Modulus-------\n" ,
        file=outfile)
156 cat("-----------------------------------------------------------------\n",
        file=outfile, append = TRUE)
157 cat("---------Coefficients Mean testing---------\n", file=
        outfile, append = TRUE)
158 cat("VE vs. Ins &\t $t_0$ &\t $\\alpha$ \t & df &\t $t_{crit}$ \t &\t
        Level\\\\ \n" , file=outfile, append = TRUE)
159 cat("5\t", format(t1.src[[1]] , digits=3,nsmall=2),"\\\\ \n" , file=
        outfile, sep="&\t",append = TRUE)
160 cat("50\t", format(t1.src[[2]] , digits=3,nsmall=2),"\\\\ \n" , file=
        outfile, sep="&\t",append = TRUE)
161 cat("500\t", format(t1.src[[3]] , digits=3,nsmall=2),"\\\\ \n" , file=
        outfile, sep="&\t",append = TRUE)
162 cat("---------Coefficients Mean testing---------\n", file=
        outfile, append = TRUE)
163 cat("VE vs. Ins &\t $t_0$ &\t $\\alpha$ \t & df &\t $t_{crit}$ \t &\t
        Level\\\\ \n" , file=outfile, append = TRUE)
164 cat("5\t", format(f1.src[[1]] , digits=3,nsmall=2),"\\\\ \n" , file=
        outfile, sep="&\t",append = TRUE)
165 cat("50\t", format(f1.src[[2]] , digits=3,nsmall=2),"\\\\ \n" , file=
        outfile, sep="&\t",append = TRUE)
166 cat("500\t", format(f1.src[[3]] , digits=3,nsmall=2),"\\\\ \n" , file=
        outfile, sep="&\t",append = TRUE)
```

C.2.3 Listing For Shear Strength Obtained From $[\pm 45o]_{2s}$ Laminate

```
rm(list=ls())
source('D:/current/Program/R/PM45/PM45-gen.R')
Src.const <- "All"
# ------------------------------ Shear Failure strain tau [12]----------------------------------------
RawD$t12 <- 1000*RawD$t12
CI <- !is.na(RawD$t12) & RawD$t12 >0
RawD <- RawD[CI,]

xcut  <- c(min(RawD$SR12), max(RawD$SR12))
ycut <- max(RawD$t12)
# Co Plot with respect to Source
win.graph(width = 7, height = 3.5, pointsize=10)
coplot(RawD$t12~RawD$SR12|RawD$FailLoc *RawD$Source , data=RawD,
    xlab= c(expression(paste("Strain Rate log [mi",n^{-1},"]")), "Given : Failure Location"),
    ylab = c("Shear stress at failure", "Given : DA Source"),
#     ylim=c(0,max(RawD$G12)) ,
    pch=as.integer(RawD$CR), col=as.integer(RawD$CR))

# Plot vs. Sustained Shear Strain rate
win.graph(width = 7, height = 3.5, pointsize=10)
plot(RawD$SR12,RawD$t12, main="Shear Failure Stress vs. Shear Strain rate",
    xlab=expression(paste("Shear Strain rate log [mi",n^{-1},"]")),
    ylab = "Shear Failure Stress [MPa]", ylim=c(0,max(RawD$t12)),
    pch=as.integer(RawD$CR), col=as.integer(RawD$CR))
legend(xcut[1], ycut/2, c("5[mm/min]", "50[mm/min]", "500[mm/min]"),
        pch=as.integer(labels(RawD$CR)),col=as.integer(labels(RawD$Source))
        )
legend(mean(xcut), ycut/2 , c("Linear", "Quadratic"), lty=1:2, col=1:2)

wrong <- identify( RawD$SR12,RawD$t12,labels=RawD$ID)
CI <- rep(TRUE, length(RawD$CR))
CI[wrong] <- c(FALSE)
GMT.bak  <- RawD
RawD <- RawD[CI,]

SR12.ord_order(RawD$SR)
t12.lm <- lm(t12~RawD$SR12, data=RawD)
t12.lm2 <- lm(t12~RawD$SR+ I((RawD$SR)^2), data=RawD)
t12.hat2 <- predict(t12.lm2)
lines(RawD$SR[SR12.ord], t12.hat2[SR12.ord], lty=2, col=2)
abline(lsfit(RawD$SR12, RawD$t12), lty=1,col=1)

```

```
win.graph(width = 7, height = 3.5,pointsize=10)
coplot(RawD$t12~RawD$SR12|RawD$FailLoc , data=RawD,
    xlab= c(expression(paste("Strain Rate log [mi",n^{-1},"]")) , "Given : Failure location"),
    ylab = "Shear stress at failure" , ylim=c(0,max(RawD$t12)),
    pch=as.integer(RawD$CR) , col=as.integer(RawD$CR))


#---------------------  STATISTICS CALCS  ----------------------------
rm(GMT.stats.t12)
GMT.stats.t12 <-  list( CR = c(5, 50, 500),
              ave = c(mean(RawD$t12[RawD$CR==5]) , mean(RawD$t12[RawD$CR
                  ==50],na.rm=TRUE) ,
                        mean(RawD$t12[RawD$CR==500],na.rm=TRUE) ) ,
              sd= c(sd(RawD$t12[RawD$CR==5]) , sd(RawD$t12[RawD$CR==50]) , sd(
                  RawD$t12[RawD$CR==500]) ) )
GMT.stats.t12$CV <- GMT.stats.t12$sd/GMT.stats.t12$ave
# EQUALITY OF MEANS
t0.func(5,50,alpha=.05, Property="t12")
t0.func(50,500,alpha=.05, Property="t12")
t0.func(5,500,alpha=.05, Property="t12")
t1 <- list(f1 =as.vector(t0.func(5,50,alpha=.05, Property="t12")),
        f2= as.vector(t0.func(50,500,alpha=.05, Property="t12"))
         ,f3 =as.vector(t0.func(5,500,alpha=.05, Property="t12")) )

# EQUALITY OF Variances
Var.f(5,50,alpha=.05, Property="t12")
Var.f(50,500,alpha=.05, Property="t12")
Var.f(5,500,alpha=.05, Property="t12")
f1 <- list(f1 =as.vector(Var.f(5,50,alpha=.05, Property="t12")),
        f2= as.vector(Var.f(50,500,alpha=.05, Property="t12"))
         ,f3 =as.vector(Var.f(5,500,alpha=.05, Property="t12")) )


win.graph(width = 7, height = 3.5,pointsize=10)
xpdf <- c(0,1.5*max(RawD$t12))
ypdf <- c(0,max(c(density(RawD$t12[RawD$CR==5])$y,
    density(RawD$t12[RawD$CR==50])$y, density(RawD$t12[RawD$CR==500])$y)))
par(mfrow=c(1,1))
plot(density(RawD$t12),
    main=" a) Complete data set",
    xlab=expression(tau[12]),
    ylab="Probability density",
    xlim=xpdf, ylim=ypdf)

win.graph(width = 6, height = 3,pointsize=12)
par(mfrow=c(1,3))
```

```
plot(density(RawD$t12[RawD$CR==5]),
     xlab=expression(tau[12]),
     ylab="Probability density",
     main="b) 5[mm/min]",
     xlim=xpdf, ylim=ypdf)
plot(density(RawD$t12[RawD$CR==50]),
     xlab=expression(tau[12]),
     ylab="Probability density",
     main="c) 50[mm/min]",
     xlim=xpdf, ylim=ypdf)
plot(density(RawD$t12[RawD$CR==500]),
     xlab=expression(tau[12]),
     ylab="Probability density",
     main="d) 500[mm/min]",
     xlim=xpdf, ylim=ypdf)

# GOODNESS OF FIT
win.graph(width = 7, height = 3.5,pointsize=10)
chi2.Prop(0,alpha=.01,cl=9,Property="t12", Dataset="RawD")
chi2.Prop(5,alpha=.05,cl=4,Property="t12", Dataset="RawD")
chi2.Prop(50,alpha=.05,cl=4,Property="t12",Dataset="RawD")
chi2.Prop(500,alpha=.05,cl=4,Property="t12",Dataset="RawD")
chi2.t12 <-  list(chi0 =as.vector(chi2.Prop(0,alpha=.05,cl=6,Property="t12
    ", Dataset="RawD")),
             chi1=as.vector(chi2.Prop(5,alpha=.05,cl=6,Property="t12",
                 Dataset="RawD")),
             chi2=as.vector(chi2.Prop(50,alpha=.05,cl=6,Property="t12",
                 Dataset="RawD")),
             chi3=as.vector(chi2.Prop(500,alpha=.05,cl=6,Property="t12",
                 Dataset="RawD")) )

#------------------------ OUTPUT ------------------------------
outfile <- "PM45_t12.txt"
cat("                    Shear Failure Stress t12 -------------\
    n", file=outfile)
cat("Using ", Src.const, " data.\n", file=outfile ,append = TRUE)
cat("-------------------------------------------------------\n",
    file=outfile , append = TRUE)
cat("Crosshead Rate\t\t", GMT.stats.t12[[1]] ,"\\\\\n", file=outfile ,
    sep="&\t",append = TRUE)
cat("Mean\t\t\t", format(GMT.stats.t12[[2]] , digits=3,nsmall=2),"\\\\\n"
     , file=outfile , sep="&\t",append = TRUE)
cat("Standard Deviation\t", format(GMT.stats.t12[[3]] , digits=3,nsmall=2)
    ,"\\\\\n" , file=outfile , sep="&\t",append = TRUE)
cat("Coef. of Variance\t\t", format(GMT.stats.t12$sd/GMT.stats.t12$ave ,
    digits=3,nsmall=2),"\\\\\n" , file=outfile , sep="&\t",append = TRUE)
```

```
122 cat("------------------------------------------------------------\n",
    file=outfile, append = TRUE)
123 cat("----------Coefficients Mean testing----------\n", file=
    outfile, append = TRUE)
124 cat("Crosshead Rate &\t $t_0$ &\t $\\alpha$ \t &df &\t $t_{crit}$ \t &
    \t Level\\\\\n" , file=outfile, append = TRUE)
125 cat("5 vs. 50\t", format(t1[[1]] , digits=3,nsmall=2),"\\\\\n" , file=
    outfile, sep="&\t",append = TRUE)
126 cat("50 vs. 500\t", format(t1[[2]] , digits=3,nsmall=2),"\\\\\n" , file=
    outfile, sep="&\t",append = TRUE)
127 cat("5 vs. 500\t", format(t1[[3]] , digits=3,nsmall=2),"\\\\\n" , file=
    outfile, sep="&\t",append = TRUE)
128 cat("----------Coefficients Variance testing----------\n",
    file=outfile, append = TRUE)
129 cat("Crosshead Rate &\t $F_0$ &\t $\\alpha$ \t &df1 \t &df1 &\t F_{
    crit} &\t Level\\\\\n" , file=outfile, append = TRUE)
130 cat("5 vs. 50\t", format(f1[[1]] , digits=3,nsmall=2),"\\\\\n" , file=
    outfile, sep="&\t",append = TRUE)
131 cat("50 vs. 500\t", format(f1[[2]] , digits=3,nsmall=2),"\\\\\n" , file=
    outfile, sep="&\t",append = TRUE)
132 cat("5 vs. 500\t", format(f1[[3]] , digits=3,nsmall=2),"\\\\\n" , file=
    outfile, sep="&\t",append = TRUE)
133 cat("----------Normality Check----------\n", file=outfile,
    append = TRUE)
134 cat("Crosshead Rate \t &$\\chi^2_0$ &$\\alpha$ &df \t &$\\chi^2_{crit
    } &Level\\\\\n" , file=outfile, sep="", append = TRUE)
135 cat("ALL\t\t\t", format(chi2.t12[[1]] , digits=3,nsmall=2),"\\\\\n" ,
    file=outfile, sep="&\t",append = TRUE)
136 cat("5\t\t\t", format(chi2.t12[[2]] , digits=3,nsmall=2),"\\\\\n" , file=
    outfile, sep="&\t",append = TRUE)
137 cat("50\t\t\t", format(chi2.t12[[3]] , digits=3,nsmall=2),"\\\\\n" , file
    =outfile, sep="&\t",append = TRUE)
138 cat("500\t\t\t", format(chi2.t12[[4]] , digits=3,nsmall=2),"\\\\\n" ,
    file=outfile, sep="&\t",append = TRUE)
139 cat("------------------------------------------------------------\n",
    file=outfile, append = TRUE)
140 cat("----------Coefficients of Material Models----------\n",
    file=outfile, append = TRUE)
141 cat("Model\t\t& Intercept &\t log(SR) &\t log^2(SR) \t& $R^2$ \n", file=
    outfile, append = TRUE)
142 cat("MC.lm1\t",format(t12.lm$coe ,digits=3,nsmall=2),"        ", format(
    summary(t12.lm)[8],digits=3),"\\\\\n", file=outfile, sep="+\t",
    append = TRUE)
143 cat("MC.lm2\t",format(t12.lm2$coe ,digits=3,nsmall=2), format(summary(t12.
    lm2)[8],digits=3),"\\\\\n" , file=outfile, sep="+\t", append = TRUE)
144 cat("----------ANOVA----------\n", file=outfile, append =
    TRUE)
```

```
145 cat(names(anova(t12.lm, t12.lm2)),"\\\\\n" , file=outfile, sep=" &\t",
    append = TRUE)
146 write.table(format(anova(t12.lm, t12.lm2), digits=3,nsmall=2), file =
    outfile,
147             quote=FALSE, sep = " &", append =TRUE, col.names = FALSE)
```

C.2.4 Listing For Transverse Strain Obtained From $[+45o]_8$ Laminate

```
 1 rm(list=ls())
 2 source('D:/current/Program/R/P45/P45-gen.R')
 3 Src.const <- "Ins"
 4 CI <- !is.na(RawD$eps22)  & RawD$eps22<.02 & RawD$FailType == "Cat"
 5 RawD <- RawD[CI,]
 6 xcut  <- c(min(RawD$SR22), max(RawD$SR22))
 7 ycut <- max(RawD$eps22)
 8 win.graph(width = 7, height = 3.5,pointsize=10)
 9 coplot(RawD$eps22~RawD$SR22|RawD$FailLoc*RawD$Source, data=RawD,
10     xlab=c(expression(paste("Transverse Strain Rate log [mi",n^{-1},"]")),
           "Given: Failure Location"),
11     ylab =c( expression(paste("Transverse Failure strain ", epsilon[22])),
           "Given: Source"),
12     #ylim=c(0,max(RawD$eps22))
13     pch=as.integer(RawD$CR), col=as.integer(RawD$CR))
14 #  source
15 win.graph(width = 7, height = 3.5,pointsize=10)
16 coplot(RawD$eps22~RawD$SR22|RawD$Source, data=RawD,
17     xlab=c(expression(paste("Transverse Strain Rate log [mi",n^{-1},"]")),
           , "Given: Source"),
18     ylab =expression(paste("Transverse Failure strain ", epsilon[22],"
           [] ")),
19     #ylim=c(0,max(RawD$eps22))
20     pch=as.integer(RawD$CR), col=as.integer(RawD$CR))
21
22 CI <- RawD$Source==Src.const
23 RawD <- RawD[CI,]
24 xcut <- c(min(RawD$SR22), max(RawD$SR22))
25 ycut <- max(RawD$eps22)
26 # Plot vs. Sustained Strain Rate
27 win.graph(width = 7, height = 3.5,pointsize=10)
28 plot(RawD$SR22,RawD$eps22, main="Transverse Failure Strain vs. Strain Rate
   ",
29     xlab=expression(paste("Transverse Strain Rate log [mi",n^{-1},"]")),
30     ylab =expression(paste("Transverse Failure strain ", epsilon[22])),
           ylim=c(0,max(RawD$eps22)),
31     pch=as.integer(RawD$CR), col=as.integer(RawD$CR))        # Plot Young's
           Modulus vs. crosshead speed
```

```
legend(xcut[1], ycut, c("5[mm/min]", "50[mm/min]", "500[mm/min]"),
       pch=as.integer(labels(RawD$CR)),col=as.integer(labels(RawD$CR)))
legend(mean(xcut), ycut, c("Linear", "Quadratic"), lty=1:2, col=1:2)
#------------------------------ TREATMENT OF OUTLIERS
wrong <- identify( RawD$SR22,RawD$eps22,labels=RawD$ID)
CI <- rep(TRUE, length(RawD$CR))
CI[wrong] <- c(FALSE)
GMT.bak  <- RawD
RawD <- RawD[CI,]

# model Fitting
SR22.ord_order(RawD$SR22)    #vector with ascending order of the Strain
    rate
eps22.lm <- lm(eps22~RawD$SR22, data=RawD)
eps22.lm2 <- lm(eps22~RawD$SR22+ I((RawD$SR22)^2), data=RawD)
eps22.hat2 <- predict(eps22.lm2)
lines(RawD$SR22[SR22.ord], eps22.hat2[SR22.ord],lty=2, col=2)
abline(lsfit(RawD$SR22, RawD$eps22), lty=1,col=1)
# Final figure

ycut <- max(RawD$eps22)
xcut  <- c(min(RawD$SR22), max(RawD$SR22))
win.graph(width = 7, height = 3.5,pointsize=10)
plot(RawD$SR22,RawD$eps22, main="Transverse_Failure_Strain_vs._Strain_Rate
    ",
     xlab=expression(paste("Transverse_Strain_Rate_log_[mi",n^{-1},"]")),
     ylab =expression(paste("Transverse_Failure_strain__", epsilon[22])),
         ylim=c(0,max(RawD$eps22)),
     pch=as.integer(RawD$CR), col=as.integer(RawD$CR))          # Plot Young's
         Modulus vs. crosshead speed
legend(xcut[1], ycut, c("5[mm/min]", "50[mm/min]", "500[mm/min]"),
       pch=as.integer(labels(RawD$CR)),col=as.integer(labels(RawD$CR)))
legend(mean(xcut), ycut, c("Linear", "Quadratic"), lty=1:2, col=1:2)
lines(RawD$SR22[SR22.ord], eps22.hat2[SR22.ord],lty=2, col=2)
abline(lsfit(RawD$SR22, RawD$eps22), lty=1,col=1)

#------------------------ STATISTICS CALCS ------------------------------
rm(GMT.stats.eps22)
GMT.stats.eps22 <-   list( CR = c(5, 50, 500),
              ave = c(mean(RawD$eps22[RawD$CR==5]),
                      mean(RawD$eps22[RawD$CR==50],na.rm=TRUE),
                      mean(RawD$eps22[RawD$CR==500],na.rm=TRUE) ),
              sd= c(sd(RawD$eps22[RawD$CR==5]),
                      sd(RawD$eps22[RawD$CR==50]),
                      sd(RawD$eps22[RawD$CR==500]) ))
GMT.stats.eps22$CV <- GMT.stats.eps22$sd/GMT.stats.eps22$ave
# EQUALITY OF MEANS
```

```
t0.func(5,50,alpha=.05, Property="eps22")
t0.func(50,500,alpha=.05, Property="eps22")
t0.func(5,500,alpha=.05, Property="eps22")
t1 <- list(f1 =as.vector(t0.func(5,50,alpha=.05, Property="eps22")),
        f2= as.vector(t0.func(50,500,alpha=.05, Property="eps22"))
         ,f3 =as.vector(t0.func(5,500,alpha=.05, Property="eps22")) )

# EQUALITY OF Variances
Var.f(5,50,alpha=.05, Property="eps22")
Var.f(50,500,alpha=.05, Property="eps22")
Var.f(5,500,alpha=.05, Property="eps22")
f1 <- list(f1 =as.vector(Var.f(5,50,alpha=.05, Property="eps22")),
        f2= as.vector(Var.f(50,500,alpha=.05, Property="eps22"))
         ,f3 =as.vector(Var.f(5,500,alpha=.05, Property="eps22")) )


# Probability density functions of the results.----------PDF plot
win.graph(width = 7, height = 3.5,pointsize=10)
xpdf <- c(0,1.1*max(RawD$eps22))
ypdf <- c(0,max(c(density(RawD$eps22[RawD$CR==5])$y,
    density(RawD$eps22[RawD$CR==50])$y, density(RawD$eps22[RawD$CR==500])$
        y)))

par(mfrow=c(1,1))
plot(density(RawD$eps22),
    main="a) Complete data set",
    xlab=expression(epsilon[22]),
    ylab="Probability density",
    xlim=xpdf, ylim=ypdf)

win.graph(width = 6, height = 3,pointsize=12)
par(mfrow=c(1,3))
plot(density(RawD$eps22[RawD$CR==5]),
    xlab=expression(epsilon[22]),
    ylab="Probability density",
    main="b) 5[mm/min]",
    xlim=xpdf, ylim=ypdf)
plot(density(RawD$eps22[RawD$CR==50]),
    xlab=expression(epsilon[22]),
    ylab="Probability density",
    main="c) 50[mm/min] ",
    xlim=xpdf, ylim=ypdf)
plot(density(RawD$eps22[RawD$CR==500]),
    xlab=expression(epsilon[22]),
    ylab="Probability density",
    main="d) 500[mm/min] ",
    xlim=xpdf, ylim=ypdf)
```

```
121
122 # GOODNESS OF FIT
123 win.graph(width = 7, height = 3.5,pointsize=10)
124 chi2.Prop(0,alpha=.01,cl=9,Property="eps22", Dataset="RawD")
125 chi2.Prop(5,alpha=.05,cl=4,Property="eps22", Dataset="RawD")
126 chi2.Prop(50,alpha=.05,cl=4,Property="eps22",Dataset="RawD")
127 chi2.Prop(500,alpha=.05,cl=4,Property="eps22",Dataset="RawD")
128 chi2.eps22 <-  list(chi0 =as.vector(chi2.Prop(0,alpha=.05,cl=6,Property="
    eps22", Dataset="RawD")),
129             chi1=as.vector(chi2.Prop(5,alpha=.05,cl=6,Property="eps22",
                Dataset="RawD")),
130             chi2=as.vector(chi2.Prop(50,alpha=.05,cl=6,Property="eps22",
                Dataset="RawD")),
131             chi3=as.vector(chi2.Prop(500,alpha=.05,cl=6,Property="eps22",
                Dataset="RawD")) )
132
133 outfile <- "P45_eps22.txt"
134 cat("                    Transverse Failure Strain
    \n", file=outfile)
135 cat("Crosshead Rate\t\t", GMT.stats.eps22[[1]] ,"\\\\\n", file=outfile,
    sep="&\t",append = TRUE)
136 cat("Mean\t\t\t", format(GMT.stats.eps22[[2]] , digits=3,nsmall=2),"\\\\\
    n", file=outfile, sep="&\t",append = TRUE)
137 cat("Standard Deviation\t", format(GMT.stats.eps22[[3]] , digits=3,nsmall
    =2),"\\\\\n", file=outfile, sep="&\t",append = TRUE)
138 cat("Coef. of Variance\t\t", format(GMT.stats.eps22$sd/GMT.stats.eps22$ave
    , digits=3,nsmall=2),"\\\\\n", file=outfile, sep="&\t",append =
    TRUE)
139 cat("-----------------------------------------------------------\n",
    file=outfile, append = TRUE)
140 cat("          Coefficients Mean testing          \n", file=
    outfile, append = TRUE)
141 cat("Crosshead Rate&\t$t_0$&\t$\\alpha$\t&df&\t$t_{crit}$\t&
    \tLevel\\\\\n", file=outfile, append = TRUE)
142 cat("5 vs. 50\t", format(t1[[1]] , digits=3,nsmall=2),"\\\\\n", file=
    outfile, sep="&\t",append = TRUE)
143 cat("50 vs. 500\t", format(t1[[2]] , digits=3,nsmall=2),"\\\\\n", file=
    outfile, sep="&\t",append = TRUE)
144 cat("5 vs. 500\t", format(t1[[3]] , digits=3,nsmall=2),"\\\\\n", file=
    outfile, sep="&\t",append = TRUE)
145 cat("          Coefficients Variance testing          \n",
    file=outfile, append = TRUE)
146 cat("Crosshead Rate&\t$F_0$&\t$\\alpha$\t&df1\t&df1&\tF_{
    crit}&\tLevel\\\\\n", file=outfile, append = TRUE)
147 cat("5 vs. 50\t", format(f1[[1]] , digits=3,nsmall=2),"\\\\\n", file=
    outfile, sep="&\t",append = TRUE)
```

```
148 cat("50 vs. 500\t", format(f1[[2]], digits=3,nsmall=2),"\\\\ \n", file=
    outfile, sep="&\t",append = TRUE)
149 cat("5 vs. 500\t", format(f1[[3]], digits=3,nsmall=2),"\\\\ \n", file=
    outfile, sep="&\t",append = TRUE)
150 cat("          Normality Check          \n", file=outfile,
    append = TRUE)
151 cat("Crosshead Rate \t& $\\chi^2_0$& $\\alpha$& df \t& $\\chi^2_{crit
    }& Level\\\\ \n", file=outfile, sep="", append = TRUE)
152 cat("ALL\t\t\t", format(chi2.eps22[[1]], digits=3,nsmall=2),"\\\\ \n",
    file=outfile, sep="&\t",append = TRUE)
153 cat("5\t\t\t", format(chi2.eps22[[2]], digits=3,nsmall=2),"\\\\ \n",
    file=outfile, sep="&\t",append = TRUE)
154 cat("50\t\t\t", format(chi2.eps22[[3]], digits=3,nsmall=2),"\\\\ \n",
    file=outfile, sep="&\t",append = TRUE)
155 cat("500\t\t\t", format(chi2.eps22[[4]], digits=3,nsmall=2),"\\\\ \n",
    file=outfile, sep="&\t",append = TRUE)
156 cat("                                                                \n",
    file=outfile, append = TRUE)
157 cat("          Coefficients of Material Models          \n",
    file=outfile, append = TRUE)
158 cat("Model\t\t& Intercept &\t log(SR22) &\t log^2(SR22) \t& $R^2$ \n",
    file=outfile, append = TRUE)
159 cat("MC.lm1\t",format(eps22.lm$coe, digits=3,nsmall=2)," ", format(
    summary(eps22.lm)[8], digits=3),"\\\\ \n", file=outfile, sep=" +\t",
    append = TRUE)
160 cat("MC.lm2\t",format(eps22.lm2$coe, digits=3,nsmall=2), format(summary(
    eps22.lm2)[8], digits=3),"\\\\ \n", file=outfile, sep=" +\t", append =
    TRUE)
161 cat("          ANOVA          \n", file=outfile, append =
    TRUE)
162 cat(names(anova(eps22.lm, eps22.lm2)),"\\\\ \n", file=outfile, sep="&\t
    ",append = TRUE)
163 write.table(format(anova(eps22.lm, eps22.lm2), digits=3,nsmall=2), file =
    outfile,
164             quote=FALSE, sep = "& ", append =TRUE, col.names = FALSE)
```

C.2.5 Listing For Critical Transverse Damage Limit Obtained From $[\pm 45^{\circ}]_{2s}$ Laminate

```
1 rm(list=ls())
2 source('D:/current/Program/R/PM67/PM67-gen.R')
3 Src.const <- "VE"
4 CI <- !is.na(RawD$Yct) & RawD$Yct >0 & RawD$Yct <3
5 RawD <- RawD[CI,]
6 xcut <- c(min(RawD$SR22), max(RawD$SR22))
```

```
7  ycut  <- max(RawD$Yct )
8
9  win.graph(width = 7, height = 3.5,pointsize=10)
10 coplot(RawD$Yct~RawD$SR22|RawD$FailLoc*RawD$Source, data=RawD,
11      xlab=c(expression(paste("Transverse Strain Rate log [mi",n^{-1},"]")),
            "Given: Failure Location"),
12      ylab =c( expression(paste("Critical transverse damage limit ", Y*
            minute[c], " [GPa]")), "Given: Source"),
13      #ylim=c(0,max(RawD$Yct))
14      pch=as.integer(RawD$CR), col=as.integer(RawD$CR))
15 win.graph(width = 7, height = 3.5,pointsize=10)
16 coplot(RawD$Yct~RawD$SR22|RawD$Source, data=RawD,
17      xlab=c(expression(paste("Transverse Strain Rate log [mi",n^{-1},"]")),
            , "Given: Source"),
18      ylab =expression(paste("Critical transverse damage limit ", Y*minute[c
            ], " [GPa]")),
19      #ylim=c(0,max(RawD$Yct))
20      pch=as.integer(RawD$CR), col=as.integer(RawD$CR))
21
22 CI <- RawD$Source == Src.const
23 RawAll <- RawD
24 RawVE <- RawD[CI,]
25 RawIns <- RawD[!CI,]
26 # Plot vs. Sustained Strain Rate
27 for (counter in c("All","VE", "Ins")) {
28      RawD <- eval(parse(text=paste("Raw",counter, sep="")))
29      xcut  <- c(min(RawD$SR22), max(RawD$SR22))
30      ycut  <- max(RawD$Yct )
31
32      cat("Calculations for ", counter, ".\n")
33      win.graph(width = 7, height = 3.5,pointsize=10)
34      plot(RawD$SR22,RawD$Yct, main=paste("Critical transverse damage limit
           vs. Strain Rate (", counter,").", sep=""),
35           xlab=expression(paste("Strain Rate log [mi",n^{-1},"]")),
36           ylab = expression(paste("Critical transverse damage limit ", Y*
                minute[c], " [GPa]")), ylim=c(0,ycut),
37           pch=as.integer(RawD$CR), col=as.integer(RawD$CR))
38      legend(xcut[1], ycut, c("5[mm/min]", "50[mm/min]", "500[mm/min]"),
39           pch=as.integer(labels(RawD$CR)), col=as.integer(labels(RawD$Source
                )))
40      legend(mean(xcut), ycut, c("Linear","Quadratic"),lty=1:2, col=1:2)
41
42      #------------------------------ TREATMENT OF OUTLIERS
43      wrong <- identify( RawD$SR22,RawD$Yct,labels=RawD$ID)
44      CI <- rep(TRUE, length(RawD$CR))
45      CI[wrong] <- c(FALSE)
46      RD.bak  <- RawD
```

```
47  RawD <- RawD[CI,]
48
49  # model Fitting
50  SR.ord_order(RawD$SR22)   #vector with ascending order of the Strain
        rate
51  Yct.lm <- lm(Yct~RawD$SR22, data=RawD)
52  Yct.lm2 <- lm(Yct~RawD$SR22+ I((RawD$SR22)^2), data=RawD)
53  Yct.hat2 <- predict(Yct.lm2)
54  lines(RawD$SR22[SR.ord], Yct.hat2[SR.ord],lty=2, col=2)
55  abline(lsfit(RawD$SR22, RawD$Yct), lty=1, col=1)
56  #---------------------  STATISTICS CALCS
        ---------------------------------
57  eval(parse(text=paste("rm(RD.stats.Yct.",counter,")", sep="")))
58  eval(parse(text=paste("RD.stats.Yct.",counter,"<-- list(CR=c
        (5,50,500),",
59            "ave=c(mean(RawD$Yct[RawD$CR==5]),mean(RawD$Yct[RawD$CR
                ==50],na.rm=TRUE),",
60                  "mean(RawD$Yct[RawD$CR==500],na.rm=TRUE)),",
61            "sd=c(sd(RawD$Yct[RawD$CR==5]),sd(RawD$Yct[RawD$CR==50]),sd
                (RawD$Yct[RawD$CR==500]))", sep="")))
62  eval(parse(text=paste("RD.stats.Yct.",counter, "$CV","<-",
63      "RD.stats.Yct.",counter, "$sd/RD.stats.Yct.",counter, "$ave",sep="
            ")))
64
65  RD.stats.Yct <-  eval(parse(text=paste("RD.stats.Yct.",counter,sep="")
        ))
66      # EQUALITY OF MEANS
67  t1 <- list(f1 =as.vector(t0.func(5,50,alpha=.05, Property="Yct")),
68          f2 = as.vector(t0.func(50,500,alpha=.05, Property="Yct")),
69          f3 =as.vector(t0.func(5,500,alpha=.05, Property="Yct")) )
70
71      # EQUALITY OF Variances
72  f1 <- list(f1 =as.vector(Var.f(5,50,alpha=.05, Property="Yct")),
73          f2= as.vector(Var.f(50,500,alpha=.05, Property="Yct")),
74          f3 =as.vector(Var.f(5,500,alpha=.05, Property="Yct")) )
75
76  win.graph(width = 7, height = 3.5,pointsize=10)
77  xpdf <- c(0,max(RawD$Yct))
78  ypdf <- c(0,max(c(density(RawD$Yct[RawD$CR==5])$y,
79          density(RawD$Yct[RawD$CR==50])$y,
80          density(RawD$Yct[RawD$CR==500])$y)))
81  par(mfrow=c(1,1))
82  plot(density(RawD$Yct),
83      main=paste("a)Complete_data_set(",counter,").", sep=""),
84      xlab=expression(paste(Y*minute[c])),
85      ylab="Probability_density",
86      xlim=xpdf, ylim=ypdf)
```

```
87
88      win.graph(width = 6, height = 3,pointsize=12)
89      par(mfrow=c(1,3))
90      plot(density(RawD$Yct[RawD$CR==5]),
91           xlab=expression(paste(Y*minute[c])),
92           ylab="Probability density",
93           main=paste("b) 5[mm/min] (", counter,").", sep=""),
94           xlim=xpdf, ylim=ypdf)
95      plot(density(RawD$Yct[RawD$CR==50]),
96           xlab=expression(paste(Y*minute[c])),
97           ylab="Probability density",
98           main=paste("c) 50[mm/min] (", counter,").", sep=""),
99           xlim=xpdf, ylim=ypdf)
100     plot(density(RawD$Yct[RawD$CR==500]),
101          xlab=expression(paste(Y*minute[c])),
102          ylab="Probability density",
103          main=paste("d) 500[mm/min] (", counter,").", sep=""),
104          xlim=xpdf, ylim=ypdf)
105
106     # GOODNESS OF FIT
107     win.graph(width = 7, height = 3.5,pointsize=10)
108     chi2.Prop(0,alpha=.01,cl=9,Property="Yct", Dataset="RawD")
109     chi2.Prop(5,alpha=.05,cl=4,Property="Yct", Dataset="RawD")
110     chi2.Prop(50,alpha=.05,cl=4,Property="Yct",Dataset="RawD")
111     chi2.Prop(500,alpha=.05,cl=4,Property="Yct",Dataset="RawD")
112     chi2.Yct <-  list(chi0 =as.vector(chi2.Prop(0,alpha=.05,cl=6,Property=
            "Yct", Dataset="RawD")),
113                  chi1=as.vector(chi2.Prop(5,alpha=.05,cl=6,Property="Yct",
                         Dataset="RawD")),
114                  chi2=as.vector(chi2.Prop(50,alpha=.05,cl=6,Property="Yct",
                         Dataset="RawD")),
115                  chi3=as.vector(chi2.Prop(500,alpha=.05,cl=6,Property="Yct"
                         ,Dataset="RawD")) )
116
117     #------------------------ OUTPUT ------------------------------
118     outfile <- paste("PM67_Yct_",counter,".txt",sep="")
119     cat("           ", counter," Critical transverse damage limit
            -----------\n" , file=outfile)
120     cat("-----------------------------------------------------------\
            n", file=outfile, append = TRUE)
121     cat("Crosshead Rate\t\t", RD.stats.Yct[[1]] ,"\\\\ \n" , file=outfile
            , sep=" &\t",append = TRUE)
122     cat("Mean\t\t\t", format(RD.stats.Yct[[2]] , digits=3,nsmall=2),"
            \\\\ \n" , file=outfile, sep=" &\t",append = TRUE)
123     cat("Standard Deviation\t", format(RD.stats.Yct[[3]] , digits=3,nsmall
            =2),"\\\\ \n" , file=outfile, sep=" &\t",append = TRUE)
```

```
124 cat("Coef. of Variance\t\t", format(RD.stats.Yct$sd/RD.stats.Yct$ave
        , digits=3,nsmall=2),"\\\\ \n" , file=outfile , sep="&\t",append
        = TRUE)
125 cat("----------------------------------------------------------\
    n", file=outfile , append = TRUE)
126 cat("--------Coefficients Mean testing---------\n" ,
    file=outfile , append = TRUE)
127 cat("Crosshead Rate&\t $t_0$&\t $\\alpha$ \t&df &\t $t_{crit}$
    \t&\t Level\\\\ \n" , file=outfile , append = TRUE)
128 cat("5 vs. 50\t", format(t1[[1]] , digits=3,nsmall=2),"\\\\ \n" , file
    =outfile , sep="&\t",append = TRUE)
129 cat("50 vs. 500\t", format(t1[[2]] , digits=3,nsmall=2),"\\\\ \n" ,
    file=outfile , sep="&\t",append = TRUE)
130 cat("5 vs. 500\t", format(t1[[3]] , digits=3,nsmall=2),"\\\\ \n" ,
    file=outfile , sep="&\t",append = TRUE)
131 cat("--------Coefficients Variance testing---------\n"
    , file=outfile , append = TRUE)
132 cat("Crosshead Rate&\t $F_0$&\t $\\alpha$ \t&df1 \t&df1 &\t F_
    {crit}&\t Level\\\\ \n" , file=outfile , append = TRUE)
133 cat("5 vs. 50\t", format(f1[[1]] , digits=3,nsmall=2),"\\\\ \n" , file
    =outfile , sep="&\t",append = TRUE)
134 cat("50 vs. 500\t", format(f1[[2]] , digits=3,nsmall=2),"\\\\ \n" ,
    file=outfile , sep="&\t",append = TRUE)
135 cat("5 vs. 500\t", format(f1[[3]] , digits=3,nsmall=2),"\\\\ \n" ,
    file=outfile , sep="&\t",append = TRUE)
136 cat("--------Normality Check---------\n", file=outfile
    , append = TRUE)
137 cat("Crosshead Rate\t&$\\chi^2_0$&$\\alpha$&df \t&$\\chi^2_{
    crit}&Level\\\\ \n" , file=outfile , sep="", append = TRUE)
138 cat("ALL\t\t", format(chi2.Yct[[1]] , digits=3,nsmall=2),"\\\\ \n"
     , file=outfile , sep="&\t",append = TRUE)
139 cat("5\t\t", format(chi2.Yct[[2]] , digits=3,nsmall=2),"\\\\ \n" ,
    file=outfile , sep="&\t",append = TRUE)
140 cat("50\t\t", format(chi2.Yct[[3]] , digits=3,nsmall=2),"\\\\ \n" ,
    file=outfile , sep="&\t",append = TRUE)
141 cat("500\t\t", format(chi2.Yct[[4]] , digits=3,nsmall=2),"\\\\ \n"
     , file=outfile , sep="&\t",append = TRUE)
142 cat("----------------------------------------------------------\
    n", file=outfile , append = TRUE)
143 cat("--------Coefficients of Material Models---------\
    n", file=outfile , append = TRUE)
144 cat("Model\t\t& Intercept &\t log(SR) &\t log^2(SR) \t&$R^2$ \n" ,
    file=outfile , append = TRUE)
145 cat("MC.lm1\t",format(Yct.lm$coe ,digits=3,nsmall=2)," ", format
    (summary(Yct.lm)[8],digits=3),"\\\\ \n" , file=outfile , sep="+\t",
    append = TRUE)
```

```
146     cat("MC.lm2\t",format(Yct.lm2$coe ,digits=3,nsmall=2), format(summary(
            Yct.lm2)[8],digits=3),"\\\\ \n" , file=outfile , sep="+\t", append
            = TRUE)
147     cat("---------ANOVA----------\n", file=outfile , append
            = TRUE)
148     cat(names(anova(Yct.lm, Yct.lm2)),"\\\\ \n" , file=outfile , sep="&\t
            ",append = TRUE)
149     write.table(format(anova(Yct.lm, Yct.lm2), digits=3,nsmall=2), file =
            outfile ,
150                 quote=FALSE, sep = "&", append =TRUE, col.names = FALSE)
151 }
152
153 RawD <- RawAll
154 t1.src <- list(f5 =as.vector(t0.src(5,alpha=.05, Property="Yct")),
155          f50 = as.vector(t0.src(50, alpha=.05, Property="Yct")),
156          f500 = as.vector(t0.src(500, alpha=.05, Property="Yct")) )
157
158 f1.src <- list(f1 =as.vector(Var.src(5,alpha=.05, Property="Yct")),
159              f2= as.vector(Var.src(50,alpha=.05, Property="Yct")),
160              f3 =as.vector(Var.src(500,alpha=.05, Property="Yct")) )
161
162 outfile <- "PM67_Yct_Src.txt"
163 cat("-----Comparison of Source for Critical transverse damage limit
      -------\n" , file=outfile)
164 cat("-----------------------------------------------------------------\n",
      file=outfile , append = TRUE)
165 cat("---------Coefficients Mean testing---------\n", file=
      outfile , append = TRUE)
166 cat("VE vs. Ins &\t $t_0$ &\t $\\alpha$ \t &df &\t $t_{crit}$ \t &\t
      Level\\\\ \n" , file=outfile , append = TRUE)
167 cat("5\t", format(t1.src[[1]] , digits=3,nsmall=2),"\\\\ \n" , file=
      outfile , sep="&\t",append = TRUE)
168 cat("50\t", format(t1.src[[2]] , digits=3,nsmall=2),"\\\\ \n" , file=
      outfile , sep="&\t",append = TRUE)
169 cat("500\t", format(t1.src[[3]] , digits=3,nsmall=2),"\\\\ \n" , file=
      outfile , sep="&\t",append = TRUE)
170 cat("---------Coefficients Mean testing---------\n", file=
      outfile , append = TRUE)
171 cat("VE vs. Ins &\t $t_0$ &\t $\\alpha$ \t &df &\t $t_{crit}$ \t &\t
      Level\\\\ \n" , file=outfile , append = TRUE)
172 cat("5\t", format(f1.src[[1]] , digits=3,nsmall=2),"\\\\ \n" , file=
      outfile , sep="&\t",append = TRUE)
173 cat("50\t", format(f1.src[[2]] , digits=3,nsmall=2),"\\\\ \n" , file=
      outfile , sep="&\t",append = TRUE)
174 cat("500\t", format(f1.src[[3]] , digits=3,nsmall=2),"\\\\ \n" , file=
      outfile , sep="&\t",append = TRUE)
```

C.3 Experimental Vs. FE Comparison- Visual Basic For Applications.

Visual Basic was used to compare the experimental vs. the Finite Element simulations.

Also, Visual Basic scripts have been created for the extraction of parameter of the global composite ply, however they have been replaced by Matlab because of performance issues(C.1.1.

```
1  Attribute VB_Name = "FEvExp"
2  ' This module contains The following functions/subroutines
3      ' expFeCompStart
4  Option Base 1
5  Option Explicit
6  Dim Msg As String
7  'Const instronFilesDir = "D:\current\Ladeveze"
8  'Const fEprocFilesDir = "D:\Papadakis\PhD\Chapters\FE\files\processed"
9  'Const compFilesDir = "D:\Papadakis\PhD\Chapters\ExpFeComp\files"
10
11 Private Sub expFeCompFull()
12     Call importCompFiles
13     Call expFeCompRead
14 End Sub
15                          '
16                          ' IMPORT both Comp FILES
17                          '
18 Private Sub importCompFiles(Optional comWkBk As Variant, _
19         Optional expSheet As Variant, Optional fESheet As Variant, _
20         Optional compSheet As Variant)
21
22 On Error GoTo Errorhandler
23     If IsMissing(comWkBk) Then
24         Set comWkBk = Application.Workbooks.Add
25         Set compSheet = comWkBk.activeSheet
26         compSheet.Name = "Comparison"
27         Set fESheet = comWkBk.Worksheets.Add
28         fESheet.Name = "FE"
29         Set expSheet = comWkBk.Worksheets.Add
30         expSheet.Name = "Experimental"
31     End If
32
33 On Error GoTo 0
34 On Error Resume Next
35     ChDir "D:\Papadakis\PhD\Chapters\FE\files"
```

```
36
37
38  '     ChDir fEprocFilesDir
39      Dim pssWkBk As Variant, expWkBk As Variant
40      Call importPssFilename
41      Set pssWkBk = ActiveWorkbook
42      cells.Copy
43      comWkBk.Activate
44      fESheet.Paste
45      Application.CutCopyMode = False
46      pssWkBk.Close
47
48  '     ChDir instronFilesDir
49      Call importInstronFile
50      Set expWkBk = ActiveWorkbook
51      cells.Copy
52      comWkBk.Activate
53      expSheet.Activate
54      Selection.PasteSpecial Paste:=xlValues, Operation:=xlNone, SkipBlanks _
            := _
55          False, Transpose:=False
56      Application.CutCopyMode = False
57      expWkBk.Close
58
59  '           input files.
60  '     ChDir compFilesDir
61      Dim fileToSave As Variant
62      comWkBk.Activate
63
64      fileToSave = Application _
65          .GetSaveAsFilename(fileFilter:="Excel File (*.xls), *.xls")
66      If fileToSave <> False Then
67          MsgBox "The filename is : " & fileToSave
68      Else
69          MsgBox "Restart and select a valid .xls name"
70          Exit Sub
71      End If
72      ActiveWorkbook.SaveAs filename:=fileToSave _
73          , FileFormat:=xlNormal, Password:="", WriteResPassword:="", _
74          ReadOnlyRecommended:=False, CreateBackup:=False
75
76      Exit Sub
77  Errorhandler:
78      MsgBox "An unexpected error occured"
79  End Sub
80
81
```

```
82                      ' Read and make interpolation.
83
84  Private Sub expFeCompRead(Optional comWkBk As Variant, _
85          Optional expSheet As Variant, Optional fESheet As Variant, _
86          Optional compSheet As Variant)
87
88      Dim count1 As Integer, count2 As Integer
89      Dim fEDataLength As Integer, expDatalength As Integer
90      Dim tempSheet As Variant
91      Dim noSpec As Integer
92      Dim maxFE(2) As Double, maxExp(2) As Double
93      Dim CRR(2) As Double, PCC(2) As Double
94
95
96      On Error GoTo noCompWkBk
97      ChDir "D:\Papadakis\PhD\Chapters\FE\files"
98      If IsMissing(comWkBk) Then
99          If ActiveWorkbook.Sheets.Count = 3 Then
100             Set comWkBk = ActiveWorkbook
101             Set compSheet = ActiveWorkbook.Sheets("Comparison")
102             Set fESheet = ActiveWorkbook.Sheets("FE")
103             Set expSheet = ActiveWorkbook.Sheets("Experimental")
104         End If
105     End If
106     On Error GoTo 0
107
108     '         8 8
109         '       Pearson Correlation factor
110     Set tempSheet = Worksheets.Add
111     tempSheet.Name = "Temp"
112 '    tempSheet.visible = False
113
114     ' Reading of FE
115     fESheet.Activate
116     Range("A1").Activate
117     fEDataLength = Range(ActiveCell, ActiveCell.End(xlDown)).Rows.Count _
            - 2
118
119     Dim iVecFE() As Double, iVecExp() As Double       ' FE And Exp input _
            vector 2xExpDataLength
120     Dim tempArray() As Double
121     Dim sVecFe() As Variant, sVecExp() As Variant
122     ReDim tempArray(fEDataLength, 3)
123
124     maxFE(1) = 0
125     maxFE(2) = 1
126     For count1 = 1 To fEDataLength
```

```
127         tempArray(count1 , 1) = ActiveCell.Offset(count1 + 1, 0).Value
128         tempArray(count1 , 2) = ActiveCell.Offset(count1 + 1, 1).Value
129         tempArray(count1 , 3) = ActiveCell.Offset(count1 + 1, 2).Value
130         If maxFE(1) < tempArray(count1 , 3) Then
131             maxFE(1) = tempArray(count1 , 3)
132             maxFE(2) = count1
133         End If
134     Next
135
136     ReDim iVecFE(fEDataLength , 3)
137     For count1 = 1 To maxFE(2)
138         iVecFE(count1 , 1) = tempArray(count1 , 1)
139         iVecFE(count1 , 2) = tempArray(count1 , 2)
140         iVecFE(count1 , 3) = tempArray(count1 , 3)
141     Next
142
143
144     MsgBox ("maximum␣Stress␣:␣" & maxFE(1) & vbCrLf & _
145             "@␣point␣" & maxFE(2))
146
147 '
148
149                             ' Reading of Experimental Data
150     noSpec = 1
151     compSheet.Activate
152     Range("A1").Activate
153     ActiveCell.Offset(0, 0).Value = "Specimen␣Number"
154     ActiveCell.Offset(0, 1).Value = "PCC1"
155     ActiveCell.Offset(0, 2).Value = "CRR1"
156     ActiveCell.Offset(0, 3).Value = "PCC2"
157     ActiveCell.Offset(0, 4).Value = "CRR2"
158
159     expSheet.Activate
160     While noSpec <= Range("A2", Range("A2").End(xlToRight)).Columns.Count _
            / 4
161 '
162         MsgBox ("Importing␣specimen␣#" & noSpec)
163         expSheet.Activate
164         Range("A2").Offset(0, 4 * (noSpec - 1)).Activate
165         expDatalength = Range(ActiveCell, ActiveCell.End(xlDown)).Rows. _
              Count
166
167         ReDim tempArray(expDatalength , 3)
168         maxExp(1) = 0
169         maxExp(2) = 1
170         count2 = 1
171         For count1 = 1 To expDatalength
```

```
172         '   : T
173         '       INSTRON.
174             If maxExp(1) < ActiveCell.Offset(count1 - 1, 2).Value Then
175                 tempArray(count2, 1) = ActiveCell.Offset(count1 - 1, 1). _
                        Value
176                 tempArray(count2, 2) = ActiveCell.Offset(count1 - 1, 3). _
                        Value
177                 tempArray(count2, 3) = ActiveCell.Offset(count1 - 1, 2). _
                        Value
178                 maxExp(1) = tempArray(count2, 3)
179                 maxExp(2) = count2
180                 count2 = count2 + 1
181             End If
182         Next
183
184         ReDim iVecExp(UBound(tempArray, 1), 3)
185         For count1 = 1 To UBound(tempArray, 1)
186             iVecExp(count1, 1) = tempArray(count1, 1)
187             iVecExp(count1, 2) = tempArray(count1, 2)
188             iVecExp(count1, 3) = tempArray(count1, 3)
189         Next
190
191         If maxExp(1) > maxFE(1) Then
192             maxExp(1) = maxFE(1)
193         End If
194
195         On Error Resume Next
196             sVecFe = updateVecf(iVecFE, maxExp(1), 101)
197             Call printVecToTemp(sVecFe, tempSheet, 1)
198
199             sVecExp = updateVecf(iVecExp, maxExp(1), 101)
200             Call printVecToTemp(sVecExp, tempSheet, 2)
201
202     ' Calculations
203             tempSheet.Activate
204             PCC(1) = -1
205             PCC(2) = -1
206             CRR(1) = -1
207             CRR(2) = -1
208             PCC(1) = Application.WorksheetFunction.Pearson(Range("B2:B102" _
                    ), Range("G2:G102"))
209             CRR(1) = iVecFE(maxFE(2), 1) / iVecExp(maxExp(2), 1)
210             PCC(2) = WorksheetFunction.Pearson(Range("C2:C102"), Range("H2 _
                    :H102"))
211             CRR(2) = iVecFE(maxFE(2), 2) / iVecExp(maxExp(2), 2)
212         On Error GoTo 0
213         compSheet.Activate
```

```
214
215         MsgBox "Specimen no: " & noSpec & "    Data points:" &  _
                expDatalength & vbCrLf & _
216              "exp: Stress: " & maxExp(1) & "    @ point " & maxExp(2) &  _
                    vbCrLf & _
217              "FE: Stress: " & maxFE(1) & "   @ point " & maxFE(2) & vbCrLf _
                    & _
218              "exp: LS: " & iVecExp(maxExp(2), 1) & "   TS: " & iVecExp( _
                    maxExp(2), 2) & "    S: " & iVecExp(maxExp(2), 3) & vbCrLf _
                    & _
219              "FE: LS: " & iVecFE(maxFE(2), 1) & "   TS: " & iVecFE(maxFE _
                    (2), 2) & "    S: " & iVecFE(maxFE(2), 3)
220
221
222         '       correlation
223         compSheet.Activate
224         Range("A1").Activate
225         ActiveCell.Offset(noSpec, 0).Value = noSpec
226         ActiveCell.Offset(noSpec, 1).Value = PCC(1)
227         ActiveCell.Offset(noSpec, 2).Value = CRR(1)
228         ActiveCell.Offset(noSpec, 3).Value = PCC(2)
229         ActiveCell.Offset(noSpec, 4).Value = CRR(2)
230         '   specimen.
231         expSheet.Activate
232         noSpec = noSpec + 1
233     Wend
234     tempSheet.Delete
235     Exit Sub
236 noCompWkBk:
237     MsgBox "Open a valid file and try again"
238     tempSheet.Delete
239     Exit Sub
240 End Sub
241
242                             '
243                             ' Auxilliary files
244                             '
245 Private Sub compInstronBiCSVConv()
246
247     Dim CountI As Integer
248     Dim counterII As Integer
249     Dim TestName As String
250     Dim BatchName As String
251     Dim SpecimenNo As Integer
252     Dim DatashtName As String, SSDatashtName As String
253     Dim ContinueLoop As Boolean
254     Dim CELGL As Double, CEIGL As Double
```

```
255     Dim NoPlies As Integer
256     Dim plyThick As Double
257
258     DatashtName = "'" & Sheets(1).Name & "'"
259     SSDatashtName = "'SS-" & Sheets(1).Name & "'"
260     BatchName = InputBox("Designation of the specimen")
261     SpecimenNo = InputBox("First specimen No:", "Specimen #", 1)
262     NoPlies = InputBox("Plies", "Number of Plies :", 8)
263     plyThick = InputBox("Ply thickness", "Ply thickness :", 0.22)
264     CELGL = InputBox("Longitudical Contact Extensiometer [mm]", "
            Longitudinal Gauge Length:", 50)
265     CETGL = InputBox("Transverse Contact Extensiometer [mm]", "Transverse
            Gauge Length:", 10)
266     counterII = 0
267
268     Application.ScreenUpdating = False
269
270
271 ' Create a stress vs. strain sheet
272     Worksheets(Sheets(1).Name).Copy After:=Worksheets(Sheets(1).Name)
273     activeSheet.Name = "SS-" & Sheets(1).Name
274     Range("B1").Select
275     ActiveCell.FormulaR1C1 = "='" & Sheets(1).Name & "'!RC/" & CELGL
276     Range("C1").Select
277     ActiveCell.FormulaR1C1 = "='" & Sheets(1).Name & "'!RC/(" &
278         NoPlies * plyThick / 1000 * CETGL & ")"
279     Range("D1").Select
280     ActiveCell.FormulaR1C1 = "=-" & Sheets(1).Name & "'!RC/" & CETGL
281
282     Range("b1:D1").AutoFill Destination:=Range("B1:D11291")
283
284     Do
285         counterII = counterII + 1
286         Worksheets(1).Activate
287         Range("A1").Select
288         TestName = BatchName & "-" & counterII + SpecimenNo - 1
289         CountI = 1
290         While ActiveCell.Offset(CountI, 0) > 1
291             CountI = CountI + 1
292         Wend
293         ' Naming Specimens and columns
294         Range("A1:D1").Insert Shift:=xlDown
295         Range("B1").Value = "Long. Displ:" & TestName
296         Range("C1").Value = "Force:" & TestName
297         Range("D1").Value = "Tran. Displ:" & TestName
298
299         ' Chart
```

```
300 '        Call ChkChartBi("LD-Curves", CountI, TestName, DatashtName, _
    SSDatashtName)
301 '
302 '        If counterII > 1 Then
303 '            ActiveChart.SeriesCollection.NewSeries
304 '            ActiveChart.SeriesCollection(2 * counterII).XValues = "=" & _
    DatashtName & "!R2C2:R" & CountI & "C2"
305 '            ActiveChart.SeriesCollection(2 * counterII).Values = "=" & _
    DatashtName & "!R2C3:R" & CountI & "C3"
306 '            ActiveChart.SeriesCollection(2 * counterII).Name = "=" & _
    DatashtName & "!R1C3"
307 '            ActiveChart.SeriesCollection.NewSeries
308 '            ActiveChart.SeriesCollection(2 * counterII + 1).XValues _
     = "=" & SSDatashtName & "!R2C2:R" & CountI & "C2"
309 '            ActiveChart.SeriesCollection(2 * counterII + 1).Values _
     = "=" & SSDatashtName & "!R2C3:R" & CountI & "C3"
310 '            ActiveChart.SeriesCollection(2 * counterII + 1).Name = "=" & _
    SSDatashtName & "!R1C3"
311 '        End If
312
313     ' Checking whether thereis a following block of data
314         Sheets(1).Select
315         ContinueLoop = False
316         If IsEmpty(Range("A" & CountI + 2)) = False Then
317             ContinueLoop = True
318         End If
319
320     ' Shifting and moving Blocks of data
321         Range("A1:D" & CountI + 1).Cut
322         Range("A1").Offset(0, 4 * counterII).Select
323         activeSheet.Paste
324         Range("A1:D" & CountI + 1).Delete Shift:=xlUp
325
326         If ContinueLoop = False Then
327             Columns("A:D").Delete
328             Range("A1").Select
329         End If
330
331 ' Stress vs. Strain sheet
332         Worksheets(2).Activate
333         Range("A1").Select
334         ' Naming Specimens and columns
335         Range("A1:D1").Insert Shift:=xlDown
336         Range("B1").Value = "Long. Strain: " & TestName
337         Range("C1").Value = "Stress: " & TestName
338         Range("D1").Value = "Tran. Strain: " & TestName
339
```

```
340         Range("A1:D" & CountI + 1).Cut
341         Range("A1").Offset(0, 4 * counterII).Select
342         activeSheet.Paste
343         Range("A1:D" & CountI + 1).Delete Shift:=xlUp
344
345
346         If ContinueLoop = False Then
347             Columns("A:D").Delete
348             Range("A1").Select
349         End If
350
351
352     Loop While ContinueLoop = True
353     Application.ScreenUpdating = True
354 End Sub
355
356                             ' IMPORT INSTRON FILE
357
358 Private Sub importInstronFile()
359     '     dc.
360     Dim fileToOpen As Variant
361
362     fileToOpen = Application _
363         .GetOpenFilename("Instron Files (*.csv), *.csv")
364     If fileToOpen <> False Then
365         Workbooks.OpenText filename:=fileToOpen, Origin:= _
366         xlWindows, StartRow:=1, DataType:=xlDelimited, TextQualifier:= _
367         xlNone, ConsecutiveDelimiter:=False, Tab:=False, Semicolon:=False _
                , _
368         Comma:=True, Space:=False, Other:=False, FieldInfo:=Array(Array _
                (1, 1), _
369         Array(2, 1), Array(3, 1))
370     End If
371
372     Call compInstronBiCSVConv
373 End Sub
374
375                             ' IMPORT PSS FILE
376
377 Private Sub importPssFilename()
378     '     pss.
379     Dim fileToOpen As Variant
380
381     fileToOpen = Application _
382         .GetOpenFilename("PamCrash Stress vs strain files (*.pss), *.pss")
383     If fileToOpen <> False Then
384         Workbooks.OpenText filename:=fileToOpen, Origin:= _
```

```
385         xlWindows , StartRow:=1 , DataType:=xlDelimited , TextQualifier:= _
386         xlNone , ConsecutiveDelimiter:=False , Tab:=False , Semicolon:=False _
                , _
387         Comma:=True , Space:=False , Other:=False , FieldInfo:=Array(Array _
                (1 , 1) , _
388         Array(2 , 1) , Array(3 , 1))
389     End If
390 End Sub
391                                 ' IMPORT VEFILE
392
393 Private Sub importVEFile()
394     '       dc.
395     Dim fileToOpen As Variant
396
397     fileToOpen = Application _
398         .GetOpenFilename("PamCrash files (*.dc),*.dc")
399     If fileToOpen <> False Then
400         Workbooks.OpenText filename:=fileToOpen , Origin:= _
401         xlWindows , StartRow:=1 , DataType:=xlDelimited , TextQualifier:= _
402         xlDoubleQuote , ConsecutiveDelimiter:=True , Tab:=False , Semicolon:= _
                False , _
403         Comma:=False , Space:=True , Other:=False , FieldInfo:=Array(Array _
                (1 , 1) , _
404         Array(2 , 1) , Array(3 , 1))
405     End If
406 End Sub
407
408
409
410                             ' update Vector
411
412 Private Function updateVecf(iVec As Variant , maxS As Variant , _
413         Optional uVecLen As Integer) As Variant
414
415     If IsMissing(uVecLen) Then
416         uVecLen = 101
417     End If
418
419     Dim intP1 As Integer
420     Dim sVec As Variant
421     Dim L0 As Double , R0 As Double          '
422     Dim L0i As Integer , R0i As Integer      '
423
424     ReDim sVec(1 To uVecLen , 1 To 3)
425     On Error GoTo updateVecErrHandler
426     sVec(1 , 1) = 0
427     sVec(1 , 2) = 0
```

```
428     sVec(1, 3) = 0
429     L0i = 1
430     R0i = 2
431
432     For intP1 = 2 To uVecLen
433         sVec(intP1, 3) = (intP1 - 1) / uVecLen * maxS
434         '     stress
435         L0i = R0i - 1
436         While iVec(R0i, 3) < sVec(intP1, 3) And R0i <= UBound(iVec, 1)
437             R0i = R0i + 1
438         Wend
439         If R0i = L0i Then
440             R0i = L0i + 1
441         End If
442         sVec(intP1, 1) = iVec(R0i, 1) - (iVec(R0i, 1) - iVec(L0i, 1)) / ( -
              iVec(R0i, 3) - iVec(L0i, 3)) * (iVec(R0i, 3) - sVec(intP1, 3))
443         sVec(intP1, 2) = iVec(R0i, 2) - (iVec(R0i, 2) - iVec(L0i, 2)) / ( -
              iVec(R0i, 3) - iVec(L0i, 3)) * (iVec(R0i, 3) - sVec(intP1, 3))
444 '         If intP1 > 0.9 * uVecLen Then
445 '             MsgBox "Updated :" & intP1 & "   Ls(1):" & sVec(intP1, 1) -
    & "   Ts():" & sVec(intP1, 2) & "   stress:" & sVec(intP1, 3)
446 '         End If
447     Next
448
449     updateVecf = sVec
450     Exit Function
451 updateVecErrHandler:
452     MsgBox ("There was an error in update vec Function")
453 End Function
454
455 Private Sub printVecToTemp(sVec As Variant, tempSheetName As Variant, -
    posOnSheet As Integer)
456
457     Dim activeSheetName As Variant
458     Set activeSheetName = activeSheet
459     Dim cnt1 As Integer
460
461     '
462     tempSheetName.Activate
463     Range("A1").Activate
464     ActiveCell.Offset(0, (posOnSheet - 1) * 5).Value = "# of obs."
465     ActiveCell.Offset(0, (posOnSheet - 1) * 5 + 1).Value = "LS"
466     ActiveCell.Offset(0, (posOnSheet - 1) * 5 + 2).Value = "TS"
467     ActiveCell.Offset(0, (posOnSheet - 1) * 5 + 3).Value = "Stress"
468     For cnt1 = 1 To UBound(sVec)
469         ActiveCell.Offset(cnt1, (posOnSheet - 1) * 5 + 0).Value = cnt1
470         ActiveCell.Offset(cnt1, (posOnSheet - 1) * 5 + 1).Value = sVec( -
```

```
            cnt1, 1)
471         ActiveCell.Offset(cnt1, (posOnSheet - 1) * 5 + 2).Value = sVec( _
            cnt1, 2)
472         ActiveCell.Offset(cnt1, (posOnSheet - 1) * 5 + 3).Value = sVec( _
            cnt1, 3)
473     Next
474
475     activeSheetName.Activate
476 End Sub
```

Appendix D

Statistical Processing of Experimental Results

Chapter Objectives

- Present the statistical processing methodology for all results categorised by the layup;

D.1 Properties Obtained From $[0°]_4$ Test.

D.1.1 Strain Rate.

Figure D.1 presents the measured strain rate of the material vs. the crosshead displacement rate.

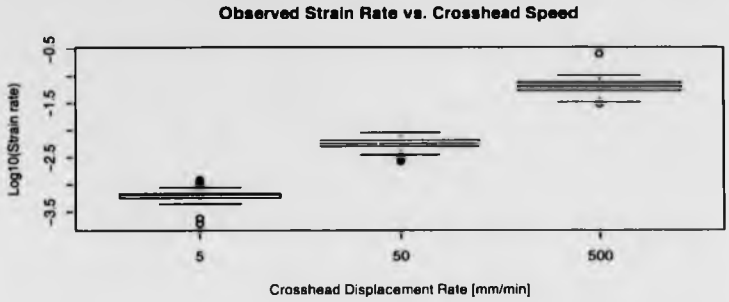

Figure D.1: Longitudinal tensile modulus vs. logarithm of strain rate.

Statistics: Table D.1 presents the statistics of the measured strain rate at different crosshead displacement rates.

Table D.1: Statistics for measured strain rate at different crosshead displacement rates.

Crosshead Rate		5	50	500
Mean	log[1/s]	-3.33	-2.41	-1.23
Standard Deviation	log[1/s]	0.1431	0.0848	0.1022
Coef. of Variance		0.0429	0.0351	0.0829

The mean of the strain rate increases a decade (the strain rate values are presented after the log transformation) for the different crosshead displacement rate. The standard deviation is lower for the 50[mm/min] crosshead displacement rate and higher for the 5[mm/min] displacement

crosshead rate. The coefficient of variance is again lower for the 50[mm/min] crosshead displacement rate but higher for the the 500[mm/min] displacement crosshead rate. The increase of the coefficient of variance is attributed to the proximity of the strain rate means to zero, while the variability is not affected in the same degree.

D.1.2 Strain Rate Effects On Elasticity

D.1.2.1 Poisson's ratio ν_{12}

Figure D.2 presents a conditional plot of the Poisson's ratio with respect to the data acquisition source. There is no visible difference in the location (there is difference in scatter) between the 5 and 50[mm/min] crosshead displacement rates, however for the 500[mm/min] crosshead displacement rate a discrepancy in the trends is visible. This is the reason that the data acquired by Instron will be used for the statistical purposes.

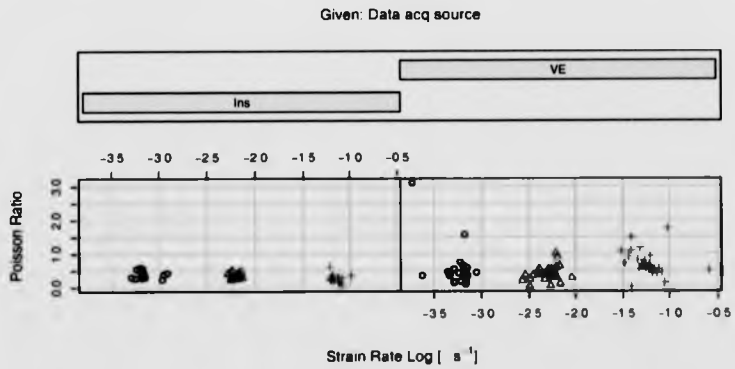

Figure D.2: Poisson's ratio vs. logarithm of strain rate.

Figure D.3 presents the Poisson's ratio vs. strain rate log and a linear and a quadratic model of

the log of the strain rate are fitted. The labeled observations have been identified as outliers and have not be included in the statistical treatment.

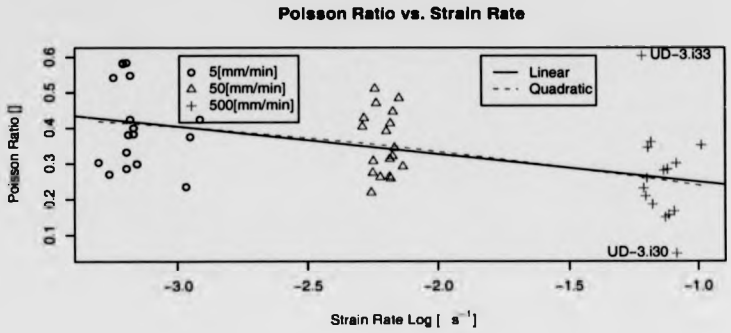

Figure D.3: Poisson's ratio vs. strain rate logarithm.

Statistics: Table D.2 presents the statistics of the Poisson's ratio at different crosshead displacement rates of a unidirectional laminate composite material.

Table D.2: Statistics for the Poisson's ratio at different crosshead displacement rates.

Crosshead Rate		5	50	500
Mean	[]	0.409	0.356	0.252
Standard Deviation	[]	0.1185	0.0894	0.0755
Coef. of Variance	[]	0.29	0.251	0.299

The mean of the Poisson's ratio decreases with increasing crosshead displacement rate. The standard deviation is lowest again for the 500[mm/min] crosshead displacement rate and highest at the 5 [mm/min] crosshead displacement rate. The lowest coefficient of variance is for the 50[mm/min] crosshead displacement rate and highest at the 500 [mm/min] crosshead displacement rate.

Hypothesis testing: The null hypothesis (H_0) is that the Poisson's ratio is not strain rate dependent. Therefore, the mean of the Poisson's ratio for one crosshead displacement rate results should be equal to the mean of the Poisson's ratio for another crosshead displacement rate, e.g. $H_0 : \overline{\nu}_{12,5} = \overline{\nu}_{12,50}$. The alternative hypothesis is that the Poisson's ratio is strain rate dependent. The statistics for the equality of means test are presented in table D.3. The table columns are similar to those of table 4.16.

Table D.3: Hypothesis testing statistics for equality of means of Poisson's ratio.

Crosshead Rate	t_0	α	df	t_{crit}	Level
5 vs. 50	1.495	0.05	31	1.696	0.927
50 vs. 500	3.472	0.05	30	1.697	0.999
5 vs. 500	4.4	0.05	28	1.7	1

The Poisson's ratio at 500 [mm/min] crosshead displacement rate appear to be statistically different to the other crosshead displacement rates, at 5% level of confidence. Therefore, there is indication that Poisson's ratio *is* dependent on the strain rate.

The statistics for the equality of variances test are presented in table D.4. The table columns are similar to those of table 4.17.

Table D.4: Hypothesis testing for equality of variances statistics of Poisson's ratio.

Crosshead Rate	F_0	α	df1	df2	F_{crit}	Level
5 vs. 50	1.76	0.05	17	18	2.29	0.87
50 vs. 500	1.402	0.05	18	13	2.583	0.721
5 vs. 500	2.47	0.05	17	13	2.6	0.94

The results presented in table D.4 suggest that there is no strong indication to reject the hypothesis that the variance of the Poisson's ratio at different crosshead displacement rates is statistically different for any of the possible pairs, at a significance level of 5%.

Distribution: Figure D.4 presents the probability density function plots of the Poisson's ratio (ν_{12}) at different crosshead displacement rates. Figure D.4(a) present the p.d.f. of the complete data set. Figures D.4 (b),(c) and (d) group the data set according to the crosshead displacement rate: 5, 50 and 500[mm/min] respectively.

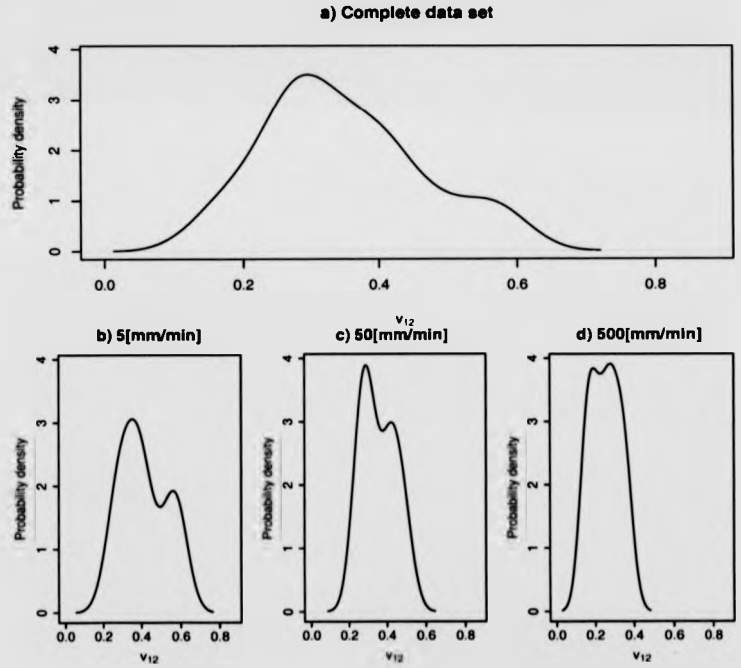

Figure D.4: Density plots of Poisson's ratio at a) all displacement rates, and b),c) and d) at each different crosshead displacement rate separately.

The p.d.f. of the Poisson's ratio for the complete data set (presented in figure D.4(a)) appears generally follow a normal distribution slightly skewed with 2 points of inflection. Figure D.4(b), D.4(c) and D.4(d)) appear to follow a normal distribution with two distinctive peaks. The secondary peaks are attributed to the sample size.

The computed values of the χ_0^2 statistic for the complete data set and for the different crosshead displacement rates are presented in table D.5, together with other information required for the calculations of the critical value.

Table D.5: Statistics for the Goodness-of-Fit of Poisson's ratio probability density function.

Crosshead Rate	χ_0^2	α	# of Classes	χ_{crit}^2	Level
ALL	1.25	0.05	6	7.815	0.259
5	5.235	0.05	6	7.815	0.845
50	2.667	0.05	6	7.815	0.554
500	2.231	0.05	6	7.815	0.474

According to the data from table D.5 there is no indication that at different crosshead displacement rates the Poisson's ratio results follow a Gaussian distribution.

Model fitting: A linear model of the Poisson's ratio with respect to the logarithm of the strain rate has the following form:

$$\nu_{12}(\dot{\varepsilon}_{11}) = 0.1716 - 0.0777 \cdot \log_{10}(\dot{\varepsilon}_{11}) \tag{D.1}$$

A quadratic model of the Poisson's ratio with respect to the logarithm of the strain rate has the following form:

$$\nu_{12}(\dot{\varepsilon}_{11}) = 0.1176 - 0.1353 \cdot \log_{10}(\dot{\varepsilon}_{11}) - 0.0133 \cdot \log_{10}(\dot{\varepsilon}_{11})^2 \tag{D.2}$$

The statistics for the comparison of the two strain rate models of Poisson's ratio are presented in table D.6. According to the data, the null hypothesis cannot be rejected i.e. the equation for the linear model (eq. D.1) describes adequately the set of results (strong conclusion).

Table D.6: ANOVA results for the selection of the strain rate model order of the Poisson's ratio.

Model	Res.Df	RSS	Df	Sum of Sq	F	$Pr(>F)$
Linear	46	0.43				
Quadratic	45	0.428	1	0.00218	0.23	0.634

The coefficient of determination R^2 value for the quadratic model is 0.282.

D.1.3 Strain Rate Effects On Strength

D.1.3.1 Longitudinal Tensile Failure Strain ε_{11}

Figure D.5 presents a conditional plot of the tensile failure strain with respect to the data acquisition source. There is no visible difference in the location (there is difference in scatter) between the 5 and 50[mm/min] crosshead displacement rates, however for the 500[mm/min] crosshead displacement rate a discrepancy in the trends is visible. The discrepancy is attributed to the better data acquisition capabilities of Instron, which allows higher sampling frequencies, thus allowing at high velocities the longitudinal tensile failure strain to be captured more accurately. This is the reason that the data acquired by Instron will be used for the statistical purposes.

Figure D.6 presents the longitudinal tensile failure strain vs. strain rate log and a linear and a quadratic model of the log of the strain rate are fitted. The labeled observation has been identified as an outlier and has not been included in the statistical treatment.

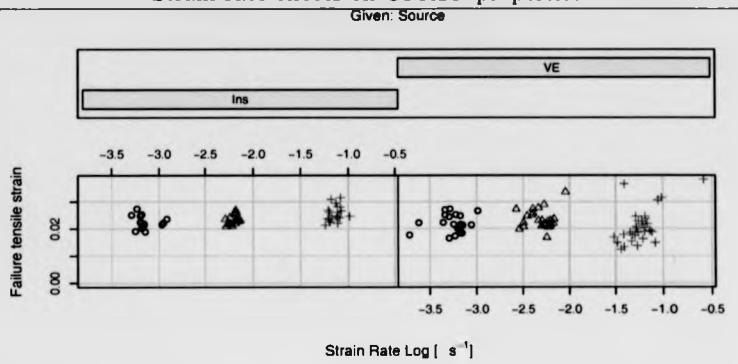

Figure D.5: Longitudinal tensile failure strain vs. logarithm of strain rate.

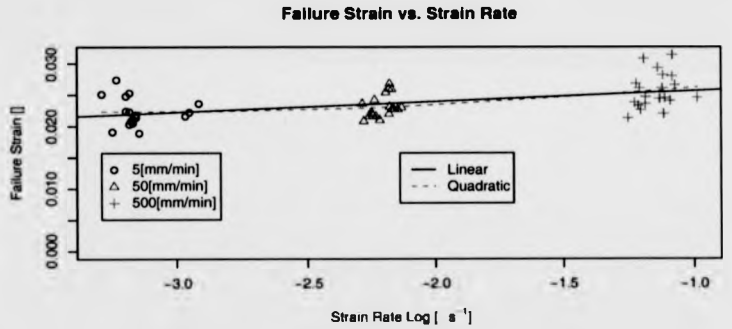

Figure D.6: Longitudinal tensile failure strain vs. strain rate logarithm.

Statistics: Table D.7 presents the statistics of longitudinal tensile failure strain at different crosshead displacement rates of a unidirectional laminate composite material.

The mean of longitudinal tensile failure strain increases for increasing displacement rate. The standard deviation is lowest for the 50[mm/min] crosshead displacement rate results and highest for the 500 [mm/min] crosshead displacement rate. Similarly, the coefficient of variance is lowest for the 50[mm/min] crosshead displacement rate results and highest at the 500 [mm/min] crosshead

Table D.7: Statistics for the longitudinal tensile failure strain at different crosshead displacement rates.

Crosshead Rate		5	50	500
Mean	[]	0.0223	0.0231	0.0256
Standard Deviation	[]	0.00231	0.00177	0.00283
Coef. of Variance	[]	0.1035	0.0767	0.1106

displacement rate.

Hypothesis testing: The null hypothesis (H_0) is that the longitudinal tensile failure strain is not strain rate dependent. Therefore, the mean of the longitudinal tensile failure strain for one crosshead displacement rate results should be equal to the mean of the longitudinal tensile failure strain for another crosshead displacement rate, e.g. $H_0 : \bar{\varepsilon}_{11,5} = \bar{\varepsilon}_{11,50}$. The alternative hypothesis is that the longitudinal tensile failure strain is strain rate dependent.

The statistics for the equality of means test are presented in table D.8. The table columns are similar to those of table 4.16.

Table D.8: Hypothesis testing statistics for equality of means of longitudinal tensile failure strain.

Crosshead Rate	t_0	α	df	t_{crit}	Level
5 vs. 50	1.215	0.05	31	1.696	0.883
50 vs. 500	3.341	0.05	33	1.692	0.999
5 vs. 500	3.97	0.05	36	1.69	1

The longitudinal tensile failure strain at 500[mm/min] crosshead displacement rate appear to be statistically different to the failure tensile strain at other crosshead displacement rates, at 5% level

of confidence. Therefore, there is indication that longitudinal tensile failure strain *is* dependent on the strain rate.

The statistics for the equality of variances test are presented in table D.9. The table columns are similar to those of table 4.17.

Table D.9: Hypothesis testing for equality of variances statistics of longitudinal tensile failure strain.

Crosshead Rate	F_0	α	df1	df2	F_{crit}	Level
5 vs. 50	1.69	0.05	17	19	2.25	0.86
50 vs. 500	2.557	0.05	20	19	2.203	0.974
5 vs. 500	1.509	0.05	20	17	2.288	0.795

The results presented in table D.9 suggest that only variances of the 5 and 50 [mm/min] crosshead displacement rate appear to be statistically different at a 5% significance level. Therefore, caution should be exercised in the interpretation of the regression analysis results.

Distribution: Figure D.7 presents the probability density function plots of the longitudinal tensile failure strain (ε_{11}) at different crosshead displacement rates. Figure D.7(a) present the p.d.f. of the complete data set. Figures D.7 (b),(c) and (d) group the data set according to the crosshead displacement rate: 5, 50 and 500[mm/min] respectively.

The p.d.f. of the longitudinal tensile failure strain which are presented in figure D.7(a) appears to have a primary and a secondary point of inflection. The low D.7(b) and high D.7(d) crosshead displacement rates (5 and 500[mm/min]) appear to follow a normal distribution with a secondary point of inflection. The p.d.f. for the 50[mm/min] crosshead displacement rate in figure D.7(c)

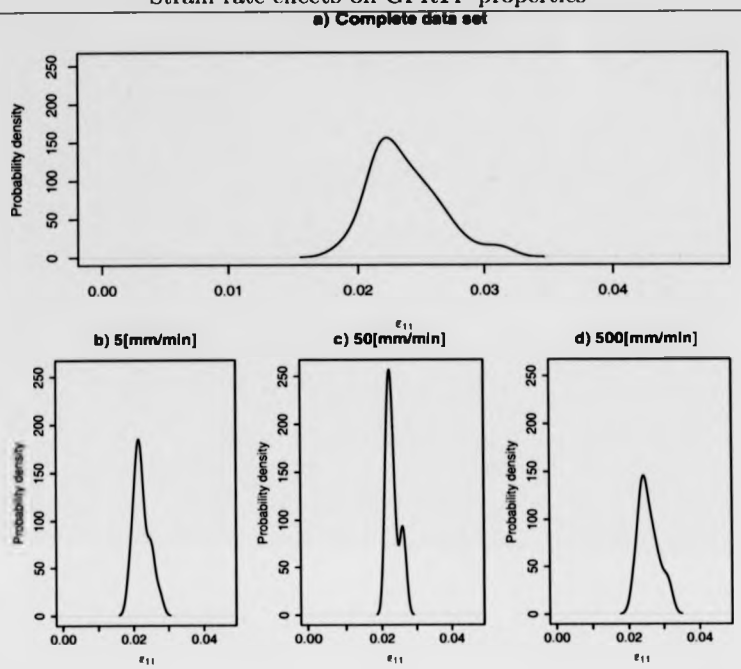

Figure D.7: Density plots of longitudinal tensile failure strain at a) all displacement rates, and b),c) and d) at each different crosshead displacement rate separately.

appears to follow a distribution with a primary and a secondary peak (there are two peaks present). The computed values of the χ_0^2 statistic for the complete data set and for the different crosshead displacement rates are presented in table D.10, together with other information required for the calculations of the critical value.

According to the data in table D.10, there is no indication that the probability distributions of the longitudinal tensile failure strain do not follow the normal distribution.

Table D.10: Statistics for the Goodness-of-Fit of longitudinal tensile failure strain probability density distribution.

Crosshead Rate	χ_0^2	α	# of Classes	χ_{crit}^2	Level
ALL	3.36	0.05	6	7.81	0.66
5	3.118	0.05	6	7.815	0.626
50	7.211	0.05	6	7.815	0.935
500	1.6	0.05	6	7.815	0.341

Model fitting: A linear model of the longitudinal tensile failure strain with respect to the logarithm of the strain rate has the following form:

$$\varepsilon_{11}(\dot{\varepsilon}_{11}) = 0.0274 + 0.00172 \cdot \log_{10}(\dot{\varepsilon}_{11}) \tag{D.3}$$

A quadratic model of the longitudinal tensile failure strain with respect to the logarithm of the strain rate has the following form:

$$\varepsilon_{11}(\dot{\varepsilon}_{11}) = 0.030811 + 0.005494 \cdot \log_{10}(\dot{\varepsilon}_{11}) + 0.000887 \cdot \log_{10}(\dot{\varepsilon}_{11})^2 \tag{D.4}$$

The statistics for the comparison of the two strain rate models of longitudinal tensile failure strain are presented in table D.11. According to the data, the null hypothesis cannot be rejected, i.e. the equation for the linear model (eq. D.3) describes adequately the set of results.

The coefficient of determination R^2 value for the linear model for longitudinal tensile failure strain is 0.259.

Table D.11: ANOVA results for the selection of the strain rate model order of the longitudinal tensile failure strain.

Model	Res.Df	RSS	Df	Sum of Sq	F	$Pr(>F)$
Linear	54	0.000298				
Quadratic	53	0.000287	1	1.08e-05	1.99	0.164

D.1.3.2 Longitudinal Tensile Failure Stress σ_{11}

Figure D.8 presents a conditional plot of the longitudinal tensile failure stress with respect to the data acquisition source. There is no visible difference between the two data acquisition sources so both of them will be used.

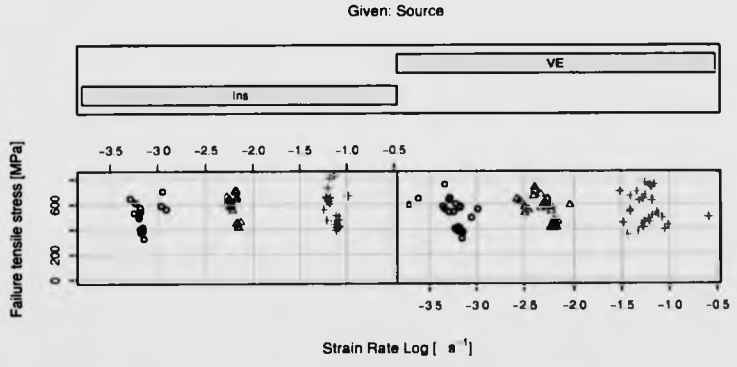

Figure D.8: Longitudinal tensile failure stress vs. logarithm of strain rate.

Figure D.9 presents the longitudinal tensile failure stress vs. strain rate log and a linear and a quadratic model of the log of the strain rate are fitted.

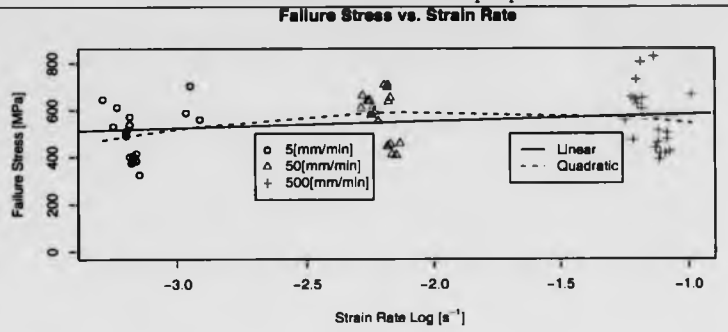

Figure D.9: Longitudinal tensile failure stress vs. strain rate logarithm.

Statistics: Table D.12 presents the statistics of the longitudinal tensile failure stress at different crosshead displacement rates of a unidirectional laminate composite material.

Table D.12: Statistics for the longitudinal tensile failure stress at different crosshead displacement rates.

Crosshead Rate		5	50	500
Mean	[MPa]	496.47	581.68	564.2
Standard Deviation	[MPa]	109.88	99.71	133.03
Coef. of Variance		0.221	0.171	0.236

The mean of the longitudinal tensile failure stress increases initially for increasing crosshead displacement rate from 5 to 50[mm/min]. Further increase of the crosshead displacement rate to 500[mm/min] crosshead displacement rate resulted in a decrease of the longitudinal tensile failure stress. In figure D.9, both models appear to increase with strain rate. The standard deviation is lowest for the 50[mm/min] crosshead displacement rates and highest at the 500 [mm/min] crosshead displacement rate. Similarly, the coefficient of variance is lowest for the 50[mm/min]

crosshead displacement rate and highest at the 500 [mm/min] crosshead displacement rate.

Hypothesis testing: The null hypothesis (H_0) is that the longitudinal tensile failure stress is not strain rate dependent. Therefore, the mean of the longitudinal tensile failure stress for one crosshead displacement rate results should be equal to the mean of the longitudinal tensile failure stress for another crosshead displacement rate, e.g. $H_0 : \overline{\sigma}_{11,5} = \overline{\sigma}_{11,50}$. The alternative hypothesis is that the longitudinal tensile failure stress is strain rate dependent.

The statistics for the equality of means test are presented in table D.13. The table columns are similar to those of table 4.16.

Table D.13: Hypothesis testing statistics for equality of means of longitudinal tensile failure stress.

Crosshead Rate	t_0	α	df	t_{crit}	Level
5 vs. 50	2.43	0.05	34.00	1.69	0.99
50 vs. 500	0.466	0.05	36.000	1.688	0.678
5 vs. 500	1.696	0.05	36.000	1.688	0.951

The longitudinal tensile failure stress at 5[mm/min] crosshead displacement appears to be statistically different to the longitudinal tensile failure stress at other crosshead displacement rates at 5% confidence level. Therefore, there is strong indication that longitudinal tensile failure stress *is* dependent on the strain rate.

The statistics for the equality of variances test are presented in table D.14. The table columns are similar to those of table 4.17.

The results presented in table D.14 suggest that there is *no* strong indication that the variance of the longitudinal tensile failure stress changes with crosshead displacement rate.

Table D.14: Hypothesis testing for equality of variances statistics of longitudinal tensile failure stress.

Crosshead Rate	F_0	α	df1	df2	F_{crit}	Level
5 vs. 50	1.214	0.05	17	19	2.25	0.657
50 vs. 500	1.78	0.05	20	19	2.203	0.886
5 vs. 500	1.466	0.05	20	17	2.288	0.778

Distribution: Figure D.10 presents the probability density function plots of the longitudinal tensile failure stress (σ_{11}) at different crosshead displacement rates. Figure D.10(a) present the p.d.f. of the complete data set. Figures D.10 (b),(c) and (d) group the data set according to the crosshead displacement rate: 5, 50 and 500[mm/min] respectively.

The p.d.f. of the longitudinal tensile failure stress for the complete data set (figure D.10(a)) and the 5[mm/min crosshead displacement rate (see figure D.10(b)) appear to have two distinct peaks, indicating two distinct populations. The p.d.f. for the 50 (D.10(c)) and 500[mm/min] (figure D.10(d)) crosshead displacement rates appear to follow a distribution with a primary peak and a secondary point of inflection. In all cases, a secondary peak can be distinguished indicating two distinct populations. This is attributed to the variability imposed by the manufacturing route, which effects primarily the strength of the material.

The computed values of the χ_0^2 statistic for the complete data set and for the different crosshead displacement rates are presented in table D.15, together with other information required for the calculations of the critical value.

According to the results presented in table D.15 there is no strong indication that the p.d.f. of the longitudinal tensile failure stress at all crosshead displacement rate groups does not follow normal

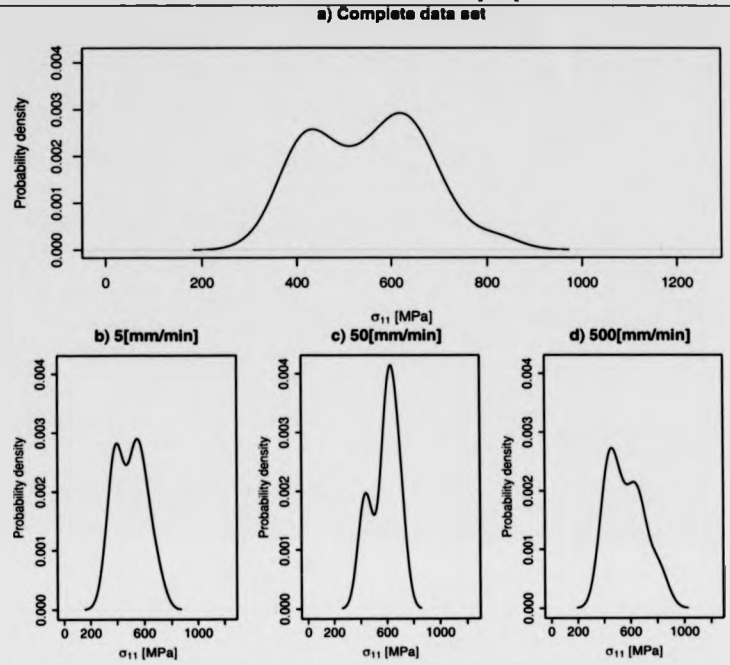

Figure D.10: Density plots of longitudinal tensile failure stress at a) all displacement rates, and b),c) and d) at each different crosshead displacement rate separately.

Table D.15: Statistics for the Goodness-of-Fit of longitudinal tensile failure stress distribution.

Crosshead Rate	χ_0^2	α	# of Classes	χ_{crit}^2	Level
ALL	6.357	0.05	6	7.815	0.905
5	1.706	0.05	6	7.815	0.364
50	5.947	0.05	6	7.815	0.886
500	4.000	0.05	6	7.815	0.739

distribution, however, the complete data set pdf has the highest χ^2 value.

Model fitting: A linear model of the longitudinal tensile failure stress with respect to the logarithm of the strain rate has the following form:

$$\sigma_{11}(\dot{\varepsilon}_{11}) = 612.31 + 29.67 \cdot \log_{10}(\dot{\varepsilon}_{11}) \tag{D.5}$$

A quadratic model of the longitudinal tensile failure stress with respect to the logarithm of the strain rate has the following form:

$$\sigma_{11}(\dot{\varepsilon}_{11}) = 374.26 - 233.23 \cdot \log_{10}(\dot{\varepsilon}_{11}) - 61.8 \cdot \log_{10}(\dot{\varepsilon}_{11})^2 \tag{D.6}$$

The statistics for the comparison of the two strain rate models of tensile longitudinal tensile failure stress are presented in table D.16. The null hypothesis is not rejected, i.e. the equation for the linear model (eq. D.5) describes adequately the set of results (weak conclusion).

Table D.16: ANOVA results for the selection of the strain rate model order of the longitudinal tensile failure stress.

Model	Res.Df	RSS	Df	Sum of Sq	F	$Pr(>F)$
Linear	54.00	7.47e+05				
Quadratic	53.00	6.95e+05	1.00	52267.71	3.99	0.051

The coefficient of determination R^2 value for the linear model is 0.0247, which is extremely low. The fitted model only explains 2.47% of the variability of the data. Therefore, other factors (like choice of manufacturing route) effect the longitudinal tensile failure stress more significantly. This outcome indicates the importance of manufacturing route on the material properties.

Despite the fact that the variability was significant, the statistical process revealed strain rate captured the strain rate dependency, which infers marked strain rate dependency of the longitudinal tensile failure stress. This is supported by figure D.9 where it is possible to observe that the highest values of longitudinal tensile failure stress for each crosshead displacement rate appear to increase with strain rate.

D.1.4 Strain Energy Density Up To Failure

Figure D.11 presents a conditional plot of the strain energy density up to failure with respect to the data acquisition source. There is no visible difference in the location (there is difference in scatter) in the mean between the two data acquisition sources, however the Instron results will be used because of the lowest scatter.

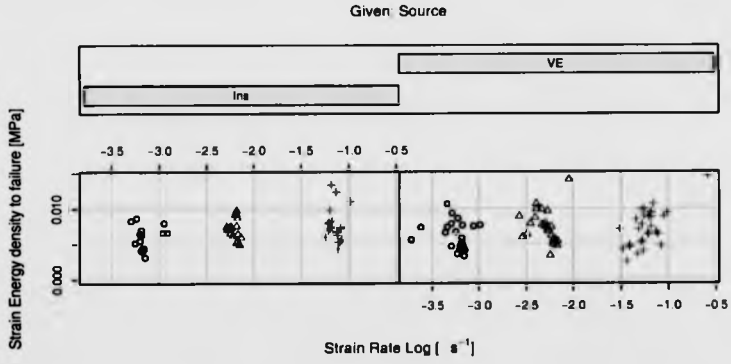

Figure D.11: Strain energy density up to failure vs. logarithm of strain rate.

Figure D.12 presents the strain energy density to failure vs. strain rate log and a linear and a quadratic model of the log of the strain rate are fitted.

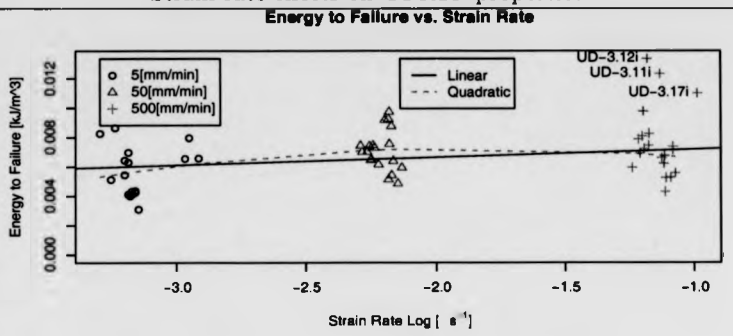

Figure D.12: Strain energy density to failure vs. strain rate logarithm.

Statistics: Table D.17 presents the statistics of the Strain energy density up to failure at different crosshead displacement rates of a unidirectional laminate composite material.

Table D.17: Statistics for the strain energy density up to failure at different strain rates.

Crosshead Rate	5	50	500
Mean	0.00568	0.0071	0.00683
Standard Deviation	0.00168	0.00138	0.00133
Coef. of Variance	0.296	0.195	0.195

The mean of strain energy increase with crosshead displacement rate and then marginally decreases for further increases of the crosshead displacement rate. The standard deviation is lowest at 500 [mm/min] crosshead displacement rate and highest for the 5[mm/min] crosshead displacement rate results. The coefficient of variance is lowest for the 50 and 500[mm/sec] crosshead displacement rate and highest at the 5[mm/min] crosshead displacement rate.

Hypothesis testing: The null hypothesis (H_0) is that the strain energy density up to failure is not strain rate dependent. Therefore, the mean of the strain energy density to failure for one crosshead displacement rate results should be equal to the mean of the energy density to failure for another crosshead displacement rate, e.g. H_0 : $\overline{SE}_{11,5} = \overline{SE}_{11,50}$. The alternative hypothesis is that the strain energy density to failure is strain rate dependent.

The statistics for the equality of means test are presented in table D.18. The table columns are similar to those of table 4.16.

Table D.18: Hypothesis testing statistics for equality of means of strain energy density to failure.

Crosshead Rate	t_0	α	df	t_{crit}	Level
5 vs. 50	2.752	0.05	32	1.694	0.995
50 vs. 500	0.608	0.05	35	1.69	0.726
5 vs. 500	2.204	0.05	32	1.694	0.983

The failure strain energy density at 5[mm/min] crosshead displacement appears to be statistically different to the failure strain energy density at other crosshead displacement rates at 5% confidence level. Therefore, there *is* indication that strain energy density to failure *is* dependent on the strain rate.

The statistics for the equality of variances test are presented in table D.19. The table columns are similar to those of table 4.17.

The results presented in table D.19 suggest that there is no strong indication to reject the hypothesis that the variance of the energy density to failure at different crosshead displacement rates is statistically different for any of the possible pairs.

Table D.19: Hypothesis testing for equality of variances statistics of strain energy density to failure.

Crosshead Rate	F_0	α	df1	df2	F_{crit}	Level
5 vs. 50	1.478	0.05	17	19	2.25	0.789
50 vs. 500	1.079	0.05	19	17	2.302	0.557
5 vs. 500	1.59	0.05	17	17	2.33	0.82

Distribution: Figure D.13 presents the probability density function plots of the energy density to failure at different crosshead displacement rates. Figure D.13(a) present the p.d.f. of the complete data set. Figures D.13 (b),(c) and (d) group the data set according to the crosshead displacement rate: 5, 50 and 500[mm/min] respectively.

The probability distribution of the material's strain energy density to failure appears to retain a Gaussian distribution shape at all crosshead displacement rates. The p.d.f. of the strain energy density to failure in figure D.13(a) appears to have a primary peak and two secondary points of inflection. The 5[mm/min] and 500[mm/min] crosshead displacement rates presented respectively in (figure D.13(b) and D.13(d)) appear to follow a normal distribution with one secondary of inflection on the higher values side. It appears that the results for the 50[mm/min] D.13(c) also follow a normal distribution but there is a distinctive peak present for increasing values of the strain energy density.

The computed values of the χ_0^2 statistic for the complete data set and for the different crosshead displacement rates are presented in table D.20, together with other information required for the calculations of the critical value.

All the different distributions of failure strain energy density appear to follow a normal distribution.

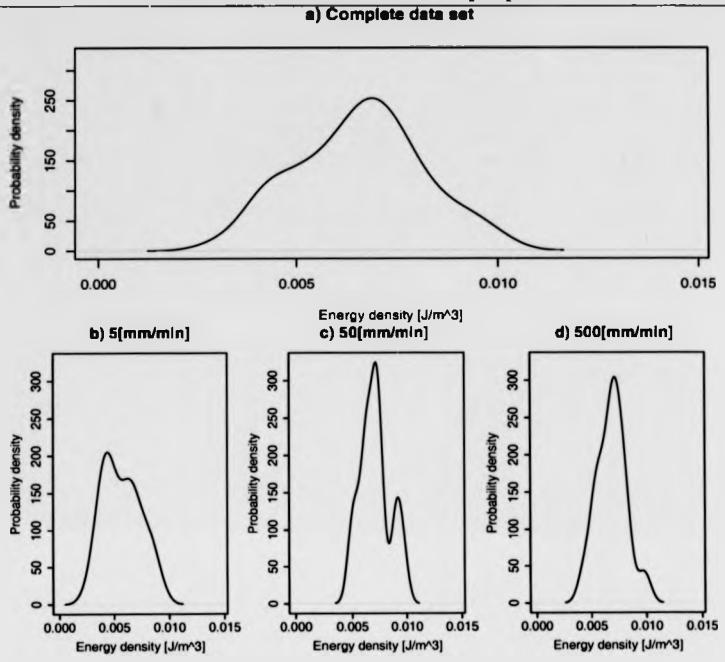

Figure D.13: Density plots of strain energy density up to failure at a) all displacement rates, and b),c) and d) at each different crosshead displacement rate separately.

Table D.20: Statistics for the Goodness-of-Fit of strain energy density to failure distribution.

Crosshead Rate	χ_0^2	α	# of Classes	χ_{crit}^2	Level
ALL	0.5472	0.05	6	7.8147	0.0916
5	3.824	0.05	6	7.815	0.719
50	5.947	0.05	6	7.815	0.886
500	1	0.05	6	7.815	0.199

Model fitting: A linear model of the strain energy up to failure with respect to the logarithm of the strain rate has the following form:

$$S.E.(\dot{\varepsilon}_{11}) = 0.007728 + 0.000539 \cdot \log_{10}(\dot{\varepsilon}_{11}) \tag{D.7}$$

A quadratic model of the strain energy up to failure with respect to the logarithm of the strain rate has the following form:

$$S.E.(\dot{\varepsilon}_{11}) = 0.004003 + -0.003502 \cdot \log_{10}(\dot{\varepsilon}_{11}) - 0.000942 \cdot \log_{10}(\dot{\varepsilon}_{11})^2 \tag{D.8}$$

The null hypothesis for the analysis of variance is that the linear model explains the behaviour as adequately as the quadratic model. The statistics for the comparison of the two strain rate models of tensile strain energy up to failure are presented in table D.21. The null hypothesis is rejected, i.e. the equation for the quadratic model (eq. D.8) describes better the set of results.

Table D.21: ANOVA results for the selection of the strain rate model order of the strain energy up to failure.

Model	Res.Df	RSS	Df	Sum of Sq	F	$Pr(>F)$
Linear	51	0.000118				
Quadratic	50	0.000106	1	1.16e-05	5.45	0.0236

The coefficient of determination R^2 value for the linear model is 0.136, which is quite low. It should be noted that although statistically it appears that the quadratic model describes better the data set, that does not necessarily mean that the physics should follow a linear model.

D.2 Properties Obtained From $[\pm 45^\circ]_4$ Test.

D.2.1 Shear Strain Rate.

Figure D.14 presents the logarithm of the measured shear strain rate of the material vs. the crosshead displacement rate.

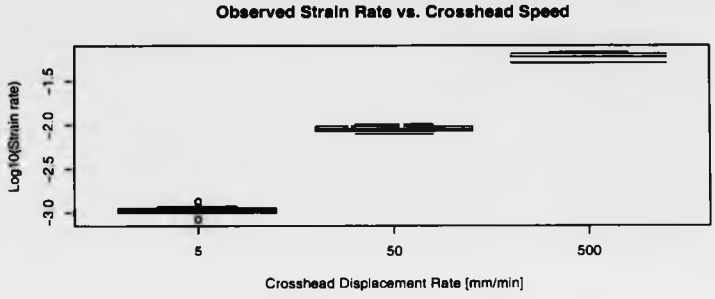

Figure D.14: Logarithm of shear strain rate vs. Crosshead displacement rate as obtained from the tensile testing of a $[\pm 45]_{2s}$ laminate.

Statistics: Table D.22 presents the statistics of the measured shear strain rate at different crosshead displacement rates.

Table D.22: Statistics for measured shear strain rate at different crosshead displacement rates.

Crosshead Rate	5	50	500	
Mean	log[1/s]	-2.97	-2.04	-1.24
Standard Deviation	log[1/s]	0.0635	0.0388	0.0559
Coef. of Variance		0.0213	0.019	0.0452

The mean of the logarithm of shear strain rate increases by approximately .9 per test. The standard

deviation appears to be in the same order of magnitude for the different crosshead displacement rates and the lowest value for standard deviation is for the 50[mm/min] crosshead displacement rate. The lowest value for the coefficient of variance is for the 5[mm/min] crosshead displacement rate.

D.2.2 Strain Rate Effects On Elasticity

D.2.2.1 Shear Modulus G_{12}

Figure D.15 presents the conditional plot of Shear modulus vs. shear strain rate with respect to data acquisition source and Failure location. The discrepancy of the trends between the sources of acquired data led use of the Instron data for the statistical analysis.

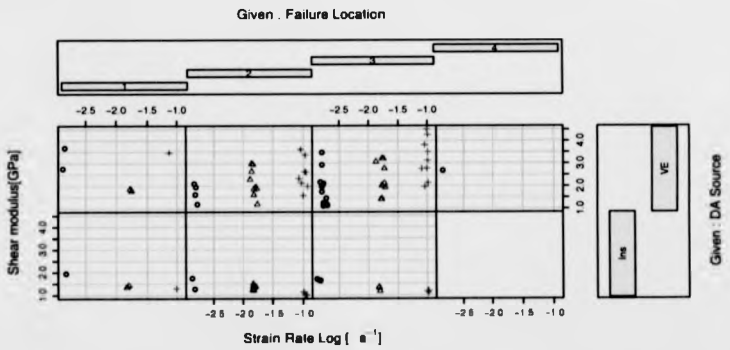

Figure D.15: Conditional plot of Shear modulus vs. logarithm of shear strain rate as obtained from the tensile testing of a $[\pm 45]_{2s}$ laminate, conditioned with respect of data acquisition source and Failure location.

Figure D.16 presents the Shear modulus vs. shear strain rate and two models (a linear and a quadratic model) of the logarithm of the shear strain rate are fitted. The labeled results on figure

D.16 were regarded outliers and were not included in the subsequent statistical treatment.

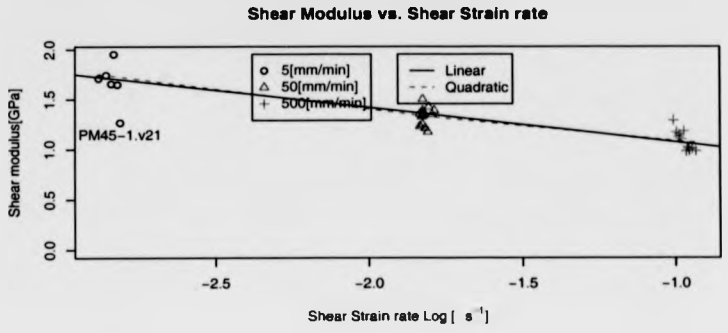

Figure D.16: Shear modulus vs. logarithm of shear strain rate as obtained from the tensile testing of a $[\pm 45]_{2s}$ laminate.

Statistics: Table D.23 presents the statistics of the shear modulus at different crosshead displacement rates as obtained from a $[\pm 45]_{2s}$ laminate.

Table D.23: Statistics for shear modulus at different crosshead displacement rates as obtained from a $[\pm 45]_{2s}$ laminate.

Crosshead Rate		5	50	500
Mean	[GPa]	1.74	1.33	1.08
Standard Deviation	[GPa]	0.124	0.0919	0.098
Coef. of Variance	[]	0.0712	0.0691	0.0907

The mean of the shear modulus appears to decrease with crosshead displacement rate. The standard deviation of the 50[mm/min] is the lowest. The standard deviation is lowest for the 50[mm/min] crosshead displacement rate and highest for the 5[mm/min] crosshead displacement

rate. Similarly the coefficient of variance is lowest for the 500[mm/min] crosshead displacement rate.

Hypothesis testing: The null hypothesis (H_0) is that shear modulus is not strain rate dependent. Therefore, the mean of the shear modulus for one crosshead displacement rate results should be equal to the mean of the shear modulus for another crosshead displacement rate, e.g. $H_0: \overline{G_{12,5}} = \overline{G_{12,50}}$. The alternative hypothesis (H_1 which is accepted automatically if the null hypothesis is rejected) is that shear modulus is shear strain rate dependent.

The statistics for the equality of means test are presented in table D.24. The table presents the calculated test statistic t_0, the α-type error probability, the degrees of freedom df and the calculated critical value t_{crit}. In the final column, the level of confidence is presented (i.e. the value of α-type error probability for which the calculated critical value t_{crit} is equal to the statistic t_0).

Table D.24: Hypothesis testing statistics for the equality of means of shear modulus.

Crosshead Rate	t_0	α	df	t_{crit}	Level
5 vs. 50	6.74	0.05	6	1.94	1
50 vs. 500	6.7	0.05	25	1.71	1
5 vs. 500	10.7	0.05	7	1.9	1

The shear modulus at different crosshead displacement rates is statistically different for all the possible pairs for a 5% α-type error. Therefore, there is strong indication that shear modulus *is* dependent on the strain rate. The level of confidence is high, and for the pair of 5 and 500[mm/min] crosshead displacement rates results it is practically 100%.

The statistics for the equality of variances test are presented in table D.25. The table presents the

calculated test statistic F_0, the α-type error probability, the degrees of freedom $df1$ and $df2$ and the calculated critical value F_{crit}. In the last column, the level of confidence is presented (i.e. the value of α-type error for which the critical value (F_{crit}) is equal to the statistic (F_0)).

Table D.25: Hypothesis testing for equality of variances statistics of shear modulus.

Crosshead Rate	F_0	α	df1	df2	F_{crit}	Level
5 vs. 50	1.82	0.05	5	13	3.26	0.81
50 vs. 500	1.138	0.05	13	13	2.687	0.587
5 vs. 500	1.601	0.05	5	13	3.259	0.763

The results presented in table D.25 suggest that the variances at all crosshead displacement rate are statistically equal at a 5% α-type error.

Distribution: Figure D.17 presents the probability density function plots of the shear modulus (G_{12}) at different crosshead displacement rates. Figure D.17(a) present the p.d.f. of the complete data set. Figures D.17 (b),(c) and (d) group the data set according to the crosshead displacement rate: 5, 50 and 500[mm/min] respectively.

The p.d.f. of the shear modulus which are presented in figure D.17(a) appears follow a skewed distribution with several peaks and points of inflection. The 5[mm/min] crosshead displacement rate (see figure D.17(b)) appears to follow a normal distribution with a distinctive secondary peak. The 50 and 500[mm/min] crosshead displacement rates (respectively figures D.17(c) and D.17(d))appear to follow a normal distribution, with a secondary point of inflection.

The computed values of the χ_0^2 statistic for the complete data set and for the different crosshead displacement rates are presented in table D.26, together with other information required for the

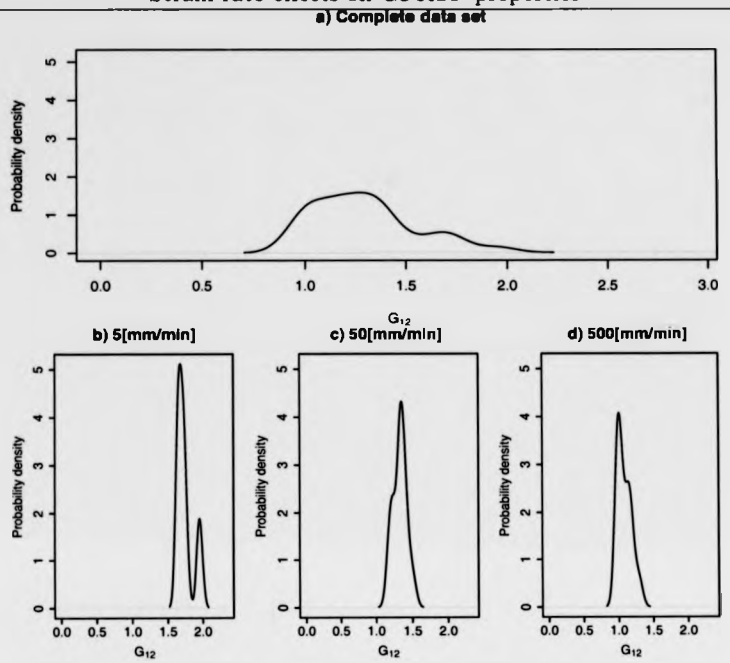

Figure D.17: Density plots of the shear modulus of at a) all displacement rates, and b),c) and d) at each different crosshead displacement rate separately.

calculations of the critical value.

If the computed χ_0^2 statistic is smaller than the χ_{crit}^2 the conclusion is that there is no reason to reject the assumption that the distribution of the shear modulus is normally distributed.

The results in table D.26 suggest all of the examined groups of crosshead displacement rate appear to follow a normal distribution.

Table D.26: Statistics for the Goodness-of-Fit of Shear modulus probability density distribution.

Crosshead Rate	χ_0^2	α	# of Classes	χ_{crit}^2	Level
ALL	11.68	0.05	9	16.81	0.93
5	3.4	0.05	6	7.815	0.666
50	3.154	0.05	6	7.815	0.631
500	6.846	0.05	6	7.815	0.923

Model fitting: A linear model of the shear modulus with respect to the logarithm of the shear strain rate has the following form:

$$G_{12}(\dot{\gamma}_{12}) = 0.731 - 0.344 \cdot \log_{10}(\dot{\gamma}_{12}) \tag{D.9}$$

A quadratic model of the shear modulus with respect to the logarithm of the shear strain rate has the following form:

$$G_{12}(\dot{\gamma}_{12}) = 0.8735 - 0.1625 \cdot \log_{10}(\dot{\gamma}_{12}) + 0.0497 \cdot \log_{10}(\dot{\gamma}_{12})^2 \tag{D.10}$$

The null hypothesis for the analysis of variance is that the linear model explains the behaviour as adequately as the quadratic model. The statistics for the comparison of the two shear strain rate models of shear modulus are presented in table D.27. The 24.8% probability which is presented in the table D.27 is the probability that the null hypothesis is true but instead the null hypothesis is rejected. In this case, accepting that the quadratic model explain better the variability of the data is related to a probability of 24.8% that the assumption is wrong. Usually α type of error higher than 5% are considered unacceptable, and therefore the null hypothesis is not rejected, i.e. the equation for the linear model (eq. D.9) describes adequately the set of results.

The coefficient of determination R^2 value for the quadratic model is 0.847, which is very high, and

Table D.27: ANOVA results for the selection of the shear strain rate model order for the shear modulus.

Model	Res.Df	RSS	Df	Sum of Sq	F	$Pr(>F)$
Linear	29	0.284				
Quadratic	28	0.27	1	0.0134	1.39	0.248

indicates good correlation.

D.2.3 Strain Rate Effects On Strength.

D.2.3.1 Shear Failure Strain γ_{12}

Figure D.18 presents the conditional plot of shear failure strain vs. shear strain rate with respect to data acquisition source and Failure location. The discrepancy of the trends between the sources of acquired data led use of the Instron data for the statistical analysis.

Figure D.19 presents the shear failure strain vs. shear strain rate log and a linear and a quadratic model of the log of the shear strain rate is fitted. The labeled results were regarded outliers and were not included in the subsequent statistical treatment.

Statistics: Table D.28 presents the statistics of shear failure strain at different crosshead displacement rates of $[\pm 45°]_{2s}$ laminate.

The mean of shear failure strain decreases from 43.8% to 40.6% and further increases to 42.3% for increasing crosshead displacement rate. The standard deviation is lowest at the 500[mm/min] crosshead displacement rate and is highest at the 5 and 50[mm/min] crosshead displacement rate. The coefficient of variance is lowest for the 500 [mm/min] crosshead displacement rate and highest

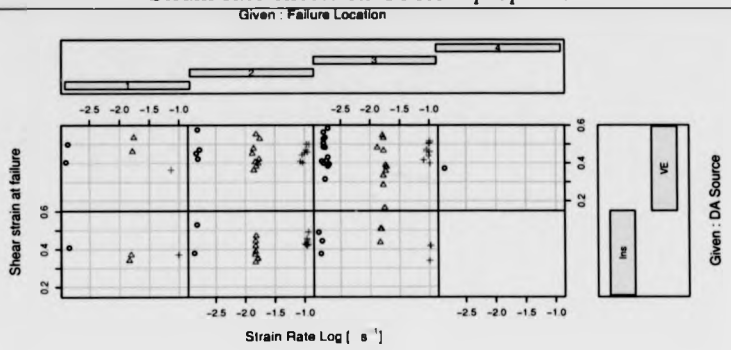

Figure D.18: Conditional plot of shear strain at failure vs. logarithm of shear strain rate as obtained from the tensile testing of a $[\pm 45]_{2s}$ laminate, conditioned with respect of data acquisition source and failure location.

Table D.28: Statistics for the shear failure strain at different crosshead displacement rates.

Crosshead Rate		5	50	500
Mean	[]	0.438	0.406	0.423
Standard Deviation	[]	0.0618	0.0618	0.0368
Coef. of Variance	[]	0.1412	0.1523	0.0871

for the 50[mm/min] crosshead displacement rate.

Hypothesis testing: The null hypothesis (H_0) is that the shear failure strain is not strain rate dependent. Therefore, the mean of the shear failure strain for one crosshead displacement rate results should be equal to the mean of the shear failure strain for another crosshead displacement rate, e.g. $H_0 : \overline{\gamma}_{12,5} = \overline{\gamma}_{12,50}$. The alternative hypothesis is that the shear failure strain is shear strain rate dependent.

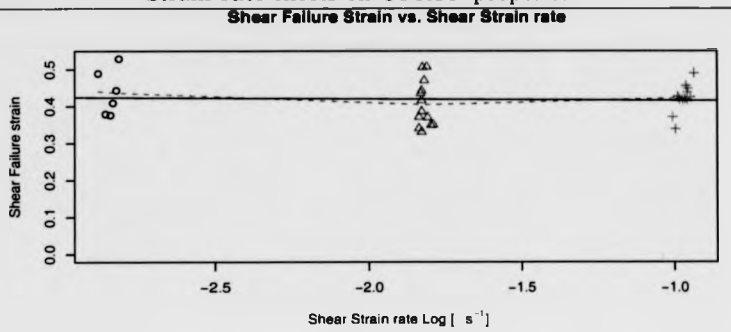

Figure D.19: Shear failure strain vs. shear strain rate logarithm.

The statistics for the equality of means test are presented in table D.29. The table columns present similar information to those of table D.24.

Table D.29: Hypothesis testing statistics for equality of means of shear failure strain.

Crosshead Rate	t_0	α	df	t_{crit}	Level
5 vs. 50	1.046	0.05	11	1.796	0.841
50 vs. 500	0.856	0.05	20	1.725	0.799
5 vs. 500	0.544	0.05	7	1.895	0.698

The shear failure strain does not appear to be statistically different at a 5% level of confidence by changes of the crosshead displacement rate. There is *no* indication that the shear failure strain is shear strain rate dependent.

The statistics for the equality of variances test are presented in table D.30. The table columns present similar information to those of table D.25.

The results presented in table D.30 suggest that there is strong indication to reject the hypothesis that the variance of the shear failure strain between the 50 and 500[mm/min] different crosshead

Table D.30: Hypothesis testing for equality of variances statistics of shear failure strain.

Crosshead Rate	F_0	α	df1	df2	F_{crit}	Level
5 vs. 50	1.001	0.05	13	6	4.678	0.459
50 vs. 500	2.814	0.05	13	13	2.687	0.957
5 vs. 500	2.811	0.05	6	13	3.106	0.934

displacement rates is statistically different at a 5% significance level.

Distribution: Figure D.20 presents the probability density function plots of the shear failure strain (γ_{12}) at different crosshead displacement rates. Figure D.20(a) present the p.d.f. of the complete data set. Figures D.20 (b),(c) and (d) group the data set according to the crosshead displacement rate: 5, 50 and 500[mm/min] respectively.

The p.d.f. of the shear failure strain which is presented in figure D.20(a) appears to follow a normal distribution a number of secondary points of inflection (which indicates that the result might come from different populations). The 5 and 50[mm/min] crosshead displacement rates (respectively figures D.20(b) and D.20(c)) appear to follow a skewed normal distribution with a single secondary point of inflection. Finally, the shear failure strain p.d.f. at the 500[mm/min] crosshead displacement rate in figure D.20(d) appears to follow a tighter distribution however a number of secondary peaks are present.

The computed values of the χ_0^2 statistic for the complete data set and for the different crosshead displacement rates are presented in table D.31, together with other information required for the calculations of the critical value.

The values in table D.31 suggest that all different groupings of the shear failure strain results

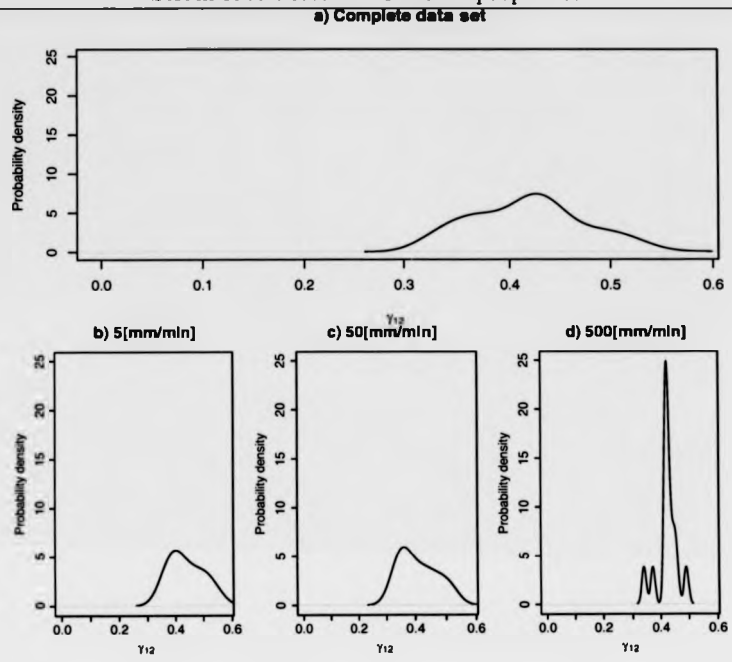

Figure D.20: Density plots of shear failure strain at a) all displacement rates, and b),c) and d) at each different crosshead displacement rate separately.

follow a normal distribution.

Model fitting: The shear failure strain at different crosshead displacement was not statistically different, which is in accordance to observations in the figure D.19.

Since no strain rate dependency was statistically determined for the shear failure stress, the mean value of the complete data set is used. This value was computed 41.85[].

Table D.31: Statistics for the Goodness-of-Fit of shear failure strain probability density distribution.

Crosshead Rate	χ_0^2	α	# of Classes	χ_{crit}^2	Level
ALL	1.375	0.05	6	7.815	0.289
5	2	0.05	6	7.815	0.428
50	3.154	0.05	6	7.815	0.631
500	5.923	0.05	6	7.815	0.885

D.2.3.2 Shear Failure Stress τ_{12}.

Figure D.21 presents the conditional plot of shear failure stress vs. shear strain rate with respect to data acquisition source and Failure location.

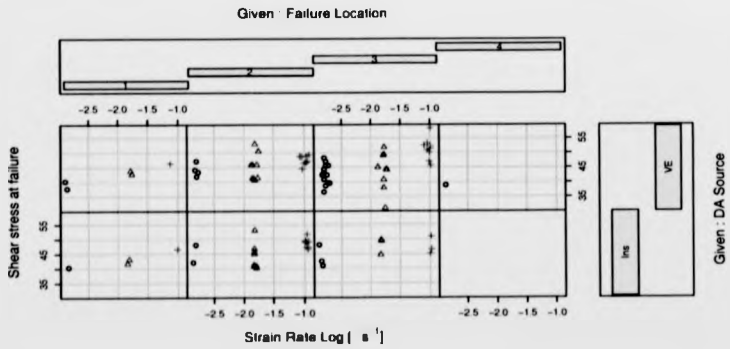

Figure D.21: Conditional plot of Shear stress at failure vs. logarithm of shear strain rate as obtained from the tensile testing of a $[\pm 45]_{2s}$ laminate, conditioned with respect of data acquisition source and failure location.

Figure D.22 presents the shear failure stress vs. shear strain rate log and a linear and a quadratic

model of the log of the shear strain rate are fitted. The labeled items were regarded outliers and were not included in the subsequent statistical treatment.

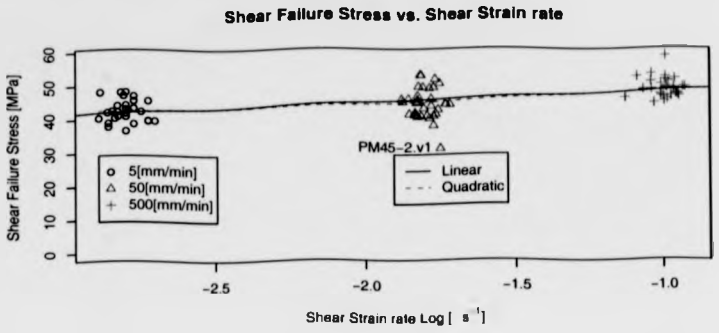

Figure D.22: Shear failure stress vs. shear strain rate logarithm.

Statistics: Table D.32 presents the statistics of the shear failure stress at different crosshead displacement rates.

Table D.32: Statistics for the shear failure stress at different crosshead displacement rates.

Crosshead Rate		5	50	500
Mean	[GPa]	42.57	44.87	48.85
Standard Deviation	[GPa]	3.32	4	2.9
Coef. of Variance	[GPa]	0.078	0.0891	0.0594

The mean of the shear failure stress increases with strain rate. The standard deviation of the shear failure stress at 500[mm/min] crosshead displacement rate is lowest and the highest standard deviation for the shear failure stress is at the 50[mm/min] crosshead displacement rate. Similarly the lowest coefficient of variance is for the shear failure stress at 500[mm/min] crosshead displacement

rate and the highest is for the shear failure stress at 50[mm/min] crosshead displacement rate.

Hypothesis testing: The null hypothesis (H_0) is that the shear failure stress is not strain rate dependent. Therefore, the mean of the shear failure stress for one crosshead displacement rate results should be equal to the mean of the shear failure stress for another crosshead displacement rate, e.g. $H_0 : \overline{\tau}_{12,5} = \overline{\tau}_{12,50}$. The alternative hypothesis is that the shear failure stress is shear strain rate dependent.

The statistics for the equality of means test are presented in table D.33. The table columns present similar information to those of table D.24.

Table D.33: Hypothesis testing statistics for equality of means of shear failure stress.

Crosshead Rate	t_0	α	df	t_{crit}	Level
5 vs. 50	2.428	0.05	59	1.671	0.991
50 vs. 500	4.57	0.05	60	1.67	1
5 vs. 500	7.61	0.05	53	1.67	1

The shear failure stress at all crosshead displacement rate groups are statistically different at 5% confidence level. Therefore, there *is* strong indication that shear failure stress is dependent on the strain rate.

The statistics for the equality of variances test are presented in table D.34. The table columns present similar information to those of table D.25.

The results presented in table D.34 suggest that there is strong indication that only the variances of the shear failure stress between 50 and 500[mm/min] crosshead displacement rate are different.

Table D.34: Hypothesis testing for equality of variances statistics of shear failure stress.

Crosshead Rate	F_0	α	df1	df2	F_{crit}	Level
5 vs. 50	1.452	0.05	33	27	1.889	0.833
50 vs. 500	1.9	0.05	33	31	1.83	0.96
5 vs. 500	1.309	0.05	27	31	1.87	0.763

Distribution: Figure D.23 presents the probability density function plots of the shear failure stress (τ_{12}) at different crosshead displacement rates. Figure D.23(a) present the p.d.f. of the complete data set. Figures D.23 (b),(c) and (d) group the data set according to the crosshead displacement rate: 5, 50 and 500[mm/min] respectively.

The shear failure stress p.d.f. for the complete data set appear to have secondary peak bug generally appears to follow a normal distribution. The shear failure stress appears to retain a Gaussian distribution shape at all crosshead displacement rates. The lesser peaks are attributed to the random effects (statistical artifacts due to the relatively small sample size). The distribution of the shear failure stress at 50[mm/min] crosshead displacement rate appears to be wider than the other two crosshead displacement rates.

The computed values of the χ_0^2 statistic for the complete data set and for the different crosshead displacement rates are presented in table D.35, together with other information required for the calculations of the critical value.

The values in table D.35 suggest that only the shear failure strain distribution at 500[mm/min] crosshead displacement rate of the results does not follow a normal distribution. The complete data set appear to have a lower level of confidence.

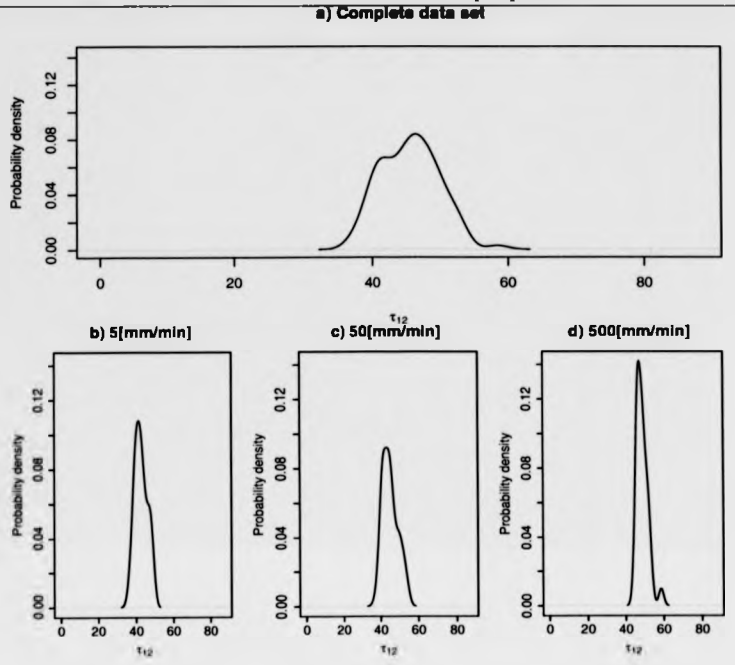

Figure D.23: Density plots of shear failure stress at a) all displacement rates, and b),c) and d) at each different crosshead displacement rate separately.

Model fitting: A linear model of the shear failure stress with respect to the logarithm of the shear strain rate has the following form:

$$\tau_{12}(\dot{\gamma}_{12}) = 51.81 + 3.44 \cdot \log_{10}(\dot{\gamma}_{12}) \tag{D.11}$$

A quadratic model of the shear failure stress with respect to the logarithm of the shear strain rate has the following form:

$$\tau_{12}(\dot{\gamma}_{12}) = 56.07 + 8.68 \cdot \log_{10}(\dot{\gamma}_{12}) + 1.38 \cdot \log_{10}(\dot{\gamma}_{12})^2 \tag{D.12}$$

The statistics for the comparison of the two shear strain rate models of shear failure strain are

Table D.35: Statistics for the Goodness-of-Fit of the shear failure stress distribution.

Crosshead Rate	χ_0^2	α	# of Classes	χ_{crit}^2	Level
ALL	7.04	0.05	6	7.81	0.93
5	3	0.05	6	7.815	0.608
50	5.364	0.05	6	7.815	0.853
500	9.84	0.05	6	7.81	0.98

presented in table D.36. The null hypothesis is not rejected, i.e. the equation for the linear model (eq. D.11) describes adequately the set of results (weak conclusion).

Table D.36: ANOVA results for the selection of the shear strain rate model order of the shear failure stress.

Model	Res.Df	RSS	Df	Sum of Sq	F	$Pr(>F)$
Linear	89	1085.27				
Quadratic	88	1058.64	1	26.63	2.21	0.14

The coefficient of determination R^2 value for the linear model is 0.341.

D.2.4 Strain Rate Effects On Damage Evolution.

D.2.4.1 Initial Shear Damage Limit Value Y_0

Figure D.24 presents the conditional plot of initial shear damage limit value vs. shear strain rate with respect to data acquisition source and Failure location. The difference of scatter from the VE between the sources of acquired data led use of the Instron data for the statistical analysis. Figure D.25 presents the initial shear damage limit value vs. shear strain rate log and a linear and

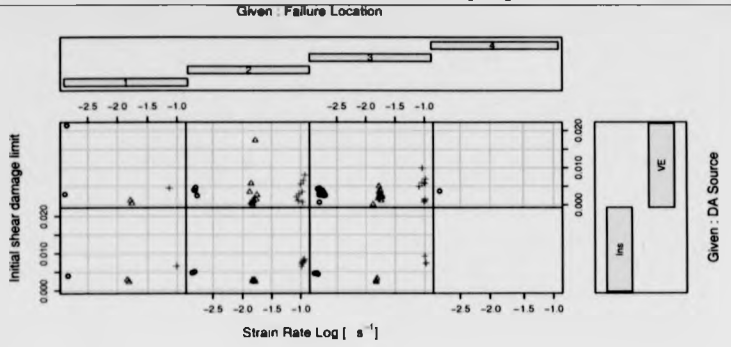

Figure D.24: Conditional plot of initial shear damage limit value vs. logarithm of shear strain rate as obtained from the tensile testing of a $[\pm 45]_{2s}$ laminate, conditioned with respect of data acquisition source and failure location.

a quadratic model of the log of the shear strain rate is fitted. The labeled results were regarded outliers and were not included in the subsequent statistical treatment.

Statistics: Table D.37 presents the statistics of the initial shear damage limit value at different crosshead displacement rates.

Table D.37: Statistics for the initial shear damage limit value at different crosshead displacement rates.

Crosshead Rate		5	50	500
Mean	$[\sqrt{GPa}]$	0.0046	0.00268	0.0077
Standard Deviation	$[\sqrt{GPa}]$	0.000374	0.000254	0.000748
Coef. of Variance	[]	0.0813	0.0948	0.0972

The mean of the initial shear damage limit value appears to decrease initially for increasing

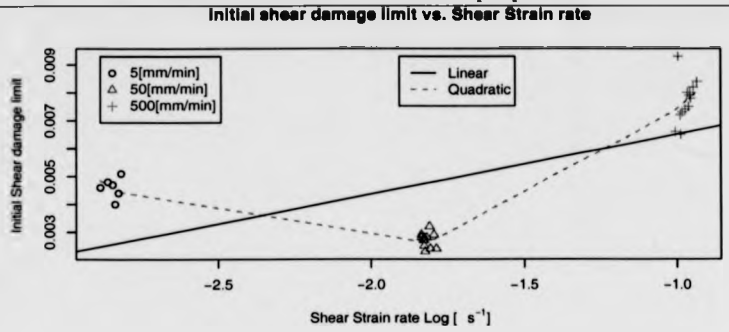

Figure D.25: Initial shear damage limit value vs. shear strain rate logarithm.

crosshead displacement rate and further decrease with increasing crosshead displacement rate . The standard deviation of the initial shear damage limit value is lowest at the 50[mm/min] displacement rate and highest at the 500[mm/min] displacement rate. The coefficient of variance is the lowest for the 5[mm/min] crosshead displacement rate, and highest for the 500[mm/min] crosshead displacement rate.

Hypothesis testing: The null hypothesis (H_0) is that the initial shear damage limit value is not strain rate dependent. Therefore, the mean of the initial shear damage limit value for one crosshead displacement rate results should be equal to the mean of the Initial shear damage limit value for another crosshead displacement rate, e.g. $H_0 : \overline{Y}_{0,5} = \overline{Y}_{0,50}$. The alternative hypothesis is that the initial shear damage limit value is shear strain rate dependent.

The statistics for the equality of means test are presented in table D.38. The table columns present similar information to those of table D.24.

The Initial shear damage limit value at 5[mm/min] crosshead displacement rate appear to be statistically different at different crosshead displacement rates, at 5% level of confidence. Therefore,

Table D.38: Hypothesis testing statistics for equality of means of initial shear damage limit value.

Crosshead Rate	t_0	α	df	t_{crit}	Level
5 vs. 50	11.38	0.05	8	1.86	1
50 vs. 500	22.88	0.05	15	1.75	1
5 vs. 500	12.03	0.05	18	1.73	1

there *is* indication that the initial shear damage limit value is shear strain rate dependent.

The statistics for the equality of variances test are presented in table D.39. The table columns present similar information to those of table D.25.

Table D.39: Hypothesis testing for equality of variances statistics of Poisson's ratio initial shear damage limit value.

Crosshead Rate	F_0	α	df1	df2	F_{crit}	Level
5 vs. 50	2.162	0.05	6	13	3.106	0.873
50 vs. 500	8.65	0.05	13	13	2.69	1
5 vs. 500	4	0.05	13	6	4.678	0.932

The results presented in table D.39 suggest that there is strong indication that the variance of the initial shear damage limit value at 50[mm/min] crosshead displacement rates is statistically different to the 500[mm/min] crosshead displacement rates, at a significance level of 5%.

Distribution: Figure D.26 presents the probability density function plots of the Initial shear damage limit value (Y_0) at different crosshead displacement rates. Figure D.26(a) present the p.d.f. of the complete data set. Figures D.26 (b),(c) and (d) group the data set according to the crosshead displacement rate: 5, 50 and 500[mm/min] respectively.

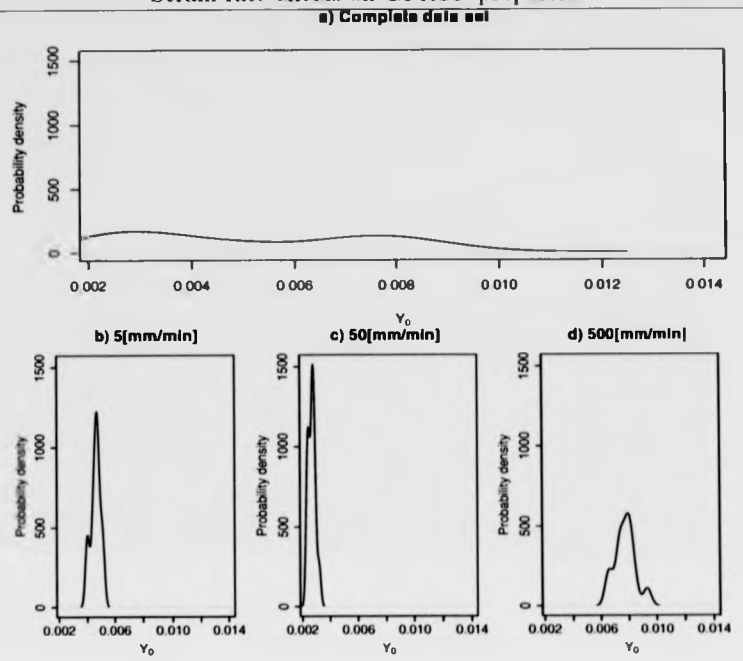

Figure D.26: Density plots of unitial shear damage limit value at a) all displacement rates, and b),c) and d) at each different crosshead displacement rate separately.

The p.d.f. of the Initial shear damage limit value for the complete data set (presented in figure D.26(a)) appears to follow a flat Gaussian distribution. The complete data set distribution has two peaks, however because the distribution is flat it is not possible to determine them accurately. At 5, 50 and 500[mm/min] crosshead displacement rates, the p.d.f.s appear to follow normal distributions with secondary peaks.

The computed values of the χ_0^2 statistic for the complete data set and for the different crosshead displacement rates are presented in table D.10, together with other information required for the calculations of the critical value.

Table D.40: Statistics for the Goodness-of-Fit of the initial shear damage limit probability density function.

Crosshead Rate	χ_0^2	α	# of Classes	χ_{crit}^2	Level
ALL	7.75	0.05	6	7.815	0.949
5	0	0.05	6	7.81	0
50	6.846	0.05	6	7.815	0.923
500	2.231	0.05	6	7.815	0.474

According to the data from table D.40 the null hypothesis cannot be rejected at any crosshead displacement rate.

Model fitting: A linear model of the initial shear damage limit value with respect to the logarithm of the shear strain rate has the following form:

$$Y_0(\dot{\gamma}_{12}) = 0.00865 + 0.00214 \cdot \log_{10}(\dot{\gamma}_{12}) \tag{D.13}$$

A quadratic model of the Initial shear damage limit value with respect to the logarithm of the shear strain rate has the following form:

$$Y_0(\dot{\gamma}_{12}) = 0.02074 + 0.01748 \cdot \log_{10}(\dot{\gamma}_{12}) + 0.00415 \cdot \log_{10}(\dot{\gamma}_{12})^2 \tag{D.14}$$

The statistics for the comparison of the two shear strain rate models of Initial shear damage limit value are presented in table D.41. According to the data, the null hypothesis can be rejected, i.e. the quadratic model (eq. D.14) describes better the set of results.

The coefficient of determination R^2 value for the linear model is 0.955.

Table D.41: ANOVA results for the selection of the shear strain rate model order of the Initial shear damage limit value.

Model	Res.Df	RSS	Df	Sum of Sq	F	$Pr(>F)$
Linear	30	1.05e-04				
Quadratic	29	7.36e-06	1	9.75e-05	384	2.85e-18

D.2.4.2 Critical Shear Damage limit Value Y_c

Figure D.27 presents the conditional plot of critical shear damage limit vs. shear strain rate with respect to data acquisition source and failure location. The discrepancy of the trends between the sources of acquired data led use of the Instron data for the statistical analysis.

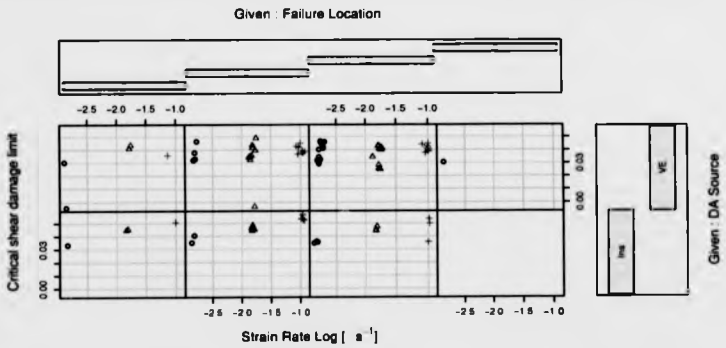

Figure D.27: Conditional plot of critical shear damage limit vs. logarithm of shear strain rate as obtained from the tensile testing of a $[\pm 45]_{2s}$ laminate, conditioned with respect of data acquisition source and Failure location.

Figure D.28 presents the critical shear damage limit value vs. shear strain rate log and a linear and a quadratic model of the log of the shear strain rate is fitted. The labeled results were regarded

Table D.41: ANOVA results for the selection of the shear strain rate model order of the Initial shear damage limit value.

Model	Res.Df	RSS	Df	Sum of Sq	F	$Pr(>F)$
Linear	30	1.05e-04				
Quadratic	29	7.36e-06	1	9.75e-05	384	2.85e-18

D.2.4.2 Critical Shear Damage limit Value Y_c

Figure D.27 presents the conditional plot of critical shear damage limit vs. shear strain rate with respect to data acquisition source and failure location. The discrepancy of the trends between the sources of acquired data led use of the Instron data for the statistical analysis.

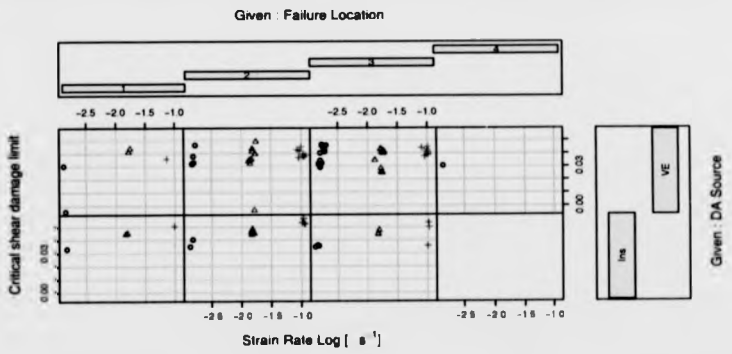

Figure D.27: Conditional plot of critical shear damage limit vs. logarithm of shear strain rate as obtained from the tensile testing of a $[\pm 45]_{2s}$ laminate, conditioned with respect of data acquisition source and Failure location.

Figure D.28 presents the critical shear damage limit value vs. shear strain rate log and a linear and a quadratic model of the log of the shear strain rate is fitted. The labeled results were regarded

outliers and were not included in the subsequent statistical treatment.

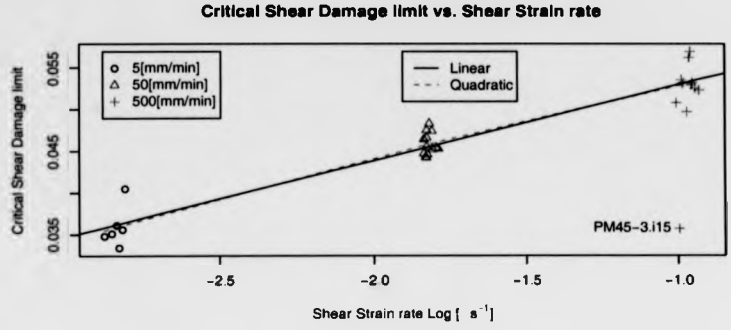

Figure D.28: Critical shear damage limit value vs. shear strain rate logarithm.

Statistics: Table D.42 presents the statistics of the critical shear damage limit value at different crosshead displacement rates.

Table D.42: Statistics for the critical shear damage limit value at different crosshead displacement rates.

Crosshead Rate		5	50	500
Mean	$[\sqrt{GPa}]$	0.0359	0.0458	0.0531
Standard Deviation	$[\sqrt{GPa}]$	0.00242	0.00132	0.00196
Coef. of Variance	[]	0.0675	0.0289	0.0369

The mean of the critical shear damage limit value appears to increase with crosshead displacement rate. The standard deviation of the critical shear damage limit value is lowest at the 50[mm/min] displacement rate and highest at the 5[mm/min] displacement rate. Similarly The coefficient of variance is lowest at the 50[mm/min] crosshead displacement rate, and highest at the 5[mm/min]

crosshead displacement rate.

Hypothesis testing: The null hypothesis (H_0) is that the critical shear damage limit value is not strain rate dependent. Therefore, the mean of the critical shear damage limit value for one crosshead displacement rate results should be equal to the mean of the critical shear damage limit value for another crosshead displacement rate, e.g. $H_0 : \overline{Y}_{c,5} = \overline{Y}_{c,50}$. The alternative hypothesis is that the critical shear damage limit value is shear strain rate dependent.

The statistics for the equality of means test are presented in table D.43. The table columns present similar information to those of table D.24.

Table D.43: Hypothesis testing statistics for equality of means of critical shear damage limit value.

Crosshead Rate	t_0	α	df	t_{crit}	Level
5 vs. 50	9.36	0.05	6	1.94	1
50 vs. 500	10.83	0.05	20	1.73	1
5 vs. 500	15.08	0.05	9	1.83	1

The critical shear damage limit value appears to be statistically different at the different crosshead displacement rates, at 5% level of confidence. Therefore, there *is* indication that the critical shear damage limit value is shear strain rate dependent.

The statistics for the equality of variances test are presented in table D.44. The table columns present similar information to those of table D.25.

The results presented in table D.44 suggest that there is strong indication that the variance of the critical shear damage limit value at 5[mm/min] crosshead displacement rates is statistically different to the 50[mm/min] crosshead displacement rates, at a significance level of 5%.

Table D.44: Hypothesis testing for equality of variances statistics of critical shear damage limit value.

Crosshead Rate	F_0	α	df1	df2	F_{crit}	Level
5 vs. 50	3.36	0.05	6	13	3.11	0.96
50 vs. 500	2.188	0.05	12	13	2.717	0.903
5 vs. 500	1.534	0.05	6	12	3.204	0.743

Distribution: Figure D.29 presents the probability density function plots of the Critical shear damage limit value (Y_c) at different crosshead displacement rates. Figure D.29(a) present the p.d.f. of the complete data set. Figures D.29 (b),(c) and (d) group the data set according to the crosshead displacement rate: 5, 50 and 500[mm/min] respectively.

The p.d.f. of the critical shear damage limit value for the complete data set (presented in figure D.29(a)) appears to follow a flat Gaussian distribution with several inflection points. The critical shear damage limit value at 50[mm/min] crosshead displacement rate appears to follow a normal distribution with a secondary point of inflection. The pdf's at 5 and 500[mm/min] crosshead displacement rates appear to follow a distribution with several distinct secondary peaks.

The computed values of the χ_0^2 statistic for the complete data set and for the different crosshead displacement rates are presented in table D.45, together with other information required for the calculations of the critical value.

According to the data from table D.45 the complete data set and the 500[mm/min] crosshead displacement rate does not follow a normal distribution. The normal distribution hypothesis at the 5 and 500[mm/min] crosshead displacement rate cannot be rejected for any of the shear strain rate partitions of the data.

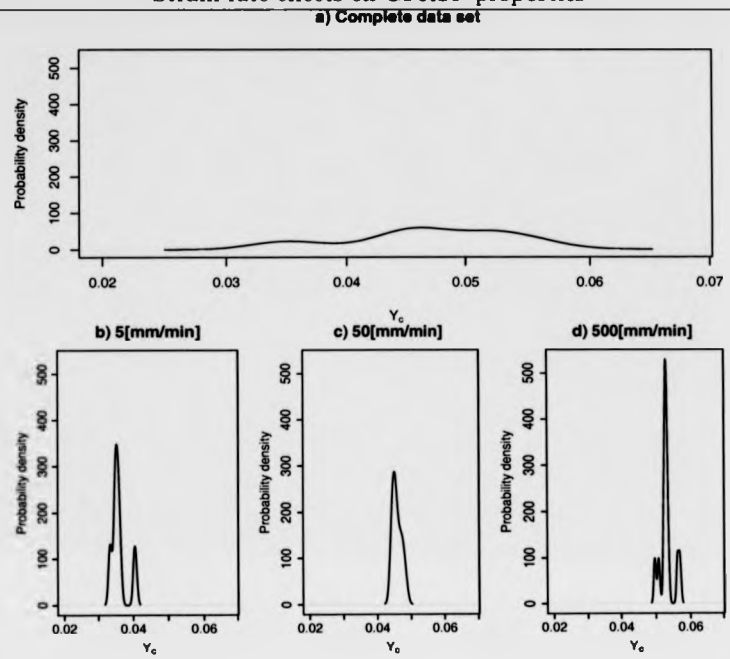

Figure D.29: Density plots of critical shear damage limit value at a) all displacement rates, and b),c) and d) at each different crosshead displacement rate separately.

Model fitting: A linear model of the critical shear damage limit value with respect to the logarithm of the shear strain rate has the following form:

$$Y_c(\dot{\gamma}_{12}) = 0.0621 + 0.00912 \cdot \log_{10}(\dot{\gamma}_{12}) \tag{D.15}$$

A quadratic model of the critical shear damage limit value with respect to the logarithm of the shear strain rate has the following form:

$$Y_c(\dot{\gamma}_{12}) = 0.060262 + 0.006805 \cdot \log_{10}(\dot{\gamma}_{12}) - 0.000625 \cdot \log_{10}(\dot{\gamma}_{12})^2 \tag{D.16}$$

The statistics for the comparison of the two shear strain rate models of critical shear damage limit

Table D.45: Statistics for the Goodness-of-Fit of the critical shear damage limit probability density function.

Crosshead Rate	χ_0^2	α	# of Classes	χ_{crit}^2	Level
ALL	9.065	0.05	6	7.815	0.972
5	2	0.05	6	7.815	0.428
50	3.154	0.05	6	7.815	0.631
500	9	0.05	6	7.81	0.97

value are presented in table D.46. According to the data, the null hypothesis cannot be rejected, i.e. the linear model (eq. D.15) describes adequately the set of results.

Table D.46: ANOVA results for the selection of the shear strain rate model order of the Critical shear damage limit value.

Model	Res.Df	RSS	Df	Sum of Sq	F	$Pr(>F)$
Linear	29	9.08e-05				
Quadratic	28	8.86e-05	1	2.18e-06	0.69	0.413

The coefficient of determination R^2 value for the linear model is 0.927.

D.2.4.3 Critical Shear Damage Limit Value Y_R

Figure D.30 presents the conditional plot of elementary shear damage limit vs. shear strain rate with respect to data acquisition source and failure location. The discrepancy of the trends between the sources of acquired data led use of the Instron data for the statistical analysis.

Figure D.31 presents the elementary shear damage limit value vs. shear strain rate log and a linear and a quadratic model of the log of the shear strain rate is fitted. The labeled results were

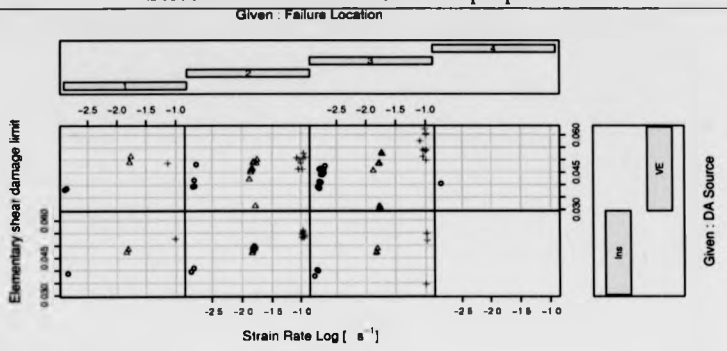

Figure D.30: Conditional plot of elementary shear damage limit vs. logarithm of shear strain rate as obtained from the tensile testing of a $[\pm 45]_{2s}$ laminate, conditioned with respect of data acquisition source and Failure location.

regarded outliers and were not included in the subsequent statistical treatment.

Statistics: Table D.47 presents the statistics of the elementary shear damage limit value at different crosshead displacement rates.

Table D.47: Statistics for the elementary shear damage limit value at different crosshead displacement rates.

Crosshead Rate		5	50	500
Mean	$[\sqrt{GPa}]$	0.0395	0.0482	0.0541
Standard Deviation	$[\sqrt{GPa}]$	0.001108	0.000906	0.001214
Coef. of Variance	[]	0.0281	0.0188	0.0225

The mean of the elementary shear damage limit value appears to increase with crosshead displacement rate. The standard deviation of the elementary shear damage limit value is lowest at the

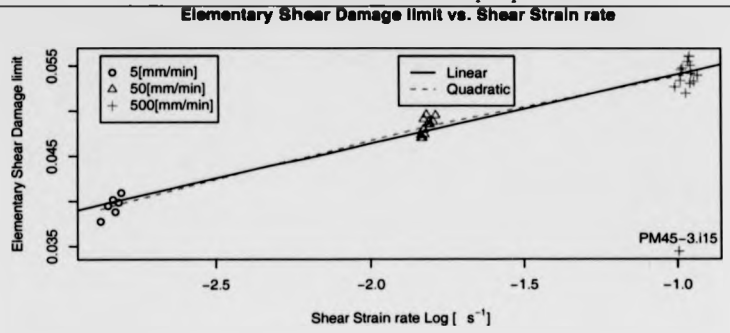

Figure D.31: Elementary shear damage limit value vs. shear strain rate logarithm.

50[mm/min] displacement rate and highest at the 500[mm/min] displacement rate (7 fold increase almost). The coefficient of variance is lowest for the 50[mm/min] crosshead displacement rate, and it is highest at the 5[mm/min] crosshead displacement rate.

Hypothesis testing: The null hypothesis (H_0) is that the elementary shear damage limit value is not strain rate dependent. Therefore, the mean of the elementary shear damage limit value for one crosshead displacement rate results should be equal to the mean of the elementary shear damage limit value for another crosshead displacement rate, e.g. $H_0 : \overline{Y}_{R,5} = \overline{Y}_{R,50}$. The alternative hypothesis is that the elementary shear damage limit value is shear strain rate dependent.

The statistics for the equality of means test are presented in table D.48. The table columns present similar information to those of table D.24.

The elementary shear damage limit value appears to be statistically different between all crosshead displacement rate groups. Therefore there *is* strong indication that the elementary shear damage limit is strain rate dependent.

The statistics for the equality of variances test are presented in table D.49. The table columns

Table D.48: Hypothesis testing statistics for equality of means of elementary shear damage limit value.

Crosshead Rate	t_0	α	df	t_{crit}	Level
5 vs. 50	16.87	0.05	9	1.83	1
50 vs. 500	13.57	0.05	21	1.72	1
5 vs. 500	25.48	0.05	13	1.77	1

present similar information to those of table D.25.

Table D.49: Hypothesis testing for equality of variances statistics of elementary shear damage limit value.

Crosshead Rate	F_0	α	df1	df2	F_{crit}	Level
5 vs. 50	1.495	0.05	6	13	3.106	0.738
50 vs. 500	1.793	0.05	12	13	2.717	0.835
5 vs. 500	1.199	0.05	12	6	4.704	0.552

The results presented in table D.49 suggest that there is *no* strong indication that the variance of the elementary shear damage limit value is statistically different at different crosshead displacement rates, at a significance level of 5%.

Distribution: Figure D.32 presents the probability density function plots of the Elementary shear damage limit value (Y_R) at different crosshead displacement rates. Figure D.32(a) present the p.d.f. of the complete data set. Figures D.32 (b),(c) and (d) group the data set according to the crosshead displacement rate: 5, 50 and 500[mm/min] respectively.

The p.d.f. of the elementary shear damage limit value for the complete data set (presented in

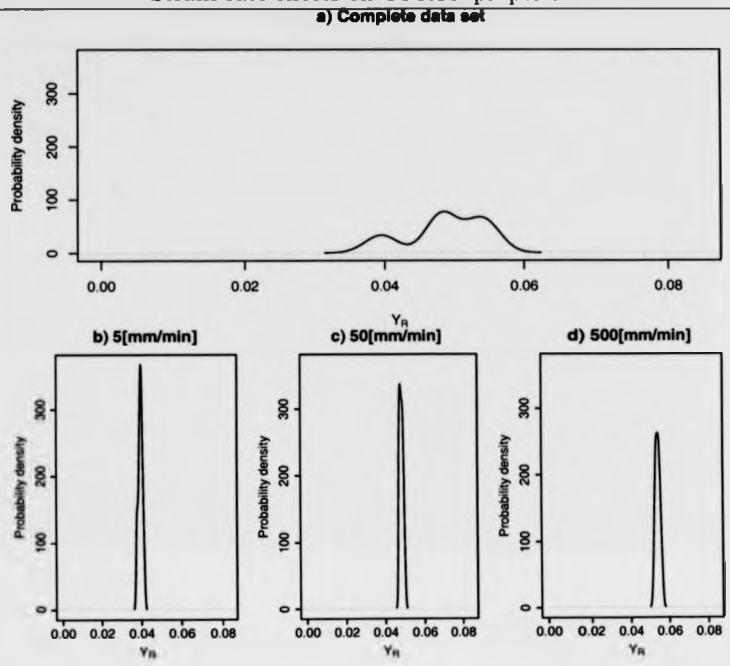

Figure D.32: Density plots of elementary shear damage limit value of at a) all displacement rates, and b),c) and d) at each different crosshead displacement rate separately.

figure D.32(a)) appears to follow a distribution with 3 distinctive peaks. The p.d.f.s of the group of different crosshead displacement rates appear to follow a noraml distribution. Figure D.32(d) has a Gaussian distribution with two distinctive peaks. The lower peak is suspected to be a mistake of the instrumentation.

The computed values of the χ_0^2 statistic for the complete data set and for the different crosshead displacement rates are presented in table D.50, together with other information required for the calculations of the elementary value.

Table D.50: Statistics for the Goodness-of-Fit of the elementary shear damage limit probability density function.

Crosshead Rate	χ_0^2	α	# of Classes	χ_{crit}^2	Level
ALL	7.129	0.05	6	7.815	0.932
5	0	0.05	6	7.81	0
50	2.231	0.05	6	7.815	0.474
500	2	0.05	6	7.815	0.428

According to the data from table D.50 the null hypothesis cannot be rejected for the any of the examined crosshead displacement rate groups.

Model fitting: A linear model of the elementary shear damage limit value with respect to the logarithm of the shear strain rate has the following form:

$$Y_R^*(\dot{\gamma}_{12}) = 0.0618 + 0.0077 \cdot \log_{10}(\dot{\gamma}_{12}) \tag{D.17}$$

A quadratic model of the elementary shear damage limit value with respect to the logarithm of the shear strain rate has the following form:

$$Y_R^*(\dot{\gamma}_{12}) = 0.059086 + 0.004299 \cdot \log_{10}(\dot{\gamma}_{12}) - 0.000919 \cdot \log_{10}(\dot{\gamma}_{12})^2 \tag{D.18}$$

The statistics for the comparison of the two shear strain rate models of elementary shear damage limit value are presented in table D.51. According to the data, the null hypothesis is rejected, i.e. the quadratic model (eq. D.18) describes adequately the set of results.

The coefficient of determination R^2 value for the linear model is 0.966.

Table D.51: ANOVA results for the selection of the shear strain rate model order of the elementary shear damage limit value.

Model	Res.Df	RSS	Df	Sum of Sq	F	$Pr(>F)$
Linear	29	3.29e-05				
Quadratic	28	2.82e-05	1	4.73e-06	4.69	0.039

D.3 Properties Obtained From $[+45°]_8$ Test.

D.3.1 Transverse Strain Rate.

Figure D.33 present the logarithm of the transverse strain rate of the material vs. the crosshead displacement rate.

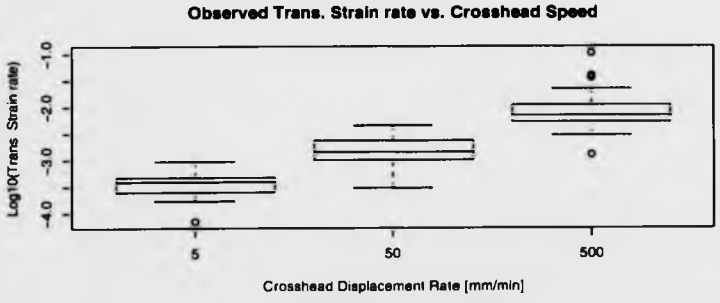

Figure D.33: Logarithm of Transverse Strain Rate vs. Crosshead displacement rate as obtained from the tensile testing of a $[+45]_8$ laminate.

Statistics: Table D.52 presents the statistics of the measured strain rate at different crosshead displacement rates.

The mean of the logarithm of strain rate increases by approximately .9 when increasing the

Table D.52: Statistics for measured strain rate at different crosshead displacement rates.

Crosshead Rate	5	50	500	
Mean	log[1/s]	-3.46	-2.84	-2.08
Standard Deviation	log[1/s]	0.238	0.324	0.390
Coef. of Variance		-0.0689	-0.1140	-0.1876

crosshead displacement rate from 5 to 50[mm/min] and then increases by less than .4 units when increasing the crosshead displacement rate further to 500[mm/min]. The standard deviation appears to be in the same order of magnitude for the different crosshead displacement rates and the lowest value for standard deviation is at 5[mm/min] crosshead displacement rate. The lowest value for the coefficient of variance is at 5[mm/min] crosshead displacement rate.

D.3.2 Strain Rate Effects On Elasticity

D.3.2.1 Transverse Tensile Modulus E_{22}

Figure D.34 presents the conditional plot of transverse tensile modulus vs. transverse strain rate with respect to data acquisition source and failure location. The discrepancy of the trends between the sources of acquired data led use of the Instron data for the statistical analysis.

Figure D.35 presents the transverse tensile modulus vs. strain rate and two models (a linear and a quadratic model) of the logarithm of the strain rate are fitted. The labeled observations on figure D.35 were regarded outliers and were not included in the statistical treatment.

One important feature of the graph is that for a given crosshead displacement rate the transverse tensile failure stress increases for increasing values of the calculated strain rate. This is attributed to the fact that specimens with lower transverse tensile modulus deform more and as a result a

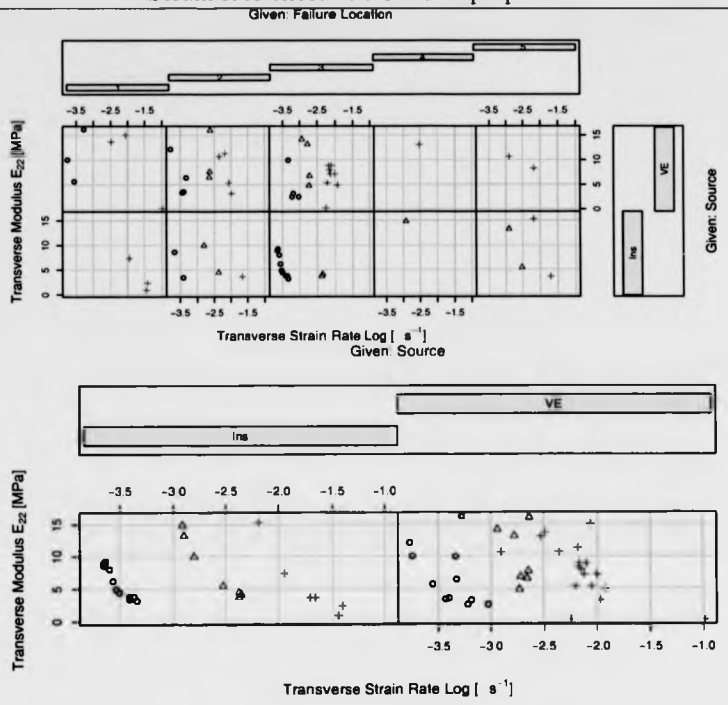

Figure D.34: Conditional plot of transverse tensile modulus vs. logarithm of shear strain rate as obtained from the tensile testing of a $[+45]_8$ laminate, conditioned with respect of data acquisition source and failure location.

higher level of strain rate is calculated.

Statistics: Table D.53 presents the statistics of the transverse tensile modulus at different crosshead displacement rates as obtained from $[+45]_8$ laminates.

The mean of the transverse tensile modulus appears to initially increase with crosshead displacement rate and the decrease with further increase of the strain rates. The standard deviation of the transverse tensile modulus is lowest at the 5[mm/min] crosshead displacement rate . The co-

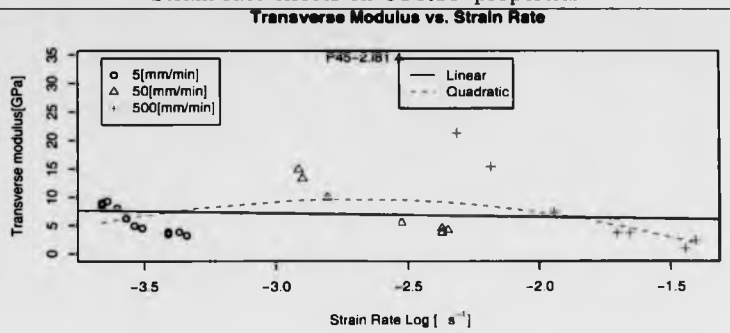

Figure D.35: Transverse tensile modulus vs. logarithm of strain rate as obtained from the tensile testing of a $[+45]_8$ laminate.

Table D.53: Statistics for the transverse tensile modulus at different crosshead displacement rates as obtained from a $[+45]_8$ laminate.

Crosshead Rate		5	50	500
Mean	[GPa]	5.85	7.97	7.78
Standard Deviation	[GPa]	2.4	4.68	7.64
Coef. of Variance	[]	0.41	0.587	0.983

efficient of variance is lowest for the 5[mm/min] crosshead displacement rate and highest at the 500[mm/min] crosshead displacement rate.

Hypothesis testing: The null hypothesis (H_0) is that the transverse tensile modulus is not strain rate dependent. Therefore, the average of the transverse tensile modulus for one crosshead displacement rate results should be equal to the average of the transverse tensile modulus for another crosshead displacement rate, e.g. $H_0 : \overline{E}_{22,5} = \overline{E}_{22,50}$. The alternative hypothesis (H_1) which is accepted automatically if the null hypothesis is rejected is that the transverse tensile

modulus is strain rate dependent.

The statistics for the equality of means test are presented in table D.54. The table presents the calculated test statistic t_0, the α-type error probability, the degrees of freedom df and the calculated critical value t_{crit}. In the final column, the level of confidence is presented (i.e. the value of α-type error probability for which the calculated critical value t_{crit} is equal to the statistic t_0).

Table D.54: Hypothesis testing statistics for the equality of averages of transverse tensile modulus.

Crosshead Rate	t_0	α	df	t_{crit}	Level
5 vs. 50	1.11	0.05	8	1.86	0.85
50 vs. 500	0.0569	0.05	11	1.796	0.522
5 vs. 500	0.646	0.05	7	1.895	0.731

The transverse tensile modulus is *not* statistically different between the different crosshead displacement rates, for a 5% α-type error. Therefore, there is *no* indication that transverse tensile modulus is dependent on the strain rate.

The statistics for the equality of variances test are presented in table D.55. The table presents the calculated test statistic F_0, the α-type error probability, the degrees of freedom $df1$ and $df2$ and the calculated critical value F_{crit}. In the last column, the level of confidence is presented (i.e. the value of α-type error for which the critical value (F_{crit}) is equal to the statistic (F_0)).

The results presented in table D.55 suggest that the variance of the transverse tensile modulus at 5[mm/min] crosshead displacement rate is statistically different at a 5% α-type error to the variances of the transverse tensile modulus at 50[mm/min] and 500[mm/min] crosshead displacement rate.

Table D.55: Hypothesis testing for equality of variances statistics of transverse tensile modulus.

Crosshead Rate	F_0	α	df1	df2	F_{crit}	Level
5 vs. 50	3.8	0.05	7	11	3.22	0.97
50 vs. 500	2.671	0.05	7	7	4.284	0.871
5 vs. 500	10.14	0.05	7	11	3.22	1

Distribution: Figure D.36 presents the probability density function plots of the transverse tensile modulus (E_{22}) at different crosshead displacement rates. Figure D.36(a) present the p.d.f. of the complete data set. Figures D.36 (b),(c) and (d) group the data set according to the crosshead displacement rate: 5, 50 and 500[mm/min] respectively.

The p.d.f. of the transverse tensile modulus which is presented in figure D.36(a) appears to be skewed with a single primary peak, however several points of inflection can be observed indicating secondary peaks. The grouped data sets in figures D.36(b) D.36(c) and D.36(d) all have a primary peak at the lower at a low value of the transverse tensile modulus and a secondary peak at a higher value.

The computed values of the χ_0^2 statistic for the complete data set and for the different crosshead displacement rates are presented in table D.56, together with other information required for the calculations of the critical value.

If the computed χ_0^2 statistic is smaller than the χ_{crit}^2 the conclusion is that there is no reason to reject the assumption that the distribution of the transverse tensile modulus is normally distributed.

The results in table D.56 suggest that only the 5[mm/min] crosshead displacement group follows a normal distribution at a 5% α-type error, and the 50 and 500[mm/min] crosshead displacement

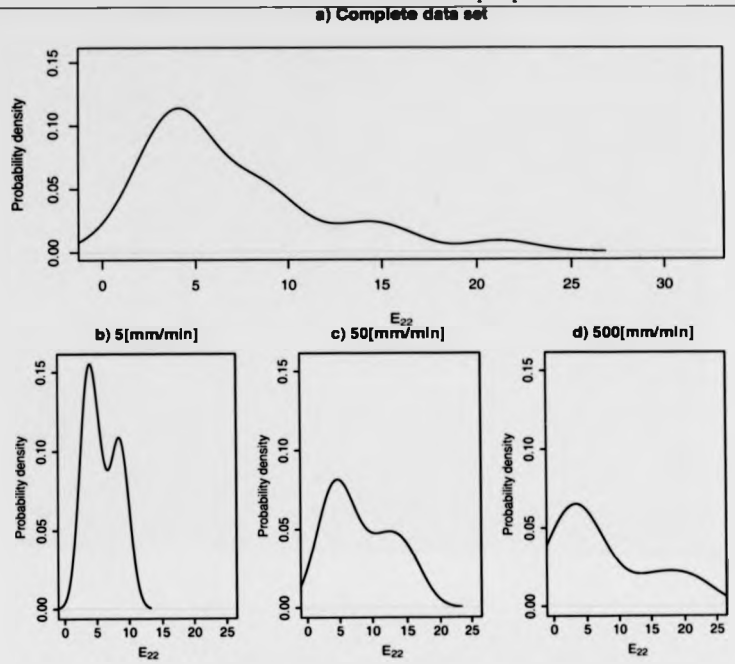

Figure D.36: Density plots of the transverse tensile modulus at a) all displacement rates, and b),c) and d) at each different crosshead displacement rate separately.

Table D.56: Statistics for the Goodness-of-Fit of Transverse tensile modulus probability density distribution.

Crosshead Rate	χ_0^2	α	# of Classes	χ_{crit}^2	Level
ALL	19.4	0.05	6	7.81	1
5	2.636	0.05	6	7.815	0.549
50	11	0.05	6	7.815	0.988
500	11	0.05	6	7.815	0.988

rates follow a normal distribution at a 1% α-type error.

Model fitting: The transverse tensile modulus mean of all observed values is proposed since the no strain rate sensitivity could be determined statistically. The calculated value is 6.986[GPa].

D.3.3 Strain Rate Effects On Strength.

D.3.3.1 Transverse Failure Strain ε_{22}

Figure D.37 presents the conditional plot of transverse tensile failure strain vs. transverse strain rate with respect to data acquisition source and failure location. The discrepancy of the trends between the sources of acquired data led use of the Instron data for the statistical analysis.

Figure D.38 presents the transverse tensile failure strain vs. strain rate log and a linear and a quadratic model of the log of the strain rate is fitted. The labeled observations are removed as outliers from the statistical treatment.

One important feature of the graph is that for a given crosshead displacement rate, the transverse tensile failure strain increases with strain rate. This is attributed to the fact that the specimens at a given crosshead displacement rate fail at the same stress. Higher observed values of the strain rate are equivalent to lower modulus. The assumption of Hooke's law[1] suggests that for lower modulus specimens, higher strains are required to obtain a given stress level.

Statistics: Table D.57 presents the statistics of transverse tensile failure strain at different crosshead displacement rates of P45.

The mean of transverse tensile failure strain initially increases for increasing crosshead displace-

[1]Hooke's law is suitable for the transverse properties because of the linear/brittle failure of the material.

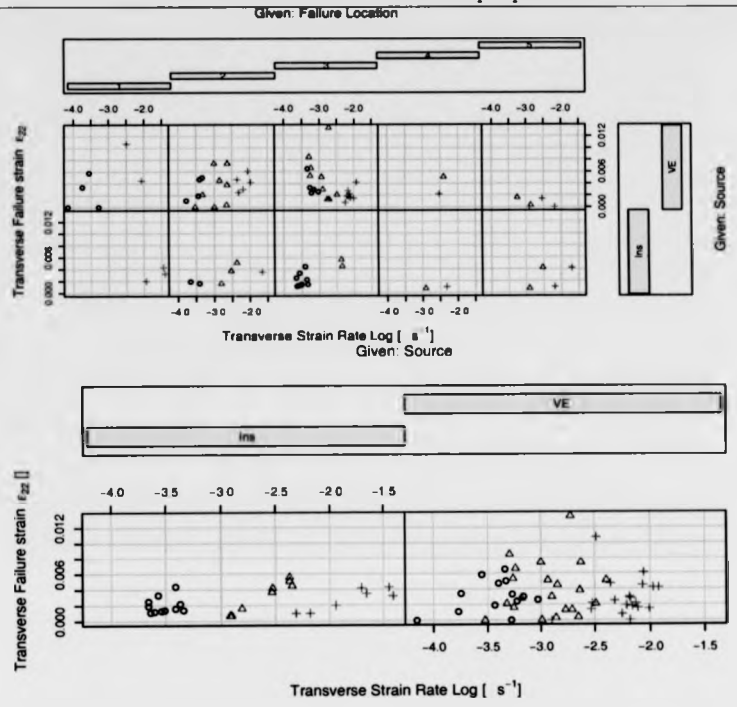

Figure D.37: Conditional plot of transverse tensile failure strain vs. logarithm of shear strain rate as obtained from the tensile testing of a $[+45]_8$ laminate, conditioned with respect of data acquisition source and failure location.

ment rate and decreases for increasing crosshead displacement rate. The standard deviation is lowest at the 5[mm/min] crosshead displacement rate and highest at the 50[mm/min] crosshead displacement rate. The coefficient of variance is lowest at the 5 [mm/min] crosshead displacement rate and highest at the 500[mm/min] crosshead displacement rate.

Hypothesis testing: The null hypothesis (H_0) is that the transverse tensile failure strain is not strain rate dependent. The alternative hypothesis is that the transverse tensile failure strain

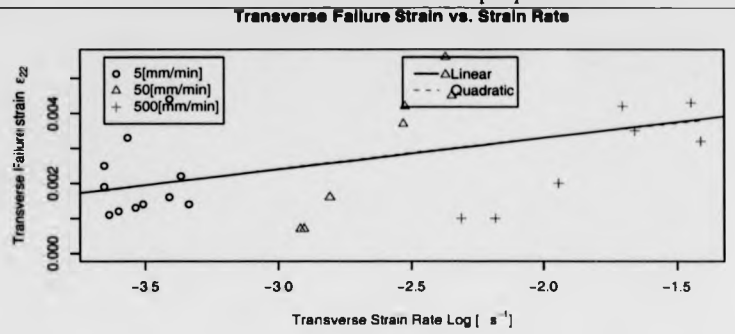

Figure D.38: Transverse tensile failure strain of vs. strain rate logarithm.

Table D.57: Statistics for the transverse tensile failure strain at different crosshead displacement rates.

Crosshead Rate	5	50	500	
Mean	[]	0.00266	0.00326	0.00234
Standard Deviation	[]	0.00124	0.00198	0.00146
Coef. of Variance	[]	0.467	0.606	0.623

is strain rate dependent.

The statistics for the equality of means test are presented in table D.58. The columns are similar to the table D.54.

Table D.58: Hypothesis testing statistics for equality of means of transverse tensile failure strain.

Crosshead Rate	t_0	α	df	t_{crit}	Level
5 vs. 50	0.675	0.05	12	1.782	0.744
50 vs. 500	0.965	0.05	12	1.782	0.823
5 vs. 500	0.373	0.05	9	1.833	0.641

The transverse tensile failure strain does not appear to be statistically statistically different at a 5% level of confidence at different crosshead displacement rates. Therefore, there is *no* indication that the transverse tensile failure strain is strain rate dependent.

The statistics for the equality of variances test are presented in table D.59. The columns are similar to the table D.55.

Table D.59: Hypothesis testing for equality of variances statistics of transverse tensile failure strain.

Crosshead Rate	F_0	α	df1	df2	F_{crit}	Level
5 vs. 50	2.531	0.05	8	5	6.094	0.807
50 vs. 500	1.835	0.05	8	5	6.094	0.709
5 vs. 500	1.379	0.05	5	5	6.388	0.619

The results presented in table D.59 suggest that the variances of the transverse tensile failure strain at different crosshead crosshead displacement rates variance are not statistically different at a 5% significance level.

Distribution: Figure D.39 presents the probability density function plots of the transverse tensile failure strain (ε_{22}) at different crosshead displacement rates. Figure D.39(a) present the p.d.f. of the complete data set. Figures D.39 (b),(c) and (d) group the data set according to the crosshead displacement rate: 5, 50 and 500[mm/min] respectively.

All p.d.f. of the transverse tensile failure strain are presented in figure D.39 appears to follow a normal distribution with a secondary point of inflection (which indicates that the result might come from two or more populations).

The computed values of the χ_0^2 statistic for the complete data set and for the different crosshead

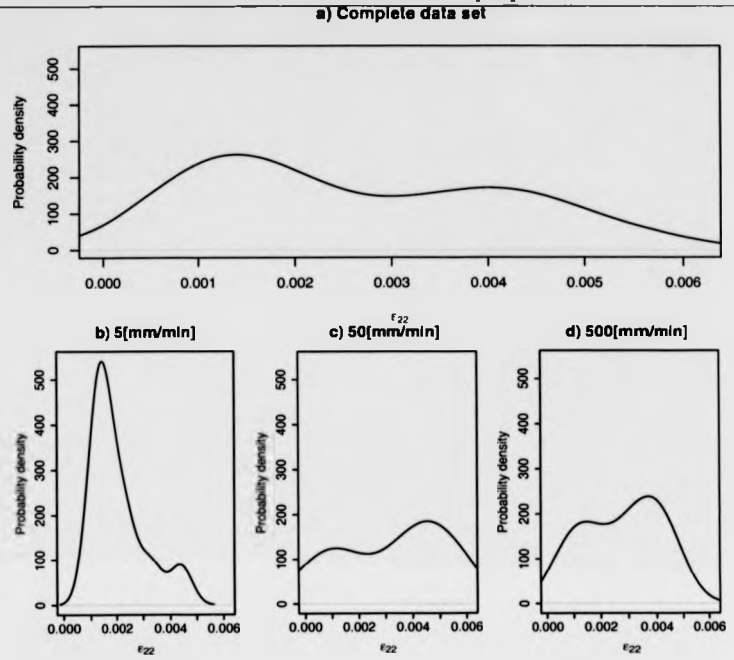

Figure D.39: Density plots of transverse tensile failure strain at a) all displacement rates, and b),c) and d) at each different crosshead displacement rate separately.

displacement rates are presented in table D.60, together with other information required for the calculations of the critical value.

The values in table D.60 suggest that all different groupings of the transverse tensile failure strain results follow a normal distribution.

Model fitting: Since, the transverse tensile failure strain at different crosshead displacement was not statistically different, despite the fact that both the fitted models exhibited an increase with strain rate in the figure 4.22. This is attributed to manufacturing and also in the instrumentation,

Table D.60: Statistics for the Goodness-of-Fit of transverse tensile failure strain probability density distribution.

Crosshead Rate	χ_0^2	α	# of Classes	χ_{crit}^2	Level
ALL	3.333	0.05	6	7.815	0.657
5	1	0.05	6	7.815	0.199
50	4	0.05	6	7.815	0.739
500	3.4	0.05	6	7.815	0.666

due to the very low strains to failure which can be observed for this class of laminates.

Since no strain rate dependency was statistically determined for the transverse tensile failure strain, the mean value of the complete data set is used. This value was computed 0.00284[].

D.3.3.2 Transverse Tensile Failure Stress σ_{22}

Figure D.40 presents the conditional plot of transverse tensile failure stress vs. transverse strain rate with respect to data acquisition source and failure location.

Figure D.41 presents the transverse tensile failure stress vs. strain rate log and a linear and a quadratic model of the log of the strain rate is fitted. The labeled observations are removed as outliers from the statistical treatment.

It should be noted that the prematurely failed specimens were already removed from the analysis. However, we can observe 3 distinct values between 5 an 6[MPa] (1 for the 5[mm/min] and 2 for the 50[mm/min] crosshead displacement rates). This values are almost certainly because of resin rich areas, attributable to manufacturing. They act as a reminder of the relatively low properties that materials of this class potentially have if not used/prepared properly.

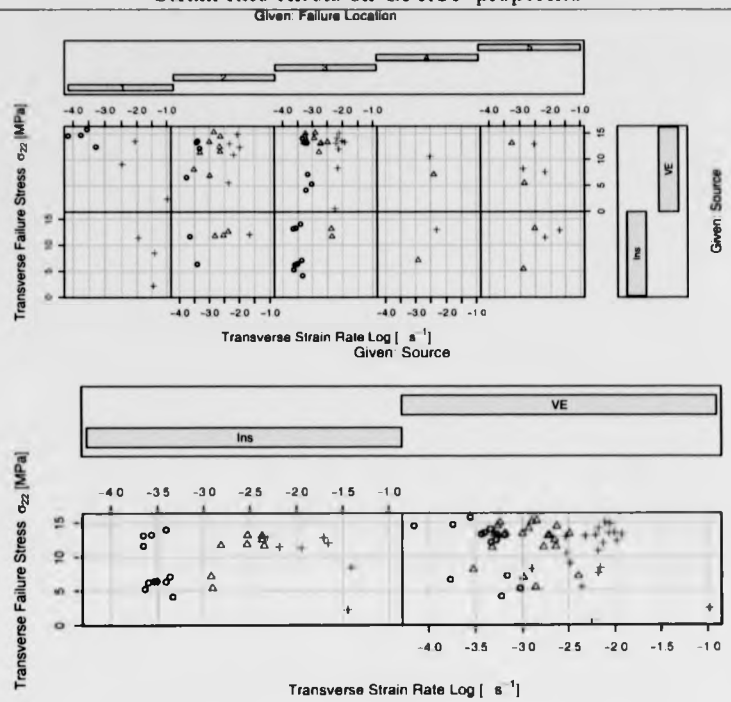

Figure D.40: Conditional plot of transverse tensile failure stress vs. logarithm of shear strain rate as obtained from the tensile testing of a $[+45]_8$ laminate, conditioned with respect of data acquisition source and failure location.

Statistics: Table D.61 presents the statistics of transverse tensile failure stress at different crosshead displacement rates of $[+45]_8$ laminate.

The mean of transverse tensile failure stress decreases for increasing crosshead displacement rate. The standard deviation is lowest at the 50[mm/min] crosshead displacement rate and highest at the 5[mm/min] crosshead displacement rate. The coefficient of variance is lowest for the 50[mm/min] crosshead displacement rate and highest for the 5[mm/min] crosshead displacement rate.

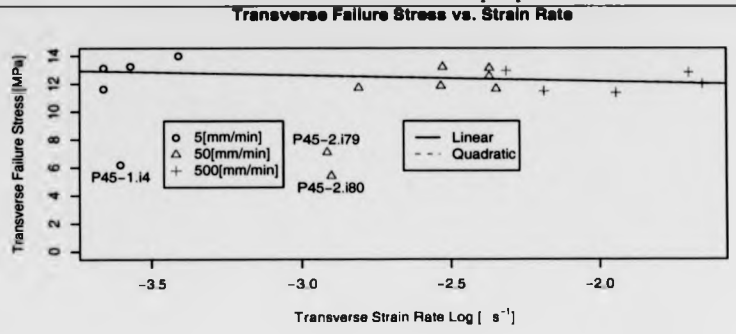

Figure D.41: Transverse tensile failure tensile stress vs. strain rate logarithm.

Table D.61: Statistics for the transverse tensile failure stress at different crosshead displacement rates.

Crosshead Rate		5	50	500
Mean	[MPa]	12.99	12.34	12.12
Standard Deviation	[MPa]	0.993	0.708	0.74
Coef. of Variance	[MPa]	0.0764	0.0574	0.0611

Hypothesis testing: The null hypothesis (H_0) is that the transverse tensile failure stress is not strain rate dependent. The alternative hypothesis is that the transverse tensile failure stress is strain rate dependent.

The statistics for the equality of means test are presented in table D.62. The columns are similar to the table D.54.

The transverse tensile failure stress at different crosshead displacement rates is not statistically different at a 5% level of confidence. Therefore, there is *no* indication that the transverse tensile failure stress is strain rate dependent.

The statistics for the equality of variances test are presented in table D.63. The columns are similar

Table D.62: Hypothesis testing statistics for equality of means of transverse tensile failure stress.

Crosshead Rate	t_0	α	df	t_{crit}	Level
5 vs. 50	1.14	0.05	6	1.94	0.85
50 vs. 500	0.51	0.05	10	1.812	0.689
5 vs. 500	1.469	0.05	6	1.943	0.904

to the table D.55.

Table D.63: Hypothesis testing for equality of variances statistics of transverse tensile failure stress.

Crosshead Rate	F_0	α	df1	df2	F_{crit}	Level
5 vs. 50	1.965	0.05	4	6	5.409	0.762
50 vs. 500	1.09	0.05	5	6	5.19	0.55
5 vs. 500	1.798	0.05	4	5	6.591	0.713

The results presented in table D.63 suggest that variances of the transverse tensile failure stress different crosshead crosshead displacement rates are *not* statistically different at a 5% significance level to the other crosshead displacement rates.

Distribution: Figure D.42 presents the probability density function plots of the transverse tensile failure stress (σ_{22}) at different crosshead displacement rates. Figure D.42(a) present the p.d.f. of the complete data set. Figures D.42 (b),(c) and (d) group the data set according to the crosshead displacement rate: 5, 50 and 500[mm/min] respectively.

The p.d.f. of the transverse tensile failure stress which is presented in figure D.42(a) appears to follow distribution with two primary peaks (which indicates that the result might come from more that one populations). The p.d.f. of transverse tensile failure stresses at the low D.42(b),

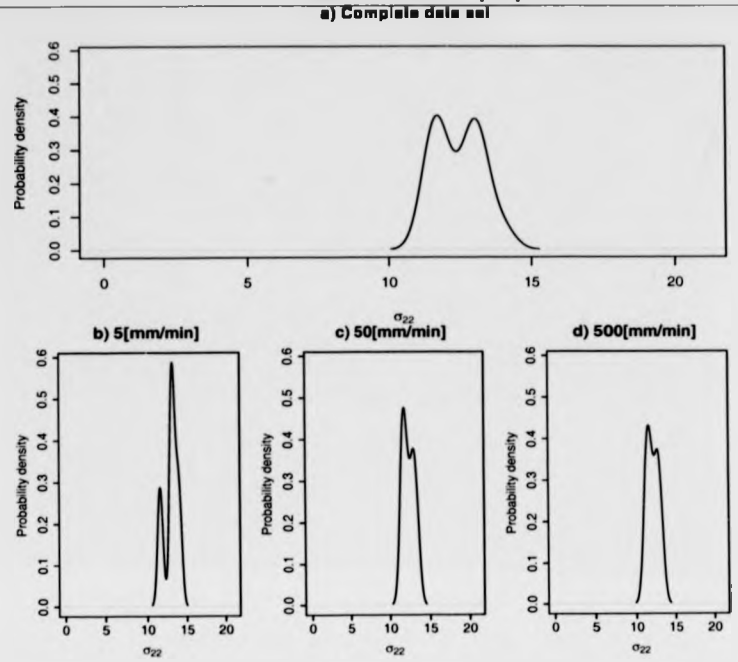

Figure D.42: Density plots of transverse tensile failure stress at a) all displacement rates, and b),c) and d) at each different crosshead displacement rate separately.

medium D.42(c) and high D.42(d) crosshead displacement rate appear to follow tighter normal distributions with a primary and a secondary peak.

The computed values of the χ_0^2 statistic for the complete data set and for the different crosshead displacement rates are presented in table D.64, together with other information required for the calculations of the critical value.

The values in table D.64 suggest that all different groupings of the transverse tensile failure stress results follow a normal distribution, which does not indicate the presence of strain rate sensitivity.

Table D.64: Statistics for the Goodness-of-Fit of transverse tensile failure stress probability density distribution.

Crosshead Rate	χ_0^2	α	# of Classes	χ_{crit}^2	Level
ALL	7	0.05	6	7.815	0.928
5	5	0.05	6	7.815	0.828
50	4	0.05	6	7.815	0.739
500	1	0.05	6	7.815	0.199

Model fitting: The transverse tensile failure stress at different crosshead displacement was not statistically different, which is in accordance to observations in the figure 1.22.

Since no strain rate dependency was statistically determined for the transverse tensile failure stress, the mean value of the complete data set is used. This value was computed 12.439[MPa].

D.3.3.3 Coupling Factor Between Plastic And Shear Strains A^2

Figure D.43 presents the conditional plot of the coupling factor between plastic and shear strains vs. transverse strain rate with respect to data acquisition source and failure location.

Figure D.44 presents the coupling factor between plastic and shear strains vs. strain rate log and a linear and a quadratic model of the log of the strain rate is fitted. The labeled observations are removed as outliers from the statistical treatment.

Statistics: Table D.65 presents the statistics of coupling factor between plastic and shear strains at different crosshead displacement rates of $[+45]_8$ laminates.

The mean of coupling factor between plastic and shear strains decreases for increasing crosshead displacement rate. The standard deviation is lowest at the 50[mm/min] crosshead displacement

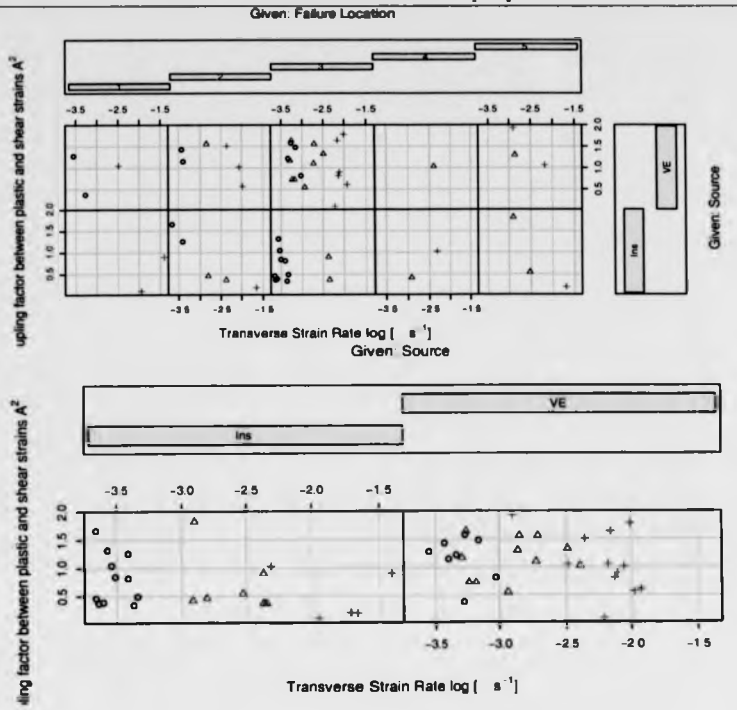

Figure D.43: Conditional plot of the coupling factor between plastic and shear strains vs. logarithm of shear strain rate as obtained from the tensile testing of a $[+45]_8$ laminate, conditioned with respect of data acquisition source and failure location.

rate and highest at the 500[mm/min] crosshead displacement rate. The coefficient of variance is lowest for the 50[mm/min] crosshead displacement rate and highest for the 500[mm/min] crosshead displacement rate.

Hypothesis testing: The null hypothesis (H_0) is that the coupling factor between plastic and shear strains is not strain rate dependent. The alternative hypothesis is that the coupling factor between plastic and shear strains is strain rate dependent.

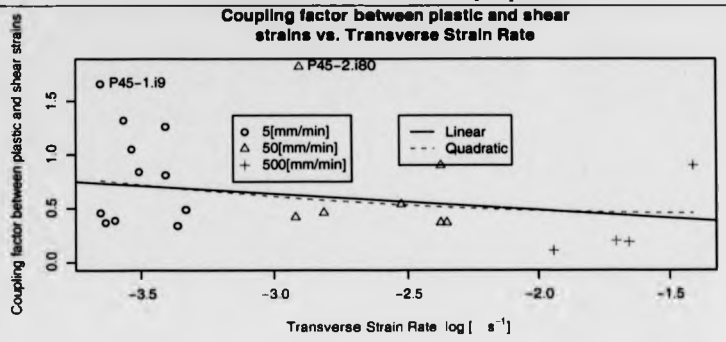

Figure D.44: Coupling factor between plastic and shear strains vs. strain rate logarithm.

Table D.65: Statistics for the coupling factor between plastic and shear strains at different crosshead displacement rates.

Crosshead Rate		5	50	500
Mean	[]	0.733	0.51	0.486
Standard Deviation	[]	0.377	0.201	0.441
Coef. of Variance	[]	0.514	0.395	0.908

The statistics for the equality of means test are presented in table D.66. The columns are similar to the table D.54.

Table D.66: Hypothesis testing statistics for equality of means of transverse tensile failure stress.

Crosshead Rate	t_0	α	df	t_{crit}	Level
5 vs. 50	1.54	0.05	15	1.753	0.928
50 vs. 500	0.112	0.05	6	1.943	0.543
5 vs. 500	1.072	0.05	8	1.86	0.842

The average of the coupling factor between plastic and shear strains at different crosshead dis-

placement rates are not statistically different at a 5% level of confidence. There is *no* indication that the coupling factor between plastic and shear strains is strain rate dependent.

The statistics for the equality of variances test are presented in table D.67. The columns are similar to the table D.55.

Table D.67: Hypothesis testing for equality of variances statistics of coupling factor between plastic and shear strains.

Crosshead Rate	F_0	α	df1	df2	F_{crit}	Level
5 vs. 50	3.5	0.05	10	6	4.77	0.91
50 vs. 500	4.796	0.05	5	6	5.192	0.942
5 vs. 500	1.37	0.05	5	10	3.633	0.682

The results presented in table D.67 suggest that there is no indication that the variances of the coupling factor between plastic and shear strains at different crosshead displacement rates are statistically different at a 5% significance level.

Distribution: Figure D.45 presents the probability density function plots of the coupling factor between plastic and shear strains (A^2) at different crosshead displacement rates. Figure D.45(a) present the p.d.f. of the complete data set. Figures D.45 (b),(c) and (d) group the data set according to the crosshead displacement rate: 5, 50 and 500[mm/min] respectively.

The p.d.f. of the coupling factor between plastic and shear strains which is presented in figure D.45(a) appears to follow a distribution with a primary and a secondary peak (which indicates that the result might come from a larger population). All the p.d.f.'s of crosshead displacement rate grouped data sets (figures D.45(b), D.45(c) and D.45(d)) appear to follow a distribution with

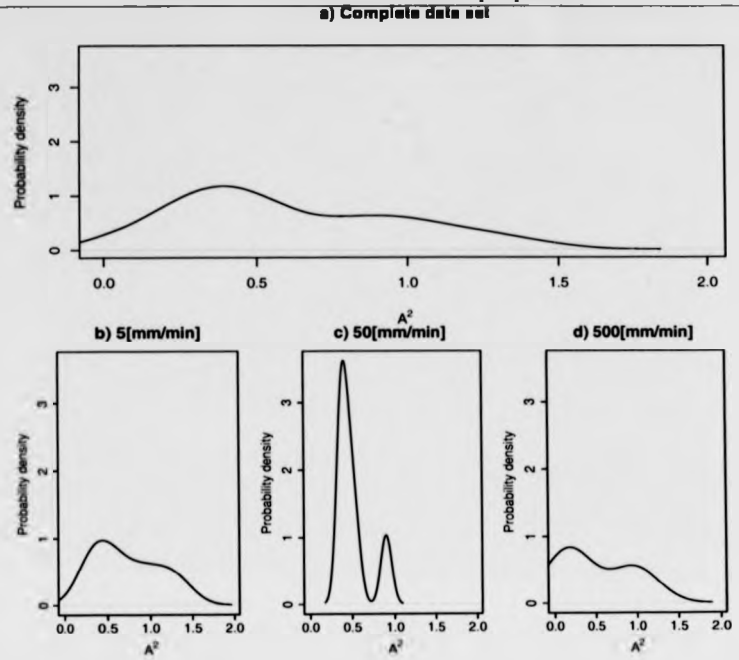

Figure D.45: Density plots of coupling factor between plastic and shear strains at a) all displacement rates, and b),c) and d) at each different crosshead displacement rate separately.

a primary and a secondary peak.

The computed values of the χ_0^2 statistic for the complete data set and for the different crosshead displacement rates are presented in table D.68, together with other information required for the calculations of the critical value.

The values in table D.68 suggest that only the 500[mm/min] crosshead displacement rate results are the only one that rejects the null hypothesis (i.e. the coupling factor between plastic and shear strains results follow a normal distribution).

Table D.68: Statistics for the Goodness-of-Fit of coupling factor between plastic and shear strains probability density distribution.

Crosshead Rate	χ_0^2	α	# of Classes	χ_{crit}^2	Level
ALL	5.571	0.05	6	7.815	0.866
5	5.6	0.05	6	7.815	0.867
50	6	0.05	6	7.815	0.888
500	8.2	0.05	6	7.815	0.958

Model fitting: The mean of the coupling factor between plastic and shear strains of all observed values is proposed since the no strain rate sensitivity could be determined statistically. The calculated value is 0.61048.

D.4 Properties Obtained From $[\pm 67.5°]_4$ Test.

D.4.1 Strain Rate.

D.4.1.1 Transverse Strain Rate.

Figure D.46 presents the logarithm of the transverse strain rate of the material vs. the crosshead displacement rate.

Statistics: Table D.69 presents the statistics of the transverse strain rate at different crosshead displacement rates.

The mean of the logarithm of transverse strain rate increases by approximately .9 when increasing the crosshead displacement rate from 5 to 50[mm/min] and then increases by less than .3 units

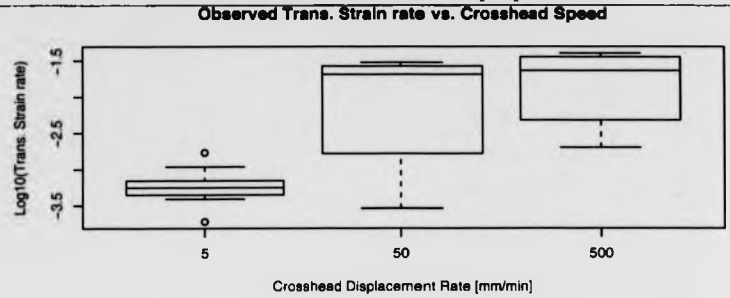

Figure D.46: Logarithm of Transverse Strain Rate vs. Crosshead displacement rate as obtained from the tensile testing of a $[\pm 67]_{2s}$ laminate.

Table D.69: Statistics for transverse strain rate at different crosshead displacement rates.

Crosshead Rate	5	50	500	
Mean	log[1/s]	-3.24	-2.16	-1.88
Standard Deviation	log[1/s]	0.203	0.679	0.484
Coef. of Variance		-0.0626	-0.3135	-0.2572

when increasing the crosshead displacement rate further to 500[mm/min]. The standard deviation appears to be in the same order of magnitude for the different crosshead displacement rates and the lowest value for standard deviation is at 50[mm/min] crosshead displacement rate. The lowest value for the coefficient of variance is at the 5[mm/min] crosshead displacement rate and the highest at the 50[mm/min] crosshead displacement rate .

D.4.1.2 Shear Strain Rate.

Figure D.48 presents the logarithm of the Shear strain rate of the material vs. the crosshead displacement rate.

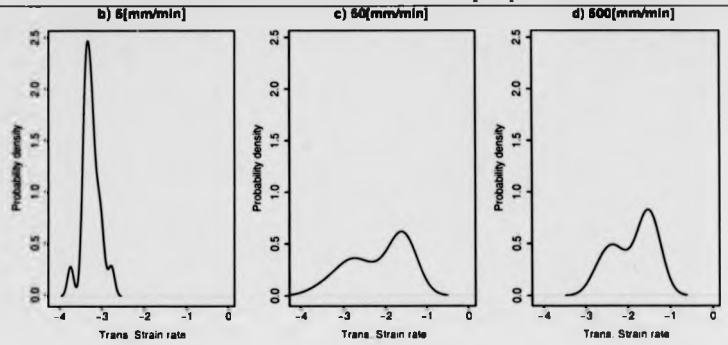

Figure D.47: Density plots of transverse strain rate for the different displacement rates.

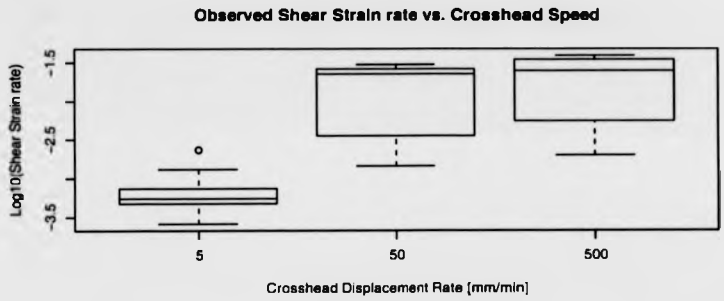

Figure D.48: Logarithm of Shear Strain Rate vs. Crosshead displacement rate as obtained from the tensile testing of a $[\pm 67]_{2s}$ laminate.

Statistics: Table D.70 presents the statistics of the Shear strain rate at different crosshead displacement rates.

The mean of the logarithm of shear strain rate increases by approximately .8 when increasing the crosshead displacement rate from 5 to 50[mm/min] and then increases by less than .3 units when increasing the crosshead displacement rate further to 500[mm/min]. The standard deviation appears to be in the same order of magnitude for the different crosshead displacement rates and the lowest value for standard deviation is at the 50[mm/min] crosshead displacement rate. The

Table D.70: Statistics for shear strain rate at different crosshead displacement rates.

Crosshead Rate	5	50	500	
Mean	log[1/s]	-3.21	-2.01	-1.86
Standard Deviation	log[1/s]	0.21	0.517	0.463
Coef. of Variance		-0.0654	-0.2577	-0.2489

lowest value for the coefficient of variance is at the 5[mm/min] crosshead displacement rate and the highest at 50[mm/min] crosshead displacement rate.

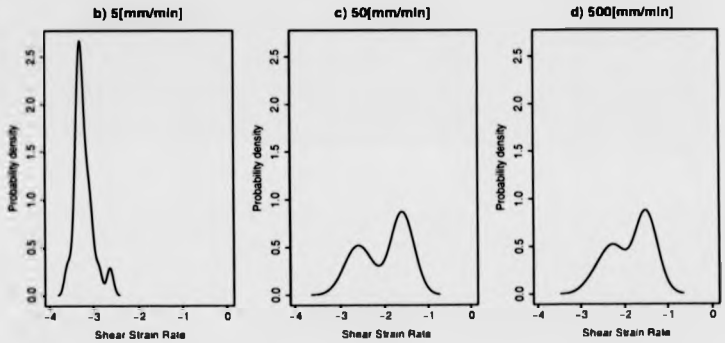

Figure D.49: Density plots of shear strain rate for the different displacement rates.

D.4.2 Strain Rate Effects On Transverse Damage Evolution

D.4.2.1 Initial Transverse Damage Limit Y_0'

Figure D.50 presents the conditional plot of initial transverse damage limit vs. transverse strain rate with respect to data acquisition source and failure location. The discrepancy of the trends between the sources of acquired data led use of the Instron data for the statistical analysis.

Figure D.51 presents the initial transverse damage limit vs. strain rate and two models (a linear

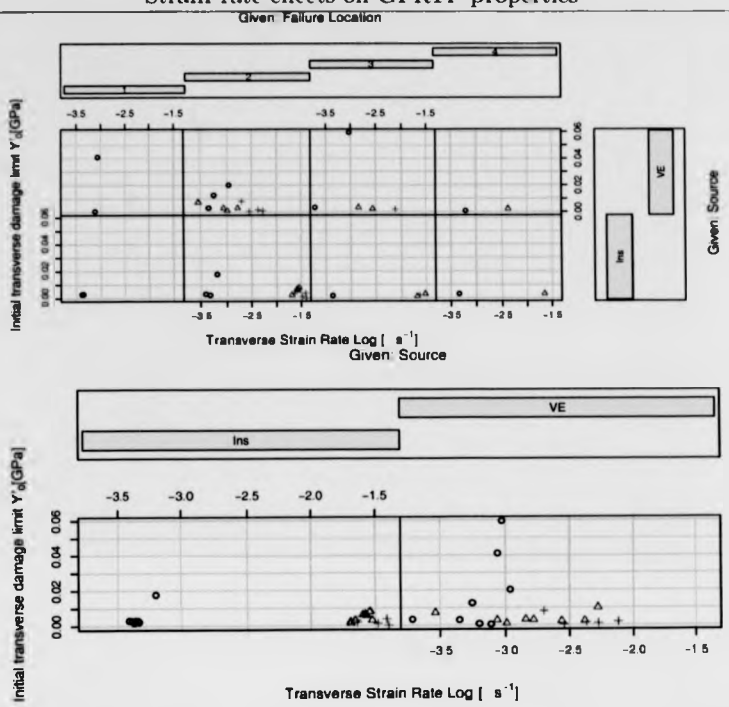

Figure D.50: Conditional plot of initial transverse damage limit vs. logarithm of shear strain rate as obtained from the tensile testing of a $[\pm 67]_{2s}$ laminate, conditioned with respect of data acquisition source and failure location.

and a quadratic model) of the logarithm of the strain rate are fitted. The labeled observations on figure D.51 were regarded outliers and were not included in the statistical treatment.

Statistics: Table D.71 presents the statistics of the initial transverse damage limit at different crosshead displacement rates as obtained from a $[\pm 67]_{2s}$ laminate.

The mean of the initial transverse damage limit appears to increase with crosshead displacement rate and then decrease. The standard deviation of the 5[mm/min] crosshead displacement rate

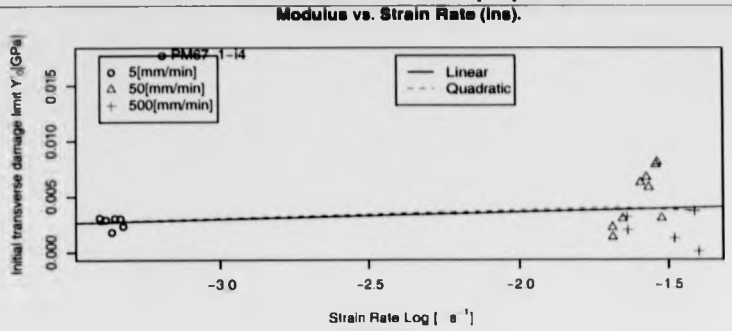

Figure D.51: Initial transverse damage limit vs. logarithm of strain rate as obtained from the tensile testing of a $[\pm 67]_{2s}$ laminate.

Table D.71: Statistics for the initial transverse damage limit at different crosshead displacement rates as obtained from a $[\pm 67]_{2s}$ laminate.

Crosshead Rate		5	50	500
Mean	$[\sqrt{GPa}]$	0.0027	0.00491	0.00201
Standard Deviation	$[\sqrt{GPa}]$	0.000519	0.002538	0.001457
Coef. of Variance	[]	0.192	0.516	0.724

is the lowest and is highest at the 50[mm/min] crosshead displacement rate. The coefficient of variance is lowest for the 5[mm/min] crosshead displacement rate and highest at the 500[mm/min] crosshead displacement rate.

Hypothesis testing: The null hypothesis (H_0) is that the initial transverse damage limit is not strain rate dependent. Therefore, the average of the initial transverse damage limit for one crosshead displacement rate results should be equal to the average of the initial transverse damage limit for another crosshead displacement rate, e.g. $H_0: \overline{Y}'_{0,5} = \overline{Y}'_{0,50}$. The alternative hypothesis

(H_1) which is accepted automatically if the null hypothesis is rejected is that the initial transverse damage limit is strain rate dependent.

The statistics for the equality of means test are presented in table D.72. The table presents the calculated test statistic t_0, the α-type error probability, the degrees of freedom df and the calculated critical value t_{crit}. In the final column, the level of confidence is presented (i.e. the value of α-type error probability for which the calculated critical value t_{crit} is equal to the statistic t_0).

Table D.72: Hypothesis testing statistics for the equality of averages of the initial transverse damage limit.

Crosshead Rate	t_0	α	df	t_{crit}	Level
5 vs. 50	2.534	0.05	9	1.833	0.984
50 vs. 500	2.716	0.05	13	1.771	0.991
5 vs. 500	1.01	0.05	5	2.02	0.82

The initial transverse damage limit at 5[mm/min] crosshead displacement rate *is* statistically different to the 50 and 500[mm/min] crosshead displacement rate at a 5% α-type probability error. Therefore, there is strong indication that initial damage limit *is* strain rate dependent.

The statistics for the equality of variances test are presented in table D.73. The table presents the calculated test statistic F_0, the α-type error probability, the degrees of freedom $df1$ and $df2$ and the calculated critical value F_{crit}. In the last column, the level of confidence is presented (i.e. the value of α-type error for which the critical value (F_{crit}) is equal to the statistic (F_0)).

The results presented in table D.73 suggest that the variance of the 5[mm/min] crosshead displacement rate is statistically different to the other crosshead displacement rates at a 5% α-type probability error.

Table D.73: Hypothesis testing for equality of variances statistics of the initial transverse damage limit.

Crosshead Rate	F_0	α	df1	df2	F_{crit}	Level
5 vs. 50	23.936	0.05	9	6	4.818	0.999
50 vs. 500	3.03	0.05	9	5	6.04	0.85
5 vs. 500	7.89	0.05	5	6	5.192	0.978

Distribution: Figure D.52 presents the probability density function plots of the initial transverse damage limit (Y_0') at different crosshead displacement rates. Figure D.52(a) present the p.d.f. of the complete data set. Figures D.52 (b),(c) and (d) group the data set according to the crosshead displacement rate: 5, 50 and 500[mm/min] respectively.

The p.d.f. of the initial transverse damage limit which is presented in figure D.52(a) appears to have one primary peak, but also a secondary peak is present. The grouped data sets at 5[mm/min] crosshead displacement rates D.52(b) appear to have a primary peak and a secondary point of inflection. As expected, the probability distribution function at the 50[mm/min] crosshead displacement rate (presented figure D.52(c)) of the initial transverse damage limit appears to follow a flat distribution with 2 peaks (however, it is generally flat). The probability distribution function at the 500[mm/min] crosshead displacement rate (presented figure D.52(d)) appears to follow a flat normal distribution.

The computed values of the χ_0^2 statistic for the complete data set and for the different crosshead displacement rates are presented in table D.74, together with other information required for the calculations of the critical value.

If the computed χ_0^2 statistic is smaller than the χ_{crit}^2 the conclusion is that there is no reason

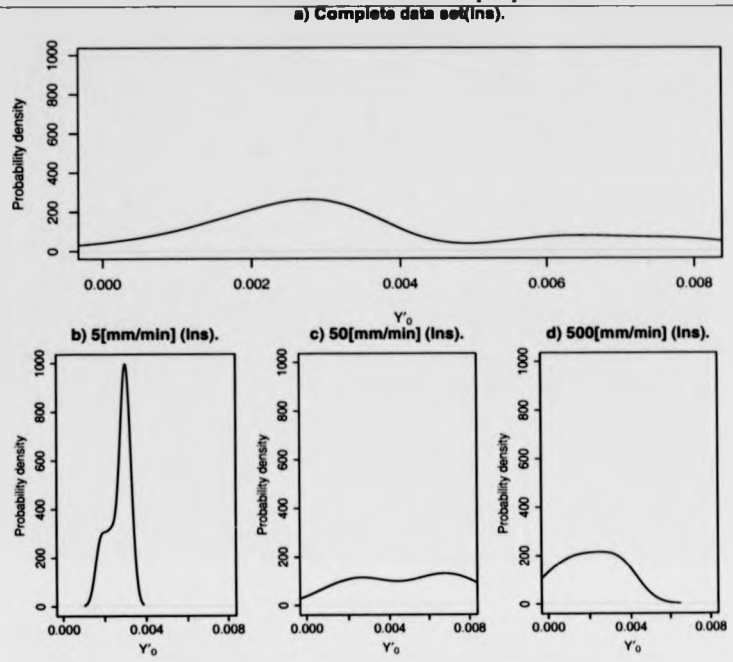

Figure D.52: Density plots of initial transverse damage limit at a) all displacement rates, and b),c) and d) at each different crosshead displacement rate separately.

Table D.74: Statistics for the Goodness-of-Fit of initial transverse damage limit probability density distribution.

Crosshead Rate	χ_0^2	α	# of Classes	χ_{crit}^2	Level
ALL	10	0.05	6	7.815	0.981
5	6	0.05	6	7.815	0.888
50	2.333	0.05	6	7.815	0.494
500	1	0.05	6	7.815	0.199

to reject the assumption that the distribution of the initial transverse damage limit is normally distributed.

The results in table D.74 suggest that only the complete data set does not appear to follow a normal distribution, which indicates strain rate dependency.

Model fitting: A linear model of the initial transverse damage limit with respect to the logarithm of the strain rate has the following form:

$$Y_0'(\dot{\varepsilon}) = 0.004879 + 0.000643 \cdot \log_{10}(\dot{\varepsilon}) \tag{D.19}$$

A quadratic model of the initial transverse damage limit with respect to the logarithm of the strain rate has the following form:

$$Y_0'(\dot{\varepsilon})) = -0.000145 - 0.004080 \cdot \log_{10}(\dot{\varepsilon}) - 0.000961 \cdot \log_{10}(\dot{\varepsilon})^2 \tag{D.20}$$

The null hypothesis for the analysis of variance is that the linear model explains the behaviour as adequately as the quadratic model. The statistics for the comparison of the two strain rate models of the initial transverse damage limit are presented in table D.75. The 29.8% probability which is presented in the table D.75 is the probability that the null hypothesis is true but instead the the null hypothesis is rejected. In this case, accepting that the quadratic model explain better the variability of the data is related to a probability of 79.6% that the assumption is wrong. Usually α type of error higher than 5% are considered unacceptable, and therefore the null hypothesis is not rejected, i.e. the equation for the linear model (eq. D.19) describes adequately the set of results. The coefficient of determination R^2 value is very low (.00777) which suggests that the initial transverse damage limit is dominated by other factors.

Table D.75: ANOVA results for the selection of the strain rate model order for the initial transverse damage limit.

Model	Res.Df	RSS	Df	Sum of Sq	F	$Pr(>F)$
Linear	18	8.85e-05				
Quadratic	17	8.82e-05	1	3.58e-07	0.0691	0.796

D.4.2.2 Critical Transverse Damage Limit Y_c'

Figure D.53 presents the conditional plot of critical transverse damage limit vs. transverse strain rate with respect to data acquisition source and failure location. The discrepancy of the trends between the sources of acquired data led use of the Instron data for the statistical analysis.

Figure D.54 presents the critical transverse damage limit vs. strain rate log and a linear and a quadratic model of the log of the strain rate is fitted. Also a magnified version is presented when the outliers are removed. The labeled observations are removed as outliers and they are not included in the statistical treatment.

Statistics: Table D.76 presents the statistics of critical transverse damage limit at different crosshead displacement rates of $[\pm 67.5]_{2s}$ laminate.

Table D.76: Statistics for the critical transverse damage limit at different crosshead displacement rates.

Crosshead Rate		5	50	500
Mean	$[\sqrt{GPa}]$	0.00364	0.00392	0.01524
Standard Deviation	$[\sqrt{GPa}]$	0.00194	0.00398	0.00758
Coef. of Variance	[]	0.533	1.015	0.497

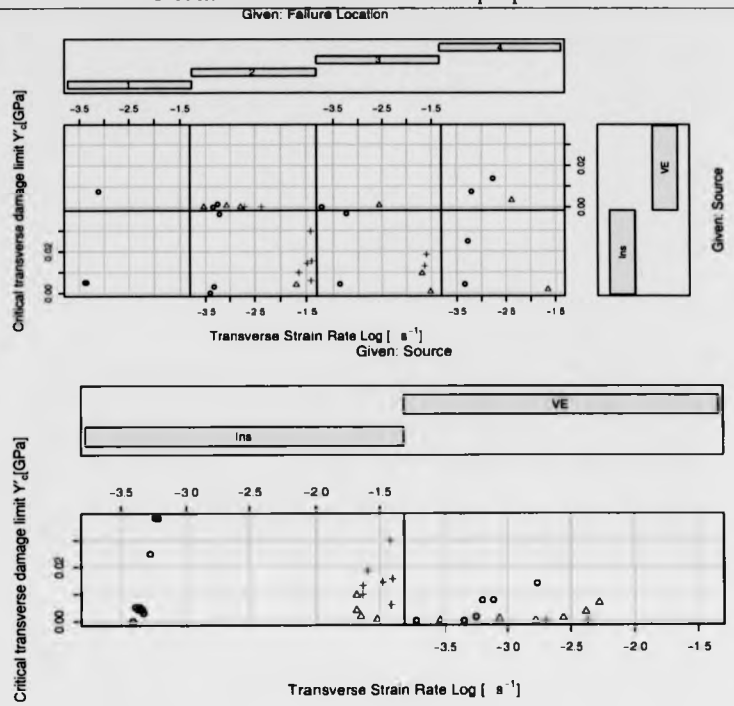

Figure D.53: Conditional plot of critical transverse damage limit vs. logarithm of shear strain rate as obtained from the tensile testing of a $[\pm 67]_{2s}$ laminate, conditioned with respect of data acquisition source and failure location.

The mean of critical transverse damage limit increases with increasing crosshead displacement rate. The standard deviation is lowest at the 5[mm/min] crosshead displacement rate and is highest at the 500[mm/min] crosshead displacement rate. The absolute value of the coefficient of variance is lowest at the 500 [mm/min] crosshead displacement rate and highest at the 50[mm/min] crosshead displacement rate.

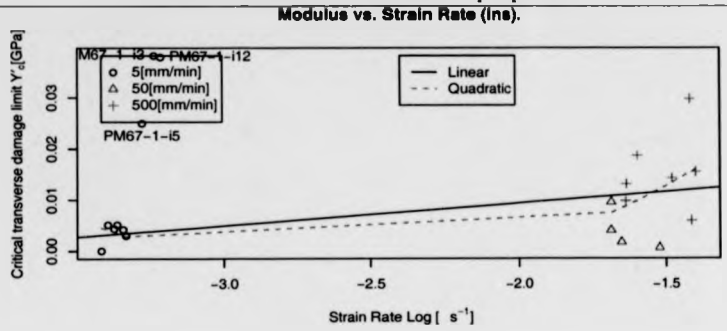

Figure D.54: Critical transverse damage limit vs. strain rate logarithm.

Hypothesis testing: The null hypothesis (H_0) is that the critical transverse damage limit is not strain rate dependent. The alternative hypothesis is that the critical transverse damage limit is strain rate dependent.

The statistics for the equality of means test are presented in table D.77. The columns are similar to the table D.72.

Table D.77: Hypothesis testing statistics for equality of means of critical transverse damage limit.

Crosshead Rate	t_0	α	df	t_{crit}	Level
5 vs. 50	0.133	0.05	4	2.132	0.55
50 vs. 500	3.244	0.05	10	1.812	0.996
5 vs. 500	3.904	0.05	7	1.895	0.997

The critical transverse damage limit at 500[mm/min] crosshead displacement rates is statistically different at a 5% level of confidence to the critical transverse damage limit at 5 and 50[mm/min] crosshead displacement rates. There *is* indication that the critical transverse damage limit is strain rate dependent.

The statistics for the equality of variances test are presented in table D.78. The columns are similar to the table D.73.

Table D.78: Hypothesis testing for equality of variances statistics of critical transverse damage limit.

Crosshead Rate	F_0	α	df1	df2	F_{crit}	Level
5 vs. 50	4.224	0.05	4	6	5.409	0.923
50 vs. 500	3.623	0.05	7	4	8.941	0.841
5 vs. 500	15.303	0.05	7	6	4.95	0.996

The results presented in table D.78 suggest that there is strong indication that, the variances of the critical transverse damage limit at 5 and 500[mm/min] crosshead displacement rates are statistically different at a 5% significance level for any given pair.

Distribution: Figure D.55 presents the probability density function plots of the critical transverse damage limit (Y_c') at different crosshead displacement rates. Figure D.55(a) present the p.d.f. of the complete data set. Figures D.55 (b),(c) and (d) group the data set according to the crosshead displacement rate: 5, 50 and 500[mm/min] respectively.

The p.d.f. of the critical transverse damage limit which is presented in figure D.55(a) appears to follow a flat skewed distribution with a single peak. The different crosshead displacement rate data sets behave differently. The 5[mm/min] crosshead displacement rate (figure D.55(b)) appears to follow a distribution with a primary and a secondary peak (the peak is at a lower value of the critical transverse damage limit). Similarly, the 50 and 500 [mm/min] crosshead displacement rate (presented respectively in figures D.55(c)) and D.55(d)) appears to follow a distribution with a

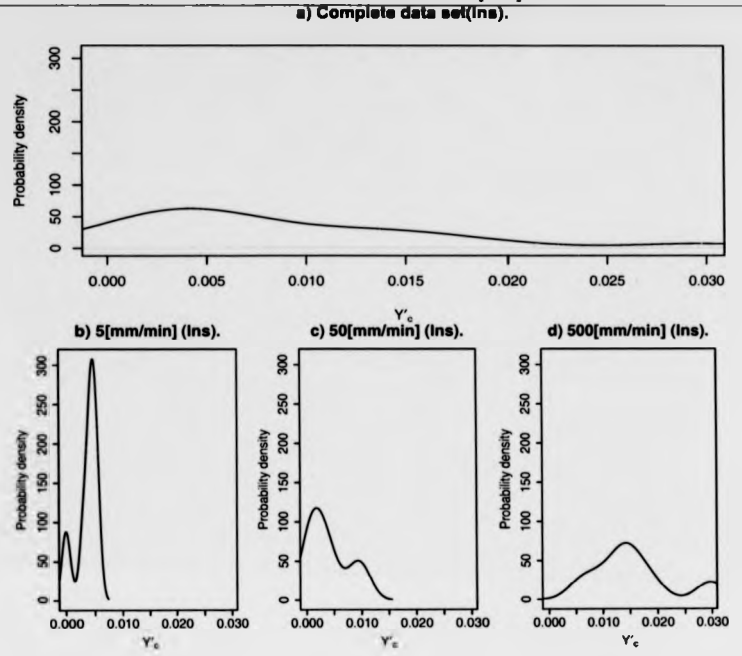

Figure D.55: Density plots of critical transverse damage limit at a) all displacement rates, and b),c) and d) at each different crosshead displacement rate separately.

primary peak and a secondary peak (the peak is at a higher value of the critical transverse damage limit).

The computed values of the χ_0^2 statistic for the complete data set and for the different crosshead displacement rates are presented in table D.79, together with other information required for the calculations of the critical value.

The values in table D.79 suggest that there *is* indication to reject the hypothesis that the critical transverse damage limit results follow a normal distribution at a 5% α type error only for the complete data set. This indicates strain rate dependency.

Table D.79: Statistics for the Goodness-of-Fit of critical transverse damage limit probability density distribution.

Crosshead Rate	χ_0^2	α	# of Classes	χ^2_{crit}	Level
ALL	8.059	0.05	6	7.815	0.955
5	4	0.05	6	7.815	0.739
50	5	0.05	6	7.815	0.828
500	0.714	0.05	6	7.815	0.13

Model fitting: A linear model of the critical transverse damage limit with respect to the logarithm of the strain rate has the following form:

$$Y_c'(\dot{\varepsilon}) = 0.01821 + 0.00443 \cdot \log_{10}(\dot{\varepsilon}) \tag{D.21}$$

A quadratic model of the critical transverse damage limit with respect to the logarithm of the strain rate has the following form:

$$Y_c'(\dot{\varepsilon}) = 0.0898 + 0.0722 \cdot \log_{10}(\dot{\varepsilon}) + 0.0138 \cdot \log_{10}(\dot{\varepsilon})^2 \tag{D.22}$$

The statistics for the comparison of the two strain rate models of critical transverse damage limit are presented in table D.80. According to the data, the null hypothesis is not rejected at a significance level, i.e. the equation for the linear model (eq. D.21) describes adequately the set of results.

The coefficient of determination R^2 value for the linear model is very low (.214). Such a low value and the fact that only one of the comparison pairs is statistically different could indicate that there is actually no strain rate effect on the critical transverse damage limit or that other factors are as equally important for the explanation of the variability of the results.

Table D.80: ANOVA results for the selection of the strain rate model order of the critical transverse damage limit.

Model	Res.Df	RSS	Df	Sum of Sq	F	$Pr(>F)$
Linear	15	0.000703				
Quadratic	14	0.000616	1	8.68e-05	1.97	0.182

D.4.2.3 Brittle Transverse Damage Limit Y_S'

Figure D.56 presents the conditional plot of brittle transverse damage limit vs. transverse strain rate with respect to data acquisition source and failure location. The discrepancy of the trends between the sources of acquired data led use of the Instron data for the statistical analysis.

Figure D.57 presents the brittle transverse damage limit vs. strain rate log and a linear and a quadratic model of the log of the strain rate is fitted. The labeled observations are removed as outliers and they are not included in the statistical treatment.

Statistics: Table D.81 presents the statistics of Brittle transverse damage limit at different crosshead displacement rates of $[\pm 67.5]_{2s}$ laminate.

Table D.81: Statistics for the brittle transverse damage limit at different crosshead displacement rates.

Crosshead Rate		5	50	500
Mean	$[\sqrt{GPa}]$	0.00638	0.00685	0.00993
Standard Deviation	$[\sqrt{GPa}]$	0.001225	0.000801	0.001851
Coef. of Variance	[]	0.192	0.117	0.187

The mean of brittle transverse damage limit increases with increasing crosshead displacement rate.

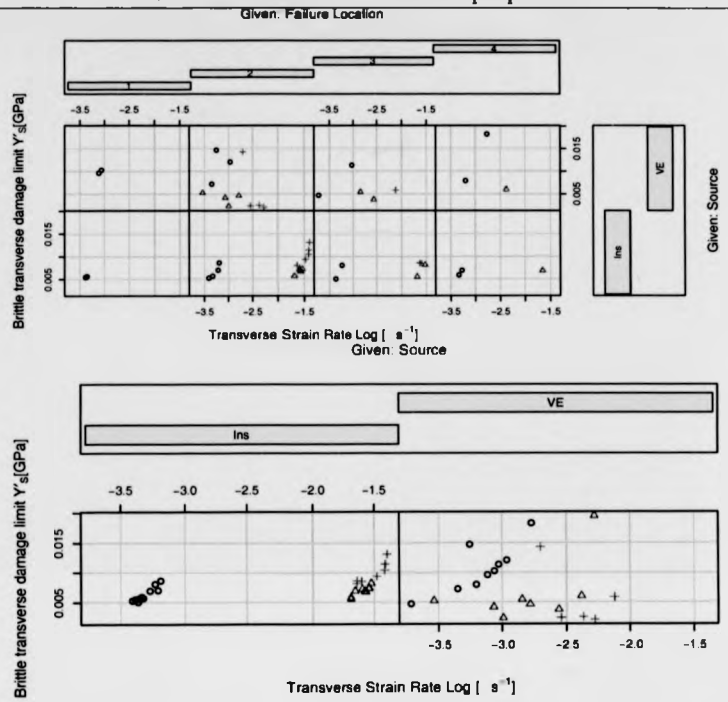

Figure D.56: Conditional plot of brittle transverse damage limit vs. logarithm of shear strain rate as obtained from the tensile testing of a $[\pm 67]_{2s}$ laminate, conditioned with respect of data acquisition source and failure location.

The standard deviation is lowest again at the 50[mm/min] crosshead displacement and highest at the 500[mm/min] crosshead displacement rate. The coefficient of variance is lowest for the 50 [mm/min] crosshead displacement rate and highest at the 5[mm/min] crosshead displacement rate.

Hypothesis testing: The null hypothesis (H_0) is that the brittle transverse damage limit is not strain rate dependent. The alternative hypothesis is that the brittle transverse damage limit is strain rate dependent.

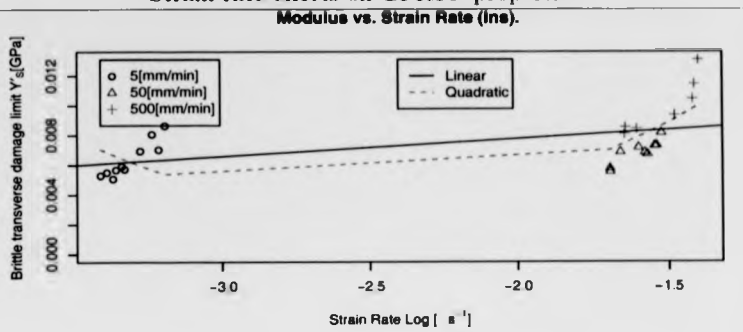

Figure D.57: Brittle transverse damage limit vs. strain rate logarithm.

The statistics for the equality of means test are presented in table D.82. The columns are similar to the table D.72.

Table D.82: Hypothesis testing statistics for equality of means of brittle transverse damage limit.

Crosshead Rate	t_0	α	df	t_{crit}	Level
5 vs. 50	0.985	0.05	17	1.74	0.831
50 vs. 500	4.111	0.05	8	1.86	0.998
5 vs. 500	4.429	0.05	10	1.812	0.999

The brittle transverse damage limit at 500[mm/min] crosshead displacement rates is statistically different at a 5% level of confidence to the brittle transverse damage limit at 5 and 50[mm/min] crosshead displacement rates. There is indication that the brittle transverse damage limit is strain rate dependent.

The statistics for the equality of variances test are presented in table D.83. The columns are similar to the table D.73.

The results presented in table D.83 suggest that there is indication that the variances of the brittle

Table D.83: Hypothesis testing for equality of variances statistics of brittle transverse damage limit.

Crosshead Rate	F_0	α	df1	df2	F_{crit}	Level
5 vs. 50	2.338	0.05	10	9	3.388	0.877
50 vs. 500	5.34	0.05	7	9	3.581	0.983
5 vs. 500	2.284	0.05	7	10	3.374	0.872

transverse damage limit at 50 and 500[mm/min] crosshead displacement rates are statistically different at a 5% significance level. There is no indication for the other pairs.

Distribution: Figure D.58 presents the probability density function plots of the brittle transverse damage limit (Y_S') at different crosshead displacement rates. Figure D.58(a) present the p.d.f. of the complete data set. Figures D.58 (b),(c) and (d) group the data set according to the crosshead displacement rate: 5, 50 and 500[mm/min] respectively.

The p.d.f. of the brittle transverse damage limit which is presented in figure D.58(a) appears to follow a skewed flat normal distribution. The p.d.f.'s for the brittle transverse damage limit at 5 and 500[mm/min] crosshead displacement rates (figures D.58(b), and D.58(d)) appear to follow a skewed distribution with a primary peak and a secondary point of inflection. The p.d.f. for the brittle transverse damage limit at 50[mm/min] crosshead displacement rates (figure D.58(c)) appears to follow a distribution with multiple distinctive peaks.

The computed values of the χ_0^2 statistic for the complete data set and for the different crosshead displacement rates are presented in table D.84, together with other information required for the calculations of the brittle transverse damage limit value.

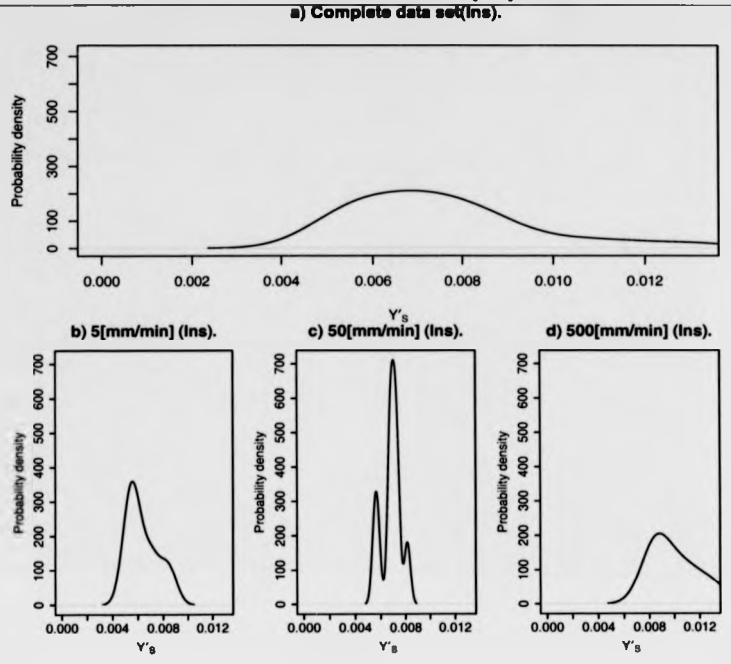

Figure D.58: Density plots of brittle transverse damage limit at a) all displacement rates, and b),c) and d) at each different crosshead displacement rate separately.

Table D.84: Statistics for the Goodness-of-Fit of brittle transverse damage limit probability density distribution.

Crosshead Rate	χ_0^2	α	# of Classes	χ_{crit}^2	Level
ALL	4	0.05	6	7.815	0.739
5	5.6	0.05	6	7.815	0.867
50	2.333	0.05	6	7.815	0.494
500	0.714	0.05	6	7.815	0.13

The values in table D.84 suggest that there is no indication that null hypothesis should be rejected (i.e. the results for a brittle transverse damage limit results follow a normal distribution at all crosshead displacement rates).

Model fitting: A linear model of the brittle transverse damage limit with respect to the logarithm of the strain rate has the following form:

$$Y'_S(\dot{\varepsilon}) = 0.01016 + 0.00119 \cdot \log_{10}(\dot{\varepsilon}) \tag{D.23}$$

A quadratic model of the brittle transverse damage limit with respect to the logarithm of the strain rate has the following form:

$$Y''_S(\dot{\varepsilon}) = 0.03646 + 0.02609 \cdot \log_{10}(\dot{\varepsilon}) + 0.00512 \cdot \log_{10}(\dot{\varepsilon})^2 \tag{D.24}$$

The statistics for the comparison of the two strain rate models of Brittle transverse damage limit are presented in table D.85. According to the data, the null hypothesis is rejected at a 5% significance level, i.e. the equation for the quadratic model (eq. D.24) better describes the set of results.

Table D.85: ANOVA results for the selection of the strain rate model order of the brittle transverse damage limit.

Model	Res.Df	RSS	Df	Sum of Sq	F	$Pr(>F)$
Linear	24	6.95e-05				
Quadratic	23	5.43e-05	1	1.52e-05	6.45	0.0183

The coefficient of determination R^2 value for the linear model is relatively high. (.39).

D.4.3 Coupling Factor Between Transverse And Shear Damage b

Figure D.59 presents the conditional plot of coupling factor between transverse and shear damage vs. transverse strain rate with respect to data acquisition source and failure location. The discrepancy of the trends between the sources of acquired data led use of the Instron data for the statistical analysis.

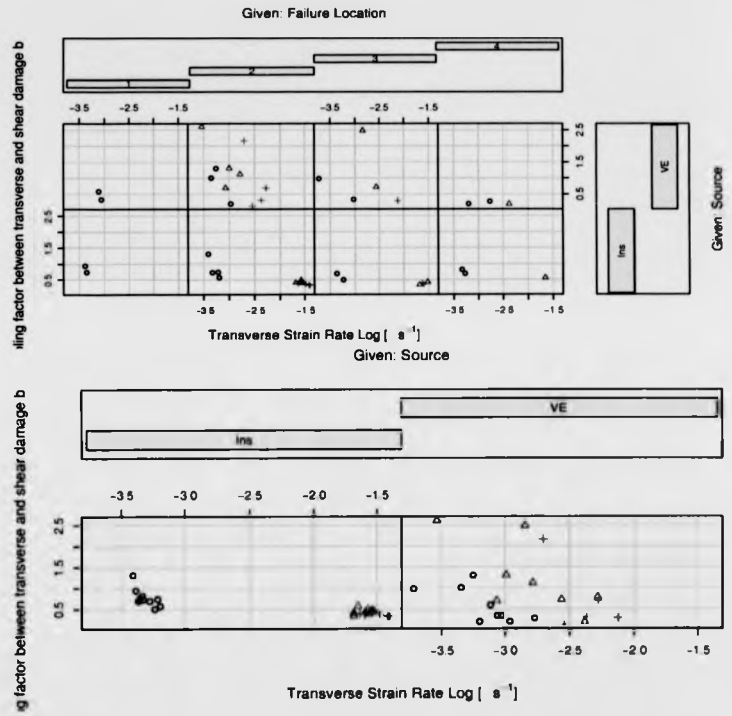

Figure D.59: Conditional plot of coupling factor between transverse and shear damage vs. logarithm of transverse strain rate as obtained from the tensile testing of a $[\pm 67]_{2s}$ laminate, conditioned with respect of data acquisition source and failure location.

Figure D.60 presents the coupling factor between transverse and shear damage vs. strain rate log

and a linear and a quadratic model of the log of the strain rate is fitted. The labeled observations are removed as outliers and they are not included in the statistical treatment. Figure D.60 presents the coupling factor between the transverse and shear damage after the outliers have been removed.

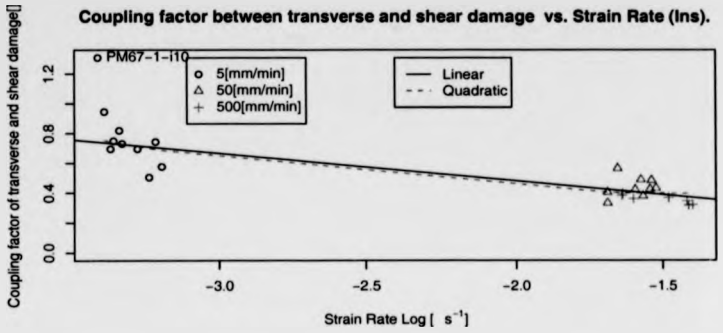

Figure D.60: Coupling factor between transverse and shear damage vs. strain rate logarithm.

Statistics: Table D.86 presents the statistics of coupling factor between transverse and shear damage at different crosshead displacement rates of $[\pm 67.5]_{2s}$ laminate.

Table D.86: Statistics for the coupling factor between transverse and shear damage at different crosshead displacement rates.

Crosshead Rate		5	50	500
Mean	[]	0.776	0.437	0.356
Standard Deviation	[]	0.2222	0.0679	0.0298
Coef. of Variance	[]	0.2862	0.1555	0.0838

The mean of coupling factor between transverse and shear damage decreases with increasing crosshead displacement rate. The standard deviation is lowest at the 500[mm/min] crosshead

displacement rate and highest at the 5[mm/min] crosshead displacement rate. The coefficient of variance is lowest for the 500 [mm/min] crosshead displacement rate and highest for the 5[mm/min] crosshead displacement rate.

Hypothesis testing: The null hypothesis (H_0) is that the coupling factor between transverse and shear damage is not strain rate dependent. The alternative hypothesis is that the coupling factor between transverse and shear damage is strain rate dependent.

The statistics for the equality of means test are presented in table D.87. The columns are similar to the table D.72.

Table D.87: Hypothesis testing statistics for equality of means of coupling factor between transverse and shear damage.

Crosshead Rate	t_0	α	df	t_{crit}	Level
5 vs. 50	4.6	0.05	11	1.8	1
50 vs. 500	3.186	0.05	12	1.782	0.996
5 vs. 500	5.91	0.05	9	1.83	1

The coupling factor between transverse and shear damage *is* statistically different at a 5% level of confidence to the coupling factor between transverse and shear damage at all given pairs of crosshead displacement rates. There *is* indication that the coupling factor between transverse and shear damage *is* strain rate dependent.

The statistics for the equality of variances test are presented in table D.88. The columns are similar to the table D.73.

The results presented in table D.88 suggest that the variances of the coupling factor between

Table D.88: Hypothesis testing for equality of variances statistics of coupling factor between transverse and shear damage.

Crosshead Rate	F_0	α	df1	df2	F_{crit}	Level
5 vs. 50	10.712	0.05	10	9	3.388	0.999
50 vs. 500	5.18	0.05	9	7	4.15	0.97
5 vs. 500	55.44	0.05	10	7	4.1	1

transverse and shear damage at different crosshead displacement rates *are* statistically different at a 5% significance level for any given pair. This reduces the validity of the regression analysis.

Distribution: Figure D.61 presents the probability density function plots of the coupling factor between transverse and shear damage (bcf) at different crosshead displacement rates. Figure D.61(a) present the p.d.f. of the complete data set. Figures D.61 (b),(c) and (d) group the data set according to the crosshead displacement rate: 5, 50 and 500[mm/min] respectively.

The p.d.f. of the coupling factor between transverse and shear damage which is presented in figure D.61(a) appears to follow a flat distributiona with a primary and a secondary peak (which indicates that the result might come from a larger population). The p.d.f.'s of the 5[mm/min] crosshead displacement rate (presented in figure D.61(b)) appear to follow a multimodal distribution. Finally, the p.d.f. of the 50 and 500[mm/min] crosshead displacement rate (presented in figures D.61(c) and D.61(d) respectively) appear to follow normal distribution with with a primary peak and a point of inflection.

The computed values of the χ_0^2 statistic for the complete data set and for the different crosshead displacement rates are presented in table D.89, together with other information required for the

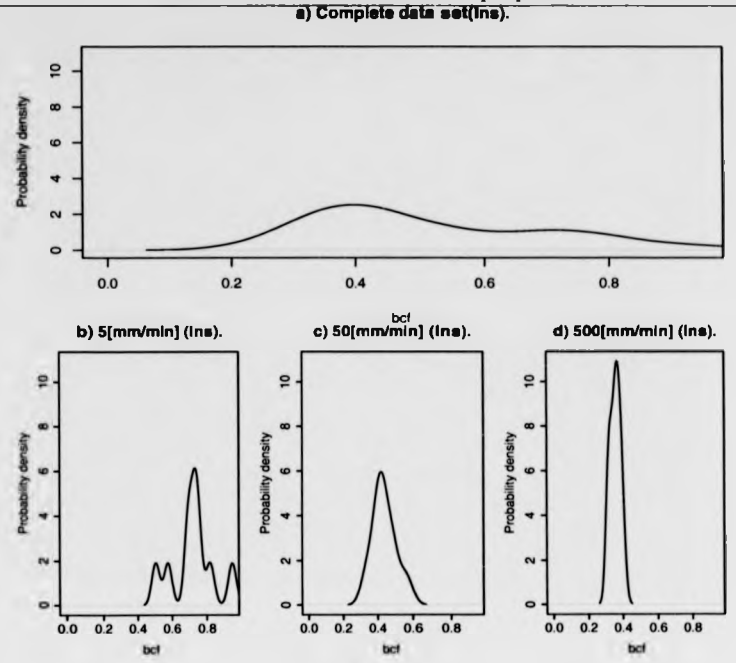

Figure D.61: Density plots of coupling factor between transverse and shear damage at a) all displacement rates, and b),c) and d) at each different crosshead displacement rate separately.

calculations of the brittle value.

Table D.89: Statistics for the Goodness-of-Fit of coupling factor between transverse and shear damage probability density distribution.

Crosshead Rate	χ_0^2	α	# of Classes	χ_{crit}^2	Level
ALL	18.31	0.05	6	7.81	1
5	8	0.05	6	7.815	0.954
50	3.67	0.05	6	7.81	0.7
500	2.429	0.05	6	7.815	0.512

The values in table D.89 suggest that there *is* indication the null hypothesis should be rejected for the complete data set and the 5[mm/min] crosshead displacement rate (i.e. the coupling factor between transverse and shear damage results do not follow a normal distribution).

Model fitting: A linear model of the coupling factor between transverse and shear damage with respect to the logarithm of the strain rate has the following form:

$$b(\dot{\varepsilon}) = 0.0546 - 0.2199 \cdot \log_{10}(\dot{\varepsilon}) \tag{D.25}$$

A quadratic model of the coupling factor between transverse and shear damage with respect to the logarithm of the strain rate has the following form:

$$b(\dot{\varepsilon}) = 1.426 + 1.079 \cdot \log_{10}(\dot{\varepsilon}) + 0.267 \cdot \log_{10}(\dot{\varepsilon})^2 \tag{D.26}$$

The statistics for the comparison of the two strain rate models of coupling factor between transverse and shear damage are presented in table D.90. According to the data, the null hypothesis is *not* rejected at a significance level, i.e. the linear function (eq. D.25) describes adequately the set of results.

Table D.90: ANOVA results for the selection of the strain rate model order of the coupling factor between transverse and shear damage.

Model	Res.Df	RSS	Df	Sum of Sq	F	$Pr(>F)$
Linear	24	0.457				
Quadratic	23	0.416	1	0.0414	2.29	0.144

The coefficient of determination R^2 value for the linear model is quite high(.655).

Index